Use of unconventional activation methods for the oxidative cleavage of lignin by dioxygen

Louay Al-Hussaini

Sorbonne Université

Ecole doctorale n°397

Programme Génie des Procédés

Laboratoire de Réactivité de Surface

Utilisation de moyens d'activation non-conventionnels pour le clivage oxydant de la lignine par le dioxygène

Louay AL-HUSSAINI

Thèse de doctorat de Physique et Chimie des matériaux

Dirigée par Franck LAUNAY

Présentée et soutenue publiquement le 16 Octobre 2019

Devant un jury composé de :

Mme. DUFAUD-NICCOLAI Véronique, Directrice de Recherche, Université Claude Bernard Lyon 1	Rapportrice
M. LAMATY Frédéric, Directeur de Recherche, Université de Montpellier	Rapporteur
Mme. VALANGE Sabine, Maître de Conférences (HDR), ENSI de Poitiers	Examinatrice
M. DA COSTA Patrick, Professeur, Sorbonne Université	Examinateur
M. LAUNAY Franck, Professeur, Sorbonne Université	Directeur
Mme. GALVEZ Elena, Maître de Conférences (HDR), Sorbonne Université	Co-directrice
Mme. ROUSSEAU Brigitte, Maître de Conférences, Sorbonne Université	Invitée
M. DELMAS Guo-Hua, Responsable R&D, BioEB	Invité

Sommaire

Liste des figures

Liste des tableaux :

REMERCIEMENTS

Je tiens tout naturellement à exprimer ma gratitude à mes directeurs de thèse et encadrants Franck LAUNAY (LRS) et Elena GALVEZ (∂'Alembert) de me donner ma chance, pour leurs conseils et leur aide que ce soit pour le déroulement des travaux, pour surmonter les difficultés que nous avons pu rencontrer, pour les présentations réalisées durant les congrès auquel j'ai eu la chance de pouvoir participer ainsi que pour l'écriture de ce présent manuscrit de thèse. Franck, merci pour ta rigueur scientifique, pour ton écoute et de m'avoir fait partager tes connaissances que ce soit dans la catalyse ainsi qu'en ce qui concerne le monde de la recherche et de m'avoir incité à me surpasser. J'admets que j'ai pu te donner du fil à retordre avec mon caractère parfois un peu « têtu ». Elena, merci pour ta patience et ton calme à tout épreuve qui m'ont aidé à surmonter les mauvais moments de cette thèse et de m'avoir initié au monde fou de l'intensification sono-chimique.

Je tiens à remercier les directeurs des deux laboratoires (Hélène PERNOT au LRS et Pierre-Yves LAGREE à ∂'Alembert) de m'avoir accueilli durant ces trois ans.

Je voudrais aussi exprimer ma gratitude envers les membres du LRS et plus largement de Sorbonne Université et du CNRS qui m'ont aidé durant ces trois ans de thèse et m'ont formé à diverses techniques, plus particulièrement Jean-Marc KRAFFT (Spectroscopie Raman), Vincent HUMBLOT (FT-IR), Mohamed SELMANE (DRX), Claire TROUFFLARD et Aurélie BERNARD (RMN) et Florie LOPIS pour la fabrication du montage pour irradiation sous ultrasons au LRS. Vos contributions m'ont permis d'avancer dans mes travaux.

J'ai eu aussi la chance d'avoir été impliqué dans plusieurs collaborations qui se sont avérées fructueuses. Je tiens à exprimer ma plus profonde gratitude à Martine TEISSIER et à Brigitte ROUSSEAU pour m'avoir fait partager leurs connaissances sur la chimie de la lignine, de leur aide pour caractériser ce polymère qui m'a bien donné du fil à retordre. Martine, je te souhaite une bonne retraite ! Une nouvelle vie t'attend. Aussi, je voudrais exprimer ma gratitude la plus profonde à Sabine VALANGE et à Prince AMANIAMPONG pour leur aide et pour m'avoir accueilli dans les locaux de l'IC2MP (Institut De Chimie des Milieux et des Matériaux de Poitiers) afin que je puisse réaliser les tests sous pression et irradiation par ultrasons. Enfin, je voudrais dire merci aux fournisseurs de lignine Guo-Hua et Michel DELMAS. Je n'oublie pas que Michel est celui qui m'a initié à la chimie de la lignine quand j'étais étudiant à l'ENSIACET (Ecole Nationale Supérieure des Ingénieurs en Arts Chimiques et Technologiques) et qui m'a fait partager non seulement ses connaissances mais aussi son enthousiasme sur ce polymère plein de surprises et aussi plein d'avenir.

J’espère que ces collaborations continueront à porter leurs fruits, même après mon départ.
Je voudrais aussi dire un grand merci à Gautier, à Elie et à Zahia de m’avoir aidé durant mes travaux, que ce soit pour la synthèse des modèles, la purification de la lignine, les premières ébauches de catalyse hétérogène ou à dompter le montage d’irradiation par ultrasons à Saint-Cyr l’Ecole.

Evidemment, je voudrais exprimer ma plus profonde gratitude envers mes collègues du LRS et de ∂’Alembert (la liste est longue !). Merci pour ces rencontres enrichissantes, pour les rires et pour les moments que nous avons partagés que ce soit au laboratoire ou durant les soirées. J’ai une pensée toute particulière pour Asma et Matthieu avec qui j’ai partagé le bureau durant ma thèse. Asma, de tout mon cœur merci pour ta disponibilité et ta gentillesse. Merci pour toute l’aide que tu m’as apportée et je tiens à te souhaiter bonne chance pour ta vie d’enseignante. Matthieu, merci de tout mon cœur pour m’avoir soutenu, surtout au moment de la rédaction du manuscrit, la période la plus stressante de la thèse. Je tiens à te souhaiter bon courage pour la dernière ligne droite. Ce n’est pas la période la plus évidente…

Enfin, je voudrais remercier mes parents (Nabil et Chantal), ma sœur Hana et mon frère Houssam. Merci de m’avoir permis de devenir ce que je suis, pour votre soutien sans faille durant toute ma thèse et plus largement durant tout mon parcours, de m’avoir aidé à surmonter toutes les difficultés auxquelles j’ai été confronté. Je n’aurai jamais pu en être là où je suis actuellement sans cela. Une famille soudée est un refuge sur lequel on peut toujours compter.

INTRODUCTION GENERALE

De nos jours, la synthèse d'une grande majorité de composés aromatiques dépend de ressources fossiles et notamment du pétrole. Par exemple, la vanilline est produite en grande majorité (85%) à partir de ce dernier, les 15% restants sont obtenus à partir de la masse lignocellulosique [1]. Alors que les ressources fossiles sont en voie d'épuisement et que leur utilisation massive dans le domaine de l'énergie contribue au changement climatique, leur consommation est toujours croissante du fait, entre autres, de la démographie mondiale galopante et d'un prix bas actuellement [2]. Dans ce contexte, l'utilisation de la biomasse lignocellulosique attire néanmoins une attention croissante, en tant qu'alternative verte au pétrole, du fait qu'elle soit bon marché, biosourcée, respectueuse de l'environnement et renouvelable [3]. En revanche, afin que l'utilisation de la biomasse puisse entrer dans le contexte d'un développement durable, cette dernière ne doit pas entrer en compétition avec les ressources agricoles, ce qui est le cas de la biomasse de première génération (huile de colza, amidon de maïs [4]). Les biomasses de deuxième (paille de blé, miscanthus…) et de troisième (micro-algues) génération n'ont pas cet inconvénient, mais leur exploitation industrielle est encore immature [5].

Les trois composantes de la biomasse sont la cellulose, l'hémicellulose et la lignine. Alors qu'il existe déjà des voies de valorisation de la cellulose à l'échelle industrielle (papier, cellophane, nitrate de cellulose etc…), la lignine est en très grande partie utilisée en tant que source d'énergie, notamment dans l'industrie papetière et une très faible minorité est valorisée chimiquement. Cependant, la lignine est le deuxième composé le plus abondant sur notre planète et c'est un polymère riche en fonctions aromatiques, ce qui fait d'elle l'alternative durable majeure au pétrole pour la production de produits aromatiques [6].

L'objectif de ce travail de thèse est de pouvoir synthétiser des molécules plateformes telles que la vanilline ou l'acide syringique par dépolymérisation oxydante de la lignine. Les deux oxydants les plus propres sont le dioxygène et le peroxyde d'hydrogène car leur sous-produit est l'eau. Le peroxyde d'hydrogène est un oxydant fort, mais il doit être synthétisé à partir du dioxygène et du dihydrogène selon un procédé qui n'est pas sans impact environnemental [7]. Ainsi, le choix de l'oxydant se portera sur le dioxygène. Vu que ce dernier est à l'état triplet dans son état fondamental et que la lignine est elle-même à l'état singulet, un catalyseur est nécessaire afin d'activer soit le substrat via une réaction d'oxydation (un électron est retiré au substrat), soit le dioxygène par une transformation en espèce active ($O_2^{\cdot -}$, $HO^{\cdot}$ …).

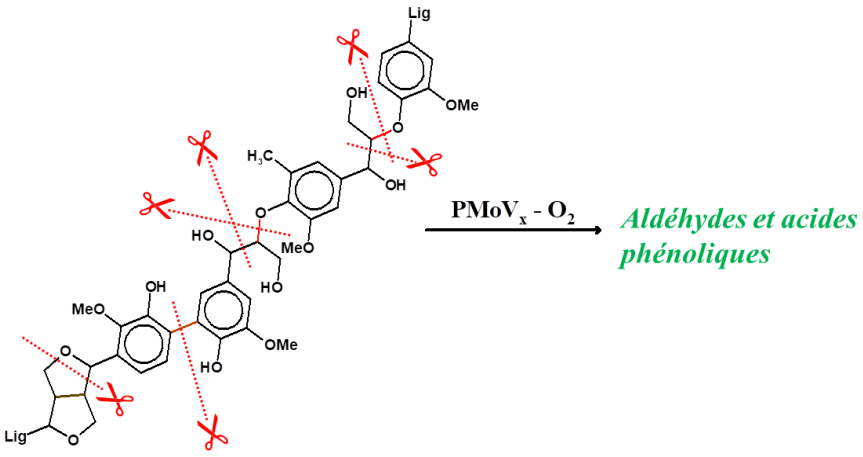

Figure : Schéma de principe du clivage oxydant de la lignine catalysée par les $PMoV_x$

La structure de la lignine étant très complexe, il est courant, dans la littérature, que les systèmes catalytiques (et parmi eux des catalyseurs au vanadium) soient d'abord testés sur des modèles dimériques, notamment ceux qui imitent en priorité la liaison β-O-4, la plus représentée dans la lignine native. Lors de travaux précédents réalisés au Laboratoire, les molybdovanadophosphates de KEGGIN ($H_{3+x}PMo_{12-x}V_xO_{40}$, notés $PMoV_x$) se sont montrés efficaces pour le clivage aérobie oxydant des liaisons C-C dans des molécules plus simples telles que les 2-hydroxyacétophénones [8]. Ces catalyseurs seront donc utilisés dans cette thèse. La mise au point d'un procédé vert, ne se cantonnant pas au choix de l'oxydant et du catalyseur, il nous est apparu judicieux de rechercher des voies plus économes en énergie pour la synthèse des catalyseurs d'une part et pour la mise en œuvre de la réaction catalytique d'autre part en exploitant, respectivement, la mécanochimie et l'intensification sonochimique [9, 10]. L'utilisation d'une intensification sonochimique basée sur le phénomène de cavitation peut être une solution pertinente pour un meilleur transfert de masse et éventuellement pour générer des conditions favorables à l'activation du dioxygène, ce qui peut aboutir à la formation de l'eau oxygénée *in situ*.

Le présent manuscrit est divisé en quatre parties.

- La **partie I** est consacrée à une étude bibliographique donnant un état de l'art sur **IA)** la dépolymérisation de la lignine et de ses modèles par voie catalytique en présence du dioxygène, **IB)** la synthèse, les modes de caractérisation et les applications des $PMoV_x$ en catalyse d'oxydation de l'alcool benzylique par le dioxygène puis **IC)** l'utilisation de la sonochimie dans le cadre des réactions d'oxydation de l'alcool benzylique et dérivés

- La **partie II** traite de l'utilisation des $PMoV_x$ pour catalyser le clivage oxydant de deux modèles dimériques (2-phenoxy-1-phényléthanol (**A1**$_{HH}$) et 2-phenoxyacétophénone (**K1**$_{HH}$)) qui miment la liaison β-O-4. Une fois que les $PMoV_x$ seront synthétisés par voie hydrothermale, une étude de faisabilité sera réalisée en partant de **K1**$_{HH}$ moyennant des ajustements des conditions opératoires puis une transposition à **A1**$_{HH}$ sera proposée.
- La **partie III** propose d'améliorer la synthèse hydrothermale des $PMoV_x$ en ayant recours au ball-milling des oxydes précurseurs puis, après une caractérisation poussée des matériaux obtenus, de les tester, à leur tour, comme catalyseurs du clivage aérobie de **K1**$_{HH}$ et **A1**$_{HH}$. Cette partie se termine par des tests préliminaires sur de la lignine extraite à partir de la paille de blé (biomasse de deuxième génération) selon un procédé Organosolv ® et purifiée.
- Enfin, la **partie IV** vise à améliorer les performances catalytiques des $PMoV_x$ dans le cadre du clivage oxydant, réputé plus difficile, du modèle **A1**$_{HH}$ ainsi que de la lignine. Plusieurs fréquences seront testées à pression atmosphérique ou plus élevée afin de déterminer les effets d'une cavitation physique (basse fréquence) et chimique (haute fréquence).

N.B. Cette thèse est rédigée en français et en anglais. L'auteur prie les lecteurs de l'excuser pour la gêne occasionnée.

Références

[1]: M. Fache, B. Boutevin, S. Caillol, *ACS Sustainable Chem. Eng.* **2016**, 4, 35-46.
[2]: BP, *BP Statistical Review of World Energy* **2018**, 67th Edition.
[3]: P. A. Anastas, J. C. Warner, *Green Chemistry Theory and Practice*, **1998**, Oxford University Press, New York.
[4]: UN, *Sustainable Development Goals*, disponible sur https://sustainabledevelopment.un.org/sdgs, consulté le 13/09/19.
[5]: S. S. Hassan, G. A. Williams, A. K. Jaiswal, *Renew. Sustainable Energy Rev.* **2019**, 101, 590-599.
[6]: D. Da Silva Perez, B. Andrioletti, M. Beyerle, C. Cabral-Almada, C. Crestini, L. Djakovitch, V. Dufaud-Niccolai, P. Fongarland, E. Framery, L. Jean-Gerard, R. Kieffer, A. Nunes Coelho, S. Woldemichael, S. Tapin-Lingua, *251st ACS National Meeting & Exposition*, **2016 march**, San Diego, CA, United States.
[7]: J. M. Campos-Martin, G. Blanco-Brieva, J. L. G. Fierro, *Angew. Chem. Int. Ed.* **2006**, 45, 6962-6984.
[8]: L. El Aakel, F. Launay, J-M. Brégeault, A. Atlamsani, *Chem. Commun.* **2001**, 2218-2219.
[9]: A. Beillard, X. Bantreil, T-X. Métro, J. Martinez, F. Lamaty, *Chem. Rev.* **2019**, 119, 7529-7609.
[10]: L. Parizot, T. Chave, M-E. Galvez, H. Dutilleul, P. Da Costa, S. I. Nikitenko, *Appl. Catal. B.* **2019**, 241, 570-577.

Partie bibliographique

IA. Aerobic oxidative cleavage of lignin and its surrogates towards platform molecules: a review

IA. 1. Introduction

In our days, an overwhelming majority of aromatic compounds are made from fossil resources that are on the way of depletion [1]. The interest on the use of alternative and more sustainable resources, such as lignocellulosic biomass, is therefore increasing exponentially. Moreover, lignocellulose has the advantage to avoid competition with food industry [2].

Cellulose, hemicellulose and lignin are the three main polymers present in lignocellulose. Among these three constituents, cellulose is the most exploited one [3]. Due to its non-negligible heat value, the lignin recovered as a by-product from the bleaching of wood pulp, or wood delignification [4] has been used for a long time as power and heat source. Current examples of practical lignin chemical valorization are scarce. Due to its antioxidant properties, lignin is used nowadays as an additive for bitumen [5]. In the near future, it may be also used as a source of carbon fibers, owing to its high carbon content and its low price compared to polyacrylonitrile [6]. Some research works propose the utilization of lignin as a substitute of bisphenol to produce polyurethanes and other types of lignin-based polymers [7]. However, lignin is an important source of aromatic molecules that can be recovered either by reductive or by oxidative depolymerization, affording biofuels and valuable aromatic compounds. Hydrogenolysis pathways normally lead to relatively poorly functionalized molecules [8]. Therefore, it is generally employed when biofuels are the targeted products. Further than the production of biofuels, the chemical use of lignin through oxidative cleavage opens the door to the promising production of bio-based highly functionalized building blocks. Generally, the targeted molecules of this reaction are aromatic aldehydes, such as vanillin and syringaldehyde. Research in this area has been the subject of several recent reviews that will be discussed later in this Introduction.

The very early studies dealing with bleaching and lignin depolymerization can be considered as the starting point of its chemical valorization through oxidative processes. The first reagents considered were chlorine derivatives such as ClO_2 [9]. However, the use of cheapest, non-dangerous reagents avoiding toxic wastes was highly recommended. This issue incited the search for delignification processes (as well as lignin chemical valorization processes) mediated by oxygenated and "greener" oxidants such as O_2 [10] or H_2O_2 [11]. Moreover, since hydrogen peroxide has to be synthesized from O_2 through the

alkylanthraquinone process, molecular oxygen can be considered as a more attractive oxidant from both the economic and the environmental point of view [12]. These "greener" processes for lignin oxidative valorization generally imply the use of a catalyst. Actually, more active catalysts are needed, which can soften the reaction conditions, while affording a better control of product selectivity. However, molecular oxygen is less active than H_2O_2 and consequently, more drastic conditions, or more active/selective catalysts, are needed to oxidize lignin with O_2.

Several published reviews already did the effort to summarize the latest advances on lignin isolation and its catalytic valorization (Table IA. 1).

The reviews published so far (Table IA. 1), as well as the different publications cited therein, bring forward several important facts about lignin oxidative depolymerization:

- The oxidative cleavage of C-C and/or C-O bonds in lignin leads to the production of highly functionalized aromatics, valuable chemicals and building blocks;
- the lignin structure strongly depends on the pre-treatment applied to isolate lignin from lignocellulosic biomass, as well as on biomass origin, *i.e.* plant type;
- sometimes lignin surrogates/models are used in an aim to emulate the bonds present in real technical lignin;
- catalytic oxidation is the most widely used method for the cleavage of C–C bonds in lignin and/or in lignin models (C-C bonds being stronger than C-O linkages);
- different oxidants can be used, *i.e.* H_2O_2 or O_2;
- oxidative lignin oxidation can be intensified using microwaves, ultrasounds, or employing ionic liquids as solvent, among other innovative approaches.

The reviews of GUADIX-MONTERO and SANKAR [31] and of WANG *et al* [32], both published in 2018, further insist on the need to seek for each time more active and selective catalysts for C-C oxidative cleavage. However, as already commented on Table IA. 1, the results obtained using different model molecules or lignin types are generally mixed, and, moreover, no clear distinction is made between aerobic oxidation and the use of H_2O_2. The aim of the present review is therefore to focus on the most recently published results from 2000 on catalytic aerobic cleavage, both of models and of several types of lignin. An important part of this review will be devoted to model classification (IA. 2). Then, the state-of-the-art of catalytic aerobic cleavage of lignin surrogates will be given (IA. 3). The catalytic systems will be classified as a function of their metal and special attention will be paid to the reaction conditions

employed. Finally, the catalytic cleavage of technical lignin will be described (IA. 4) with a special attention on the reaction conditions and on the impact of lignin type.

Table IA. 1: Reviews about lignin dpolymerization published from 2010

Authors	Year	Content	Ref.
ZAKESKI	2010	Catalytic processes for chemicals production from lignin.	[13]
PANDEY and KIM	2011	Thermochemical methods for lignin depolymerization and conversion into value-added chemicals, including oxidation.	[14]
CRESTINI *et al.*	2010	Active and selective catalysts for lignin oxidative depolymerization by H_2O_2 or O_2 in presence of biocatalysts, organometallic and biomimetic catalysts and plasma oxidation process. Updated in 2013.	[15]
LANGE, DECINA and CRESTINI	2013		[16]
LANGE *et al*	2013	Enzymes in lignin oxidation & different lignin characterization techniques, an important issue concerning lignin valorization.	[17]
CHATEL and ROGERS	2013	Lignin oxidation processes in ionic liquid media.	[18]
DAI *et al*	2016	Recent advances on the utilization of ionic liquids for lignin oxidation.	[19]
CHATEL *et al*	2014	Utilization of ultrasonic intensification to boost production of chemicals from lignin. Mostly focused on lignin extraction.	[20]
KUNA *et al.*	2017	Examples of ultrasonic intensification for lignin processing in the presence of either homogeneous or heterogeneous catalysts.	[21]
KANG *et al*	2015	Hydrothermal lignin valorization, including wet oxidation, as an effective way for the recovery of aromatic aldehydes.	[22]
MA *et al.*	2014	Production and key characteristics of several representative biorefinery lignins, comparing their behavior in catalytic oxidation.	[23]
MA *et al*	2018	General compilation of recent updates on oxidative lignin valorization.	[24]
LI *et al.*,	2014	Catalytic transformation of lignin for the production of chemicals and fuels including oxidative depolymerization. Impact of extraction methods on lignin structure and reactivity.	[25]
BEHLING *et al*	2016	Mechanochemical, sonochemical, microwave and electrochemical approaches for heterogeneous catalytic cleavage of lignin and lignin models.	[26]
RINALDI *et al.*	2016	Prevalence of β-O-4 bond type depends not only on the origin of biomass but also on the extraction process.	[27]
SCHUTYSER *et al*	2017	Importance of keeping the C^{β}-O bond in native lignin during the extraction, avoiding the formation of recalcitrant C-C bonds	[28]
SUN *et al*	2018	State-of-the-art about lignin and lignocellulosic biomass depolymerization towards the synthesis of lignin-based platform molecules	[29]
DEUSS and BARTA	2016	Transition metal-catalyzed reductive or oxidative cleavage of lignin models and in technical lignins.	[30]

IA. 2. Lignin and its models

IA. 2.1. Lignin composition and structure

Lignin is a non-fermentiscible phenylpropanoid polymer mainly present in plants. This polymer is the second most abundant on our planet, after cellulose, and accounts for almost 30% of the organic carbon present in our biosphere [33, 34]. In living vegetals, its role is to orientate and regulate the flow of water and nutrients and to protect the plant against external attacks [34]. It is chemically linked to hemicelluloses by either an ester or an ether bond. The structure of this racemic aromatic heteropolymer (Fig. IA. 1) is based on alternating three

different units that differ in their degree of methoxylation: p-coumaryl alcohol, noted H for hydroxyphenyl; coniferyl alcohol, noted G for guaiacyl and syringyl alcohol, noted S for syringyl (Fig IA. 2.) [35]. The relative amount of the three monolignols depends on plant type and growth. Generally, hardwood lignins contain mostly G and S units and only traces of H units, whereas softwood lignins consist principally of G units and traces of H ones [36, 37].

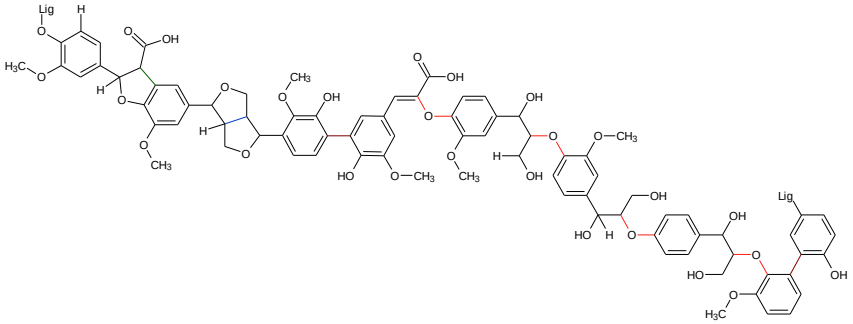

Figure IA. 1: Example of lignin structure

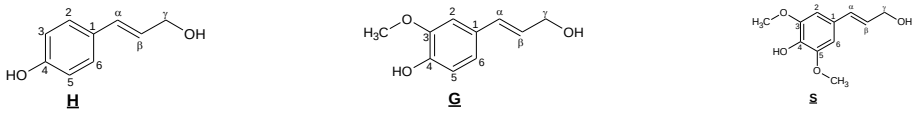

Figure IA. 2: H, G and S lignin monomers

The construction of the lignin polymer is called lignification and usually takes place through radical coupling reactions between the three monolignols [38]. These H, G and S units appear randomly distributed and linked through different C-O and C-C bonds (Fig. IA. 2), thus constituting a three-dimensional network [34, 39]. The relative abundance of these bonds is presented in Table IA. 2, for various origins of lignin. Generally speaking, the β-O-4 linkage is the most frequent, independently of the biomass source. This bond is moreover the most easily cleaved. Conifer lignins, composed mainly of G units, contain relatively important amounts of more recalcitrant β-5, 5-5 and 5-O-4 bond types (Fig. IA. 3), due to the availability of the C_5 position for coupling [34]. Other bonds like spirodienone or α-O-4 are rare.

Herbaceous lignin has a simpler structure, since some linkages are not represented, such as the recalcitrant diphenyl bond. Besides, the β-O-4 linkage in herbaceous lignin generally represents more than 50% [40]. For example, herbaceous species such as *Miscanthus* X *giganteus*, are quite rich in lignin with a relatively simple structure that contains only traces of the β-1 bond, not invasive and grows quickly and require low land occupation. Furthermore, this kind of biomass does not compete with food industry [41]. Let us note here, however, that as discussed in many previous studies on lignin valorization [23, 25-28], the global structure of lignin depends not only on the vegetal specimen of origin, but also on the conditions of its

growth and other environmental factors, being moreover conditioned by the extraction process employed for its separation from cellulose and hemicellulose.

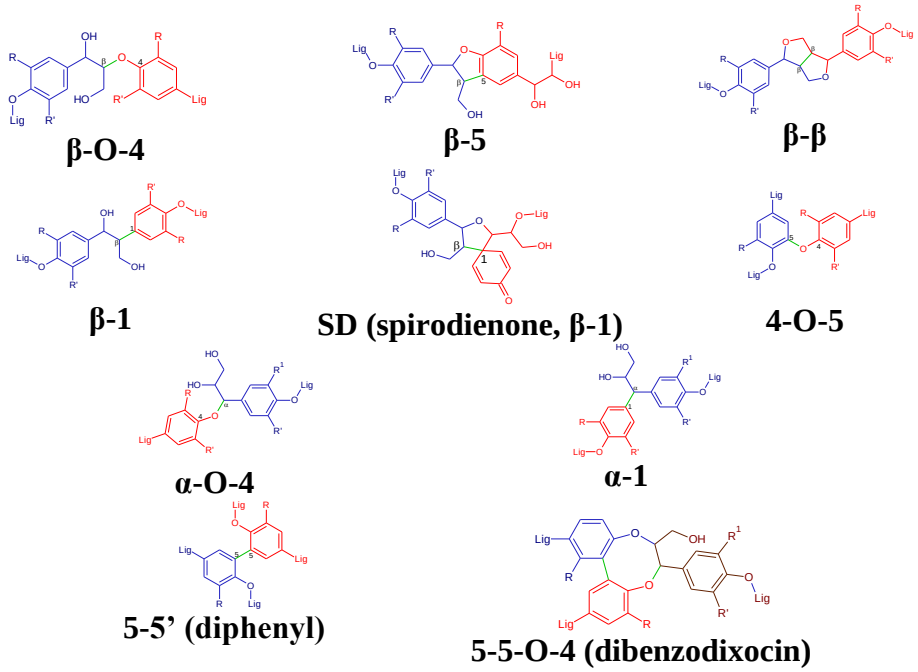

Figure IA. 3: Bonds between the different monomers in lignin.

Table IA. 2: Relative presence of the different bonds in herbaceous, softwood and hardwood lignin. [42-46]

	Bond	β-O-4	β-β	β-5	β-1	5-5 + 5-5-O-4	4-O-5
Abundance (%)	Herbaceous	63-93	0-8	3-37	0-6	0	0
	Softwood	27.5-72	1-11	9-18	0-10	9.5-27	4-8
	Hardwood	41-80	0-19	3-14.6	7-15	2.3-9	6.5-9

IA. 2.2. Influence of the extraction process on lignin structure

The different processes involved in the isolation of lignin from lignocellulosic biomass have been traditionally used for the production of pulp for paper manufacture [47]. Lignin extraction basically consists in its chemical separation from cellulose and hemicellulose, as depicted in Fig IA. 4a. The reactions involved in this step are the cleavage of the ester bonds (saponification or acidic solvolysis) and ether bonds (nucleophilic substitution) between lignin and hemicellulose (Fig. IA. 4b) [48]. Actually, this extraction cannot be performed without inducing any modification of the native structure.

The two main industrial pulping processes leading to lignin extraction, *i.e.* the so-called Kraft and Bisulfite processes, are schematized in Fig IA. 5. The core of both procedures is the production of what has been generally named “black liquor”. They differ however in the protocol used for the precipitation of the extracted lignin. While Kraft lignin precipitation is

based on an acidification using concentrated H_2SO_4, lignosulfonate precipitation involves a nucleophilic addition of the $-SO_3^-$ moiety. As a consequence, Kraft lignin generally contains lower amount of sulfur than the one isolated through the Bisulfite process.

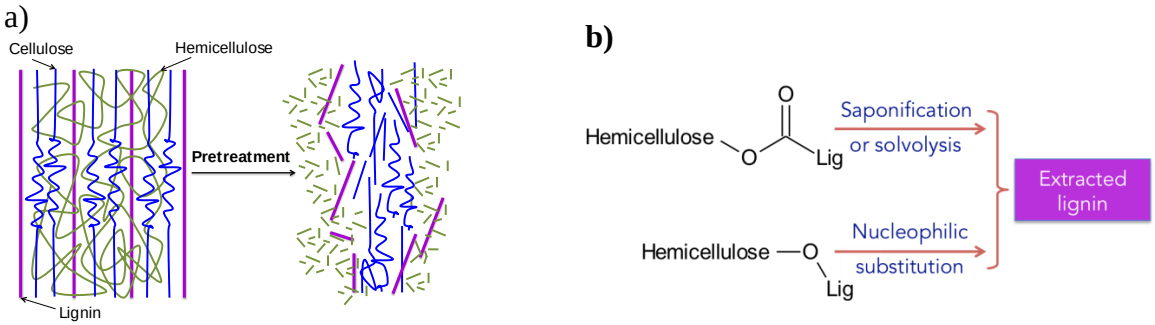

Figure IA. 4: Lignin extraction: (a) pretreatment for the separation of lignin, cellulose and hemicellulose, and (b) reactions involved in lignin extraction

A relatively more recent route for lignin extraction, called Organosolv extraction, makes use of water-organic solvents having a low-boiling point, such as ethanol or dioxane [49, 50]. The core reaction is a solvolysis (alcoholysis or acidolysis). After filtration, the lignin is precipitated in acidic aqueous medium. The most famous example is the Alcell® or Lignol® process involving ethanol and water [51]. Some other more innovative processes, such as the CIMV one [52-54], consider the recycling of the solvents used in lignin isolation (water-formic acid- acetic acid). In general, as discussed later on, Organosolv lignin is sulfur-free, since no sulfur compounds are employed.

The severity of the extraction process is moreover a key point that needs to be taken into account in order to understand the reactivity of the resulting isolated lignin [7, 55]. More stringent conditions favor the formation of C-C bonds through the recombination of radical lignin fragments [56].

Table IA. 3 summarizes the main features found in lignin extracted through different processes, the price, as well as some estimates on the annual worldwide production. Lignosulfonates are the cheapest and the most widely produced lignins. Kraft lignin production and price are generally average and its sulphur content is rather low. Actually, Kraft lignin is mainly used as an internal source of energy in paper mills. Still, even if the Kraft process is the most representative lignin extraction process, its volume production is smaller than lignosulfonates. Organosolv lignin production is considerably more expensive, main reason why its production remains relatively marginal, compared to the other extraction processes. Organosolv lignin is however purer and presents lower structure modifications than Kraft and Bisulfite lignins.

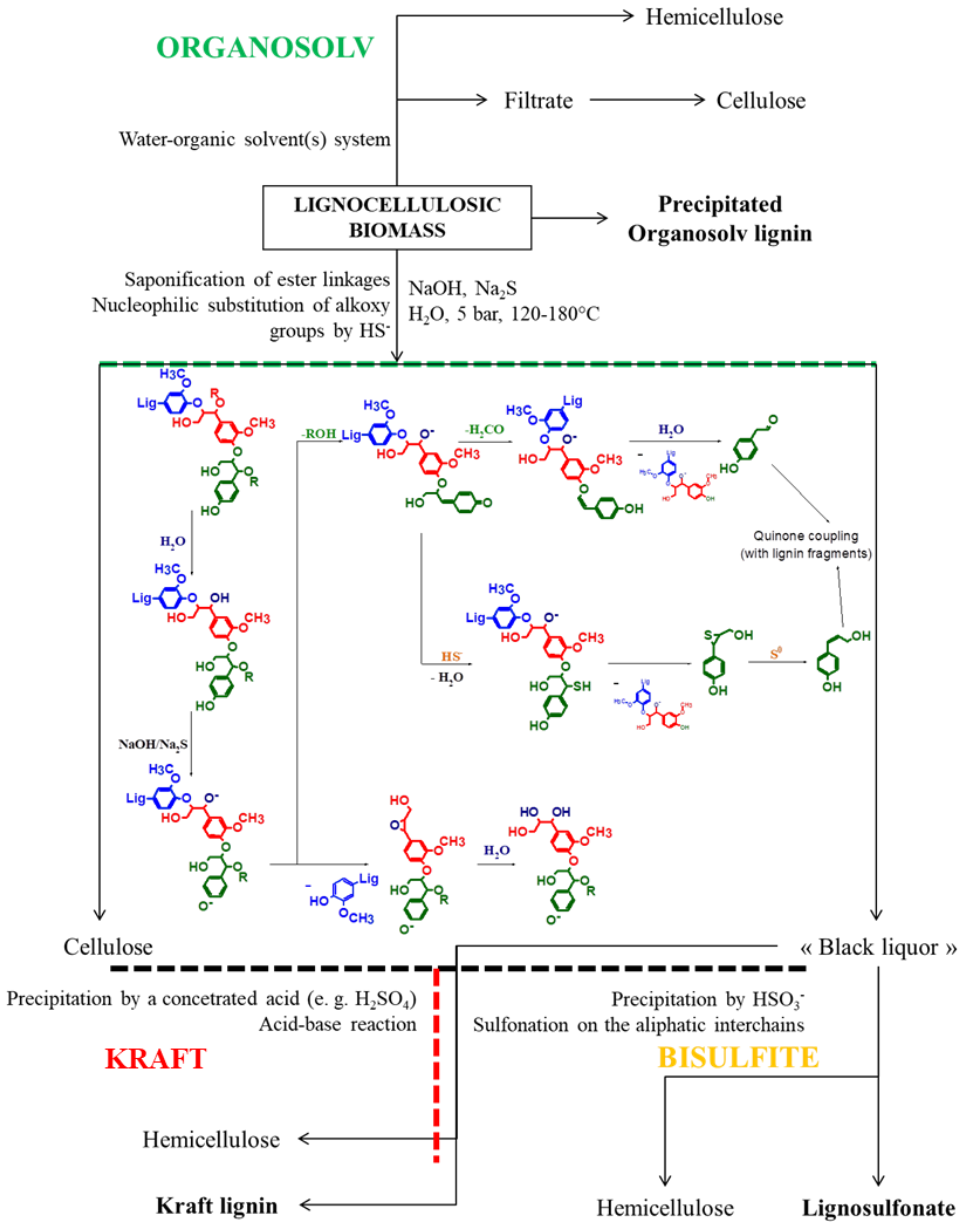

Figure IA. 5: Lignin extraction processes: Kraft and Bisulfite routes vs. Organosolv processes

Table IA. 3: Main features, price and worldwide production of lignin extracted through Kraft, Bisulfite and Organosolv processes (2011) [57-62]

Process	Structure modifications	Purity	Sulfur content	Added value	Cost	Worldwide production (kTon/year, 2011)
Kraft	High	+	Low	High	Average	27-60 [59, 60]
Bisulfite	High	-	High	Low	Low	~1,000 [59, 61]
Organosolv	Low	+	S free	High	High	0.5-3 [53, 62]

Another lignin extraction process is the Ionosolv® process which is based on the use of ionic liquid [63-69]

As pointed by LANGE *et al* [16] chemical valorization through oxidative cleavage requires to take into account that lignin is heterogeneous by nature and the extraction process has a critical impact on its biomass. Moreover, the characterization of the different resulting products of technical lignin oxidation requires extra efforts as well as the use of sophisticated analytical techniques, such as 2D NMR and SEC [35, 39, 70]. Lignin models have been often used to represent lignin structure in fundamental analysis.

IA. 2.3. Lignin surrogates/models

The relevant models used as lignin surrogates need to be at least dimers containing the β-O-4 linkage, considering the predominant abundance of these bonds in most lignin sources (Table IA. 2). As a consequence, the present review will be focused on the cleavage of this type of bond. In 1997, CRESTINI and D'AURIA [71] already suggested some models representative of lignin structure. Later on, ZAKZESKI *et al* [13] reviewed the different models used until 2010. According to ZAKZESKI, two types of dimer models can be found: alcohols and ketones.

Here, these compounds will be noted **A**$\mathbf{N}_{XY}$ and **K**$\mathbf{N}_{XY}$ respectively, in an aim to unify the notation given to the different dimer models used as lignin surrogates in the already published literature. The number N (see Table IA. 4 and Fig. IA. 6) is determined by the nature of the groups R^1 and R^2 (R^1 may be a proton (H), a hydroxyl (OH) or an alkyloxy group (OMe/OEt). R^2 located within the interchain can be a proton (H) or a CH_2OH group). X and Y stand for the monomer type and are determined by the nature of the radicals R, R', R'' and R''' (see Table IA. 4 and Fig. IA. 6). If all the groups are set as proton, the model will be noted **K**1_{HH} (Fig. IA. 6). Its alcohol analogue will be thus noted **A**1_{HH}. These two models are the simplest ones and they can be synthesized in a relatively simple way.

Table IA. 4 gathers the different structures tested. For example, a more sophisticated surrogate, closer to native lignin, is the alcoholic model containing R^1 = OH, R^2 = CH_2OH, R = R' = R'' = OMe and R''' = H, *i.e.* the dimer noted **A**$\mathbf{4}_{SG}$. Such model allows a better understanding of the influence of the CH_2OH group and of phenolic moieties present in native lignin. The influence of the etherification of the phenolic function in the β-O-4 [72] cleavage can be explored through the comparison of the reactivity of **A**$\mathbf{5}_{XY}$ and **A**$\mathbf{6}_{XY}$ with that of **A**$\mathbf{3}_{XY}$ and **A**$\mathbf{4}_{XY}$ models.

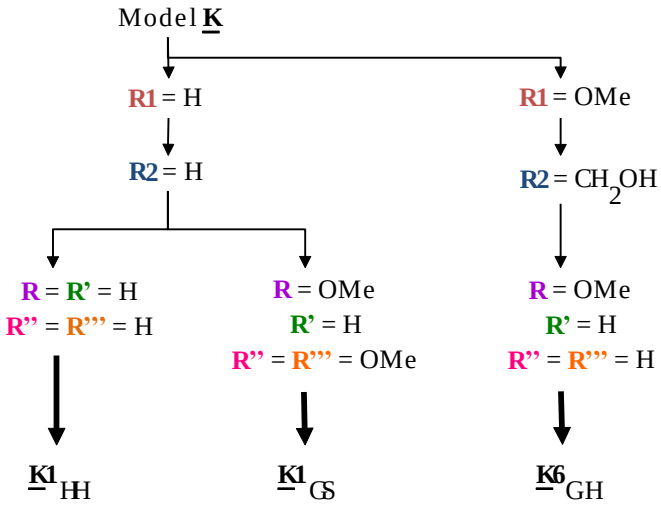

Figure IA. 6: A detailed example of the model nomenclature used in the present review

According to our classification and taking into account all the possible combinations, 126 different dimer structures can be thus considered. Here, we have surveyed the different studies published since 2000, considering such dimers as lignin surrogates and using either molecular oxygen or air as the cleaving reagent. The results (presented in Table IA. 4) clearly evidence that only a small fraction (36 models) were tested.

Complex A-type models closest to native lignin structure such as **A**6_{XY}, have been more frequently used as surrogates, compared to other simpler structures such **A**1_{XY}. Studies considering **K**N_{XY} dimer cleavage [86, 122-128] are less numerous in the literature (8 refs for **KN**$_{XY}$ vs 23 refs for **AN**$_{XY}$). A striking difference with A-type models is the scarcity of examples of studies using phenolic substrates (only one occurrence in the case of **KN**$_{XY}$!).

Table IA. 4: Nomenclature proposed for the different dimer models

<table>
<tr><td colspan="3"></td><td colspan="3"> 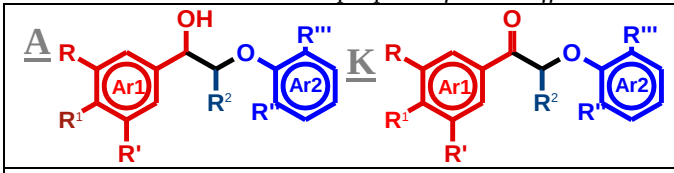
R, R’, R’’, R’’’ = H or OMe
R¹ = H or OMe or OEt
R² = H or CH₂OH</td></tr>
<tr><td colspan="3"></td><td colspan="3">R²</td></tr>
<tr><td colspan="3"></td><td>H</td><td colspan="2">CH₂OH</td></tr>
<tr><td rowspan="3">A</td><td rowspan="3">R¹</td><td>H</td><td> 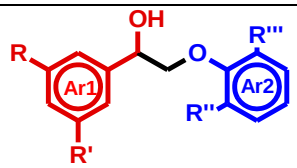
A1XY</td><td> 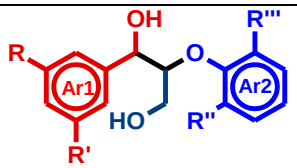
A2XY</td><td></td></tr>
<tr><td>OH</td><td> 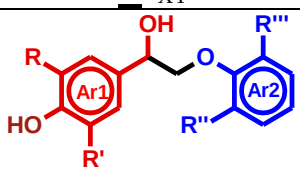
A3XY</td><td> 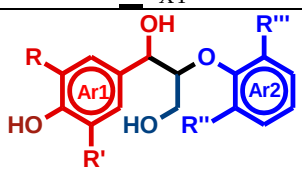
A4XY</td><td></td></tr>
<tr><td>OMe/
OEt</td><td> 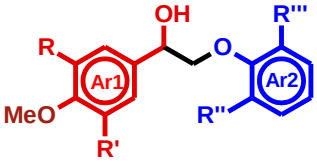
A5XY</td><td> 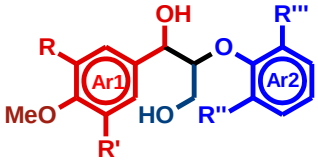
A6XY</td><td> 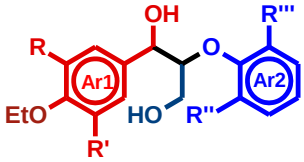
A6’XY</td></tr>
<tr><td rowspan="3">K</td><td rowspan="3">R¹</td><td>H</td><td> 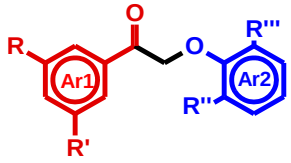
K1XY</td><td> 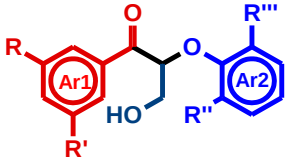
K2XY</td><td></td></tr>
<tr><td>OH</td><td> 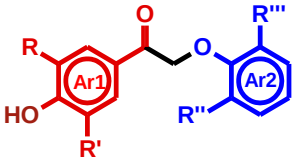
K3XY</td><td> 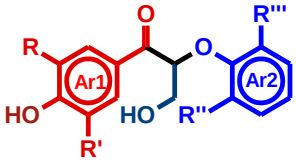
K4XY</td><td></td></tr>
<tr><td>OMe/
OEt</td><td> 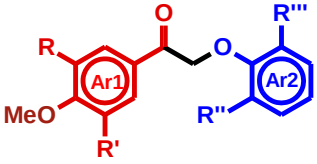
K5XY</td><td> 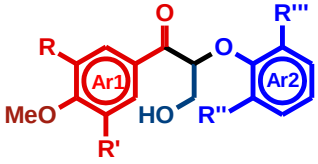
K6XY</td><td> 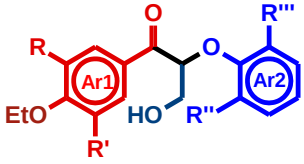
K6’XY</td></tr>
<tr><td colspan="6">X = H ⇒ R=R’=H, X = G ⇒ R=OMe and R’=H, X = S ⇒ R=R’=OMe
Y = H ⇒ R’’=R’’’=H, Y = G ⇒ R’’=OMe and R’’’=H, Y = S ⇒ R’’=R’’’=OMe</td></tr>
</table>

Table IA. 5: Literature survey on the different A and K dimers used in aerobic cleavage

Model	Substrate	Times used	References	Total amount of records per **A**N_{XY} or **K**N_{XY} type
A	**A**1_{HH}	7	83-85, 87, 102, 108	10
	A1_{HG}	2	102, 108	
	A1_{HS}	1	102	
	A2_{HG}	1	110	7
	A2_{SG}	6	73, 86, 88-89, 103-104	
	A3_{GG}	1	97	4
	A3_{SG}	2	73, 97	
	A3_{SS}	1	73	
	A4_{HG}	1	101	9
	A4_{GG}	3	84 101, 105, 111	
	A4_{SG}	4	73, 88-89, 103	
	A4_{SS}	1	73	
	A5_{HH}	1	102	4
	A5_{HG}	1	102, 113	
	A5_{HS}	1	102	
	A5_{GG}	1	97	
	A6_{HH}	1	106	15
	A6_{HG}	4	101, 105, 117-118	
	A6_{GG}	5	102, 112-113, 117-118	
	A6$_{SG}$	2	117-118	
	A$6'_{GG}$	3	92, 115-116	
K	**K**1_{HH}	6	122-125, 127-128	13
	K1_{HG}	4	122-124, 128	
	K1_{HS}	1	122	
	K1_{GH}	2	125-126	
	K2_{HH}	1	126	2
	K2_{SG}	1	86	
	K3_{HH}	1	122	1
	K5_{HH}	2	122-123	16
	K5_{HG}	4	122-124, 126	
	K5_{GH}	2	122-123	
	K5_{GG}	4	122-124, 126	
	K5_{GS}	3	122-124	
	K6_{GG}	4	122-124, 126	4

IA. 3. Aerobic oxidation of lignin models

This part is devoted to the study of the aerobic oxidative cleavage of lignin dimeric models presented in Table IA. 6. The main aims will be to compare the catalysts to find the most adequate conditions for each kind of model and for lignin aerobic cleavage.

IA. 3.1. C-C, C-O bond cleavage and products obtained

A better understanding of cleavage reactions is needed in order to compare the results obtained in the catalytic aerobic cleavage of the β-O-4 linkage. In this section, we intend to comprehensively describe β-O-4 cleavage, presenting the list of the most frequent products obtained through the different C-C and C-O cleavage reactions.

Fig IA. 7 shows the different pathways of C-C and C-O bond cleavage involved for the **A**N$_{XY}$ and **K**N$_{XY}$ models. The main products, excluding formic acid and CO_2, are shown in Table IA. 6.

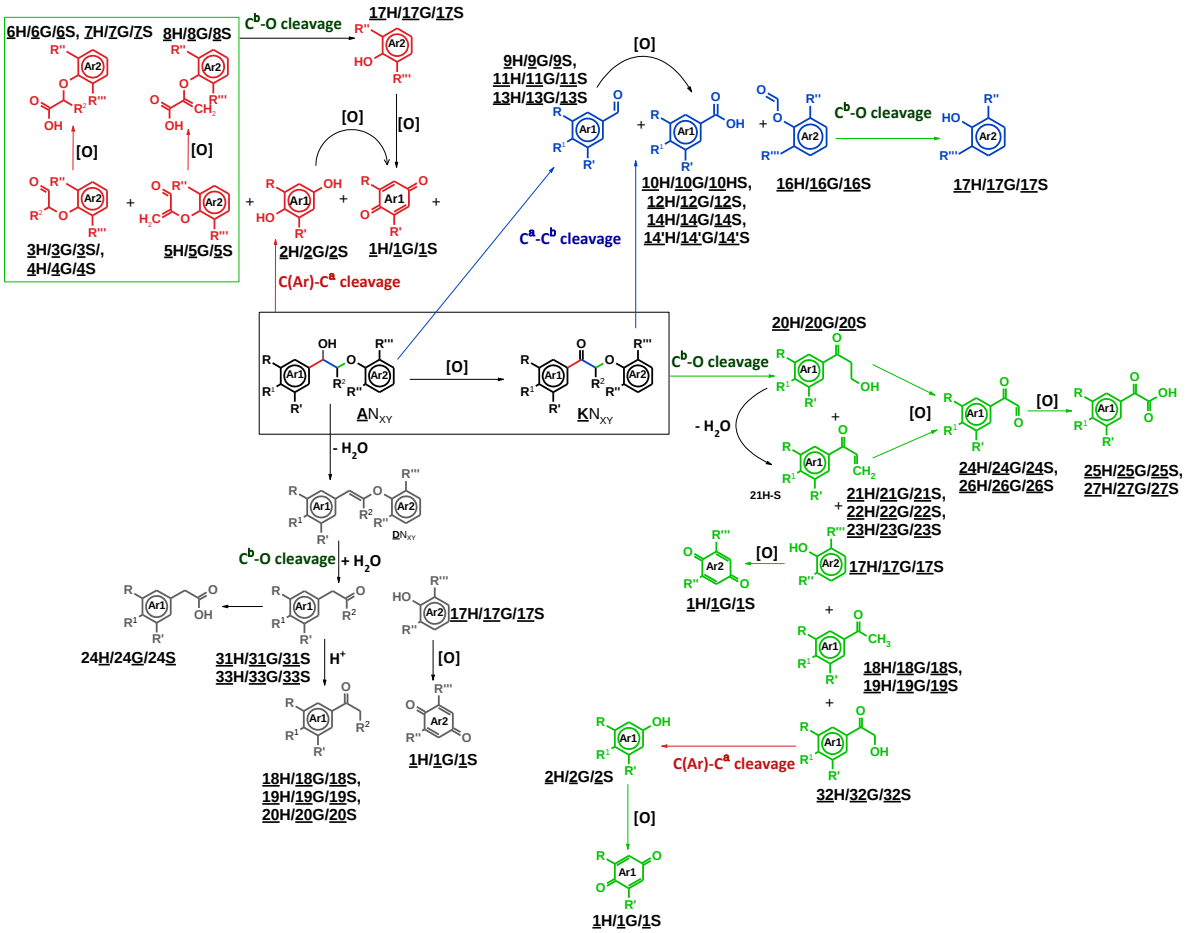

Figure IA. 7: Cleavage of C-C and C-O bonds in AN$_{XY}$ and KN$_{XY}$ dimeric lignin models

The three main reactions are C(Ar)-C$^\alpha$, C$^\alpha$-C$^\beta$ and C$^\beta$-O cleavage.

- C(Ar)-C$^\alpha$ cleavage in **AN**$_{XY}$ leads, on one hand, to hydroquinones **2** (**2**H, **2**G or **2**S) and/or quinones **1**, coming from Ar1 moiety and, on the other hand, phenoxyacetaldehyde (**3** and **4**) and/or 2-phenoxyacroleins noted **5** or, after over-oxidation, phenoxyacetic acid derivatives noted **6**, **7** and/or **8**, coming from Ar2 moieties. The products (**3**, **4** and **5**) coming from Ar2 moiety may then undergo C$^\beta$-O cleavage as described by BIANNIC and BOZELL [73]. Quinones **1** are also formed through phenols **16** over-oxidation. As a consequence, quinones are not quite characteristic of C(Ar)-C$^\alpha$ cleavage.
- Typical C$^\alpha$-C$^\beta$ cleavage products are benzaldehydes (**9**, **11**, **13**) and benzoic acids (**10**, **12**, **14**, **14'**) coming from Ar1. The side products from Ar2 moiety are phenylformiates, noted **16**. Very often, C$^\beta$-O cleavage can simultaneously take place, resulting in phenols **17** formation.

- Oxidative C^{β}-O cleavage, followed by dehydration can lead to the formation of 3-phenylacroleins (**21**, **22**, **23**). These products may be further oxidized to phenylglyoxal (**24**, **26**) or phenylglyoxylic acid (**25**, **27**) derivatives.

Furthermore, **AN**$_{XY}$ may be dehydrated, resulting in the formation of enol ethers **DN**$_{XY}$ that, through hydrolysis, can lead to phenylacetaldehydes (**31**, R^2 = H) or HIBBERT ketones (**31**) (Hibbert ketones, R^2 = OMe) [74-79]. The side products of enol ether hydrolysis are phenols (**17**). In acidic conditions, phenylacetaldehydes (**31**) isomerize to acetophenones (**18**). **31**H may isomerize into **H1**, **H2** and **H3** (see Fig. IA. 8 in the case of **A2**$_{HH}$).

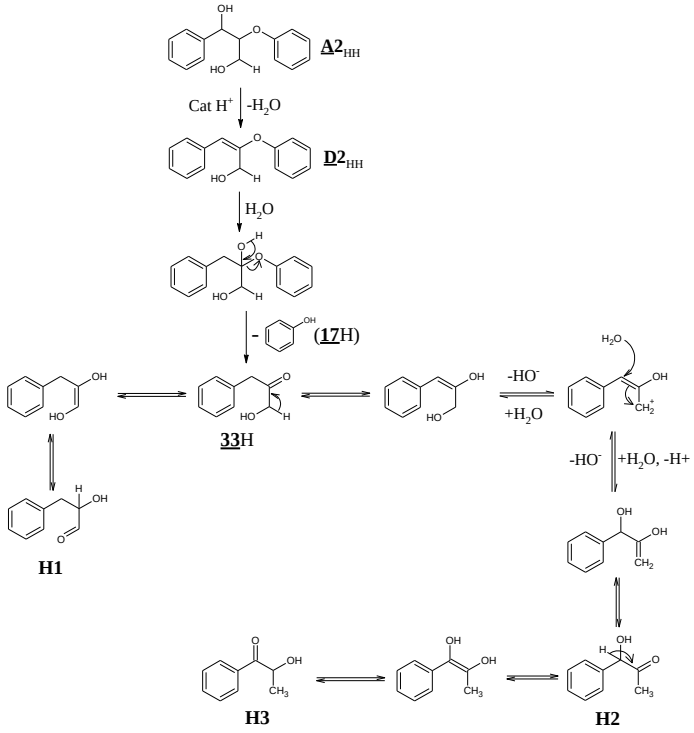

Figure IA. 8: Hibbert ketones isomerization

Hibbert ketones and quinones (among others) can be involved in parasite oxidative condensation reactions leading to the regeneration of different dimers and/or to other polyaromatic products, such as tars [80, 81]. These condensation reactions are rather difficult to control and may yield β-1 or diphenyl 5-5' bonds [82], which are quite recalcitrant to oxidation.

Table IA. 6: Products obtained through the oxidative cleavage of C-C and C-O bonds in dimeric lignin models containing the β-O-4 linkage

C^{α}-C^{β} cleavage		C(Ar)-C^{α} cleavage	C^{β}-O cleavage	dehydration
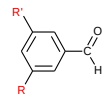 **9**H/**9**G/**9**S	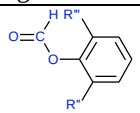 **16**H/**16**G/**16**S	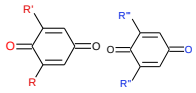 **1**H/**1**G/**1**S	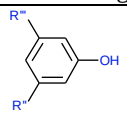 **17**H/**17**G/**17**S	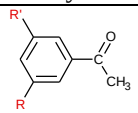 **18**H/**18**G/**18**S
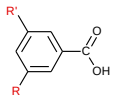 **10**H/**10**G/**10**S		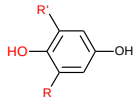 **2**H/**2**G/**2**S	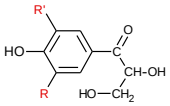 **20**H/**20**G/**20**S	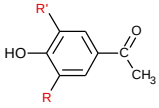 **19**H/**19**G/**19**S
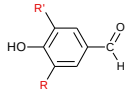 **11**H/**11**G/**11**S		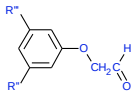 **3**H/**3**G/**3**S	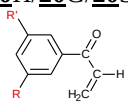 **21**H/**21**G/**21**S	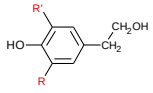 **29**H/**29**G/**29**S
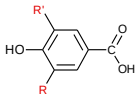 **12**H/**12**G/**12**S	Methyl ester derivate : **12-OMe**	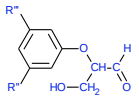 **4**H/**4**G/**4**S	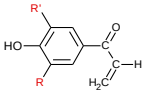 **22**H/**22**G/**22**S	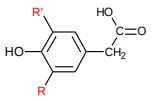 **30**H/**30**G/**30**S
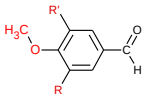 **13**H/**13**G/**13**S		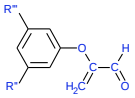 **5**H/**5**G/**5**S	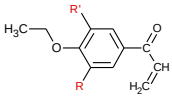 **23**H/**23**G/**23**S	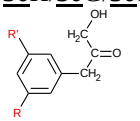 **31**H/**31**G/**31**S
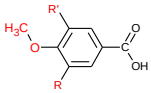 **14**H/**14**G/**14**S	Methyl ester derivate : **14-OMe** Amide derivate : **14-Npip**	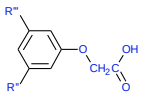 **6**H/**6**G/**6**S	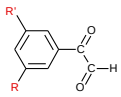 **24**H/**24**G/**24**S	Acetal derivatives : **24-acMe / 24-acEt**
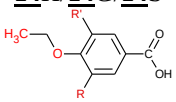 **14'**H/**14'**G/**14'**S	Methyl ester derivate : **14'-OMe**	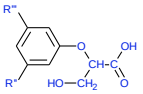 **7**H/**7**G/**7**S	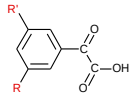 **25**H/**25**G/**25**S	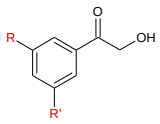 **32**H/**32**G/**32**S
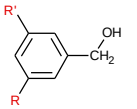 **15**H/**15**G/**15**S		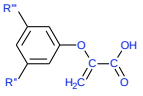 **8**H/**8**G/**8**S	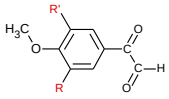 **26**H/**26**G/**26**S	Amide derivate : **26-Npip**
			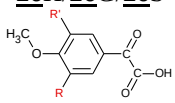 **27**H/**27**G/**27**S	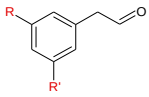 **33**H/**33**G/**33**S
			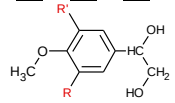 **28**H/**28**G/**28**S	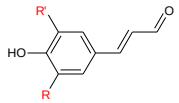 **34**H/**34**G/**34**S
				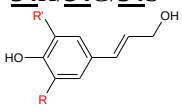 **35**H/**35**G/**35**S

1H : *p*-quinone, **1**G : 2-methoxyquinone, **1**S : 2,5-DMBQ; **2**H : dihydroquinone; **3**H : phenoxyacetaldehyde; **5**H : 2-phenoxyacrolein ; **6**H : phenoxyacetic acid; **7**H : 3-hydroxy-2-phenoxypropanoic acid; **7**H : 2-phenoxyacrylic acid ; **9**H : benzaldehyde; **10**H : benzoic acid; **11**H : *p*-hydroxy-benzaldehyde; **11**G : vanillin; **11**S : syringaldehyde ; **12**H : *p*-hydroxybenzoic acid; **12**G : vanillic acid; **12**S : syringic acid ; **13**H : *p*-hydroxybenzaldehyde; **13**G : veratraldehyde; **13**S : eudesmic aldehyde ; **14**H : *p*-methoxybenzoic acid; **14**G : veratric acid; **14**S : eudesmic acid ; **15**H : benzyl alcohol; **16**H : phenylformiate; **17**H : phenol, **17**G : guaiacol, **17**S : syringol; **18**H : acetophenone ; **19**H : *p*-hydroxyacetophenone, **24**G : phenylglyoxal, **25**H : phenylglyoxylic acid, **34**G : Coniferyl aldehyde, **35**G : coniferyl alcohol, **35**S : sinapyl alcohol

Moreover, other important side reactions that do not involve any cleavage must be considered. We have cited before (Fig. IA. 7) the formation of **K1**$_{HH}$ and **D1**$_{HH}$ from alcohol oxidation and dehydration. Plenty of other structures of dimers are possible:

- For instance, **A2**$_{XY}$, **A4**$_{XY}$ and **A6**$_{XY}$ models (R^2 = -CH_2OH) can be dehydrated into two types of enol ethers **DN**$_{XY}$ and **D'N**$_{XY}$ whose remaining alcohol function can be oxidized into ketone (**E'N**$_{XY}$ acrolein) or aldehyde / acid (**EN**$_{XY}$, **FN**$_{XY}$ acrolein) (see Fig. IA. 9).
- Moreover, oxidation of **A2**$_{XY}$, **A4**$_{XY}$ and **A6**$_{XY}$ models (R^2 = -CH_2OH) can lead to the aldehyde **BN**$_{XY}$ (oxidation of primary alcohol). Then, further oxidation of **BN**$_{XY}$ can lead to the β-oxo aldehyde **LN**$_{XY}$ or the **L'N**$_{XY}$ acid. Further oxidation of both leads to the **MN**$_{XY}$ dimer.
- Additionally, in the presence of an alcohol or of a carboxylic acid (solvent), esterification and etherification of dimers (**Est**$^{\alpha}$**AN**$_{XY}$, **Est**$^{\gamma}$**AN**$_{XY}$, **Eth**$^{\alpha}$**AN**$_{XY}$, **Eth**$^{\gamma}$**AN**$_{XY}$ and **Est**$^{\gamma}$**KN**$_{XY}$) and monomers are possible. These reactions can have a crucial influence as they may hide the active site for dimer cleavage.

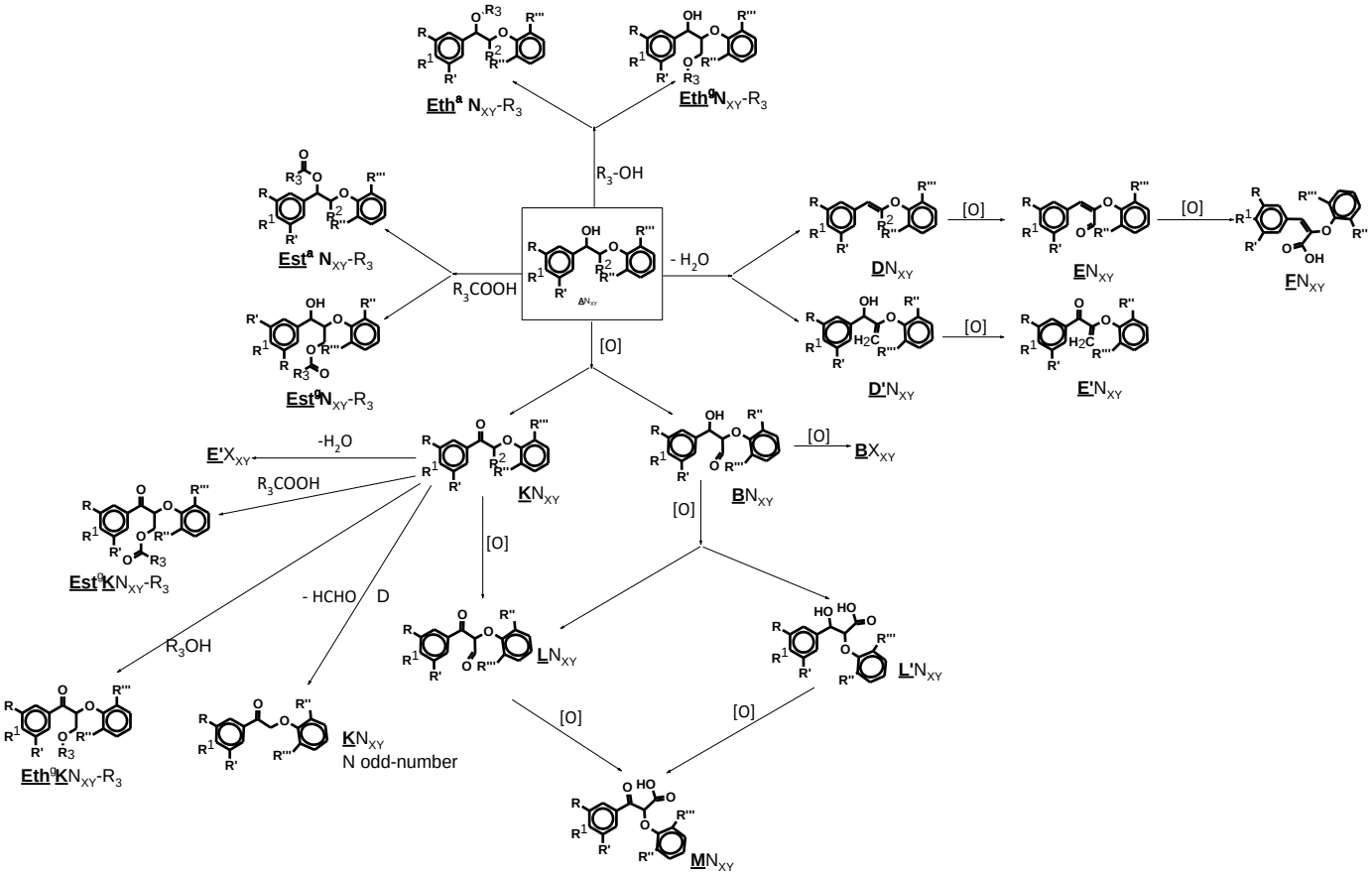

Figure IA. 9. Other side reactions not involving C-C and C-O bond cleavage

IA. 3.2. Aerobic oxidation of **A**N$_{XY}$ models

Most of the studies considering **A**N$_{XY}$ models focus on the selective oxidation of **A1**$_{XY}$ and **A6**$_{XY}$ while phenolic models such as **A3**$_{XY}$ are being slightly less tested.
Table IA. 7 compiles the results obtained in the catalytic aerobic oxidation of **A1**$_{XY}$ compounds. Table IA. 8 compares the data reported when using phenolic **A3**$_{XY}$ and etherified **A5**$_{XY}$ compounds. Such a comparison is helpful when assessing the influence of the phenolic group in the aerobic cleavage reactions, and can be moreover useful when relating lignin surrogates to *real* lignin behavior. Table IA. 9 summarizes the results reported for **A2**$_{XY}$ compounds and compares the results obtained when employing **A2**$_{SG}$ and **A4**$_{SG}$ models as substrates. Other **A4**$_{XY}$-type models are considered in Table IA. 10. The last two tables in this section, Table IA. 11 and Table IA. 12, recapitulate the works considering **A6**$_{XY}$ (R^1 = OMe) and **A6'**$_{XY}$ (R^1 = OEt) type, as well as other miscellaneous models. These last and more complicated compounds can be seen as transition to *real* lignin.

The results obtained, *i.e.* in terms of conversion and product yield (C^{α}-C^{β}, C^{β}-O cleavage, and/or other side reactions) are analyzed and discussed in detail within this section, paying special attention to the catalytic system employed, as well as to the operating conditions. These systems have been classified according to: i) homogeneous and ii) heterogeneous catalysis. Process intensification strategies, such as photochemistry, have been also revised.

IA. 3.2.1. Homogeneous catalytic systems

Among the different homogeneous systems employed in the aerobic oxidation of **A**N$_{XY}$-type models, vanadium, copper and cobalt-containing catalysts have been often described to show important activity, with a product yield distribution strongly depending on the type of model used as lignin surrogate, as well as on the reaction conditions, as it will be discussed in the following sub-sections.

*Table IA. 7: Aerobic oxidation of **A1**-type substrates*

Entry	Substrate	Conc. (M)	Catalyst	Solvent	Oxidant P (bar)	T (°C)	t (h)	Conv. (%)	Product yield (%)					Ref.
									C^{α}-C^{β} cleavage	C^{β}-O cleavage	[O]	-H_2O	others	
1	**A**1$_{HH}$	0.16	**V1** 10 mol.%	DMSO-d_6	air atm.	100	168	95	**10**H: 81	**17**H: 77	**K**1$_{HH}$: 9	-	HCOOH 46	83
2a		0.15	**V2** 5 mol.%	DMSO-d^6	air atm.	100	96	93[a]	-	(**18**H +**17**H) / **K1**$_{HH}$ = 1.43	-	-	-	84
2b			**V3** 5 mol.%					60[a]	-	(**18**H +**17**H) / **K1**$_{HH}$ = 1.80	-	-	-	
3a		0.5	VO(acac)$_2$ 10 mol%	MeCN				53	**9**H: 7 ; **10**H: 25 ; **16**H: 19	**17**H: 19	**K**1$_{HH}$: 18	-	12	85
3b		0.5		MeCN + 10% AcOH				89	**9**H: 4 ; **10**H: 29 ; **16**H: 9	**17**H: 44	**K**1$_{HH}$: 6	-	7	
3c		0.5		MeCN + 10% Et_3N				38	**9**H: 10 ; **10**H: 0 ; **16**H: 0	**17**H: 29	**K**1$_{HH}$: 32	-	29	
4		0.18	CuCl-TEMPO 20 mol.%	$CDCl_3$ – Lut – Toluene 1:0.14:6	O_2 Atm.	100	40	67	**10**H: 1	**17**H: 2	**K**1$_{HH}$: 1	-	**Est**$^{\gamma}$**A1**$_{HH}$-H-H: 18 TEMPO-adduct: 14	87
5		0.02	CeO_2 (80 wt.%)	MeOH	O_2 10	185	24	9.1	**18**H: 0 ; **10**H: 0.3 **10-OMe**-H: 3	**17**H: 0	**K**1$_{HH}$: 0	-	-	108
6		0.01	Pd-CeO_2	MeOH	O_2 10	185	24	64[a]; 68[b]	**10**H: 0.03[a] ; 0.07[b] **10-OMe**-H: 14[a] ; 25[b]	**17**H: 48[a] ; 39[b] **18**H: 38[a] ; 27[b]	**K**1$_{HH}$: 12[a] ; 12[b]	-	-	
7		0.1	Cu(OAc)$_2$-phen 20 mol.%	KOH 2M in DMSO	O_2 4	80	6	99	**10**H: 79	-	-	-	-	102
8						100	2	99	**10**H: 73	-	-	-	-	
9	**A**1$_{HG}$	0.01	Pd-CeO_2 (42 mol.% Pd)	MeOH	O_2 10	185	24	90	**10-OMe**-H: 25	**17**G: 68 **18**H: 38	**K**1$_{HH}$: 11	-	**Eth**$^{\gamma}$**K1**$_{HH}$: 6.4	108
10	**A**1$_{HS}$	0.1	Cu(OAc)$_2$-phen 20 mol.%	KOH 2M in DMSO	O_2 4	100	2	99	**10**H: 70	-	-	-	-	102

[a]fresh catalyst, [b]upon catalyst recycling, 5th consecutive runs.

*Table IA 8: Aerobic oxidation of **A3**$_{XY}$ and **A5**-type substrates*

Entry	Substrate	Conc. (M)	Catalyst	Solvent	Oxidant P (bar)	T (°C)	t (h)	Conv. (%)	Product yield (%)						Ref.
									C(Ar)-C$^{\alpha}$ cleavage	C$^{\alpha}$-C$^{\beta}$ cleavage	C$^{\beta}$-O cleavage	[O]	-H_2O	others	
1	**A3**$_{GG}$	$5.2\cdot10^{-3}$	$PMoV_5$ (38 mol.%)	Acetone-H_2O 30:70	O_2 5	90	0.33	100	**3**G: 16; **6**G: 7; **2**G : 4	-	**17**G: 77	-	**18**G: 3	-	97
2	**A3**$_{SG}$	$4.6\cdot10^{-3}$	$PMoV_5$ (42 mol.%)						**3**G: 17; **6**G: 9; **2**S: 8	-	**17**G: 75	-	**18**S: tr.		
3	**A3**$_{SS}$	0.2	Co(salen)**1** (5 mol.%)	MeOH	O_2 3.4	r. T	16	n. i.	**1**S: 86	-	**1**G: 17	**K**3$_{GS}$: tr.	-		73
4									**1**S: 81[a]	-		**K**3$_{SS}$: tr.	-		
5	**A5**$_{HH}$	0.1	$Cu(OAc)_2$-phen 20 mol.%	KOH 2M in DMSO	O_2 4	100	2	99	-	**14**H: 72	-	-	-		102
6									-	**14**H: 64	-	-	-		
7[b]	**A5**$_{HG}$	0.08	hydroquinone 10 mol.% + Cu/AlO(OH), 2 mol.% of Cu	$PhCF_3$-Acetone 3:1	O_2 atm	r. T.	40	low	-	**13**H: 22	**17**G: 12	-	-		113
8	**A5**$_{HS}$	0.1	$Cu(OAc)_2$-phen 20 mol.%	KOH 2M in DMSO	O_2 4	100	2	99	-	**14**H: 75	-	-	**-**		102
9	**A5**$_{GG}$	$4.9\cdot10^{-3}$	$PMoV_5$ (38 mol.%)	Acetone-H_2O 30:70	O_2 5	90	0.33	20	-	**11**G ~ 1 **12**G ~ 1 **15**G ~ 1.5 **13**G ~ tr.	**17**G ~ 1.5 **28**G ~ 4.5 **2G** ~ 1	-	**13G**: tr.		97

[a]Both from C(Ar)-C$^{\alpha}$ and from C$^{\beta}$–O cleavage, relative to 2 equivalents of substrate ; [b]Photocatalytic intensification

*Table IA. 9: Aerobic oxidation of **A2**$_{XY}$-type and **A4**$_{SG}$ substrates*

Entry	Substrate	Conc. (M)	Catalyst	Solvent	Oxidant P (bar)	T (°C)	t (h)	Conv. (%)	Product yield (%)						Ref.
									C(Ar)-C$^{\alpha}$ cleavage	C$^{\alpha}$-C$^{\beta}$ cleavage	C$^{\beta}$-O cleavage	[O]	-H_2O	others	
1	**A2**$_{HG}$	0.41	Co(salen)/GO 10 mol% of Co	MeCN	air atm.	80	24	90	-	-	**17**G: n.i.			**K**1$_{HG}$ 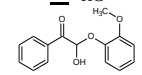 yield n. i.	110
2		0.017	CuOTf-TEMPO (20 mol%)	$CDCl_3$ – Lut – Toluene 1:0.14:6	O_2 atm.	100	40	95	-	**10**S: 1; **9**S: 54	**17**G: 10; **1**G: 5	**K**2$_{SG}$: 7 **A2**$_{SG}$-γ-estMe: 2	**E'2**$_{SG}$: 5	**A2**$_{SG}$-γ-estMe: 18	103-104
3		0.067	**V4** 10 mol%	pyr-d_5	air atm.	80	48	~ 65	-	-	-	**K**2$_{SG}$: 55	**E'2**$_{SG}$: 10	-	88
4	**A2**$_{SG}$	0.095	**V5** (10 mol%)	Toluene-d_8	air atm.	100	48	84	-	**10**S: 6; **9**S: 4	**5**S : 26 ; **4**S : 14	**K**2$_{SG}$: 27			89
5		0.086	**V1** 10 mol%	DMSO-d_6	air atm.	100	48	> 95	-	**10**S: 11; **9**S: 2	**17**G: n. q.; **21**S: 14	**K**2$_{SG}$: 65	**E'2**$_{SG}$: 5	HCOOH: 4	86
6		0.104		pyr-d_5				~ 85	-	**10**S: 6; **9**S: 4	**17G**: n. i.; **21**S: 29	**K**2$_{SG}$: 27	**E'2**$_{SG}$: 14	HCOOH: < 1	86
7		0.086	$V^V(O)(O^iPr)_3$ (10 mol%)	DMSO-d_6				~ 75	-	**10**S: 12; **9**S: 7	**17**G : n. i.; **21**S: 16	**K**2$_{SG}$: 39		HCOOH: 7	86
8		0.089	CuCl-TEMPO 100 mol%	pyr-d_5	O_2 atm.	100	40	89	-	**10**S: 13; **9**S: 43	**17**G: 7	**K**2$_{SG}$: 1	**E'2**$_{SG}$:2	HCOOH: 7 Condensation products	86
9		0.2	Co(salen)**1** (10 mol%)	MeOH	O_2 3.4	r. T.	48	n. i.	**1**S : 64	-	**1**G: 21	**K**4$_{SG}$: tr.			73
10	**A4**$_{SG}$	0.017	CuOTf-TEMPO (10 mol%)	$CDCl_3$ – Lut – Toluene 1:0.14:6	O_2 atm.	100	18	98	**5**G : 12 ; **1**S : 22	-	-	**K**4$_{SG}$: 44	**D'2**$_{SG}$: 7		88
11		0.080	**V4** (10 mol%)	pyr-d^5	air atm.	80	48	100	**5**G : 34 ; **1**S : 30	-	-	**K**4$_{SG}$: 27			89
12		0.057	**V5** (10 mol%)	Toluene-d_8	air atm.	100	48	20	**5**G : tr. ; **1**S : tr.	-	-	**K**4$_{SG}$: 19			

*Table IA. 10: Aerobic oxidation of other **A4**-type substrates*

Entry	Substrate	Conc. (M)	Catalyst	Solvent	Oxidant P (bar)	T (°C)	t (h)	Conv. (%)	Product yield (%)						Ref.
									C(Ar)-C$^{\alpha}$ cleavage	C$^{\alpha}$-C$^{\beta}$ cleavage	C$^{\beta}$-O cleavage	[O]	-H_2O	others	
1	**A4**$_{HG}$	0.06	Co(salen)**2** (10 mol.%)	chloroform	O_2 10	r. T.	48	98, 83[a] (1h: 83)	**1**H: 3 ; **5**G: 20	**11**H: tr.	-	-	-	-	101
2		0.06						99 (1h: 99[a])	**1**G: 16 ; **5**G: 81	-	-	-	-	-	
3	**A4**$_{GG}$	0.005	$Cu(phen)_2$ (5 mol.%)	NaOH 0.5 M	O_2 2.7	r. T.	20	97	-	**11**G: 51 ; **12**G: 1	**17G**: 0	-	-	-	105
4		0.15	**V2** (5 mol.%)	DMSO-d_6	air atm.	100	24	100	-	-	**21**G + **17**G	-	-	-	84
5		0.007	GO 1.5 mg	MeCN	O_2 5	140	24	100	**1**G: 15	**11**G: 7 ; **30**G: 5; **34**G: 2	**17**G: 87		**D4**$_{GG}$: 6		111
6	**A4**$_{SS}$	0.2	Co(salen)**1** (10 mol.%)	MeOH	O_2 3.4	r. T.	48	n. i.	**1**S: 10[b]	-	-	-	-	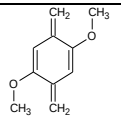 14 Aldehydes 30	73

[a]After 1 h, [b]Both from C(Ar)-C$^{\alpha}$ and from C$^{\beta}$–O cleavage, relative to 2 equivalents of substrate.

*Table IA. 11: Aerobic oxidation of **A6**-type substrates*

Entry	Substrate	Conc. (M)	Catalyst	Solvent	Oxidant P (bar)	T (°C)	t (h)	Conv. (%)	Product yield (%)					Ref.
									C^{α}-C^{β} cleavage	C^{β}-O cleavage	[O]	-H_2O	others	
1	**A6**$_{HH}$	0.25	CuCl-bipy-TEMPO 20 mol.% + NMI 0.4 eq	MeCN	air atm.	r. T.	20	23	**13**H: 13	**17**H: 6		-		106
2	**A6**$_{HG}$ (racemic)	0.06	Co(salen)$_2$ 10 mol.%	$CHCl_3$	O_2 10	r. T.	48	98	**13**H: tr.	-	Uncharacterized polymer			101
3		0.06	Cu(phen)$_2$ (5 mol.%)	NaOH 0.5 M	O_2 2.7	r. T.	24	75	**14**G: 50 ; **13**G: 2	-	-	-	-	105
4[a]		0.3	saturated DCA 12.9 mol.%	5% aq. MeCN	O_2 atm.	r. T.	7	50	**13**H: 26	**17**G: tr.	**K**6$_{GG}$: tr.	-	-	117-118
5	**A6**$_{GG}$	0.1	Cu(OAc)$_2$-phen 20 mol.%	KOH 2M in DMSO	O_2 4	140	2	92	**14**G: 49	-	-	-	-	102
6[a]	**A6**$_{GG}$ (racemic)	0.08	10 mol.% hydroquinone + Cu/AlO(OH), 2 mol.% of Cu	TFT-AcMe 3:1	O_2 atm	r. T.	66	low	**13**G: 7	**17**G: 7	-	-	-	113
7a	**A6**$_{GG}$ (racemic)	0.1	HTc-Cu-V (20 wt.%)	Toluene	O_2 5	135	16	> 99	-	**13**G: 38 ; **14**G: 31	**K**6$_{GG}$: 5	**D'6**$_{GG}$: 3	-	112
7b			HTc-Zn-Cu-V (20 wt.%)	Pyridine				>99[a] 76[b]	-	**13G**: 30 [a]; 22 [b] **14G**: 22 [a]; 14 [b]	**K**6$_{GG}$: 7	**D'6**$_{GG}$: 2 [a]; 3 [b]	-	
8[a]	**A6**$_{GG}$ (erythro)	0.3	saturated DCA 12.9 mol.%	5% aq. MeCN	O_2 atm.	r. T.	7	88	**13**G: 45	**17G**: 3	**K**6$_{GG}$: 4	-	-	117-118
9[a]	**A6**$_{GG}$ (threo)							90	**13**G: 5	**17G**: 5	**K**6$_{GG}$: 20	-	-	
10	**A6**$_{SG}$	0.3						51	**13**S: 10	**17**G: tr.	**K**6$_{GG}$: 0	-	-	
11a	**A6'**$_{GG}$	0.3	**V6** (10 mol.%)	CD_3CN	air atm.	80	24	> 95	-	**17G**: 57 ; **23'**G: 80	**K**6'$_{GG}$: 7	-	-	92
11b			**V6 dimer** (10 mol.%)						-	**17G**: 58 ; **23'**G: 80	**K**6'$_{GG}$: 1	-	-	
11c			**V6** 10 mol.%	AcOEt					-	**17**G: 70 ; **23'**G: 93	**K**6'$_{GG}$: 3	-	-	
12[a]		0.05	**V7b** 10 mol.%	CD_3CN	O_2 atm.	r. T.	24	76	**13'**G: 68 ; **16**G: 51	**17**G: 14 ; HCOOH: 16	-	-	-	115-116

[a]Photocatalytic intensification ; [b]fresh catalyst, [c]After recycling 3 times

Table IA. 12: Aerobic oxidation of miscellaneous models (dimers to tetramers)

Entry	Substrate	Conc. (M)	Catalyst	Solvent	Oxidant P (bar)	T (°C)	t (h)	Conv. (%)	Product yield (%)					Ref.
									C^{α}-C^{β} cleavage	C^{β}-O cleavage	[O]	-H_2O	others	
1	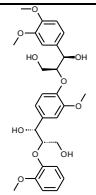	0.1	**V5** (10 mol.%)	AcOEt	air atm.	80	24	> 95	-	**17**G : 61; **23'**G : 83 ; **22**G : 63	-	-	-	92
2	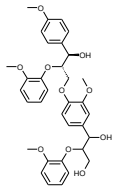	0.075	saturated DCA 51.4 mol.%	5% aqueous MeCN	O_2 atm.	r. T.	1	39	**13**H : 4	**16G** : tr. 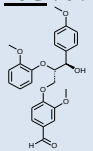 18	-	-	-	117-118
3	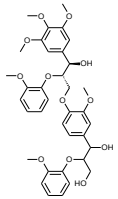							21	**13**S: 3	**16**G : tr.; 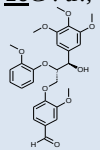 12	-	-	-	
4	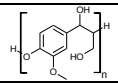	0.005	$Cu(phen)_2$ (5 mol%)	NaOH 0.5 M	O_2 2.7	r. T.	24	n. i.	**11**G: 13 ; **12**G: 1	-	-	-	-	105

- *Vanadium-based catalysts*

Vanadium-containing complexes have been often used in the aerobic oxidation of **AN**$_{XY}$ dimeric lignin models. In particular, complexes with O/N donor ligands (Table IA. 13) have been reported as promising homogeneous catalysts leading to the production of highly functionalized monomers.

Table IA. 13: Notation and molecular structures of V-catalysts used in the aerobic cleavage of AN$_{XY}$

Notation	**V1** (dipic)V^{V}(O)(O^{i}Pr)	**V2** V(+V)	**V3** V(+V)	**V4** $(HQ)_2V^{V}$(O)(O^{i}Pr)
Formula	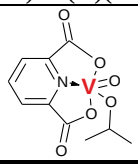	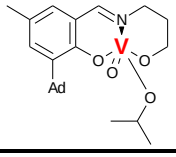	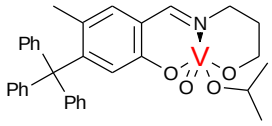	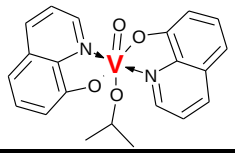

Notation	**V5** V(+V)	**V6** V(+V)	**V7a-c** (V(+V)) a : R^1=R^2=H b : R^1=H; R^2=NO_2 c : R^1=R^2=NO_2	**V(O)salen-IL** V(+IV)
Formula	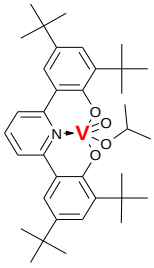	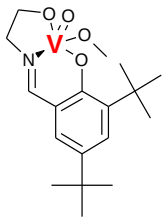	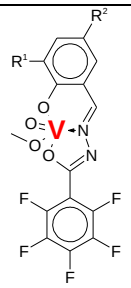	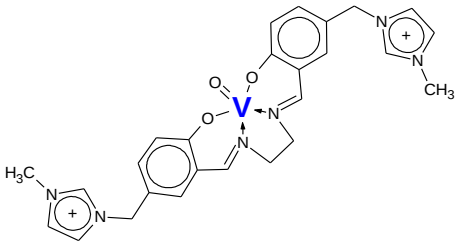

Such V-containing catalysts have shown to be quite efficient when operating in mild conditions, under either atmospheric O_2 (Table IA. 11, entry 12), or most commonly, in atmospheric air (Table IA. 7 – entries 1, 2a, 2b and 3; Table IA. 9 – entries 3-7 and 11-12, Table IA. 10 – entry 4; and Table IA. 11 – entries 11a-c).

- Case of **A1**$_{HH}$

HANSON *et al.* reported, for the first time in 2010, on the aerobic C-C cleavage of 1,2-hydroxyether lignin models in atmospheric air – among them **A1**$_{HH}$ – in the presence of a dipicolinate vanadium (V) catalyst, *i.e.* (dipic)V^{V}(O)O^{i}Pr, **V1** structure [83]. In deuterated dimethyl sulfoxide (DMSO-d_6), used for ^{1}H NMR monitoring, in ambient air conditions and at 100°C, a **A1**$_{HH}$ conversion of 95% was reached but only after 7 days reaction time! The main oxidation products were formic acid (46%), benzoic acid (**10**H, 81%), phenol (**17**H, 77%) and 2-phenoxyacetophenone (**K1**$_{HH}$, 9%) (see Table. IA. 7, entry 1). According to the authors, **A1**$_{HH}$ degradation occurred through benzylic oxidation resulting in the formation of **K1**$_{HH}$, which was subsequently oxidized to benzoic acid, phenol and formic acid. Within the conclusions of this work, HANSON *et al.* already anticipated that a proper choice of the ligand of these

homogeneous catalysts might lead to improved activity and selectivity. Few years later, PARKER *et al.* studied the aerobic oxidation of **A1**$_{HH}$ in the presence of different Schiff-base V-complexes (**V3** and **V2**) [84]. They observed that, in DMSO-d_6 and at 100°C (same conditions as before, but during 4 days instead of 7), the use of highly electro-donating and bulky ligands, such as the one with a trityl substituent (**V3** in Table. IA. 7, entry 2b), resulted in an improved selectivity towards the cleavage of C-O bonds (acetophenone (**18**H) and phenol (**17**H)) compared to **V2** (adamantyl substituent, Table IA. 7, entry 2a). On the contrary, a ligand with an electron-withdrawing substituent gave rise to poor catalytic activity. **V2** and **V3** did not give rise to C^{α}-C^{β} cleavage on the contrary of **V1** as **10**H was never observed.

With **A1**$_{HH}$, MA *et al* [85] have recently demonstrated, using $V^{IV}O(acac)_2$ as a catalyst (10 mol%), that the nature of the solvent might strongly influence the dimer conversion, as well as the products selectivity (Table IA. 7, entry 3). The cleavage of C-C bonds was particularly favored in a mixture of acetonitrile (MeCN) and acetic acid (10 wt.%), (conversion: 89% and cleavage selectivity 85% after 96 h!) whereas other solvents, such as MeCN + 10 wt% triethylamine (Et_3N) and dimethyl sulfoxide (DMSO) seemed to favor side reactions, mostly alcohol oxidation. The authors of this work claimed that DMSO molecules can either be coordinated to the vacant vanadium coordination site in $V^{IV}O(acac)_2$, thus competing with the dimeric substrate or even ligands, which substantially affect the oxidation reaction and its yield. To explain the better performances obtained in presence of acetic acid, the authors therefore concluded that, during oxidation, the carboxylic group of acetic acid could coordinate to vanadium(IV) by exchanging with the acetylacetonato ligand in $VO(acac)_2$. MA *et al.* also tested different types of vanadium complexes, such as $VO(mal)_2$ (mal = malonate), $VOSO_4 \cdot xH_2O$, VOC_2O_4, $VO(OEt)_3$, and $VO(O^iPr)_3$. They reported, however, very similar activity and selectivity in all cases, and related this fact to the formation of very similar V(IV) active complexes in all these reaction systems.

- Case of **A2**$_{SG}$ 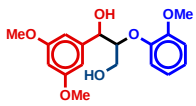

In further studies, HANSON *et al* [86, 88-89] considered the oxidation of the relatively more complex **A2**$_{SG}$ model in atmospheric air and in the presence of different homogeneous vanadium catalysts (**V1** already tested on **A1**$_{HH}$ and **V4** and **V5**, structure in Table IA. 13), also clearly evidencing in this case the key importance of the choice of the catalytic system.
They reported almost complete conversion of the **A2**$_{SG}$ dimer upon 48 h reaction under air at 100°C, in DMSO-d_6 (Table IA. 9, entry 5) and in the presence of the $(dipic)V^{V}(O)(O^iPr)$

catalyst (**V1** structure in Table IA. 6), whereas in the presence of $V^{V}(O)(O^{i}Pr)_3$, the reaction was somehow slower, reaching only 75% conversion (Table IA. 9, entry 7) [86]. Important differences in selectivities were also observed, (see Table IA. 9, entries 5 and 7), *i.e.* the dipicolinate vanadium catalyst (entry 5) led mostly to the production of the **K2**$_{SG}$ (as a result of the oxidation of the alcohol group of **A2**$_{SG}$), and catalyzed also the C^{α}-C^{β} in this ketone, leading to the formation of 3,5-dimethoxybenzoic acid (**10**S). The use of pyridine-d_5 as solvent, instead of DMSO-d_6, had a significant impact on the product distribution (Table IA. 9, entry 6 vs 5). In pyridine-d_5, the non-oxidative cleavage of C-O bonds is favored, resulting in an increased yield of the alkene **21**S, and the dehydration of the **K2**$_{SG}$ ketone (yielding **E'2**$_{SG}$) seems to occur also to a greater extent than when using the DMSO-d_6. The conversion in pyridine-d_5 reached 85% upon 48 h reaction.

Comparing **A2**$_{SG}$ to **A1**$_{HH}$ [83], in the presence of the same catalyst (**V1**) and under similar reaction conditions (in DMSO-d_6 at 100°C and same catalytic loading of **V1**), one can observe that, although the reaction time was much longer in the case of the simplest **A1**$_{HH}$ model, its oxidation led to higher yields of the different C-C and C-O cleavage products, whereas the formation of the corresponding ketone (secondary alcohol oxidation) was much higher when using the more complicated **A2**$_{SG}$ model. Separate oxidation of **K2**$_{SG}$ (conversion: 40%, Table IA. 15, entry 2) yielded the dehydrated ketone **E'2**$_{SG}$ (14%), a mixture of guaiacol (3%, **17**G), 2,6-dimethoxybenzoic acid (**10**S, 19%) and formic acid (7%) in DMSO-d_6 and in the presence of the dipic V-complex (**V4**) [86, 87], confirming that this ketone can be an intermediate in the formation of these products starting from **A2**$_{SG}$.

HANSON *et coll* considered as well the oxidation of **A2**$_{SG}$ in the presence of two more types of V-complexes: 8-quinolinate complexes ($(HQ)_2V^{V}(O)(O^{i}Pr)$, **V4** (Table IA. 9, entry 3) [88] and tridentate bis(phenolate)pyridine ($(BPP)V^{V}(O)(O^{i}Pr)$, **V5** Table IA. 9, entry 4) complexes [89]. In pyridine-d_5 (Table IA. 9, entry 3), the 8-quinolinate V-complex (**V4**) led to approximately 65% conversion of the **A2**$_{SG}$ substrate at 80°C and after 48 h. No cleavage was observed in this case, since the products obtained were the ketone **K2**$_{SG}$ and the dehydrated ketone **E'2**$_{SG}$ (Table IA. 9, entry 3). This catalyst showed thus much lower activity and selectivity for the aerobic cleavage than the other ones previously reported and tested using **A2**$_{SG}$, *i.e.* **V1** and $V^{V}(O)(O^{i}Pr)_3$. In toluene, the bis(phenolate)pyridine V-complex (**V5**) mostly favored the C-O cleavage and alcohol oxidation in **A2**$_{SG}$, yielding also relatively important amounts of the **K2**$_{SG}$ ketone (Table IA. 9, entry 4).

- **Case of <u>A4</u>$_{SG}$** (R' = OMe), **<u>A4</u>$_{GG}$** (R' = H) 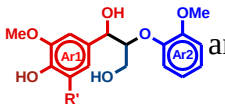 and **<u>A4</u>$_{HH}$**

In these last two works of HANSON *et al.* [88, 89], the reactivity of **<u>A2</u>$_{SG}$** has also been compared to that of **<u>A4</u>$_{SG}$**, bearing a phenol function (R^1 = OH). Phenolic moieties are abundant in real lignin [90]. HANSON *et al* aimed to demonstrate the influence of these phenolic groups on the course of the oxidation in atmospheric air in the presence of the 8-quinolinate and the bis(phenolate)pyridine V-complexes (**V4** and **V5,** Table IA. 9, entries 11 and 12).

In pyridine-d_5 and in the presence of the 8-quinolate catalyst (**V4**) [88], complete conversion of the **<u>A4</u>$_{SG}$** dimer was achieved upon 48 h of reaction at 80°C. The oxidation reaction was therefore faster on the phenolic substrate than on the non-phenolic one (conversion: 65%, Table IA. 9, entry 3). Moreover, the reaction yielded C(Ar)-C^{α} cleavage products such as 2-(2-methoxyphenyl)acrolein (**<u>5</u>G**, 34%) and 2,6-dimethoxybenzoquinone (**<u>1</u>S**, 30%), proving that the 8-quinolinate complex (**V4**) at 80°C in pyridine was catalytically active in breaking this bond in **<u>A4</u>$_{SG}$** (100% of conv. within 48 h) while no cleavage was observed for **<u>A2</u>$_{SG}$** in the same conditions. So, the phenolic is the active site for cleavage. Moreover, it is important to note that the bis(phenolate)pyridine V-catalyst (**V5**) led to slower **<u>A4</u>$_{SG}$** substrate oxidation despite a higher reaction temperature [89] (entry 12). In toluene at 100°C, only 20% conversion was obtained upon 48 h. In both cases (**V4** in pyridine-d^5 at 80°C and **V5** in toluene at 100°C), the reaction of **<u>A4</u>$_{SG}$** under air afforded the ketone **<u>K4</u>$_{SG}$** and only trace amounts of the C^{α}-C^{β} cleavage products were detected. It therefore seemed that the presence of the phenolic group did not have any definitive influence on the reaction rate and selectivity, this being mostly determined by the type of V-catalyst used.

Another phenolic dimer, **<u>A4</u>$_{GG}$** (guaiacylglycerol-β-guaiacyl) was also considered by PARKER *et al.* [84]. The reaction was performed in DMSO-d_6 at 100°C under air and in the presence of the V-complex **V2** (Table IA. 10, entry 4,). Complete conversion of this phenolic substrate was obtained after 24 h of reaction with 100% selectivity towards C^{β}-O bond cleavage (no evidences of ketone oxidation products).

JIANG *et al.* [91] recently performed density functional theory (DFT) calculations, in order to gain more evidence on the mechanism of C^{β}-O and C(Ar)-C^{α} bond cleavage in dimeric lignin models. Mechanistic observations pointed that C^{β}-O cleavage proceeds *via* the formation of a V(IV) complex through ligand exchange with the benzylic group of the lignin model that gives rise to the complex TDTS2 followed by intramolecular hydrogen transfer (TOF-determining step) leading to a V(III)-complex (pathway (2)). C(Ar)-C^{α} cleavage proceeds *via* a hydrogen radical from the phenolic moiety by the V(V) complex resulting to a phenoxy

radical and to a V(IV) complex. Dioxygen withdraws then an electron to the reduced vanadium complex, which gives rise to a peroxo V(V) complex and then to the complex noted TDTS1 (pathway (1)). The TOF-determining step is the O-O homolytic cleavage in TDTS1. The understanding of the role of both TOF-determining steps enables to anticipate the selectivity of vanadium-based catalysts. Indeed, if O-O cleavage in TDTS1 is favored, the catalyst will be more selective for C(Ar)-C^{α} cleavage whereas if the hydrogen transfer giving rise to the V(III)-complex is favored, the catalyst will be selective for C^{β}-O cleavage.

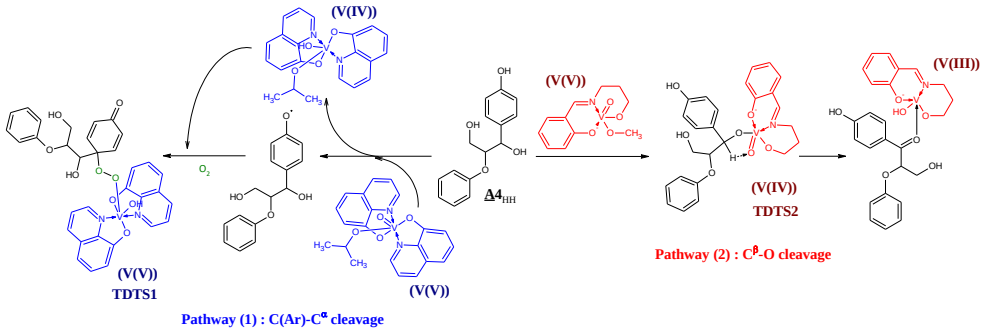

Figure IA. 10: Two examples of interactions between the substrate A4$_{HH}$ and a V-catalyst [90]

- **Case of A6'$_{GG}$**

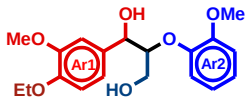

As remarked by PARKER *et al* [84], the catalytic performance of V-complexes in the oxidation of dimeric lignin models might be the result of a balance of steric and electronic effects. The work of SON and TOSTE [92], which substantially inspired the investigations of HANSON *et al.*, established a relationship between the increased selectivity of the catalysts towards C^{β}-O cleavage and the high bite angles values of the ligands in the corresponding V-complexes (see **V6** in Table IA. 13). This and other V-complexes were tested in the oxidation of **A6**$_{GG}$-like dimers (**A6'**$_{GG}$, R^1 = OEt, see Table IA. 11) in atmospheric air. The results obtained with **V6** or its dimer in three sets of reaction conditions (Table IA. 11, entries 11a, 11b and 11c) emphasized a very important selectivity for the products of the C^{β}-O cleavage (1-(4-ethoxy-3-methoxyphenyl)-2-propen-1-one, **23**'G: 93%, **17**G: 70%, entry 11c). Similar trends were also obtained by the same authors using another V-compound, **V5**, (Table IA. 12, entry 1) in the oxidation of a trimeric lignin model. SON and TOSTE claimed that, through subtle changes in the ligand structure, the reactivity of the V-catalyst can be tuned from simple alcohol oxidation to the cleavage of the C^{β}-O bond in the lignin model. SON and TOSTE aimed to assess as well the role of dioxygen in this aerobic oxidation reaction and concluded that dioxygen was not essential for the catalyst turnover but it did increase the reaction rate. They

proposed a one-electron process as the most probable reaction mechanism involving V(IV) and V(V) species. Based on this and according to their different observations, HANSON *et coll* concluded that electron-rich ligands might accelerate the catalyst regeneration, *i.e.* the reaction of V(IV) with air, whereas the oxidation of the alcohol group by the V(V)-catalyst in these A-type models would be promoted by more electron deficient ligands [89].

- **Case of <u>A3</u>$_{SG}$** (R^1 = OH, R' = OMe), **<u>A3</u>$_{GG}$** (R^1 = OH, R' = H) and **<u>A5</u>$_{GG}$** (R^1 = OMe, R' = H)

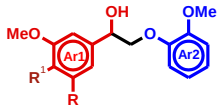

Vanadium-containing heteropolyacids (HPAs) have also been used as catalysts in the aerobic oxidation of dimeric lignin models under 5 bar of dioxygen. The $H_8[PMo_7V_5O_{40}]$ complex, noted $PMoV_5$, was tested on **<u>A3</u>$_{GG}$**, **<u>A3</u>$_{SG}$** and **<u>A5</u>$_{GG}$** (Table IA. 8 – entries 1, 2 and 9). Such HPAs behave as relatively strong acids [94] and have shown several times to be highly selective catalysts in oxidative organic synthesis and in oxygen-mediated lignin delignification [95, 96]. EVTUGUIN *et al* [97] observed that, at 5 bar and 90°C, $PMoV_5$ was five times more active on the phenolic compounds (**<u>A3</u>$_{GG}$** and **<u>A3</u>$_{SG}$** : total conversion, entries 1-2) than on the non-phenolic one, **<u>A5</u>$_{GG}$** (conversion = 20%, entry 9). Given the products obtained (phenoxyacetaldehyde **<u>3</u>**G (16%), phenoxyacetic acid **<u>6</u>**G (7%), 2-methoxyhydroquinone **<u>2</u>**G (4%) from aerobic C(Ar)-C^{α} cleavage and guaiacol **<u>17</u>**G (77%) from acidic C^{β}-O cleavage) for **<u>A3</u>$_{GG}$** and (phenoxyacetaldehyde **<u>3</u>**G (17%), phenoxyacetic acid **<u>6</u>**G (9%), 2,5-dimethoxyhydroquinone **<u>2</u>**S (8%) from C(Ar)-C^{α} cleavage and guaiacol **<u>17</u>**G (75%) from C^{β}-O cleavage) for **<u>A3</u>$_{SG}$**), the authors claimed that the oxidation of the phenolic compounds (**<u>A3</u>$_{GG}$** and **<u>A3</u>$_{SG}$**) would proceed through heterolytic mechanisms involving the hydrolytic splitting of the C(Ar)-C^{α} linkage in Int1 (Fig. IA. 11) and the acidolytic cleavage of the β-O-4 bond (*via* the intermediate **<u>D3</u>$_{GG}$** or **<u>D3</u>$_{SG}$**) as on Fig. IA. 9.

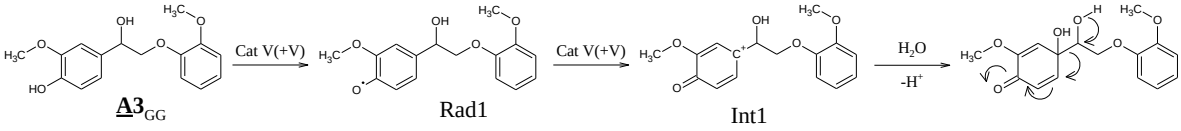

Figure IA. 11: Mechanism of $PMoV_5$-catalyzed C(Ar)-C^{α} cleavage inspired by Ref 97

On the other hand, the cleavage of the non-phenolic model would occur through a one-electron oxidation mechanism followed by the homolytic splitting of the C^{β}-O (**<u>17</u>**G (1.5%), 1-(3,4-dimethoxyphenyl)-1,2-ethanediol **<u>28</u>**G (4.5%) and **<u>2</u>**G (1%)) and of the C^{α}-C^{β} linkages (3-methoxybenzylic alcohol **<u>15</u>**G (1.5%), vanillin **<u>11</u>**G (1%) and vanillic acid **<u>12</u>**G (1%)) instead of C(Ar)-C^{α} cleavage. In both cases, the $PMoV_5$ (actually VO_2^+ from $PMoV_5$ decomposition [97-100]) would withdraw an electron from the aromatic ring Ar1 and from the alcohol II

moiety. On phenolic substrates, the oxidation is easier due to a high electro-donating effect of the phenol group.

> *Homogeneous vanadium complexes tend to be quite active and selective catalysts whose performances can be tailored by properly choosing the ligands (HANSON et coll. [83, 86-89]). Indeed,* ***V1*** *is active for* C^{α}-C^{β} *cleavage in* ***A1****$_{HH}$ (and even the most active for such reaction in non-phenolic models (****A1****$_{XY}$,* ***A2****$_{XY}$,* ***A5****$_{XY}$ and* ***A6****$_{XY}$), yield of benzoic acid of 81%). The catalyst* ***V2*** *proved to be the most active for the cleavage of* C^{β}*-O bond (combined yield of* ***17****H +* ***18****H = 54%). The cleavage of C(Ar)-*C^{α} *linkage was observed only in the oxidation of phenolic models. Two strategies have been used: oxidation i) in atmospheric air during a long time (48 h,* ***V4*** *10 mol%, pyridine 100°C) and ii) under a higher pressure of dioxygen (5 bar) during a short time (20 min,* $PMoV_5$ *38 mol%, acetone-water 3-7 90°C). The first option was more adequate for C(Ar)-*C^{α} *cleavage whereas the second one was the best solution for* C^{β}*-O cleavage.*

- ***Cobalt-based catalysts: Co(salen)***

Co(salen) catalysts are the sole homogeneous Co(+II)-containing systems that have been considered for the aerobic cleavage of C-C and C-O bonds in **AN**$_{XY}$-type lignin models at room temperature.

Table IA. 14: Notation and molecular structures of Co^{II}*(salen) catalysts used for aerobic clivage of* ***AN****$_{XY}$ models*

Name	Co(salen)1	Co(salen)2
	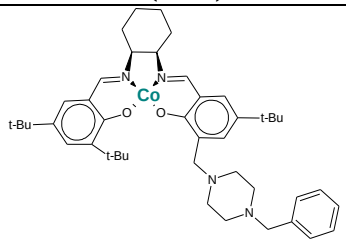	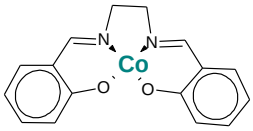

BIANNIC and BOZELL assessed impact of different ligands on the activity and the selectivity for phenolic lignin model aerobic cleavage in the presence of Co-Schiff base catalysts in MeOH [73] at room temperature and under O_2, at approximately 3 bar. The results obtained with Co(salen)**1** are presented in Table IA. 8, entries 3 and 4 for **A3**$_{SG}$ and **A3**$_{SS}$ models, Table IA. 9, entry 9 for **A4**$_{SG}$ and Table IA. 10, entry 6 for **A4**$_{SS}$ model.

The main products obtained from the oxidation of such phenolic models were the corresponding benzoquinones **1**G (yield 17% from **A3**$_{SG}$) and **1**S (yield 81% from **A3**$_{SS}$ and 86% from **A3**$_{SG}$). The authors claimed that the conversion of the dimer into benzoquinones

occurred through the simultaneous cleavage of the C(Ar)-C^{α} and the C^{β}-O bond (see Fig. IA. 7). The presence of a bulky sterically hindered N-benzylpiperazine as substituent in the **Co(salen)1** catalyst was suggested to be at the origin of this highly selective C(Ar)-C^{α} bond cleavage. The authors also claimed that product distribution could be further tailored by using differently substituted Schiff bases and playing with the symmetry of the Co(salen) catalyst.

In the presence of **Co(salen)1**, the CH_2OH group in **A4**$_{SG}$ and **A4**$_{SS}$ dimers does not seem to impact the selectivity but considerably affects both the yield and the reaction rate, due to further steric hindrance. For these substrates, the oxidation reaction mechanism would involve the formation of a superoxo complex [Co^{III}(salen)(ArOH)($O_2^{\cdot}$)]. The cleavage is initiated by the oxidation of the phenolic moiety into a phenoxy radical. Afterwards, the addition of another superoxo complex on the carbon C(Ar) gives rise to the intermediate presented on Fig. IA. 12 (case of **A4**$_{SG}$). This intermediate would then undergo C(Ar)-C^{α} cleavage, yielding the dimethoxybenzoquinone **1**S. Other products would either undergo re-dimerization, or further react with another superoxo Co-complex yielding the methoxybenzoquinone **1**G (but with a yield of 17% only). Such mechanism is somehow similar to that suggested by JIANG *et al.* [92] for V-complexes, but differs to the reaction pathway proposed for V-substituted HPAs [97]. Indeed, $[PMo_7V_5O_{40}]^{8-}$ was also quite selective towards C(Ar)-C^{α} cleavage, but the main product was a hydroquinone derivative **2**G or **2**S instead of a benzoquinone. This could be explained by the different reaction mechanisms. The key intermediate in presence of $PMoV_5$ (substrate: **A3**$_{GG}$ or **A3**$_{SG}$) is the diol formed through the hydratation of the cationic oxidation product depicted in Fig. IA. 11.

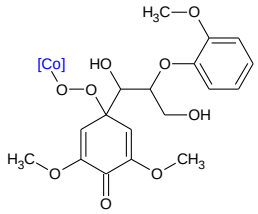

Figure IA. 12: Simplified structure of IntCo

CANEVALI *et al* [101] assayed the reactivity of Co(salen)**2** in the aerobic oxidation of **A4**$_{HG}$, **A4**$_{GG}$ (Table IA. 10 – entries 1 and 6) and **A6**$_{HG}$ (Table IA. 11 – entry 2) in chloroform at room temperature but the O_2 pressure used was three times higher than in the work of BIANNIC and BOZELL [73]. In the case of the **A4**$_{HG}$ and **A4**$_{GG}$ models, almost complete conversion was observed upon 48 h. Co(salen)**2** was quite selective towards C(Ar)-C^{α} cleavage affording the conjugated aldehyde (**5**G) and the quinones (**1**H or **1**G), as the main products. Yields were higher for the oxidation of **A4**$_{GG}$ than for **A4**$_{HG}$. In the case of the non-phenolic substrate **A6**$_{HG}$, the oxidation reaction was considerably slower and yielded no cleavage products at all. Instead, undetermined polymerization products were detected.

***Co(salen)** catalysts were essentially tested on phenolic substrates. Only one test was carried out on a non-phenolic **A6**$_{XY}$ model (CANEVALI et al, see Table IA. 11, entry 2). Instead of aerobic cleavage, polymerization took place.*
*The **Co(salen)1** (O_2 3 bar, 10 mol%, methanol r. T) catalyst showed to be more suitable for C(Ar)-C^{α} cleavage than $PMoV_5$ in **A3**$_{XY}$ models (yield of **2**S until 86% from **A3**$_{SG}$ vs 34% (combined yield of **3**G, **6**G, **2**S) in the case of $PMoV_5$). However, **Co(salen)1** was less active on **A4**$_{XY}$ substrates. So, **Co(salen)2** is the most suitable Co-catalyst for **A4**$_{XY}$ aerobic cleavage (it should be noted that the dioxygen pressure was 10 bar).*

- ***Copper-based catalysts***

Cu homogeneous catalysts have also been used often as V-complexes for the aerobic cleavage of C-C and C-O bonds in **AN**$_{XY}$ molecules.

- *$Cu^{+II}(OAc)_2$/phenantroline/KOH*

Using Cu(II) acetate in the presence of 1,10-phenanthroline and KOH, WANG *et al.* [102] worked on seven non-phenolic substrates: **A1**$_{HH}$, **A1**$_{HG}$, **A1**$_{HS}$, **A5**$_{HH}$, **A5**$_{HG}$, **A5**$_{HS}$ and **A6**$_{GG}$. $Cu(OAc)_2$ itself was found to be inactive for alcohol oxidation and several organic ligands, as well as base additives were tested. In DMSO, 1,10-phenanthroline was found to be the most effective ligand for C^{α}-C^{β} bond cleavage. **A1** and **A5** dimeric models were successfully oxidized using $Cu(OAc)_2$/1,10-phenanthroline/KOH, yielding important amounts of the corresponding benzoic acids **10**H (70-79%) and **14**H (72-75%) (see Table IA. 7 – entries 7, 8 and 10 and Table IA. 8 – entries 5, 6 and 8). The presence of the methoxy substituents in the **A1** $_{XY}$ models (Table IA. 7, entries 8 and 10) showed relatively low effect on the catalytic performance compared to **A5**$_{XY}$ ones (Table IA. 8, entries 6 and 8). However, **A6**$_{GG}$, with its additional -CH_2-OH substituent in β position, was found to be more reluctant to oxidation and higher temperature had to be applied, *i.e.* 140°C instead of 100°C, still yielding lower amounts of the corresponding monomeric aromatic acid (**14**G, veratric acid) than **A1** and **A5** models (see Table IA. 11 – entry 5). Steric hindrance of the additional -CH_2-OH would be responsible of the low reactivity of **A6**$_{GG}$.

- *Cu^{+I}(OTf)/2,6-lutidine/TEMPO*

SEDAI and BAKER, together with HANSON *et coll.* have published several papers dealing with the copper-catalytic oxidation of different dimeric lignin models [86, 87, 103-104]. The activity of such Cu(I)-catalysts was often compared to that observed for the V-complexes (see section IA. 3.2.1.1. of this review). TEMPO, (2,2,6,6,-tetramethylpiperidin-1-yl)oxyl, was used as a co-catalyst in the Cu-mediated oxidation.

In the presence of stoichiometric amounts CuCl-TEMPO in pyridine [86], 89% conversion of **A2**$_{SG}$ was reached after 40 h at 100°C under O_2 at ambient pressure (see Table IA. 9 – entry 8). In these conditions, the reaction yielded important amounts of C^{α}-C^{β} cleavage products, such as the correspondingly substituted benzaldehyde (**10**S) and benzoic acid (**9**S). The yields of these monomeric compounds were considerably higher than the ones obtained under relatively similar reaction conditions but in the presence of **V1**. Indeed, the yield of **9**S increased from 4 to 43% when using CuCl-TEMPO. Moreover, the formation of the **K2**$_{SG}$ and the dehydrated ketone **E'2**$_{SG}$ was almost negligible. Such results pointed out the occurrence of different reaction mechanisms for both types of catalysts. SEDAI *et al* [86] claimed that Cu-catalysts tend to cleave directly the C-C linkage whereas V-catalysts lead first to the oxidation of the aliphatic hydroxyl group generating the ketone intermediate that undergoes subsequent C-C or C-O bond cleavage. It must be nevertheless noted that, although the oxidation of **A2**$_{SG}$ by O_2/CuCl-TEMPO resulted in higher yields of C^{α}-C^{β} bond cleavage products, the reaction conditions were slightly different compared to those used in the presence of **V1**. Indeed, O_2 was used instead of air and the catalytic loading was 100%, *i.e.* ten times higher than for **V1**. In subsequent studies [103, 104], the CuOTf/2,6-lutidine/TEMPO catalytic system was presented to be more active than CuCl/pyridine/TEMPO. Under optimized reaction conditions, the production of the 2,6-dimethoxybenzaldehyde (**9**S) from **A2**$_{SG}$ increased from 43% (see Table IA. 9 – entry 8, for CuCl) to 54% (see Table IA. 9 – entry 2) and the combined yield of **9**S and **10**S did not change significantly (55% *vs* 56%).

More recently, the oxidation of the simplest model, **A1**$_{HH}$, was assayed [87] in the presence of 20 mol% of CuCl/TEMPO/2,6-lutidine (see Table IA. 7 – entry 4). In toluene and at 100°C, the conversion reached 67% after 40 h and the product distribution obtained was completely different from that in the oxidation of **A2**$_{SG}$ (see Table IA. 9 – entry 4). Indeed, the oxidation did not seem to proceed through direct C^{α}-C^{β} bond cleavage. Several by-products related to substrate formylation (by formic acid from the CH_2 group in **A1**$_{HH}$) and radical coupling with the TEMPO reagent were observed. It can be noted that the carbon balances of

the Cu-catalyzed oxidations seemed to be poor (conversion much higher than the yield of cleavage product and default of products from Ar2 moiety) and the formation of small amounts of condensation and uncharacterized reaction products was observed.

SEDAI *et al* also considered the influence of the presence of a phenolic –OH group in the lignin model used as substrate [103, 104] also in a dioxygen atmosphere at 100°C (but the duration was shortened from 40 to 18 h). As previously detailed within this review, the comparison between the oxidation of **A2**$_{SG}$ (w/o phenol group) and **A4**$_{SG}$ (w phenol group) was analogously performed in the case of V-catalysts with Cu(OTf) (Table IA. 9). Complete conversion of the **A4**$_{SG}$ model was observed upon 18 h at 100°C (Table IA. 10, entry 10). However, the product distribution obtained from the oxidation of **A4**$_{SG}$ importantly differed from that of the non-phenolic **A2**$_{SG}$ compound. A lot of ketone **K4**$_{SG}$ (44%) was formed, along with C(Ar)-C$^{\alpha}$ cleavage products (**5**G (12%) and **1**S (22%)). This can be attributed to a shortened duration. No 4-hydroxy-3,5-dimethoxybenzaldehyde and no 2-methoxyphenol (direct C$^{\alpha}$-C$^{\beta}$ cleavage products) were detected, which was expected due to the presence of the phenolic moiety. The same observation was made for **V4**-catalyzed oxidation of **A4**$_{SG}$ [88].

- *Cu^{+II}(phenantroline)/NaOH*

Still dealing with phenolic models, AZAPIRA *et al.* [105] considered the oxidation of **A4**$_{GG}$ in the presence of a copper-phenantroline complex (Table IA. 10, entry 3) [105]. Almost complete conversion of the **A4**$_{GG}$ dimer was observed upon 20 h at room temperature and under 2.7 bar of O_2 in alkaline media. The main products obtained were vanillic acid (**12**G), vanillin (**11**G) and guaiacol (**17**G), emphasizing the high selectivity of the Cu(phen)$_2$ catalyst towards C$^{\alpha}$-C$^{\beta}$ and C$^{\beta}$-O bond cleavage. However, as reaction proceeded, the yield of all cleavage products decreased, suggesting that they are not stable under the reaction conditions employed. Upon 20 h, the only major reaction product was vanillin, **11**G (51% yield, see Table IA. 10 – entry 3). Increasing O_2 pressure from 2.7 to 12.4 bar led to complete conversion of **A4**$_{GG}$ but resulted in lower cleavage products yields. Many new and unidentified products were formed, pointing to the occurrence of side reactions as a consequence of increased O_2 pressure. Suspecting that the free phenolic group in **A4**$_{GG}$ was responsible for the low yields of cleavage products obtained, AZAPIRA *et al* [105] also studied the catalytic oxidation of a non-phenolic dimer, **A6**$_{HG}$ (Table IA. 11 – entry 3). Under the same reaction conditions and after 24 h (O_2 2.7 bar), the conversion of **A6**$_{HG}$ reached only 75%. The yield of veratric acid (**14**G) and veratraldehyde (**13**G) increased with reaction time, whereas the production of guaiacol (**17**G)

increased and then dropped to zero. After 24 h, veratric acid, **14**G, was the main reaction product (50% yield, see Table IA. 11 – entry 3). The conversion of **A6**$_{HG}$ was almost complete at 12.4 bar O_2 pressure and an increased veratric acid yield was obtained, in comparison to the reaction performed at 2.7 bar. Considering these results, the authors concluded that the oxidation of phenolic and of etherified models most probably involved different mechanisms. Moreover, after conducting alkaline catalytic oxidations experiments on the separate reaction products, they claimed that the prompter degradation of vanillic acid (**12**G) in comparison to veratric acid (**14**G) might be linked to the presence of the free hydroxyl group *para* to the side chain in Ar1 ring. This phenolic group seemed to play thus a decisive role concerning product stability under reaction conditions. A β-ether oligomer with an average degree of polymerization of 10 was also submitted to catalytic oxidation (O_2 2.7 bar) in the presence of the same Cu(phen)$_2$ complex (5 mol%). The yield of vanillic acid and vanillin reached a maximum after 12 h of reaction and then gradually decreased reaching 13% vanillin yield after 24 h (see Table IA. 12 – entry 4). The results of the oxidation of this oligomer seemed to match those obtained in the oxidation of the phenolic model **A4**$_{GG}$.

- *Cu^{+I}Cl/bipyridine-NMI/TEMPO*

PATIL and YAN [106] assayed the oxidation of **A6**$_{HH}$, in the presence of a CuCl/bipyridine/TEMPO catalytic system and using 1-Methylimidazole (NMI) as an additive (ligand) [107] in atmospheric air. The choice of this catalyst was based on the previous results published by BAKER *et coll* on dimeric lignin models [103, 104], as well as on the observations of HOOVER and STAHL [107], who used a similar CuX salt/bipy/TEMPO system in the ambient air oxidation of primary alcohols in other compounds (from aliphatic substrates to others containing different functional groups such as heterocycles as well as unprotected secondary alcohols). Under an atmosphere of air, the results evidenced a low conversion (23%) and a low extent of C^{α}-C^{β} and C^{β}-O bond cleavage in **A6**$_{HH}$ (see Table IA. 11 – entry 1). PATIL and YAN [106] observed that the oxidation of primary alcohols in dimeric models might be sometimes strongly hindered by steric constraints, thus motivating to oxidize the benzylic alcohol into a ketone and then to perform the cleavage of the substrate.

*To sum up, Cu-catalysts were tested for the cleavage of both phenolic and non-phenolic **AN**$_{XY}$. For the direct cleavage, a base was often used as an additive to boost the oxidation of the substrate via the deprotonation of the alcohol (WANG et al). Cu-catalysts are the most adapted for C^{α}-C^{β} cleavage. Cu(OAc)$_2$/phenantroline/KOH showed to be the most suitable for such cleavage for **A1** (yield of **10**H comparable to **V1** in DMSO at 100°C,*

*but with a reaction duration shortened 84 times !!) , phenolic **A4**, non-phenolic **A5** models. However, in the case of non-phenolic models, the presence of the CH_2OH group gave rise to a decrease of the yield of cleavage products. CuOTf/lutidine/TEMPO was the only catalytic system that gave rise to C^{α}-C^{β} cleavage products in **A2** models with a correct yield.*

IA. 3.2.3. Heterogeneous catalytic systems

Although the use of homogeneous catalytic systems constitutes the core of a huge majority of the works in the field of the aerobic cleavage of C-C and C-O bonds in **AN**$_{XY}$-type lignin models, some interesting attempts have been as well made in the presence of different heterogeneous catalysts.

Hence, DENG *et al* [108] assayed the catalytic performance of several metal oxides, *i.e.* Al_2O_3, SiO_2, CeO_2 and MgO, in the oxidation of **A1**$_{HH}$, under 10 bar of dioxygen at 185°C in methanol. The conversions obtained after 24 h time-on-stream were low, between 2.1-9.4%, as well as the yields of the different cleavage products (mainly methyl benzoate, **10-OMe-H** (3%) see Table IA. 7– entry 5). These authors, therefore, prepared several 1.5 wt.% Pd catalysts using different metal oxides as support. The conversions as well as the yields of **A1**$_{HH}$ cleavage products considerably increased, ranging from 10 to 70%. The highest conversion was obtained when using Pd/CeO_2 as a catalyst (see Table IA. 7 – entry 6). In this case, the main reaction products were phenol (**17**H, 48%), acetophenone (**18**H, 38%), methyl benzoate (**10-OMe**-H, 14%), **K1**$_{HH}$ (12%) and benzoic acid (**10**H, 0.03%). Very similar conversion and product yield distribution was obtained upon five consecutive 24-h consecutive runs, pointing to a good recyclability of the catalytic system.

Given the results obtained in their mechanistic studies, DENG *et al.* [108] concluded that the conversion of **A1**$_{HH}$ proceeded through the oxidation of the C^{α}-hydroxyl group to the corresponding carbonyl group, *i.e.* through the conversion of **A1**$_{HH}$ to the ketone **K1**$_{HH}$. This observation seems to be in agreement with the results reported in the presence of the previously discussed Cu containing homogenous catalyst (WANG *et al* [103]). The authors therefore stated that Pd/CeO_2 was able to catalyze the oxidation of C^{α}-OH leading to a significant enhancement in the conversion and yield of cleavage products, since such pre-oxidation would reduce the energy barrier for the cleavage of the β-O-4 bond [109]. In methanol and in the absence of O_2, β-O-4 bond hydrogenolysis (by methanol dehydrogenation) was found to take place to a certain extent, yielding phenol and acetophenone. However, under such conditions, no C^{α}-C^{β} cleavage was observed. Then, in methanol and in the presence of O_2, the proposed reaction mechanism excluded the direct hydrogenolysis of the C^{α}-C^{β} bond and involved the pre-oxidation of C^{α}-OH

to C^{α}=O (**K1**$_{HH}$), followed by the cleavage of the β-O-4 bond leading to the formation of phenol (**17**H), acetophenone (**18**H) and an oxidized intermediate such as 2-hydroxyacetophenone (**32**H) and phenylglyoxal (**21**H). Such reaction intermediate would undergo rapid C^{α}-C^{β} bond cleavage yielding benzoic acid (**10**H), further converted to methyl benzoate

DENG *et al.* [108] also investigated the aerobic cleavage of **A1**$_{HG}$, in order to assess the influence of methoxy functional groups on Ar2 moiety. Under the reaction conditions used for **A1**$_{HH}$ (MeOH 185°C, O_2 10 bar, 24 h), **A1**$_{HG}$ was found to be more reactive (see Table IA. 7 – entry 9). The conversion reached was as high as 90%, whereas the yields of the different cleavage products (**10-OMe-H**: 25% *vs* 14% from **A1**$_{HH}$, **17**G: 68% *vs* **17**H: 48% from **A1**$_{HH}$ cleavage and **18**H: 38% *vs* 38% from **A1**$_{HH}$ cleavage) were higher than those obtained for **A1**$_{HH}$. The electron-donating properties of the CH_3O- group seemed to facilitate the cleavage of the β-O-4 bond.

Homogeneous catalysts, especially Co(salen) have also been grafted onto supports. Hence, ZHOU *et al.* have considered the aerobic oxidation of **A2**$_{HG}$ (air atm, MeCN 80°C, 24 h) in the presence of Co(salen) covalently anchored onto the surface of graphene oxide (GO) [110]. Graphene oxide was found to stabilize the Co-phase on its surface, leading to the conversion of 90% of **A2**$_{HG}$ (Table IA. 9 – entry 1). Various products issued from β-O-4 cleavage were seemingly observed, along with a certain extent of alcohol oxidation at the side chain and deformylation (**K1**$_{HH}$ was formed). Such reaction may proceed *via* the oxidation of **A2**$_{HG}$ to **K2**$_{HG}$. Indeed, the oxidized substrate **K2**$_{HH}$ so as **K6'**$_{GH}$ were tested also and such conditions led to **K1**$_{HH}$ or **K5'**$_{GH}$ and phenol formation. However, the authors did not provide further details on the yields. It has to be noted that graphene oxide itself was used as a heterogeneous catalyst in the oxidation of **A4**$_{GG}$ under O_2 at 5 bar and at 140°C in acetonitrile (see Table IA. 10 – entry 5) [111]. Complete conversion of **A4**$_{GG}$ upon 24 h was observed, leading to an important production of guaiacol (**11**G, 87% yield). The authors compared the activity and selectivity of graphene oxide to other carbonaceous materials, such as commercial graphite, a hydrothermally reduced graphite oxide, and to cokes obtained in the pyrolysis of either borate-doped alginate or in the pyrolysis of chitosan. This last one was highly inefficient in the aerobic oxidation of **A4**$_{GG}$, whereas the others showed intermediate conversions (32 and 44%, for commercial graphite and for the pyrolysis coke from borate-doped alginate, 65% for the reduced graphene oxide). In all cases, the cleavage of the C-O bond was favored compared to C-C cleavage, *i.e.* guaiacol (**17**G) was the major product obtained. The solvent used was found as well to have a significant influence on the selectivity of the aerobic oxidation in the presence of graphene oxide. Among the different solvents assayed, ethyl acetate allowed the

highest yields in guaiacol (**17**G, 94%), vanillic acid (**12**G, 9%) and vanillin (**11**G, 7%). Water, ethanol and toluene were not appropriate media for the aerobic cleavage, resulting mostly in a large extent of mineralization. The experiments performed at different oxygen pressures, *i.e.* 1, 2.5 and 5 bar, pointed to 2.5 bar as the optimal pressure leading to the highest guaiacol yield. It is noteworthy that **A4**$_{GG}$ underwent full conversion in Ar atmosphere, yielding guaiacol as the main product, together with propiophenone (as a consequence of the oxidation of C^{α}-OH to C^{α}=O) and coniferyl aldehyde (**34**G). Considering these results, the authors concluded that the oxygenated groups in graphene oxide might be responsible of the oxidation of **A4**$_{GG}$, with molecular oxygen in the gas phase contributing to its regeneration. They further claimed that the acid sites in graphene oxide would contribute as well to the oxidative cleavage, affecting the selectivity of the process.

MOTTWEILER *et al.* evaluated the activity of transition-metal-containing hydrotalcites in the aerobic cleavage of **A6**$_{GG}$ [112]. At 135°C with a dioxygen pressure of 6 bar, using pyridine as solvent, the Cu-containing catalyst (20 wt.%) led to 77% conversion of **A6**$_{GG}$. In toluene, this material was found to be inactive towards oxidation of the **A6**$_{GG}$. In order to boost the catalytic activity, vanadates were also introduced into the interlayer of hydrotalcite. Indeed, almost complete conversion of **A6**$_{GG}$ was obtained in the presence of the HTc-Cu-V (9 wt% Cu and 29 wt% V) and HTc-Fe-V (4 wt% Fe, 30 wt% V), even in toluene (13 h) and the main reactions were C^{α}-C^{β} cleavage and alcohol oxidation into the corresponding ketone. The reaction in toluene was however rather unselective. Interestingly, the use of pyridine as solvent resulted in almost complete conversion after 17 h, together with the production of important amounts of veratric acid and veratraldehyde (**14**G and **13**G, 31 and 38% yield, respectively, see Table IA. 11 – entries 7a-b). Therefore, the presence of vanadates was found to be quite beneficial in terms of oxidation activity. However, the β-O-4 bond cleavage selectivity was only enhanced with the combination of Cu and V in the HTc catalyst, since a vanadium-containing HTc without Cu was found to be active but not selective towards the cleavage products! The uses of dimethyl carbonate as solvent (instead of pyridine) and air (as oxidant) were also assayed. A HTc-Zn-Cu-V catalyst was recycled two times. The role of Zn consists in lowering the activity of the catalyst to avoid full conversion of **A6**$_{GG}$ substrate. Its activity remained almost the same during the first two runs (89-91% conversion), but slightly decreased during the third one (76% conversion, see Table IA. 11 – entry 7b). Although no important structural changes occurred in the recovered HTc, the authors have identified a non-negligible leaching of V and Cu into the liquid reaction media. In order to assess the importance of the "homogeneous reaction" in the whole catalytic process, $V(acac)_3$ (2.5 mol%) and

$Cu(NO_3)_2 \cdot 3H_2O$ (1 mol%) were employed under equivalent reaction conditions and in the absence of the heterogeneous HTc-Cu-V catalyst. Lower activity and selectivity were obtained for this homogeneous catalytic system. EPR spectroscopy was used, in order to gain more details about the nature of the active V and Cu homogeneous species. Very similar behavior in RPE was observed for both the leached species from the HTc-Cu-V catalyst and the homogeneous catalytic system. MOTTWEILER *et al* thus concluded that the HTc catalyst might be acting as a dispenser of the catalytically active homogeneous species that deactivate over time, possibly due to agglomeration or a resting state of the catalyst.

*To sum up, only a few heterogeneous catalysts were tested. Among them, GO proved to be active for C^{β}-O cleavage (87%), which is comparable to homogeneous catalysts such as **V6** catalyst. However, their activity for oxidative cleavage of C(Ar)-C^{α} and C^{α}-C^{β} is quite low compared to homogeneous catalysts.*

IA. 3.2.4. Intensification strategies: Photochemistry

Process intensification, as a general concept, aims to a substantial increase in process efficiency through the utilization of innovative process equipment, technologies and methods. Among the available strategies, the use of different sources and types of light irradiation has proven to be a feasible way for the acceleration of liquid-phase oxidation reactions. This has been applied as well to the oxidation of lignin and its models, either itself or in combination to different catalytic systems.

A first reference to the use of light irradiation in combination to a heterogeneous catalytic system is the work of MITCHELL and MOODY [113]. They studied the aerobic oxidation of **A5**$_{HG}$ (Table IA. 8, entry 7) and **A6**$_{GG}$ (racemic, Table IA. 11, entry 6) under visible light (400 W HQI-T metal halide lamp) and in the presence of a Cu/AlO(OH)-hydroquinone catalytic system. Cu/AlO(OH) was prepared as described in the work of PARK *et al.* [114]. No further details, other than their XPS characterization, were provided. The reaction was performed at ambient conditions, under dioxygen atmosphere, and in trifluorotoluene/acetone. C^{α}-C^{β} and C^{β}-O cleavage such as guaiacol (**17**G, 12% from **A5**$_{HG}$ and 7% from **A6**$_{GG}$), *p*-anisaldehyde (**13**H, 22% from **A5**$_{HG}$) and veratraldehyde (**13**G, 7% from **A6**$_{GG}$) were obtained. No results were however provided about the non-intensified catalytic reaction.

Recently, GAZI *et al* [115] have considered the photo-oxidation of an **A6**$_{GG}$-like lignin model, in the presence of different vanadium complexes (noted **V7a**, **V7b** and **V7c**, see Table IA. 13). Acetonitrile was used as solvent and the reaction was performed at room temperature

under dioxygen atmosphere and a 48 W light emitting diode (LED) was used as the light source. The highest conversion under such reaction conditions was obtained in the presence of **V7b** (76% upon 24 h, see Table IA. 11 – entry 12). The reaction yielded important amounts of C^{α}-C^{β} products, such as 4-ethoxy-3-methoyxybenzaldehyde (**13'**G, 68%) and 2-methoxyphenylformiate (**16**G, 51). The formation of C^{β}-O cleavage products was also observed, *i.e.* guaiacol (**17**G, 14%) and formic acid (16%). GAZI *et al.* moreover performed both kinetics and DFT analyses revealing that the incorporation of electron-withdrawing groups at selected sites of the ligand in the V-complexes was essential. In a previous work, GAZI *et al* reported on the selective photocatalytic C-C bond cleavage in **A6'**$_{GG}$ (Atm. O_2, r. T.) in the presence of similar V-complexes but using concentrated sunlight (300 W solar simulator, visible light filter > 420 nm) [116]. In the presence of **V7b** without light irradiation, no conversion at all was obtained at ambient temperature, whereas no cleavage and only the oxidation of the **A6**$_{GG}$-like model was observed at 80°C. Under photocatalytic conditions, more than 40% of the dimeric model was selectively converted to the C^{α}-C^{β} cleavage products *p*-ethoxybenzaldehyde **13'**G (68%) and guaiacyl formate **16**G (51%), proving therefore the acceleration of this process as a consequence of visible light irradiation. However, the cleavage activity of other V-complexes did not seem to be enhanced through light irradiation, which pointed out to an important influence of the ligand structure. Supported by the results of their DFT calculations, GAZI *et al.* stated that the V-catalysts bearing an appropriate conjugated hydrazine-imidate ligand could indeed absorb visible light and activate the sp^3 C-C bonds via a ligand-to-metal charge transfer mechanism. Moreover, when assessing the influence of phenolic groups in the lignin models, they found that their presence impeded the C^{α}-C^{β} bond cleavage, and thus suggested that, in the case of processing natural lignin, that these phenolic groups should be passivated prior to its oxidative depolymerization. Indeed, GAZI *et al.* further observed that under certain conditions, phenolic cleavage products, such as guaiacol, would slowly but irreversibly deactivate some of the V-complexes assayed [116].

LIM *et al.* [117] and CHO *et al.* [118] studied the SET-promoted photochemical oxidation of **A6**$_{HG}$, **A6**$_{GG}$ and **A6**$_{GS}$ models, using 9,10-dicyanoantracene (DCA) as the excited state electron acceptor (Table IA. 11, entries 4, 8-10). DCA was expected to absorb light irradiation at longer wavelengths (> 350 nm) than the lignin models itself (*c.a.* 280 nm). Therefore DCA-containing 5% aqueous MeCN solutions were irradiated using a visible light source (λ > 330 nm), leading to the formation of several cleavage products, such as *p*-hydroxybenzaldehyde (**13**H, 26%) veratrylaldehyde (**13**G, 45%), eudesmic aldehyde (**13**S, 10%) and guaiacol (**17**G, ≤ 3%), along with their corresponding dimeric ketones (≤ 3%), even

under ambient pressure and temperature conditions (Table IA. 11 – entries 4, 8-10). The aerobic oxidation was quite selective towards C^{α}-C^{β} cleavage, but this strongly depended on the type of substrate employed. Indeed, such conditions gave rise to a yield of **13**G of 45% from *erythro* **A6**$_{GG}$ and only 5% from *threo* **A6**$_{GG}$.

Other works report as well on the photochemical intensification of A-type lignin models in the presence of $^1O_2$ sensitizers, such as Rose Bengal. As an example, MCNALLY *et al* studied the kinetics of the photodegradation of **A4**$_{GH}$, **A4**$_{GG}$ and **A4**$_{GS}$ dimers in the presence of such reagent [119]. The presence of methoxy groups in the phenolic ring accelerated the photosensitized lignin model degradation. These authors proposed that ketones might behave themselves as photosensitizers in the degradation of lignin dimeric models under such conditions. Contrary to these observations, D'AURIA and FERRI [120] reported higher reactivity of guaiacyl units compared to syringyl units when assessing the photosensitized photodegradation of **A4**$_{GG}$ and **A4**$_{GS}$ models under similar reaction conditions. They demonstrated it by the superposition of DFT *ab initio* studies and experimental tests.

IA. 3.2.5. Impact of the secondary alcohol oxidation to ketone on the reactivity of lignin dimeric model

Before shifting to **KN**$_{XY}$ substrates, a digression about the noteworthy reactivity of phenolic models may be relevant. **AN**$_{XY}$ compounds have at least 3 possible sites for oxidation (see Fig. IA. 13). The site ② corresponds to the Markó oxidation which was observed for several vanadium-based catalysts. The site ① (aromatic ring oxidation especially in the case of phenolic models **A3**$_{XY}$ and **A4**$_{XY}$) is the active site for catalysts such as $PMoV_x$. The site ③ corresponds to the primary alcohol oxidation. Such a reaction has been observed in this review through the dehydromethylation product formation in presence of Co(salen)-GO.

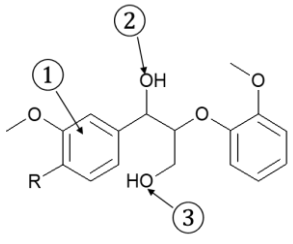

Figure IA. 13: Active sites of the etherified phenolic model for aerobic oxidation

According to the DFT calculations by PARTHASARATHI *et al* [121], the etherification of phenolic moieties should weaken the C-C and C-O bonds in **A3** and **A4** models. Experimentally, phenolic substrates were shown to be generally more reactive than the non-

phenolic ones, which seems to be antagonist to the DFT calculations as C-C and C-O bonds should be weaker in **A5**$_{XY}$ and **A6**$_{XY}$ models than in **A3**$_{XY}$ and **A4**$_{XY}$ models. Yet, for the phenolic models, a potential active site is unlocked and catalysts such as PMoVx or homogeneous Co(salen) may abstract a H radical to the phenolic moiety, thus producing a phenoxy radical ($ArO^{\cdot}$), which is quite stable. Consequently, the radical intermediate formation is easier that boosts the oxidation and oxidative cleavage of C-C and C-O bonds.

The cleavage of **AN**$_{XY}$ substrates may be direct or made in two steps. In the latter case, the first one is an alcohol oxidation (site ②) giving rise to **KN**$_{XY}$. Some DFT calculations were carried out by PARTHASARATHI *et al* [121] and by BECKHAM *et al* [109] showing that the secondary alcohol oxidation on the side chain weakens the C-O bond in β position, which is in good agreement with the observations of McNALLY, MOODY and McNEILL [119] and MOODY and by WANG *et al* [102]. The enthalpy of the ether bond in the case of the phenolic models (Table IA. 13) decreases at each alcohol oxidation (for instance, enthalpy of C-O bond in **A4**$_{HH}$ = 69.5 kcal/mol, in **K4**$_{HH}$ = 60.6 kcal/mol, in **B4**$_{HH}$ = 59.1 kcal/mol, in **L4**$_{HH}$ = 55.6 kcal/mol, structures: see Fig. IA. 14). Such drop of the enthalpy of the C-O is also observed for etherified phenolic groups. So, progressive oxidation of alcohols has a critical impact on the oxidative cleavage (easier with **KN**$_{XY}$ than **AN**$_{XY}$).

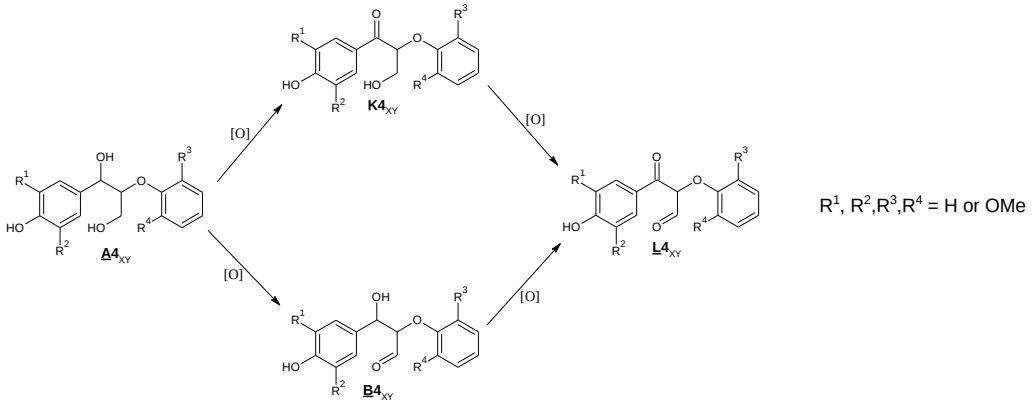

Figure IA. 14: General structure of the studied models

*As a partial conclusion, plenty of catalysts were tested on **AN**$_{XY}$ models operating with atmospheric dioxygen or even atmospheric air (case of vanadium-based ones). Heterogeneous catalysts are much less represented than homogeneous ones. A drawback is the leaks observed with some heterogeneous vanadium-based catalysts.*

IA. 3.3. Aerobic oxidation of KN$_{XY}$ models

The first difference with **AN**$_{XY}$ models is that phenolic compounds are barely represented (only one occurrence). The simplest, as well as the most complex models are well represented in the literature. At first glance to the tables IA. 15-17, it can be observed that copper-based catalysts are the most used (about 92% of the tests). The studies involving these catalysts can give an overview of the different oxidation strategies.

For instance, WANG *et coll* investigated three methods for **KN**$_{XY}$ cleavage. In a first strategy, after a preliminary selective oxidation of the benzylic alcohol in **AN**$_{XY}$ catalyzed by $VOSO_4$-TEMPO (O_2 4 bar) [122], the authors performed the oxidative cleavage of **KN**$_{XY}$ by O_2 (4 bar) in the presence of $Cu(OAc)_2$/phenantroline without any additive in methanol at 80-150°C during 3 h to get carboxylic acids and phenols. The second step procedure was tested on **K1** substrates (Table IA. 15, entries 2, 7, 11), **K3**$_{HH}$ (Table IA. 16, entry 3), **K5** substrates (Table IA. 16, entries 5, 7, 11 and Table IA. 17, entries 2, 6) and **K6**$_{GG}$ (Table IA. 17, entry 9). Benzoic acids (**10**H, **10**G and **10**S from **K1**$_{XY}$, **12**H from **K3**$_{HH}$ and **14**H, **14**G and **14**S from **K5**$_{XY}$ and **K6**$_{GG}$) were obtained with a maximum yield of 99% from **K1** substrates (Table IA. 15, entry 11), 95% from **K5** substrates (Table IA. 16, entry 11) and 92% from **K6**$_{GG}$ (Table 17, entry 9). However, the yield of *p*-hydroxybenzoic acid (**12**H) from **K3**$_{HH}$

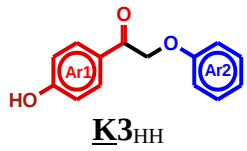

K3$_{HH}$

*Table IA. 15: Oxidation o f **K1** substrates*

Entry	Substrate	Conc. (M)	Catalyst	Solvent	Oxidant P (bar)	T (°C)	t (h)	Conv. (%)	Product yield (%)		Ref
									C^{α}-C^{β} cleavage	C^{β}-O cleavage	
1a[c]	**K**1$_{HH}$	0.5	Cu-pyr (15 mol%)	MeOH	air atm.	65	24	99.9	**10-OMe**-H : 33	**17**H : 91 **24-acMe**-H : 57	125
1b[c]				EtOH					**10-OEt**-H : 18	**17**H : 89 **24-acEt**-H : 52	
2		0.1	$Cu(OAc)_2$-phen (20 mol%)	MeOH	O_2 4	80	3	94	**10**H : 95	**17**H : 85	122
3		0.5	$Cu(NO_3)_2$ (20 mol%)	MeCN	O_2 6	120	10	100	**10**H : > 99	**17**H : 43	124
4a[b]		0.1	$Cu(OAc)_2$ (20 mol%)	MeOH	O_2 4	100	3	99	**10-OMe**-H : 96	**17**H : 95	123
4b[b]				EtOH		100	6	n. i.	**10-OEt**-H : 86	**17**H : 87	
5		1 mmol/g of IL	[BnMIm][NTf_2] + 2.7 wt% H_3PO_4 + 4.6 wt% H_2O		O_2 10	130	3	100	**10**H : 89	-	127
6			[OMIm][OAc] + 2.5 wt% H_2O		O_2 15	100	2	> 99	**10**H : 86	-	128
7	**K**1$_{HG}$	0.1	$Cu(OAc)_2$-phen (20 mol%)	MeOH	O_2 4	80	3	95	**10**H : 95	**17**G : 27	122
8		0.5	$Cu(NO_3)_2$ (20 mol%)	MeCN	O_2 6	120	10	100	**10**H : > 99	**17**G : 18	124
9[b]		0.1	$Cu(OAc)_2$ (20 mol%)	MeOH	O_2 4	100	3	> 99	**10-OMe**-H : 84	**17**G : 46	123
10		1 mmol/g of IL	[OMIm][OAc] (1 g) + 25 wt% H_2O		O_2 15	100	2	> 99	**10**H : 85	-	128
11	**K**1$_{HS}$	0.1	$Cu(OAc)_2$-phen (20 mol%)	MeOH	O_2 4	90	3	96	**10**H : 99	**17**S : 3	122
12[c]	**K**1$_{GH}$	0.5	Cu-pyr (15 mol%)	MeOH	air atm.	65	24	99.9	**10-OMe**-G : 15	**17**H : 62 **24-acMe**-G : 39	125
13[a]		0.25	CuI (10 mol%)	toluene	O_2 atm.	70	6	n. i.	**10-Npip**-G : 17	**17**H : 72 **24-Npip**-G : 68	126

[a]With 5 equivalents of piperidine, [b]With 2 equivalents of BF_3-Et_2O, [c]With 1 equivalent of BF_3-Et_2O

*Table IA. 16: Oxidation of **K2** and **K3**, **K5**$_{HG}$ and **K5**$_{GH}$ substrates*

Entry	Substrate	Conc. (M)	Catalyst	Solvent	Oxidant P (bar)	T (°C)	t (h)	Conv. (%)	Product yield (%)		others	Ref
									C^{α}-C^{β} cleavage	C^{β}-O cleavage		
1[a]	**K**2$_{HH}$	0.25	CuI (10 mol%)	toluene	O_2 atm.	70	6	n. i.	**10-OMe**-H : 18	**17**H : 65 **24-Npip**-H : 81	-	126
2	**K**2$_{SG}$	0.1	(dipic)V(O)(O^iPr) 10 mol%	DMSO-d^6	air atm.	100	48	40	**10**S : 19	**17**G : n. q.	**E'**1$_{SG}$: 14 ; HCOOH : 7	86
3	**K**3$_{HH}$	0.1	$Cu(OAc)_2$-phen (20 mol%)	MeOH	O_2 4	80	3	99	**12**H : 68	**17**H : 81		122
4a[b]	**K**5$_{HH}$	0.1	$Cu(OAc)_2$ (20 mol%)	MeOH	O_2 4	100	6	> 99	**14-OMe**-H : 94	**17**H : 99	-	123
4b[b]				EtOH		100	6	n. i.	**14-OEt**-H : 82	**17**H : 77	-	
5			$Cu(OAc)_2$-phen (20 mol%)	MeOH		90	3	99	**14**H : 94	**17**H : 90	-	122
6[b]	**K**5$_{HG}$	0.1	$Cu(OAc)_2$ (20 mol%)	MeOH	O_2 4	100	3	99	**14-OMe**-H : 93	**17**G : 73	-	123
7			$Cu(OAc)_2$-phen (20 mol%)			80	3	98	**14**H : 85	**17**G : 10	-	122
8		0.5	$Cu(NO_3)_2$ (20 mol%)	MeCN	O_2 6	120	10	100	**14H** : >99	**17**G : 69	-	124
9[a]		0.25	CuI (10 mol%)	Toluene	O_2 atm.	70	6	n. i.	**10-Npip**-H : 21	**26-Npip**-H : 71 ; **17**G : 52	-	126
10a[b]	**K**5$_{GH}$	0.1	$Cu(OAc)_2$ (20 mol%)	MeOH	O_2 4	100	3	>99	**14-OMe**-G : 98	**17**H : 75	-	123
10b[b]				EtOH		150	3	n. g.	**14-OEt**-G 91	**17**H : 66	-	
11			$Cu(OAc)_2$-phen (20 mol%)	MeOH		90	3	98	**14**G : 95	**17**H : 80	-	122

[a]With 5 equivalents of piperidine, [b]With 2 equivalents of BF_3-Et_2O

Table IA. 17: Oxidation of ***K5****$_{GY}$ substrates and* ***K6*** *substrates*

Entry	Substrate	Conc. (M)	Catalyst	Solvent	Oxidant P (bar)	T (°C)	t (h)	Conv. (%)	Product yield (%)			Ref
									C^{α}-C^{β} cleavage	C^{β}-O cleavage	others	
1[b]	**K**5$_{GG}$	0.1	$Cu(OAc)_2$ (20 mol%)	MeOH	O_2 4	100	3	>99	**14-OMe**-G : 96	**17**G : 72	-	123
2			$Cu(OAc)_2$-phen (20 mol%)			100	3	98	**14**G : 85	**17**G : 0	-	122
3		0.5	$Cu(NO_3)_2$ (20 mol%)	MeCN	O_2 6	120	10	100	**14**G : >99	**17**G : 80	-	124
4		0.25	CuI (10 mol%)	Toluene	O_2 atm.	70	6	n. g.	**10-Npip**-G : 27	**17**G : 51 **26-Npip**-G : 58	-	126
5[b]	**K**5$_{GS}$	0.1	$Cu(OAc)_2$ (20 mol%)	MeOH	O_2 4	100	6	>99	**14-OMe**-G : 82	**17**S : 0	-	123
6			$Cu(OAc)_2$-phen (20 mol%)				3	96	**14**G : 93	**17**S : 21	-	122
7		0.5	$Cu(NO_3)_2$ (20 mol%)	MeCN	O_2 6	120	10	100	**14**G : >99	**17**S : <5	-	124
8a[b]	**K**6$_{GG}$	0.1	$Cu(OAc)_2$ (20 mol%)	MeOH	O_2 4	150	6	82	**14-OMe**-G : 82	**17**G : n. q.	-	123
8b[b]				EtOH			6	>99	**14-OEt**-G : 76	**17**G : n. q.	-	
9			$Cu(OAc)_2$-phen (20 mol%)	MeOH			3	>99	**14**G : 92	**17**G : n. q.	-	122
10		0.5	$Cu(NO_3)_2$ (20 mol%)	MeCN	O_2 6	120	10	>99	**14**G : 20	**17**G : <5	-	124
11[a]		0.25	CuI (10 mol%)	Toluene	O_2 atm.	70	6	n. g.	**10-Npip**-G : 24	**17**G : 56 **26-Npip**-G : 58	-	126
12[a, c]			CuBr-phen (10 mol%)	Toluene	O_2 atm.	70	6	n. g.	**14-Npip**-G : 28	**17**G : 41 **26-Npip**-G : 48	-	
13[a, d]	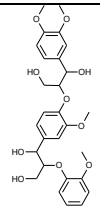		CuBr-phen 10 mol%	Toluene	O_2 atm.	90 then 70	1.5 then 6	n. g.	**14-Npip**-G : 19	**17**G : 0 **26**G-Npip : 40	-	126

[a]With 5 equivalents of piperidine, [b]With 2 equivalents of BF_3-Et_2O, [c]Synthesized *in situ* through oxidation by DEAD (1.1 eq) catalyzed by K_2CO_3 2.2 eq (90°C, 1.5 h),
[d]Synthesized *in situ* through oxidation by DEAD (2.2 eq) catalyzed by K_2CO_3 4.4 eq (90°C, 1.5h)

cleavage was 68% only (Table IA. 16, entrée 3). The yield of phenols from C^{β}-O cleavage decreased with the content of methoxy groups (**17**H: 81-90%, **17**G: 0-21%, **17**S: 3-21%). An interpretation that can be made is that the phenolic moieties were oxidized in such conditions, leading to a lower yield of **12**H and of the phenols.

In a second strategy, the authors used BF_3-Et_2O to weaken the C^{α}-C^{β} bond and $Cu(OAc)_2$ in methanol (100-150°C, O_2 4 bar, 3 h) to synthesize methyl esters of benzoic acid derivatives [123]. This method was tested on **K1** substrates (Table IA. 14, entries 4a-b and 9), **K5** substrates (Table IA. 15, entries 4a-b, 6, 10a-b and Table IA. 16, entries 1, 5) and **K6**$_{GG}$ (Table IA. 16, entries 8a-b). Benzoate methyl esters (**10-OMe** from **K1**$_{XY}$ substrate cleavage) and *p*-methoxybenzoate methyl esters (from **K5**$_{XY}$ and **K6**$_{XY}$ oxidation) were obtained with a maximum yield of 96% (Table IA. 15, entry 4a) and 98% respectively (Table IA. 15, entry 10a). The presence of the CH_2OH group was shown to have a negative influence on the conversion of the substrate (**14-OMe**-G, yield 82%, see Table IA. 16, entry 8a). This method was assayed also in ethanol instead of methanol (Table IA. 15, entry 4b, Table IA. 15, entries 4b and 10b and Table IA. 16, entry 8b). Generally, the yields of ethyl esters were lower compared to those of methyl esters.

In a third strategy, oxidation of **KN**$_{XY}$ by O_2 (6 bar) in the presence of $Cu(NO_3)_2$ in acetonitrile at 120°C during 10 h [124] was performed. This method was tested on **K1** substrates (Table IA. 15, entries 3 and 8), **K5** substrates (Table IA. 16, entry 8 and Table IA. 17, entries 3 and 7) and **K6**$_{GG}$ (Table IA. 17, entry 10). Benzoic acids and *p*-methoxybenzoic acids were obtained with a yield higher than 99%, whatever the nature of the Ar2 moiety (see Table IA. 4). However, the presence of CH_2OH was detrimental for the selectivity of the oxidation into *p*-methoxybenzoic acid derivative (conversion > 99% and **14**G yield: 20% only). Also, there was a default of phenol (maximum yield of **17**H, **17**G and **17**S : 43%, 80% and <5% respectively, see Table IA. 15, entry 3, Table IA. 17, entry 3 and Table IA. 17, entry 7) since these compounds are not very stable to such operative conditions (O_2 6 bar, 120°C !).

Those methods differ from the copper salt, the presence or not of the BF_3-Et_2O additive and the solvent. An alcoholic solvent (methanol, ethanol…) enables the shifting of the balance of the cleavage. The key intermediate is the hydroperoxide from the addition of dioxygen on the position C^{β}. All of the three catalysts were selective for C^{α}-C^{β} and C^{β}-O cleavage. The yield of benzoic acid derivatives, except for **K6**$_{GG}$ was higher than 66%. The yield of phenol

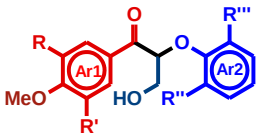

K6$_{GG}$

derivatives depends mainly on the number of methoxy radicals. The higher is this number, the least the phenol derivative is yielded. This is certainly due to the oxidation of the product favored by the electro-donating effect of the methoxy radicals. Among these three methods, the oxidation without additive and in acetonitrile (third strategy) gave the highest yield of benzoic acid derivatives, except for the oxidation of **K6**$_{GG}$. However, this method is obviously not the most adapted if phenols are also targeted as the best yield of phenol derivatives is up to 80% and syringol (**17**S) is not stable for stringent operative conditions.

The effect of BF_3-Et_2O in refluxing alcohols was also investigated by LIU *et al* on the oxidation of **K1**$_{HH}$ and **K1**$_{GH}$ (Table IA. 15, entries 1a-b and 12) [125] in atmospheric air in presence of $CuCl_2$/pyridine/BF_3-Et_2O (15 mol% of Cu and 1 equivalent of BF_3) in methanol and in ethanol. The conditions are therefore milder compared to the tests carried out by WANG *et coll*. The conversion was also close to 100% and a good activity for C^{β}-O cleavage was observed since the yield of phenol (**17**H) as weel as of the methyl acetal of phenylglyoxal (**24-acMe**-H) were 91 and 57% respectively. However, the activity for C^{α}-C^{β} seemed to be lower as the yield of methyl benzoate was 33% only. The presence of the methoxy group on the Ar1 moiety (see Table IA. 4) so as the substitution of methanol by ethanol did not give rise to higher yields of methyl *m*-methoxybenzoate and ethyl benzoate. Such conditions enabled the formation of α-oxoacetals (**24-acMe**-H, **24-acEt**-H, **24-acMe**-G) issued from C^{β}-O cleavage thanks to softer conditions.

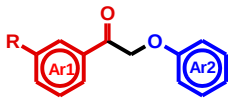

K1$_{HH}$ (R^1 = H)
K1$_{GH}$ (R^1 = OMe)

ZHANG *et al* performed oxidative cleavage-amidification by the system CuI/piperidine of several non-phenolic ketone models (**K1**$_{GH}$ (Table IA. 15, entry 12), **K5**$_{HG}$ (Table IA. 16, entry 9), **K5**$_{GG}$ (Table IA. 17, entry 4) and **K6**$_{GG}$ (Table IA. 17, entry 11) in mild conditions (atmospheric oxygen, 70°C) [126]. The amine on the same way as methanol enables the equilibrium shifting. The main products were α-keto amides (48-71%) and phenols (51-72%) from C^{β}-O cleavage and amides issued from C^{α}-C^{β} cleavage (17-24%). For instance, the amides, N-(3-methoxybenzoyl)piperidine (**10-Npip**-G) and 1-(3-methoxyphenyl)-2-(1-piperidinyl)-1,2-ethanedione (**25-Npip**-G) were obtained from **K1**$_{GH}$ with a yield of 17 and 68% and phenol (**17**H) was also obtained (72%, see Table IA. 15, entry 13). Similarly, these conditions were assayed for the cleavage of **K6**$_{GG}$ (Table IA. 17, entry 11), a more complex substrate and the products were 1-(3,4-dimethoxyphenyl)-2-(1-piperidinyl)-1,2-ethanedione (**27-Npip**-G, 58%) and guaiacol (**17**G, 56%) from C^{β}-O cleavage and N-(3,4-

dimethoxybenzoyl)piperidine (**14-Npip**-G, 24%) from C^{α}-C^{β} cleavage. So, the catalyst was more selective for C^{β}-O cleavage than C^{α}-C^{β} cleavage. Compared to Cu-pyr-BF_3, the yield of C^{β}-O cleavage products was higher because atmospheric molecular oxygen was used instead of atmospheric air. What if these substrates are produced *in situ* by the secondary alcohol oxidation? In other terms, is a one-pot conversion of a **AN**$_{XY}$ into amides possible? This is attractive as the structure of **AN**$_{XY}$ is closer to lignin. The most performant system for this reaction was DEAD (DiEthyl AzoDicarboxylate) + K_2CO_3. The catalyst was not CuI but CuBr-phen and 2 equivalents of DEAD were used to boost alcohol oxidation. The yields of α-keto amide noted **26-Npip**-G and of guaiacol (**17**G) were 48% and 41%, respectively and the benzamide derivative was obtained with a yield of 28% (Table IA. 17, entry 12). So, the selectivity to C^{β}-O cleavage was lower compared to Cu^{I}/phenantroline-catalyzed **K6**$_{GG}$ cleavage. Also, a trimer was assessed (Table IA. 17, entry 13). Excepted for guaiacol, the yield of the main products did not decrease significantly. These promising results proved that this catalyst might be also active on lignin. In the cases of low oxygen pressure, namely one atmosphere or lower, the catalyst tended to be more selective for C^{β}-O cleavage. For a higher oxygen pressure (4 bars or more), C^{α}-C^{β} products were favored. The C^{β}-O bond is the weak point both in models and lignin, so this is cleaved more easily than the C^{α}-C^{β} bond. At higher pressure, there is enough energy to cleave the C^{α}-C^{β} bond. But, in such range of pressure, phenols undergo further oxidation to quinones.

Among the homogeneous catalysts, only one non copper-based catalyst was tested (on **K2**$_{SG}$) [86], *i.e.* **V1** (dipicV(O)(O^{i}Pr), 10 mol%), the results are already presented along with **A2**$_{SG}$ oxidation. In brief, the ketone conversion was lower than the alcohol conversion.

An ionic liquid promoter, [BnMIm][NTf_2] was assessed by YANG *et al* for **K1**$_{HH}$ oxidation by O_2 10 bar [127]. Phosphoric acid and water were the co-reactants for the radical oxidation of the substrate (Table IA. 15, entry 5). Using 1 mmol of substrate /g of [BnMIm][NTf_2], in presence of water and phosphoric acid, 100% of conversion was achieved and the yields of benzoic acid and phenol were 89% and 84%, respectively. The ionic liquid promoted the formation and transfer of the superoxide radical $HOO^{\cdot}$. The role of the acid was to exacerbate the electrophilic power of the ketone, which accelerates the transposition of the radical $HOO^{\cdot}$. More recently, the same group tested the [OMIm][OAc] ionic liquid for the cleavage of **K1**$_{HH}$ and **K1**$_{HG}$ (Table 15, entries 6 and 10) [128]. The oxygen pressure was higher (15 bar) and the temperature was 100°C instead of 130°C. The conversion of the substrates was

almost complete (> 99%) and the yield of benzoic acid was 85 (from **K1**$_{HH}$) or 89% (from **K1**$_{HG}$).

Some ketones were photo-oxidized in presence of Rose Bengal in acetonitrile-ethanol 1:1 [121]. For instance, the oxidation of **K6'**$_{GG}$ gave 70-80% of the C^{β}-O cleavage product. The aim in this paper was to show the higher sensitivity of the guaiacyl units in lignin. **K6'**$_{GS}$ was oxidized in a lesser extent. These results confirmed this hypothesis. But, in the case of the phenolic substrates.

Examples of heterogeneous catalysts for the oxidation of ketones lignin models are also scarce. The lone catalysts are supported Co(salen)-GO [111] (results detailed in IA. 3.2.3).

IA. 3.4. Partial conclusion about lignin model aerobic cleavage

At the end of the study of catalytic aerobic oxidation of **KN**$_{XY}$ catalyzed by homogeneous catalysts, a striking observation is no C(Ar)-C^{α} cleavage was observed even for phenolic substrates. This might be linked to the scarce studies of oxidation of phenolic K3 and K4 models or tend to confirm that the C(Ar)-C^{α} cleavage is unlocked by the presence of phenolic moieties. Another interpretation is Cu-catalysts are mainly active for C^{α}-C^{β} cleavage as observed for **AN**$_{XY}$ aerobic cleavage. Yet, the catalyst $Cu(NO_3)_2$ (O_2 6 bar) gave rise to best conversion of **K1**$_{XY}$ and **K5**$_{XY}$ substrates whereas for **K6**$_{XY}$, $Cu(OAc)_2$-phenantroline (O_2 4 bar) showed to be more suitable.

For the oxidation of lignin model, plenty of different catalysts and different operative conditions were assessed. Some efforts for more sustainable oxidation are made as replacing methanol by ethanol or operating in milder conditions (atmospheric oxygen or air and at a moderate temperature). However, such process requires long reaction time (until 7 days!).
However, even excellent conversion and selectivity may be observed, the transposition to "real" lignin oxidation might be problematic as a lot of complex factors are not involved in lignin model oxidation as the polymeric and heterogeneous nature of lignin and the diversity of the bonds. Indeed, lignins containing only the β-O-4 are extremely seldom. Some β-β and β-5 bonds are present and this cleavage will probably require catalyst upgrading.

Some of the listed catalysts were also tested on lignin as Co(salen)-GO or $PMoV_5$ (for delignification).

IA. 4. Aerobic oxidation of lignin

As mentioned before, technical lignin (lignosulfonates, kraft and Oganosolv mainly) is provided by three main extraction processes that have an impact on its molecular composition. However, oxidative catalytic systems used with dimeric models have proven to be very sensitive to the structure of the molecules. The purpose of this part is to identify to which extent the performances of the catalysts may be modified with the lignin considered.

IA. 4.1. From delignification to lignin valorization

Kraft lignin and lignosulfonates are present in the residue of kraft and sulfite processes. For now, less than 2% are chemically valorized. The oldest example (mid-1930s in North America) is the industrial scale vanillin manufacturing from lignosulfonate in alkaline media at high pressure (100 bar of air) [129, 130]. Nowadays, 15% of vanillin in the world is produced from lignosulfonate or Kraft lignin but such vanillin is 10-30 times more expensive than vanillin from the guaiacol route. Drawbacks of Kraft lignin and lignosulfonates are related to their sulphur and sugars impurities. The third type of technical lignin, the Organosolv one, seems to be more adapted to chemical valorization but its price is an obstacle. Despite the above considerations, studies on the aerobic oxidative cleavage of lignin have been carried starting from the three sources as it will be shown below.

Let remember first that lignin depolymerization may occur during the oxidative delignification treatment aiming at recovering pure cellulose. KEGGIN polyoxometalates (POMs) were reported to be promising catalysts for such operation that was supposed to transform the lignin polymer into CO_2 and low molecular weight compounds [131]. On the contrary, nowadays, sustainability concerns push for delignification processes providing cellulose and lignin-derivated fine chemicals as exemplified by the works of CHENG *et al.* [132] on the Southern yellow pine wood and of DE GREGORIO *et al* [133] on pretrated pine or willow wood using ionic liquids. In both cases, atmospheric O_2 was coupled with $PMoV_2$ ($H_5PMo_{10}V_2O_{40}$). With CHENG *et al.*, the lignin content was reduced by 97% in the presence of 0.5 wt% of $[C_2mim][PMoV_2]$ in 10 g of the ionic liquid, but with a loss of matter of 41%. The main product from lignin degradation was methyl vanillate with some amounts of acetovanillone (**19**G) and vanillic acid (**12**G) from C^{α}-C^{β} as shown by the authors. With DE GREGORIO *et al,* the work was focused on maximizing the lignin aerobic oxidation products.

For a pretreatment of 4 h and a catalytic charge of 5 wt% respect to lignin, the main products were phenol (0.36%), syringaldehyde (0.22%), syringol (0.22%), guaiacol (0.08%) and vanillin (0.07%). In this case, aromatic products derivated from the syringyl units were detected, on the contrary of the works of CHENG *et al.* Indeed, willow is a hardwood species whose lignin is rich in syringyl units whereas that of pine, a softwood species, is constituted of guaiacyl units. Moreover, DE GREGORIO, WELTON *et al* showed that molecular oxygen seems to be more efficient than hydrogen peroxide to get aromatic aldehydes and acids under their working conditions.

AARABI *et al.* [133] studied the synthesis of vanillin from sugar beet pulp in NaOH 2 M under 4.3 bars O_2 at 156°C and showed that, after 0.5 h, the yield of vanillin was 1.4 wt%. According to these authors, the addition of $CuSO_4$ as a potential catalyst was useless due to its tendency to favor the over-oxidation of vanillin to vanillic acid. It has to be noticed too that sugar beet pulp does not contain so much lignin. Recently, TARABANKO [134] *et al* tested CuO in alkaline media for the processing of pine wood into vanillin and glucose. The yield of vanillin was 19 %, which is much higher than in the tests in presence of $PMoV_x$.

IA. 4.2. Chemicals from lignosulfonates

Lignosulfonates which are the residue of the sulfite pulping (see IA.2) are the cheapest lignins. We will compare the different catalysts with a focus on the yield of phenolic platform molecules.

- *Copper catalysts*

The copper-based catalysts were said to be the most efficient for aerobic lignin oxidative cleavage in alkaline media. TARABANKO *et al.* [134, 135] assessed $Cu(OH)_2$ (5.4 wt.%) in 3 M NaOH for the oxidation of fir wood lignosulfonate by O_2 at 2 bar / 160°C (Table IA. 18 entry 1). The yield of vanillin (**11**G) reached 7.7 wt% after 0.67 h with respect to lignin. Similarly, SANTOS *et al* assessed $CuSO_4$ (20 wt.%) as a catalyst in alkaline media for the oxidation of eucalyptus lignosulfonate [136]. The pressure of O_2 was higher than before (6 bar), but the alkalinity was lower. Aromatic aldehydes (vanillin, **11**G and syringaldehyde, **11**S) were obtained with a higher yield (Table IA. 18 entries 2a-b). Moreover, it seemed that the concentration of the liquor (thin liquor *vs* thick liquor, see entry 2a) had not a significant influence on the yield of the aromatic aldehydes (**11**G + **11**S: 12 wt% from thin liquor *vs* 10%

from thick liquor) whereas a raise of the pH and dioxygen pressure enabled to get more aromatic aldehydes (**11**G 4.5 wt% and **11**S 16 wt%, see entry 2b).

LUGOVITSKAYA *et al* tested another system involving Cu^{2+}-Fe^{3+}-H_2SO_4-O_2 in acidic medium [137] for the oxidation of a lignosulfonate at varying temperatures and pressures of O_2 (Table IA. 18, entry 4a). Under mild conditions, the catalytic system showed a low efficiency for lignin aerobic cleavage. Hence, the hydroxyl groups of the lignin linkages were oxidized to carbonyls as expected from the work of DENG *et al* [108] on **AN**$_{XY}$ models. In more severe conditions (O_2 8 bar, 150°C, 3 h, Table IA. 18, entry 4b), the aromatic groups were destroyed into low molecular weight compounds. PACEK *et al* [138] assessed also the combination of $CuSO_4$ and NaOH (3 M) both in a dead-end reactor and a flow-through system (see Table IA. 18, entries 3a-d). The total O_2/N_2 pressure was kept at 11.5 bar.

- In the dead-end reactor, oxidation was followed by hydrolysis. Even without dioxygen, some vanillin and vanillic acid were produced by hydrolysis above 100°C (*e.g.* at 160°C with 1.3 bar of O_2, the vanillin was present at 3.7 wt% before O_2 admission). In the presence of O_2, the yields of vanillin (**11**G) and vanillic acid (**12**G) were improved with up to 6.8 and 1.4 wt%, respectively, after 0.5 h in presence of O_2 6 bar.

- In the flow-through system, the influence of the temperature was studied. The yield of vanillin was not much impacted. However, an increase of temperature seemed to disfavor vanillic acid production (1.1 wt% yield at 180°C *vs.* 2.3 wt% at 140°C). The influence of dioxygen pressure was also studied. The results are analoguous to those obtained in the dead-end reactor. The plateau yields of vanillin (**11**G) and vanillic acid (**12**G) were 6.8 and 1.1 wt% respectively.

Another important aspect deals with the NaOH consumption and the subsequent decrease of pH value (which should be higher than 12). Often the pH falls to 9 and NaOH has to be refilled.

Table IA. 18: Aerobic oxidation of sulfonated lignin

Entry	Substrate	Conc. (g/L)	Catalyst	Solvent	Oxidant P (bar)	T (°C)	t (h)	Product (yield in wt%) C^{α}-C^{β} cleavage G	C^{α}-C^{β} cleavage S	C^{β}-O cleavage	others	Ref
1a	Fir wood sodium lignosulfonate	180	$Cu(OH)_2$ 5.4 wt%	NaOH 3 M	O_2 2	160	0.67	**11**G : 7.7	-	-	-	134-135
2a	Eucalyptus magnesium lignosulfonate	5	$CuSO_4$ 20 wt%	NaOH 0.75 M	O_2 6	150	0.33	**11**G : 3.7[a] **11**G : 3.3[b]	**11**S : 12[a] **11**S : 10[b]	-	-	136
2b				NaOH 0.9 M	O_2 10			**11**G : 4.5[b]	**11**S : 16[b]	-	-	
3a[c]	Scandinavian spruce sodium lignosulfonate	220	$CuSO_4$ 1.3 wt%	NaOH 3M	O_2-N_2 (1.3-10.2)	160	0.5	**11**G : 6.8 **12**G : 1.4	-	-	-	138
4a	Lignosulfonate	13.3	Cu^{2+}-Fe^{3+} not mentionned	H_2SO_4 0.025 M	O_2 1-8	130-150	0.5-3	Mild conditions : low efficiency				137
4b					O_2 8	150	3	Severe conditions : destruction of aromatic bonds				
5a	Commercial sodium lignosulfonate M_w = 19910 g/mol M_n = 4400 g/mol	10	PMo_{12} 912 wt%	H_2O	O_2 10	170	0.33	**11**G : 6.6	-	-	-	139-141
								M_w = 4730 g/mol, M_n = 1040 g/mol				
5b				MeOH-H_2O 80:20				**11**G : 6.5 **12-OMe**-G : 6.2	-	-	-	
								M_w = 2940 g/mol, M_n = 970 g/mol, 12.7 wt% of monomers				
5c	Commercial calcium lignosulfonate M_w = 10240 g/mol M_n = 2430 g/mol			H_2O				**11**G : 5.5	-	-	-	
								M_w = 2450 g/mol, M_n = 750 g/mol				
5d				MeOH-H_2O 80:20				**11**G : 5.1 **12-OMe**-G : 4.9	-	-	-	
								M_w = 2170 g/mol, M_n = 830 g/mol				
6a	Commercial sodium lignosulfonate M_w = 52000 g/mol M_n = 7000 g/mol	15	$PMoV_2$ 579 wt%	MeOH-H_2O 90:10	O_2 25	190	0.17	Oil liquid products: 17 Solid residue: 52				142
6b	Commercial calcium lignosulfonate M_w = 18000 g/mol M_n = 2500 g/mol							Oil liquid products: 12 Solid residue: 50				

[a]Thin liquor, [b]Thick liquor , [c]Dead-end reactor.

- *KEGGIN polyoxometalates*

Being unstable in basic media, phosphomolybdic acid and derivatives had to be tested in acidic conditions. VOITL *et al* [139-141] studied the performances of PMo_{12} ($H_3PMo_{12}O_{40}$, 0.5 M in water or aqueous methanol) at 170°C under 10 bars of O_2 during 20 min, thus demonstrating a positive influence of methanol (see Table IA. 18 entries 5a-b). Indeed, the yield of vanillin (**11**G) and methyl vanillate (**12-OMe**-G) was doubled. Moreover, the decrease of the number M_n and weight average M_w molecular weights of the remaining lignin fragments was shown to be marked in aqueous MeOH than in water. Methanol would prevent condensation reactions.

ZHAO *et al* tested 0.05 M $PMoV_2$ ($H_5PMo_{10}V_2O_{40}$, 579 wt.%!!) in aqueous methanol at 190°C [142] but with more severe conditions (25 bar of O_2, Table IA. 18, entries 6a-b). Too high temperature or pressure led to gaseous compounds issued from the cleavage of aromatic rings that impact the carbon balance or promote radical coupling at the origin of condensation products. Under the best conditions, the maximum yield in oil liquid products was 17% whereas solid residue was around 50% or even more. Recyclability tests were carried out.

Lignosulfonate degradation is ensured simultaneously by oxidation and hydrolysis for a temperature above 120-170°C. The best yield of C^{α}-C^{β} products was 20.5 wt% only obtained in presence of $CuSO_4$ in NaOH 0.9 M, which is much lower compared to lignin model oxidation. Generally, in the case of Cu-catalysts, a high pH is needed to have satisfactory yields of aromatic aldehydes and acids. Some limitations are the fall of the pH and the resistance to mass-transfer. It is noteworthy that there is not any example of heterogeneous catalysts and only three metals (Cu, Mo and V) were tested.

IA. 4.3. Chemicals from Kraft lignins

Kraft lignins which contain less sulphur and are rather unexpensive are also relevant candidates for chemical revalorization (see Table IA. 3 dealing with main features of technical lignins (sulfur content, cost…)).

Tests without metal catalysts were performed by ARAÚJO *et al* (NaOH 2 M, O_2 4 bar + N_2 5 bar, 123°C, 1.25 h) [143]. They showed that oxygen pressure had an influence only on the kinetics of vanillin production (**11**G, 2.2 wt%). Also, PINTO *et al* [144-145] carried out tests in isolated and treated kraft lignin ($NaOH_{aq}$, pH > 13.8, O_2 3 bar + N_2 6.8 bar, 120°C, 20 min). Isolated lignin without treatment was oxidized more efficiently (vanillin **11**G:

1.1 wt%, syringaldehyde **11**S: 2.8 wt%, vanillic acid **12**G: 0.7 wt%, syringic acid **12**S: 1.5 wt%). Apparently, heat treatment does not preserve the chemical structure of lignin and linkages recalcitrant to oxidation are formed as shown by SCHUTYSER *et al* [28].

- *Cu and Fe homogeneous catalysts*

ALUNGA *et al* assessed $CuSO_4$ in 2 M NaOH (O_2 1.5 bar, 170°C, Table IA. 19a, entry 1) [146] for the oxidation of bamboo kraft lignin. Syringaldehyde (**11**S) was the major product (5.5%) and the global yield of aromatic monomers was 8.6 wt%. Such distribution of monomers was explained by the higher reactivity of syringyl units compared to the guaiacyl ones. Indeed, an increase of methoxy substituents should accelerate lignin degradation [120].

IMAI *et al* assessed $FeCl_3$ not only for the cleavage of **A4**$_{GG}$ but also for the oxidation of softwood kraft lignin [78] ($FeCl_3$ 29 wt%, O_2 8 bar, NaOH 0.5 M, 95°C, Table IA. 19a, entry 4). The molecular oxygen consumption by lignin turned out to be a little less than with **A4**$_{GG}$ which means that lignin is less reactive but the authors concluded that the oxidation of both substrates would follow the same mechanism.

- *KEGGIN polyoxometalates*

PMo_{12} ($H_3PMo_{12}O_{40}$) was tested on Spruce kraft lignin (10 g/L, O_2 5 bar) and on a commercial Indulin kraft lignin (50 g/L, O_2 10.8 bar) by VOITL *et al* [139-141] in batch conditions. The influence of methanol (Table IA. 19b entries 6a-h) was emphasized again and a lower solvent volume (entries 6b (20 mL) *vs* 6a (100 mL) and 6d (20 mL) *vs* 6c (100 mL)) gave rise to better yields which could be explained by a higher O_2/substrate ratio. Besides, some recyclability tests were performed (entry 6c). The yields of vanillin (**11**G) and vanillic acid (**12**G) reached a plateau (**11**G: 3.7 wt%, **12**G: 3.7 wt%) and decreased at the 11th run (2.2 wt% for both products). As lignin is unsoluble, recycling can be performed by filtrating out the lignin and then adding fresh substrate for another reaction. According the authors, catalyst deactivation would be related to its adsorption on oxidized lignin. It has to be noted that a lower amount of vanillin (**11**G) and vanillic acid (**12**G) were yielded from kraft lignin compared to lignosulfonates (Table IA. 18b, entries 6a-b). However, the lignin samples investigated in both studies were purchased from two different companies. So, the starting species may be different with non equivalent H-G-S ratio thus impacting the yield of vanillin. For $PMoV_2$ ($H_5PMo_{10}V_2O_{40}$) [145], the yield of oil liquid products was 43% (*vs.* 17% pour sodium lignosulfonate) and the solid residue represented 18% of the initial lignin (Table IA. 19b, entry

7). So, kraft lignin was more efficiently oxidized than lignosulfonate (see Table IA. 18b, entries 6a-b).

- *Heterogeneous catalysts*

On the contrary to lignosulfonate oxidation, some heterogeneous catalysts were assessed in the case of kraft lignin.

HTc-Cu-V (copper (9.2 %) and vanadium (28 %) supported on hydrotalcite) was tested for the degradation of a commercial kraft lignin (M_n = 1000 Da, HTc-Cu-V 20 wt%, O_2 10 bar, pyridine, 135°C, 48 h) by MOTTWEILER *et al* (Table IA. 19c, entries 9a-b) [112]. The successful depolymerization was shown by the decrease of the number molecular weight from 1000 to M_n = 300 Da (monitored by GPC). In particular, β-β or β-O-4 bonds were concerned as demonstrated by HSQC-NMR of the residue. In these conditions, repolymerization seemed to be a minor reaction.

In parallel, several perovskites ($LaM^1M^2_{1-x}O_3$, M = Fe, Mn or Sr) were tested in the aerobic oxidation of corn stalk kraft lignin in 2 M NaOH at 120°C under 2 bar of O_2 during 1 h (Table IA. 19c, entries 10a-f) [147]. The conversion was around of lignin was 86% and the yields of oligomers estimated to 34-39%. Among them, vanillin represented 2.6-3.0 wt% with respect to lignin. The yield of gaseous products was around 20% and the char 1.1%, which is similar to $PMoV_2$ ($H_5PMo_{10}V_2O_{40}$), but perovskites operated in milder conditions.

LUO *et al* assessed rhenium oxides supported on alumina or ceria (3 atom% of Re) in the commercial kraft lignin oxidation in liquid phenol at 120°C under 2 bars of O_2 (Table IA. 19c, entries 11a-c) [148]. Alumina turned to be a better promoter than ceria for lignin cleavage. With low lignin concentrations (52-104 g/L, entries 11a-b), the yield of vanillin (**11**G) was 7.3-7.4 wt% with a selectivity of 95%. At higher concentrations (entry 11c), the yield of vanillin (**11**G) dropped to 4.1 wt%, with a lower selectivity probably as the result of a lower catalytic loading.

Table IA.19a: Oxidation of kraft lignin catalyzed by Cu and Fe-catalysts

Entry	Substrate	Conc. (g/L)	Catalyst	Solvent	Oxidant P (bar)	T (°C)	t (h)	Conv. (wt%)	Product (yield in wt%) C^{α}-C^{β} cleavage G	C^{α}-C^{β} cleavage S	C^{β}-O cleavage G	C^{β}-O cleavage S	others	Ref
1	Bamboo kraft lignin	14.3	$CuSO_4$ 20 wt%	NaOH 2 M	O_2 1.5	170	n. i.	n. i.	**11**G : 2.1	**11**S : 5.5	**19**G : 0.4	**19**S : 1.6		146
2a	Commercial softwood kraft lignin, low sulfonate content	2.5	$CuCl_2$	MeOH-H_2O 80:20 pH = 1	O_2 48	150	0.3	n. i.	**11**G : 0.3 **12-OMe**-G : 0.2	-	-	-	(5-carbomethoxy-vanilin, 5CV) : 0.2 MDHA 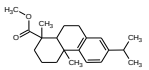 0.2	163
2b					O_2 48	210			**11**G : 3.0 12-OMe-G : 0.6	-	-	-	5CV : 0.6 MDHA : 0.3	
2c					O_2 72	230	2.10^{-4}		**11**G : 1.8 12-OMe-G : 0.7	-	-	-	5CV : 0.7 MDHA : 0.6	
2d					O_2 96	250			**11**G : 1.1 12-OMe-G : 0.4	-	-	-	5CV : 0.4 MDHA : 1.2	
3a	Calcium salt of kraft Eucalyptus lignin	17.2	CuO	NaOH 1 M	O_2 15.2	180	2	8.8	**11**G : 1.0 **12**G : 0.7	**11**S : 3.1 **12**S : 1.8	-	-		149
3b			None					9.3	**11**G : 0.9 **12**G : 0.6	**11**S : 3.3 **12**S : 1.5	-	-		
3c			CoO					6.0	**11**G : 0.9 **12**G : 0.6	**11**S : 3.3 **12**S : 1.5	-	-		
4	Softwood kraft lignin	2.5	$FeCl_3$ 29 wt%	NaOH 0.5 M	O_2 8	95	0.5	n. i.	3 mol of O_2 consumed / 200 g of lignin					78
5a	Kraft pine lignin $M_w \approx 3500$ g/mol	10	$CuSO_4$ 0.01 M	MeOH-H_2O 75:25 pH = 1	O_2 10	170	2	n. i.	**11**G : 3.1 **12-OMe**-G : 3.2	-	-	-	MDHA : 1.4 Others : 2.3 M_w = 775 g/mol	150
5b	Kraft pine lignin $M_w \approx 3500$ g/mol		$CuCl_2$ 0.01 M						**11**G : 3.2 **12-OMe**-G: 3.1	-	-	-	MDHA : 1.6 Others : 6.0 M_w = 531 g/mol	
5c	Kraft pine lignin $M_w \approx 3500$ g/mol		$FeCl_3$ 0.01 M						**11**G : 2.9 **12-OMe**-G: 2.6	-	-	-	MDHA : 1.52 Others : 4.9 M_w = 529 g/mol	
5d	Kraft pine lignin $M_w \approx 3500$ g/mol		$CoCl_2$ 0.01 M						**11**G : 2.9 **12-OMe**-G: 2.3	-	-	-	MDHA : 1.5 Others : 2.9 M_w = 753 g/mol	

Table IA.19b: Oxidation of kraft lignin catalyzed by polyoxometalates

Entry	Substrate	Conc. (g/L)	Catalyst	Solvent	Oxidant P (bar)	T (°C)	t (h)	Product (yield in wt%) C^{α}-C^{β} cleavage	C^{β}-O cleavage	others	Ref
6c	Spruce kraft lignin	10	PMo_{12} 912.5 wt%	MeOH-H_2O 80:20[a]	O_2 10	170	0.33	**11**G : 1.2 **12-OMe**-G : 1.4		Further products : 0.3	139-141
6d				MeOH-H_2O 80:20[b]				**11**G : 2.7 **12-OMe**-G: 2.5 **19**G : 0.07		n. i.	
6e	Commercial kraft lignin M_w = 9460 g/mol M_n = 2790 g/mol			H_2O[c]				**11**G : 5.9 M_w = 140830 g/mol, M_n = 1050 g/mol		-	
6f				MeOH-H_2O 90:10[c]				**11**G : 4.6 12-OMe-G : 4.2 M_w = 3370 g/mol, M_n = 990 g/mol		-	
6g				H_2O[b] MeOH-H_2O 90:10[b]	O_2 5			**11**G : 2.5 **11**G : 2.7 **12-OMe**-G : 2.5		- -	
6h	Indulin (commercial kraft lignin)	50		MeOH-H_2O 80:20[a]	O_2 10.8			**11**G : 3.7; 2.2[d] **12-OMe**-G : 3.7; 2.2[d]		CO_2: 7.8; 11[a]	
7	Commercial kraft lignin Nitrogen : 0.09% Sulfur : 3.48% M_w = 60000 g/mol M_n = 10000 g/mol	15	$PMoV_2$ 579 wt%	MeOH-H_2O 90:10	O_2 25	190	0.17	Oil liquid products: 43 (Dimethyl fumarate : 12 Dimethyl succinate : 8) Solid residue: 18		-	142
8[b]	Kraft pine lignin $M_w \approx$ 3500 g/mol	10	PMo_{12} 912.5 wt%	MeOH-H_2O 75:25				**11**G : 2.6 **12-OMe**-G : 3.2		MDHA : 1.6 Others : 0.87 M_w = 1250 g/mol	

[a]V = 100 mL, [b]V = 20 mL, [c]V = 10 mL, [d]10th recycling test

Table IA.19c: Oxidation of kraft lignin in presence of heterogeneous catalysts

Entry	Substrate	Conc. (g/L)	Catalyst	Solvent	Oxidant P (bar)	T (°C)	t (h)	Conv. (wt%)	Product (yield in wt%) C^{α}-C^{β} cleavage G	Product (yield in wt%) C^{β}-O cleavage G	others	Ref
9a	Commercial kraft lignin (1000 Da)	22.2	HTc-Cu-V 20 wt%	Pyridine	O_2 10	135	48	n. i.	Molar mass : 300 Da Minor repolymerization (4000-5000 Da) β-O-4 and β-β totally degraded			112
9b	Commercial kraft lignin (3000 Da)	22.2	HTc-Cu-V 20 wt%	Pyridine	O_2 10	135	48	n. i.	Molar mass : 200 Da Minor repolymerization (4500 Da) β -O-4 and β-β totally degraded			
10a	Corn stalks kraft lignin	10	$LaFe_{0.98}O_3$	NaOH 2 M	O_2 2	120	1	85	**12**G : 2.9; Oligomers : 38		Gas : 18 Char : 1.1	147
10b			$LaFe_{0.68}Mn_{0.32}O_3$					87	**12**G : 2.6; Oligomers : 39		Gas : 17 Char : 1.1	
10c			$LaFe_{0.45}Mn_{0.55}O_3$					87	**12**G : 2.8; Oligomers : 38		Gas : 21 Char : 1.1	
10d			$LaFe_{0.16}Mn_{0.84}O_3$					86	**12**G : 2.8; Oligomers : 36		Gas : 20 Char : 1.1	
10e			$LaMn_{1..01}O_3$					85	**12**G : 2.8; Oligomers : 37		Gas : 22 Char : 1.1	
10f			$LaSr_{0.03}Mn_{1.02}O_3$					85	**12**G : 3.0; Oligomers : 34		Gas : 23 Char : 1.1	
11a	Commercial neutral kraft lignin	104	ReO_x/γ-Al_2O_3 25 wt%	Phenol	O_2 2	120	1		**11**G : 7.3 **12**G : 0.1	**19**G : 0.1  0.3		148
11b		52	ReO_x/γ-Al_2O_3 50 wt%						**11**G: 7.4 **12**G: 0.1	**19**G : 0.1  0.3		
11c		208	ReO_x/γ-Al_2O_3 12.5 wt%						**11**G: 4.1 **12**G: 0.1	**19**G : 0.1  0.3		

Table IA. 19d: Oxidation of treated kraft lignin

Entry	Substrate	Conc (g/L)	Catalyst	Solvent	Oxidant P (bar)	T (°C)	t (h)	Product (yield in wt%) C^{α}-C^{β} cleavage	Product (yield in wt%) C^{β}-O cleavage	others	Ref
11a	Pyrolysis bio-oil from mixed hardwood kraft lignin	14.3	**V2** 10 wt% + 2.5 wt% Et_3N	AcOEt	air atm.	100	24	Alcohol oxidation preferred			152
11b			$[Cu(OTf)]_2$-toluene 20 wt% + 6 wt% TEMPO + 2-6 lutidine 42 wt%	DMF	O_2 atm	100	48	Aromatic aldehydes and acids Recombination of quinones			
11c[a]		50	**V(O)salen-IL** 10 wt% + 10 wt% DIPEA	[EMIM][OAc]		80	4	C-O cleavage preferred			
11d[a]				[MMIM][$MeOSO_3$]				C-O cleavage preferred			
12a	Microwave bio-oil from mixed hardwood kraft lignin	14.3	**V2** 10 wt% + 2.5 wt% Et_3N	AcOEt	air atm.	100	24	Alcohol oxidation preferred Microwave bio-oil more reactive			152
12b			$Cu(OTf)_2$-toluene 20 wt% + 6 wt% TEMPO + 2-6 lutidine 42 wt%	DMF	O_2 atm	100	48	Aromatic aldehydes and acids Recombination of quinones			
12c[a]		50	**V(O)salen-IL** 10 wt% + 10 wt% DIPEA	[EMIM][OAc]		80	4	C-O cleavage preferred. Easier extraction from [EMIM][$MeOSO_3$]			
12d				[MMIM][$MeOSO_3$]				C-O cleavage preferred			

[a]MW 200W

- *Comparison between catalysts*

VILLAR *et al* [149] have compared the activity of heterogeneous Cu and Co-catalysts in the aerobic oxidation of a calcium salt of kraft lignin in 1 M NaOH at 180°C under 15 bar of dioxygen. Only CuO was active for the production of aldehydes (see Table IA. 19a, entries 3a-b) whereas CoO had a negative effect on vanillin formation (entry 3c), promoting instead low molecular weight compounds arising from aromatic ring cleavage under the severe conditions used. WERHAN *et al* [150] tested also a series of catalysts: PMo_{12} ($H_3PMo_{12}O_{40}$), $CuSO_4$, $CuCl_2$, $FeCl_3$ and $CoCl_2$ (0.01 M) for the oxidation of a Pine kraft lignin (Table IA. 19a, entry 5a-d and Table IA. 19b, entry 8) by dioxygen (10 bars) in aqueous methanol (90-10) at 170°C. All the catalysts turned out to be active for lignin degradation into vanillin and derivatives. Precisely, Cu salts were the most active for vanillin (**11**G) and methyl vanillate (**12**-**OMe**-G) production (combined yield:6.3 wt%, Table IA. 19a, entries 5a-b). $CuSO_4$ yielded most of the targeted aromatic compounds, but the sulfate salt turned out to be less efficient for lignin fragmentation than $CuCl_2$ (M_w = 775 g/mol *vs* 531 g/mol) and $FeCl_3$ (529 g/mol). $FeCl_3$ was found to be less active than $CuCl_2$, thus confirming the observations made by LUGOVITSKAYA *et al* in alkaline media [137]. PMo_{12} gave rise to a combined yield of vanillin and methyl vanillate of 5.8 wt% (see Table 18b, entry 8), which is better than $FeCl_3$ and $CoCl_2$. However, PMo_{12} was the least active for lignin fragmentation (M_w = 1250 g/mol *vs* M_w = 529-775 g/mol).

As in Ref 86 (comparison between **V1**, $V(O)(O^iPr)_3$ and CuCl-TEMPO), the catalytic action of **V2** (10 wt%) in ethyl acetate (atm. air, 24 h see Table 19d, entries 11a and 12a) was compared to that of Cu(OTf)-TEMPO (20 wt%, atm. O_2, 48 h, see entries 11b and 12b) by DIAZ-URRUTIA *et al* in the case of microwave and pyrolysis bio-oils obtained from mixed hardwood kraft lignin [151]. **V2** was more selective for alcohol oxidation into ketones whereas Cu(OTf)-TEMPO was adapted to lignin cleavage and quinones recombination, which was similar to Ref 86 (**V1** and $V(O)(O^iPr)_3$ were selective for C-O cleavage whereas CuCl-TEMPO was selective for C-C cleavage). It should be noted that oxidation in presence of the Cu-catalyst took place under more stringent conditions. Also, the ionic liquid-tagged complex V**O(salen)-IL** (10 wt%) associated with DIPEA (N,N-DiIsoPropylEthylAmine, 10 wt%) was tested for the cleavage of both lignin samples in two different ionic liquids (Table 19d, entries 11c-d and 12c-d) under irradiation by microwave at 80°C during 4 h instead of 24 or 48 h. In both cases, the catalyst was selective for C-O cleavage, which shows the positive impact of irradiation.

*Overall, no selectivity of C(Ar)- C^{α} cleavage was observed. It might be because C(Ar)- C^{α} (e.g quinones **1**) or they were not analyzed because the main targets are phenolic aldehydes and acids, on the difference of phenolic lignin model oxidation. As for lignosulfonate cleavage, the best yield was obtained in presence of PMo_{12} (8.8 wt% C-C cleavage products).*

IA. 4.4. Organosolv and ionosolv lignins

It should be noted that both kraft and technical lignosulfonates are extracted in harsh conditions (high pH and high temperature). Therefore, these technical lignins are more resistant to cleavage. As a consequence, Organosolv lignin is more suitable for valorization through aerobic cleavage provided it is extracted in soft conditions. Also, aerobic cleavage of Ionosolv® lignin will be detailed as the extraction of this lignin is similar to Organosolv process.

- *KEGGIN polyoxometalates*

PMo_{12} ($H_3PMo_{12}O_{40}$, 912 wt%) was also tested as a catalyst in methanol-water 80:20 (O_2 5 bar, 170°C, 20 min) on a hardwood Organosolv lignin (Table IA. 20a, entry 1) which was depolymerized more efficiently than spruce (softwood) kraft lignin [139-141]. In both cases, the yield of vanillin **11**G and methyl vanillate **12-OMe**-G from C^{α}-C^{β} cleavage products were similar (3 wt%). However, syringaldehyde and its derivates were detected only in the case of Organosolv lignin aerobic cleavage. The difference is the production of syringaldehyde and its derivatives. Mn^{2+}-substituted $PMoV_5$ ($[Mn^{2+}]_x[H^+]_{7-2x}PMo_7V_5O_{40}$) has been also considered by GASPAR *et al* [152] for the aerobic oxidation (O_2 5 bar) of a dioxane lignin mixed with cellulose (lignin-cellulose 1:5) in water at 90°C during 1 h. The aim of such study was to mimick the behavior of residual lignin in treated lignocellulose (Table IA. 20a, entry 2). In these conditions, lignin was significantly degraded (destruction of the β-O-4, β-β and β-5 bonds) but new benzyl ether linkages resistant to cleavage were formed between residual lignin and carbohydrates. Thus, the conclusion was that impurities may have a critical impact on the cleavage of lignin.

Table IA. 20a: Oxidation of Organosolv and Ionosolv lignin in presence of homogeneous catalysts

Entry	Substrate	Conc. (g/L)	Catalyst	Solvent	Oxidant P (bar)	T (°C)	t (h)	Product (yield in wt%) Cα-Cβ cleavage G	Cα-Cβ cleavage S	Cβ-O cleavage G	Cβ-O cleavage S	others		Ref
1	Poplar organosolv lignin	10	PMo_{12} 912 wt%	MeOH-H_2O 80:20	O_2 5	170	0.33	**11**G: 0.5 **12-OMe**-G: 0.6	**11**S: 0.8 **12-OMe**-S : 1.0	**19**G : 0.03	**19**S : 0.1	Further products : 0.2		139-141
2	Eucalypt dioxane lignin	1.5	Mn^{2+}-substituted $PMoV_5$ or $PMoV_5$ 2 mM	H_2O	O_2 5	90	1	Significant lignin degradation Formation of benzyl ether linkages with carbohydrates						152
3	Beech organosolv lignin (2000 Da)	22.2	$V(acac)_3$ 5 wt% + $Cu(NO_3)_2{\cdot}3H_2O$ 5 wt%	Pyridine	O_2 10	135	48	Molar mass : 300 Da Minor repolymerization (2000 Da) β-β, β-O-4 structures totally degraded						112
4	Poplar organosolv lignin	50	Co(salen)**1** (10 wt%)	MeOH-DMSO 1:1	O_2 3.4	r. T.	72	**11**G : 0.6	11S: 1.2	-	-	 0.1	**1**S : 1.6	73
5d[a]	Mixed hardwood organosolv lignin	78	$Co^{2+}/Mn^{2+}/Zr^{4+}$/HBr 1/1/0.1/2 mol/mol (metals from hydrated acetate salts)	AcOH + 8 wt% H_2O	Air 69	140	2	**11**G: 0.8 **12**G: 1.5	**11**S: 1.8 **12**S: 2.9	-	-	-	-	153
5e[a]		84		AcOH				**11**G: 0.7 **12**G:1.4	**11**S: 2.4 **12**S: 3.3	-	-	-	-	
5f[a]		70		AcOH + 20 wt% H_2O				**11**G: 1.3 **12**G: 1.0	**11**S: 3.3 **12**S: 3.2	-	-	-	-	
5g[a]		78		AcOH + 8 wt% H_2O	Air 138			**11**G: 0.9 **12**G: 1.8	**11**S: 2.4 **12**S S: 3.8	-	-	-	-	
5i[a]		78		AcOH				**11**G: 1.0	**11**S: 2.5	-	-	-	-	
5h[b, c]	Mixed hardwood organosolv acetate	78		AcOH	Air 69			**11**G: 0.7 **12**G: 1.4	**11**S: 2.4 **12**S: 3.3	-	-	-	-	

[a][Co] = 6.9 mM, [b][Co] = 30 mM, [c]Partially bleached before isolation

Table IA. 20b: Oxidation of Organosolv and Ionosolv lignin in ionic liquids (entries 6-8) or in presence of a heterogeneous catalyst (9a-10b)

Entry	Substrate	Conc. (g/L)	Catalyst	Solvent	Oxidant P (bar)	T (°C)	t (h)	Conv. (wt%)	Product (yield in wt%) Cα-Cβ cleavage H	G	S	Cβ-O cleavage S	Ref
6	Mixed hardwood ethanolsolv lignin	0.05 g/g of IL (i.e 0.07 g/L)	$CuSO_4$ 1 wt%	[mmim] [Me_2PO_4]	O_2 25	175	1.5	Fresh catalyst : 100; 100[a]	**11**H : 6; 7[a]	**11**G : 9; 9[a]	**11**S : 15; 15[a]	-	155
7	Beech organosolv lignin	0.10 g/g of IL (i.e 0.14 g/L)	$Mn(NO_3)_2$ 22.2 wt%	[EMIM] [CF_3SO_3]	Synthetic air 84 O_2 : 17.5	100	24	66	Minor products : 11G, 11S			**1**S : 12	156
8	Rubber wood-ionosolv lignin	0.22 g/g of IL (i.e 0.15 g/L)	[mmim] [$MeOSO_3$]		O_2 atm	100	10	n. i.	-	**11**G: n. i.	-	-	154
9a[b]	Pine steam-exploded organosolv lignin	1	Rose Bengal 10^{-4} M	Acetonitrile-ethanol 1:1	air	r. T.	8	n. i.	-	**11**G : 0.2	**11**S : 0.5	**34**S : - **35**S: 1.5 *Cis*-Sinapyl alcohol : 0.03	157
9b[b]							48		-	**11**G : 0.3	**11**S : 0.7	**34**S : 0.5 **35**S: 0.8 *Cis*-Sinapyl alcohol : 0.05	
10a	Beech organosolv lignin (30-1300 Da)	22.2	HTc-Cu-V 20 wt%	Pyridine	O_2 10	135	48	n. i.	Molar mass : 60-800 Da Minor repolymerization (3000-5000 Da) Resinol structures totally degraded				112
10b	Beech organosolv lignin (300-5000 Da)	22.2	HTc-Cu-V 20 wt%	Pyridine	O_2 10	135	48	n. i.	Molar mass : 200-1300 Da Minor repolymerization (4000 Da) Resinol structures totally degraded				

[a]6th recycling, [b]Photocatalytic intensification (50 W, λ = 400 nm)

- *Combined Cu and V-catalysts*

MOTTWEILER *et al* assessed a binary mixture of $V(acac)_3$ (5 wt%) and $Cu(NO_3)_2$ (5 wt%) [112] in pyridine for the oxidation of a beech Organosolv lignin in pyridine (135°C, 48 h) under 10 bar of dioxygen (Table IA. 20a, entry 3). As for kraft lignin, a significant decrease of the molecular weight took place as the result of depolymerization: β-O-4 and β-β linkages were cleaved totally. HTc-Cu-V tested as a heterogeneous catalyst in the same operative conditions (Table IA. 20b, entries 9a-b) gave rise to similar results (M_n decreased from 2000 to 300 Da). Consequently, Organosolv lignin was oxidized on a similar extent compared to kraft lignin (Table IA. 19d, entries 12a-b) and repolymerized lignin was also noted as a by-product in both cases.

- *Co and Mn-salts*

BIANNIC and BOZELL [73] assessed **Co(salen)1** (structure in Table IA. 14, 10 wt%) for the aerobic oxidative cleavage of a Poplar Organosolv lignin in methanol-DMSO (1-1) at room temperature under 3.4 bar of dioxygen (72 h). The yield of vanillin **11**G and syringaldehyde **11**S were 0.6 and 1.2 wt%, respectively and the yield of syringol **17**S was 1.6% (Table 20a, entry 4). Hence, on the contrary to **AN$_{XY}$** substrates, **Co(salen)1** was not selective for C(Ar)-C^{α} cleavage here. PARTENHEIMER tested a 1/1/0.1/2 $Co(OAc)_2$/$Mn(OAc)_2$/$Zr(OAc)_4$ /HBr (molar) catalytic system in acetic acid with various concentrations of water for the aerobic cleavage of mixed hardwood Organosolv lignin (Table 20a-b, entries 5a-i) under 69 bars of air (dioxygen 13.8 bar) in binary AcOH-H_2O solvents (140°C, 2 h) [153]. Such system proved to be active for lignin degradation into aromatic aldehydes. Water seemed to have a positive effect on aldehydes production and a negative effect on acids. Lignin concentration (39-234 g/L) also had a negative effect on acid production, but the yield of aldehydes was rather unchanged. At [Co] > 30 mM, aromatic aldehydes and acids were barely observed (entry 5i). The lignin sample (entry 5g) and an Organosolv lignin acetate (entry 5h) in acetic acid hydrated by 8 wt% of water were oxidized under a higher pressure (138 bars of air). The pressure was found to be benefical for syringaldehyde (2.4 vs 1.8%) and syringic acid (3.8 vs 2.9%).

- *Ionic liquids*

The ionic liquid [mmim][Me_2PO_4] was tested as a solvent and a catalyst for the oxidation by atmospheric O_2 of rubber wood Ionosolv lignin at 10 wt% by SHAMSURI and

ABDULLAH [154] (Table IA. 20b, entry 8). According to the authors, the yield (n. i.) was maximized for a dioxygen flow of 20 $ft^3.h^{-1}$.

LIU *et al* tested $Cu(SO_4)$ 1 wt% in $[mmim][Me_2PO_4]$ at 175°C (Table IA. 20b, entry 6) for lignin oxidation with O_2 at 25 bar coupled with extraction by MIBK (MethylIsoButylKetone, used as a co-solvent) [155]. The conversion was as high as 100% after 1.5 h, the selectivity in aromatic aldehydes (*p*-hydroxybenzaldehyde **11**H, vanillin **11**G and syringaldehyde **11**S) reached 30% and the catalyst turned out to be still stable after 6 tests. Since the oxidation products were extracted during the reaction, the recycling procedure consisted in adding fresh substrate only on the homogeneous catalyst. No significant decline of both conversion and of the yields of aromatic products could be emphasized over the tests. Similarly, STÄRK *et al* assessed $Mn(NO_3)_2$ 22.2 wt% in another ionic liquid, $[EMIM][CF_3SO_3]$ at 100°C (Table IA. 20b, entry 7) for the catalytic oxidation of a beech organosolv lignin by synthetic air (84 bar, O_2 17.5 bar) [156]. The main product formed was DMBQ (DiMethoxyBenzoQuinone, **1**S, 11.5 wt%), an anti-tumor compound. At a lower catalytic loading (2.2 wt%), some syringol **17**G was noted as a product.

- *Photocatalytic oxidation*

A singlet oxygen (in atmospheric air at room temperature) mediated oxidation of a Pine steam-exploded organosolv lignin (1.5 g) was performed by BONINI and D'AURIA in presence of 10^{-4} M of Rose Bengal in acetonitrile-ethanol 1:1 (Table IA. 20b, entries 9a-e) [157]. The suspension was irradiated by a tungsten-halogen lamp (50 W) during 48 h. The main product was sinapyl alcohol (**35**S, max. yield of 1.5 wt% after 8 h, entry 9b). Low amounts of aromatic aldehydes (vanillin (**11**G): 0.2-0.3 wt% and syringaldehyde (**11**S): 0.5-0.8 wt%) and sinapylaldehyde **34**S (0.5 wt% after 48 h) were formed.

> *A partial conclusion from the tests on various Organosolv lignin is that several catalysts and several operative conditions were assayed. Generally, similar yields of aromatic platform molecules were obtained. Yet, $CuSO_4$ in $[mmim][Me_2PO_4]$ gave rise to an outstanding yield of aromatic aldehydes of 30%, thanks to an extraction simultaneous to the reaction, with enabled to preserve the targeted products.*

Yet, there are plenty of other extraction processes such as ball-milling, hydrolytic and pyrolytic treatments that have been used to provide lignin for oxidative depolymerisation experiments with $Cu(phen)_2$ / 0.5 M NaOH at 80°C under 2.7 bar of O_2 (24 h) (case of milled

wood lignin (15 g/L)) [105], Cu and Fe hydroxides in 2 M NaOH at 170°C under 13.8 bar of O_2 (10-30 min) [158] (case of poplar hydrolytic lignin (40 g/L)), $PMoV_2$ in methanol-water 90:10, O_2 25 bar, 190°C, 10 min (cases of pyrolytic, hydrolytic and alkali lignins (15 g/L)), [146], perovskites such as $LaMnO_3$, $LaCoO_3$, $LaCo_{0.9}Cu_{0.1}O_3$ and $LaCo_{0.8}Cu_{0.2}O_3$ (5 wt%) in 2 M NaOH at 120°C under 20 bar (40 min) of air (case of lignin from the enzymatic hydrolysis of steam-explosive cornstalk) [159-161]. The comparison of pyrolytic, hydrolytic and alkali lignins [142] showed that the yield of oil liquid products from hydrolytic lignin was lower than from alkali lignin (36 wt% vs 43 wt%) maybe as the consequence of the presence of residual sugars, which may lead to the formation of recalcitrant linkages between saccharides and residual lignin as in Ref 152. Moreover, pyrolytic lignin was oxidized more efficiently than the alkali one due to a lower degree of polymerization.

Dioxygen transfer to liquid phase has been pointed out as the main limitation parameter [162]. So, a higher pressure is often required for lignin depolymerization. WERHAN *et al* tested $CuCl_2$ in methanol/water 80/20 acidified by H_2SO_4 (pH = 1) [163] for the aerobic oxidation of a commercial softwood Kraft lignin. The reaction took place in a micro-reactor pressurized to 32-96 bar in presence of pure O_2 at 150-250°C at short reaction time (Table 19a, entries 2a-d). In these conditions, the main product was vanillin but the yield was rather low (3 wt%). Other solutions consist in adapting the reactor design or moving from a batch to a continuous mode of production. SALES *et al* [162] have compared both working at 120°C with 60 g/L of lignin during 2 h, under 5 bar of O_2 in the presence of 4 wt% Pd/γ-Al_2O_3 (2.85 wt% of Pd) in the batch reactor. In the continuous reactor, the liquid phase (30 g/L of lignin) and dioxygen (20 bar, 1000 L/h) were flowing concurrently and enabled to improve the yields of vanillin (2.2 wt% *vs.* 0.9 wt%) and syringaldehyde (3.8 wt% *vs.* 0.8 wt%). However, these yields were quite low too.

IA. 5. Conclusions

This review tried to rationalize the different types of dimeric models bearing β-O-4 lignin linkages reported in the literature and to present the main catalytic systems used in the cleavage of those models and in the depolymerization of lignin in the presence of O_2.

Active metal-based catalysts often involve Cu, V and Co. Cu-catalysts are mainly active for C^{α}-C^{β} cleavage whereas Co(salen) complexes are mainly active for C(Ar)-C^{α} cleavage.

More, it has been shown that the catalyst design can be useful to target a particular product. Indeed, the selectivity of V-based catalysts may be tuned by the choice of the ligand. In addition, a stepwise oxidation of lignin was explored. It proceeds *via* the oxidation of alcohol moieties to give rise to an oxidized lignin less resistant to cleavage. However, such approach was tested on **AN**$_{XY}$ models only and the operative conditions reported with **KN**$_{XY}$ models were actually not milder.

Lignin surrogates do not describe the reality of lignin. They do not take into account its heterogeneity, the presence of other bonds, of impurities (sugars, proteins…) and obviously the polymeric properties of lignin. So, after transposition from models to real lignin whatever its extraction mode, the yield of aromatic aldehydes or acids plummeted (maximum yield of aromatic aldehydes: 30%). Some of the reasons behind are listing below:

- Less phenolic groups are present in lignin compared to in some of the dimeric models. As said previously, these functions are the most active ones for oxidation and cleavage. Moreover, some of the phenolic groups can be transformed into quinones initializing repolymerization, giving rise to a repolymerized lignin more recalcitrant to oxidation. Therefore, operative conditions have to be further optimized.
- Lignin is a heterogeneous three-dimensional polymer actually constituted of oligomers having similar molecular weight but different structures, which may be at the origin of steric effects and heterogeneities of chemical properties. Moreover, it contains other linkages more resistant than β-O-4 [164].
- Lignin is often not soluble in conventional solvents (except in aqueous alkali), so the transfer of dioxygen has to be boosted.

The main solution is to operate at higher pressure and temperature compared to lignin model oxidation to overcome resistances to dioxygen transfer and to activate lignin. Nevertheless, this implies a higher probability of over-oxidation and aromatic cycle degradation as pointed out by GASPAR *et al* [152] and such conditions can favor radical coupling too. Some intensification processes were already explored as photochemistry and the use of microwave. An example is the use of an ionic liquid in which lignin is soluble. Some results can validate this solution as a yield of aromatic aldehydes up to 30% was obtained by LIU *et al* [155]. This is the highest obtained yield of aromatic aldehydes.

KEGGIN molybdovanadophosphates ($H_{3+x}PMo_{12-x}V_xO_{40}$, $PMoV_x$) were already used for lignin oxidative cleavage. Yet, only a few studies of $PMoV_x$-catalyzed aerobic cleavage of lignin into aromatic platform molecules were carried out. In our laboratory, such vanadium compounds were shown to be efficient for the cleavage of simple C-C bonds in simple molecules such as α-hydroxyketones. As such reaction is involved in lignin aerobic cleavage, these catalysts will be deeper studied in this thesis.

Another solution may consist in using ultrasounds to enhance dioxygen transfer. To the best of our knowledge, this solution was not exploited for lignin aerobic oxidation.

References

[1]: BP Statistical Review of World Energy June BP, London, UK, 2017.
[2]: F.H. Isikigor, C.R. Becer, *Polym. Chem.* **2015**, 6, 4497-4559.
[3]: B. Hahn-Härgerdal, M. Galbe, M.F. Gorwa-Grauslund, G. Lidén, G. Zachhi, *Trends Biotechnol.* **2006**, 24, 549-556.
[4]: A. R. Gaspar, J. A. F. Gamelas, D. V. Evtuguin, C. Pascoal Neto, *Green Chem.* **2007**, 9, 717–730.
[5]: P.J. De Wild, W.J.J. Huijgena, H.J. Heeres, *J. Anal. Appl. Pyrolysis* **2012**, 93, 95-103.
[6]: N. Smolarski, **2012**, *High-Value Opportunities for Lignin : Unlocking its Potential*, Frost & Sullivan.
[7]: S. Laurichesse, L. Avérous, *Prog. Poly. Sci.* **2014**, 39, 1266-1290.
[8]: H. Konnerth, J. Zhang, D. Ma, M. H.G. Prechtl, N. Yan, *Chem. Eng. Sc.* **2015**, 155-163.
[9]: I. A. Weinstock, R. H. Atalla, R. S. Reiner, M. A. Moen, K. E. Hammel, C. J. Houtman, C. L. Hill, M. K. Harrup, *J. Mol. Catal. A* **1997**, 116, 59-84.
[10]: D. M. Sonnen, R. S. Reiner, R. H. Atalla, Ira A. Weinstock, *Ind. Eng. Chem. Res.* **1997**, 36, 4134-4142.
[11]: M. Suchy, D. S. Argyropoulos, *ACS Symposium Series* **2011** Washington, DC.
[12]: J. M. Campos-Martin, G. Blanco-Brieva, J. L. G. Fierro, *Angew. Chem. Int. Ed.* **2006**, 45, 6962-6984.
[13]: J. Zakzeski, P. C. A. Bruijnincx, A. L. Jongerius, B. M. Weckhuysen *Chem. Rev.* **2010**, 110, 3552-3599.
[14]: M. P. Pandey, C. S. Kim, *Chem. Eng. Technol.* **2011**, 34, 29–41.
[15]: C. Crestini, M. Crucianelli, M. Orlandi, R. Saladino, *Catal. Today* **2010**, 156, 8-22.
[16]: H. Lange, S. Decina, C. Crestini, *Eur. Polym. J.* **2013**, 49, 1151–1173.
[17]: L. Munk, A. Kitarz, Dayanand. C. Kalyani, J. Dalgaard Mikkelsen, Anne S. Meyer, *Biotechnol. Adv.* **2015**, 33, 13-24.
[18]: G. Chatel, R. D. Rogers, *ACS Sustainable Chem. Eng.* **2014**, 2, 322−339.
[19]: J. Dai, A.F. Patti, K. Saito, Tetrahedron Lett. **2016**, 57, 4945-4951.
[20]: G. Chatel, K. De Oliveira Vigier, F. Jérôme, *ChemSusChem* **2014**, 7, 2774-2787.
[21]: E. Kuna, R. Behling, S. Valange, G. Chatel, J.C. Colmenares, *Top. Curr. Chem* **2017**, 375, 1-20.
[22]: Kang, X. Li, J. Fan, J. Chang, *Renew. Sus. Ener. Rev.* **2013**, 27, 546-558.
[23]: R. Ma, Y. Xu, X. Zhang, *ChemSusChem* **2015**, 8, 24-51.
[24]: R. Ma, M. Guo, X. Zhang, *Catal. Today* **2018**, 302, 50-60.
[25]: C. Li, X. Zhao, A. Wang, G. W. Huber, T. Zhang, *Chem. Rev.* **2015**, 115, 11559-11624.
[26]: R. Behling, S. Valange, G. Chatel, *Green Chem.* **2016**, 18, 1839-1854.
[27]: R. Rinaldi, R. Jastrzebski, M. T. Clough, J. Ralph, M. Kennema, P. C. A. Bruijnincx, B. M. Weckhuysen, *Angew. Chem. Int. Ed.* **2016**, 55, 8164-8215.
[28]: W. Schutyser, T. Renders, S. Van den Bosch, S.-F. Koelewijn, G. T. Beckham, B. F. Sels, *Chem. Soc. Rev.*, 2018, 47, 852-908.
[29]: Z. Sun, B. Fridrich, A. de Santi, S. Elangovan, K. Barta, *Chem. Rev.* **2018**, 118, 614-678
[30]: P.J. Deuss and K. Barta, *Coord. Chem. Rev.* **2016**, 306, 510-532.
[31]: S. Guadix-Montero, M. Sankar, *Top. Catal.* **2018**, 61, 183-198.
[32]: M. Wang, J. Ma, H. Liu, N. Luo, Z. Zhao, F. Wang, *ACS Catal.* **2018**, 8, 2129-2165.

[33]: M. Leisola, O. Pastinen, D.D. Axe, *BIO-Complexity* **2012**, 3, 1-11.
[34]: W. Boerjan, J. Ralph, M. Baucher, *Annu. Rev. Plant Bio.* **2003**, 54, 519-546.
[35]: M. Sette, R. Wechselberger, C. Crestini, *Chem. Eur. J.* **2011**, 17, 9529-9535.
[36]: M. M. Campbell, R. R. Sederoff, *Plant. Physiol.* **1996**, 110, 3-13.
[37]: J. H. Wei, Y. R. Song, *J. Integr. Plant Biol.* **2001**, 43, 771-779.
[38]: K. Freudenberg, *Nature* **1959**, 183, 1152-1155.
[39]: J. Banoub, G-H. Delmas Jr., N. Joly, G. Mackenzie, N. Cachet, B. Benjelloun-Mlayah, M. Delmas, *J. Mass Spectrom.*, **2015**, 50, 5-48.
[40]: S. Bauer, H. Sorek, V. D. Mitchell, A. B. Ibáñez, D. E. Wemmer, *J. Agric. Food Chem.* **2012**, 60, 8203-8212.
[41]: P. Azadi, O. R. Inderwildi, R. Farnood, D. A. King, *Renew. Sustainable Ener. Rev.* **2013**, 21, 506-523.
[42]: J.S. Lupoi, S. Singh, R. Parthasarathi, B. A. Simmons, R. J. Henry, *Renew. Sustainable Ener. Rev.* **2015**, 49, 871-906.
[43]: J. J. Villaverde, J. Li, M. Ek, P. Ligero, A. De Vega, *J. Agric. Food Chem.* 2009, 57, 6262-6270.
[44]: F.S. Chakar, A.J. Ragauskas, *Ind. Crop. Prod.* **2004**, 20, 131-141.
[45]: M. P. Pandey, C. S. Kim, *Chem. Eng. Technol.* 2011, 34, 29-41.
[46]: J. C. Del Río, J. Rencoret, G. Marques, A. Gutiérrez, D. Ibarra, J. I. Santos, J. Jiménez-Barbero, L. Zhang, Á. T. Martínez, *J. Agric. Food Chem.* 2008, 56, 9525-9534.
[47]: F. S. Chakar, A. J. Ragauskas, *Ind. Crops. Prod.* **2004**, 20, 131-141.
[48]: A. Brandt, J. Gräsvik, J. P. Hallett, T. Welton, *Green Chem.* **2013**, 15, 550-583.
[49]: T.N. Kleinert, *U.S. Pat. 3585104* **1971**.
[50]: J. Quesada-Medina, F. J. Lopez-Cremades, P. Olivares-Carrillo, *Biores. Technol.* **2010**, 101, 8252-8260
[51]: A. Ferrer, A. Vega, L. Rodriguez, L. Jimenez, *Bioresour Technol* **2013**, 132, 115-120.
[52]: G. Avignon, M. Delmas, *U.S. Pat 7402224* **2008**.
[53]: M. Delmas, *Chem. Eng. Technol.* **2008**, 31, 792-797.
[54]: G. H. Delmas, B. Benjelloun-Mlayah, Y. L. Bigot, M. Delmas, *J. Appl. Polym. Sci.* **2011**, 121, 491-501.
[55]: S. Constant, H. L. Wienk, A. E. Frissen, P. De Peinder, R. Boelens, D. S. Van Es, R. J. H. Grisel, B. M. Weckhuysen, W. J. J. Huijgen, R. J. A. Gosselink, P. C. A. Bruijnincx, *Green Chem.* **2016**, 18, 2651-2665.
[56]: M. Funaoka, T. Kako, I. Abe, *Wood Sci. Technol.* **1990**, 24, 277-288.
[57]: M. McCoy, *Chem. Eng. News.* **2016**, 94, 35-37.
[58]: S. H. Mood, A. H. Golfeshan, M. Tabatabaei, G. S. Jouzani, G. H. Najafi, M. Gholami, M. Ardjmand, *Renew. Sustainable Ener. Rev.* **2013**, 27, 77-93.
[59]: A. Berlin, M. Balakshin, Bioener. Res. Adv. Appl. **2014**, 315-336.
[60]: K. Christoffersson, H. Grundberg, B. Joensson, *Proceedings 3rd Nordic Wood Biorefinery Conference* **2011**, 106-108.
[61]: R. J. A. Gosselink, M. H. B. Snijder, A. Kranenbarg, E. R. P. Keijsers, E. de Jong, L. L. Stigsson, *Ind. Crops Prod.* **2004**, 20, 121-129.
[62]: J. Michels, K. Wagemann, *Biofuels Bioprod. Bior.* **2010**, 4, 263-267.
[63]: A. Brandt, J. Gräsvik, J. P. Hallett, T. Welton, *Green Chem.* **2013**, 15, 550-583.
[64]: P. Verdía, A. Brandt, J. P. Hallett, M. J. Ray, T. Welton, *Green Chem.* **2014**, 16, 1617-1627.
[65]: A. Brandt-Talbot, F. J. V. Gschwend, P. S. Fennell, T. M. Lammens, B. Tan, J. Weale, J. P. Hallett, *Green Chem.* **2017**, 19, 3078-3102.
[66]: L. Weigand, S. Mostame, A. Brandt-Talbot, T. Welton, J. P. Hallett, *Faraday Discuss.* **2017**, 202, 331-349.
[67]: N. Pareek, T. Gillgren, L. J. Jönsson, *Bioresour. Technol.* **2013**, 148, 70-77.
[68]: M. Zahedifar, F. B. Castro, E. R. Ørskova, *Anim. Feed Sci. Technol.* **2002**, 95, 83-92.
[69]: G. Bentivenga, C. Bonini, M. D'Auria, A. De Bona, *Biomass Bioenergy* **2003**, 24, 233-238.
[70]: R. El Hage, N. Brosse, L. Chrusciel, C. Sanchez, P. Sannigrahi, A. Ragauskas, *Polym. Degrad. Stab.* **2009**, 94, 1632-1638.
[71]: C. Crestini, M. D'auria, *Tetrahedron* **1997**, 53, 7877-7888.
[72]: G. Brunow, J. Sipilä, T. Mäkelä, *Holzforschung* **1989**, 43, 55-59.
[73]: B. Biannic, J. J. Bozell, *Org. Lett.* **2013**, 15, 2730-2732.
[74]: E. West, A. S. MacInnes, H. J. Hibbert, *J. Am. Chem. Soc.* **1943** 65 (1943) 1187.

[75]: P. J. Deuss, M. Scott, F. Tran, N. J. Westwood, J. G. de Vries, K. Barta, *J. Am. Chem. Soc.* **2015**, 137, 7456-7467.
[76]: S. Jia, B. J. Cox, X. Guo, Z. C. Zhang, J. G. Ekerdt, *ChemSusChem* **2010**, 3, 1078-1084.
[77]: R. El Hage, N. Brosse, P. Sannigrahi, A. Ragauskas, *Polym. Degrad. Stab.* **2010**, 95, 997-1003.
[78]: T. Imai, T. Yokoyama, Y. Matsumoto, *J. Wood. Sci.* **2011**, 57, 219-225.
[79]: J. Li, G. Henriksson, G. Gellerstedt, *Bioresour. Technol.* **2007**, 98, 3061-3068.
[80]: T. Hosoya, H. Kawamoto, S. Saka, *J. Anal. Appl. Pyrolysis* **2008**, 83, 78-87.
[81]: C. P. Masuku, *J. Anal. Appl. Pyrolysis* **1992**, 23, 195-208.
[82]: C. Fabbri, M. Bietti, O. Lanzalunga, *J. Org. Chem.* **2005**, 70, 2720-2728.
[83]: S. K. Hanson, R. T. Baker, J. C. Gordon, B. L. Scott, D. L. Thorn, *Inorg. Chem.* **2010**, 49, 5611-5618.
[84]: H. J. Parker, C. J. Chuck, T. Woodman, M. D. Jones, *Catal. Today* **2016**, 269, 40-47.
[85]: Y. Ma, Z. Du, J. Liu, F. Xia, J. Xu, *Green Chem.* **2015**, 17, 4968-4973.
[86]: B. Sedai, C. Diaz-Urrutia, R. T. Baker, R. Wu, L. A. Silks, S. K. Hanson, *ACS Catal.* **2011**, 1, 794-804.
[87]: C. Diaz-Urrutia, B. Sedai, K.C. Leckett, R.T. Baker, S.K. Hanson, *ACS Sustainable Chem. Eng.* **2016**, 4, 6244-6251.
[88]: S. K. Hanson, R. Wu, L. A. Silks, *Angew. Chem. Int. Ed.* **2012**, 51, 3410-3413.
[89]: G. Zhang, B. L. Scott, R. Wu, L. A. Silks, S. K. Hanson, *Inorg. Chem.* **2012**, 51, 7354−7361.
[90]: E. Alder, Lignin Chemistry – Past, present and future, *Wood Sci. Technol.* **1977**, 11, 169-218.
[91]: Y-Y. Jiang, L. Yan, H-Z. Yu, Q. Zhang, Y. Fu, *ACS Catal.* **2016**, 6, 4399-4410.
[92]: S. Son, F. D. Toste, *Angew. Chem. Int. Ed.* **2010**, 49, 3791-3794.
[93]: B. N. Wigington, M. L. Drummond, T. R. Cundari, D. L. Thorn, S. K. Hanson, S. L. Scott, *Chem. Eur. J.* **2012**, 18, 14981-14988.
[94]: M. M. Heravi, T. Benmorada, K. Bakhtiari, F. F. Bamoharramb, H. H. Oskooie, *J. Mol. Catal. A* **2007**, 264, 318-321
[95]: R. Neumann, *Prog. Inorg. Chem.* **1997**, 47, 317-370.
[96]: I. V. Kozhevnikov, *Chem. Rev* **1998**, 98, 171-198.
[97]: D. V. Evtuguin, A. I. D. Daniel, A. J. D. Silvestre, F. M. L. Amado, C. Pascoal Neto, *J. Mol. Catal. A*, **2000**, 154, 217–224.
[98]: J. Arichi, M. Eternot, B. Louis, Catal. Today **2008**, 138, 117-122.
[99]: A. Gaspar, D. V. Evtuguin, C. Pascoal Neto, *Holzforschung* **2004**, 58, 640-649.
[100]: D. V. Evtuguin, C. Pascoal Neto, J. Rocha, J. D. Pedrosa de Jesus, *Appl. Catal. A* **1998**, 167, 123-139.
[101]: C. Canevali, M. Orlandi, L. Pardi, B. Rindone, R. Scotti, J. Sipila, F. Morazzoni, *J. Chem. Soc., Dalton Trans.* **2002**, 3007-3014.
[102]: M. Wang, J. Lu, L. Li, H. Li, H. Liu, F. Wang, *J. Catal.* **2017**, 348, 160-167.
[103]: B. Sedai, T. Baker, *Adv. Synth. Catal.* **2014**, 356, 3563-3574.
[104]: S. K. Hanson, R. T. Baker, *Acc. Chem. Res.* **2015**, 48, 2037-2048.
[105]: A. Azarpira, J. Ralph, F. Lu, *Bioenerg. Res.* **2014**, 7, 78-86.
[106]: N. D. Patil, N. Yan, *Tetrahedron Lett.* **2016**, 57, 3024-3028.
[107]: J. M. Hoover, S. S. Shannon, *J. Am. Chem. Soc.* **2011**, 133, 16901-16910.
[108]: W. Deng, H. Zhang, X. Wu, R. Li, Q. Zhang, Y. Wang, *Green Chem.* **2015**, 17, 5009-5018.
[109]: S. Kim, S. C. Chmely, M. R. Nimlos, Y. J. Bomble, T. D. Foust, R. S. Paton, G. T. Beckham, *J. Phys. Chem.* **2011**, 2, 2846-2852.
[110]: X-F. Zhou, X-J. Lu, *J. Appl. Polym. Sci.* **2016**, 44, 44133-44141.
[111]: J. F. Blandez, S. Navalon, M. Alvaro, H. Garcia, *ChemCatChem* **2015**, 7, 3020-3026.
[112]: J. Mottweiler, M. Puche, C. Räuber, T. Schmidt, P. Concepción, A. Corma, C. Bolm, *ChemSusChem* **2015**, 8, 2106-2113.
[113]: L. J. Mitchell, C. J. Moody, *J. Org. Chem.* **2014**, 79, 11091-11100.
[114]: I. S. Park, M. S. Kwon, Y. Kim, J. S. Lee, J. Park, *Org. Lett.* **2008**, 10, 497-500.
[115]: S. Gazi, M. Đokić, A. Mangala P. Moeljadi, R. Ganguly, H. Hirao, H. Sen Soo, *ACS Catal.* **2017**, 7, 4682-4691.
[116]: S. Gazi, W. K. H. Ng, R. Ganguly, A. M. P. Moeljadi, H. Hirao, H. S. Soo, *Chem. Sci.* **2015**, 6, 7130-7142.

[117]: S. H. Lim, K. Nahm, C. S. Ra, D. W. Cho, U. C. Yoon, J. A. Latham, D. Dunaway-Mariano, P. S. Mariano, *J. Org. Chem.* **2013**, 78, 9431-9443.
[118]: D. W. Cho, R. Parthasarathi, A. S. Pimentel, G. D. Maestas, H. J. Park, U. C. Yoon, D. Dunaway-Mariano, S. Gnanakaran, P. Langan, P. S. Mariano, *J. Org. Chem.* **2010**, 75, 6549-6562.
[119]: A. M. Mcnally, E. C. Moody, K. Mcneill, *Photochem. Photobiol. Sci.* **2005**, 4, 268-274.
[120]: M. D'auria, R. Ferri, *J. Photochem Photobiol* **2003**, 157, 1-4.
[121]: R. Parthasarathi, R. A. Romero, A. Redondo, S. Gnanakaran, *J. Phys. Chem. Lett.* **2011**, 2, 2660-2666.
[122]: M. Wang, J. Lu, X. Zhang, L. Li, H. Li, N. Luo, F. Wang, *ACS Catal.* **2016**, 6, 6086-6090.
[123]: M. Wang, L. H. Li, J. M. Lu, H. J. Li X. C. Zhang, H. F. Liu, N. C. Luo, F. Wang, *Green Chem.* **2017**, 19, 702-706.
[124]: H. Liu, M. Wang, H. Li, N. Luo, S. Xu, F. Wang, *J. Catal.*, **2017**, 346, 170-179.
[125]: X. Liu, H. Xu, Z. Ma, H. Zhang, C. Wu, Z. Liu, *RSC Adv.* **2016**, 6, 27126-27129.
[126]: J. Zhang, Y. Liu, S. Chiba, T-P. Loh, *Chem. Commun.* **2013**, 49, 11439-11441.
[127]: Y. Yang, H. Fan, J. Song, Q. Meng, H. Zhou, L. Wu, G. Yang, B. Han, *Chem. Commun.* **2015**, 51, 4028-4031.
[128]: Y. Yang, H. Fan, Q. Meng, Z. Zhang, G. Yang, B. Han, *Chem. Commun.* **2017**, 53, 8850-8853.
[129]: M. B. Hocking, *J. Chem. Educ.* **1997**, 74, 9, 1055-1059.
[130]: E. W. Schoeffel, *Pat. US 2598311*.
[131]: F. Cheng, H. Wui, R. D. Rogers, *ACS Sustainable Chem. Eng.* **2014**, 2, 2859-2865.
[132]: G. F. De Gregorio, R. Prado, C. Vriamont, X. Erdocia, J. Labidi, J. P. Hallett, T. Welton, *ACS Sustainable Chem. Eng.* **2016**, 4, 6031-6036.
[133]: A. Aarabi, M. Mizani, M. Honarvar, *Int. J. Biol. Macromol.* **2017**, 94, 345-354.
[134]: V. E.Tarabanko, K. L. Kaygorodov, E. A. Skiba, N. Tarabanko, Y. V. Chelbina, O. V. Baybakova, B. Kuznetsov, L. Djakovich, *J. Wood. Chem. Technol.* **2017**, 37, 43-51.
[135]: V. E. Tarabanko, D. V. Petukhov, G. E. Selyutin, *Kinect. Catal.* **2004**, 45, 569-577.
[136]: S. G. Santos, A. P. Marques, D. L. D. Lima, D. V. Evtuguin, V. I. Esteves, *Ind. Eng. Chem. Res.* **2011**, 50, 291-298.
[137]: T. N. Lugovitskaya, K. N. Bolatbaev, S. S. Naboichenko, *Russ. J. Gen. Chem.* **2013**, 84, 309-312.
[138]: A. W. Pacek, P. Ding, M. Garrett, G. Sheldrake, A. W. Nienow, *Ind. Eng. Chem. Res.* **2013**, 52, 8361-8372.
[139]: T. Voitl, P. R. von Rohr, *ChemSusChem* **2008**, 1, 763-769.
[140]: T. Voitl, P. R. von Rohr, *Ind. Eng. Chem. Res.* **2010**, 49, 520-525.
[141]: T. Voitl, M. V. Nagel, P. R. von Rohr, *Holzforschung* **2010**, 64, 2010.
[142]: Y. Zhao, Q. Xu, T. Pan, Y. Zuo, Y. Fu, Q-X. Guo, *Appl. Catal. A* **2013**, 467, 504-508.
[143]: J. D. P. Araújo, C. A.Grande, A. E. Rodrigues, *Chem. Eng. Res. Des.* **2010**, 88, 1024-1032.
[134]: P. C. Rodrigues Pinto, E. A. Borges da Silva, A. E. Rodrigues, *Ind. Eng. Chem. Res.* **2011**, 50, 741-748.
[145]: P. C. Rodrigues Pinto, E. A. Borges da Silva, A. E. Rodrigues, *Ind. Eng. Chem. Res.* **2010**, 49, 1231-12318.
[146]: K. R. Alunga, Y-Y. Ye, S-R. Li, D. Wang, Y-Q. Li, *Catal. Sci. Technol.* **2015**, 5, 3746-3753.
[147]: P. Gao, C. Li, H. Wang, X. Wang, A. Wang, *Chin. J. Catal.* **2013**, 34, 1811-1815.
[148]: J. Luo, P. Melissa, W. Zhao, Z. Wang, Y. Zhu, *ChemistrySelect* **2016**, 1, 4596-4601.
[149]: J. C. Villar, A. Caperos, F. García-Ochoa, *Wood. Sci. Tchnol.* **2001**, 245-255.
[150]: H. Werhan, J. M. Mir, T. Voitl, P. R. von Rohr, *Holzforschung* **2011**, 65, 703-709.
[151]: C. Díaz-Urrutia, B. B. Hurisso, P. M. P. Gauthier, B. Sedai, R. D. Singer, R. T. Baker, *J. Mol. Catal. A* **2016**, 423, 414-422.
[152]: A. Gaspar, D. V. Evtuguin, C. Pascoal Neto, *Holzforschung* **2005**, 58, 640-649.
[153]: W. Partenheimer, *Adv. Synth. Catal.* **2009**, 351, 456-466.
[154]: A. A. Shamsuri, D. K. Abdullah, *Oxid. Commun.* **2012**, 35, 767-775.
[155]: S. Liu, Z. Shi, L. Li, S. Yu, C. Xiec, Z. Song, *RSC Adv.* **2013**, 3, 5789-5793.
[156]: K. Stärk, N. Taccardi, A. Bössman, P. Wassercheid, *ChemSusChem* **2010**, 3, 719-723.
[157]: C. Bonini, M. D'Auria, *Ind. Crop. Prod.* **2004**, 20, 243-259.
[158]: Q. Xiang, Y. Y. Lee, *Appl. Biochem. Biotechnol.* **2000**, 84, 153-162.
[159]: H. Deng, L. Lin, Y. Sun, C. Pang, J. Zhuang, P Ouyang, Z Li, S. Liu, *Catal Lett* **2008**, 126, 106-111.

[160]: H. Deng, L. Lin, Y. Sun, C. Pang, J. Zhuang, P. Ouyang, J. Li, S. Liu, *Ener. Fuels* **2009**, 23, 19-24.
[161]: H. Deng, L. Lin, S. Liu, *Ener. Fuels* **2010**, 24, 4797-4802.
[162]: F. G. Sales, L. C. A. Maranhão, N. M. Lima Filho, C. A. M. Abreu, *Chem. Eng. Sci.* **2007**, 62, 5386-5391.
[163]: H. Werhan, N. Assmann, P. R. von Rohr, *Chem. Eng. Process.* **2013**, 73, 29-37.
[164]: H. Lange, P. Schiffels, M. Sette, O. Sevastyanova, C. Crestini, *ACS Sustainable Chem. Eng.* **2013**, 73, 29-37.

IB. PMoVx et oxydation aérobie

IB. 1. Introduction

Précédemment, dans le point bibliographique sur le clivage oxydant aérobie de la lignine en molécules plateformes aromatiques, nous avons indiqué que les $PMoV_x$ ont déjà été utilisés pour la dégradation oxydante de la lignine en présence de dioxygène. Excepté dans l'article de DE GREGORIO *et al.* [1], les acides phosphomolybdovanadiques notés $PMoV_x$, sont généralement utilisés en assez grande quantité par rapport à la lignine, voire même en excès. Ces catalyseurs ont fait leur preuve par ailleurs lors de travaux portant sur i) le clivage aérobie de la liaison C-C dans des molécules simples telles que la 2-hydroxyacétophénone [2] et ii) l'oxydation des alcools. Revoir cette littérature nous permettra de mieux appréhender les tests d'oxydation de la lignine et de ses modèles. En effet, ceci pourra donner une idée de comment agit le catalyseur sur les différents groupements présents sur la lignine.
Dans cette partie, un état des lieux sur les méthodes de caractérisation de la structure des $PMoV_x$ de KEGGIN est réalisé. Nous nous focaliserons ensuite sur l'oxydation aérobie de l'alcool benzylique vu que la lignine contient généralement des fonctions alcool secondaire en α d'un noyau aromatique.

IB. 1 1. Généralités sur les polyoxométallates

La toute première synthèse d'un polyoxométallate (POM) par BERZELIUS remonte à 1826 [3]. Il s'agissait du phosphomolybdate d'ammonium connu aujourd'hui sous la formule $(NH_4)_3PMo_{12}O_{40}$, obtenu par ajout d'un excès de molybdate d'ammonium dans de l'acide phosphorique. Mais, il a fallu attendre les travaux de MARIGNAC [4] qui aboutirent à la découverte de l'acide silicotungstique ($H_4SiW_{12}O_{40}$) en 1862 pour connaître les proportions des éléments constituant les POM. Néanmoins, la structure de ces composés reste à élucider. PAULING a fait un pas dans cette direction en 1929 en suggérant la présence d'octaèdres WO_6 dans l'acide silicotungstique [5]. Finalement, la structure complète fut découverte par KEGGIN en 1933 par analyse DRX de l'acide phosphotungstique ($H_3PMo_{12}O_{40}$) [6]. Tous les POM mentionnés sont anioniques et ont pour formule générale $XM_{12}O_{40}^{n-}$. Ces POM dits de KEGGIN sont constitués d'un tétraèdre XO_4 au centre de l'édifice où X est l'hétéroatome central et d'un réseau de 12 d'octaèdres MO_6 où M désigne un addenda, un métal à haut degré d'oxydation.

Depuis ces travaux, de nombreuses autres structures ont été découvertes. Parmi elles, on peut citer celle de DAWSON [7] ainsi que des POM de KEGGIN lacunaires [8]

généralement instables. Comme indiqué dans l'introduction générale, le catalyseur envisagé est un POM de KEGGIN. Nous nous intéresserons donc principalement à ces derniers et plus particulièrement aux molybdovanadophosphates de KEGGIN de formule $PMo_{12-x}V_xO_{40}^{(3+x)-}$. Par la suite, ils seront notés $PMoV_x$.

IB. 1.2. Structure et composition des POM de KEGGIN

La structure générale de KEGGIN est dessinée sur la Figure 1a. Les octaèdres MO_6 se regroupent en triades M_3O_{13} *via* les atomes d'oxygène notés O_e (e = *edge-sharing*) comme sur la Figure IB. 1b. Les 4 triades se lient par les atomes d'oxygène O_c (c = *corner sharing*). Les atomes d'oxygène restants sont les atomes d'oxygène terminaux notés O_t (t = *terminal*). On peut donc dénombrer 4 O_a, 12 O_e, 12 O_c et 12 O_t. Enfin, il reste les 4 atomes d'oxygène O_a qui sont liés à l'hétéroatome central X (Figure 1c) [9, 10]. Les $PMoV_x$ sont composés de métaux dont les configurations électroniques sont en d^0 ou en d^1. Par exemple, dans les $PMoV_x$ sous forme oxydée, les métaux ont leur couche d vide. Ils ont donc un degré d'oxydation élevé (+VI pour le molybdène et +V pour le vanadium) ce qui explique leur pouvoir oxydant.

Figure IB. 1a : Structure générale de l'anion de KEGGIN

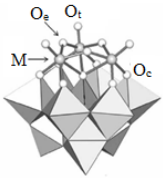

Figure IB. 1b : Structure des groupements $[M_3O_{13}]$

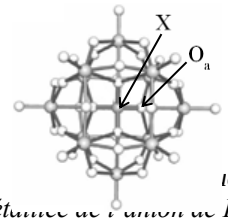

ıcture détaillée de l'anion de KEGGIN

Déjà dans le cas de l'acide phosphomolybdique, il existe 5 isomères théoriques de la structure de KEGGIN. Parmi eux, on trouve l'isomère α (Figure IB. 1a) qui est le plus souvent observé. L'isomère β est obtenu par rotation de 60° d'une des triades M_3O_{13} sur l'axe X-O. Ceci a pour conséquence un changement de symétrie de T_d pour α vers C_{3v} pour β. Ces isomères ont des structures différentes, ce qui peut aboutir à des propriétés différentes [11].

La DRX permet de montrer la structure de KEGGIN notamment par l'apparition de pics autour de $2\theta = 9°$. Ces pics n'apparaissent pas dans le cas des oxydes de départ MoO_3 (JCPDS 05-0508) et V_2O_5 (JCPDS 9-387). En fait, les $PMoV_x$ sont obtenus sous une forme hydratée. Leur formule réelle est donc : $H_{3+x}PMo_{12-x}V_xO_{40}$, nH_2O où n représente l'indice d'hydratation. Ce dernier a une forte influence sur leur structure cristalline (Tableau IB. 1).

Tableau IB. 1: Evolution de la structure des PMoVx avec la température

Température	n	Géométrie
A froid	30-36	Cubique
ambiante	12-13	Triclinique
60°C	6-8	Cubique
150-200°C	0	Quadratique

L'estimation de l'indice d'hydratation peut être affinée par une analyse en ATG. Il y a deux pertes de masse. La première est liée à l'eau d'hydratation alors que la deuxième est liée à l'eau de constitution. La perte d'eau d'hydratation se fait en plusieurs étapes avec changement de structure cristalline comme indiqué dans le tableau IB. 1 [12]. Elle a lieu jusqu'aux alentours de 200°C. La DRX ne permet pas de conclure clairement sur la présence du vanadium. Il est donc judicieux de compléter cette dernière par une analyse par RMN du ^{31}P (abondance isotopique : 100%, spin 1/2) et du ^{51}V (abondance isotopique 99,75%, spin 5/2). En RMN dans D_2O, on peut trouver des signaux caractéristiques autour de -3 ppm en ^{31}P et autour de -530 ppm en ^{51}V. Pour x = 0 et x = 1, il y a un pic principal en ^{31}P et en ^{51}V comme observé par NOMIYA *et coll* [13] ainsi que par PARKER Jr et CAVANI plus récemment [14]. Par contre, pour une teneur en vanadium plus élevée, plusieurs isomères sont présents, ce qui fait que l'on observe plusieurs signaux différents en ^{31}P et en ^{51}V. En effet, pour x = 2, il y a déjà 5 isomères différents. PETTERSSON est parvenu à identifier ces derniers par RMN ^{31}P et ^{51}V en solution (Tableau IB. 2) [15].

Les déplacements chimiques sont donc aussi influencés par le pH. Un désavantage est que pour x élevé, les spectres peuvent vite se révéler complexes. De plus, il est possible de montrer la présence de composés à 1 et 2 atomes de vanadium tels que les cations pervanadyle et de composés lacunaires, du phosphomolybdate de DAWSON qui peut être vu comme un produit de « dimérisation » de la structure de KEGGIN ainsi que la présence de l'acide phosphorique qui donne un pic à 0 ppm (pH = 0-0,85).

La structure à l'état solide des POM peut être caractérisée par XPS [16]. Le vanadium (V) donne des pics à 525 (V $2p_{1/2}$) et à 518 (V $2p_{3/2}$) eV alors que le molybdène (VI) donne des pics à 236 (Mo $2p_{3/2}$) et à 233 (Mo $2p_{5/2}$) eV. Ceci a permis à SHE *et al* de montrer la délocalisation électronique du vanadium au molybdène et au phosphore. La nature des liaisons peut être caractérisée par FT-IR et la spectroscopie RAMAN (Tableau IB. 3), des techniques simples à mettre en œuvre. En effet, les liaisons entre chaque type d'atome d'oxygène et les addenda donnent des signaux bien distincts en FT-IR et en spectroscopie RAMAN comme indiqué dans le Tableau 3 [17-18]. D'ailleurs, McGARVEY est aussi parvenu à identifier en

spectroscopie RAMAN un signal à 925 cm^{-1} qui correspond à l'espèce lacunaire $[PMo_{11}O_{39}]^{7-}$ [17].

Tableau IB. 2: Signaux observés pour $PMoV_2$ en solution dans D_2O [13, 15]

Formule de l'ion	Type of POM	Isomère	pK_a	Déplacement chimique (ppm) ^{31}P	^{51}V
$[PMo_{10}V_2O_{40}]^{5-}$	KEGGIN	α-1,4	-	-3,65	-515,7
		α-1,2	-	-3,63	-531,8
		α-1,5	-		-533,8
		α-1,6	-	-3,60	534,5
		α-1,11	-		
		β-4,10	-	-3,43 ; -3,51	
		β-4,11	-		534,7
$H[PMo_{10}V_2O_{40}]^{4-}$		α-1,4	0,48	-2,95	-543,2
		α-1,2	0,26	-3,09	-544,1
		α-1,5	0,26		-541,9
		α-1,6	0,04	-3,16	-544,1
		α-1,11	0,04		
		β-4,10	0,35	-3,17 ; 2,98	
		β-4,11	0,35		-546,4
$[PMo_{11}VO_{40}]^{4-}$		n. i.	-	-3,9	-532
$[P_2M_{18}O_{62}]^{6-}$	DAWSON	n. i.	-	-2,5	n. i.
$[PMo_{11}O_{39}]^{7-}$	Monolacunary KEGGIN	n. i.	-	-1,3	-
$[PMo_9O_{34}]^{9-}$	Trilacunary KEGGIN	n. i.	-		-
VO_2^+	-	n. i.	n. i.	-	-544
H_3PO_4	-	n. i.	2,14	0	-

Tableau IB. 3 : Attribution des pics observés en FT-IR et en RAMAN (Refs 17-18)

Liaison	FT-IR (cm^{-1})	RAMAN (cm^{-1})
M-O_a	n. i.	240
M-O_c-M	780	600
M-O_e-M	870	814
M=O_t	960	990
P-O_a	1060	n. i.

- *Composition élémentaire*

Les méthodes précédentes donnent un indice qualitatif sur la présence des éléments qui composent le $PMoV_x$. Pour obtenir des informations quantitatives, il faut donc déterminer la composition élémentaire. Une technique qui vient naturellement est la spectrométrie à couplage inductif ou ICP (Inductively Coupled Plasma). Le désavantage notable de cette technique est qu'elle est destructive. Pour pallier ceci, il est possible d'utiliser la fluorescence des rayons X (FRX), qui requiert moins de préparation et donc plus simple à mettre en œuvre. Enfin, la dernière information en ce qui concerne la composition élémentaire est l'acidité des $PMoV_x$. Un grand classique est le dosage pH-métrique par une solution de soude. Cette technique est destructive surtout que le complexe de KEGGIN est instable à pH basique. L'analyse thermogravimétrique (ATG) présente également un intérêt. Plus précisément, la deuxième perte en masse permet d'obtenir x [19-20]. L'eau de constitution fait partie intégrante de la structure

primaire et est donc bien plus liée au $PMoV_x$ que l'eau d'hydratation. Plus la valeur de x est élevée, plus l'eau de constitution part tôt, comme sur la Figure IB. 2 comme montré par VILLABRILE *et al*, ce qui est lié à une plus grande mobilité du vanadium [20]. Ceci a été prévu par l'étude quantique mené par JANIK *et al* [21]. L'énergie de formation de lacunes suit cet ordre : $PMoV_2$ < $PMoV_1$ << PMo_{12}. Pour $PMoV_2$, la lacune se forme préférentiellement entre deux atomes de vanadium. La proportion en vanadium peut être aussi déterminée par voltamétrie.

Figure IB. 2: Allures des courbes d'ATG en fonction de x (Réf 21)

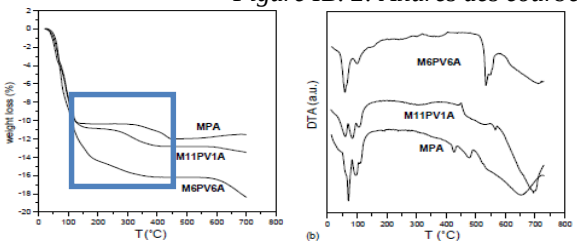

MPA: $H_3PMo_{12}O_{40}$
M**11**PV**1**A: $H_4PMo_{11}V_1O_{40}$
M_6PV_6A: $H_9PMo_6V_6O_{40}$

La spectrophotométrie UV-Visible peut donner des indices sur le nombre de vanadium comme montré par SHE *et al.* Ces POM étaient en solution (à 2 mM) dans l'acétonitrile. Le maximum d'absorption dans le visible, plus précisément dans le bleu, se décale vers la droite quand x augmente [16].

- *Spéciation du vanadium*

Dans les paragraphes précédents ont été décrites la caractérisation de la structure de l'anion de KEGGIN puis la détermination de la proportion des éléments, mais il peut être nécessaire de déterminer la proportion des états d'oxydation du vanadium qui est généralement le site actif pour l'oxydation [22], notamment durant des tests d'oxydation. Le vanadium (+V) capte un électron, ce qui donne du vanadium (+IV) paramagnétique actif en RPE. Aussi, le $PMoV_x$ oxydé étant orange alors que la forme réduite est bleue si bien que la spectrophotométrie UV-Visible peut également apporter des informations sur l'état d'oxydation du vanadium [16]. Par ailleurs, plus le $PMoV_x$ contient de vanadium, plus le potentiel rédox est élevé [23, 24].

IB. 2. Applications des $PMoV_x$ de KEGGIN en catalyse d'oxydation

Un des $PMoV_x$ qui a beaucoup d'occurrences dans la littérature est $PMoV_2$. Ce dernier peut être utilisé seul ou associé à un co-catalyseur comme le palladium pour de multiples réactions telles que l'oxydation des alcools [25], de méthylarènes comme le toluène [26] donnant du benzaldéhyde ou de 5-HMF (issu de la cellulose) en anhydride maléique [27]. $PMoV_2$ a également été utilisé pour l'hydroxylation du benzène en phénol [28] ou pour la désulfurisation de la lignine extraite par les procédés Kraft ou bisulfite [29]. Aussi, les $PMoV_x$ se sont montrés être des catalyseurs efficaces pour des réactions qui nécessitent un acide fort telles l'acylation [30] du phénol ou encore l'estérification d'alcools [31].

Vu la structure de la lignine, on regardera plus particulièrement les dérivés de l'alcool benzylique. Dans la suite, nous visons à étudier les cas de substrats qui ont des structures plus complexes pour aller progressivement vers la lignine. Généralement, les articles sont sortis entre 2000 et 2019.

IB. 2.1. Oxydation de l'alcool benzylique et dérivés

- *Test de catalyse en phase aqueuse*

Les $PMoV_x$ et notamment le $PMoV_2$ sont solubles dans l'eau. Ils peuvent donc être utilisés pour l'oxydation d'alcools dans l'eau et ainsi éviter d'utiliser des solvants organiques. Par exemple, HUANG *et al* [32] ont synthétisé des nanoparticules d'or et y ont fixé des cations 1,3,5-tris [(3-methylimidazolio)methyl]-2,4,6-trimethylbenzene permettant ainsi d'ancrer les anions issus du $PMoV_2$ (1 mol% par rapport au substrat). Les entités en résultant, notées $Au@IL@PMoV_2$, sont amphiphiles de par la présence du spacer et de l'anion de KEGGIN. Elles ont été utilisées comme catalyseurs pour l'oxydation aérobie de l'alcool benzylique (100 mM) en benzaldéhyde noté **9**H (Tableau IB. 4, entrée 1a-d) dans l'eau.

$Au@IL@PMoV_2$ catalyse efficacement l'oxydation de l'alcool benzylique et de ses dérivés en aldéhyde/cétone sans suroxydation (entrée 1d, rendement en benzaldéhyde > 99%). Le $PMoV_2$ seul (entrée 1a), puis associé au cation considéré avec (entrée 1c) et sans nanoparticules d'or (entrée 1b) ont été testés pour servir de témoins. Dans aucun de ces cas, le rendement n'a pas dépassé 76%, ce qui suggère une synergie entre les différents éléments constitutifs de $Au@IL@PMoV_2$, à savoir l'or, le bras espaceur et $PMoV_2$. Des bulles d'air générées par l'agitation se forment durant la réaction. D'après les auteurs, le catalyseur agit à l'interface entre les bulles d'air et l'eau qui contient le réactif. D'autres substrats tels que 1-

phényléthanol (entrée 2), l'alcool *p*-méthoxybenzylique (entrée 3) ont été testés. Le rendement en produit carbonylé obtenu est au minimum de 98%, ce qui démontre l'activité du catalyseur sur les alcools primaires et secondaires et sa sélectivité pour les aldéhydes et cétones. Des tests de recyclage ont été réalisés. Les nanoparticules ont été récupérées par centrifugation. Après 5 recyclages, le rendement en benzaldéhyde est de 90% (*v.s.* > 99% pour le catalyseur frais). Les auteurs ont expliqué cette perte d'activité par l'agglomération des nanoparticules durant la centrifugation.

Tableau IB. 4: Activité des $PMoV_x$ pour l'oxydation de l'alcool benzylique en phase aqueuse

Entrée	Substrat	Catalyseur	TON	TOF (h^{-1})	Produits (rdt en %)	Réf
1a	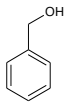 Alcool benzylique	$[H^+]_5[PMo_{10}V^{5+}_2O_{40}^{5-}]$	52	17	**9**H: 52	
1b		$[H^+]_5[PMo_{10}V^{5+}_2O_{40}^{5-}]/IL^b$	68	23	**9**H: 68	
1c		$[H^+]_5[PMo_{10}V^{5+}_2O_{40}^{5-}]/IL^b$ + Au NPs^c	76	25	**9**H: 76	
1d		$[H^+]_5[PMo_{10}V^{5+}_2O_{40}^{5-}]/IL^b$/Au NPs	99 33^c	33 30^c	**9**H: > 99 **10**H: 0 **9**H: 90^c	
2	 1-phenyl-ethanol	$[H^+]_5[PMo_{10}V^{5+}_2O_{40}^{5-}]/IL^b$/Au NPs	99	33	**18**H: > 99	32
3	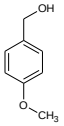 Alcool *p*-méthoxy-benzylique	$[H^+]_5[PMo_{10}V^{5+}_2O_{40}^{5-}]/IL^b$/Au NPs	98	33	**13**H: 98 **14**H: 0	

Substrat 100 mM, O_2 atm, $PMoV_2$ 1 mol%, eau, 75% conversion et produits mineurs: n. i. [a]Charge du $PMoV_x$ par rapport au substrat; [b] IL= 1,3,5-tris-[(3-methylimidazolio)methyl]-2,4,6-trimethylbenzene; [c]Stabilisé au polyvinylpyrrolidone; [d]Après 4 recyclages ; **9**H = benzaldéhyde; **10**H = acide benzoïque; **13**H = *p*-méthoxybenzaldéhyde; **14**H = acide *p*-méthoxybenzoïque; **18**H = acétophénone

- *Test de catalyse homogène dans des solvants binaires eau-alcool*

Le procédé idéal devrait effectivement être mis en œuvre dans l'eau, un solvant disponible à grande échelle et non dangereux pour l'homme et respectueux de l'environnement. Cependant, d'une part de nombreux substrats organiques y sont très peu solubles et d'autre part, O_2 présente une mauvaise solubilité dans ce solvant, ce qui fait du transfert un facteur limitant. En conséquence, les travaux reportés dans la littérature ont plus tendance à faire intervenir des solvants organiques. Une autre piste consiste à ajouter un co-solvant avec l'eau qui permet de mieux solubiliser le substrat. Un exemple est donné par KRICKL *et al* [33]. Ces derniers ont testé $PMoV_2$ (2 mol%) pour l'oxydation de l'alcool benzylique (100 mM) dans un mélange binaire, soit d'eau et d'éthanol, soit d'eau et de ^{t}BuOH (Tableau IB. 5a, entrées 1a-c). Le milieu réactionnel a été illuminé par une LED bleue (455 nm, 1.12 W) pendant 16 h à 25°C. $PMoV_2$ absorbe la lumière issue de la LED et cette dernière remplace l'apport thermique. Les auteurs

ont montré que l'irradiation est indispensable à la formation du benzaldéhyde (**9**H). En ce qui concerne le premier binaire, l'ajout d'éthanol ne change rien à la structuration du mélange ternaire eau-EtOH-alcool benzylique. La conséquence principale est une meilleure solubilité du dioxygène, ce qui améliore le transfert du gaz et logiquement le rendement en benzaldéhyde. Dans le cas du mélange eau-^{t}BuOH, les auteurs de l'article ont montré que le solvant organique apporte une structuration au système eau-solvant organique-substrat. En d'autres termes, ceci peut donner lieu à la création de deux pseudo-phases. L'une d'elles serait riche en eau et solubiliserait préférentiellement le $PMoV_x$ alors que la seconde serait riche en *tertio*-butanol et contiendrait le substrat et le dioxygène. Ceci peut être défavorable à la réaction malgré une solubilité du dioxygène plus élevée (entrées 1a-b) pour cause d'un contact plus difficile entre les composantes du système catalytique. Par exemple, le rendement en **9**H est plus faible dans H_2O-^{t}BuOH 10-90 (12%) que dans H_2O-^{t}BuOH 38-62 (9%). Par conséquent, le contact entre le substrat et le catalyseur se fait moins bien, ce qui provoque une diminution du rendement en benzaldéhyde. Il a été démontré qu'il fallait que la fraction volumique en tertio-butanol soit supérieure à 94% pour avoir un impact positif sur le rendement en benzaldéhyde (entrée 5c). Il atteint alors un maximum de 22%. Il faut noter que les auteurs ont limité l'avancement de la réaction pour s'intéresser davantage à l'impact de la structuration du solvant. Des tests avec une durée de 72 h ont été réalisés avec les mêmes proportions de solvants. Le rendement en benzaldéhyde (29-32%) n'est que très peu impacté par la structuration du mélange réactionnel ainsi que par la solubilité du dioxygène.

- *Tests de catalyse homogène dans des solvants organiques*

La plupart des équipes ont testé des solvants organiques purs, plutôt polaires dans lesquels les $PMoV_x$ sont également solubles comme l'acétonitrile ou le méthanol. D'autres exemples sont les polyéthylène glycols (PEG). Ces derniers ont été testés par HAIMOV et NEUMANN [34] pour l'oxydation de l'alcool benzylique (1 M) sous 2 bar de dioxygène en présence de $PMoV_2$ (2 mol%) à 100°C pendant 2 h (Tableau IB. 5a, entrée 2). Une conversion complète en benzaldéhyde a été obtenue, ce qui montre que $PMoV_2$ est bien actif pour l'oxydation du benzaldéhyde dans le PEG-200. De la même manière, l'alcool *p*-méthylbenzylique a aussi été quantitativement oxydé en *p*-méthylbenzaldéhyde (Tableau IB. 5c, entrée 1). En revanche, en ce qui concerne le 1-phényléthanol (Tableau IB. 5b, entrée 1), le catalyseur est plus sélectif pour la déshydratation en styrène (66%), ce qui est lié à son caractère acide. La déshydratation est une réaction secondaire qu'il faudra prendre en compte

pour le cas des modèles de la lignine. De plus, on peut déjà remarquer une réaction de clivage de liaison C-C par la formation du benzaldéhyde (9%), mais dans une plus faible mesure.

Les $PMoV_x$ ont aussi été testés en association avec des co-oxydants. Par exemple, BEN-DANIEL *et al* [35] ont utilisé $PMoV_2$ (1 mol%) en association avec le TEMPO (3 mol%) pour l'oxydation de l'alcool benzylique (6,7 M) dans l'acétone (100°C) sous 2 bar de dioxygène pendant 6 h (Tableau IB. 5a, entrées 3a-b). En présence de TEMPO, le rendement en benzaldéhyde atteint presque 100% alors qu'avec $PMoV_2$ seul, sa valeur a été divisée par plus que 10. Des études cinétiques ont montré que la vitesse de la réaction ne dépend ni de la pression du dioxygène, ni de la concentration en substrat. En conséquence, les seuls facteurs qui influent sur la cinétique sont les concentrations en catalyseur et en TEMPO ainsi que la température. Le 1-phényléthanol a été oxydé dans les mêmes conditions en présence de TEMPO. Le rendement en acétophénone a atteint 98% et le styrène n'a pas été détecté. Le mécanisme proposé par les auteurs est décrit sur la Figure IB. 4

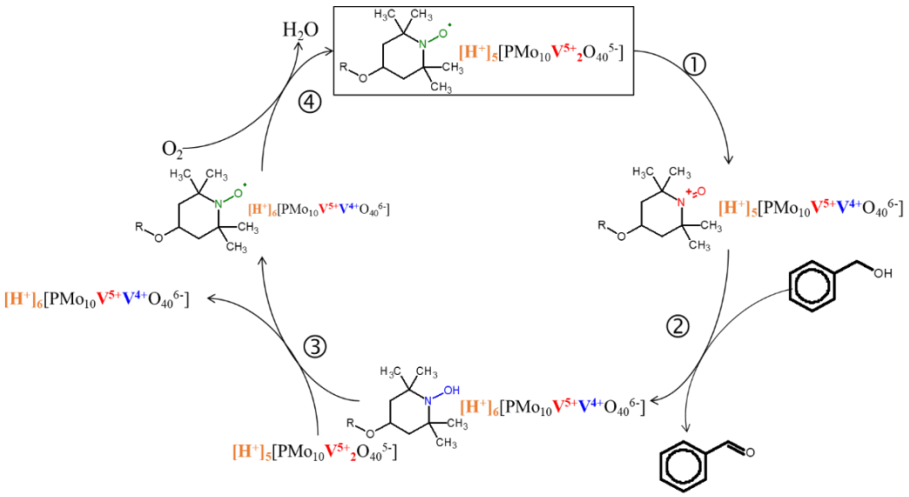

Figure IB. 3: Mécanisme d'oxydation de l'alcool benzylique en présence d'un système $PMoV_2$-TEMPO modifié [35]

Le vrai oxydant pour l'oxydation du substrat est le TEMPO oxydé par le $PMoV_2$ (étape ①). Il est réduit en hydroxylamine par le substrat (étape ②). La régénération du catalyseur est réalisée dans un premier temps par le $PMoV_2$ oxydé (étape ③) puis par le dioxygène pour le $PMoV_2$ (étape ④).

Un autre exemple de co-catalyseur a été donné par HUANG *et al.* [36] qui ont testé l'anion $PMoV_2$ (0,625 mol%) associé à un complexe cationique du palladium (1,25 mol%) pour oxyder l'alcool benzylique à 0,5 M dans le DMSO à 130°C sous atmosphère de dioxygène pendant 8 h (Tableau IB. 5a, entrée 4a). Le sel de départ avait pour formule générale $[Pd(dpa)(DMSO)_2^{2+}]_2[HPMo_{10}V_2O_{40}]^{4-}$ où dpa représente la 2,2'-dipyridylamine. La

conversion a atteint 99,8% et la sélectivité en benzaldéhyde. Des tests de recyclage ont été réalisés, ce qui est plutôt rare dans les tests en catalyse homogène. Ils ont consisté à ajouter du substrat frais au milieu réactionnel. Ceci a été répété à trois reprises. Le catalyseur ne s'est pas montré moins actif. Au contraire, la réaction est devenue quantitative en 6 h au lieu de 8 h (Tableau IB. 5a, entrée 4b). Le catalyseur est donc devenu plus actif. D'après les auteurs, il se serait transformé en une autre entité, $[Pd^{+II}(dpa)_2\{V^{+IV}O(DMSO)_5\}][PMo_{12}O_{40}]^{3-}$, où le vanadium a été éjecté du POM. Ils ont montré que le palladium, le vanadium et le phosphomolybdate sont tous les trois actifs pour l'oxydation et opèrent en synergie (voir Fig. IB. 5). Lorsque le palladium et l'ion phosphomolybdate sont isolés, la conversion est au mieux divisée par 2,7 (36.9% pour le phosphomolybdate et 18.3% pour le palladium). Dans le cas du complexe $[Pd(dpa)(DMSO)_2]_2^{2+}[HPMo_{12}O_{40}]^{4-}$, la conversion atteint 99%, mais après 10 h au lieu de 6.

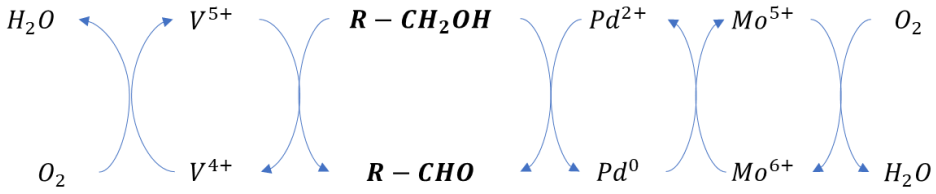

Figure IB. 4: Mécanisme simplifié de l'oxydation d'alcools catalysé par $[Pd^{+II}(dpa)_2\{V^{+IV}O(DMSO)_5\}][PMo_{12}O_{40}]^{3-}$

En outre, un des produits détectés est le diméthylsulfolane, $(CH_3)_2SO_2$, obtenu par oxydation du DMSO, ce qui montre qu'ici le solvant ne joue pas le rôle d'oxydant au contraire de ce qu'ont décrit NEUMANN *et al* [37]. Le 1-phényléthanol (Tableau IB. 5b, entrée 3) et l'alcool *p*-méthylbenzylique (Tableau IB. 5c, entrée 2) ont été oxydés dans les mêmes conditions et l'acétophénone et le *p*-méthoxybenzaldéhyde ont été obtenus avec des rendements de 98 et 96% respectivement.

En 1991, NEUMANN et LEVIN [38] ont déposé $PMoV_2$ sur du charbon actif (10 wt% de $PMoV_2$). Le matériau qui en a résulté s'est montré efficace pour l'oxydation de l'alcool benzylique (0.33 M dans le toluène) en benzaldéhyde sous air à 100°C pendant 22 h avec une charge apportée en $PMoV_2$ de 1 mol%. Dans le cas des dérivés de l'alcool *p*-hydroxybenzylique, la condensation oxydante est la réaction majoritaire conduisant à la formation d'un goudron par polymérisation rendue possible par la présence du groupement phénol. Noter que dans les conditions utilisées par les auteurs, en partant de l'alcool *p*-méthylbenzylique (Tableau IB. 5c, entrées 3a-b), le $PMoV_2$ sous forme acide, non supporté (entrée 3a), conduit plutôt à la formation au 4,4'-diméthyldibenzyléther (rendement : 95%), ce

qui montre que le caractère acide peut parfois s'exprimer aux dépens du pouvoir oxydant du $PMoV_2$. Cependant, les sels non acides se sont montrés inactifs pour l'oxydation de l'alcool benzylique et de l'alcool *p*-méthylbenzylique en aldéhydes (entrée 3b). De plus, il est apparu que le charbon actif est le seul support qui soit adapté à la conversion de l'alcool benzylique en benzaldéhyde. D'après les auteurs, le charbon joue le rôle d'un support non innocent. Pour le démontrer, ils ont associé $PMoV_2$ à des quinones (*p*-chloranil *i.e.* 2,3,5,6-tétrachloro-1,4-benzoquinone) en solution. Ces dernières sont intrinsèquement des oxydants qui peuvent servir de co-catalyseurs pour l'oxydation des alcools [39] et le charbon actif comporte des fonctions quinones. Cela a été vérifié pour l'oxydation de dérivés de l'alcool benzylique (Tableau 5a, entrées 5a-b). Deux méthodes ont été testées. La première implique le catalyseur sous forme d'un sel de sodium dans un mélange biphasique eau-décaline porté à 90°C. L'intérêt principal est que la séparation du catalyseur est facile vu qu'il est insoluble dans la phase organique contrairement au substrat et au produit d'oxydation. La seconde, plus classique, implique le catalyseur sous forme d'un sel d'ammonium en solution dans l'acétonitrile à 110°C. En milieu biphasique, le rendement en benzaldéhyde a été de 81% (entrée 5a) alors qu'en milieu monophasique, le rendement tombe à 62% (entrée 5b). L'approche impliquant le sel de sodium apparaît donc la plus efficace malgré une température de travail plus basse. Aucune explication n'a été clairement formulée par les auteurs. Dans le cas du milieu biphasique, on peut supposer qu'une catalyse par transfert de phase a lieu. La même tendance s'est dégagée pour l'alcool *p*-méthoxybenzylique (Tableau IB. 5d, entrées 3a-b) et l'alcool *p*-méthylbenzylique (Tableau IB. 5c, entrées 3a-b) alors que pour le 1-phényléthanol (Tableau IB. 5b, entrées 3a-b) la différence entre les deux méthodes est plus faible. Le mécanisme réactionnel est similaire au cas avec le TEMPO mis à part que le vrai oxydant est un intermédiaire semi-quinone-$[PMo_{10}V^{4+}V^{5+}O_{40}]^{(6+x)-}$ [40].

Dans les exemples avec les quinones notamment, le catalyseur est en solution. Or, il est judicieux, de faciliter sa séparation au moins en fin de réaction afin de le recycler plus aisément. De plus, les composés du vanadium (V) étant connus pour avoir une certaine toxicité [41], il faut veiller à les séparer le plus efficacement possible des produits désirés. Une solution consiste à procéder par une hétérogénéisation post-réaction.

Tableau IB. 5a: Activité des $PMoV_x$ pour l'oxydation aérobie de l'alcool benzylique et du benzaldéhyde en solution

Entrée	Substrat	Conc. (mM)	Catalyseur Formule	Charge[a] (mol%)	Co-catalyseur (charge[a] en mol%)	Solvant	Oxydant (press)	T (°C)	t (h)	Conv. (%)	TON	TOF (h^{-1})	Produits (rdt en %) Oxydation	Produits (rdt en %) Catalyse acide	Réf
1a						Eau-^{t}BuOH[b] 38-62 v/v				n. i.	6		**9**H: 12		
1b		100	$[H^+]_5[PMo_{10}V^{5+}_2O_{40}^{5-}]$	2	-	Eau-^{t}BuOH[b] 10-90 v/v	O_2 (atm, bullage)	25	16	n. i.	4	< 1	**9**H: 8	n. i.	33
1c						Eau-^{t}BuOH[b] 6-94 v/v				n. i.	11		**9**H: 22		
2		1000				PEG-200	O_2 2	100	16	≈100	50	3	**9**H: 100	0	34
3a		6700	$[H^+]_5[PMo_{10}V^{5+}_2O_{40}^{5-}]$	1	TEMPO (3)	Acétone	O_2 2	100	6	n. i.	100	17	**9**H: 99,6	n. i.	35
3b					-					n. i.	8	1	**9**H: 8,4		
4a		500	$[\{Pd\}^{2+}]_2[H^+]_1[PMo_{10}V^{5+}_2O_{40}^{5-}]$	0.6	$\{Pd\}^{2+}$[b] (1.25)	DMSO	O_2 Atm	130	8	≥ 99	160	20	**9**H: 97	tr.	
4b[c]									6		220	26	**10**H: tr.		
5a	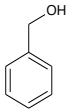	7,5	$[Na^+]_5[PMo_{10}V^{5+}_2O_{40}^{5-}]$	1.5	*p*-chloranil (5)	Décaline-eau 1.1 v/v (biphasique)	O_2 Atm	90	18	n. i.	54	3	**9**H: 81	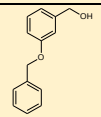 < 4	36
5b		15	$[Bu_4N^+]_5[PMo_{10}V^{5+}_2O_{40}^{5-}]$			MeCN		110		n. i.	41	2	**9**H: 62	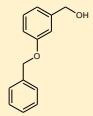 < 3	
6a[e]		2	$[H^+]_4[PMo_{10}V^{5+}_1O_{40}^{4-}]$	0.05	-	DMSO	Air (Atm)	150	1,7	78	1400	840	**9**H: 70	n. i.	42
6b[f]			$[Coumarin]_3[H^+]_1[PMo_{10}V^{5+}_1O_{40}^{4-}]$							99	1980	1200	**9**H: 99	n. i.	
6c[g]			$[Coumarin]_4[PMo_{10}V^{5+}_1O_{40}^{4-}]$							45	900	540	**9**H: 45	n. i.	
7a		200	$[H^+]_3[PMo_{12}V^{5+}_0O_{40}^{3-}]$	2,7	-	MeCN	O_2 (Atm)	80	20	n. i.	-	< 1	**9**H: 6	n. i.	40
7b			$[H^+]_{3,8}[PMo_{11,2}V^{5+}_{0,8}O_{40}^{3,8-}]$	2,8	-			80	12		12	21	**9**H: 35		
8	**9**H	1000	$[H^+]_5[PMo_{10}V^{5+}_2O_{40}^{5-}]$	0,4	-	AcOH-H_2O 9-1 v/v	O_2 (Atm)		24	97	240	10	**10**H: 97	n. i.	55

[a]Charge par rapport au substrat; [b]Proportions volumiques calculées à partir de fractions molaires ; [c]Après 3 recyclages ; [d]{Pd} = [Pd(dpa)(DMSO)$_2$], dpa = 2,2'-dipyridylamine ; [e]S_{BET} = 9 m²/g; [f]S_{BET} = 31m²/g; [e]S_{BET} = 26 m²/g ; **9**H = benzaldéhyde; **10**H = acide benzoïque.

Tableau IB. 5b: Activité des $PMoV_x$ pour l'oxydation aérobie du 1-phényléthanol en solution

Entrée	Substrat	Conc. (mM)	Catalyseur Formule	Charge[a] (mol%)	Co-catalyseur (charge[a] en mol%)	Solvant	Press. O_2 (bar)	T (°C)	t (h)	Conv. (%)	TON	TOF (h^{-1})	Produits (rdt en %) Oxydation	Catalyse acide	Réf
1	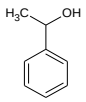 1-phényl-éthanol	20	$[H^+]_5[PMo_{10}V^{5+}_2O_{40}^{5-}]$	2	-	PEG-200	O_2 2	100	16	≈100	17	1	**18**H: 26 **9**H: 8	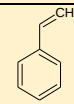 66	34
2		6700	$[H^+]_5[PMo_{10}V^{5+}_2O_{40}^{5-}]$	1	TEMPO (3)	Acétone	O_2 2	100	6	n. i.	98	16	**9**H: 98	n. i.	35
3		500	$[\{Pd\}^{2+}]_2[H^+]_1[PMo_{10}V^{5+}_2O_{40}^{5-}]$	0,6	$\{Pd\}^{2+,b}$ (1.25)	DMSO	O_2 Atm	130	8	98	160	19	**18**H: 93	n. i.	36
4a		7,5	$[Na^+]_5[PMo_{10}V^{5+}_2O_{40}^{5-}]$	1,5	*p*-chloranil (5)	Décaline-eau 1-1 v/v (biphasique)	O_2 Atm	90	18	n. i.	56	3	**18**H: 87	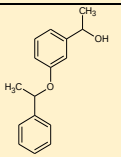 < 4	37
4b		15	$[Bu_4N^+]_5[PMo_{10}V^{5+}_2O_{40}^{5-}]$			MeCN		110		n. i.	53	2	**18**H: 80	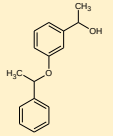 < 4	

[a]Charge par rapport au substrat; [b]$\{Pd^{2+}\}$ = $[Pd(dpa)(DMSO)_2]^{2+}$; **9**H = benzaldéhyde, **13**H = *p*-méthoxybenzaldéhyde; **14**H = acide *p*-méthoxybenzoïque; **18**H = acétophénone; *p*-$MePhCH_2OH$ = Alcool *p*-méthoxybenzylique; *p*-PhCHO = *p*-méthoxybenzaldéhyde.

Tableau IB. 5c : Activité des PMoV$_x$ pour l'oxydation aérobie de l'alcool p-méthylbenzylique en solution

Entrée	Substrat	Conc. (mM)	Catalyseur Formule	Charge[a] (mol%)	Co-catalyseur (charge[a] en mol%)	Solvant	Press. O_2 (bar)	T (°C)	t (h)	Conv. (%)	TON	TOF (h^{-1})	Produits (rdt en %) Oxydation	Catalyse acide	Réf
1	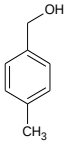 Alcool *p*-méthyl-benzylique	1000	$[H^+]_5[PMo_{10}V^{5+}_2O_{40}^{5-}]$	2	-	PEG-200	O_2 2	100	16	≈100	50	3	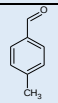 100	n. i.	34
2[b]		500	$[\{Pd\}^{2+}]_2[H^+]_1[PMo_{10}V^{5+}_2O_{40}^{5-}]$	0.6	$\{Pd\}^{2+,b}$ (1.25)	DMSO	O_2 Atm	130	6	> 99	160	27	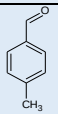 96  tr	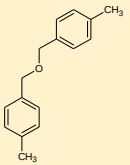 tr	35
3a		1000	$[H^+]_5[PMo_{10}V^{5+}_2O_{40}^{5-}]$	1,4	-	MeCN	O_2 Atm	110	24	100	3,5	-	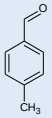 5	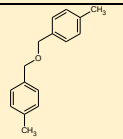 95	36
3b			$[Na^+]_5[PMo_{10}V^{5+}_2O_{40}^{5-}]$							0	0	-	-	-	
4a		7,5	$[Na^+]_5[PMo_{10}V^{5+}_2O_{40}^{5-}]$	1,5	*p*-chloranil (5)	Décaline-eau 1-1 v/v	O_2 Atm	90	18	56	54	3	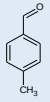 82	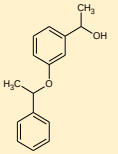 < 4	
4b		15	$[Bu_4N^+]_5[PMo_{10}V^{5+}_2O_{40}^{5-}]$			MeCN		110		53	42	2	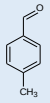 63	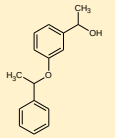 < 4	

[a]Charge par rapport au substrat; [b]{Pd^{2+}} = $[Pd(dpa)(DMSO)_2]^{2+}$; **13**H = *p*-méthoxybenzaldéhyde; **14**H = acide *p*-méthoxybenzoïque; **18**H = acétophénone; *p*-$MePhCH_2OH$ = Alcool *p*-méthoxybenzylique; *p*-PhCHO = *p*-méthoxybenzaldéhyde.

Tableau IB. 5d: Activité des $PMoV_x$ pour l'oxydation aérobie de l'alcool p-méthoxybenzylique en solution

Entrée	Substrat	Conc. (mM)	Catalyseur Formule	Charge[a] (mol%)	Co-catalyseur (charge[a] en mol%)	Solvant	Press. O_2 (bar)	T (°C)	t (h)	Conv. (%)	TON	TOF (h^{-1})	Produits (rdt en %) Oxydation	Catalyse acide	Réf
1	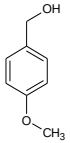 Alcool *p*-méthoxy-benzylique	20	$[H^+]_5[PMo_{10}(V^{5+})_2O_{40}^{5-}]$	2	-	PEG-200	O_2 2	100	16	≈100	50	3	**13**H: 100	n. i.	34
2		500	$[\{Pd\}^{2+}]_2[H^+]_1[PMo_{10}V^{5+}_2O_{40}^{5-}]$	0.6	$\{Pd\}^{2+,\,b}$ (1.25)	DMSO		130	8	> 99	170	20	**13**H: 99		35
3a		7,5	$[Na^+]_5[PMo_{10}V^{5+}_2O_{40}^{5-}]$	1.5	*p*-chloranil (5)	Décaline-eau 1-1 v/v	O_2 Atm	90	18	n. i.	57	3	**13**H: 85	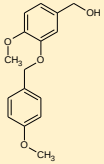 < 4	38
3b		15	$[Bu_4N^+]_5[PMo_{10}V^{5+}_2O_{40}^{5-}]$			MeCN	Atm	110		n. i.	50	3	**13**H: 75	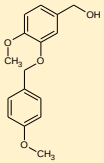 < 4	
4	**13**H	1000	$[H^+]_5[PMo_{10}V^{5+}_2O_{40}^{5-}]$	0,4	-	AcOH-H_2O 9-1 v/v	1	70	48	30	65	3	**14**H: 26	n. i.	39

[a]Charge par rapport au substrat; [b]$\{Pd^{2+}\} = [Pd(dpa)(DMSO)_2]^{2+}$; **13**H = *p*-méthoxybenzaldéhyde; **14**H = acide *p*-méthoxybenzoïque.

- *Tests d'activité des $PMoV_x$ en catalyse pseudo-hétérogène et hétérogène*

XU *et al* [42] ont réalisé l'oxydation de l'alcool benzylique sous air dans le DMSO à 150°C pendant environ 1,7 h en présence d'un $PMoV_1$ (0.05 mol%) modifié par une coumarine fonctionnalisée par un groupement n-$C_6H_{13}NMe_3^+$ (Tableau IB. 5a, entrées 6a-c). On se trouve donc en présence d'un surfactant qui diminue la solubilité du $PMoV_1$ modifié, ce qui est lié à la substitution des H^+ par la coumarine modifiée, un gros cation. On se trouve alors en présence d'une pseudo-phase. Les coumarines dimérisant réversiblement sous irradiation UV, le catalyseur a pu être séparé du milieu par précipitation après réaction. Le catalyseur où l'intégralité des ions H^+ a été remplacée (entrée 6b) apparaît moins actif que $PMoV_1$ sous forme acide libre (entrée 6a). Il semblerait que les ions ammonium associés à la coumarine masquent $PMoV_1$. Le catalyseur $H(Coumarine)_3PMoV_1$ est plus actif que $PMoV_1$ (entrée 6c). Ceci serait lié, d'après les auteurs, à l'existence d'interactions π-π* entre la surface de la coumarine modifiée et l'alcool benzylique et aussi à une plus grande surface de contact entre le catalyseur et le milieu réactionnel. De plus, ces résultats semblent indiquer que le catalyseur $H(Coumarine)_3PMoV_1$ présente un TON (1980) et un TOF (1200 h^{-1}) bien plus élevés que les systèmes catalytiques précédemment cités, notamment ceux menés en présence de palladium (Tableau IB. 5a, entrée 4b, TON et TOF de 220 et 26 h^{-1}, respectivement).

Cette méthodologie basée sur l'ajout d'une étape de séparation par hétérogénéisation est néanmoins peu simple à mettre en place car elle suppose de modifier au préalable le $PMoV_x$. On peut, à l'inverse, opérer en hétérogène dès le départ. L'option la plus simple alors est d'utiliser un solvant dans lequel le $PMoV_x$ n'est pas soluble, par exemple le toluène. $PMoV_2$ (5,8 mol%) a été testé par NOROUZI *et al* [43] pour l'oxydation de l'alcool benzylique (Tableau IB. 7, entrée 1) et certains de ses dérivés dans ce solvant à 110°C. Ainsi, les aldéhydes et cétones sont obtenus avec des rendements assez élevés. Cependant, alors que la conversion de l'alcool *p*-méthoxybenzylique (entrée 6) semble être assez rapide (après 0,04 h seulement), celle de l'alcool benzylique est plutôt lente (2 h), ce qui montre un effet positif de l'effet donneur du groupement méthoxy. Celle de la benzoïne (entrée 10) est la plus ralentie (3 h). De plus, $PMoV_2$ semble être plus actif sur les alcools secondaires que sur les alcools primaires comme montré par les exemples du 1-phényléthanol, du 1-phénylpropanol et du styrène-1,2-diol (Tableau IB. 7, entrées 4, 8, 9). MAAYAN *et al* [44] ont testé le CO_2 supercritique en tant que solvant pour l'oxydation de l'alcool benzylique en présence de $PMoV_2$. L'avantage principal du CO_2 supercritique est que les produits peuvent être plus facilement récupérés vu que CO_2 est facilement évaporé. La pression en dioxygène était de 2 bar et la pression totale de

170 bar. La durée a été fixée à 2 h et la température à 100°C. Une charge en catalyseur de 1 mol% est suffisante pour convertir totalement l'alcool benzylique (Tableau IB. 7, entrées 2a-c) en benzaldéhyde. Cependant, pour le 1-phényléthanol, il y a eu déshydratation de l'alcool au lieu de l'oxydation en cétone, ce qui a été déjà constaté par HAIMOV et NEUMANN (Réf 43) en catalyse homogène.

Le désavantage d'utiliser des $PMoV_x$ dans des anti-solvants est que ces derniers sont insolubles uniquement dans les solvants organiques apolaires. Le choix est donc plutôt restreint. Un moyen d'y remédier, consiste à faire précipiter les $PMoV_x$ à l'aide d'une source de contre-cations volumineux tel Fe^{3+}. Cette option a été suivie par NAGARAJU *et al* [45] en 2006. Deux tests témoins (en homogène) en présence de $PMoV_1$ ou de PMo_{12} ont été menés pour étudier l'oxydation aérobie de l'alcool benzylique dans l'acétonitrile à 80°C (Tableau IB. 5a, entrées 7a-b). Contrairement au PMo_{12}, $PMoV_1$ semble avoir une activité, mais assez faible vu que le rendement en benzaldéhyde est de 24% et le TON de 12. $PMoV_1$ ainsi que PMo_{12} ont ensuite été précipités par ajout d'ions Fe^{3+} (Tableau IB. 7, entrées 3a-b). Les catalyseurs qui en résultent se sont montrés plus actifs. Notamment, $PMoV_1$ précipité par Fe^{3+} est le plus efficace d'entre tous avec un TON de 107 et le rendement en benzaldéhyde est de 93% après 4 recyclages, ce qui est presque 4 fois plus élevé qu'avec $PMoV_1$ non supporté. Le catalyseur hétérogène $FePMoV_1$ est stable de surcroît. En fait, la surface spécifique est plutôt faible (de 7 à 10 m^2/g), ce qui semble indiquer que l'amélioration de l'activité du catalyseur est liée au fait que le vanadium et le fer agissent en synergie, surtout que Fe^{3+} est aussi un oxydant. Le 1-phényléthanol (Tableau IB. 7, entrée 5) et l'alcool *p*-méthoxybenzylique (Tableau IB. 7, entrée 7) ont également été sélectivement oxydés en produits carbonylés sans formation d'un produit de déshydratation ou d'un acide carboxylique par sur-oxydation. Des tests analogues ont été réalisés en présence de $PMoV_x$ précipités par des sels d'argent sur l'alcool cinnamique dans le toluène [46]. Comme pour le fer, les auteurs ont mis en évidence une synergie entre l'argent et le vanadium. Les ions Ag^+ sont des bons oxydants et les $PMoV_x$ réduits activent le dioxygène. Des solvants tels que l'acétonitrile ou le DMSO ont donné des rendements moins bons, ce qui est lié à un plus mauvais transfert de dioxygène (voir Tableau IB. 6). La précipitation des $PMoV_x$ par des métaux de transition est une méthode qui finalement permet d'opérer avec deux catalyseurs qui agissent en synergie dans des conditions de catalyse hétérogène. On peut remarquer en effet que la surface spécifique ne varie que très peu contrairement au cas avec la coumarine évoqué précédemment [42].

Tableau IB. 6: Solubilité du dioxygène dans des solvants usuels utilisés pour l'oxydation des alcools benzyliques

Solvant	Solubilité du dioxygène (mM)	Référence
Toluène	9,2	47
Acétonitrile	2,3	48
DMSO	0,33	49
Eau	0,012	50

Solubilité à 25°C.

- *Tests d'activité des $PMoV_x$ ancrés sur des supports neutres*

Une autre option qui devrait avoir plus d'impact sur la surface spécifique consiste à supporter les POMs sur des matériaux dotés de grandes surfaces spécifiques. Cette façon de faire est assez développée. Un exemple est le charbon actif sur lequel des sels non acides de $PMoV_2$ ont été ancrés. Il est connu pour sa grande surface spécifique et est riche en fonction oxygénées telles que les quinones, ce qui nous amène à supposer que le POM peut se lier au support par des forces de Van der Waals. Nous pouvons le qualifier de support non-innocent (cf modélisation de sa co-activité par des quinones, voir paragraphe IB. 3. 1c) vu qu'il a eu priori un rôle décisif pour l'oxydation de l'alcool *p*-méthylbenzylique en dérivé carbonylé, obtenu avec un rendement de 95% (Tableau IB. 8b, entrée 1) en présence de sels non acides de $PMoV_2$.

Dans l'acétonitrile ainsi que dans le DMSO, pour favoriser l'oxydation de l'alcool benzylique en benzaldéhyde, il est nécessaire de modifier le système catalytique :

- Par l'ajout d'un co-catalyseur (NEUMANN *et al*)
- Par l'ajout d'un métal de transition à haut degré d'oxydation (Pd^{2+} ou Fe^{3+} ou Ag^{+}) (NAGARAJU *et al* et HUANG *et al*).
- En améliorant le contact entre le substrat et le catalyseur par l'ajout d'un surfactant, une coumarine modifiée s'est révélée être une comme montré par XU *et coll*.

Il est à noter que la solubilité du dioxygène dans ces solvants est plutôt faible surtout comparé à l'acide acétique (7,5 mM) [47] ou au toluène (voir Tableau 6), ce qui permet de montrer que le transfert du dioxygène est un des facteurs limitants principaux.

Tableau IB. 7: Activité des $PMoV_x$ pour l'oxydation de l'alcool benzylique et de ses dérivés en présence d'un $PMoV_x$ hétérogène non supporté

Entrée	Substrat	Conc. (mM)	Catalyseur Formule	Charge[a] (mol%)	Surface spécifique (m^2/g)	Co-catalyseur (charge[a] en mol%)	Solvant	T (°C)	t (h)	TON	TOF (h^{-1})	Produits (rdt en %) Oxydation	Réf
1	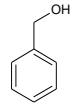	100	$[H^+]_5[PMo_{10}V^{5+}_2O_{40}^{5-}]$	5,8	n. i.	-	Toluène	110	2	16	8	**9**H: 90	43
2a[b]				1		-				100	6	**9**H: 100	
2b[b]		39	$[H^+]_5[PMo_{10}V^{5+}_2O_{40}^{5-}]$	0,4	n. i.	-	$scCO_2$	100	16	230	14	**9**H: 91	44
2c[b]				0,2		-				410	25	**9**H: 81	
3a		200	$[Fe^{3+}]_{0,8}[H^+]_{0,5}[PMo_{12}V^{5+}_0O_{40}^{3-}]$	2,7	8,5	Fe^{3+} (2,1)	MeCN	80	20	21	< 1	**9**H: 35	45
3b		200	$[Fe^{3+}]_{1,1}[H^+]_{0,8}[PMo_{11}V^{5+}_1O_{40}^{4-}]$	2,7	11	Fe^{3+} (3,0)			12	107 107[c]	9 9[c]	**9**H: 93[c]	
4		100	$[H^+]_5[PMo_{10}V^{5+}_2O_{40}^{5-}]$	5,8		-	Toluène	110	0,4	16	39	**18**H: 90	43
5		200	$[Fe^{3+}]_{1,1}[H^+]_{0,8}[PMo_{11}V^{5+}_1O_{40}^{4-}]$	2,7	11	Fe^{3+} (3,0)	MeCN	80	15	107	9	**18**H: 94	45
6	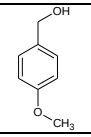	100	$[H^+]_5[PMo_{10}V^{5+}_2O_{40}^{5-}]$	5,8		-	Toluène	110	0,04	16	405	**13**H: 94	43
7		200	$[Fe^{3+}]_{1,1}[H^+]_{0,8}[PMo_{11}V^{5+}_1O_{40}^{4-}]$	2,7	11	Fe^{3+} (3,0)	MeCN	80	12	107	34	**13**H: 93	45
8	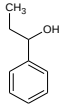				n. i.				2	16	8	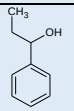 95	
9	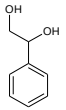	100	$[H^+]_5[PMo_{10}V^{5+}_2O_{40}^{5-}]$	5,8	n. i.	-	Toluène	110	0,2	16	79	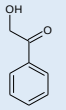 92	43
10	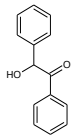				n. i.				3	16	5	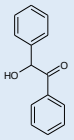 90	

Sans indication: O_2 à pression atmosphérique; conversion et produits mineurs non indiqués; Conversion : n. i. (not indicated) ; [a]Charge par raport au substrat ; [b]Pression d'oxygène : 2 bar, pression totale : 170 bar; [c]Après 4 recyclages

Tableau IB. 8a: Activité des $PMoV_x$ pour l'oxydation de l'alcool benzylique, du 1-phenyléthanol et du benzaldéhyde en présence d'un $PMoV_x$ hétérogène supporté

Entrée	Substrat	Conc. (mM)	Catalyseur/Support Forme $PMoV_x$ (teneur en $PMoV_x$)	Charge[a] (mol%)	Surface spécifique (m^2/g)	Co-catalyseur (charge[a] en mol%)	Solvant	Oxydant (press)	T (°C)	t (h)	Conv. (%)	TON	TOF (h^{-1})	Produits (rdt en %) Oxydation	Réf
1	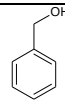	50	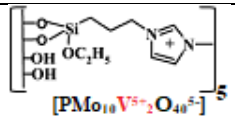 $[PMo_{10}V^{5+}_2O_{40}^{5-}]$ (30)	0,02	714	-	MeCN	Air (3,4)	100	12	n. i.	4900	410	**9**H: 98	52
2		130	**[ImidTEMPO]**$_5$[$PMo_{10}V^{5+}_2O_{40}^{5-}$] /$SiO_2$/$Fe_3O_4$ (20)	0,005	n. i.	**ImidTEMPO** 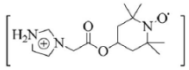 (0,025)	Toluène	O_2 (2)	80	5	98	19400	3900	**9**H: 97; 77[b]	51
3a	**9**H	-	**[H^+]**$_4$[$PMo_{11}V^{5+}_1O_{40}^{4-}$]/MCM-41 (10)	0,01	950	-	-	O_2 (atm)	50	1	n. i.	4900	4900	**10**H: 55	53
3b			**[H^+]**$_4$[$PMo_{11}V^{5+}_1O_{40}^{4-}$]/MCM-41 (30)	0,03	932							1900	1900	**10**H: 64	
3c			**[H^+]**$_4$[$PMo_{11}V^{5+}_1O_{40}^{4-}$]/MCM-41 (40)	0,04	897							1850	1850	**10**H: 83	
3d			**[H^+]**$_4$[$PMo_{11}V^{5+}_1O_{40}^{4-}$]/MCM-41 (50)	0,06	875							1690	1690	**10**H: 95	
3e			**[H^+]**$_4$[$PMo_{11}V^{5+}_1O_{40}^{4-}$]/MCM-41 (60)	0,07	845							1350	1350	**10**H: 91	
3f			**[H^+]**$_3$[$PMo_{12}V^{5+}_0O_{40}^{3-}$]/MCM-41 (50)	0,06	685							790	790	**10**H: 43	
4		50	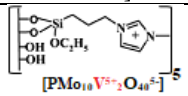 $[PMo_{10}V^{5+}_2O_{40}^{5-}]$ (30)	0,02	714	-	MeCN	Air (3,4)	100	6	n. i.	4950	825	**18**H: 99	52
5		130	**[ImidTEMPO]**$_5$[$PMo_{10}V^{5+}_2O_{40}^{5-}$] /$SiO_2$/$Fe_3O_4$ (20)	0,005	n. i.	**ImidTEMPO** (0,025)	Toluène	O_2 (2)	80	18	70	13600	760	**18**H: 68	51

[a]Charge par raport au substrat ; [b]Après 9 recyclages ; n. i. = not indicated

Tableau IB. 8b: Activité des $PMoV_x$ pour l'oxydation de dérivés de l'alcool benzylique en présence d'un $PMoV_x$ hétérogène supporté

Entrée	Substrat	Conc. (mM)	Catalyseur/Support Forme $PMoV_x$ (teneur en $PMoV_x$)	Charge[a] (mol%)	Surface spécifique (m^2/g)	Co-catalyseur (charge[a] en mol%)	Solvant	Oxydant (press)	T (°C)	t (h)	Conv. (%)	TON	TOF (h^{-1})	Produits (rdt en %) Oxydation	Réf
1	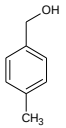	1000	$[Na^+]_5[PMo_{10}V^{5+}_2O_{40}^{5-}]$/C (10)	1,4	n. i.	-	Toluène	Atm	100	24	n. i.	68	3	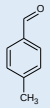 95	39
2		50	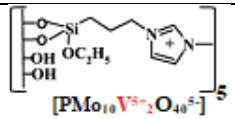 (30)	0,02	714	-	MeCN	Air (3,4)	100	6	n. i.	4800	800	**9**H: 96	52
3		130	**[ImidTEMPO]**$_5[PMo_{10}V^{5+}_2O_{40}^{5-}]$ /SiO_2/Fe_3O_4 (20)	0,005	n. i.	**ImidTEMPO** (0,025)	Toluène	O_2 (2)	80	5	99	19600	3920	**9**H: 98	51
4	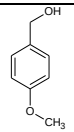	50	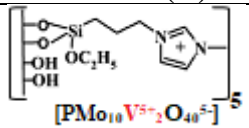 (30)	0,02	714	-	MeCN	Air (3,4)	100	6	n. i.	4800	800	**9**H: 96	52
5		130	**[ImidTEMPO]**$_5[PMo_{10}V^{5+}_2O_{40}^{5-}]$ /SiO_2/Fe_3O_4 (20)	0,005		**ImidTEMPO** (0,025)	Toluène	O_2 (2)	80	5	97	19000	3800	**9**H: 95	51
6	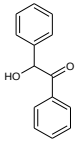	50	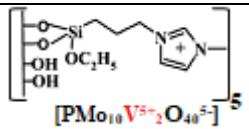 (30)	0,02	714	-	MeCN	Air (3,4)	100	7	n. i.	4750	680	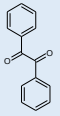 95	52

[a]Charge par raport au substrat

ZHU *et al* [51] ont opté pour un système associant, ioniquement, $PMoV_2$ à un imidazolium fonctionnalisé par du TEMPO, noté ImidTEMPO. Le tout a été supporté sur des nanoparticules $Fe_3O_4@SiO_2$ pour catalyser l'oxydation de dérivés de l'alcool benzylique en leurs analogues carbonylés dans le toluène à 80°C sous 2 bar de dioxygène. Fe_3O_4 est magnétique, ce qui facilite la récupération et est protégé de l'oxydation par la couche de silice. Le mode d'ancrage du $PMoV_2$ n'a pas été abordé par les auteurs. Néanmoins, on peut supposer qu'il se fait par des liaisons de type VAN DER WAALS. La charge du catalyseur était de 20 wt% par rapport au support ((0.005 mol% $PMoV_x$ par rapport au substrat), Tableaux. 8a-b, entrées 2, 5, 8, 10). La conversion de l'alcool benzylique (entrée 2) ainsi que les dérivés fonctionnalisés en *para* (entrées 2 et 5) a atteint 97-99% après 5 h avec des rendements en aldéhyde autour de 95-98%. De plus, on peut noter que des TON (presque 20000 !!) et des TOF (presque 4000) bien plus élevés que pour les systèmes catalytiques cités précédemment ont été obtenus. Cependant, il faut signaler que la pression en dioxygène est plus élevée (2 bar). Le même constat a été fait dans les travaux de NOROUZI *et al* [43]. Le 1-phényléthanol a également été testé. Malgré une durée de 18 h, ce qui est trois fois plus que pour l'alcool benzylique, la conversion n'est que de 70% et le rendement en acétophénone est de 68%. Ce système est donc plus efficace pour l'oxydation des alcools primaires que des alcools secondaires. Les auteurs n'ont pas constaté de suroxydation des aldéhydes formés et pas de réaction de déshydratation des alcools secondaires, sans doute en raison du caractère acide atténué du $PMoV_x$. Le mécanisme proposé par les auteurs est analogue à celui décrit par BEN-DANIEL *et coll* [35].

- *Tests d'activité des $PMoV_x$ ancrés sur des supports cationiques*

Vu que les $PMoV_x$ sont des anions, les supports cationiques devraient être plus adaptés pour ancrer de telles structures. Un exemple donné par BORDOLOI *et al* [53] implique l'utilisation d'un liquide ionique greffé sur une silice SBA-15. La structure générale adaptée de cette référence est donnée dans la Figure IB. 5. Du $PMoV_2$ (0,02 mol%) a été supporté sur cette silice modifiée (30 wt%) (Tableaux IB. 8a-b). Une première chose à noter est que la surface BET (714 m^2/g) est environ 100 fois plus élevée que celle de $PMoV_2$ non supporté. Ce système a été testé pour l'oxydation de l'alcool benzylique (Tableau IB. 8a, entrée 1) sous 3,4 bar d'air (O_2 0,7 atm) dans l'acétonitrile à 100°C pendant 12 h. Le benzaldéhyde a été obtenu avec un rendement de 98% et le TON est d'un peu moins de 5000. Des rendements supérieurs à 95% en *p*-méthoxybenzaldéhyde (Tableau IB. 8b, entrée 4), en *p*-méthylbenzaldéhyde (entrée 2) et en

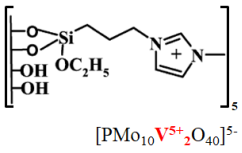

Figure IB.5: $PMoV_2$ ancré sur la SBA modifiée

acétophénone (Tableau IB. 8a, entrée 4) ont été obtenus, mais après 6 h au lieu de 12 h. De plus, en ce qui concerne l'oxydation de la benzoïne (entrée 6), le rendement en benzile est de 95% après 7 h. En conséquence, le catalyseur est plus actif sur les alcools benzyliques secondaires ou activés par des substituants donneurs d'électrons. L'alcool cinnamique a aussi été oxydé dans les mêmes conditions. Un rendement de 98% a été obtenu, mais après 13 h.

Nous venons de voir que l'alcool benzylique est un substrat abondamment étudié dans le cadre de la mise au point de catalyseurs d'oxydation aérobie des alcools. L'aldéhyde est dans la plupart des cas le produit prépondérant. Les trois leviers trouvés dans la littérature consistent à :

- *utiliser un solvant qui a une bonne affinité avec le dioxygène (toluène…). Le désavantage est que l'utilisation d'un tel solvant implique des risques élevés pour la santé et pour l'environnement. Par exemple, le toluène est un CMR.*
- *utiliser un co-oxydant en quantité catalytique (Fe^{3+}, Ag^{+} ou quinones).*
- *améliorer le contact entre le $PMoV_x$ et le substrat (ajout de la coumarine modifiée qui a pu donner un TON allant jusqu'à presque 2000 ou hétérogénéisation sur support).*

Généralement, la substitution du molybdène par le vanadium se révèle déterminante pour l'activité du catalyseur pour l'oxydation de l'alcool en aldéhyde ou cétone.
En solution (et milieu pseudo-hétérogène), les sels non acides sont inactifs. L'acidité se révèle donc nécessaire pour oxyder le substrat, mais ceci est une arme à double tranchant vu que ce paramètre est favorable à la formation d'un éther par dimérisation du substrat comme montré par NEUMANN et coll et par SRIVANI et coll. L'étude d'autres substrats, à l'instar du 1-phényléthanol, a permis de montrer que l'acidité accélère aussi les réactions de déshydratation qui aboutissent au styrène comme montré par NEUMANN et coll. Dans ce cas, des TON allant jusqu'à presque 2000 ont été obtenus, ce qui est le meilleur résultat pour les $PMoV_x$ en solution et en milieu pseudo-hétérogène.

Trois pistes ont été envisagées pour réaliser des réactions de catalyse hétérogène :

- *Utiliser les $PMoV_x$ (sous forme acide libre ou de sel) dans un anti-solvant. Le $PMoV_2$ s'est révélé être actif pour l'oxydation dans le toluène et davantage dans le CO_2 supercritique. L'acide libre étant soluble dans les solvants polaires et protiques, le choix est plutôt limité. Il peut donc être plus intéressant d'ajouter un gros cation comme Fe^{3+} ou Ag^{+} qui sont aussi de bons oxydants afin de les rendre insoluble dans des solvants*

tels que l'acétonitrile et atténuer le caractère acide. Comme montré par NAGARAJU et al, ces cations et les $PMoV_x$ ont opéré en synergie pour l'oxydation des alcools benzyliques en benzaldéhydes et ont donné des résultats comparables aux $PMoV_x$ sous forme d'acide libre, mais dans l'acétonitrile, un solvant moins dangereux que le toluène.

- *La structure des $PMoV_x$ étant connue pour être peu stable, il a pu être avantageux de les supporter sur un matériau neutre. Trois exemples ont été traités : le charbon actif, les nanoparticules SiO_2/Fe_3O_4 et TiO_2. Leur étude a permis de voir deux modes d'influence du support. Le charbon actif joue le rôle d'un co-oxydant (NEUMANN et coll) alors que TiO_2 permet de stabiliser la structure du POM (RANA et al). Les deux systèmes catalytiques ont donné de bons rendements. La différence est que le système $PMoV_2$-TEMPO modifié supporté sur la silice est bien plus actif et plus stable (TON et TOF plus élevés). D'ailleurs, c'est le catalyseur qui a donné les meilleurs résultats en termes de TON et TOF. Cependant, cette stabilité tend à diminuer au fur et à mesure des recyclages.*
- *Comme les $PMoV_x$ sont négativement chargés, un support cationique peut être plus adapté. Un exemple a été donné par BORDOLOI et coll. Le $PMoV_2$ supporté s'est montré plus rapide que les catalyseurs supportés précédemment cités, mais le TON est plus faible.*

Une généralité sur les $PMoV_x$ supportés est qu'ils sont plus actifs que les $PMoV_x$ en homogène. En effet, pour ces derniers, le TON ne dépasse pas 2000 alors que des valeurs de presque 20000 ont pu être atteintes dans le cas des $PMoV_x$ supportés. Aussi, les $PMoV_x$ sont dans la majorité des cas plus actifs sur les alcools benzyliques secondaires.

IB. 2.2. Benzaldéhyde

L'acide benzoïque est l'un des principaux sous-produits de l'oxydation de l'alcool benzylique en benzaldéhyde. Il est obtenu par sur-oxydation de ce dernier. EL AMRANI *et al* ont testé $PMoV_2$ (0,4 mol%) dans un mélange $AcOH/H_2O$ 4,5-0,5 pour l'oxydation du benzaldéhyde (Tableau IB. 5a, entrée 8) en acide benzoïque [55]. La réaction a été effectuée sous atmosphère de dioxygène, à 70°C pendant 24 h. Dans ces conditions, le benzaldéhyde est

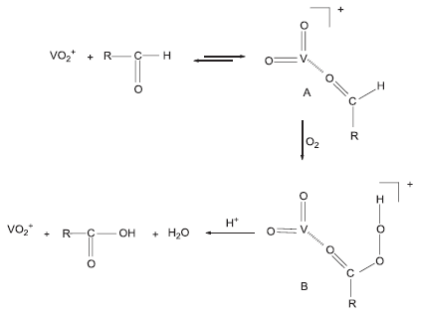

Figure IB. 6: Mécanisme proposé par EL AMRANI et al

converti en acide benzoïque avec un rendement de 97%. L'explication donné par les auteurs est que l'oxydation du benzaldéhyde nécessite la formation d'ions pervanadyle, un oxydant plus fort que $PMoV_2$ [56]. Le mécanisme proposé est donné dans la Figure IB. 6:

La formation de cations pervanadyle a été déjà signalée par HUANG *et al* dans les cas d'oxydation des alcools benzyliques dans le DMSO. Mais, dans leur cas, l'acide benzoïque ne se forme qu'à l'état de traces au plus. Cette différence pourrait être liée d'une part à une meilleure solubilité du dioxygène dans l'acide acétique (7,5 mmol/L, [47]) que dans le DMSO (0,33 mM) et au fait que les cations pervanadyle (la forme active du catalyseur) peuvent être stabilisés par l'acide acétique comme signalé par ZHIZHINA *et al* [57]. Aussi, les auteurs ont proposé l'absence de régénération du $PMoV_x$ et que ce dernier ne sert donc que de précurseur aux formes solubles du vanadium (+IV) et (+V). Le *p*-méthoxybenzaldéhyde a été comparé avec le benzaldéhyde (tableau IB. 5d, entrée 4) [55]. Malgré un temps deux fois plus long (48 h vs 24 h), la conversion ainsi que le rendement en acide ont été divisés par plus que 3 (rendement de 26% *vs* 97% pour l'acide benzoïque). Les groupements donneurs auraient donc un fort effet négatif sur l'oxydation. Ce résultat est contraire au cas avec les dérivés de l'alcool benzylique qui sont eux activés par des groupements donneurs. Les auteurs l'ont expliqué par le fait qu'une réaction de réarrangement qui aboutit à des phénols a été favorisée aux dépens de l'oxydation. Ceci peut être un indicateur des produits d'oxydation attendus pour la lignine. En effet, les substituants sur les groupements aromatiques ayant principalement un effet donneur, on peut donc espérer obtenir préférentiellement des aldéhydes tels que la vanilline à partir de la lignine.

Une piste intéressante et novatrice a été envisagée par RANA *et al* [53] pour réaliser l'oxydation aérobie des aldéhydes par voie de catalyse hétérogène. Elle consiste à supporter $PMoV_1$ sur de la silice MCM-41 (S_{BET} = 1250 m²/g) afin de réaliser la réaction en l'absence de solvant (Tableau IB. 8a, entrées 3a-f). Un des paramètres d'étude est la teneur en $PMoV_1$ dans le catalyseur hétérogène. En présence de $PMoV_1$, la surface BET a diminué jusqu'à 685 m²/g pour une teneur en $PMoV_1$ de 60 wt% (entrée 3f). Les auteurs ont montré qu'une teneur de 50 wt%, ce qui donne une charge en $PMoV_1$ de 0,06 mol%, est l'optimum pour l'oxydation du benzaldéhyde en acide benzoïque. La conversion atteint alors 95%. Un témoin sans vanadium a été aussi testé. Il s'est montré moins actif que le $PMoV_1$ supporté vu que la conversion a été divisée par plus que 2 (43%, entrée 3f vs 95%, entrée 3c). Le vanadium a donc un rôle à jouer, ce qui a déjà été montré à plusieurs reprises, notamment par NAGARAJU *et coll* (Réfs 50-51). En fait, le dioxygène a pu être activé par le catalyseur réduit. En d'autres termes, il a été réduit en un radical superoxyde $HOO^{\cdot}$. De plus, le catalyseur s'est montré stable vu que la conversion diminue de 3% au plus après recyclage. Le dioxygène est donc activé par le catalyseur alors

que dans le cas d'EL AMRANI *et al* [55], c'est le substrat qui est activé par la coordination d'un cation pervanadyle. Ceci peut être lié à la surface spécifique qui stabilise le catalyseur et facilite son action qui consiste à accrocher une fonction hydroperoxyde au vanadium. D'ailleurs, ce cation n'est pas mentionné dans le cas du $PMoV_1$ supporté et on peut supposer que le $PMoV_1$ reste sous forme de POM de KEGGIN. La structure du catalyseur à la fin de la réaction n'a pas été analysée par RANA *et al*, donc, on ne peut pas dire si le POM garde une structure de KEGGIN ou non. En effet, ce n'est pas parce qu'il y a pas de perte d'activité que la structure reste inchangée, comme démontré par HUANG *et coll*. En revanche, ceci peut faire penser qu'il n'y a pas de « fuites » de vanadium, mais ceci mériterait des études plus approfondies.

IB. 2.3. Clivage des α- hydroxycétones

Des α-hydroxycétones peuvent se former au moment du clivage de la lignine et de ses modèles, notamment après la rupture de la liaison C^{β}-O, là où des liaisons β-O-4 sont présentes. Comme proposé par DE GREGORIO *et al* [1] dans le cas du modèle **A4**$_{GG}$ (Fig. IB. 7), une réaction de déshydratation de l'alcool secondaire a lieu libérant un équivalent d'eau et donnant lieu à la formation d'un éther d'énol intermédiaire ①. Ce produit est ensuite hydrolysé pour libérer du guaïacol ③ et une cétone d'HIBBERT ② qui peut subir elle-même des réactions de réarrangement (Figure IA. 8).

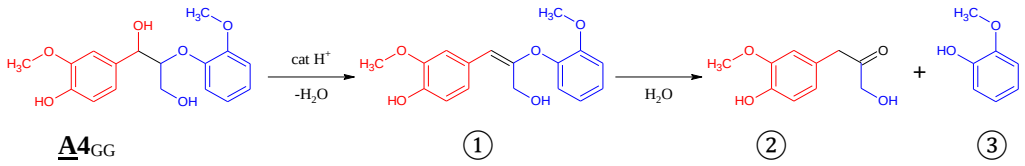

Figure IB. 7: Formation d'une cétone de HIBBERT

Ceci donne lieu à des transformations assez complexes et multiples qu'il faudra en compte dans l'étude du clivage oxydant de la lignine et de ses modèles. Auparavant, on se propose d'examiner la réactivité vis-à-vis de du dioxygène d'α-hydroxycétones plus simples telles que la 2-hydroxyacétophénone et les benzoïnes. La réaction visée est décrite sur la Figure IB. 8.

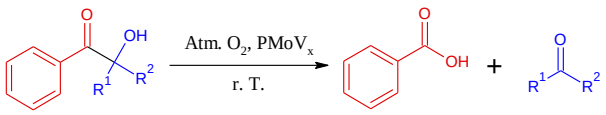

Figure IB. 8: Clivage oxydant aérobie des 2-hydroxyacétophénones

EL ALI *et al* [58] ont utilisé un $PMoV_x$, en l'occurrence $PMoV_2$ (1 mol%) pour l'oxydation de la benzoïne (0,33 M) en benzil sous atmosphère de dioxygène. Dans ^tBuOH, le THF, l'acétonitrile et le DME (DiMéthoxyEthane), l'oxydation de la benzoïne en benzil est quantitative à 50°C en 8 h alors qu'à 25°C, elle n'a pas lieu. Dans le DMF, aucune réaction ne se passe, même à 50°C. Dans le propan-1-ol et plus généralement dans les alcools primaires, la benzoïne est clivée même à température ambiante en présence d'un $PMoV_x$ sous forme d'acide libre, ce qui montre l'importance de l'acidité de Brönsted pour le clivage du substrat (Tableau 9, entrée 2b-e). De plus, PMo_{12} ($H_3PMo_{12}O_{40}$) est inactif pour la réaction ciblée (entrée 2a), même à 50°C, ce qui implique que le vanadium est le centre actif pour le clivage de la benzoïne.

Un an après, EL AAKEL *et al* [2] ont également testé un $PMoV_3$ pour catalyser le clivage aérobie de la 2-hydroxyacétophénone et dérivés soit dans le méthanol, soit en milieu acide acétique-eau 9-1 à température ambiante sous pression atmosphérique de dioxygène (Tableau IB. 9, entrées 1a-b, 3a-5b). Le $PMoV_3$ est un catalyseur efficace pour le clivage à température ambiante des 2-hydroxyacétophénones (voir Figure IB. 8) avec une conversion de 100% en général. Le solvant a une influence majeure. En effet, lors de l'oxydation de la benzoïne dans AcOH-H_2O, du benzile, un produit d'oxydation sans clivage se forme avec un rendement de 47% (Table IB. 9, entrée 1b), ce qui n'est pas le cas dans le méthanol (entrée 1a). Aussi, la 1-hydroxycyclohexylphenylcétone est moins clivée (conversion : 60%) dans AcOH-H_2O (Tableau IB. 9, entrée 5b) que dans le méthanol (entrée 5a, conversion totale), malgré une moins bonne solubilité de l'oxygène dans ce dernier. Ceci peut être lié à la réaction d'estérification entre l'acide issu de l'hydroxyacétophénone et le méthanol qui permet de déplacer l'équilibre vers le clivage, ce qui a été constaté de manière analogue par EL ALI *et coll*. Noter que la cyclohexanone obtenue n'est pas stable à une température plus élevée. Elle subit elle-même une réaction de clivage conduisant à l'acide adipique. Cette réaction a d'ailleurs été exploitée par BALLARANI *et al* plus récemment (en 2011) [59]. On peut remarquer que les rendements en produits de clivage dans le cas de $PMoV_3$ sont plus élevés que dans les travaux précédents. Ceci pourrait être lié à une solubilité du dioxygène plus faible dans le propan-2-ol.

Tableau IB. 9: Activité des $PMoV_x$ pour le clivage oxydant des α-hydroxyacétophénones

Entrée	Substrat	Conc. (mM)	Catalyseur	Solvant	t (h)	TON	TOF (h^{-1})	Conv. (%)	Produits d'oxydation (rdt en %) Clivage Acides	Clivage Aldehydes	Sans clivage	Réf
1a	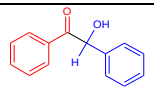 Benzoine	1100	$[H^+]_6[PMo_9V^{5+}_3O_{40}^{6-}]$	MeOH	5	100	17	100	**10**-**OMe**H: 110	**9**H: 45 $PhCH(OMe)_2$: 45		2
1b				AcOH-H_2O 9-1		100	15	100	**10**H: 81	**9**H: 1	 47	
2a[b]		330	$[H^+]_3[PMo_{12}V^{5+}_0O_{40}^{3-}]$	Propan-1-ol	8	-	-	-	**10**-**OPr**H: tr **10**H: tr	**9**H: tr		58
2b			$[H^+]_4[PMo_{11}V^{5+}_1O_{40}^{4-}]$			53	7	n. i.	**10**-**OPr**H: 46 **10**H: 6,7	**9**H: 43		
2c			$[H^+]_5[PMo_{10}V^{5+}_2O_{40}^{5-}]$			17	2		**10**-**OPr**H: 15 **10**H: 0,6	**9**H: 17		
2d			$[H^+]_6[PMo_9V^{5+}_3O_{40}^{6-}]$			42	5		**10**-**OPr**H: 37 **10**H: 4,7	**9**H: 36		
2e			$[H^+]_7[PMo_8V^{5+}_4O_{40}^{7-}]$			42	5		**10**-**OPr**H: 39 **10**H: 3,3	**9**H: 39		
2f			$[Na^+]_5[PMo_{10}V^{5+}_2O_{40}^{5-}]$ ou $[NH_4^+]_5[PMo_{10}V^{5+}_2O_{40}^{5-}]$			-	-		**10**-**OPr**H: tr **10**H: tr	**9**H: tr		
2g[c]			$[H^+]_5[PMo_{10}V^{5+}_2O_{40}^{5-}]$	MeCN		-	-	-	-	-	-	
2h[b, c]						100	13	100	-	-	 100	
3a	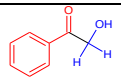	1100	$[H^+]_6[PMo_9V^{5+}_3O_{40}^{6-}]$	MeOH	5	97	17	100	**10**-**OMe**H: 97	Formaldehyde : n. i.		2
3b				AcOH-H_2O 9-1		100	20	100	**10**H: 100	Acide formique: n. i.		
4a	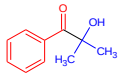			MeOH		97	19	100	**10**-**OMe**H: 97	Acétone: n. i.		
4b				AcOH-H_2O 9-1		100	20	100	**10**H: 100			
5a	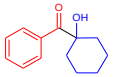			MeOH		100	20	100	**10**-**OMe**H: 100	Cyclohexanone: 100		
5b				AcOH-H_2O 9-1		60	12	60	**10**H: 54	Cyclohexanone: 60		

O_2 à pression atmosphérique, POM 1 mol% par rapport au substrat, r. T. **9**H = benzaldéhyde; **10**H = acide benzoïque; **10**-**OMe**H = Benzoate de méthyle; **10**-**OPr**H = Benzoate de propyle.

La 2-hydroxycyclohexanone et sa version O-méthylée ont été testées dans les mêmes conditions dans le méthanol. La version éthérée est moins active, ce qui a montré que le groupement hydroxy a un rôle clé dans l'activation de la liaison C-C en vue de son clivage

IB. 2.4. Conclusions sur les tests catalytiques

Les oxydations de molécules simples telles que l'alcool benzylique et le 2,6-diméthylphénol permettent d'appréhender la réactivité des $PMoV_x$ sous leurs différentes formes (en fonction du contre-cation et de leur teneur en vanadium). Dans les cas de l'alcool benzylique et du 1-phényléthanol, il a été montré que les $PMoV_x$ sont des catalyseurs versatiles efficaces pour l'oxydation d'alcools en cétones ou aldéhydes. Par contre, en phase homogène, il faut avoir des sites acides. Le problème est que les $PMoV_x$ sous forme d'acide libre peuvent donner lieu à des réactions secondaires (déshydratation et sur-oxydation principalement) et n'ont une bonne activité que dans des solvants qui ont une bonne affinité pour le dioxygène (acide acétique par exemple). Donc, il peut se révéler nécessaire d'ajouter un co-oxydant ou de modifier le $PMoV_x$ par ajout d'un surfactant. Cette dernière option développée par XU *et al* s'est révélée être la plus efficace. La présence de vanadium est donc une condition nécessaire mais pas suffisante pour l'acte catalytique de l'oxydation des alcools ainsi que de la lignine. Les $PMoV_x$ ont été plus souvent utilisés en catalyse hétérogène qu'en homogène. Les avantages principaux sont une meilleure activité grâce à une surface spécifique élevée et à l'effet stabilisant sur la structure du $PMoV_x$ dans certains cas. Parmi toutes les solutions envisagées, celle développée par ZHU *et al* est celle qui a donné le catalyseur le plus actif. L'oxydation d'aldéhyde en acide carboxylique a été réalisée en homogène par ATLAMSANI *et al* et en hétérogène, sans solvant organique ajouté, par PARIDA *et al*. En homogène, le $PMoV_x$ n'est pas stable et la formation de cations pervanadyles est nécessaire. Le choix du solvant peut s'expliquer par la nécessité d'avoir un bon transfert de dioxygène et de stabiliser les cations pervanayles qui sont les vrais catalyseurs d'oxydation. En hétérogène, il n'y a pas de perte d'activité après recyclage et la formation de VO_2^+ n'a pas été constatée. Les réactions de clivage de la liaison C-C ont été surtout constatées pour les acétophénones activées par une fonction dérivée de l'oxygène en α. En effet, à part dans le cas de l'oxydation du 1-phényléthanol dans les PEG où le benzaldéhyde obtenu par clivage est un produit mineur, cette réaction n'a jamais été constatée dans les travaux sur les acéophénones non activées. Deux exemples sont la 2-hydroxyacétophénone et la benzoïne qui peuvent tous les deux êtres clivées pour donner comme produits un aldéhyde et l'acide benzoïque ou un ester de cet acide. Les deux leviers utilisés sont

d'une part le choix d'un solvant dans lequel le dioxygène est bien soluble et d'autre part d'opérer dans un alcool afin de favoriser le clivage à l'aide d'une réaction d'estérification.

IB. 3. Les différentes voies de synthèse conventionnelles des $PMoV_x$

Dans la littérature, trois voies de synthèse reviennent souvent : la voie éthérate, la voie hydrothermale et la voie oxo-peroxo. Le paramètre principal est la valeur de x obtenue.

IB. 3.1. Voies éthérates

La voie éthérate ainsi que ses variantes sont celles qui reviennent le plus souvent dans la littérature. Elles ont pour point commun le passage par un éthérate de formule $PMoV_x$-Et_2O et partent généralement des sels de vanadium(V) et de molybdène(VI). Une acidification par un acide minéral fort tel que H_2SO_4 ou HCl est réalisée afin d'obtenir le $PMoV_x$ souhaité. Le pH à la fin doit être très bas au vu du caractère acide fort des $PMoV_x$, ce qui implique l'ajout d'une grande quantité d'acide minéral. Le $PMoV_x$ sous forme d'acide libre est ensuite extrait à l'aide de diéthyléther. S'ensuit la formation d'un complexe $PMoV_x$-diéthyléther avec obtention d'une phase supplémentaire rouge foncée voire noire. En fin de synthèses, trois phases doivent être observées : la phase aqueuse qui contient l'acide minéral, la phase $PMoV_x$-éther et la phase éther. Après extraction du $PMoV_x$-diéthyléther et évaporation de l'éther sous flux d'air, le $PMoV_x$ est obtenu. Ce dernier est ensuite dissous dans de l'eau et recristallisé par évaporation lente de cette dernière afin de le purifier.

Les réactions mises en jeu sont décrites sur le schéma suivant (Fig IB. 9) :

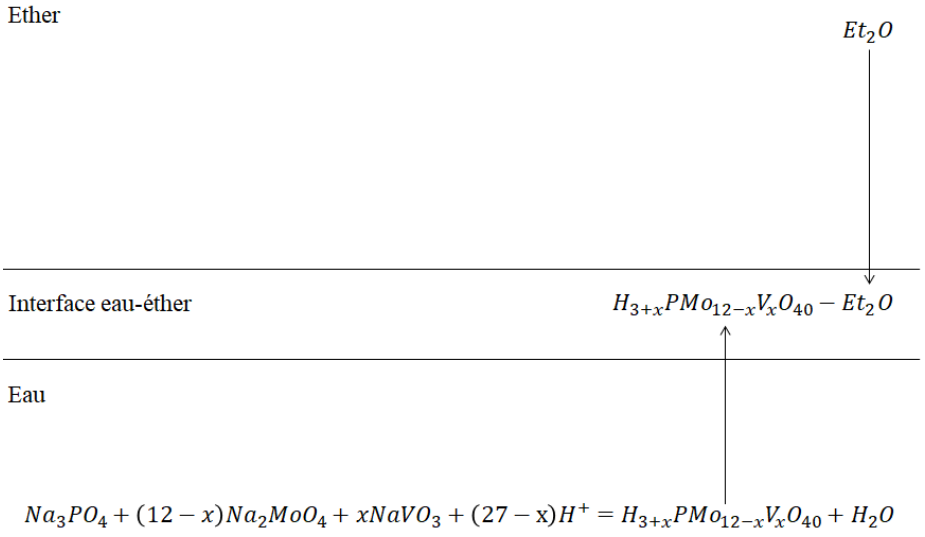

Figure IB. 9: Principe général de la synthèse des $PMoV_x$ par la voie étherate

La version la plus connue de ce type de protocole et celle qui apparait le plus souvent dans la littérature est celle de TSIGDINOS et HALLADA [65]. Dans cette approche, les sels de départ sont Na_2MoO_4, $NaVO_3$ et Na_3PO_4 et l'acidification est réalisée avec H_2SO_4 concentré. Le $PMoV_x$ est enfin recristallisé par évaporation lente dans un dessicateur. La proportion volumique diéthyléther/phase aqueuse est de 8/10. Des adaptations permettant de consommer moins d'éther ont été publiées telles que celle de SHE *et al* [16]. Le rapport éther/phase aqueuse est alors de 3/10 et la source de vanadium est V_2O_5, un composé moins dangereux car moins toxique que $NaVO_3$. Ces deux voies ont été essayées pour x = 3. Elles se sont révélées assez faciles à mettre en œuvre dans nos mains, mais il y a un fort risque de présence d'impuretés tels que les composés de l'acide sulfurique ou encore les sels de sodium de départ qui n'ont pas réagi. Ces voies ont été appliquées pour x allant jusqu'à 3 et les rendements peuvent dépasser les 80% surtout pour x =1, mais, il a été constaté que la voie de TSIGDINOS et HALLADA donne de faibles rendements pour x = 3, e qui a été expliqué par les auteurs par la formation d'une espèce lacunaire et de cations pervanadyles.

IB. 3.2. Voies hydrothermales

Les voies hydrothermales partent des oxydes de vanadium(V) et de molybdène(VI) et de l'acide orthophosphorique. La suspension est chauffée à reflux dans l'eau pendant plusieurs heures pour obtenir le $PMoV_x$. Ce sont les voies les plus simples à mettre en œuvre vu qu'elles procèdent en une seule étape. Elles ont été l'objet de brevets déposés dans les années 1970 [66]. L'équation de la réaction mise en œuvre est :

$$H_3PO_4 + (12 - x)MoO_3 + \frac{x}{2}(V_2O_5 + H_2O) = H_{3+x}PMo_{12-x}V_xO_{40} \text{ (Eq. IB. 1)}$$

Le désavantage de cette approche est la durée de la réaction qui peut atteindre 21 jours et le fait que les rendements sont plutôt modestes en lien avec la présence de résidus d'oxydes (avec une teneur plus forte en V_2O_5). Aussi, ces voies sont peu adaptées pour x élevé à cause du manque de solubilité de l'oxyde de vanadium. Deux exemples de voies hydrothermales sont celle de KERN *et al* [67] et celle de ZHANG *et al* [68]. La première a été décrite pour x = 1 alors que la seconde a été décrite pour x = 2. Les rendements annoncés sont proches de 100%. La différence entre ces deux voies est que l'eau est évaporée à chaud dans le protocole de KERN *et al* alors que le POM est recristallisé dans le protocole de ZHANG *et al*.

IB. 3.3. Voies oxo-peroxo

Cette approche part des oxydes comme la voie hydrothermale. Comme son nom l'indique, l'attaque des oxydes implique l'utilisation de H_2O_2 dans le but de former des complexes oxo-peroxo du molybdène(VI) et du vanadium(V) qui bien sont plus solubles dans l'eau que les oxydes de départ. Cette approche est tout à fait possible à basse température. Il faut même refroidir le récipient où est réalisée l'attaque de V_2O_5. Contrairement aux deux voies précédentes, il n'y a pas un protocole général (Tableau IB. 10).

Tableau IB. 10: Complexes intermédiaires et x visés

Auteurs	Complexes synthétisés		x visés
	Mo	V	
ATLAMSANI *et al.* [69]	$[PO_4\{Mo_2O_2(\mu\text{-}O_2)_2(O_2)_2\}_2]^{3-}$	$[\{V(\mu\text{-}O_2)_2O\}_2O]^-$	4
MATVEEV *et al.* [70]	$H_3PMo_{12}O_{40} + MoO_3$	$H_{14}PV_{14}O_{42}$	2, 3, 5 et 6

Dans la voie d'ATLAMSANI *et al*, d'une part, V_2O_5 a été attaqué à 0°C et d'autre part, MoO_3 a été attaqué par H_2O_2 et H_3PO_4 à 50°C. Après dissolution complète et refroidissement à température ambiante, la solution contenant MoO_3 a été versée à la solution de vanadium attaqué. L'eau a été ensuite évaporée sous air. En ce qui concerne la voie de MATVEEV, V_2O_5 est le seul oxyde à avoir été attaqué par le peroxyde d'hydrogène. Celle-ci s'est faite en présence d'acide phosphorique. La réaction qui a lieu aboutit à un complexe de KEGGIN. Aussi, la principale différence est que la voie de MATVEEV *et al* passe par des POM de KEGGIN alors que la voie d'ATLAMSANI *et al* passe par des intermédiaires oxo-peroxo. Le rendement n'a pas été précisé. Le désavantage est le manque de stabilité de ces complexes, surtout celui du vanadium qui a tendance à donner un gel de V_2O_5 si la température tend à remonter trop vite. Les deux voies citées ont été testées pour la synthèse de $PMoV_x$ pour $x \geq 3$, des composés qui sont peu accessibles par les voies hydrothermales.

La voie de TSIGDINOS et HALLADA (Tableau IB. 11) est celle qui revient le plus souvent. Le x visé était alors généralement de 1 ou 2 sauf dans les travaux de SRIVANI *et al* où un $PMoV_3$ a été synthétisé. Une voie hydrothermale a été utilisée pour synthétiser un $PMoV_1$. Ceci peut être expliqué par le fait que les voies étherates sont plus faciles à mettre en œuvre et moins longues. Comme les deux voies citées ne sont pas adaptés pour x élevés, les $PMoV_x$ à x élevé ont plutôt été synthétisés par des voies oxo-peroxo vu qu'elles permettent de contourner le problème de la faible solubilité de l'oxyde de vanadium.

Tableau IB. 11: Occurrences des voies de synthèse des $PMoV_x$

Auteur [Réf]	Voie de synthèse des $PMoV_x$	$PMoV_x$ utilisé
HUANG *et al.* [32]	Etherate (TSIGDINOS)	$PMoV_2$
KRICKL *et al.* [33]	Etherate (TSIGDINOS)	$PMoV_2$
HAIMOV *et al.* [34]	n. i.	$PMoV_2$
BEN-DANIEL *et al.* [35]	Etherate (TSIGDINOS)	$PMoV_2$
HUANG *et al.* [36]	Etherate (TSIGDINOS)	$PMoV_2$
NEUMANN *et al.* [39]	Etherate (TSIGDINOS)	$PMoV_2$
XU *et al.* [42]	n. i.	$PMoV_1$
NOROUZI *et al.* [43]	n. i.	$PMoV_2$
MAAYAN *et al.* [44]	Etherate (TSIGDINOS)	$PMoV_2$
NAGARAJU *et al.* [45]	Etherate (TSIGDINOS)	$PMoV_1$
NAGARAJU *et al.* [46]	Etherate (TSIGDINOS)	$PMoV_1$
ZHU *et al.* [51]	n. i.	$PMoV_2$
RANA *et al.* [52]	Hydrothermal	$PMoV_1$
BORDOLOI *et al.* [53]	Etherate (TSIGDINOS)	$PMoV_2$
SRIVANI *et al.* [54]	Etherate (TSIGDINOS)	$PMoV_x$ (x = 1-3)
EL AMRANI *et al.* [55]	Oxo-peroxo (ATLAMSANI)	$PMoV_2$
EL AAKEL *et al.* [2]	Oxo-peroxo (ATLAMSANI)	$PMoV_3$
MATVEEV *et al.* [62]	Oxo-peroxo (MATVEEV)	$PMoV_4$
KOLESNIK *et al.* [63-64]	Oxo-peroxo (MATVEEV)	$PMoV_x$ (x = 1-9)

IB. 3.4. Une voie méchano-chimique : le ball-milling

Le ball-milling est une piste d'intérêt car elle peut aider à améliorer le contact (granulométrie plus fine) entre les deux oxydes à l'état solide et ainsi à solubiliser V_2O_5 notamment par attaque avec H_2O [71]. Il s'agit de broyer les oxydes en présence de billes « dures » dans un autoclave tapissé de la même matière que les billes afin d'obtenir un oxyde mixte qui sera ensuite attaqué par H_3PO_4 à plus basse température et à une durée réduite. Ce protocole nous semble être plus économe en énergie que la voie hydrothermale notamment. MOLCHANOV *et coll* ont réalisé un travail précurseur. Ils ont étudié l'influence du ratio billes/oxydes, du temps de broyage ainsi que des conditions opératoires de l'attaque. Cependant, les PMoVx obtenus n'ont jamais été testés pour l'oxydation de la lignine (et de ses modèles) et leur caractérisation mérite d'être plus approfondie, notamment en ce qui concerne l'oxyde mixte.

IB. 3.5. Conclusion - quel choix opérer ?

Même si la voie de TSIGDINOS est prépondérante, il ne faut pas ignorer les inconvénients liés à l'utilisation de réactifs additionnels (éther diéthylique, acide minéral, voir Tableau IB. 12) et que c'est la seule voie dans laquelle on part de sels. Il y a donc un risque accru de présence d'impuretés. Les voies oxo-peroxo sont difficiles à mettre en œuvre et nécessitent l'utilisation de peroxyde d'hydrogène afin de « solubiliser » les oxydes de départ. Les voies hydrothermales sont simples à mettre en œuvre mais nécessitent un long temps de

chauffage surtout pour x élevé. Malgré cet inconvénient, cette dernière sera choisie dans les travaux de cette thèse.

Tableau IB. 12: Avantages et inconvénients des voies conventionnelles

	Voies étherate	Voies hydrothermales	Voies « oxo-peroxo »
+	Rapide et simple à réaliser Séparation facile (éthérate à récupérer)	La plus simple à mettre en œuvre Pas de sels de Na donc pas d'ajout d'un acide minéral et donc moins de risques de pollution des $PMoV_x$	Meilleure solubilisation des oxydes de départ grâce à H_2O_2 Température plus basse / hydrothermale Rendements plus élevés/hydrothermale
-	Le diéthyléther est nocif, inflammable Risque de présence d'impuretés accrue	Long à mettre en œuvre Résidus de Mo et V donc pertes en réactifs	Plus difficile à gérer du fait de l'instabilité des complexes oxo-peroxo du Mo et V qu'il faut « fabriquer » en simultané. Dangers liés à H_2O_2

IB. 4. Mécanismes proposés pour le clivage oxydant de la lignine

La base du mécanisme est l'oxydation du substrat par le vanadium (V). Ensuite, le dioxygène peut avoir plusieurs rôles. Dans certains rôles, il peut uniquement régénérer le catalyseur sous sa forme oxydée, ce qui est souvent le cas en présence d'un co-oxydant. Sans co-oxydant, il se peut que l'oxygène soit activé par le catalyseur réduit, ce qui permet de régénérer le catalyseur et d'activer le dioxygène. En d'autres termes, le catalyseur active nécessairement le substrat et aussi le dioxygène dans sa forme réduite. En ce qui concerne des dérivés de l'alcool benzylique tels que le styrènediol, l'alcool secondaire est plus actif que l'alcool primaire, ce qui a été expliqué par NOROUZI *et coll* par une énergie de la liaison C-H plus faible en position benzylique.

IB. 4.1. Transformations de la lignine

Tout au long de ce paragraphe, la lignine sera modélisée par des modèles du type **A4**$_{GG}$ (R^1 = OH) ou **A6**$_{GG}$ (R^1 = OMe) (Figure IB. 10). Comme montré par EVTUGUIN *et al* (voir partie IA), les groupements OH phénoliques sont bien plus réactifs que les groupements OH non phénoliques. En présence des PMoVx sous leur forme oxydée (V^V) réputés pour être des oxydants monoélectroniques, le clivage oxydant doit passer au départ par des radicaux cations, dont certains peuvent perdre un proton pour donner des radicaux. Trois voies différentes ont été suggérées (Fig IB. 10).

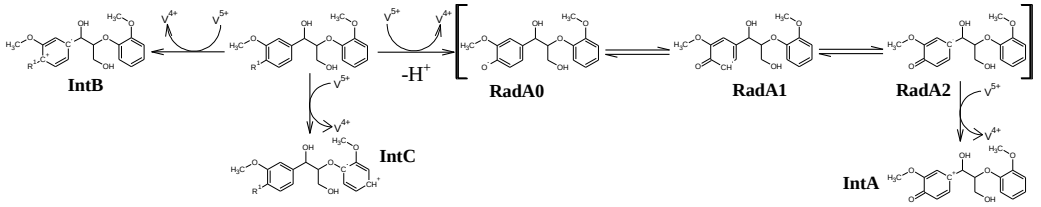

Figure IB. 10: Génération des radicaux possibles à partir des modèles A4GG et A6GG (adapté de Réf. 65)

D'une part, un OH phénolique peut transférer un électron et un proton au catalyseur, ce qui donne un radical cation (les formes mésomères sont notées RadA). Un équivalent supplémentaire du vanadium (+V) peut capter un électron en plus, ce qui conduit au cation intermédiaire IntA. En présence d'eau, l'intermédiaire IntA peut subir une addition nucléophile (Figure IB. 11). La liaison C(Ar)-C^{α} est ensuite clivée pour donner lieu à la formation d'un dérivé du 1,4-dihydroxybenzène et d'un aldéhyde qui peut subir une sur-oxydation catalysée par le vanadium (V) ou encore une déshydratation pour former un dérivé de l'acroléine vu que le catalyseur est un acide fort [61, 72]. Dans le cas d'EVTUGUIN *et al*, le catalyseur était à forte teneur en vanadium ($PMoV_5$) et opérait en homogène. Il est donc plus probable que le vanadium ait été éjecté de la structure de KEGGIN comme montré dans les paragraphes sur les tests d'oxydation.

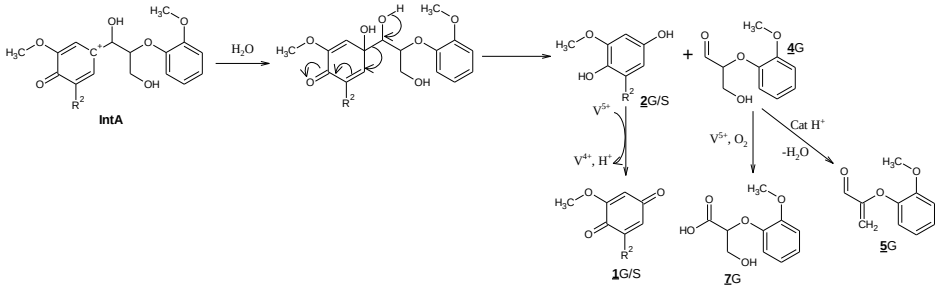

Figure IB. 11: Clivage de l'intermédiaire IntA

Dans le cas des modèles ne comportant pas de fonction phénol, comme vu dans la partie IA, le clivage de la liaison C(Ar)-C^{α} n'a jamais été observé dans la littérature. Le groupement phénol est donc essentiel au clivage de la liaison C(Ar)-C^{α}. A la place, le clivage de la liaison C^{α}-C^{β} est favorisé selon un mécanisme hétérolytique décrit à la Figure IB. 12.

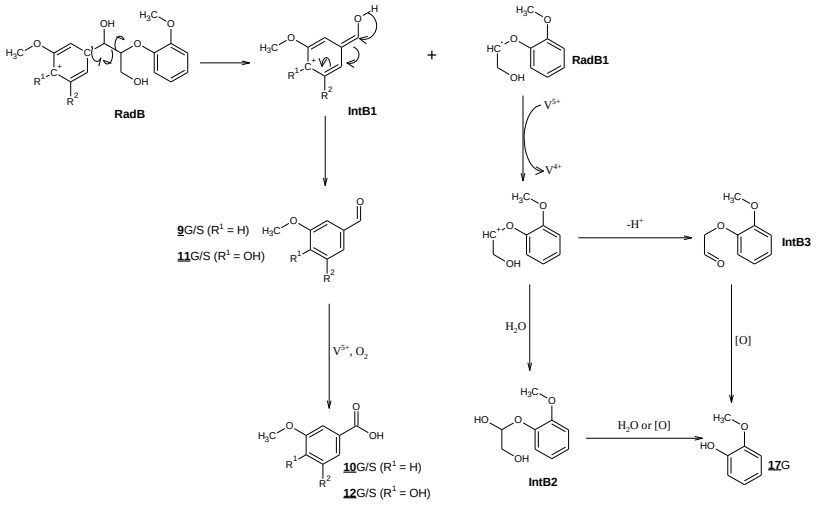

Figure IB. 12: Clivage de l'intermédiaire RadB

D'après EVTUGUIN *et al*, dans le cas des modèles non-phénoliques, le clivage du radical RadB2 peut avoir lieu. Ceci donne les intermédiaires IntB1 et un radical RadB1. Par tautomérie, un aldéhyde est obtenu à partir de IntB1 puis un acide carboxylique par oxydation aérobie. RadB1 peut céder un électron au vanadium (V) pour former un cation qui peut soit perdre un proton pour donner IntB3, soit être hydrolysé en IntB2. Dans les deux cas, une réaction de clivage a lieu pour donner le guaïacol. Il faut prendre en compte que les radicaux alkyle (RadB1 par exemple) ont une forte affinité avec le dioxygène comme indiqué par NEUMANN et KHENKIN [40]. Ainsi, le dioxygène peut s'additionner pour donner un radical peroxyde puis un hydroperoxyde dont la liaison O-O est clivée pour donner un alcool. Ainsi, on peut obtenir des aldéhydes et acides aromatiques.

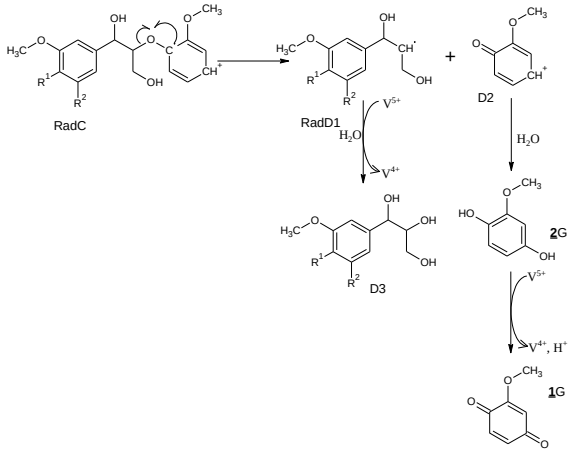

Figure IB. 13: Clivage de l'intermédiaire RadC

Le radical RadC peut subir clivage hétérolytique de la liaison C^{β}-O (Fig IB. 13). Ceci aboutit alors au radical RadD1 et au cation D2. De la même manière que pour le radical RadB,

soit le vanadium retire un électron à RadD1, ce qui forme un cation qui après hydrolyse donne un dérivé du glycérol noté D3, soit le dioxygène s'additionne, ce qui donne en milieu acide un hydroperoxyde puis le même dérivé du glycérol. Le cation D2 est quant à lui hydrolysé en hydroquinone puis oxydé en quinone (voir Fig. IB. 13). Le produit D3 peut à son tour subir l'action des $PMoV_x$, ce qui peut amener à la formation d'α-hydroxycétones comme montré par GASPAR *et al* [73]. En présence de VO_2^+, le mécanisme de la Figure IB. 11 [73] décrit par EL ALI *et al* peut être impliqué [58]. En effet, l'alcool en position benzylique est le plus facile à oxyder comme montré dans le paragraphe IB. 3. 1.

De plus, des réactions secondaires telles que l'oxydation de l'alcool secondaire en cétone sans clivage du modèle de départ (**A4**$_{GG}$ (R^1 = OH) ou **A6**$_{GG}$ (R^1 = OMe)) peuvent avoir lieu comme montré par les tests sur les dérivés de l'alcool benzylique. Il a été montré que les alcools en position benzylique sont plus faciles à oxyder (notamment par SRIVANI *et coll*). Puisque les $PMoV_x$ sont des catalyseurs acides, il est possible que des réactions de déshydratation-hydrolyse opèrent également, comme décrit par DE GREGORIO *et al* [1], pour aboutir à des cétones de HIBBERT. Mais, ces dernières n'ont pas encore été observées dans la littérature en présence de $PMoV_x$.

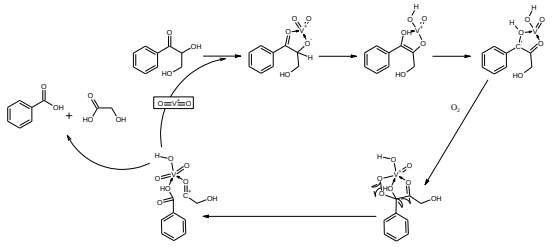

Figure IB. 14: Clivage d'un 2-hydroxyacétophénone issu du clivage oxydant d'un modèle de la lignine

Dans les cas d'oxydations plus poussées, il peut y avoir clivage des cycles aromatiques et formation ultimement de CO_2 comme sur Fig. IB. 15. Ceci peut passer par des réactions d'oxydation décrites par NEUMANN et KHENKIN en 2006 [63] lesquelles impliquent la formation d'*o*- et *p*-quinones intermédiaires.

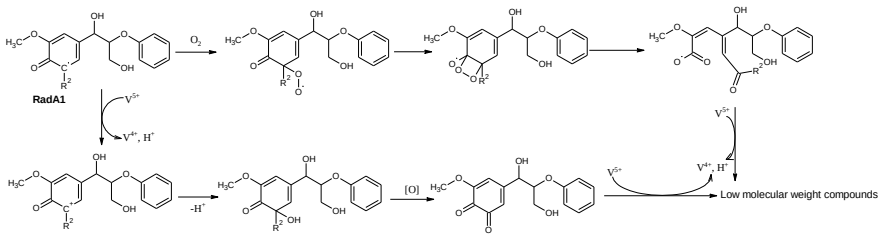

Figure IB. 15: Clivage d'un 2-hydroxyacétophénone issu du clivage oxydant d'un modèle de la lignine

IB. 4.2. Réactivité des $PMoV_x$ et régénération de la forme active

Pour comprendre les mécanismes proposés dans la littérature, il faut aussi s'intéresser à l'évolution des $PMoV_x$ pendant ces réactions. Il y a assez peu d'informations mais on peut néanmoins affirmer que le vanadium est le site actif pour l'oxydation du substrat [22]. Aussi, dans le cas de $PMoV_2$, le $PMoV_x$ le plus étudié dans la littérature, les isomères les plus réactifs sont ceux qui ont des atomes de vanadium vicinaux (isomères 1,2 ; 1,4 ; 1,5) [21]. On peut déjà distinguer deux mécanismes différents : un mécanisme avec une structure de KEGGIN gardée intacte et un mécanisme avec départ de cations VO_2^+ ou VO^{2+} qui jouent le rôle de catalyseur accompagné de la formation d'un anion de KEGGIN lacunaire. Dans l'étude bibliographique sur l'oxydation d'alcools (voir paragraphe IB. 2), les réactions en catalyse homogène se font selon le premier mécanisme dans les cas où il y a présence de TEMPO comme montré par NEUMANN *et al*. Dans les autres cas, le second mécanisme a pu être observé, notamment dans les travaux de HUANG *et al* et les travaux d'oxydation du benzaldéhyde et de clivage oxydant des 2-hydroxyacétophénones qui nécessitent la formation d'un cation pervanadyle. En ce qui concerne la catalyse hétérogène, la structure de KEGGIN est généralement maintenue, ce qui montre que le mécanisme sans génération de cations VO_2^+ ou VO^{2+} est prépondérant. Dans les cas sans détachement d'ions VO_2^+, les équations [40] des réactions mises en jeu sont :

$$[PMo_{12-x}\boldsymbol{V_x^{(V)}}O_{40}]^{(3+x)-} + mSu - H = \left[PMo_{12-x}\boldsymbol{V_{x-m}^{(V)}}\boldsymbol{V_m^{(IV)}}O_{40}\right]^{(3+x+m)-} + mH^+ + mSu^{\cdot}$$

(Eq. IB. 2)

$$\left[PMo_{12-x}\boldsymbol{V_{x-m}^{(V)}}\boldsymbol{V_m^{(IV)}}O_{40}\right]^{(3+x+m)-} + \frac{m}{4}O_2 + mH^+ = [PMo_{12-x}\boldsymbol{V_x^{(V)}}O_{40}]^{(3+x)-} + \frac{m}{2}H_2O$$

(Eq. IB. 3)

Le $PMoV_x$ retire des électrons au substrat (Su-H, Eq. IB. 2). Ceci se manifeste par un changement de couleur. A l'origine de couleur orange, le $PMoV_x$ devient vert, voire bleu après réduction complète de V par le substrat. Le $PMoV_x$ à l'état oxydé est régénéré par O_2 (Eq. IB. 3). En accord avec la loi de NERNST, l'acidité permet d'augmenter le pouvoir oxydant des $PMoV_x$.

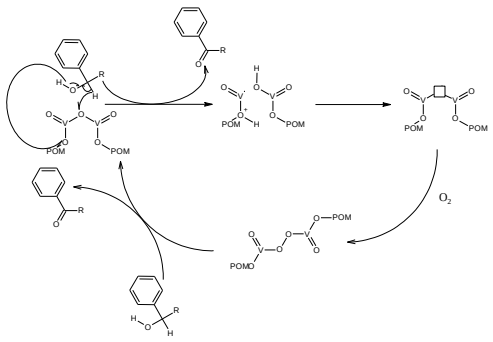

Figure IB. 16: Oxydation des alcools benzyliques selon un mécanisme de MARS-VAN KREVELEN [74]

Pour un mécanisme plus précis, il est possible de s'inspirer de la revue de KWON *et al* [74] portant sur l'activation du dioxygène via

un mécanisme de MARS-VAN KREVELEN (Figure IB. 16) proposé pour une catalyse hétérogène gaz solide sur la base d'une étude cinétique. Or, l'étude théorique menée par JANIK *et al* a montré que cette lacune se forme préférentiellement entre deux addenda du vanadium, ce qui permet de justifier l'activité accrue des complexes qui contiennent deux atomes de vanadium vicinaux. Ainsi, le catalyseur capte deux protons et deux électrons au substrat. Ceci est accompagné d'un départ d'eau et de la formation d'une lacune d'oxygène. Ensuite, le vanadium réduit se lie à une molécule de dioxygène au niveau de la lacune. On se retrouve alors avec un complexe peroxo qui peut oxyder un équivalent de substrat à son tour pour revenir à la forme initiale. Aussi, il existe d'autres mécanismes où les $PMoV_x$ réduits peuvent donner un atome d'oxygène au substrat [37]. Un tel exemple a été donné par KHENKIN et NEUMANN dans le cas du clivage du 2-phényléthanol en formaldéhyde et en benzaldéhyde. Le POM de formule $[PMo_{12-x}V^{(IV)}_xO_{39}]^{(3+x)-}$ est donc formé. Le vanadium (IV) peut ensuite capter l'oxygène pour revenir à la forme oxydée.

Afin que ces mécanismes opèrent, il faut que le $PMoV_x$ soit stable. Or, la réduction du $PMoV_x$ tend à accentuer la distorsion des octaèdres VO_6. La réduction (Eq. IB. 3) est accompagnée par une élongation de la distance entre les atomes P et V de 3,5-3,7 Å à au-delà de 5 Å [75]. Ceci aboutit à l'éjection d'un cation vanadyle et d'une lacune au niveau du POM. Ainsi, plus la valeur de x est élevée, plus la structure de KEGGIN est instable et donc la génération de cations VO^{2+} s'en trouve favorisée (Eq. IB. 4) [76]. Selon l'équation (Eq. IB. 4), des cations pervanadyle VO_2^+ peuvent se former par oxydation aérobie (Eq. IB. 5). D'après BUJANOVIC *et al* [56], ces cations peuvent avoir, un potentiel redox plus élevé que ceux que des $PMoV_x$ de départ et être les « vrais » oxydants (Eq. IB. 6). Un tel cas revient régulièrement dans la littérature, surtout pour des valeurs de x élevées.

$$[PMo_{12-x}\boldsymbol{V}^{(\boldsymbol{V})}_{\boldsymbol{x}}O_{40}]^{(3+x)-} + Su - H = \left[PMo_{12-x}\boldsymbol{V}^{(\boldsymbol{V})}_{\boldsymbol{x-1}}O_{39}\right]^{(3+x)-} + \boldsymbol{V}^{(\boldsymbol{IV})}O^{2+} + Su^{\cdot} \text{ (Eq. IB. 4)}$$

$$2\boldsymbol{V}^{(\boldsymbol{IV})}O^{2+} + O_2 + 4H^+ = 2\boldsymbol{V}^{(\boldsymbol{V})}O_2^+ + 2H_2O \text{ (Eq. IB. 5)}$$

$$\boldsymbol{V}^{(\boldsymbol{V})}O_2^+ + Su - H + 2H^+ = \boldsymbol{V}^{(\boldsymbol{IV})}O^{2+} + Su^{\cdot} + H_2O \text{ (Eq. IB. 6).}$$

L'éq. IB. 4 correspond à la réduction du $PMoV_x$ par le substrat, qui est la cause de la déstabilisation du $PMoV_x$. Les cations pervanadyle peuvent être ensuite obtenus par oxydation par O_2 (Eq. IB. 5). Aussi, les cations vanadyle peuvent être oxydés par $PMoV_x$. L'équation impliquée (Eq. IB. 7) est :

$$[PMo_{12-x}\boldsymbol{V}^{(\boldsymbol{V})}_{\boldsymbol{x}}O_{40}]^{(3+x)-} + VO^{2+} + H_2O = [PMo_{12-x}\boldsymbol{V}^{(\boldsymbol{V})}_{\boldsymbol{x-1}}V^{(IV)}O_{40}]^{(4+x)-} + \boldsymbol{V}^{(\boldsymbol{V})}O_2^+ + 2H^+$$

En théorie, le vanadium pourrait retourner dans la structure du POM. Cependant, ces structures finissent par se détruire pour former à la fin l'acide phosphomolybdique et des ions vanadyles comme suggéré par MARCHAL-ROCH *et al* [77]. Aussi, l'acidité a pour effet d'éjecter les cations pervanadyles de la structure du POM. La réaction décrite par (Eq. IB. 8) a alors lieu :

$$H_{3+x}PMo_{12-x}\boldsymbol{V_x^{(V)}}O_{40} + H^+ = H_{4+x}PMo_{12-x}\boldsymbol{V_{x-1}^{(V)}}O_{38} + VO_2^+ \quad \text{(Eq. IB. 8)}$$

Qu'advient-il du dioxygène ? Est-il réduit directement en H_2O et ne sert-il qu'à régénérer la forme active du catalyseur en récupérant les électrons du vanadium (IV) ? Ou y-a-t-il interaction de O_2 avec le POM et formation d'un adduit ?

Pour NEUMANN et KHENKIN [40], le dioxygène ne sert qu'à régénérer la forme oxydée. Dans d'autres cas, il est proposé que le vanadium (+IV) donne un électron à O_2 ce qui a été montré par ZHIZHINA *et al* [77] ou encore par WEINSTOCK *et al* [26], et ainsi initie la formation d'espèces actives tels que l'anion superoxyde $O_2^{\cdot -}$ (E = 1,55 eV) ou le radical hydroxyle $HO^{\cdot}$ (E = 2,80 eV). Ces oxydants forts ne sont pas sélectifs et sont réputés agir soit sur les groupements aromatiques, soit sur les chaînes aliphatiques.

IB. 5. Conclusion

L'étude bibliographique sur la réactivité des $PMoV_x$ pour l'oxydation des dérivés de l'alcool benzylique a permis de constater qu'un des paramètres clés est le transfert du dioxygène. En catalyse homogène sans co-oxydant, l'acidité est primordiale à l'activité du catalyseur. Néanmoins, ceci est à double tranchant car des réactions secondaires telles que l'étherification ou la déshydratation sont favorisées et la structure de KEGGIN peut ne pas être stable à cause de la réduction du vanadium (V) ou de l'acidité. Ainsi, il est nécessaire d'opérer dans un solvant qui a une bonne affinité avec le dioxygène ou d'ajouter un co-oxydant tel que le TEMPO ou le chloranil. En catalyse hétérogène, on peut obtenir des catalyseurs plus actifs et plus stables (avec un TON qui peut aller jusqu'à presque 20000). Le rôle du support est soit de servir de co-oxydant (charbon actif), soit de stabiliser la structure du $PMoV_x$ (TiO_2). Les $PMoV_x$ peuvent être synthétisés de diverses manières. Le choix de la méthode a été influencé par le x visé. Vu que $PMoV_2$ a été le plus utilisé, le protocole de TSIGDINOS est celui qui revient le plus souvent même s'il implique des solvants organiques et des acides minéraux comme l'acide sulfurique, ce qui pose des problèmes de pollution. Divers mécanismes ont été proposés dans la littérature pour rendre compte des réactions d'oxydation aérobie catalysées par les $PMoV_x$. Ils reposent en général sur l'activation du substrat par le $PMoV_x$ oxydé et aussi,

dans certains cas sur l'activation du dioxygène par le catalyseur réduit (mécanisme type MARS-VAN KREVELEN) qui a pour conséquence la génération d'espèces actives du dioxygène.

Références

[1]: G. F. De Gregorio, R. Prado, C. Vriamont, X. Erdocia, J. Labidi, J. P. Hallett, T. Welton, *ACS Sustainable Chem. Eng*. **2016**, 4, 6031-6036.
[2]: L. El Aakel, F. Launay, A. Atlamsani, J-M. Brégeault, *Chem. Commun*., 2001, 2218-2219.
[3]: J. J. Berzelius, *Ann. Phys. Chem*. **1826**, 6, 369-392.
[4]: J. C. De Marignac, *Ann. Phys. Chem*. **1864**, 3, 1.
[5]: L. Pauling, *J. Am. Chem. Soc.* **1929**, 51, 2868-2880.
[6]: J. F. Keggin, *Nature* **1933**, 131, 75-100.
[7]: B. Dawson, *Acta Cryst.* **1953**, 6, 113-126.
[8]: A. I. G. Petrehele, D. Rusu, A. Ungurean, G. L. Turdean, E. Indrea, L. David, M. Rusu, *Rev. Chim.* **2014**, 65, 265-271.
[9]: A. J. Bridgeman, *Chemical Physics* **2003**, 287, 55-69.
[10]: Y-R. Guo, Q-J. Pan, Y-D. Wei, Z-H. Li, X. Li, *J. Mol. Struct.* **2004**, 676, 55-64.
[11]: K. Y. Matsumoto, *Bull. Chem. Soc. Jpn.* **1975**, 48, 3148-3151.
[12]: D. Barats-Damatov, L. J. W. Shimon, Y. Feldman, T. Bendikov, R. Neumann, *Inorg. Chem.* **2015**, 54, 628-634.
[13]: K. Nomiya, S. Matsuoka, T. Hasegawa, Y. Nemoto, *J. Mol. Catal. A* **2000**, 156, 143-152.
[14]: W. O. Parker Jr, F. Cavani, *J. Phys. Chem.* C **2015**, 119, 24003-24015.
[15]: L. Pettersson, *Mol. Eng.* **1993**, 3, 29-42.
[16]: J. She, Z. Fu, J. Li, B. Zeng, S. Tang, W. Wu, H. Zhao, D. Yin, S. R. Kirk, *Appl. Catal. B* **2016**, 182, 392-404.
[17]: A. J. Bridgeman, *Chem. Phys.* **2003**, 287, 55-69.
[18]: G. B. McGarvey, J. B. Moffat, *J. Mol. Catal.* **1991**, 69, 137-155.
[19]: M. Fournier, C. Feumi-Jantou, C. Rabia, G. Herve, S. Launay, *J. Mater. Chem.* **1992**, 2, 971-978.
[20]: P. Villabrille, G. Romanelli, P. Vazquez, C. Caceres, *Appl. Catal. A*, **2004**, 270, 101-111.
[21]: M. J. Janik, B. B. Bardin, R. J. Davis, M. Neurock, *J. Phys. Chem. B* **2006**, 110, 4170-4178.
[22]: H. Hirao, D. Kumar, H. Chen, R. Neumann, S. Shaik, *J. Phys. Chem. C* **2007,** 111, 7711-7719.
[23]: V.F. Odyakov, E.G. Zhizhina, K.I. Matveev, J. Mol. Catal. A **2000**, 158, 453-456.
[24]: E.G. Zhizhina, V.F. Odyakov, *Appl. Catal A* **2009**, 358, 254-258.
[25]: J. E. Molinari, L. Nakka, T. Kim, I. E. Wachs, *Acs Catal.* **2011**, 1, 1536-1548.
[26]: I. A. Weinstock, R. E. Schreiber, R. Neumann, *Chem. Rev.* 2018, 118, 2680-2717.
[27]: J. Lan, J. Lin, Z. Chen, G. Yin, *Acs Catal.* **2015**, 5, 2035-2041.
[28]: Y. Leng, J. Wang, D. Zhu, L. Shen, P. Zhao, M. Zhang, *Acs Catal.* **2015**, 5, 2035-2041.
[29]: M. Shi, D. Zhang, X. Yu, Y. Li, X. Wang, W. Yang, *Fuel Process. Technol.* **2017**, 160, 136-142.
[30]: S. Farhadi, M. Taherimehr, *Catal. Commun.* **2008**, 9, 703-708.
[31]: R. Tayebee, *Chem. Technol.* **2010**, 6, 54-57.
[32]: Z. Huang, F. Li, B. Chen, G. Yuan, *Green Chem.* **2015**, 17, 2325-2329.
[33]: S. Krickl, T. Buchecker, A. Uwe Meyer, I. Grillo, D. Touraud, P. Bauduin, B. König, A. Pfitzner, W. Kunz, *Phys.Chem.Chem.Phys.* **2017**, 19, 23773-23780.
[34]: A. Haimov, R. Neumann, *Chem. Commun*. **2002**, 876-877.
[35]: R. Ben-Daniel, P. Alsters, R. Neumann, *J. Org. Chem.* **2001,** 66, 8650-8653.
[36]: X. Huang, X. Zhang, D. Zhang, S. Yang, X. Feng, J. Li, Z. Lin, J. Cao, R. Pan, Y. Chi, B. Wang, C. Hu, *Chem. Eur. J.* **2014**, 20, 2557-2564.
[37]: A. M. Khenkin, R. Neumann, *J. Org. Chem.* **2002**, 67, 7075 –7079.
[38]: R. Neumann, M. Levin, *J. Org. Chem.* **1991**, 56, 5707-5710.
[39]: R. Neumann, A. M. Khenkin, I. Vigdergauz, *Chem. Eur. J.* **2000**, 6, 875-882.
[40]: R. Neumann, A. Khenkin, *Chem. Commun.* **2006**, 2529-2538.
[41]: O. A. Kholdeeva, O. V. Zalomaeva, *Coord. Chem. Rev.* **2016**, 306, 302-330.
[42]: Q. Xu, S. Li, M. K. Banks, W. Xu, R. Wu, *Catal. Commun*. **2018**, 114, 24-27.
[43]: M. Norouzi, F. Ashrafi, M. Taharimehr, F. Bagheri, *Int. J. Chem. Tech. Res*. **2010**, 2, 1666-1672.
[44]: G. Maayan, B. Ganchegui, W. Leitner, R. Neumann, *Chem. Commun.* **2006**, 2230-2232.
[45]: P. Nagaraju, N. Pasha, P. S. Sai Prasad, N. Lingaiah, *Green Chem*. **2007**, 9, 1126-1129.
[46]: P. Nagaraju, M. Balaraju, K. Mohan Reddy, P.S. Sai Prasad, N. Lingaiah, *Catal. Commun*. **2008**, 9, 1389-1393.

[47]: X. Wu, Z. Deng, J. Yan, Z. Zhang, F. Zhang, Z. Zhang, *Ind. Eng. Chem. Res.* **2014**, 53, 9932-9937.
[48]: M. Quaranta, M. Murkovic, I. Klimant, *Analyst* **2013**, 138, 6243-6245.
[49]: F. S. Gittleson, R. E. Jones, D. K. Ward, M. E. Foster, *Energy Environ. Sci.* **2017**, 10, 1167-1179.
[50]: D. Tromans, *Ind. Eng. Chem. Res.* 2000, 39, 805-812.
[51]: J. Zhu, P-C. Wang, M. Lu, *Chempluschem* **2014**, 79, 8265-8268.
[52]: S. Rana, S. Mallick, K. M. Parida, *J. Porous Mater.* **2012**, 19, 397-404.
[53]: A. Bordoloi, S. Sahoo, F. Lefebvre, S.B. Halligudi, *J. Catal.* **2008**, 259, 232-239.
[54]: A. Srivani, K. T. Venkateswara Rao, P. S. Sai Prasad, N. Lingaiah, *J. Chem. Sci.* **2014**, 126, 467-472.
[55]: I. El Amrani, A. Atlamsani, M. Dakkach, M. Rodriguez, I. Romero, S. Amthiou, *C. R. Chimie* **2017**, 20, 888-895.
[56]: B. Bujanovic, S. Ralph, R. Reiner, K. Hirth, R. Atalla, *Mater.* **2010**, 3, 1888-1903.
[57]: E. G. Zhizhina, Y. A. Rodikova, V. N. Parmon, *Chemselect* **2017**, 2, 4686-4690.
[58]: B. El Ali, A. M. El-Ghanam, M. Fettouhi, *J. Mol. Catal. A* **2001**, 165, 283-290.
[59]: N. Ballarini, L. Casagrandi, F. Cavani, T. D'alessandro, A. Frattini, P. Accorinti, S. Alini, P. Babini, *DGMK Tagungsbericht* **2008**.
[60]: D. V. Evtuguin, A. I. D. Daniel, A. J. D. Silvestre, F. M. L. Amado, C. Pascoal Neto, *J. Mol. Catal. A* **2000**, 154, 217-224.
[61]: J. M. Campos-Martin, G. Blanco-Brieva, J. L. G. Fierro, *Angew. Chem. Int. Ed.* **2006**, 45, 6962-6984.
[62]: K.I. Matveev, V.F. Odyakov, E.G. Zhizhina, *J. Mol. Catal. A: Chem*. **1996**, 114, 151-160.
[63]: I.G. Kolesnik, E.G. Zhizhina, K.I. Matveev, *React. Kinet. Catal. Lett*. **1999**, 68, 339-346.
[64]: I.G. Kolesnik, E.G. Zhizhina, K.I. Matveev, *J. Mol. Catal. A* **2000**, 153, 147-154.
[65]: G. A. Tsigdinos, C. J. Hallada, *Inorg. Chem.* **1968**, 7, 437-441.
[66]: M. Otake, T. Onoda, *Pat. Fr 7715134*, 1977.
[67]: F. Kern, S. Ruf, G. Emig, *App. Catal. A* 1997, 150, 143-151.
[68]: F. Zhang, M. Guo, H. Ge, J. Wang, *Chin. J. Chem. Eng.* **2007**, 15, 895-898.
[69]: A. Atlamsani, J.-M. Bregeault, M. Ziyad, *J. Org. Chem.* **1993**, 58, 5663-5665.
[70]: V. F. Odyakov, E. G. Zhizhina, R. I. Maksimovskaya, *Appl. Catal. A* **2008**, 342, 126-130.
[71]: V. V. Molchanov, R. A. Buyanov, Kinetics and Catal. 2001, 42, 3, 366-374.
[72]: A. R. Gaspar, D. V. Evtuguin, C. Pascoal Neto, *Ind. Eng. Chem. Res.* **2004,** 43, 7754-7761.
[73]: G. Zhang, B. L. Scott, R. Wu, L. A. Silks, S. K. Hanson, *Inorg. Chem.* **2012**, 51, 7354−7361.
[74]: S. Kwon, P. Deshlara, E. Iglesia, *J. Catal.* **2018**, 364, 228-247.
[75]: I. Efremenko, R. Neumann, *J. Am. Chem. Soc.* **2012**, 134, 20669-20680.
[76]: C. Marchal-Roch, R. Bayer, J. F. Moisan, A. Tézé, G. Hervé, *Top. Catal.* **1996**, 3, 407-419.
[77]: E. G. Zhizhina, V. F. Odyakov, M. V. Simonova, K. I. Matveev, *React. Kinet. Catal. Lett.* **2003**, 78, 373-379.

IC. La cavitation ultrasonore

IC. 1. Introduction

Comme montré dans la partie IB, les $PMoV_x$ procèdent généralement par une voie radicalaire. Le vanadium au degré d'oxydation V retire un électron au substrat. Ensuite, il y a des cas où le vanadium réduit active le dioxygène en lui cédant un électron. L'anion superoxyde puis les radicaux hydroxyle, des oxydants forts se forment. Ces catalyseurs se sont montrés performants pour l'oxydation d'alcools, notamment des fonctions alcool benzyliques présents dans la lignine et pour le clivage oxydant de liaisons C-C et C-O dans les α-hydroxycétones (paragraphe IB. 3.2) ainsi que dans des modèles de la lignine (paragraphe IA. 3.2.1.1) avec des conversions quantitatives et une sélectivité totale pour le clivage. Cependant, déjà pour des modèles non phénoliques, de faibles conversions ont été obtenues (paragraphe IA. 3.2.1.1). En ce qui concerne le clivage oxydant aérobie de lignines extraites, les rendements en molécules aromatiques ne sont que très modestes (de l'ordre de 10% au maximum). En s'inspirant des conclusions des parties IA et IB, il est possible d'expliquer en partie ces faibles rendements par une limitation du transfert d'oxygène. Dans la littérature sur le clivage de la lignine (parte IB), diverses méthodes d'intensification ont été testées telles que la photocatalyse [1-7], les micro-ondes [8] ou encore d'opérer dans des liquides ioniques [8-15]. Cette dernière méthode s'est révélée être adaptée pour le clivage oxydant de la lignine, vu que le rendement en aldéhydes phénoliques a atteint 30%. Par contre, la sonochimie n'a été que très peu testée pour le clivage oxydant de la lignine (qu'une seule référence) et même pas du tout sur les modèles de la lignine. Ce procédé peut être un choix pertinent car il permet d'accélérer les transferts de masse, notamment celui du dioxygène [16]. Ce procédé s'appuie sur le phénomène de cavitation. Des bulles dans lequel du dioxygène est emprisonné se forment, ce qui permet d'améliorer les phénomènes de transfert. Ces bulles oscillent et peuvent finir par imploser, ce qui provoque de très fortes augmentations de température et de pression, ce qui donne des conditions favorables à la formation de radicaux. La seule occurrence de cette méthode d'intensification concerne les travaux de NAPOLY *et al* [17] qui ont consisté à réaliser le clivage oxydant d'une lignine kraft (40 g/L dans acétone-eau 1:1 ou acétate d'éthyle à 40°C) par le peroxyde d'hydrogène (2 équivalents) et non pas par le dioxygène en présence d'un catalyseur au tungstène (5 mol%) pendant une heure sous ultrasons à basse fréquence (0,38 W/mL, 20 kHz).

Tableau IC.1: Impact des ultrasons sur les rendements en produits de clivage [16]

Entrée	Solvant	Amplitude (W/mL)[a]	Rendement (wt%)			
			11G	**12**G	**19**G	**17**G
1	Acetone-eau 1:1	0	0.20	0.10	0.20	0.01
2		0.36	0.15	0.08	0.03	0.03
3[b]		0.36	0	0	0	0
4	Acétate d'éthyle	0	0.20	0.05	0.09	0.03
5		0.36	0.16	0.06	0	0.02
6[c]	NaOH 1 M	0	0.03	0.08	0.28	0.02
7[c]		0.36	0.05	0.05	0.14	0.02

Lignine kraft 40 g/L, 5 mol% Na_2WO_4, $2H_2O$, 1 h, 45°C, 20 kHz ; [a]Amplitude de 0 W/mL = condition silencieuse ; [b]4 équivalents de H_2O_2 ; [c]T = 80°C ; **11**G = vanilline, **12**G = acide vanillique, **19**G = acétovanillone, **17**G = gaïacol

Ainsi, que ce soit dans le binaire acétone-eau (Tableau IC.1, entrées 1 et 2) ou dans l'acétate d'éthyle (entrées 4 et 5) ou dans la soude (entrées 6 et 7), les ultrasons ont eu un impact négatif sur le rendement combiné en vanilline et acide vanillique (acétone-eau : -26%, acétate d'éthyle : -13%) ainsi que le rendement global en produits de clivage (jusqu'à -43% dans le binaire acétone-eau). Les auteurs l'ont expliqué par le fait que les radicaux superoxyde ($HO_2^{\cdot}$) et les radicaux hydroxyle ($HO^{\cdot}$) favorisent les condensations oxydantes plutôt que le clivage. Un test a été fait avec plus d'équivalents d'oxydant (entrée 3). Les produits visés n'ont pas été détectés, ce qui peut signifier que les conditions sont trop oxydantes et que les réactions de condensation ont lieu. En effet, des conditions rudes favorisent généralement les réactions de condensation oxydantes qui génèrent des liaisons C-C résistantes au clivage oxydant comme montré dans la partie IA.

Ceci motive donc à utiliser le dioxygène, un oxydant moins fort que le peroxyde d'hydrogène afin d'adoucir les conditions oxydantes. De plus, la voie sono-chimique peut être une voie prometteuse pour améliorer le transfert de dioxygène dans un milieu liquide. Par conséquent, nous nous intéresserons dans un premier lieu au phénomène de cavitation puis nous nous focaliserons sur la cavitation ultrasonore et ses conséquences. Ensuite, de la même manière que dans la partie IB, nous étudierons les applications des ultrasons pour l'oxydation aérobie des dérivés de l'alcool benzylique.

IC. 2. Généralités sur le phénomène de cavitation

IC. 2.1. Formation des bulles de cavitation

Sous l'effet d'une dépression (Figure IC.1a) dans un liquide incompressible, ce dernier entre en rupture d'équilibre, ce qui amène à la formation de bulles de vapeur (nucléation) qui oscillent. La nucléation peut se faire soit à partir de vapeurs de liquide, soit à partir d'un gaz dissous ou encore d'impuretés. Le phénomène de cavitation a alors lieu [16]. Les bulles peuvent finir par imploser (Figure IC.1b), ce qui crée un « hot spot » caractérisé par une température et une pression très élevées.

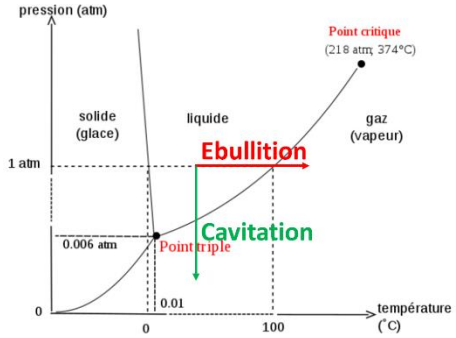

Figure IC. 1a: Cavitation dans le cas de l'eau

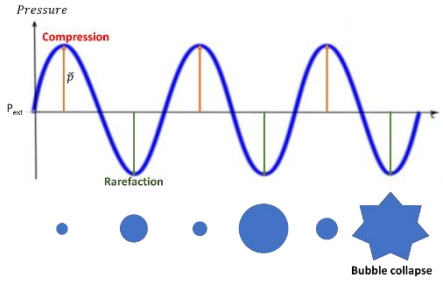

Figure IC. 1b: Représentation schématique du phénomène de cavitation [17]

En fonction du type de perturbation provoquée dans le milieu liquide, on fait la distinction entre trois types de cavitation : i) hydrodynamique ii) optique iii) acoustique.

La cavitation hydrodynamique fait intervenir des écoulements à forte vitesse, ainsi, les moteurs, les hélices ou les pompes peuvent être sujets à l'usure liée à ce phénomène. Cependant, elle peut donner lieu à des phénomènes qui peuvent être exploités notamment dans la synthèse de nanomatériaux [18] ou le prétraitement de la biomasse lignocellulosique [19]. La cavitation optique, découverte par LAUTERBORN [20] se base sur l'exposition d'un liquide à une source lumineuse intense ou à un laser. La température s'élève alors localement, ce qui provoque la cavitation. La cavitation acoustique se déclenche au moment du passage d'une onde sonore. Cette onde peut être soit induite par un choc violent par un piston par exemple (cavitation par impact) [21] soit émise par un transducteur (cas des ultrasons). Nous nous intéressons plus particulièrement à la cavitation ultrasonore dans la suite de ce paragraphe.

IC. 2.2. Dynamique des bulles de cavitation

Le phénomène a été pour la première fois détecté par REYNOLDS en 1894 par l'observation de l'eau bouillante dans un tube ouvert dans les conditions normales de température et de pression (cavitation hydrodynamique). Ce phénomène a été étudié plus en

détail par RAYLEIGH [22] puis par PLESSET [23] en 1949. L'équation qui en résulte, dite de RAYLEIGH-PLESSET est : $R\frac{d^2R}{dt^2}+\frac{3}{2}\left(\frac{dR}{dt}\right)^2=\frac{P(R,t)-P(ext)}{\rho_L}-\frac{1}{\rho_L}\left(\frac{2\sigma}{R}+\frac{4\mu}{R}\frac{dR}{dt}\right)$ (Eq. IC.1)

P(R) correspond alors à la pression dans la bulle de rayon R, P(ext) est la pression qui règne dans le liquide loin de la bulle et ρ_L est la masse volumique du liquide. Le membre écrit en bleu correspond aux contributions de la viscosité dynamique du liquide (notée μ) et de la tension de surface du liquide (notée σ).

De cette équation, il est possible de déduire le seuil de BLAKE [24] à partir duquel la cavitation est possible, c'est-à-dire le seuil à partir duquel les forces qui donnent lieu à la formation de la bulle l'emportent sur les forces de cohésion du liquide. Il est possible de le calculer à partir de l'équation (Eq IC.2), supposant

- Une détente quasi-statique isotherme (donc proches des états d'équilibres).
- Le rayon de la bulle est très inférieur au rayon de résonance
- Le gaz est un gaz parfait

Donc, le seuil de BLAKE noté P_B est défini par l'équation (Eq. IC.2) obtenue à partir de l'équation (Eq IC.2):

$P_B=P(R)+\frac{4\sqrt{3}}{9}\sqrt{\frac{\left(\frac{2\sigma}{P_0R_0}\right)^3}{1+\frac{2\sigma}{P_0R_0}}}$ (Eq IC.2). P_0 et R_0 définissent alors la pression et le rayon de la bulle au repos dans les conditions de température et de pression.

Afin de simplifier l'équation (Eq. IC.1), on formule les hypothèses suivantes :

- La phase liquide est un fluide incompressible, ainsi ρ_L est une constante.
- Les gaz présents (bulles de vapeur et gaz dissous) sont des gaz parfaits.
- La pression dans la bulle est supposée uniforme et ne dépend alors que de R et de t.
- La pression à l'infini notée p(ext) est de la forme $p(ext)=\overline{p_{ext}}+\breve{p}cos(\omega t)$ où p est la surpression et est telle que $\breve{p} << \overline{p_{ext}}$.

Alors, le rayon de la bulle oscille autour de son rayon d'équilibre notée R_E avec des oscillations de faible amplitude. De plus, au moment où la bulle entre en résonance, du fait que le liquide soit incompressible et le gaz soit parfait, on a à tout moment :

$P(R,t)=P_{sat}+P_{gaz}\left(\frac{R_0}{R(t)}\right)^{3k}$ (Eq. IC.3)

P_{sat} est alors la pression de vapeur saturante, P_{gaz} la pression partielle du gaz dissous et k est la constante BOLTZMANN en J. K^{-1}. A partir des équations (Eq. IC.1) et (Eq IC.3), à la fréquence de résonance f_{res}, si on fait l'hypothèse que les bulles sont assez grosses (quelques microns) et

si on fait l'approximation $f_{res} = \frac{3}{R_E}$ [25], alors le rayon de résonance est donné par l'équation (Eq IC.4) :

$R_{res} = \sqrt{\frac{3k\overline{p_{ext}}}{\rho_L {f_{res}}^2}}$ (Eq. IC.4).

Lorsque le rayon des bulles dépasse un rayon critique dit de résonance noté R_{res}, elles finissent par imploser. Lorsqu'elles se trouvent près d'une paroi, l'implosion est alors dissymétrique, ce qui provoque la formation d'un micro-jet [26] très puissant, ce qui peut modifier la réactivité des composants du milieu réactionnel. De ces équations, nous pouvons déduire les conclusions suivantes résumées dans le tableau IC.2:

Tableau IC. 2: Influences des paramètres sur la cavitation

Equation	Conclusions
(Eq IC.2)	Une faible cohésion dans la phase liquide est favorable à la cavitation.
(Eq IC.4)	Une augmentation de la pression permet d'obtenir des plus grosses bulles de cavitation Une fréquence plus basse excite des bulles plus grosses, ce qui augmente la probabilité de formation de micro-jets et qui favorise des effets de paroi.

De plus, il est possible de déduire à partir de la Figure IC.1a qu'une augmentation de la température abaisse le seuil de BLAKE, ce qui donne aussi des conditions favorables à la cavitation.

IC. 2.3. Cas des ultrasons

Ici et jusqu'à la fin de la partie bibliographique, nous nous focaliserons maintenant sur la cavitation ultrasonore. Les ultrasons sont des ondes acoustiques dont la fréquence est comprise entre 20 kHz et 1 MHz. Le domaine entre 20 et 100 kHz correspond aux basses fréquences et celui entre 100 kHz et 1 MHz aux hautes fréquences. Elles sont émises par des transducteurs piézoélectriques qui transforment l'énergie électrique en énergie mécanique et sont constitués d'une pièce ou d'un empilement de pièces en céramique qui vibrent alors à la fréquence souhaitée.

Quand on utilise un transducteur ultrasonore, son intensité surfacique I est liée à la puissance acoustique délivrée par l'équation : $I = \frac{P_{acous}}{S} e^{-2\alpha d}$ (Eq. IC.7) où S est l'aire de la surface émettrice des ultrasons en cm², α le coefficient d'absorption du fluide et d la distance de la source des ultrasons. Aussi, comme indiqué par LUPACCHINI *et al* [27], le coefficient α peut être obtenu via l'équation $\alpha = \frac{2\pi^2 f^2}{\rho_L c}\left(\frac{4\mu}{3} + \frac{(\gamma-1)K}{C_p}\right)$ (Eq. IC.8) où K est la conductivité thermique du milieu. Donc, un fluide visqueux amortit plus les ondes ultrasonores. Aussi, plus la fréquence est élevée, plus l'onde est amortie. De plus, la puissance acoustique dépend de la capacité

calorifique du milieu. D'après l'équation (Eq IC.4), on peut montrer que les basses fréquences tendent à favoriser la formation de grosses bulles qui sont plus stables, ce qui peut laisser le temps aux radicaux formés d'initier des réactions de pyrolyse comme montré par PETRIER *et al* [28]. Les hautes fréquences, au contraire donnent lieu à des bulles plus petites mais plus nombreuses et à une puissance moins élevée, mais plus localisée. Aussi, la surface de contact entre les bulles et le milieu réactionnel est augmentée du fait du faible rayon critique, ce qui est favorable à la formation de radicaux et aux réactions sono-chimiques [29]. Néanmoins, si la fréquence devient trop élevée, il y a un grand nombre de bulles, ce qui accentue le risque de coalescence, diminue la puissance acoustique et amortit la propagation de l'onde.

IC. 3. Applications des ultrasons pour l'oxydation de dérivés de l'alcool benzylique par H_2O_2 et O_2

Dans ce paragraphe, nous nous intéressons aux applications des ultrasons à l'oxydation des dérivés de l'alcool benzylique. Cependant, il faut signaler qu'il y a peu d'occurrences dans la littérature, même lorsqu'on ne se limite pas à l'oxydation aérobie.

Les ultrasons sont en fait plus souvent utilisés pour la délignification de la biomasse lignocellulosique afin de pouvoir convertir plus facilement la cellulose (en pâte à papier blanchie ou en carburant) [19]. Il existe diverses méthodes qui peuvent présenter de fortes similitudes avec les procédés d'extractions de la lignine (voir IA. 2.1). Leur dénominateur commun est que ces procédés visent à améliorer le transfert de l'agent délignifiant sur les parois de la biomasse lignocellulosique et de rompre la liaison covalente entre la lignine et l'hémicellulose tout en préservant la structure de la lignine [30], ce qui est déterminant pour les procédés de clivage oxydant (voir IA. 6). Ainsi, il est rare de trouver des quantifications de molécules plateformes issus de l'oxydation de la lignine comme dans la partie IA, mais les rendements obtenus en aldéhydes et acides phénoliques sont très faibles [31]. L'effet positif des ultrasons a été démontré, que ce soit sur l'étape de prétraitement où dans les étapes de délignification. Dans la majorité des cas, elle s'effectue en milieu alcalin sous irradiation par ultrasons [32-39]. Les taux de délignification obtenus peuvent aller jusqu'à 60 %. Il existe aussi d'autres procédés de délignification : i) en milieu acide [32, 40] (HCl souvent car meilleur catalyseur pour le clivage de la liaison lignine-hémicellulose) (taux de délignification maximum : 80%) ii) en présence d'un surfactant qui permet de diminuer le seuil de BLAKE (voir Eq IC.2) [36, 41] iii) dans un solvant organique tel que l'éthanol [42] ou dans un DES (Deep-Eutectic Solvent), un solvant vert présenté comme une alternative à la délignification

alcaline [39]) iv) délignification oxydante [43], notamment via des réactions de sono-FENTON [44].

Comme dans la partie IB, nous nous intéresserons à l'oxydation des dérivés de l'alcool benzylique, mais nous nous ne limiterons pas à l'oxydation par le dioxygène en ce qui concerne les modèles simples et les exemples avec le peroxyde d'hydrogène seront aussi étudiés.

Il est cependant pertinent de signaler que des oxydants minéraux sont tels que $KMnO_4$ en phase hétérogène [45-46], le peroxodisulfate de choline [47], l'acide nitrique [48], le diiode [49] pour l'oxydation de dérivés de l'alcool benzylique ainsi que l'oxone® (en présence d'oxyde de graphène) pour l'oxydation du benzaldéhyde et dérivés sous l'assistance des ultrasons à basse fréquence [50-51] ont aussi été utilisés. En général, il a été montré que l'apport des ultrasons a été d'améliorer le transfert de matière et par conséquent de faciliter la réaction d'oxydation du substrat ainsi que l'action du catalyseur. Un catalyseur qui a été souvent utilisé est l'oxyde de graphène. Son action consiste soit à oxyder le substrat, soit à rendre le substrat (cas du benzaldéhyde) plus électrophile afin d'accélérer l'oxydation en acide carboxylique. Néanmoins, l'inconvénient des oxydants minéraux est que des sous-produits sont générés en quantités importantes. L'oxydation par H_2O_2 ou par O_2 ne génèrent que l'eau comme sous-produit. Le peroxyde d'hydrogène est généralement plus souvent utilisé que le dioxygène pour l'oxydation assistée par ultrasons. Un tel procédé nous a donc semblé être un bon point de départ pour comprendre l'impact des ultrasons.

MAHAMUNI *et al* ont oxydé l'alcool benzylique en benzaldéhyde dans un binaire dichlorométhane-eau sous irradiation par des ultrasons à 22 kHz pendant 2,1 h en faisant varier des paramètres comme la quantité d'oxydant et de catalyseurs (Tableau IC.3, entrées 1a-d) [52]. Les catalyseurs utilisés sont un catalyseur de transfert de phase, l'aliquat-336 et l'acide phosphotungstique. Les paramètres optimisés sont : 2,8 équivalents de peroxyde d'hydrogène, 4 mol% d'aliquat-336 et 0.6 mol% d'acide phosphotungstique (entrée 1a). Il faut noter que le rendement en benzaldéhyde n'est que de 11%. Sans ultrasons, le rendement diminue à 4.4% (entrée 1b). Cependant, sous irradiation, sans catalyseur de transfert de phase, le rendement a chuté à 0.5% (entrée 1c) et sans acide phosphomolybdique, le benzaldéhyde ne se forme même pas (entrée 1d), ce qui montre que les ultrasons ne peuvent pas remplacer les catalyseurs. BEHLING *et al* ont utilisé le même oxydant (2 équivalents) pour l'oxydation de l'alcool vanillique (0.035 M) catalysée par 63 mol% de Co_3O_4 synthétisé par co-precipitation dans l'eau à 75°C sous irradiation par des ultrasons à 20 kHz (0.25 W/mL) [52]. La conversion a atteint 38% et le rendement en vanilline est de 19% (Tableau IC.3, entrée 2a) au bout de 15 min, ce

qui est légèrement meilleur que dans le cas de MAHAMUNI *et al*. Sans catalyseur, avec ultrasons, le rendement chute à 2% (entrée 2c), mais sans diminution significative de la conversion (35% *vs* 38%) et l'acide vanillique n'a pas été détecté, ce qui montre que le catalyseur est indispensable à la synthèse de la vanilline. Sans ultrasons, avec catalyseur, la conversion a été de 32% et le rendement a été de 7% (entrée 2b) au bout de 1 h, ce qui montre l'effet positif des ultrasons. Sans ultrasons et sans catalyseur, la conversion chute à 12% sans formation de vanilline (entrée 2d).

Tableau IC .3: Impact des ultrasons sur l'oxydation de l'alcool benzylique (source US : bain à ultrasons)

Entrée	Substrat (Conc en M)	Eq H_2O_2	Catalyseur (charge en mol%)	T (°C)	t (h)	Solvant	Ultrasons f (kHz)	Ultrasons P_{acous} (W/mL)[a]	Conv. (%)	Rdt (%)	Réf
1a	Alcool benzylique  0.76	2.8	Aliquat-336[b] (4) $H_3PW_{12}O_{40}$ (0.6)	39	2.08	CH_2Cl_2-eau 3:2	22	0.20	n. i.	**9**H: 11	52
1b			Aliquat-336 (4) $H_3PW_{12}O_{40}$ (0.6)					0	n. i.	**9**H: 4.4	
1c			$H_3PW_{12}O_{40}$ (0.6)					0.20	n. i.	**9**H: 0.5	
1d			Aliquat-336 (4)					0.20	n. i.	**9**H: 0	
2a	Alcool vanillique 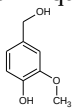 0.035	2	Co_3O_4 (63)	75	0.25	Eau	20	0.25	38	**11**G: 19	53
2b			Co_3O_4 (63)		1			0	32	**11**G: 7	
2c			-		0.25			0.25	35	**11**G: 2	
2d			-		1			0	12	**11**G: 0	

[a]Puissance acoustique ; [b]méthyl trocytl-(tricapryl)ammonium chloride

Ainsi, même si les ultrasons ont un effet positif sur l'oxydation de l'alcool en aldéhyde, ils ne peuvent se substituer aux catalyseurs dans le cas de l'oxydation par le peroxyde d'hydrogène en solution aqueuse. On peut remarquer que les rendements en aldéhydes aromatiques dans le cas de l'oxydation par le peroxyde d'hydrogène sont bien plus bas que dans les cas d'oxydation par des oxydants minéraux ($KHSO_5$, $KMnO_4$…). Comme l'eau oxygénée est un oxydant plus « vert » que les oxydants minéraux cités (l'eau est le seul sous-produit), un tel procédé d'oxydation mérite des recherches plus approfondies et il n'est qu'à ses débuts. De plus, seules des basses fréquences ont été utilisées et comme montré dans le paragraphe IC.2.2, une fréquence plus élevée peut permettre de favoriser les réactions d'oxydations par la formation d'espèces actives du dioxygène *in situ*. Il faut cependant noter que ceci peut être une arme à double tranchant comme observé dans les travaux de NAPOLY *et al*. Comme indiqué dans l'introduction de l'étude bibliographique du clivage aérobie de la lignine, il serait plus intéressant de partir du dioxygène et de former H_2O_2 *in situ*. Ainsi, pour clore cette étude, trois exemples d'oxydation par l'oxygène et sous ultrasons sont décrits.

Le premier, qui date de 2012 (MIRZA-AGHAYAN *et al*) concerne l'oxydation de l'alcool benzylique (5 mM) dans le toluène en présence d'oxyde de graphène (200 wt%)

(Tableau IC.4a, entrées 1a-b) dans le toluène à 80°C [53]. L'oxyde de graphite, soluble dans le toluène joue le rôle d'oxydant primaire et le dioxygène joue le rôle d'oxydant terminal. Deux modes d'irradiation (80 kHz) ont été comparés : avec une sonde (non indiqué dans le tableau) et dans un bain à ultrasons (entrée 1a). Dans les deux cas, une conversion supérieure à 99% a été obtenue (au bout de 45 min dans le cas de la sonotrode et au bout de 2 h dans le bain à ultrasons). Cependant, l'irradiation par une sonde a donné lieu à une sélectivité en benzaldéhyde de 58% et à la formation de produits non identifiés (41%) alors que la réaction dans le bain à ultrasons a eu pour résultat un rendement en benzaldéhyde de 98%. Ceci est lié au fait que la puissance émise par la sonotrode est plus localisée. Ainsi, la puissance autour de la sonde est élevée, ce qui donne des conditions plus dures, ce qui ne bénéficie pas à la formation du benzaldéhyde.

Dans le cas du bain à ultrasons, la puissance émise est au contraire moins localisée et plus uniforme dans le milieu réactionnel. Elle est donc plus faible, ce qui modère la réaction d'oxydation, ce qui donne une meilleure sélectivité en benzaldéhyde dans le toluène par exemple. L'alcool *p*-méthoxybenzylique a été oxydé dans les mêmes conditions (Tableau IC.4b, entrée 1). Au bout de 30 min, un faible rendement (24%) en anisaldéhyde a été obtenu, ce qui monte l'effet négatif du groupement donneur d'électrons, mais aucune indication n'est donnée sur la conversion ainsi que sur d'éventuels produits secondaires. Aussi, un autre solvant (hexane) a été testé ainsi une quantité plus faible en oxyde de graphène (50 wt% au lieu de 200 wt%, Tableau IC. 4a, entrée 1b). Ces conditions ont donné une conversion de 86% et se sont révélées plus sélectives pour l'étherification (rendement en éther de diphényle : 54%) que pour l'oxydation en benzaldéhyde (32%). Ceci peut être lié à une plus faible proportion d'oxyde de graphène qui joue le rôle d'oxydant primaire.

Tableau IC. 4a: Oxydation de l'alcool benzylique assistée par ultrasons (mode d'irradiation : bain à ultrasons)

Entrée	Conc.[a] (M)	Oxydant (éq)	Catalyseur (charge en mol%)	T (°C)	t (h)	Solvant	Ultrasons		Rdt (%)		Réf
							f (kHz)	Puissance (W)	[O]	autres	
1a	0,005	Air (atm)	Oxyde de graphène (200 mol%)	n. c.[b]	2	Toluène	80	n. i.	**9**H: 98	n. i.	56
1b			Oxyde de graphène (50 mol%)			Hexane			**9**H: 32	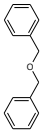 54	
2a[c]	0,25	Aucun (Ar)	Oxyde de graphène (139 mol%)	50	1,5	MeCN	37	n. i.	**10**H-Nbenzyl: 55	n. i.	55
2b[c]		O_2 (saturé)			0,5				**10**H-Nbenzyl: 95		
2c[c]		Air (atm)			1,5				**10**H-Nbenzyl: 82; 83[e]; 82[f]; 32[g]		
2d[d]					0,5				**10**H-Nphen: 82		
3	0,5	Air (atm)	MWCNTs/TiO_2 28 wtM	25	0,25-0,5	MeCN	40	n. i.	**9**H: 100, 97[f]	n. i.	56

[a]Alcool benzylique ; [b]not controlled ; [c]Avec 1 éq d'amine benzylique ; [d]Avec 1 éq d'aniline ;
[e]Après 5 recyclages ; [f]Après 6 recyclages ; [g]Après 7 recyclages

Tableau IC. 4b: Oxydation des dérivés de l'alcool benzylique fonctionnalisés sous air assistée par ultrasons

Entrée	Substrat (Conc en M)	Catalyseur (charge en mol%)	T (°C)	t (h)	Solvant	Ultrasons f (kHz)	Ultrasons Puissance (W)	Rdt (%) [O]	Rdt (%) autres	Réf
4	Alcool *p*-méthoxybenzylique 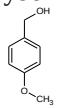 0.005	Oxyde de graphène (200 wt%)	80	0.5	Toluène	80	n. i.	**13**H: 24	n. i.	54
5	Alcool *p*-méthoxybenzylique 0.5	MWCNTs/TiO_2 (28 wt%)	25	0.25-0.5	MeCN	40	n. i.	**13**H: 94	n. i.	56
6	Alcool *p*-méthylbenzylique 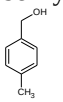 0.5	MWCNTs/TiO_2 (28 wt%)	25	0.25-0.5	MeCN	40	n. i.	 90	n. i.	56
7	Alcool vanillique  0.25	Oxyde de graphène (139 wt%)	50	1.5	MeCN	37	n. i.	**12**G-Nphen: 70	n. i.	55

Les mêmes équipes ont aussi testé l'oxyde de graphène (139 wt%) en tant que catalyseur pour l'amidification oxydante de l'alcool benzylique (0.25 M) en présence d'un équivalent d'amine benzylique dans l'acétonitrile à 50°C sous irradiations par des ultrasons à 37 kHz pendant 1,5h sous atmosphère inerte (Tableau IC.4a, entrée 2a), sous air (entrée 2b) ainsi qu'en présence d'un solvant saturé en dioxygène (entrée 2c, 30 min) [54]. Il faut noter que dans ce cas, le produit visé, un amide (carbone trivalent) est issu d'une oxydation plus poussée que dans le cas précédent où le produit ciblé est le benzaldéhyde (carbone divalent). Au bout de 1,5 h, le rendement en N-benzylbenzamide a atteint 55% sous argon et 82% sous air ce qui montre que la réaction peut certes se faire sans oxygène, mais que ce dernier permet d'accélérer l'oxydation de l'alcool benzylique en N-benzylbenzamide. La saturation du solvant en dioxygène a permis d'accélérer davantage l'oxydation vu que le rendement en amide a atteint 95% au bout de 30 min au lieu de 1,5 h. Selon le mécanisme proposé par les auteurs, l'irradiation par les ultrasons permet d'une part d'oxyder l'alcool benzylique en benzaldéhyde et d'autre part d'activer le dioxygène en présence d'oxyde de graphène. Aussi, sous irradiation, l'amine est oxydée par le dioxygène activé, ce qui forme un radical aminyle, un oxydant fort et un électrophile qui s'additionne sur le groupement carbonyle, ce qui forme un radical alkoxyle qui cède ensuite un radical $H^{\cdot}$, ce qui donne l'amide final (Fig. IC. 2). Aussi, comme l'oxyde de graphène permet d'exacerber le caractère électrophile du groupement carbonyle, l'addition électrophile de l'amine est ainsi favorisée, ce qui donne un hémiaminal qui, sous l'effet des ultrasons, est oxydé par l'oxyde de graphène pour donner lieu à la formation de l'amide visé. L'effet des ultrasons a été de nouveau d'améliorer le contact entre le catalyseur avec le dioxygène (activation) et le substrat (renforcement du caractère électrophile). Ici, l'oxydation va jusqu'à un amide, un dérivé de l'acide carboxylique. Ceci est lié à la présence d'un nucléophile (amine). En effet, dans le cas précédent, aucun nucléophile n'a été utilisé.

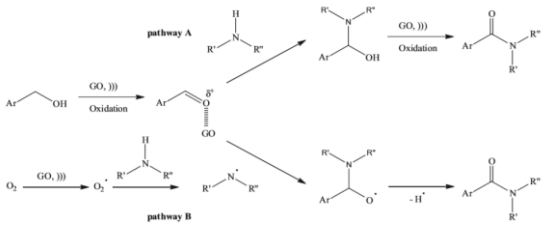

Figure IC. 2: Mécanisme d'amidification oxydante des alcools benzyliques catalysée par l'oxyde de graphène

Des tests de stabilité de l'oxyde de graphène ont été réalisés sous air. Le rendement en N-benzylbenzamide a été conservé jusqu'à après 5 recyclages. Au bout du sixième recyclage, le rendement chute de 83 à 32% (entrée 2c), ce qui est lié à une perte

du caractère oxydant du catalyseur. L'aniline a été utilisée à la place de l'amine benzylique (entrée 2d) dans les conditions d'une oxydation sous air. Le produit ciblé est alors le N-phénylbenzamide. Il a été obtenu avec un rendement de 82%, ce qui est identique à celui du N-benzylbenzamide. Cette réaction n'est donc pas sensible au type d'amine. L'alcool vanillique (0.25 M) a aussi été oxydé en N-phénylvanillamide dans les mêmes conditions (Tableau IC.4b, entrée 7) en présence d'un équivalent d'amine benzylique. Le rendement en amide est de 70% au bout de 1,5h (*vs* 82% pour le N-phénylbenzamide).

Enfin, plus récemment, MALEKI a testé un catalyseur hybride constitué de nanotubes de carbone et de TiO_2 (28 wt%) pour l'oxydation de l'alcool benzylique (0,5 M, Tableau IC.4a, entrée 3) ainsi que de l'alcool *p*-méthylbenzylique (Tableau IC.4b, entrée 6) et de l'alcool *p*-méthoxybenzylique (Tableau IC.4b, entrée 5) sous air dans l'acétonitrile à 40°C sous irradiation par des ultrasons à 40 kHz [55]. L'alcool benzylique a été quantitative oxydé en benzaldéhyde après 30 min maximum et le rendement en ce dernier est de 97% au bout de 5 recyclages au bout de la même durée, ce qui est le meilleur résultat d'oxydation sous air. De la même manière, le rendement en *p*-méthylbenzaldéhyde et en *p*-anisaldéhyde ont atteint 90% et 94% respectivement, ce qui montre qu'un groupement donneur n'a qu'un faible effet négatif sur le rendement en aldéhyde.

Ainsi, l'oxydation sous air assistée par ultrasons a déjà pu donner des résultats très prometteurs, notamment dans le cas de MALEKI avec un rendement en benzaldéhyde de 100% en moins d'une demi-heure. Ceci est non seulement lié à un meilleur transfert de dioxygène mais aussi à une meilleure activation de cet oxydant par le catalyseur comme montré par MIRZA-AGHAYAN *et al*. Ceci doit motiver à faire des recherches approfondies et à élargir la gamme des dérives de l'alcool benzylique. En effet, seules des basses fréquences ont été testées et depuis 2000, il y a seulement 3 références qui ont traité d'un tel sujet. Il faut noter que, bien que le dioxygène soit un oxydant moins fort que l'eau oxygénée, ce dernier n'a pas donné lieu à des rendements aussi élevés. Il faut cependant signaler que les solvants utilisés sont des solvants organiques et non pas l'eau (notamment dans Ref 47) contrairement aux cas d'oxydation par le peroxyde d'hydrogène. Le transfert de dioxygène est donc un facteur critique. Au vu de la fréquence utilisée, les phénomènes physiques tels que la formation de turbulences et des micro-jets et les forces de cisaillement l'emportent sur le phénomène sono-chimique dont l'efficacité

est maximisée aux alentours de 300-500 kHz [30] comme montré dans le paragraphe IC.2.2. Ceci aboutit à un meilleur transfert de dioxygène.

IC. 3. Conclusions

L'intensification sono-chimique pour le clivage aérobie de la lignine et de ses modèles n'ont pas été étudiés et il y a très peu d'occurrences concernant l'application de cette voie d'intensification pour l'oxydation aérobie des dérivés de l'alcool benzylique. Des résultats très prometteurs ont déjà pu être obtenus dans le cas de l'oxydation de l'alcool benzylique, ce qui est lié à un meilleur transfert de dioxygène. Néanmoins, ceci n'en est qu'à ses débuts et cette voie mérite d'être explorée davantage. Le dioxygène peut être un oxydant plus adapté que le peroxyde d'hydrogène pour le clivage oxydant de la lignine en aldéhydes phénoliques à conditions que le transfert de dioxygène soit optimisé comme montré à plusieurs reprises dans cette étude bibliographique. Pour ces raisons, l'intensification sono-chimique est une voie à explorer pour le clivage aérobie de la lignine et de ses modèles. La voie sono-chimique peut permettre d'activer le dioxygène et de le transformer en espèces actives ($O_2^{\cdot -}$, $HO^{\cdot}$). Aussi, il a été montré dans la partie IB que les $PMoV_x$ réduits peuvent remplir ce rôle. Ainsi l'intensification sono-chimique pourrait agir en synergie avec les $PMoV_x$ pour le clivage oxydant de la lignine par le dioxygène.

Références

[1]: L. J. Mitchell, C. J. Moody, *J. Org. Chem.* **2014**, 79, 11091-11100.
[2]: S. Gazi, M. Đokić, A. Mangala P. Moeljadi, R. Ganguly, H. Hirao, H. Sen Soo, *ACS Catal.* **2017**, 7, 4682-4691.
[3]: S. H. Lim, K. Nahm, C. S. Ra, D. W. Cho, U. C. Yoon, J. A. Latham, D. Dunaway-Mariano, P. S. Mariano, *J. Org. Chem.* **2013**, 78, 9431-9443.
[4]: D. W. Cho, R. Parthasarathi, A. S. Pimentel, G. D. Maestas, H. J. Park, U. C. Yoon, D. Dunaway-Mariano, S. Gnanakaran, P. Langan, P. S. Mariano, *J. Org. Chem.* **2010**, 75, 6549-6562.
[5]: A. M. Mcnally, E. C. Moody, K. Mcneill, *Photochem. Photobiol. Sci.* **2005**, 4, 268-274.
[6]: M. D'auria, R. Ferri, *J. Photochem Photobiol* **2003**, 157, 1-4.
[7]: C. Bonini, M. D'Auria, *Ind. Crop. Prod.* **2004**, 20, 243-259.
[8]: C. Díaz-Urrutia, B. B. Hurisso, P. M. P. Gauthier, B. Sedai, R. D. Singer, R. T. Baker, *J. Mol. Catal. A* **2016**, 423, 414-422.
[9]: Y. Yang, H. Fan, J. Song, Q. Meng, H. Zhou, L. Wu, G. Yang, B. Han, *Chem. Commun.* **2015**, 51, 4028-4031.
[10]: Y. Yang, H. Fan, Q. Meng, Z. Zhang, G. Yang, B. Han, *Chem. Commun.* **2017**, 53, 8850-8853.
[11]: F. Cheng, H. Wui, R. D. Rogers, *ACS Sustainable Chem. Eng.* **2014**, 2, 2859-2865.
[12]: G. F. De Gregorio, R. Prado, C. Vriamont, X. Erdocia, J. Labidi, J. P. Hallett, T. Welton, *ACS Sustainable Chem. Eng.* **2016**, 4, 6031-6036.
[13]: S. Liu, Z. Shi, L. Li, S. Yu, C. Xiec, Z. Song, *RSC Adv.* **2013**, 3, 5789-5793.
[14]: K. Stärk, N. Taccardi, A. Bössman, P. Wassercheid, *ChemSusChem* **2010**, 3, 719-723.

[15]: A. A. Shamsuri, D. K. Abdullah, *Oxid. Commun.* **2012**, 35, 767-775.
[16]: G. Chatel, K. de Olivera Vigier, F. Jerôme, *ChemSusChem* **2014**, 7, 2274-2287.
[17]: F. Napoly, N. Kardos, L. Jean-Gérard, C. Goux-Henry, B. Andrioletti, M. Draye, *Ind. Eng. Chem. Res.* **2015**, 5422, 6046-6051.
[18]: D. V. Pinjari, P. R. Gogate, K. Prasad, M. Ashokkumar, *Cavitation* **2014**, Pan-Stanford Publishing, 171-179.
[19]: Y. Liu, Y. Nie, X. Lu, X. Zhang, H. He, F. Pan, L. Zhou, X. Liu, X. Ji, S. Zhang, *Green Chem* **2019**, 21, 3499-3535.
[20]: W. Lauterborn, *J. Phys. Colloq.* **1979**, 40, 273-278.
[21]: H. Dutilleul, A. Partaloglu, P. Da Costa, M.E. Galvez, *Chem. Eng. Process. Process. Intensif.* **2017**, 112, 47-55
[22]: O. M. Rayleigh, *Philos. Mag.* **1917**, 34, 94-98.
[23]: M. S. Plesset, *J. Appl. Mech.* **1949**, 16, 277-282.
[24]: F. Blake Jr., Ph.D. thesis, Harvard University, 1949.
[25]: L. Parizot, *thèse de doctorat*, Sorbonne Université, 2019.
[26]: M. M. Daou, thèse de doctorat, Sorbonne Université, 2018.
[27]: M. Lupacchini, A. Mascitti, G. Giachi, L. Tonucci, N. d'Alessandro, J. Martinez, E. Colacino, *Tetrahedron* **2017**, 73, 609-653.
[28]: C. Petrier, Y. Jiang, M-F. Lamy, *Environ. Sci. Technol.* **1998**, 32, 1316-1318.
[29]: R. J. Wood, J. Lee, M. J. Bussemaker, *Ultrason. Chem.* **2017**, 38, 351-370.
[30]: M. J. Bussemaker, D. Zhang, *Ind. Eng. Chem. Res.* **2013**, 52, 3563-3580.
[31]: J-X Sun, F Xu, X-F Sun, R-C Sun, S-B Wu, *Polym. Int.* **2004**, 53, 1711-1721
[32]: H. Behesti, K. Karimi, *Eng. Life Sci.* **2016**, 16, 750-761.
[33]: D. K. Kim, K. E. O'Shea, W. J. Cooper, *Sci. Total. Env.* **2012**, 430, 246-259.
[34]: M. Brahim, S. el Kantar, N. Boussetta, N. Grimi, N. Brosse, E. Vorobiev, *Biomass Bioener.* **2016**, 95, 92-98.
[35]: R. Terán Hilares, J. César dos Santos, M. Ajaz Ahmed, S. Hwan Jeon, S. Silvério da Silva, J-I. Han, *Biores. Technol.* **2016**, 214, 609-614.
[36]: C. Zhong, H. Jia, P. Wei, *Process Biochem.* **2017**, 53, 180-187.
[37]: M. Eblaghi, M. Niakousari, M. Sarshar, G. Reza Mesbahi, *J. Food Process Eng.* **2015**, 39, 273-282.
[38]: C. Dong, J. Chen, R. Guan, X. Li, Y. Xin, *Renew. Ener* **2018**, 127, 444-451.
[39]: E. Calcio Gaudino, S. Tabasso, G. Grillo, G. Cravotto, T. Dreyer, G. Schories, S. Altenberg, L. Jashina, G. Telysheva *C. R. Chimie*, **2018**, 21, 563-571.
[40]: S. Mohapatra, S. Pattathil, H. Thatoi, *ACS Sustainable Chem. Eng.* **2017**, 5, 6486-6497.
[41]: M. Shanthi, J. Rajesh Banu, P. Sivashanmugam, *Biores. Technol.* **2018**, 264, 35-41.
[42]: M-F. Li, S-N. Sun, F. Xu, R-C. Sun, *Ultrason. Chem.* **2012**, 19, 243-249.
[43]: R. Ravindran, S. Jaiswal, N. Abu-Ghannam, A. K. Jaiswal, *Biores. Technol.* **2017**, 224, 680-687.
[44]: A. Kawee-ai, A. Srisuwun, N. Tantiwa, W. Nontaman, P. Boonchuay, A. Kuntiya, T. Chaiyaso, P. Seesuriyachan, *Ultrason. Chem.* **2016**, 31, 184-192.
[45]: T. X. Thi Luu , P. Christensen , F. Duus, T. Ngoc Le, *Synth. Commun.* **2011**, 38, 2011-2024.
[46]: S. Rahmatia, A. Khazaeib, M. Golbaghia, M. Panahimehrc, *Iran. Chem. Commun.* **2018**, 6, 109-113.
[47]: B. L. Gadilohar, D. V. Pinjari, G. S. Shankarling, *Ind. Eng. Chem. Res.* **2016**, 55, 4797-4802.
[48]: R. Naik, A. Nizam, A. Siddekha, M. A. Pasha, *Ultrason. Chem.* **2011**, 18, 1124-1127.
[49]: M. Afzal Pasha, S. Nagashree, *Ultrason. Chem.* **2013**, 20, 810-814.
[50]: M. Mirza-Aghayan, M. Molaee Tavana, R. Boukherroub, *Tetrahedron Lett.* **2014**, 55, 342-345.
[51]: M. Mirza-Aghayan, S. Zonoubi, M. Molaee Tavana, R. Boukherroub, *Ultrason. Chem.* **2015**, 22, 359-364.
[52]: N. N. Mahamuni, P. R. Gogate, A. B. Pandit, *Ind. Eng. Chem. Res.* **2006**, 45, 98-108.
[53]: R. Behling, G. Chatel, S. Valange, *Ultrason. Chem.* **2017**, 36, 27-35.
[54]: M. Mirza-Aghayan, M. Molaee Tavana, R. Boukherroub, *Tetrahedron Lett.* **2012**, 53, 4962-4965.
[55]: M. Mirza-Aghayan, N. Ganjbakhsh, M. Molaee Tavana, R. Boukherroub, *Ultrason. Chem.* **2016**, 32, 37-43.
[56]: A. Maleki, *Ultrason. Chem.* **2018**, 40, 460-464.

Partie Résultats - Discussion

II. Lignin model aerobic cleavage catalyzed by $PMoV_x$: operational parameters

II. 1. Introduction

Lignin is the second most abundant natural polymer on our planet and the only natural, renewable and abundant source of aromatic compounds. It has raised increasing interest due to the depletion of oil, from which aromatic compounds are currently mainly produced. One of the most outstanding lignin valorization routes is its oxidation to aromatic platform molecules such as vanillin obtained from C-C cleavage [1]. Aerobic lignin cleavage in alkali media was already set up in the industrial scale on the 1930's. The major problem is the elimination of caustic wastes conjugated with a rather low yield of vanillin [2]. So, such process is currently not competitive against the oil-based routes for vanillin production and has to be improved. O_2 will be used as it is the most sustainable oxidant. However, it needs to be activated by a catalyst. Several metal-containing catalysts were assessed for aerobic oxidative cleavage of lignin [3, 4] (see paragraph IA 3). . The two main metals used are copper [5-11] and vanadium [6, 11, 12]. KEGGIN molybdovanadophosporic acids ($H_{3+x}PMo_{12-x}V_vO_{40}$, nH_2O) noted $PMoV_x$ [13-15] are among the vanadium-based catalysts reported. Since two decades, KEGGIN $PMoV_x$ are well-known to be adequate for wood pulp oxygen delignification since the contributions of WEINSTOCK *and coll* [16] and EVTUGUIN *et coll* [17, 18]. Also, these catalysts already proved to be efficient catalysts for the C-C cleavage in ketones (70°C) and α-ketols in an atmosphere of dioxygen, at room temperature [18-20] as detailed in part IB.Herein, since lignin is an extremely complex molecule, preliminary studies of its oxidative cleavage are usually carried out on models. Several linkages as β-5, β-β and 5-5 are represented in lignin (paragraph IA. 2.1), but the β-O-4 bond (Fig. II.1) is always the major one [21]. As a result, many Cu [22-25] and V-catalysts [25-33] were assessed for the aerobic oxidative cleavage of models bearing these linkages. Besides, a $PMoV_5$ was tested by EVTUGUIN *et al* for the aerobic cleavage of phenolic (R^1 = H and R^2 = H or OMe) and etherified (R^1 = Me, R^2 = H) models (see Fig. II.2) in acetone-water 80-20 (O_2 5 bar, 90°C). The phenolic model was quantitatively converted in 20 min and the cleavage of the bond C(1)-C^α was

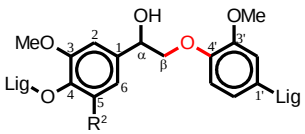

Figure II. 1: β-O-4 bond in lignin polymer

favored whereas the etherified model proved to be much more resistant to cleavage (conversion: 20%) and the catalyst was selective for C^{α}-C^{β} cleavage [34]. To the best of our knowledge, $PMoV_x$ catalysts were never tested on ketone models.

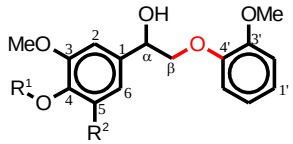

Figure II. 2: General strcture of the dimeric alcohol models tested by EVTUGUIN et al [34]

$PMoV_x$ catalysts can be synthesized either through the etherate, the hydrothermal or the oxo-peroxo routes (cf paragraph IB. 4. 3). The etherate pathway starts with aqueous soluble molybdenum and vanadium sodium salts. In this case, the $PMoV_x$ is obtained by acidification and then extracted by diethylether [35]. An obvious drawback is the use of a flammable, harmful and environmental hazardous organic solvent and of strong acids (HCl, H_2SO_4) [36]. The oxo-peroxo procedures involve hydrogen peroxide to form molecular complexes of Mo, V and P [37, 38]. However, these complexes, especially those of vanadium are rather unstable. In addition, hydrogen peroxide has to be used in excess due to its decomposition by $PMoV_x$ [39], which leads to the destabilization of the KEGGIN structure because of the transient formation of reduced $PMoV_x$ [40]. Consequently, in the present work, the hydrothermal pathway which just consists in refluxing the starting oxides and phosphoric acid in water was chosen for the synthesis of the reference $PMoV_x$ catalysts [41].

So, the aim in this part will be to set the operative conditions for the cleavage of two dimeric lignin models noted **K1**$_{HH}$ and **A1**$_{HH}$ (see paragraph IA. 2. 3, Table IA. 3). Firstly, the solvent, the catalytic loading so as the pressure and temperature will be optimized for the oxidative cleavage of the ketone **K1**$_{HH}$. A preliminary kinetic study will be carried out and a mechanism will be proposed. Afterwards, the stability of the catalyst will be assessed. The catalytic tests will be performed on **A1**$_{HH}$ in the conditions optimized for **K1**$_{HH}$ cleavage and finally some optimization essays will be performed.

II. 2. Experimental part

In this part will be described the experimental set up of catalyst characterization and lignin model aerobic cleavage monitoring.

II. 2. 1. Hydrothermal synthesis of $PMoV_x$ & characterization

Reference $PMoV_x$ ($H_{3+x}PMo_{12-x}V_xO_{40}$, nH_2O) materials were synthesized through an attack of MoO_3 (Acros Organics) and V_2O_5 (Sigma-Aldrich) by H_3PO_4 (purity 85%, Carlo Erba) in refluxing water. Two $PMoV_x$ noted V_1-HT (x = 1) and V_3-HT (x = 3) were synthesized.

For x = 1, the procedure took place according to ref. 8. 1.165 g of H_3PO_4 85% (10.1 mmol of H_3PO_4) were dissolved in 150 mL of distilled water. 14.41 g (100 mmol) of MoO_3 and 0.916 g (5 mmol) of V_2O_5 were added to the solution of H_3PO_4. The mixture was heated to reflux during 3 h. For x = 3, 0.386 g (3.3 mmol) of H_3PO_4 was dissolved in 200 mL of water and 3.93 g of MoO_3 (27.3 mmol) and 0.919 g (5.1 mmol) of V_2O_5 were added. Longer attack and more diluted conditions were needed to dissolve the oxides. So, the reflux lasted 6.5 h instead of 3 h. A reflux of 24 h was tested to enhance the dissolution but the amount of residual oxide did not decrease significantly meaning that a longer attack is not efficient. For both $PMoV_x$, after cooling, the residual oxides were removed by filtration and water was then evaporated leading to an orange powder.

The $PMoV_x$ solids were characterized by XRD on a Brüker Advance D8 diffractometer using the Cu Kα radiation (λ = 1.5406 Å) without a monochromator. The diffraction patterns were collected in an angular range of 2θ from 5° to 50°, with a scanning rate of 0.34°/min. The signals were then analyzed on the software EVA and treated with Fullprof to check the crystalline phases. The main parameters are the RIETVIELD factor R_P and Chi_2. They should be lower than 5%. The diffractograms were normalized according to the major peak. The diffractogram is impacted by the hydration of the $PMoV_x$ mainly (paragraph IB. 1.2.1)

Consequently, liquid ^{31}P NMR analyses of the PMoVx were performed on a 400 MHz Brüker apparatus. 30 mg of the solid were dissolved in 250 µL of D_2O (Eurisotop) and 250 µL of H_2O. 7.5 µL of dioxane (SDS, Carlo-Erba) were added too to the solution. For each analysis, 16 scans were recorded and the relaxation delay was set to 32 s. NMR enabled to confirm the KEGGIN structure. Moreover, as shown on Fig. SII. 6, the maximal relaxation time was established to 1.02 ± 0.11 s. So, the relaxation time set in each acquisition was higher than 5 times the relaxation delay of every phosphorous nucleus. As a result, the integration is considered to be quantitative and, because reactants were added in stoichiometric amounts, the area of the peak at 0 ppm

enables to calculate the unreacted H_3PO_4 and so the $PMoV_x$ yield. The latter corresponds to the molar fraction of phosphorous atom present in $PMoV_x$ complexes, hypothesizing that the lone impurity is H_3PO_4.

Once the KEGGIN structure was validated (Fig. II. 3), ICP analyses were carried out by Crealins on an ICP Thermo-Fischer iCAM Duo to calculate the mean number of vanadium equivalents per $PMoV_x$, noted x. Finally, TGA analysis of the $PMoV_x$ was performed on a Cp SDTQ600 system to calculate the hydration index noted n. To do this, the temperature was raised until 600°C at a heating rate of 10°C/min under an air flow of 100 mL/min. All the calculations are detailed on paragraph SII. 3 in the appendix (cf Determination of the formula of the synthesized $PMoV_x$).

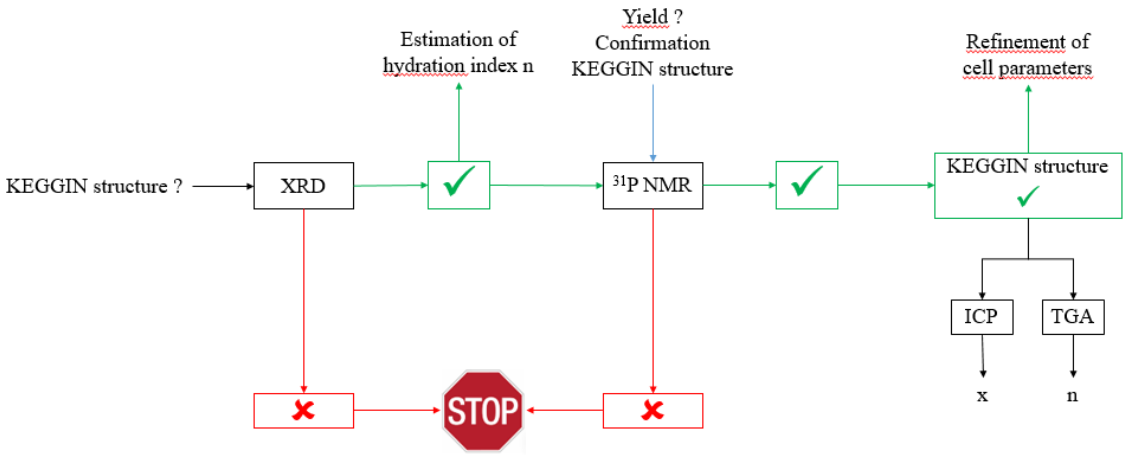

Figure II. 3: General procedure for $PMoV_x$ characterization

II. 2.2. Lignin model synthesis

Lignin models were synthesized by methods from the literature with slight modifications. The ketone models **K1**$_{HH}$ / **K1**$_{HG}$ were synthesized from 2-bromoacetophenone and phenol / guaiacol following the procedure described by NICHOLS *et al*. [42] The **K2**$_{HH}$ and **A1**$_{HH}$ models were obtained by the formylation and reduction of **K1**$_{HH}$, respectively. The **A1**$_{HH}$ alcohol was further acetylated in a 1:1 mixture of acetic anhydride-pyridine affording the acetic ester noted **Est**$^{\alpha}$**A1**$_{HH}$ [43].

The synthetic procedures are detailed in the appendix (Synthesis of dimeric lignin models).

II. 2.3. Catalytic tests in atmospheric conditions

The efficiency of the $PMoV_x$ for the aerobic cleavage in atmospheric conditions was tested on 1.5 mmol of four substrates (**K1**$_{HH}$ (0.3185 g), **K1**$_{HG}$ (0.3641 g), **A1**$_{HH}$ (0.3215 g), **K2**$_{HH}$ (0.3641 g) or **Est$^{\alpha}$A1**$_{HH}$ (0.4055 g)). If not specified, the concentration of the substrate was 100 mM. The substrates and then the catalyst were dissolved in 15 mL of the solvent in a Schlenk tube connected to gas burette system to monitor the dioxygen consumption (Fig II. 4).

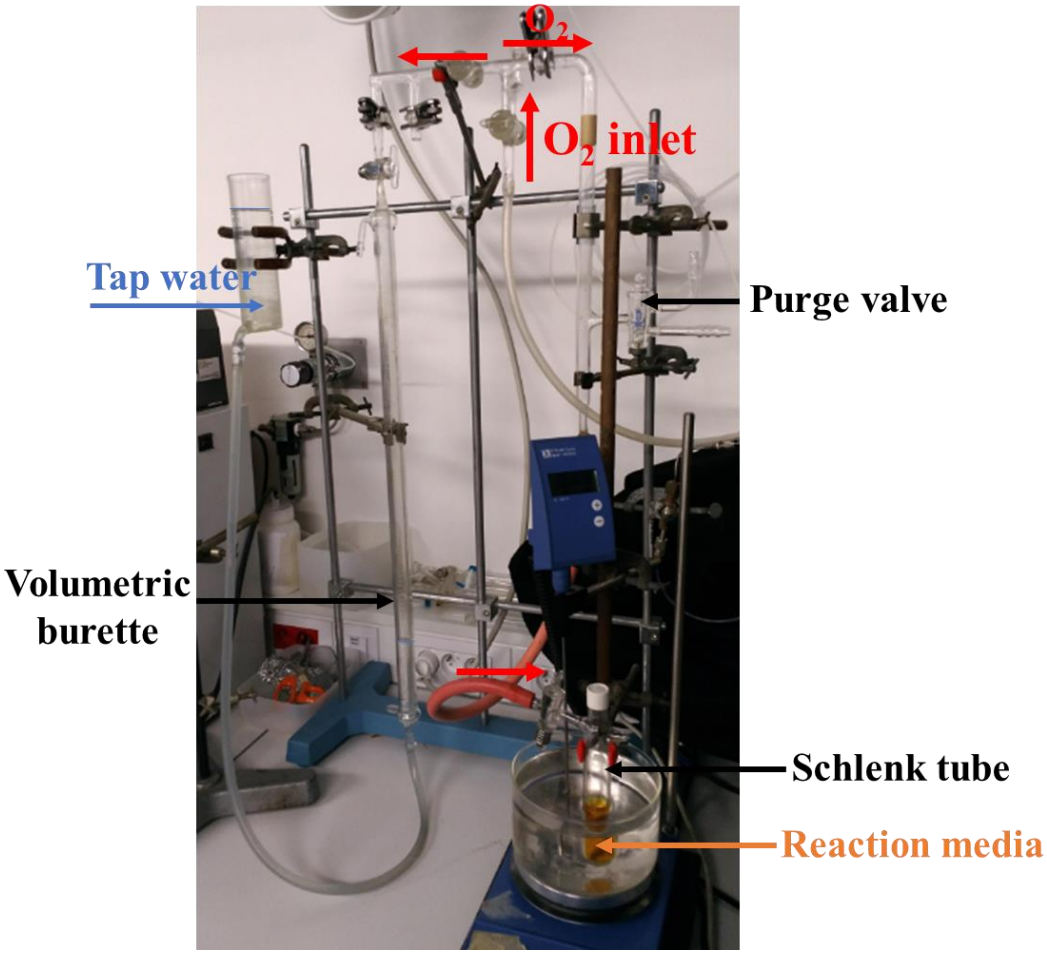

Figure II. 4: Set up of catalytic tests at atmospheric pressure

In a typical experiment, the combined loading of molybdenum and vanadium was adjusted to 15 mol%. The Schlenk tube was purged with dioxygen and then heated during 24 h at 82°C. The various sets of conditions tested at atmospheric pressure for both **K1**$_{HH}$ and **A1**$_{HH}$ are summarized in Table II.1 and Table II.2, respectively.

Table II. 1: Tests on ***K1****$_{HH}$*

Entry	Catalyst	Metal loading (mol%)	Solvent	Acetic acid volumic fraction (vol%)	Duration (h)
1			Acetonitrile	0	24
1bis					
2[a]			Methanol		
3			Acetic acid		24
4					15
5[b]			Water-Acetonitrile 14-1	100	
6	V_3-HT	15	Acetonitrile	2.5	24
7				5	
8				10	
8bis					
8ter					
9[a]				10	
10[c]				10	
11				20	
12			Water	10	
13	H_2SO_4 (5 µL)	0	Acetonitrile	10	24
14	V_3-HT	7			
15		18			
16		36			
17	PMo_{12}	15			
18	V_1-HT	15			
19		43			
20[d]	V_3-HT	15	Acetonitrile	10	24
21[e]					
22[f]					
23	V_3-HT	15	Acetonitrile	10	2
24					8
25					14
26					37
27					48
28[g]	V_3-HT	15	Acetonitrile	0.03 (5 µL)	24
29[h]				0.03 (5 µL)	
30[h]				0.13 (20 µL)	
31[h]				0.67 (100 µL)	
32[h]				3.6 (540 µL)	
33[i]	V_3-HT	15	Acetonitrile	10	24

Substrate 100 mM, P = 1 atm, T = 82°C if not specified, [a] T = 65°C; [b] T = 98°C; [c] T = r. T.; [d] PhOH instead of **K1$_{HH}$**; [e] PhCHO instead of **K1$_{HH}$**; [f] PhOH (50 mM) + PhCOOH (50 mM) instead of **K1$_{HH}$**; [g] H_2SO_4 instead of acetic acid; [h] TFA instead of acetic acid; [i] Recyclability test.

II. 2.4. Catalytic tests at higher pressure

Some tests on **A1**$_{HH}$ were carried out at higher pressure. In a typical experiment, 0.5358 g of the substrate (2.5 mmol) and 61.4 mg of V_3-HT were dissolved in 25 mL of solvent in a Teflon container that was further placed in an autoclave. The mixture became instantaneously green due to the reduction of the catalyst. Once the autoclave was sealed, the reaction medium was purged three times by dioxygen at room temperature. The pressure was set to 5 bar and then heated at 80°C or 120°C under stirring. Once the reaction is completed, the recovered solution is orange-brown. The different sets of conditions used are summarized in Table II.2.

*Table II. 2: Tests on **A1**$_{HH}$*

Entry	Catalyst	Co-oxidant (mol%)	Temperature (°C)	Pressure (bar)	Acetic acid fraction (vol%)	TFA fraction (vol%)	Duration (h)
1	V_1-HT	-	80	atm	10	-	24
2	V_3-HT				10		
3	H_2SO_4				10		
4	V_3-HT				0		
5					5		
6					100		
7					10	-	2
8							8
9							14
10							37
11							48
12			80	5	0		6
13			80				24
14			80				24
15			80				24
16			80				48
17			120		10		0.33
18			120				2
19			120				2
20			120				6
21		H_2O_2 (3)	80	atm	10	-	24
22		H_2O_2 (330)		atm			
23		TEMPO (15)		atm			
24		TEMPO (3)		5			
25		TEMPO (30)					
26		-	80	atm	0	0.67	24
27					0	1.67	
28					0	3.60	

A1$_{HH}$ 100 mM, loading of Mo + V = 15 mol%

II. 2.5. Monitoring of the catalytic tests

The reaction mixture was monitored by HPLC (Shimadzu LC-20AD) using a Shim-pack column (4.6 * 100 mm, 2.2 µm, stationary phase : C_{18}) heated to 40°C by an CT0-10AS oven. The mobile phase was constituted of aqueous AcOH (0.5 vol%) and

methanol (HPLC grade, VWR Chemicals) used at a flow rate of 0.4 mL/min. On Fig. II. 5 is given the evolution of the volumic fraction of methanol in the eluent

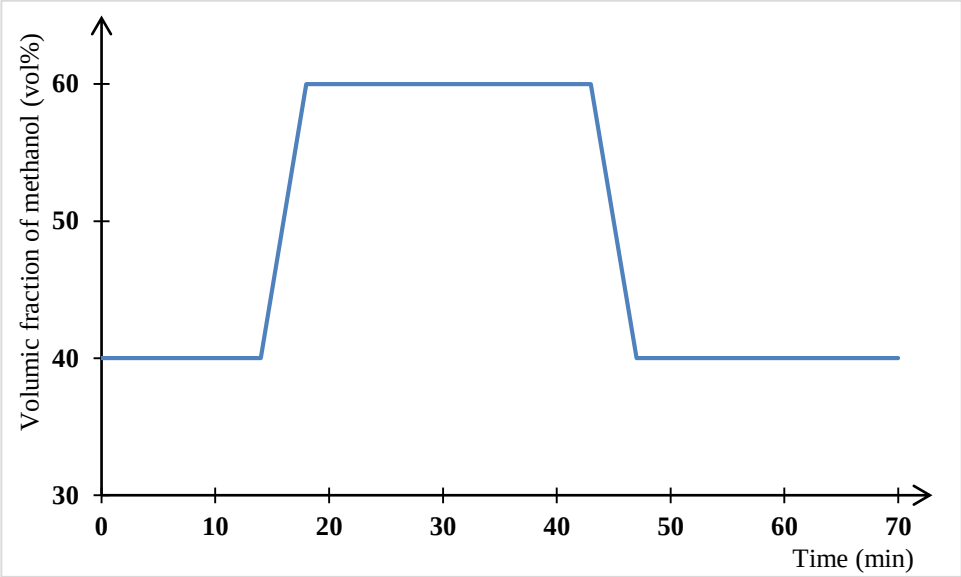

Figure II. 5: Evolution of the volumic fraction of methanol in the eluant

The substrates and the products were detected in UV (210, 220 and 254 nm) by an SPD-M20A detector. 0.5 mL of the reaction was sampled and dropped in a 20 mL volumetric flask and diluted by a ternary H_2O-MeOH-AcOH 49:49:2. In the case of the tests performed in water, for solubility reasons, the reaction mixture had to be diluted first by acetonitrile (15 mL added) and completed to 50 mL in a volumetric flask by methanol.

Benzaldehyde, benzoic acid, phenol, **K1**$_{HH}$, **A1**$_{HH}$, the acetic ester of **A1**$_{HH}$ noted **Est**$^{\alpha}$**A1**$_{HH}$ and the **A1**$_{HH}$ dehydration product noted **D1**$_{HH}$ (see paragraph IA. 3.1) were quantified according calibration curves (see Appendix, Fig SII. 1). The products of the C-O cleavage such as phenylglyoxylic acid, *etc* as well as quinones were not taken into account.

It has to be noticed that the relative error on the yield of **D1**$_{HH}$ was 10% due its determination method (by NMR, see the Appendix, Fig SII. 2-3). Therefore, $CB_{A1_{HH}}$ may be higher than 100%. A typical chromatogram obtained for **K1**$_{HH}$ oxidation in presence of V_3-HT (entry 11) is shown in Figure II.6a.

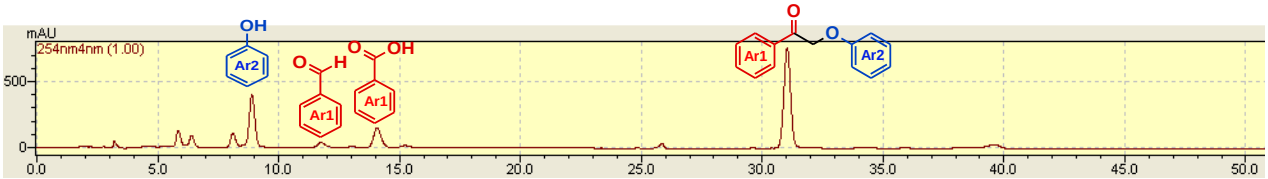

*Figure II. 6a: General HPLC profile of **K1**$_{HH}$ oxidative cleavage*

The retention times (RT) of the main products from **K1**$_{HH}$ cleavage are 8.3 min (phenol, PhOH), 10.9 min (benzaldehyde, PhCHO) and 14.0 min (benzoic acid).

Between 3 and 20 min, several minor products were also detected (Figure II.6b).

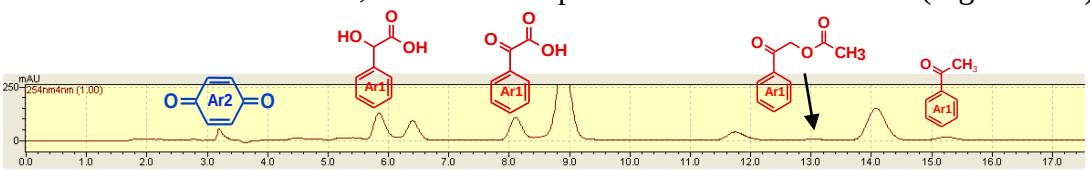

Figure II. 6b: Minor products from ***K1****$_{HH}$ oxidative cleavage detected by HPLC*

Four minor products resulting from the C-O cleavage in **K1**$_{HH}$, namely mandelic acid (5.7 min), phenylglyoxylic acid (8.0 min), acetoxyacetophenone (13.0 min) could be identified through the injection of their authentic samples. During the reaction, phenol was partly oxidized into *p*-quinone (RT = 4.7 min). Besides, **K1**$_{HH}$ may be cleaved through an acetolysis reaction (nucleophilic substitution of the phenoxy group by acetate moiety) giving rise to 2-acetoxyacetophenone (RT = 13 min).

The carbon balance, noted CB, was also calculated taking into account **K1**$_{HH}$ and the main oxidation products (PhOH, PhCHO and $PhCO_2H$, see Fig. II.6a). The expression used is: $CB_{K1_{HH}} \approx \frac{14(100-Conv)+6\eta_{PhOH}+7(\eta_{PhCHO}+\eta_{PhCOOH})}{14}$ where the yield of each product i is noted η_i.

Fig. II.7 shows a typical HPLC profile (254 nm) of the reaction mixture after the test on **A1**$_{HH}$ substrate (Table II. 3, entry 19). Three additional by-products could be detected: the ketone **K1**$_{HH}$ (RT = 31 min) provided by the oxidation of the secondary alcohol **A1**$_{HH}$, the acetic ester **Est**$^{\alpha}$**A1**$_{HH}$ (RT = 51 min) and the enol ether **D1**$_{HH}$ (RT = 29 min) obtained by the dehydration of **A1**$_{HH}$.

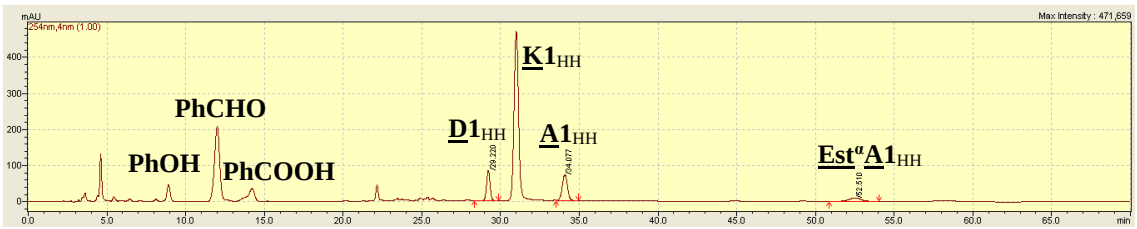

Figure II. 7: Typical HPLC profile of the catalytic tests on ***A1****$_{HH}$*

These side products had to be taken into account in the carbon balance as follows:

$$CB_{A1_{HH}} \approx \frac{14 * (100 - Conv + \eta_{A1_{HH}} + \eta_{Est^{\alpha}A1_{HH}} + \eta_{D1_{HH}}) + 6\eta_{PhOH} + 7(\eta_{PhCHO} + \eta_{PhCOOH})}{14}$$

where the yield of each product i is noted η_i.

D1$_{HH}$ could not be synthesized as a pure compound and, as a matter of fact, could not be quantified directly by HPLC. Consequently, an NMR study was carried out in order to determine the relative HPLC response factor of **D1**$_{HH}$ compared to that of **Est**$^{\alpha}$**A1**$_{HH}$ which could be quantified independently by HPLC. To do this, several reaction media were gathered in an 800 mL beaker and acetonitrile was evaporated at room temperature under air. A brown oil containing **D1**$_{HH}$, **Est**$^{\alpha}$**A1**$_{HH}$ and several other products in acetic acid was obtained. Consequently, 100 mL of water was added to lower the solubility of the organic products and especially of the dimeric ones. The latter were extracted by 2 x 100 mL of pentane (Carlo Erba) and 150 mL of cyclohexane (Carlo Erba). The aqueous phase was discarded and the organic phase was washed by 100 mL of brine and concentrated. 4 g of a pale-yellow solid were obtained. Then, 1 g of the concentrate was dissolved in 0.6 mL of $CDCl_3$ (Eurisotop). The solution was analyzed by ^{1}H NMR (300 MHz).

The Table II.3 sums up the different compounds issued from the treatment of the dimeric models in presence of $PMoV_x$ catalysts that can be detected by HPLC:

Table II. 3: List of all the products identified by HPLC

Retention time (min)	Compound	Supplier	Comments	
4.7	*p*-quinone (99%)	Merck	Identification by a commercial standard **No calibration**	Product from phenol oxidation
5.7	Mandelic acid (99%)	Aldrich		C-O cleavage product
8.0	Phenylglyoxylic acid (97%)	Aldrich		
8.3	Phenol (>99%)	Aldrich	Identification by a commercial standard. **Calibration at 210 nm**	Main products from dimeric model oxidative cleavage
9.4	Guaiacol (97%)	Sigma		
10.9	Benzaldehyde (>99%)	Aldrich		
13.0	2-phenoxyacetic acid	-	The standard was synthesized according to Ref 43 **No calibration**	Acetolysis product (non oxidative C-O cleavage)
14.0	Benzoic acid (99%)	Aldrich	Identification by a commercial standard. **Calibration at 220 nm.**	Main product from dimeric model oxidative cleavage
15.0	Acetophenone (>99%)	Fluka	Identification by a commercial standard **No calibration**	Acidic C-O cleavage product
25.0	**<u>K2</u>**$_{HH}$ 3-hydroxy-2-phenoxypropiophenone 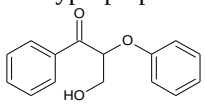	-	Identification by a synthesized standard according to Ref 42. **Calibration at 220 nm**	Ketone substrate
27.8	**<u>K1</u>**$_{HG}$ 2-(2-methoxy)-phenoxyacetophenone 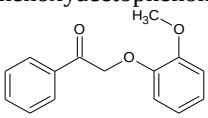	-	Identification by a synthesized standard aaccording to Ref 42. **Calibration at 220 nm**	Ketone substrate.
29.0	**<u>D1</u>**$_{HH}$ (E)-2-phenoxystyrene 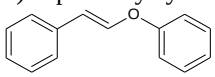	-	**Identification by NMR** Yield calculated at 254 nm.	**<u>A1</u>**$_{HH}$ dehydration product.
31.0	**<u>K1</u>**$_{HH}$ 2-phenoxyacetophenone	-	Identification by synthesized standard according to Ref 42. **Calibration at 220 nm**	Ketone substrate. **<u>A1</u>**$_{HH}$ oxidation product
34.0	**<u>A1</u>**$_{HH}$ 2-phenoxy-1-phenylethanol	-	Identification by synthesized standard according to Ref 43. **Calibration at 254 nm**	Alcohol substrate
51.0	**<u>Est</u>$^{\alpha}$<u>A1</u>**$_{HH}$ Benzenemethanol, α-(phenoxymethyl)-, 1-acetate	-		Esterification product of **<u>A1</u>**$_{HH}$

II. 2.6. Catalyst stability

Two methods were considered to test the stability of the catalyst for **K1**$_{HH}$ cleavage.

The first one consists in the addition of fresh substrate at the end of one reaction (Table II. 1, entry 8ter) (24 h, 82°C, atm. O_2). During the second run, the mixture was also heated 24 h in the same conditions (entry 33).

The second method involved the catalyst recovery from the homogeneous reaction mixture. To do this, the solvent had to be evaporated at room temperature under air overnight. Then, 5 mL of toluene and 3 x 5 mL of water were added. The organic products were solubilized in toluene whereas the catalyst was mainly dissolved in the aqueous phase. It turned green after the tests on **K1**$_{HH}$ due to reduced vanadium compounds and orange at the end of the tests on **A1**$_{HH}$. The absence of catalyst in the organic phase was checked by adding water. If the aqueous phase was colorless, it was considered that the catalyst was totally extracted. It was characterized by ^{31}P NMR after solvent evaporation. The organic phase was analyzed by GC-MS in duplicate on a GC-2010 Plus gas chromatograph using a HP-5MS ((5%-phenyl)-methylpolysiloxane) column. The temperature of the injector was set to 250°C. The temperature program of the oven was as described on Fig. II. 8.

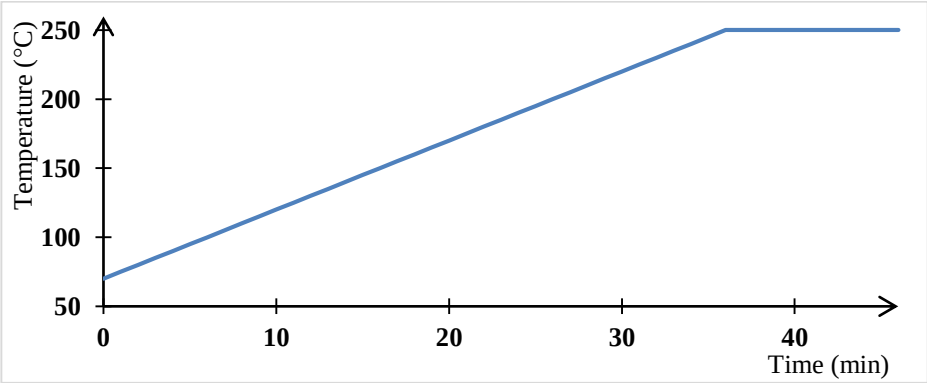

Figure II. 8: Temperature profile of the GC-MS program

Helium (1.5 mL/min) was used as the carrier gas. The products were detected by a GCMS-QP2010 SE mass spectrometer with a time delay of 4 min. The ion source and the mass detector were heated to 200 and 250°C respectively and the voltage was 0.2 kV. The mass spectra were recorded for 35 < m/z < 300 every 0.3 s.

II. 3. Features of the hydrothermal $PMoV_x$

Two $PMoV_x$ were synthesized using the hydrothermal pathway in the present work targeting x values of 1 and 3 (see experimental part, paragraph II. 2.1). V_1-HT and V_3-HT were characterized by XRD and by ^{31}P NMR to check the KEGGIN structure. The X-Ray diffractograms are shown in Figure II. 9.

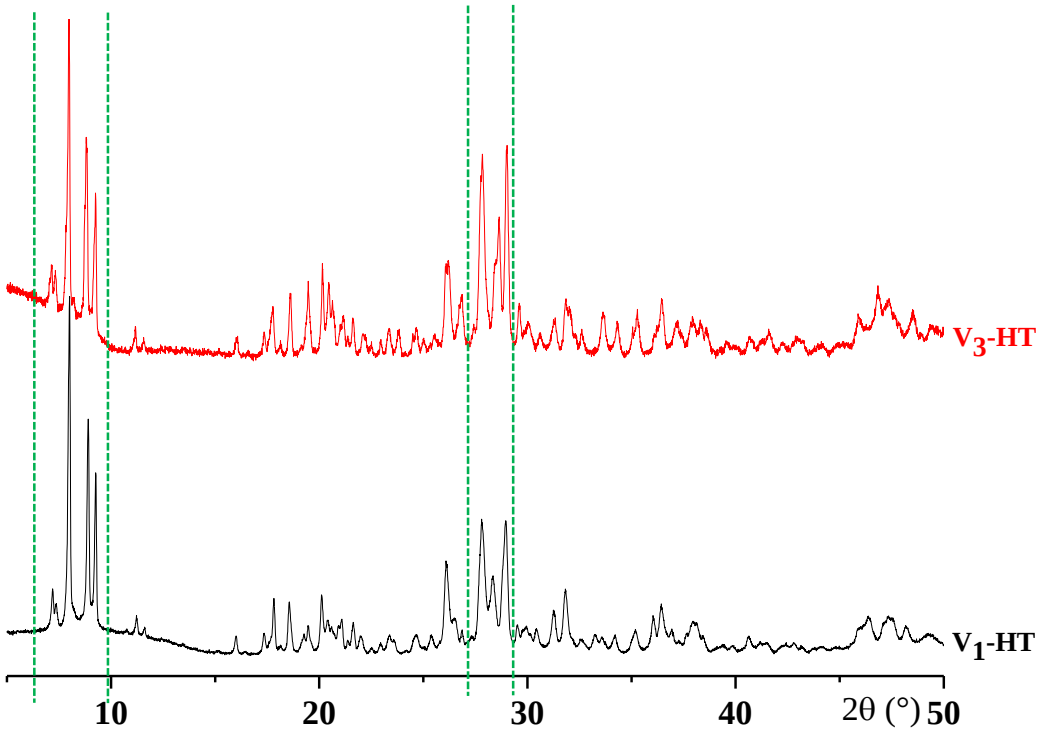

Figure II. 9: XRD profiles of V_1-HT and V_3-HT

The diffractograms of V_1-HT and V_3-HT are similar to that of tridecahydrated phosphomolybdic acid, $H_3PMo_{12}O_{40}$, 13 H_2O (see the Appendix, Fig. SII. 4) which adopts a triclinic ($P\bar{1}$) structure. The main characteristic peaks of this KEGGIN structure are expected at *c.a.* 9° and *c.a.* 28°, corresponding on one hand to the (110), ($0\bar{1}1$) and ($\bar{1}01$) reflection plans and , on the other hand, to the ($3\bar{1}1$), ($\bar{4}\bar{3}2$) and (132) plans. It has to be noted that the peaks at *c.a.* 9° are not present in the profiles of the starting oxides and are clearly related to the triclinic structure of the $PMoV_x$.

- The V_1-HT material contains only one crystalline phase as shown by a RIETVIELD refinement on Fullprof (Fig. SII. 5). Indeed, the optimized values of the RIETVIELD R_P and Chi_2 factors were lower than 10% and 5%, respectively (Table II. 4). A hypothetic formula for V_1-HT would be $H_4PMo_{11}V_1O_{40}$. $13H_2O$.

- The V_3-HT material is constituted of at least two crystalline phases since R_P > 10% (Table II. 4). The second crystalline phase may be vanadium oxide or a $PMoV_x$ having a different hydration index.

The cell parameters were calculated on Fullprof (cf. Appendix. Refinement on Fullprof Suite) and are given in Table II.4.

Table II. 4: Cell parameters of V_x-HT catalysts calculated on Fullprof by the RIETVIELD method

Material	a (Å)	b (Å)	c (Å)	α (°)	β (°)	γ (°)	R_P	Chi_2
V_1-HT	14.074	14.161	13.577	112.24	109.79	60.61	2.51	4.57
V_3-HT	14.219	14.410	13.616	112.54	110.13	60.13	15.1	13.1
PMo_{12} (JCPDS 00-043-0317)	14.100	14.130	13.550	112.10	109.80	60.70	-	-

Liquid NMR was preferred to solid NMR since $PMoV_x$ will be used as homogeneous catalysts. The structure of the $PMoV_x$ was stabilized by dioxane [44]. The final pH of the $PMoV_x$ solution was 1 as measured by a universal pH paper. The obtained NMR spectra are given and compared with a commercial phosphomolybdic acid (see Fig. II. 10).

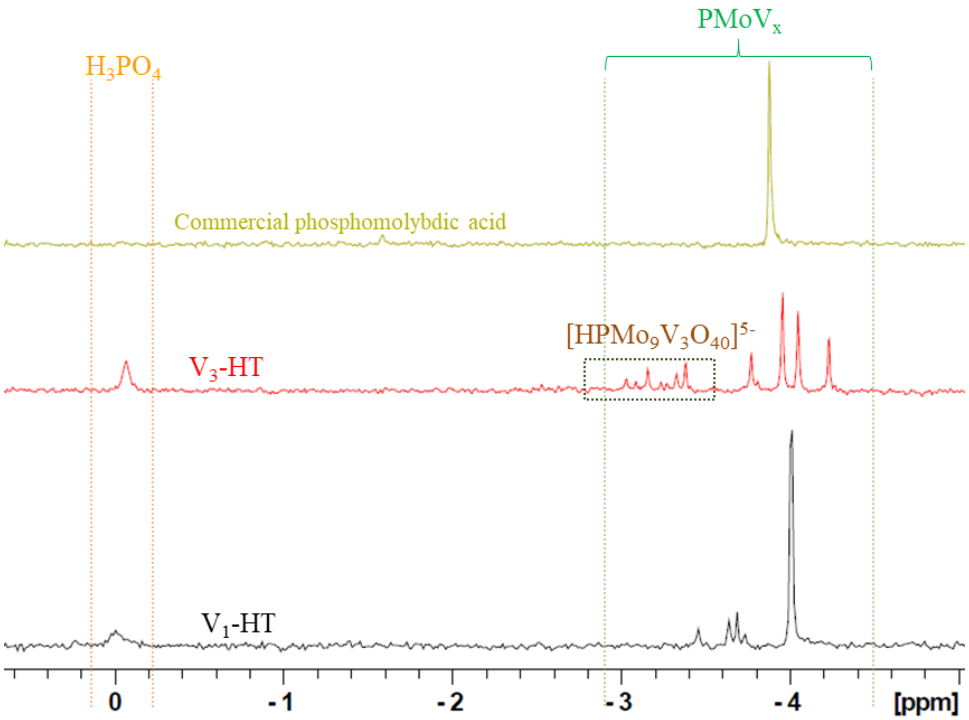

Figure II. 10: ^{31}P NMR profiles of V_x-HT (vs commercial PMo_{12})

Phosphomolybdic acid is characterized by a unique signal at -3.88 ppm which is related to the high symmetry of this anion.

- In the case of V_1-HT, the main signal is located at -4.20 ppm. The substitution of molybdenum by vanadium tends to shield the phosphorous center. There are also minor peaks in the case of V_1-HT, that may be due to coupling between phosphorous and vanadium atoms (^{51}V, spin = 3/2) and the presence of isomers. The spectrum of V_3-HT is more complex. On one hand, several isomers can be envisaged and, on the other hand, the introduction of vanadium *id* leading to a weaker acidity strength [45] ($pK_a([HPMo_9V_3O_{40}]^{5-}/[PMo_9V_3O_{40}]^{6-}) \approx 3$). As a result, the additional peaks from -2.9 to -3.25 observed for V_3-HT could be associated to protonated $PMoV_3$. Yet, only 5 pics should be added and there are 7 peaks. The additional peaks may be explained by the formation of $PMoV_x$ having different vanadium content as shown by a non-whole number of vanadium contents (Table II.5) and/or by coupling between P and V

Due to the choice of a reasonable NMR sequence (see exp part, II. 2. 1 + Fig SII. 6), ^{31}P NMR integration could be quantitative. The presence of residual phosphoric acid, at 0 ppm, then allowed us to determine the yields of V_1-HT and V_3-HT assuming that H_3PO_4 is the only by-product. The values, hence calculated, were 89% and 79% respectively.

The number of vanadium equivalents in V_x-HT solids was calculated from the weight fraction of phosphorous (w_P), molybdenum (w_{Mo}) and vanadium (w_V) obtained by ICP (Table II. 5). TGA-DSC measurements (Fig. II. 11) allowed also to determine the x values (see calculations in the Appendix, Determination of the formula of the synthesized $PMoV_x$, Fig. SII. 7) from the knowledge of the loss of constitutive water. However, the latter may start before the completion of the total evaporation of the hydration water, especially for the high values of x [46] leading to a underestimation of x. Consequently, ICP was preferred for x and TGA-DSC measurements for n (Table II. 5).

To sum up, the targeted x values could be obtained by following the hydrothermal synthesis route. The yields were rather high even if they can still be improved, especially for x = 3. In this latter case, part of the oxides did not dissolve and had to be eliminated

by filtration despite of more diluted conditions and longer heating time. The residue was found to be richer in vanadium (w_{Mo} = 23 wt%, w_v = 38 wt%). Thus, the inclusion of vanadium in the KEGGIN structure is more difficult than that of molybdenum. All of this implies that the hydrothermal procedure may be not the most adequate method for the synthesis of $PMoV_x$ with the highest amounts of vanadium. Moreover, for high x values, it has to be noted that x in the general formula corresponds more likely to an average vanadium content since V_x-HT, at least in solution, is actually a mixture of different $PMoV_x$.

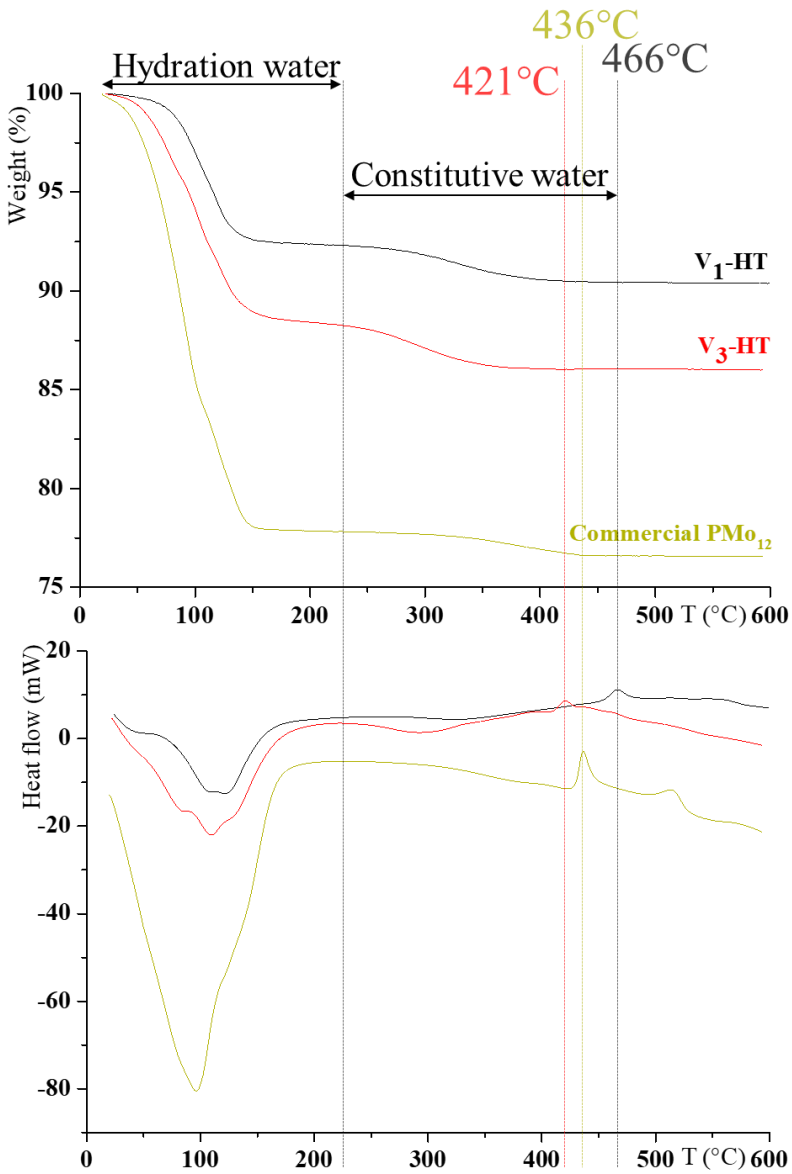

Figure II. 11: TGA-DSC profiles of V_x-HT (vs commercial PMo_{12})

Table II. 5: General formulas for the synthesized V_x-HT solids

Catalyst	%P	%Mo	%V	x_{exp}	n	Formula	Molecular weight (g/mol)
V_1-HT	1.77	49.25	2.75	1.140±0.005	8	$H_{4.14}PMo_{10.86}V_{1.14}O_{40}$, $8H_2O$	1919
V_3-HT	2.01	46.16	7.06	2.680±0.005	13	$H_{5.68}PMo_{9.32}V_{2.68}O_{40}$, $13H_2O$	1942

II. 4. Activity of the $PMoV_x$ catalysts for **K1**$_{HH}$ cleavage

II. 4.1. Optimization of the operative conditions

Firstly, V_1-HT and mainly V_3-HT were assessed as catalysts for the aerobic cleavage of **K1**$_{HH}$ under atmospheric pressure of dioxygen in pure solvents. The solution was heated to the targeted temperature (65-98°C) during 24 h. Initially, the reaction media was yellow/orange due to the presence of vanadium in its high oxidation state in the $PMoV_x$ used. During the reaction, except in water, the solution took a green color due at least to the partial reduction of vanadium. The final coloration is given in Table II. 6.

The involved reaction affords phenol, benzaldehyde and benzoic acid as the main products (Figure II. 12).

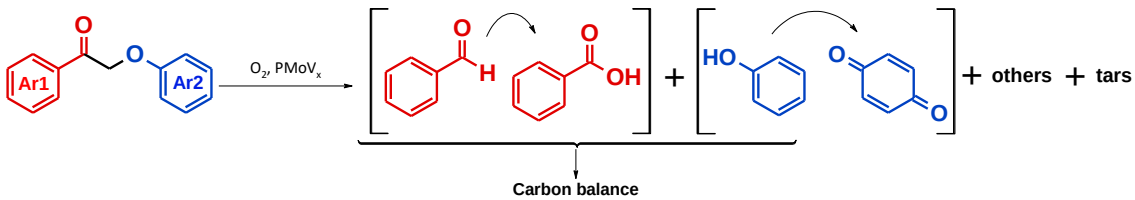

Figure II. 12: Cleavage of $K1_{HH}$ by O_2

The calculated yields are shown in Table II. 6. The amount of *p*-quinone could not be determined accurately (see exp part, paragraph II. 2.5) but only a small amount of this compound was formed. The conversion of **K1**$_{HH}$, the yields of the main products as well as the carbon balance values are given in Table II. 6. The products from both C-C (PhCHO and PhCOOH) and C-O (PhOH) cleavage and the initial substrate were taken into account in the calculation of the carbon balance. As usually observed, the carbon balance tends to decrease with increasing conversion rates as the result of the occurrence of side reactions. It has to be noted here that, the maximum value of the carbon mass balance (see calculation details in the exp part, paragraph II.2. 5) is normally lower than 100%. Indeed, C_1 products such as formaldehyde, formic acid, CO_2…coming from the transformation of the CH_2 group of **K1**$_{HH}$ could not be detected quantitatively and were

not taken into account. Assuming that **K1**$_{HH}$ was totally converted into the targeted products (PhOH, PhCHO and PhCOOH), CB_{max} should be equal to $\frac{1400-Conv}{14}$.

Several solvents were tested (Table II. 6). As a starting point, methanol and acetic acid were used like EL AAKEL *et al* did [18], for the C-C bond cleavage of cyclic α-hydroxyketones in presence of $PMoV_3$. However, on one hand, pure acids are rather corrosive and, on the other hand, methanol is known to be a vanadium reductant that are the reasons why acetonitrile was assessed too.

As evocated before, the reaction mixture was orange at the beginning (Fig. II.13a on the left). With acetonitrile, $PMoV_x$ was also reduced in contact with **K1**$_{HH}$ upon heating affording the characteristic greenish coloration and then, the mixture went back to a brown-yellow color (see Figure II. 13b). The conversion of **K1**$_{HH}$ in refluxing acetonitrile (entry 1) was not so high (48%, brown) and turned out to be lower in refluxing methanol (14%, green, entry 4). The bad performances of V_3-HT in methanol compared to V_3-HT in acetonitrile cannot be related to i) a difference of the dioxygen solubilities (Table II. 6, entries 1 and 2) but to the lower oxidation state of vanadium in MeOH which is reflected by the persistent green coloration as well as maybe to ii) the lower temperature (65°C instead of 82°C).

The highest conversion of **K1**$_{HH}$ and yields of PhOH and PhCOOH were obtained in acetic acid after a shorter time than in the earlier tests (15 h instead of 24 h). These results can be explained by the dioxygen solubility. Indeed, the concentration of dissolved O_2 is 3.5 times higher in AcOH than in MeCN and MeOH (Table II. 6). Despite the best results obtained, almost no dioxygen consumption was observed in AcOH which could be explained by an equimolar release of CO_2 less soluble in acetic acid (0.19 M) than in acetonitrile (0.24 M) (calculated from ref [47]) and uptake of O_2 in this case. However, as already mentioned, an oxidation procedure working in acetic acid would not be easy to handle for an industrial application due to corrosiveness. Consequently, in spite of these results, acetonitrile was preferred to acetic acid provided that some further optimization would be done.

*Table II. 6: Influence of the "pure" solvent on the activity of V_3-HT catalyst for **K1**$_{HH}$ aerobic oxidative cleavage*

Entry	Solvent	O_2 solubility at 20°C (mmol/L) [48, 49]	Conversion (%)	Yield (%)			$\frac{n_{PhCHO} + n_{PhCOOH}}{n_{PhOH}}$	Carbon balance (%)	O_2 consumption/ converted **K1**$_{HH}$	Color after reaction
				PhOH	PhCHO	PhCOOH				
1	Acetonitrile	2.3	48	38	2.5	19	0.57	79	n. d.	Brown
1bis			36	32	6.4	18	0.62	90	1.67	
2	Methanol (65°C)	2.1	14	8.1	0	4	0.49	91		Green
3	Acetic acid	7.5	100	80	0	80	1	74	0	Dark
4[a]			98	75	0	75	1	73	0	brown
5	Water-acetonitrile 14:1 [b]	0.28	5.6	2.5	0	11	4.4	96	6.61[c]	Orange

K1$_{HH}$ 100 mM, atm. O_2, 24 h, V_3-HT (Mo+V 15 mol%), 82°C. [a] t = 15 h, [b]T = 98°C and higher stirring rate, [c]Due to experimental error

Figure II. 13: General aspect of the reaction media a) before the catalytic test b) at the end of the catalytic tests

Mixtures of acetonitrile and acetic acid with varying AcOH concentrations ($0 \leq z \leq 20\%$ AcOH in volume) have also been tested as solvents at 82°C (Table II.7, entries 1, 5, 10-12, 14). In the present work, a positive influence of acetic acid on the conversion of **K1**$_{HH}$ into the targeted products was shown. Indeed, the conversion of **K1**$_{HH}$ as well as the yields of phenol coming from C-O and benzoic acid from C-C cleavage, respectively raised with the acetic acid content. Similarly, it has to be noted that a positive effect of acetic acid on the aerobic cleavage of dimeric model (**A1**$_{HH}$) was also shown by MA *et al* when using $VO(acac)_2$ as a catalyst [50]. In our case, a z value of 10 vol. % was found to be an optimum. Indeed, at 20 vol. % (Table II. 7, entries 11 *vs*. 8), the carbon balance decreased (72% vs 80%). Since C-O bond is weaker than C-C bond, its cleavage is favored giving rise to an enhanced phenol production compared to benzaldehyde and benzoic acid and some minor products detectable by HPLC like phenylglyoxylic acid detected for z = 2.5 and z = 5 (entries 6-7). Furthermore, benzaldehyde yield was found to be always lower than those of phenol and benzoic acid. The maximum yield of benzaldehyde was reached for z = 5 (entry 7) and the ratio PhCHO/PhCOOH was maximized for z = 2.5 (entry 6) and tends to decrease for a higher content of acetic acid until no benzaldehyde was observed in pure acetic acid (entry 3). So, acetic acid boosts benzaldehyde over-oxidation.

The test in MeCN - 10 vol% AcOH was repeated at 65°C (Table II. 7, entry 9). From the comparison with the test in methanol (Table II. 6, entry 2), the test in acidified acetonitrile gave rise to better conversion and yields of cleavage products meaning that acetonitrile is more suitable for **K1**$_{HH}$ cleavage. The ratio (PhCHO+PhCOOH)/PhOH was equal to 1.2 at 65°C and 1 at 80°C.

Additionnaly, a test was carried out in water. Prior to the reaction, a minimum amount of acetonitrile (1/15 of the total volume) had to be added to dissolve the substrate and 15 mL of water was added and the mixture was heated to 98°C with stronger stirring. However, the adjunction of water precipitated the substrate at room temperature. During heating, the substrate melted, which generated droplets of ketone (T_f = 72°C) in the water phase (see Table II. 6, entry 5). Also, a test was carried out in H_2O - 10 vol.% AcOH in order to check the possibility to perform an organic solvent-free process (Table II. 7, entry 12). Indeed, organic solvents are, at best only flammable, harmful and environmental hazardous. The temperature and the catalyst are similar to Table II. 7, entry 8. Sadly, in both cases the conversion was very low (Table II. 6, entry 5 : 5.6%, Table II. 7, entry 12

: 14%) in spite of higher temperature used due to the lack of contact between the substrate and dioxygen and the very low solubility of O_2 in water (*c.a.* 25 times less than in AcOH).

A series of experiments (Table II. 8) were performed in order to evaluate the influence of the V_1-HT (entries 15-16) V_3-HT loading (from 7 to 43 mol% of Mo + V, entries 8 and 17-19) and of the vanadium content (entries 8, 14 and 19). Logically, the higher the metal charge, the higher the conversion rate of the dimer. At low Mo+V% value (entry 17, 7 mol%), the conversion is rather low. At the highest metal charge (entries 16 and 18), the conversion rate is certainly higher but the carbon balance tends to be rather low (58% only, compared to 80% for 15 mol% Mo+V (entries 8 and 15)). For these reasons, a metal loading of 15 mol% was found to be a good compromise. Besides, in the case of the tests performed at high metal loading (entries 16 and 18), the dioxygen consumption per mole of converted substrate was slightly lower.

Vanadium was shown to have a beneficial impact on the aerobic cleavage of **K1**$_{HH}$. Indeed, the conversion and carbon balance values were lower in the presence of $H_3PMo_{12}O_{40}$ (Table II. 8, entry 14) compared to V_1-HT (entry 15) and V_3-HT (entry 8) tested at 15% of Mo+V. Besides, we also proved that the incorporation of vanadium has a positive effect on the phenol and benzaldehyde formation and on the (PhCHO+PhCOOH)/PhOH ratio (closer to 1 for V_3-HT). Amongst phosphomolybdic acid, V_1HT and V_3HT catalysts, the first one is characterized by the strongest acidic properties. In this latter case, it was important for us to check the influence of the acidity on the cleavage of **K1$_{HH}$**. This was studied owing to a reference test (no metal) performed with H_2SO_4 (Table II. 8, entry 13) which showed that the conversion of **K1**$_{HH}$ was lower than with $H_3PMo_{12}O_{40}$ as well as with the V_x-HT catalysts. With $H_3PMo_{12}O_{40}$, phenol was by far the main product meaning that the C-C cleavage requires the presence of a metallic catalyst whereas C-O linkage may be cleaved more easily, just by acidity. In other words, $H_3PMo_{12}O_{40}$ cannot be considered as inactive for the **K1**$_{HH}$ C-C bond cleavage as it proves to boost the conversion and the production of cleavage products (entry 14 vs 13) due to redox properties [51].

*Table II. 7: Influence of acetic acid content on the activity of V_3-HT on the **K1**$_{HH}$ aerobic oxidative cleavage*

Entry	Volumic fraction of acetic acid (vol%)	Conversion (%)	Yield (%)				$\frac{n_{PhCHO}+n_{PhCOOH}}{n_{PhOH}}$	$\frac{n_{PhCHO}}{n_{PhCOOH}}$	Carbon balance (%)	O_2 consumption/ converted **K1**$_{HH}$
			PhOH	PhCHO	PhCOOH	PhCOCOOH[a]				
1	0	48	32	2.5	19	n. d.	0.7	0.1	76	0.9
6	2.5	59	34	17	28	2.5	1.3	0.6	78	2.0
7	5	68	47	20	38	4.5	1.2	0.5	81	2.9[e]
8	10	72	55	12	44	n. d.	1.0	0.3	80	1.5
8bis	10	72	49	11	40	n. d.	1.0	0.3	74	n. d.
9[b]	10	44	24	5.6	24	n. d.	1.2	0.2	81	1.5
10[c]	10	9.1	7.8	2.3	6.8	n. d.	1.2	0.3	99	n. d.
11	20	80	67	0	47	n. d.	0.7	0	72	1.4
3	100	100	80	0	80	n. d.	1.0	0	74	0
12[d]	10	14	4.6	0	5.3	n. d.	1.2	0	91	1.4

K1$_{HH}$ 100 mM, Atm. O_2, V_3-HT (Mo + V 15 mol%), MeCN – 10 vol% AcOH, 82°C, 24 h; [a]Estmated by HPLC, [b]T = 65°C; [c]Test at room temperature; [d]Test in water; [e]Due to experimental error

*Table II. 8: Influence of the catalyst precursor and of the Mo+V loading on the **K1**$_{HH}$ aerobic oxidative cleavage*

Entry	Catalyst	Metal loading (mol%)		Conversion (%)	Yield (%)			$\frac{n_{PhCHO}+n_{PhCOOH}}{n_{PhOH}}$	Carbon balance (%)	O_2 consumption/ converted **K1**$_{HH}$
		V	Mo		PhOH	PhCHO	PhCOOH			
13	H_2SO_4[a]	0	0	39	35	11	0.9	0.3	82	1.3
14	PMo_{12}	0	15	69	41	11	38	1.2	73	1.4
15	V_1-HT	1.6	13.4	72	46	16	36	1.1	73	1.5
16		4.5	38.5	92	33	5.2	37	1.3	43	1.1
17	V_3-HT	2.0	5.0	43	36	8	24	0.9	88	1.4
8		4.3	10.7	72	55	12	44	1.0	80	1.5
8bis					49	11	40	1.0	74	
18		10.4	25.6	88	47	2.2	50	1.1	58	1.1
19[a]		4.3	10.7	7	6.8	0	3.4	0.5	98	-

K1$_{HH}$ 100 mM, atm. O_2, MeCN – 10 vol% AcOH, 82°C, 24 h; [a]Test in dinitrogen atmosphere

Finally, a test was also performed under a dinitrogen atmosphere in the presence of V_3-HT (entry 19). In this case, the reaction mixture remained blue during the whole test meaning that the catalyst was totally reduced at the beginning by the excess of substrate and unable to go back to its high oxidation state due to the absence of dioxygen, thus emphasizing the important role of the later in the other tests. As a result, the conversion rate of **K1**$_{HH}$ was very low as well as the yield of PhOH and PhCOOH.

Except for the tests 16 and 18 carried out with a higher catalytic loading, a general linear trend was observed for the plot of the conversion balance (%) versus the conversion rate of **K1**$_{HH}$ (%) (Figure II. 14, see black dashed line (Δ)). As expected, the mass balance (MB) including the targeted products and **K1**$_{HH}$ decreased with the increase of the conversion rate (increasing gap between the straight lines of theoretical MB and that of real MB vs conversion). In particular, phenol can be over-oxidized into quinones which may initiate oxidative condensation [52]. Indeed, the yield of *p*-quinone was 6.8% in the case of the test 18 in presence of an increased amount of catalyst whereas no quinone was detected in the case of the test 8 with an average catalytic loading.

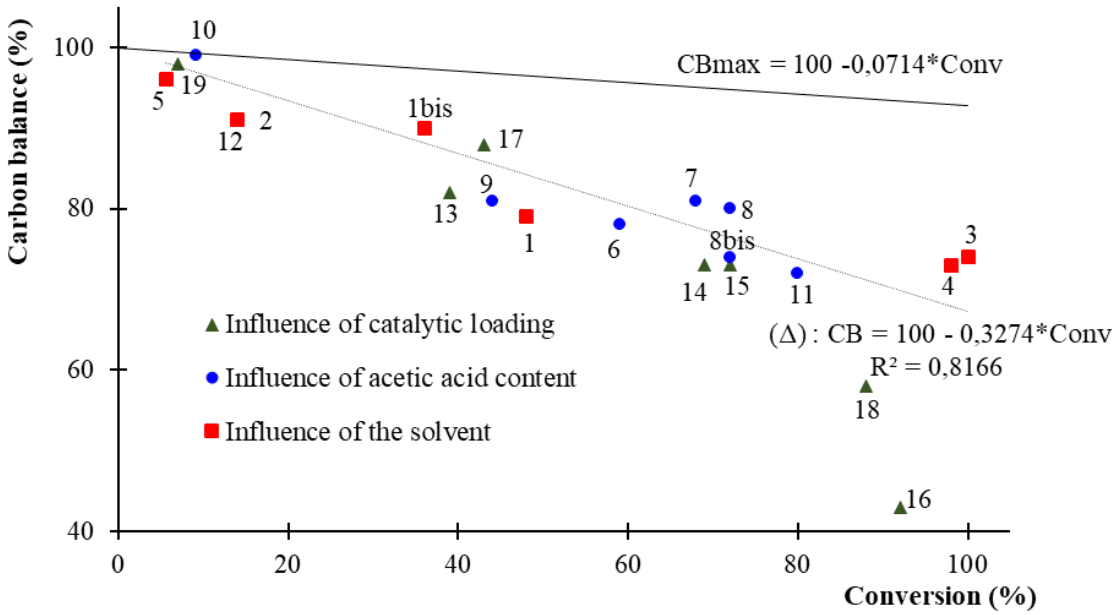

*Figure II. 14: Carbon balance vs **K1**$_{HH}$ conversion*

As a strong oxidant will be needed for lignin aerobic cleavage, a catalyst having a high vanadium content will be preferred. So, V_3-HT was chosen as the reference catalyst in this paragraph.

Phenol (Table II. 9, entry 20), benzaldehyde (Table II. 9, entry 21) and an equimolar mixture of phenol and benzoic acid (Table II. 9, entry 22) were tested instead of **K1**$_{HH}$ to check the possibility of *in situ* over-oxidations and the extent of phenyl benzoate formation through acidic catalysis.

Table II. 9: Catalytic tests on monomeric substrates

Entry	Substrate	Conversion (%)	Comments
20	PhOH (100 mM)	19	-
21	PhCHO (100 mM)	97	Yield of PhCOOH: 21% Carbon balance: 24% Another product detected by HPLC (RT = 19 min)
22	PhOH (50 mM) + PhCOOH (50 mM)	PhOH: 20 PhCOOH: 0	PhCOOH is stable

Atm O_2, V_3-HT (Mo+V 15 mol%), MeCN - 10% AcOH 82°C, 24 h

As a matter of fact, the conversion of phenol was 19% (Table II. 9, entry 20), which is much lower compared to the ketone **K1**$_{HH}$ (Table II. 7, entry 8, 72%). Benzaldehyde conversion was high (entry 21). However, the yield of benzoic acid was 21% only and another product was detected by HPLC (19 min). It may be an acetylation product of benzaldehyde as the catalyst may be active for such reaction as shown in paragraph IB. 3.1a [53]. The test carried out on an equimolar mixture of phenol and benzoic acid (entry 22) showed the stability of benzoic acid as no conversion was observed and so, no esterification was observed. So, the decrease of the carbon balance with increasing conversions as observed in Figure II. 14 may be rather due to phenol over-oxidation and side reactions during benzaldehyde over-oxidation.

Acetic acid proved to have a positive effect on **K1**$_{HH}$ cleavage (Table II. 7). This can be explained by a) the acidity b) a solvent effect. So, tests in presence of strong acids were performed. Acetic acid is a weak acid in acetonitrile (pK_a = 21.5) due to the low ability of this solvent to solvate anions [54]. Stronger acids in acetonitrile such as H_2SO_4 and TFA with pK_a values of 8 and 12.7, respectively, were also assessed for the aerobic catalytic cleavage of **K1**$_{HH}$. Hence, the tests in presence of the alternative acids took place in more acidic conditions (Table II. 10, entries 8 and 23-27). As a consequence, only a small volume of H_2SO_4 or TFA were added to avoid too strong acidic conditions (*vs* MeCN - 10% AcOH).

The presence of alternative strong acids at 0.033 vol. % (Table II. 10, entries 23-24) gave rise to moderate conversion of **K1**$_{HH}$ and yields of C-C and C-O cleavage products compared to the test with 10 vol% of acetic acid (Table II. 7, entry 8). An excess of phenol was observed meaning that C-O cleavage took place at a higher extent than C-C cleavage. Moreover, TFA seemed to give rise to a slightly better carbon balance than H_2SO_4 (84% vs 78%).

As a consequence, the effect of TFA was investigated more deeply by varying its initial concentration between 0.03 and 3.6 vol.% (Table II. 10, entries 24-27). The higher the acid concentration, the higher the conversion, as well as the yield of phenol. In presence of 0.07 vol% of TFA (entry 26), the yield of PhOH and PhCHO so as the carbon balance were similar to that obtained in the reference experiment performed in 10 vol.% of AcOH (entry 8). However, the conversion (62% *vs* 72%) so as the yield of benzoic acid (26% *vs* 44%) were lower. At higher concentrations of TFA (Table II. 10, entries 26-27), the **K1**$_{HH}$ conversion reached 80% and the yield of PhOH 70%. Actually, the excess of PhOH became more and more important whereas the yield of C-C cleavage products turned out to be limited. Indeed, the combined yield of PhCHO and PhCOOH was 38% in presence of TFA (Table II. 10, entry 27) *vs* 58% in presence of 10 vol% of acetic acid (Table II. 7, entry 8). It seems that the acidity brought by TFA preferentially catalyzes C-O cleavage through an acidolysis reaction as TFA is a much stronger acid than acetic acid. As a result, the acidity of the reaction media is likely not the key feature for **K1**$_{HH}$ cleavage since the test run in the least acidic conditions gave rise to the best yields of C-C cleavage products.

*Table II. 10: Catalytic tests on **K1**$_{HH}$ substrate in presence of alternative strong acids*

Entry	Acid (vol%)	Estimated pH	Conv. (%)	Yield (%)			$\frac{n_{PhCHO}+n_{PhCOOH}}{n_{PhOH}}$	Carbon balance (%)
				PhOH	PhCHO	PhCOOH		
23	H_2SO_4 (0.033)	5	53	41	8	19	0.7	78
24	TFA (0.033)	8	49	45	8	19	0.6	84
25	TFA (0.133)	7	50	33	13	17	0.9	79
26	TFA (0.667)	7	62	49	12	26	0.8	78
27	TFA (3.60)	7	83	71	10	28	0.5	67
8	AcOH (10)	11	72	46	12	44	1.0	79

K1$_{HH}$ 100 mM, acidified MeCN 82°C, 24 h, V_3-HT (Mo + V 15 mol%), V = 15 mL

Another effect of acetic acid would be related to its ability to improve the dioxygen solubility in acetonitrile. Thus, an increase of the content of AcOH should lead to an enhanced dioxygen transfer from the gas phase to the solution, which should be

beneficial for **K1**$_{HH}$ cleavage. This can be demonstrated thanks to the application of HANSEN parameters noted δ [55]. As shown in the appendix (Demonstration of the effect of acetic acid on dioxygen solubility), the adjunction of acetic acid gives rise to an enhanced solubility of dioxygen in the reaction media.

II. 4.2. Kinetics / mechanistic study of the V_3-HT-catalyzed aerobic oxidative cleavage of **K1**$_{HH}$

Most of the previous tests in MeCN-AcOH 10% were performed at 80°C within 24 h. Here, we propose to monitor, during 48 h, **K1**$_{HH}$ conversion, the carbon balance as well as the yields of the three main products in our reference conditions, *i.e.* **K1**$_{HH}$ 100 mM, V_3-HT (Mo+V 15.2 mol%), MeCN - 10% AcOH (15 mL), T = 82°C (see Table II. 11 and Figure II. 15). The yield of *p*-quinone was also calculated though a low precision.

*Table II. 11: Influence of the reaction duration on **K1**$_{HH}$ conversion and on the yields of cleavage products*

Entry	Time (h)	Conv. (%)	Yield (%)			$\frac{n_{PhCHO}}{n_{PhCOOH}}$	$\frac{n_{PhCHO}+n_{PhCOOH}}{n_{PhOH}}$	Carbon balance (%)	O_2 consumption / conversion
			PhOH	PhCHO	PhCOOH				
26	2	30	17	7.4	12	0.6	1.1	87	
27	7.6	49	46	8.2	26	0.3	0.7	88	1.5
28	14.1	64	67	7.4	35	0.2	0.6	86	1.5
8	24	72	46	12	44	0.3	1.0	79	1.7
29	37	78	46	12	46	0.3	1.3	71	1.6
30	48.1	87	61	8.9	43	0.2	0.9	65	1.4

K1$_{HH}$ 100 mM, atm. O_2, MeCN - 10% AcOH, V_3-HT (Mo + V 15 mol%) 15 mL, 82°C

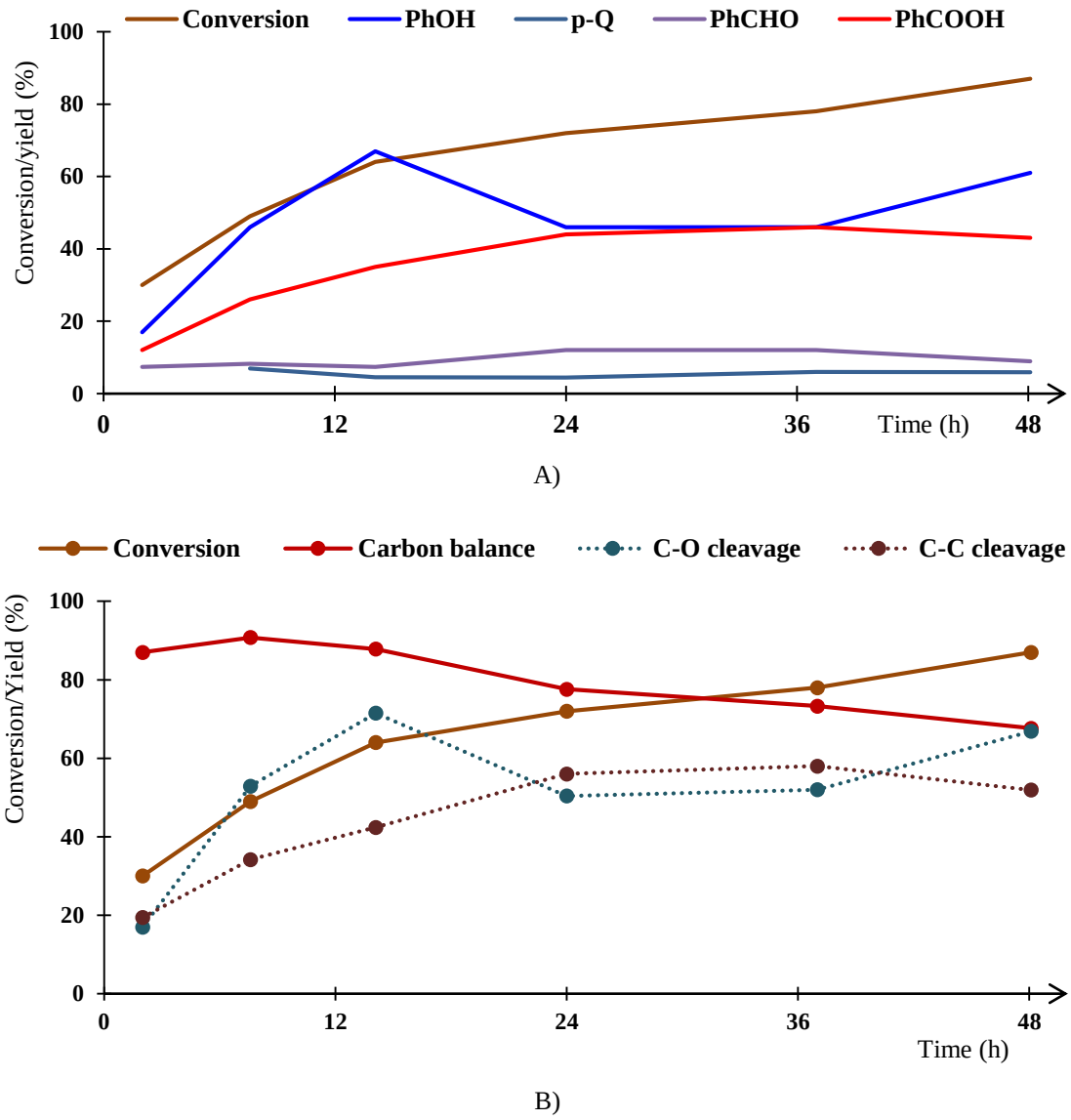

*Figure II. 15: Evolution of different reaction parameters vs time for the V_3-HT-catalyzed aerobic cleavage of **K1**$_{HH}$; a) yield of cleavage products, b) carbon balance and C-O and C-C cleavage products*

In details:

- As expected, the conversion of **K1**$_{HH}$ raised whereas the carbon balance decreased throughout the reaction.
- The yield of PhCHO increased until 24 h with a maximum of 12%, then it slowly decreased to 9%.
- PhCOOH production reached also its maximum (46%) within 37 h. After, it did not change significantly.

- First, before 24 h, the reaction duration was positive for PhOH formation with a maximum of 67%. Then, due to over-oxidation, the yield of PhOH decreased until 46% till 37 h.

For short reaction times (< 24 h), the ratio (PhCHO+PhCOOH)/PhOH was often lower than 1 meaning that PhOH is produced in greater extent than the two other main products. As a result, it is highly probable that part of phenol was issued from C-O cleavage. The detection by HPLC of C_8-products such as phenylglyoxylic acid confirms such hypothesis.

After 24 h of reaction, the carbon balance decreased significantly as the result of phenol over-oxidation into *p*-quinone. The yield of the latter could be estimated to *c.a.* 6% showing no significant evolution between 37 and 48 h. Hence, the quinone production was limited and took place at much smaller extent compared to phenol formation from the dimer $\underline{\mathbf{K1}}_{HH}$.

Furthermore, no dioxygen volume variation was observed between 37 and 48 h while the conversion of $\underline{\mathbf{K1}}_{HH}$ still raised in the meantime. We may hypothesize that carbon dioxide emission may compensate exactly the consumption during that time interval. Otherwise, the dioxygen consumption per mole of converted substrate was quite constant with a value of 1.5 mol of O_2 per mole of consumed $\underline{\mathbf{K1}}_{HH}$. Besides, the quantity of gaseous dioxygen is much higher than dissolved dioxygen. So, it can be hypothesized that dissolved oxygen is constantly renewed and so, the concentration of dioxygen is constant (order degeneration).

In a first attempt, we have tried to model the experimental results by a first-order reaction (n= 1) rate law by drawing $\ln[\underline{\mathbf{K1}}_{HH}] = f(t)$ (Figure II. 16.A). Not being satisfied by the results (low value of the regression factor, R^2), we also tested a more general expression which is valid for n order values strictly greater than 1. In this way, by applying different values of n, it appeared that the best modelling of the experimental data corresponds to $[\underline{\mathbf{K1}}_{HH}]^{-0.25} = f(t)$ (Figure II. 16.B) curve, *i.e.* n= 1.25.

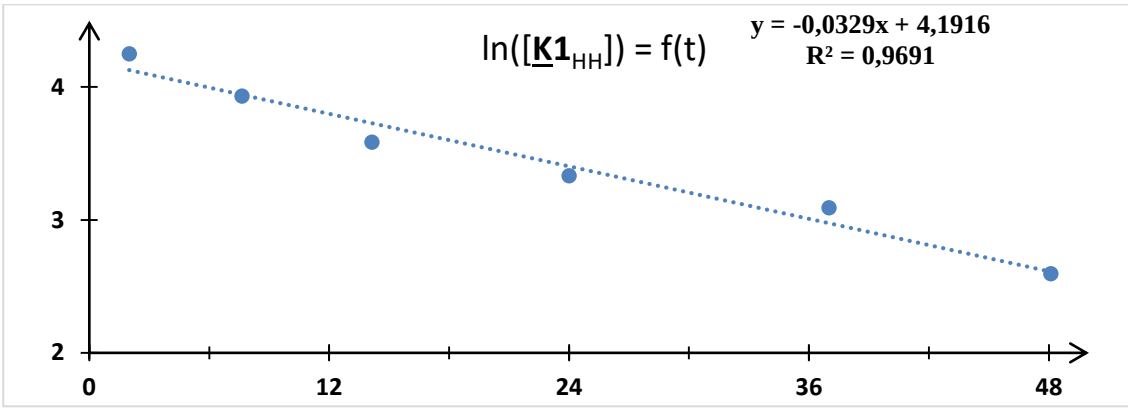

A)

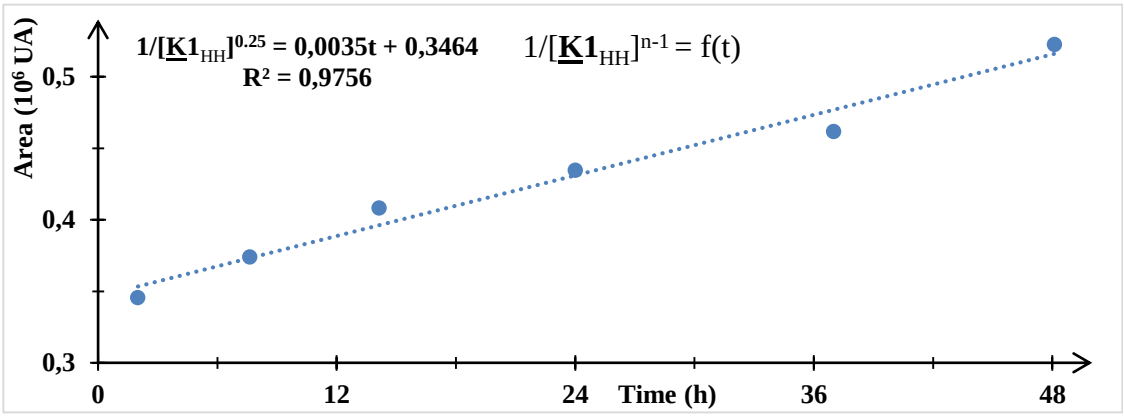

B)

Figure II. 16: Attempts for the determination of the kinetic order A) n= 1; B) n = 1.25 T = 82°C

Our attention has so far focused on the majority of the reaction products. In order to establish a plausible mechanism, we tried to identify as many other products as possible. To do this, we analyzed by GC-MS the same solution (1/40 dilution) or a concentrated organic extract obtained after removal of the catalyst (see exp. Part. II.2.6). The different monomeric compounds detected are listed in the Table II.12 depending on their origin (C-O cleavage (Table II. 12a), C-C cleavage (Table II. 12b)). Dimers were detected too (Table II. 12c).

Table II. 12a: C-O cleavage products detected by GC-MS

RT (min)	Compound	Match (%)	Area ratio /PhOH	Comments
4.0	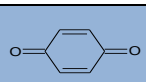 *p*-quinone	88		**Identification by HPLC** with a commercial standard. Minor product.
4.9	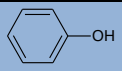 phenol	97	1	Targeted product. **Identification by HPLC** with a commercial standard. Absolute area: 2.10 10^8 UA
6.9	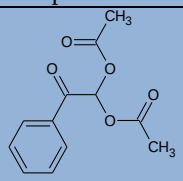 2,2-bis(acetyloxy)-1-phenylethanone	97	4.3. 10^{-2}	Phenylglyoxal stabilized by acetic acid. Phenylglyoxylic acid is a rather strong acid (pK_a = 2.1). So, it reacts more easily with water. As the peak almost disappeared, it is more probably due to this compound.
	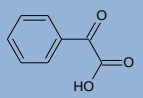 Phenylglyoxylic acid	97		**Identification by HPLC** with a commercial standard. Minor product.
15.3	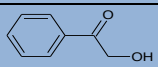 2-hydroxyacetophenone	94	6.5. 10^{-2}	Hydrolysis product. (Its formation was undirectly proved by the detection of mandelic acid).
19.60	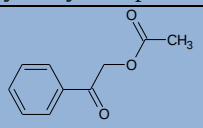 2-phenoxyacetophenone	95	5.3. 10^{-1}	**Identification by HPLC** with a synthesized standard. Acetolysis product.

Table II. 12b: C-C cleavage products detected by GC-MS

RT (min)	Compound	Match (%)	Area ratio /PhCOOH	Comments
4.7	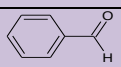 Benzaldehyde	96	4.2.10^{-3}	Targeted product. **Identification by HPLC** with a commercial standard.
4.8	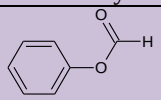 Phenyl formate	92	7.8. 10^{-1}	Formic ester of phenol.
9.8	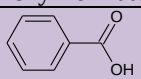 Benzoic acid	97	1	Targeted product. **Identification by HPLC** with a commercial standard. Absolute area: 3.0. 10^8 UA
17.2	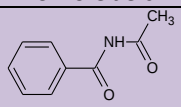 N-acetylbenzamide	93	8.5. 10^{-2}	Benzamide of benzoic acid and acetamide. Acetamide was also identified by GC-MS (3.93 min).

Table II. 12c: Dimeric products detected by GC-MS

RT (min)	Compound	Match (%)	Area ratio /**K1**$_{HH}$	Comments
25.7	**K1**$_{HH}$		1	Substrate. Absolute area: 4.0. 10^8
25.8	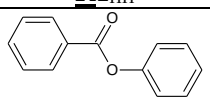 Phenyl benzoate	97	7.8. 10^{-2}	Ester obtained from phenol (from C-O cleavage) and benzoic acid (from C-C cleavage).
27.0	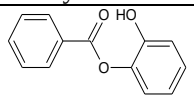 or 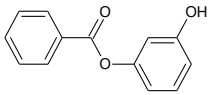	95-96	1.0. 10^{-2}	Hydroxylated phenyl benzoates from side reactions
27.9	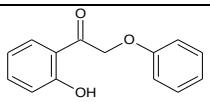 W	86	6.5. 10^{-3}	Product obtained by hydroxylation of the aromatic rings in **K1**$_{HH}$.
28.7	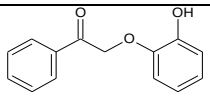 W’	90	5.4. 10^{-3}	
29.2	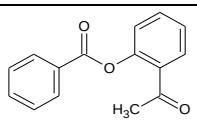 X’ ?	80	2.5. 10^{-2}	The match % was the lowest value obtained meaning probably that this structure issued from the NIST Library (NIST 14) is not the correct one.

The formation of *p*-quinone (from phenol oxidation, Table II. 12a) as well as those of phenylglyoxylic acid and 2-acetoxyacetophenone (from the acetolysis of **K1**$_{HH}$**,** Table II. 12a) were confirmed by GC-MS. In addition, N-acetylbenzamide (17.2 min, Table II. 12b) was detected too in the diluted reaction sample. This amide would result from the reaction of benzoic acid with acetamide, the latter being produced by the hydrolysis of acetonitrile (the catalyst is hydrated and water is the by-product of aerobic oxidation). Phenyl formate was also observed (Table II. 12b), meaning that formic acid maybe produced during the reaction.

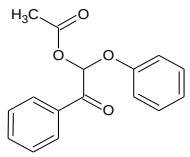

Figure II. 17: Hypothetic structure of the intermediate X

The analysis of the more concentrated sample allowed us to detect 1-(2-hydroxyphenyl)-2-phenoxyethanone (RT = 27.9 min, Table II. 12c) and the isomer 2-(2-hydroxyphenyl)-1-phenoxyethanone (RT = 28.7 min, Table II. 12c) which would be produced by the hydroxylation of the aromatic rings of **K1**$_{HH}$ by $HO^{\cdot}$ radicals. Moreover, another compound (X) detected at RT = 29.2 min could be 2-phenoxy-2-acetoxy-

1phenylethanone (Fig. II. 17). As mentioned in Table II.12c, the structure proposed by the NIST Library (X') was not satisfying. Further investigations had to be done by comparing in particular the masses of the different fragments of X with those of **<u>K1</u>**$_{HH}$ (Table II. 13).

Table II. 13: Mass table of the compound X and ***<u>K1</u>****$_{HH}$*

Compound X	**105 (100)**; **94 (43.9)**; **43 (42.8)**; 77 (33.8); 51 (9.7); **227 (8.6)**; 106 (7.9); **136 (5.3)**; 95 (4.5); 66 (3.2)
<u>K1</u>$_{HH}$	**105 (100)**; 77 (63.3); 212 (43.0); 106 (17.3); 51 (15.6); 65 (7.7); 91 (7.2); 213 (6.8); 78 (4.7); 39 (4.7)
<u>X'</u>	**105 (100)**; 77 (37.3); 51 (10.0); 106 (6.1);43 (462); 50 (2.9); 78 (2.5); 240 (2.1); 39 (209); 76 (2.0)
<u>W</u>	**121 (100)**; 39 (23.9); 65 (22.8); 77 (21.6); 51 (12.0); 228 (10.5); 93 (10.3); 122 (7.3); 63 (6.0); 53 (4.8)
<u>W'</u>	**105 (100)**; 77 (34.3); 106 (7.9); 51 (5.1); 78 (2.1); 50 (1.3); 76 (1.3); 214 (1.1); 52 (0.6); 107 (0.6)

Indeed, the molecular peak (m/z = 240) of the reference compound X' proposed by the NIST Library was absent in the mass spectrum of the compound X whereas the peaks at m/z = 94 ($PhOH^{\cdot+}$) and m/z = 136 ($PhCOCHO^{\cdot+}$) were only observed for X and not X'. Besides, the peak at m/z = 227 may correspond to an oxyradical from hydroxylated **<u>K1</u>**$_{HH}$. The peak at m/z = 121 ($HOPhCHO^{+}$) was not observed for X unlike the compound W whereas the peak at 94 was observed unlike the compound W'. Moreover, the peak at m/z = 136 ($PhCH_2OH^{+}$) is observed only for X only. As an intense peak is observed at m/z = 43 is present, it is probable the hydroxyl group is acetylated.

From these data, we have obtained some key elements that have helped us to propose a mechanistic pathway (Figure II. 18) explaining the formation of the main products, other compounds being either intermediates or products from dead-end routes. Hence, as already mentioned in the bibliographic part, benzoic acid could be generated directly from **<u>K1</u>**$_{HH}$ through a direct C-C cleavage *via* a peroxyl radical intermediate (pathway (1)) [56], or through the C-O cleavage of a phenylgyoxal hemiacetal intermediate obtained by hydroxylation of **<u>K1</u>**$_{HH}$ (pathway (2)), oxidation into phenylglyoxylic acid and then decarboxylation to benzaldehyde. The hemiacetal could not be detected due to a lack of stability.

As shown by CAVANI *et al* [57], **<u>K1</u>**$_{HH}$ may be tautomerized into its corresponding enol ether (Fig. II. 18) as a result of an acid-catalyzed process involving

$PMoV_x$. One electron oxidation of the enol by vanadium (V) can be envisaged affording X_1 and X_2 radicals. Then, X_2 may react with dioxygen giving rise to an hydroperoxyl radical, Y_1. The latter can react with a hydrogen donor, *e.g.* the substrate itself [56] affording an hydroperoxide Y_2. It has to be noted that Z could also be produced by the reaction of $O_2^{\cdot -}$ with the X_2 radical followed by a protonation step. Such superoxide anions would be formed *in-situ* by the one-electron oxidation of vanadium (+IV) by dioxygen.

Reductive cleavage of the O-O bond in Y_2 would occurs afterwards, leading to the hemiacetal Y_3 that would give, by hydrolysis, phenylglyoxal and phenol. Further oxidation of phenylglyoxal may give an α-keto carboxylic acid, phenylglyoxylic acid that can be decarboxylated, thus producing benzaldehyde and CO_2. Phenylglyoxal may be formed from 2-hydroxyacetophenone, the hydrolysis product of **K1**$_{HH}$.

Water molecules involved may be originated from the catalyst (it is hydrated) or from the alcohol oxidation reactions. For instance, the oxidation of mandelic acid into phenylglyoxylic acid catalyzed by a $PMoV_3$ can be described by the equation: $PhCHOHCOOH + ½\ O_2 = PhCOCOOH + H_2O$. Hydrolysis was shown indirectly by the presence of mandelic acid. Indeed, without the hydrolysis step leading to the formation of the HIBBERT ketone [58], the carbonyl C=O could not be transformed into an alcohol. Since benzaldehyde cannot be formed through the pathway (1), *i. e.* cleavage of the C-C bond into phenol and phenyl formate, the pathway (2) and also the oxidation *via* the hydrolysis product take place. Yet, the formation of substantial amounts of phenyl formate, and hence of formic acid shows that the oxidative cleavage takes place through pathway (1).

Finally, it has to be noted that the oxidation through i) pathway (1) consumes one equivalent of dioxygen and ii) the oxidation through an initial nucleophilic substitution reaction (either with water or acetic acid) and the oxidation through pathway (2) three equivalents of dioxygen and one equivalent of carbon dioxide is emitted. So, two equivalents of gases are consumed by the oxidative cleavage of **K1**$_{HH}$. So, the oxygen consumption (1.5 mol/ converted **K1**$_{HH}$) is adequate to this mechanism.

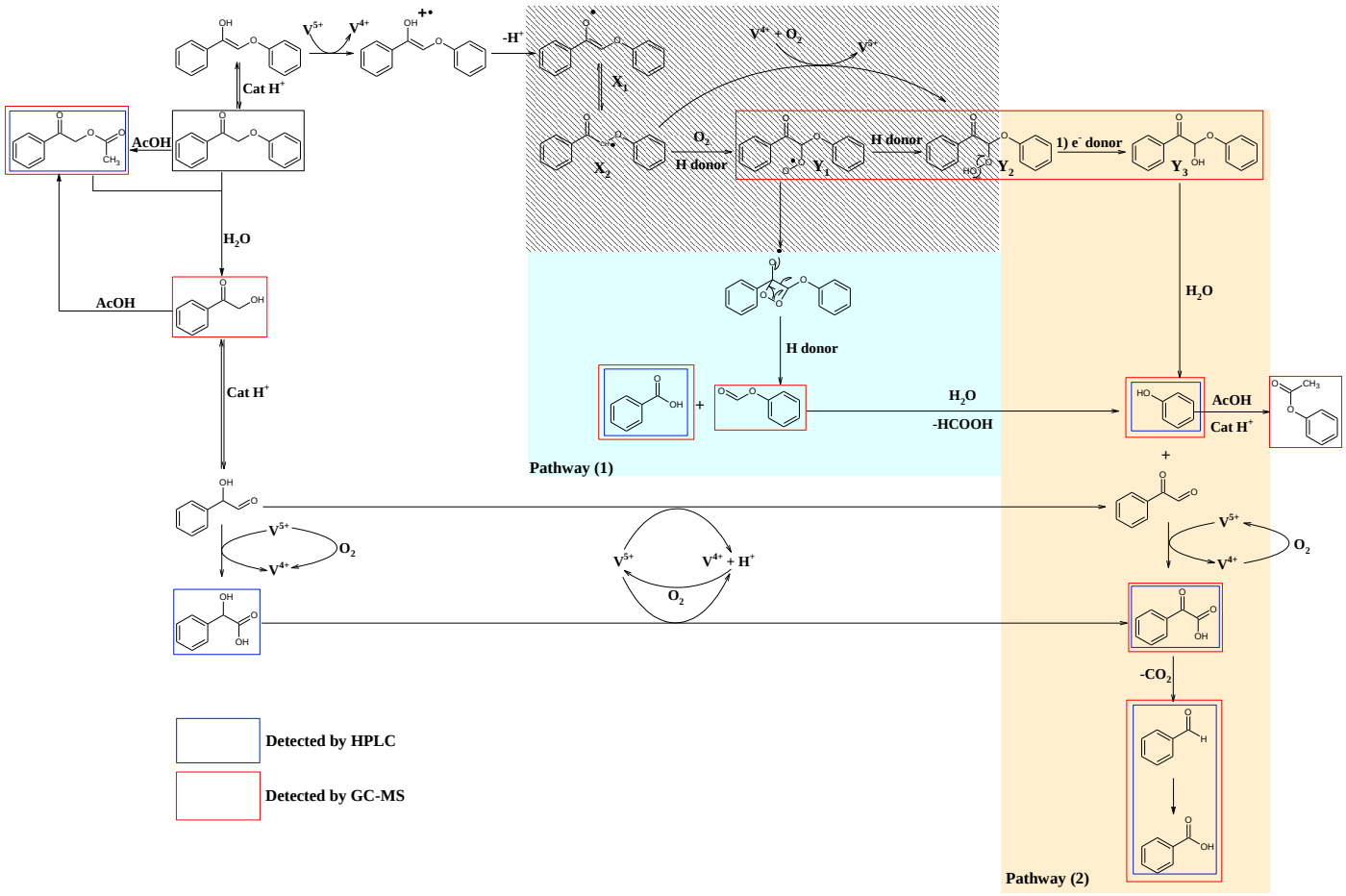

Figure II. 18: Mechanism proposal for the V3-HT catalyzed aerobic cleavage of ***K1****HH*

II. 4. 3. Study of the catalyst evolution during the reaction

We have previously demonstrated that $PMoV_x$ such as V_3-HT and V_1-HT are essential to achieve the aerobic cleavage of **K1**$_{HH}$ under kinetically favorable conditions. However, two questions arise: Are those catalysts capable of working several times? Are $PMoV_x$ themselves the catalysts or are they the precursors of more catalytically active species?

To answer the question dealing with the recyclability of those catalysts, a first reaction was carried out during 24 h under the conditions optimized before (**K1**$_{HH}$ 100 mM, V_3-HT (Mo + V 15 mol%, Atm. O_2, MeCN + 10% AcOH 82°C). As the catalysis is homogeneous, PMoVx cannot be recovered easily and, it was decided, in a preliminary approach, that we would proceed better by adding, at the end of the first run, another initial amount of **K1**$_{HH}$ and would perform again the tests by heating the reaction mixture during 24 h. Results are shown in Table II. 14.

*Table II. 14: Stability of the V_3-HT catalyst during the aerobic cleavage of **K1**$_{HH}$*

Entry	Run n°	Conv. (%)	Yield (%)			$\frac{n_{PhCHO} + n_{PhCOOH}}{n_{PhOH}}$	Carbon balance (%)
			PhOH	PhCHO	PhCOOH		
19	1	68	42	11	30	1.0	70
33	2	35	19	15	20	3.2	58

K1$_{HH}$: 19 (1.5 mmol), 33 (end of 19 + 1.5 mmol), atm. O_2, V_3-HT (Mo + V 15 mol%), MeCN + 10% AcOH 82°C, 24 h

Clearly, V_3-HT was not so active during the second run. A lower Mo+V loading (11.8 mol% and 15% / **K1**$_{HH}$ in the second and first runs, respectively) could be invoked. However, this assumption cannot be retained. Indeed, in a separate experiment conducted in the same conditions but with a Mo+V loading of only 7 mol% (Table II. 8, entry 17), the **K1**$_{HH}$ conversion was 43%.

A first possible explanation would deal with the instability of the KEGGIN structure leading to less active species. Secondly, the oxidation of phenol and benzaldehyde formed during the first run may compete with the **K1**$_{HH}$ cleavage in the second run as shown in paragraph II. 4.1 (Table II. 9). Indeed, the yield of benzoic acid was higher during the second run. As the result, it was decided that a better approach to study the catalyst stability would be to extract the remaining catalyst before re-use. The recovered catalyst was analyzed by ^{31}P NMR showing only one peak at - 4.2 ppm (Figure II. 19) instead of several ones as shown in Figure II. 10. As the pH of the aqueous solution

was lower than 1, this peak cannot correspond to phosphoric acid (signal at 0 ppm, pK_a = 2.3 in water). Therefore, it corresponds to phosphomolybdic acid. We checked, in parallel, that the structure of KEGGIN was preserved when only heating V_3-HT in MeCN – 10 vol% AcOH. Hence, we may reasonably suggest that the KEGGIN structure of the introduced $PMoV_x$ is not stable upon the reaction conditions, being transformed into a mixture of phosphomolybdate anion and, a priori, vanadyl (VO^{2+}) or pervanadyl (VO_2^+) counter-cations. Indeed, it is well-known that the KEGGIN free acids $PMoV_x$, especially those with a high vanadium content are not very stable, especially when reduced by the substrate noted H-Su, due to an increased distance between the heteroatom P and vanadium [59]. A general equation of the reaction (Eq. II. 1) involves the ejection of a vanadyl cation.

$$[PMo_9V^{+V}{}_3O_{40}]^{6-} + H - Su = [PMo_9V^{+V}{}_2O_{39}]^{9-} + V^{+IV}O^{2+} + H^+ + Su^{\cdot} \quad \text{(Eq II. 1)}$$

So, $PMoV_x$ may be considered as the precursors of *in situ*-formed pervanadyl cations that would be the true catalysts. Such ejection is accompanied by the formation of an unstable lacunary POM that generates phosphomolybdates.

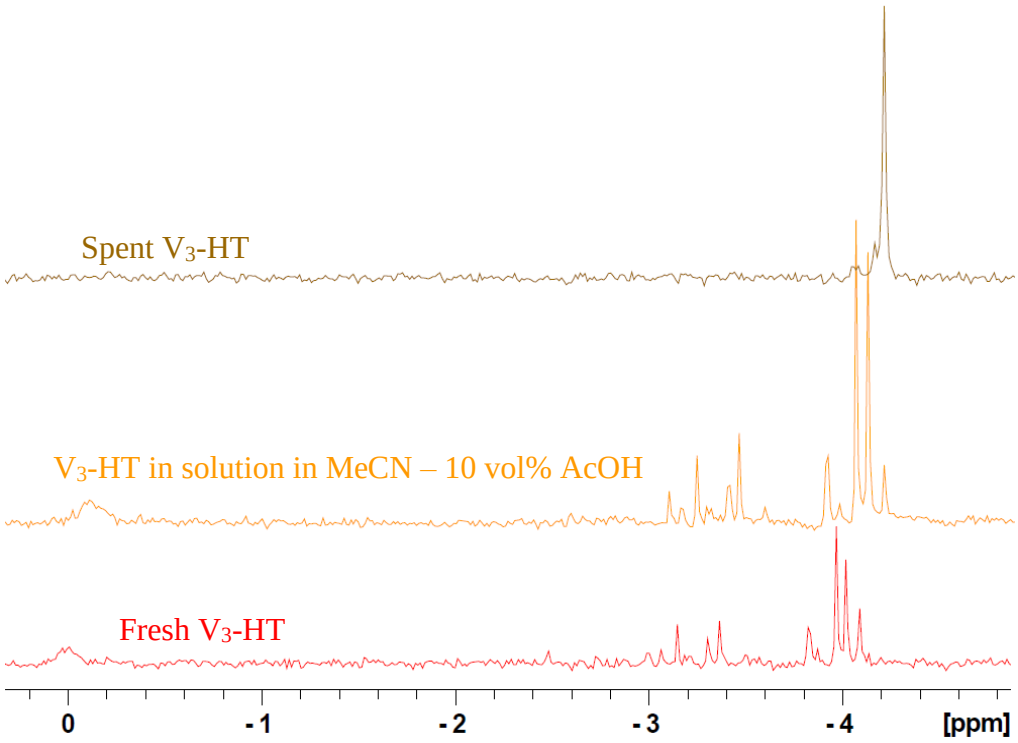

Figure II. 19: ^{31}P NMR spectra of the fresh and spent V_3-HT catalysts (catalyst 30 mg in D_2O-H_2O 50:50 500 µL + dioxane 7.5 µL)

II. 5. Activity of the $PMoV_x$ catalysts for $\underline{A1}_{HH}$ cleavage

$PMoV_x$ proved to be an active catalyst for the aerobic cleavage of $\underline{K1}_{HH}$. However, this dimer is not the best model of lignin. $\underline{A1}_{HH}$ has a structure closer to lignin and will be now considered as the substrate.

II. 5.1. Tests under atmospheric pressure

$\underline{A1}_{HH}$ was tested first in the conditions optimized for $\underline{K1}_{HH}$ (see paragraph II. 4.1), *i.e.* in the presence of V_1-HT and V_3-HT catalysts (Mo+V 15 mol%) in MeCN + 10 vol% AcOH under atmospheric pressure of O_2 (Table II. 15, entries 1-2).

Table II. 15: Activity of V_x-HT catalysts for $\underline{A1}_{HH}$ cleavage

Entry	Catalyst	Conv. (%)	Yield (%)						Carbon balance (%)
			PhOH	PhCHO	PhCOOH	$K1_{HH}$	$\underline{Est}^{\alpha}\underline{A1}_{HH}$	$D1_{HH}$	
1	V_1-HT	41	5.8	2.4	2.3	16	10	14	104
2	V_3-HT	35	4.6	2.0	2.1	17	9	13	108
3	H_2SO_4[a]	9.1	1.9	2.0	tr	tr	0	5.2	98

$\underline{A1}_{HH}$ 100 mM, MeCN + 10 vol% AcOH (15 mL), Mo+V 14.5 mol%, O_2 (1-6 bar), 24 h; [a]6.2 mol%, 0.03 vol%

Undoubtedly, $\underline{A1}_{HH}$ proved to be more resistant than $\underline{K1}_{HH}$. Under atmospheric pressure, the oxidation of the alcohol function is favored so as the formation of the esterification (by acetic acid) and dehydration products, noted $\underline{Est}^{\alpha}\underline{A1}_{HH}$ and $\underline{D1}_{HH}$ respectively. These two last compounds are favored by the acidity of $PMoV_x$ (Figure II. 20).

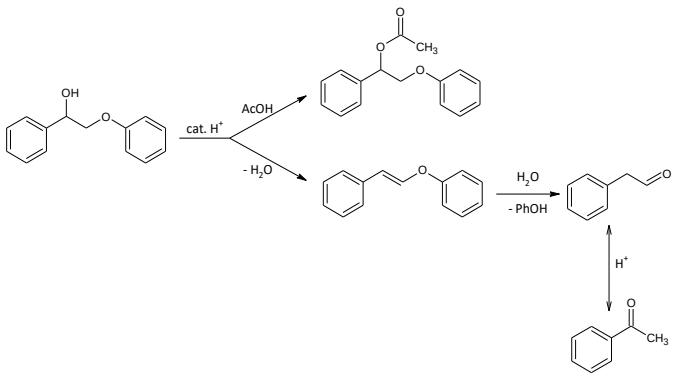

Figure II. 20: Side reactions during $\underline{A1}_{HH}$ conversion

Still, the catalyst has an activity for $\underline{A1}_{HH}$ cleavage. Indeed, in presence of H_2SO_4, (entry 3), the conversion falls to 9.1% (*vs* 35% in presence of V_3-HT, entry 2), the yield of phenol is 1.9% (*vs* 4.6%) and benzoic acid was not detected. As it was done for $\underline{K1}_{HH}$, the influence of the amount of acetic acid on the transformation rate of $\underline{A1}_{HH}$ was assessed (Table II. 16).

From the results of Table II.16, it is clear that acetic acid has a strong influence on the amount of ester produced. A yield of 51% of **Est**$^{\alpha}$**A1**$_{HH}$ was reached in pure acetic acid medium (Table II.16, entry 6) but the main product proved to be recalcitrant to cleavage (conversion: 8.2%, formation of **D1**$_{HH}$ favored and PhCHO and PhCOOH not detected). Moreover, there seems to be a competition between the formation of the ester and the dehydration product **D1**$_{HH}$, the latter being mainly formed in the absence of acetic acid (Table II.16, entry 4). The best results in terms of oxidation, i.e. cleavage and conversion of **A1**$_{HH}$ to **K1**$_{HH}$, were obtained for the acetic acid contents of 5 and 10% (Table II.16 5 vs. 2 vs. 4), the latter appearing to have a (slight) influence on the production of benzoic acid. However, acetic acid does not seem to impact the yield of PhOH, PhCHO and **K1**$_{HH}$.

In the following section, the reactions with **A1**$_{HH}$ will be carried out in MeCN + 10 vol% AcOH similarly to **K1**$_{HH}$.

II. 5.2. Kinetic and mechanistic studies

The cleavage reaction of **A1**$_{HH}$ in the presence of V_3-HT in the reference solvent, MeCN +10% AcOH, under atmospheric pressure of O_2 at 82°C was monitored for 48 h (Table II. 17 and Fig II. 21). During that time period, the conversion of **A1**$_{HH}$ raised until 67% (instead of 35% within 24 h). Clearly, the oxidation of **A1**$_{HH}$ is slow compared to that of **K1**$_{HH}$ under the same conditions. The yields of phenol and benzoic acid raised both until 10% and benzaldehyde yield was stable from 8 (entry 8) to 24 h (entry 2) meaning that its production and its oxidation took place at similar rates. **K1**$_{HH}$ formed during the **A1**$_{HH}$ cleavage process seems to accumulate (the yield of **K1**$_{HH}$ raised until 17% at 24 h, then **K1**$_{HH}$ was converted since its yield was 11% after 48 h (entry 11) showing that, in presence of **A1**$_{HH}$, V_3-HT becomes less efficient for the aerobic oxidative cleavage of **K1**$_{HH}$.

The side products **Est**$^{\alpha}$**A1**$_{HH}$ and **D1**$_{HH}$ accumulated on the course of the reaction. The selectivity to phenol was stable during the reaction and the selectivity in C-C cleavage increased during the reaction. Carbon balance decreased after 37 h (entry 10).

*Table II. 16: Influence of the acetic acid content on the activity of V_3-HT catalysts for **A1**$_{HH}$ cleavage*

Entry	z	Conv. (%)	Yield (%)						Selectivity (%)[a, b]		$\frac{n_{PhCHO}}{n_{PhCOOH}}$	Carbon balance (%)
			PhOH	PhCHO	PhCOOH	K1$_{HH}$	Est[α]A1$_{HH}$	D1$_{HH}$	C-O cleavage	C-C cleavage		
4	0	24	4.2	2.7	0.6	18	0	21	18	14	4.5	99
5	5	41	5.2	3.2	1.7	20	5.4	8.9	13	12	1.9	98
2	10	35	4.6	2.0	2.1	17	9.2	12	13	12	1.0	107[c]
6	100	83	16	4.2	16	1.6	51	16	19	24	0.3	102

A1$_{HH}$ 100 mM, Atm. O_2, MeCN + z% AcOH, V_3-HT (Mo + V 15 mol%), 82°C, 24 h
[c]Higher than 100% due to experimental error

*Table II. 17: Influence of the reaction duration on **A1**$_{HH}$ conversion and on the yields of cleavage products*

Entry	t (min)	Conv. (%)	Yield (%)						Selectivity (%)		$\frac{n_{PhCHO}}{n_{PhCOOH}}$	Oxygen consumption / conversion	Carbon balance (%)
			PhOH	PhCHO	PhCOOH	K1$_{HH}$	Est[α]A1$_{HH}$	D1$_{HH}$	C-O cleavage	C-C cleavage			
7	2	18	2.1	2.4	0.3	3.6	5.2	6.1	12	15	8		99
8	8	29	3.3	2.6	1.7	3.6	5.4	6.2	11	15	1.5	1.4	90
9	14	39	4.4	1.9	2.3	17	9.2	7.5	11	11	0.8	0.3	93
2	24	35	4.6	2.0	2.1	17	9.2	12	13	12	1.0	0.5	107[c]
10	37	61	10	4.9	8.0	9.8	13	11	16	21	0.6	0.7	82
11	48	67	10	6.4	9.9	11	13	13	15	24	0.6	0.9	83

A1$_{HH}$ 100 mM, atm. O_2, V_3-HT (Mo + V 15 mol%), MeCN + 10 vol% AcOH, 82°C
[a] $Sel(C-C\ cleavage) = \frac{\eta_{PhCHO}+\eta_{PhCOOH}}{Conv}$ [b] $Sel(C-O\ cleavage) = \frac{\eta_{PhOH}}{Conv}$ [c]Carbon balance higher than 100% due to standard deviation

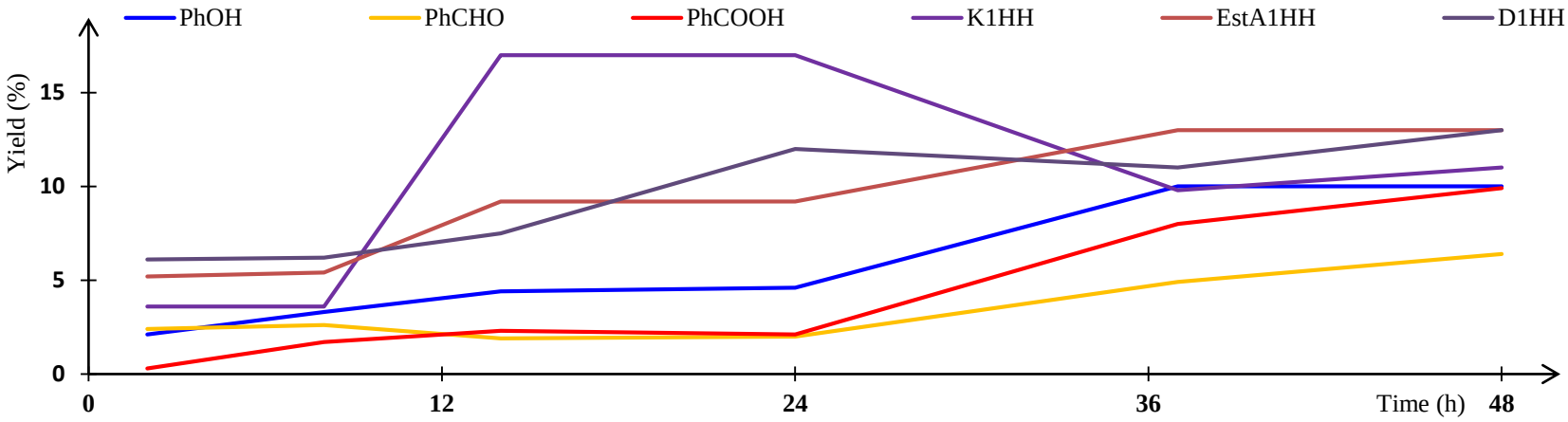

A)

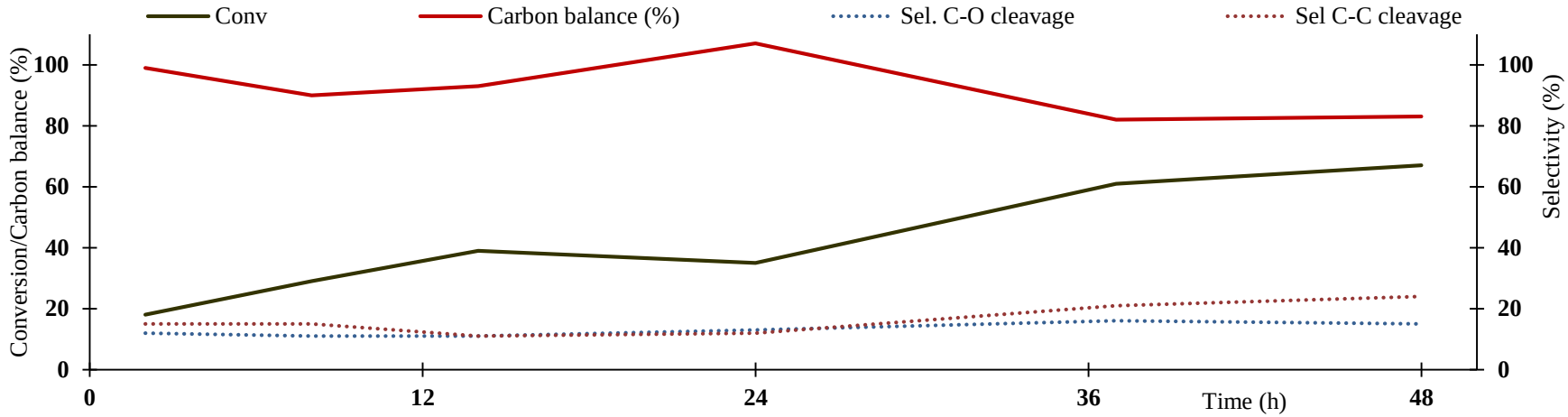

B)

*Figure II. 21: Evolution of A) yields of cleavage products, B) **A1**$_{HH}$ conversion, carbon balance and selectivity to C-O and C-C cleavage*

The general expression of the rate law for **A1**$_{HH}$ can be written $-\frac{d[\underline{A}1_{HH}]}{dt} = k_{app}[\underline{A}1_{HH}]^n$ which can be transformed, after integration ($n \neq 1$), into $[\underline{A}1_{HH}]^{-(n-1)} = k'_{app}t$, hypothesizing the concentration of dissolved oxygen is constant as for **K1**$_{HH}$ cleavage. With our experimental data, the best fit was obtained with the curve $[\underline{A}1_{HH}]^{-0.7} = f(t)$ (Regression coefficient of $R^2 = 0.9999$, Fig. II. 22). So, the kinetics law for **A1**$_{HH}$ cleavage is : $-\frac{d[\underline{A}1_{HH}]}{dt} = k_{app}[\underline{A}1_{HH}]^{1.7}$.

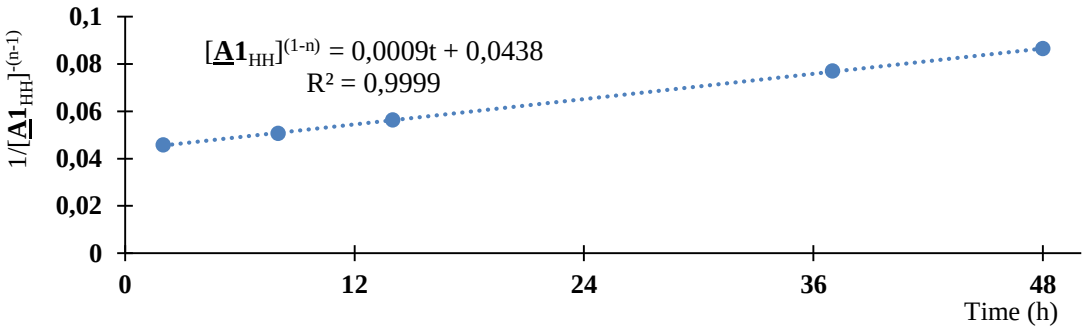

Figure II. 22: Graphical calculation of the kinetic order to ***A1****$_{HH}$ (T = 80°C, n = 1.7)*

GC-MS analyses were carried out too on the reaction media collected after the extraction of the spent catalyst. As before for **K1**$_{HH}$ (paragraph II. 4.2), the detected compounds were classified either as products arising either from C-O (Table II. 18a) and C-C (Table II. 18b) cleavage or dimers from side reactions (Table II. 18c).

Table II. 18a: GC-MS identification of products arising from C-O bond cleavage of A1$_{HH}$

RT (min)	Compound	Area ratio (/PhOH)	Match (%)	Comments
4.0	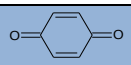 *p-quinone*	0.01	88	**Identification by HPLC** with a commercial standard. Minor product.
4.9	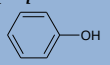 *phenol*	1	97	Targeted product. **Identification by HPLC** with a commercial standard. Absolute area: 7.4. 10^6 UAAbsolute area: 2.10 10^8 UA
6.3	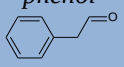 **phenylcetaldehyde**	0.01	98	Acidic cleavage product.
6.8	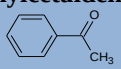 **acetophenone**	0.01	91	Acidic cleavage product from phenylacetaldehyde isomerization.
11.2	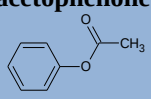 *Phenyl acetate*	0.05	88	Phenol esterified by acetic acid
19.6	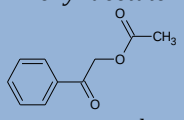 *2-acetoxyacetophenone*	0.19	95	**Identification by HPLC** with a synthesized standard. Acetolysis product.

phenol : product similar to ***K1****$_{HH}$ cleavage,* **phenylacetaldehyde : not observed after K1$_{HH}$ cleavage**

*Table II. 18b: C-C cleavage products of **A1**$_{HH}$ detected by GC-MS*

RT (min)	Compound	Area ratio (/PhCOOH)	Match (%)	Comments
4.7	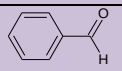 *Benzaldehyde*	0.05	96	Targeted product. **Identification by HPLC** with a commercial standard.
4.8	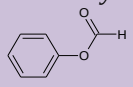 *Phenyl formate*	0.04	92	Formic ester of phenol.
9.8	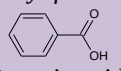 *Benzoic acid*	1	97	Targeted product. **Identification by HPLC** with a commercial standard. Absolute area: 2.95. 10^8 UA
17.2	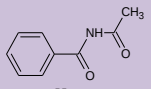 *N-acetylbenzamide*	0.10	93	Benzamide of benzoic acid and acetamide. Acetamide was also identified by GC-MS (3.93 min).

*Table II. 18c: Dimeric products of **A1**$_{HH}$ detected by GC-MS*

RT (min)	Compound	Area ratio (/**K1**$_{HH}$)	Match (%)	Comments
22.0	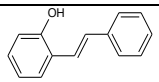 **2-hydroxystilbene**	0.003	88	Oxidative condensation product from **A1**$_{HH}$ oxidation. Detected by ^{1}H NMR.
22.82	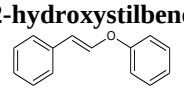 **D1**$_{HH}$	0.02	n. i.	Identified by the injection of a diluted reaction media (Molecular peak at m/z = 196)
25.66	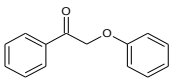 **K1**$_{HH}$	1	n. i.	Identified by the injection of a diluted reaction media (Characteristic molecular peak at m/z = 212) Absolute area: 2.6. 10^8 UA
25.8	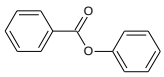 *Phenyl benzoate*	0.03	93	Ester of phenol and benzoic acid
26.9	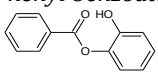 *2-hydroxyphenyl benzoate*	0.04	95-96	Oxidation side product
27.8	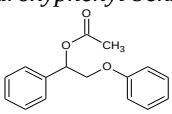 **Est$^{\alpha}$A1**$_{HH}$	1.9	n. i.	Identified by the injection of a diluted reaction media (Peaks at m/z = 43 ($COCH_3^+$) and 196)
29.2	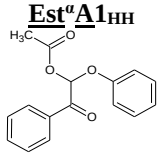 *X*	0.03	n. i.	Structure supposed from GC-MS data of **K1**$_{HH}$ cleavage (see Table II. 12c)

*Phenyl benzoate: product similar to **K1**$_{HH}$ cleavage,* **2-hydroxystilbene : not observed after K1$_{HH}$ cleavage**

As for **K1**$_{HH}$ cleavage, phenyl formate (C-C cleavage) and acetate (C-O cleavage), 2-acetoxyacetophenone (acetolysis) and phenyl benzoate were observed as minor products from **A1**$_{HH}$ cleavage. Yet, there are some products characteristic to **A1**$_{HH}$ cleavage as phenylacetaldehyde (6.3 min) and the hydroxystilbenes (22.0 min).

Phenylacetaldehyde would be generated from a dehydration of **A1**$_{HH}$ affording **D1**$_{HH}$ followed by its hydrolysis, meaning that a non-oxidative C-O cleavage of **A1**$_{HH}$ was involved. The hydroxystilbenes are oxidative condensation products.

Two different mechanisms may be proposed. The first one involves the oxidation of **A1**$_{HH}$ into **K1**$_{HH}$ as in part IA. Then, the mechanism detailed on Fig. II. 18 will be applicable. Indeed, **K1**$_{HH}$, 2-phenoxyacetophenone and the product X were also detected. However, the ratio PhCHO/PhCOOH in **A1**$_{HH}$ cleavage is higher than in **K1**$_{HH}$ cleavage. Therefore, another mechanism should be involved. A mechanism inspired by EVTUGUIN *et al* [34] can be proposed on Fig. II. 23.

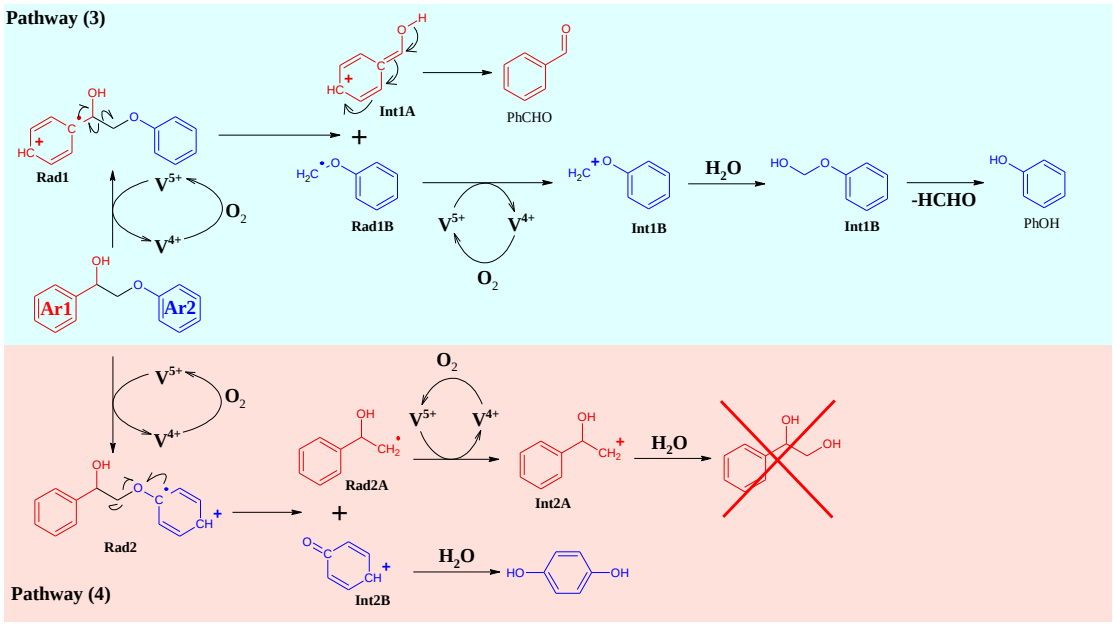

*Figure II. 23: Mechanism of direct cleavage of **A1**$_{HH}$ inspired by Ref 34*

Two pathways were suggested. The first one (pathway (3)) involves a monoelectronic oxidation of Ar1 moiety by the catalyst into Rad1. This activates the substrate for C-C cleavage into Int1A and Rad1B. Int1A is deprotonated into benzaldehyde while Rad1B is oxidized into Int1B which is hydrated into a formaldehyde hemiacetal. Finally, the hemiacetal is cleaved into phenol and formaldehyde. The second one involves a monoelectronic oxidation of Ar2 moiety into Rad2. C-O cleavage in Rad2 takes place, giving rise to Rad2A and Int2B. Int2B is hydrated into hydroquinone while Rad2A is oxidized into Int2A that is hydrated into styrenediol. However, these products were not detected by GC-MS, which invalidates the pathway (4). So, the increased ratio PhCHO/PhCOOH may be explained by **A1**$_{HH}$ oxidation according pathway (3) only.

However, this cannot explain the formation of phenylacetaldehyde and acetophenone. These products are originated from a non-oxidative C-O cleavage. The intermediate is the dehydration product **D1**$_{HH}$. **D1**$_{HH}$ is rehydrated then into an instable hemiacetal of which the cleavage gives rise to phenol and phenylacetaldehyde. The latter one isomerizes into acetophenone in acidic media. A simplified mechanism is given on Fig. II. 24.

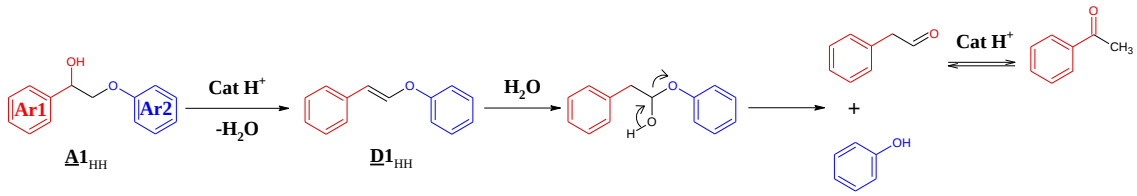

A1$_{HH}$ **D1**$_{HH}$

Figure II. 24: Formation of phenylacetaldehyde and acetophenone

So, the dehydration is not a dead-end route on the contrary of esterification. However, it essentially gives rise to non-oxidative C-O cleavage.

II. 6. Optimization essays

A1$_{HH}$ proved to be more resistant to cleavage than **K1**$_{HH}$. So, more stringent conditions were applied. As the temperature is close to the boiling point of the solvent, the pressure was raised first to 5 bar (before heating). Afterwards, the effect of temperature was assessed. As **K1**$_{HH}$ cleavage is easier, some tests in presence of a co-oxidant (TEMPO ((2,2,6,6-Tetramethylpiperidin-1-yl)oxyl) or hydrogen peroxide) to boost the alcohol oxidation into a the ketone were performed.

II. 6.1. Tests at higher pressure and temperature

In a first attempt, the O_2 pressure was raised from 1 to 5 bar without modifying the temperature (80°C; Table II.19, entries 2, 13-14). A rise of O_2 pressure boosted the conversion (54% and 65%, entries 13-14 *vs* 35%, entry 2) and the yield of PhCHO and PhCOOH (entry 14 *vs* 2) and therefore the selectivity of the catalyst for C-C cleavage products. Nonetheless, dehydration and esterification took place at a higher extent. Since then, the duration of the test was shortened to 6 h (entry 12 vs 14) instead of 24 h, **A1**$_{HH}$ conversion decreased, as expected, from 66 to 33%. The yield of **K1**$_{HH}$ was higher after 6 h than after 24 h but the selectivity to C-O and C-C cleavage products did not seem to

be impacted by the reaction time. Such observations are in agreement with the intermediate role of **K1**$_{HH}$ in the oxidative cleavage of **A1**$_{HH}$.

A test without acetic acid was carried out (entry 15). The conversion (23 *vs* 54%) so as the yield of phenol (6.9 *vs* 16%), benzaldehyde (4.8 *vs* 7.1%) and benzoic acid (1.8 *vs* 9.8%) were much lower (*vs* entry 13), which means acetic acid has a positive effect on the substrate conversion as for **K1**$_{HH}$ cleavage (paragraph II. 4.1, Table II. 7, 48% without acetic acid and 72% in presence of 10 vol% of acetic acid). Also, the absence of acetic acid gave rise to similar selectivity to C-O (30 *vs* 30%) and C-C (29% *vs* 31%) cleavage.

To boost the cleavage of **A1**$_{HH}$, the temperature was raised to 120°C and the duration was shortened to 20 min (entry 17) or 2 h (entry 18). After 2 h, the conversion was 43% (*vs* 33%, entry 12). The temperature showed to have a positive impact (entry 18 *vs* entry 12) on the selectivity for C-O (16% *vs* 11%) and C-C cleavage (32% *vs* 19%). This can be explained by the acceleration of side reactions. Moreover, **Est**$^{\alpha}$**A1**$_{HH}$ (11% *vs* 9.9%) was produced at similar extent and the carbon balance was not significantly degraded (96% vs 99%).

Part of the tests were performed with a magnetic stirrer whereas others were carried out with a mechanical helicoloidal one (14 vs 13 and 19 vs 18) showing that the agitation mode is a critical parameter. Indeed, in the case of the mechanical stirring, C-C and C-O cleavage were much more favored. For instance, after 24 h of at 80°C with a magnetical stirrer (entry 14 *vs* 13 (helicoidal stirrer)), the conversion was 65% (*vs* 54%) while the yield of phenol (6.6 *vs* 16%), benzaldehyde (6.0 *vs* 7.1%) and benzoic acid (7.8 *vs* 9.8%) were lower, which leads to a lower selectivity for C-O and C-C cleavage. This hints again that dioxygen transfer from the gas phase to the liquid reaction mixture has a strong impact on the cleavage of **A1**$_{HH}$.

A test was carried out at 120°C during 6 h with a helicoidal stirrer (entry 20). Compared to the test with a shorter duration (2 h, entry 18), the conversion was expectedly improved (90% *vs* 80%) and the yield of benzoic acid was higher (19 *vs* 7.9%). However, the yield of phenol was not improved significantly and the carbon balance fell to 55% (*vs* 78%). Finally, a test was carried out at 80°C with a duration lengthened to 48 h with a magnetical stirrer (entry 16). The conversion of **A1**$_{HH}$ does not increase (*vs* entry 14). However, the yield of cleavage products raised, which leads to a better selectivity for C-C (30 *vs* 21%) and C-O (15 *vs* 10%) cleavage.

To conclude, ideally **A1**$_{HH}$ cleavage tests should be performed at 120°C during 2 h (Table II. 19, entry 18) since a reasonable compromise was reached between the **A1**$_{HH}$ conversion rate, the yields of PhOH, PhCHO and PhCOOH and a correct mass balance.

II. 6.2. Tests in the presence of a co-oxidant

Another solution envisaged in order to increase the PMoVx performances in the aerobic oxidative cleavage of **A1**$_{HH}$ is based on the addition of a co-oxidant such as TEMPO or H_2O_2. Indeed, NEUMANN *et al* [59-60] proved that the $PMoV_x$-TEMPO system is efficient for benzylic alcohol oxidation (see paragraph IB. 3.1). Moreover, TEMPO and derivatives showed to be efficient to oxidize the alcohol function into ketone in lignin [61]. According to WANG *et al*, the alcohol oxidation reaction to ketone is beneficial for the cleavage of the C-C bond [62]. In these cases, the oxidized TEMPO is the real catalyst and the role of the $PMoV_x$ is to regenerate the oxidized TEMPO.

Table II. 20 gives details, in our hands, the yields of the cleavage products (PhOH, PhCHO and PhCOOH) and of the dimers **K1**$_{HH}$, **Est**$^{\alpha}$**A1**$_{HH}$ and **D1**$_{HH}$ in presence of TEMPO and H_2O_2 at different pressures and concentrations of co-oxidant in metal equivalents.

With TEMPO (table II. 20, entries 24-25) under 5 bar of O_2 pressure (before heating), the optimum for conversion rates was obtained with a molar loading of 3 mol% of TEMPO (molar ratio TEMPO / Mo+V of 0.2). The yields of C-C cleavage products and **K1**$_{HH}$ raised whereas phenol yield decreased (entry 24 *vs* 14) leading to a degraded selectivity to C-O cleavage and also to a decrease of carbon balance. At a higher proportion of TEMPO, the conversion was always lower. For a molar loading of 29 mol% of TEMPO (TEMPO / Mo+V = 2), the combined yield of PhCHO and PhCOOH was comparable to the one obtained with test with 3 mol% of TEMPO (entry 25 *vs* 24) whereas **K1**$_{HH}$ yield was two times lower. An interesting feature about TEMPO was that a loading of 30 mol% proved to cut down both dehydration and esterification.

*Table II. 19: Influence of temperature and pressure on **A1**$_{HH}$ cleavage*

Entry	Pressure (bar)	Temperature (°C)	Time (h)	Conv. (%)	Yield (%) PhOH	PhCHO	PhCOOH	K1$_{HH}$	Est^{a}A1$_{HH}$	D1$_{HH}$	Sel. to cleavage (%)[d] C-O	C-C	Carbon balance (%)
2 [b]	1	80	24	35	4.6	2.0	2.1	17	9.2	12	12	13	107
12[c]	5	80	6	33	3.7	2.9	3.5	8.7	9.9	10	11	19	99
13[c]	5	80	24	54	16	7.1	9.8	10	18	21	30	31	118
14[b]	5	80	24	65	6.6	6.0	7.8	3.4	13	17	10	21	85
15[a, c]	5	80	24	23	6.9	4.8	1.8	11	0	20	30	29	106
16[b]	5	80	48	66	9.6	8.9	11	7.1	9.4	19	15	30	87
17[c]	5	120	0.33	43 (?)	5.5	3.3	3.8	6.9	10	25	16	17	104
18[c]	5	120	2	44	7.1	6.4	7.5	2.7	11	16	16	32	96
19[b]	5	120	2	80	9.0	5.8	7.9	9.5	20	14	11	17	78
20[c]	5	120	6	90	7.6	2.6	19	6.7	12	12	8.4	24	55

A1$_{HH}$ 100 mM, V_3-HT (Mo+V 15 mol%), MeCN - 10 vol% AcOH

[a]Test without AcOH; [b]Use of a magnetical stirrer; [c]Use of a mechanical helicoidal stirrer; [d]$Sel(C-C\ cleavage) = \frac{\eta_{PhCHO}+\eta_{PhCOOH}}{Conv}$, $Sel(C-O\ cleavage) = \frac{\eta_{PhOH}}{Conv}$

*Table II. 20: Influence of TEMPO or H_2O_2 addition and of acetic acid replacement by TFA on **A1**$_{HH}$ cleavage*

Entry	Pressure (bar)	Co-oxidant (mol ratio / Mo+V)	Acid (vol%)	Conv. (%)	Yield (%) PhOH	PhCHO	PhCOOH	K1$_{HH}$	Est^{a}A1$_{HH}$	D1$_{HH}$	Sel. to cleavage (%)[a] C-O	C-C	Carbon balance (%)[b]
2	Atm.	-	AcOH (10)	35	4.6	2.0	2.1	17	9.2	12	12	13	107
14	5	-	AcOH (10)	54	16	7.1	9.8	10	18	21	30	31	118[b]
21		H_2O_2 (3)		47	7.0	4.4	3.8	5.5	12	13	15	17	90
22	Atm.	H_2O_2 (6)		35	4.9	3.6	1.9	2.9	n. d.	n. d.	14	16	n. d.
23		H_2O_2 (330)	AcOH (10)	77	10	7.9	14	7.3	n. d.	n. d.	13	28	n. d.
24	5	TEMPO (3)		73	10	11	12	14	20	19	14	32	96
25		TEMPO (30)		45	18	9.2	15	7.0	0	0	40	54	82
4		-	-	24	4.2	2.7	0.6	18	0	21	18	14	118[b]
26	Atm.	-	TFA (0.67)	39	4.9	3.2	1.4	3.8	6.0	6.0	13	12	79
27		-	TFA (1.67)	70	5.9	2.1	1.3	0.3	6.5	6.5	8.4	4.9	45
28		-	TFA (3.60)	69	13	4.4	7.3	3.6	11	11	19	17	61

A1$_{HH}$ 100 mM, Atm. O_2, V_3-HT (Mo+V 15 mol%), MeCN - 10 vol% AcOH, 80°C, Use of a mechanical helicoidal stirrer

[a]$Sel(C-C\ cleavage) = \frac{\eta_{PhCHO}+\eta_{PhCOOH}}{Conv}$, $Sel(C-O\ cleavage) = \frac{\eta_{PhOH}}{Conv}$, [b]Higher than 100% due to experimental errors

H_2O_2 was evaluated as a co-oxidant (Table II. 20, entries 21-22) at atmospheric pressure. A molar ratio H_2O_2/(Mo+V) of 0.2 proved to be an optimum not only for **A1**$_{HH}$ conversion but also for the aerobic cleavage since PhOH, PhCHO and PhCOOH yields were maximized and accumulated of **K1**$_{HH}$ content was lower. At a higher concentration of H_2O_2 (entry 22), the conversion was equal to 35% like in the test (entry 2) performed without H_2O_2 and it dies not give rise to substantial improvement of the selectivities to C-O and C-C cleavage products were not improved (*vs* entry 2). Then, H_2O_2 was tested as the oxidant for **A1**$_{HH}$ (330 mol%, 3.3 equivalents to substrate, entry 23). The conversion was higher compared to the test without H_2O_2 (entry 2) and even to the test under higher pressure (entry 14). However, compared to the test under 5 bar of dioxygen, the selectivity to C-O and C-C cleavage are lower (*vs* entry 14). So, dioxygen may be the most adapted oxidant for **A1**$_{HH}$ cleavage.

Thus, a rise of temperature and pressure (to 5 bar) may give rise to a boost of selectivity to C-C cleavage. It was maximized for T = 80°C and t = 24 h (Table II. 19, entry 15) and for T = 120°C, t = 2 h (entry 20). However, for a long duration (24 h) gives rise to a higher yield of acetic ester (18%). Thus, the most adequate conditions are T = 120°C and t = 2h. However, the yield of phenol is rather low, which is due to over-oxidation. The effect of TEMPO and H_2O_2 on **A1**$_{HH}$ cleavage were assessed. TEMPO gives rise to better results than H_2O_2. Indeed, the adjunction of TEMPO enabled to cut down the dead-end esterification (Table II. 20, entry 24 and 25) and the maximal selectivities to C-O and C-C cleavage were 40% and 54% respectively (entry 25). Nevertheless, TEMPO is not stable as shown in the Appendix (*cf.* Attempts of **A1**$_{HH}$ oxidation into **K1**$_{HH}$).

II. 6.3. Use of trifluoroacetic acid (TFA) as an alternative acid

As emphasized in the paragraph II. 5.2, the major parasite reaction is the esterification of **A1**$_{HH}$ by acetic acid used as a co-solvent. This has led us to envisage another carboxylic acid (RCO_2H) that do not form easily esters due to the better leaving group ability of its carboxylate moiety RCO_2^-. TFA was proposed as an alternative to acetic acid. Consequently, a series of tests with various amounts of TFA (from 0.67 to 3.6%) were carried out (Table II. 20, entries 26-28).

As for the tests on **K1**$_{HH}$ (see Table II. 10, entries 26 and 27), the volumic fraction of TFA were either 0.66, 1.67 and 3.6 vol%. A higher content of TFA would lead to too acidic conditions as the alternative acid is much stronger than acetic acid as emphasized in paragraph II. 4.1. A volumic fraction of 3.6 vol% (entry 28) was needed to boost the yields of phenol and benzoic acid. However, the carbon balance plummeted compared to the test in presence of acetic acid justifying the low amounts of TFA tested. A low amount gave rise to a degraded selectivity to C-C and C-O cleavage products (entries 26 and 27 *vs* entry 4). In general, the substitution of acetic acid by TFA gave rise to a lower yield of **K1**$_{HH}$, meaning that the in-situ formed ketone cleavage into PhOH, PhCHO and PhCOOH was easier. However, the maximum of the selectivity to C-O and C-C cleavage was 19% and 17% respectively, which does not a noteworthy improvement compared to the test without TFA (entry 4) and there is a drop of the carbon balance (61% only). Thus, TFA does not appear to be better than acetic acid and the latter one will still be used in the incoming catalytic tests.

Why such of difference of reactivity between A1$_{HH}$ and K1$_{HH}$?

Paragraphs II. 4 and II. 5 have clearly emphasized strong differences of reactivity between the substrates **A1**$_{HH}$ and **K1**$_{HH}$. The alcohol proved to be less reactive than the ketone. Indeed, the presence of the carbonyl moiety, an electron-drawing group, on the C-C bond to be broken in **K1**$_{HH}$ may activate **K1**$_{HH}$ (see paragraph IA. 3.2.6).

An important question is whether the cleavage of **A1**$_{HH}$ requires prior oxidation of the alcohol into a carbonyl derivative. Indeed, the formation of **K1**$_{HH}$ was observed but the ketone tends to accumulate as if the alcohol would be responsible of some catalyst deactivation. As a result, the ability of the $PMoV_x/O_2$ system to catalyze the aerobic oxidation of alcohols was investigated by replacing **A1**$_{HH}$ by 1-phenylethanol. In the standard conditions (Atm. O_2, V_3-HT, Mo + V 15 mol%, MeCN – 10 vol% AcOH, 82°C, 24 h), the conversion was 98% with quantitative selectivity for acetophenone, which means that the catalyst is more active for the oxidation of 1-phenylethanol into the corresponding ketone, acetophenone, than for **K1**$_{HH}$ cleavage. So, the alcohol function in **A1**$_{HH}$ does not seem to be responsible of the deactivation of the catalyst mentioned before. Besides, two additional tests were performed with V_3-HT in presence of TEMPO or H_2O_2 (2.9 mol%) affording the same conversion rate of 98% meaning that those co-oxidants

are not really efficient. We have just noticed that a little bit of benzoic acid, arising from the C-C cleavage of acetophenone, was formed in presence of TEMPO.

A1$_{HH}$ has a lower reduction potential than 1-phenylethanol as shown by ANDERSEN *et al* [63]. Consequently, two solutions containing either **A1**$_{HH}$ or 1-phenylethanol and the catalyst (room temperature, MeCN-10 vol% AcOH 5 mL, V_3-HT (Mo + V 15 mol%)) were prepared. They both reduced the catalyst as shown by the green coloration. Then, the solution containing **A1**$_{HH}$ became orange meaning that the $PMoV_x$ was oxidized back whereas the solution of 1-phenylethanol was still green. So, the $PMoV_x$ may be transformed into another catalyst of which the reduction by **A1**$_{HH}$ may be kinetically hindered.

Having demonstrated that the oxidation of alcohols is feasible with the $PMoV_x/O_2$ system, we have suspected that the lack of reactivity of the alcohol **A1**$_{HH}$ could result from secondary reactions of the $PMoV_x$ with phenol co-produced during the cleavage of **A1**$_{HH}$. As described in Table II. 9, $PMoV_x$ are active for phenols oxidation and such reaction may compete with **A1**$_{HH}$ cleavage [64]. Consequently, the aerobic cleavage of **A1**$_{HH}$ was repeated in presence of 20 mol% of phenol (see appendix, attempts for **A1**$_{HH}$ oxidation into **K1**$_{HH}$). Phenol did not show to have any impact of **A1**$_{HH}$ conversion and even seems to boost **K1**$_{HH}$ cleavage. As shown in paragraph IB. 3.1, quinones are efficient co-catalysts for alcohol oxidation catalyzed by $PMoV_x$ catalysts. So, it may be hypothesized that *p*-quinone eventually compensate the negative effect of phenol on **A1**$_{HH}$ cleavage and boosts **K1**$_{HH}$ cleavage through acceleration of the reoxidation of reduced $PMoV_x$.

II. 7. Conclusions

The $PMoV_x$ catalyst were synthesized through the hydrothermal procedure and characterized by XRD, ^{31}P NMR in D_2O-H_2O 50:50, ICP and TGA. Tridecahydrated KEGGIN $PMoV_x$ were obtained as shown by XRD with a RIETVIELD refinement and by TGA. Such pathway was adapted for a low amount of vanadium. Indeed, the yield of V_1-HT was 89% (^{31}P NMR), the experimental x was 1.14 as shown by ICP and there was only one crystalline phase as shown by RIETVIELD refinement. For x = 3, the yield was

80% only and there were several crystalline phases. Besides, the experimental x was 2.68 (*vs* 3). So, the hydrothermal procedure is not very suitable for high vanadium content.

V_1-HT and V_3-HT catalysts proved to be efficient catalysts for the aerobic cleavage of the ketone model **K1**$_{HH}$. The adjunction of 10 vol% of acetic acid showed to be beneficial for the ketone cleavage due to an enhanced solubility of oxygen and a Mo + V loading of 15 mol% is an optimum. In the optimized solvent (82°C, 24 h) and metal loading, the conversion of **K1**$_{HH}$ was 72% and the yield of PhOH, so as the combined yield of PhCHO and PhOOH were around 52% (Table II. 7, entries 8 and 8bis). Nevertheless, **K1**$_{HH}$ is quite far from lignin compared to the alcohol model **A1**$_{HH}$. The latter one proved to be more resistant and O_2 pressure had to be increased. A possible explanation is that **A1**$_{HH}$ is not reductive enough as suggested by the comparison with 1-phenylethanol. Besides, the acetate ester of **A1**$_{HH}$, formed as a main by-product, turned out to be even more resistant than **A1**$_{HH}$. Furthermore, at high pressure and temperature, the carbon balance tended to be low, implying that side reactions as hydroxystilbenes formation through oxidative condensation and tar formation.

Lignin structure being closer to **A1**$_{HH}$ than **K1**$_{HH}$, a tentative of optimization of the O_2 pressure and of the reaction temperature was carried out. Co-oxidants were used too. With TEMPO 30 mol%, the yield of phenol did not exceed 18% and the maximal combined yield of PhCHO and PhCOOH was 24%. Though TEMPO proved to cut down parasite esterification, it cannot be considered as a good alternative. Indeed, it was tested as a co-catalyst for **A1**$_{HH}$ oxidation into **K1**$_{HH}$ (see Appendix, Attempts for **A1**$_{HH}$ oxidation into **K1**$_{HH}$) associated with $VOSO_4$. It shows to be less active after recycling upon reaction conditions because of TEMPO partial degradation.

A1$_{HH}$ and **K1**$_{HH}$, the two molecules we used are particularly simple, even simplistic, models of lignin. The latter were chosen for their easy synthesis (average global yields of 80% for **K1**$_{HH}$ and 70% of **A1**$_{HH}$) but it turned out to be important to test more complex molecules with an easy access and a low cost. As a result, the cleavage of the two other keto compounds **K1**$_{HG}$ and **K2**$_{HH}$ (Table II. 21) was tested to investigate, respectively, the effects of another unit (G instead of H in **K1**$_{HG}$) and of replacing the methylenic group of **K1**$_{HH}$ with a hydroxyethyl group as in the true β-O-4 bond (Fig. II. 1). The conditions used were adapted from the optimum ones implemented in the case of **K1**$_{HH}$.

Starting from **K1**$_{HG}$, benzaldehyde and benzoic acid were also produced, as well as guaiacol. The conversion of **K1**$_{HG}$ and the yield of benzoic acid were similar to those of the test performed on **K1**$_{HH}$ (entry 29 *vs* 8). However, the yield of guaiacol was much lower than the yield of phenol with **K1**$_{HH}$. Indeed, the reaction mixture became dark red that is very characteristic of guaiacol oxidation (influence of the electron donating methoxy group on the ortho position) with the formation of a black residue.

Table II. 21: Cleavage of more complex ketonic substrates

Entry	Substrate	Conv. (%)	Yield (%)						Carbon balance (%)
			ArOH	PhCHO	PhCOOH	**K1**$_{HH}$	**A1**$_{HH}$	**D1**$_{HH}$	
8	**K1**$_{HH}$ 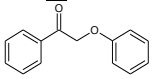	72	55	12	44	-	-	-	76
29	**K1**$_{HG}$ 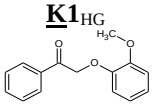	69	5.8	4.9	46	-	-	-	57
30	**K2**$_{HH}$ 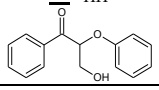	19	4.9	3.2	1.4	19	-	-	104

Substrate 100 mM, MeCN-AcOH 90:10 (15 mL), V_3-HT (Mo+V 15 mol%), atm. O_2, 24 h

K2$_{HH}$ was converted much more slowly than **K1**$_{HH}$. The main product arising from **K2**$_{HH}$ is **K1**$_{HH}$ which would be obtained by a kinetically hindered deformylation process (entry 30 *vs* 8).

Such reaction was observed by ZHOU and LU [65] (see paragraph IA. 3.2.3).

An aim will be to use a heterogenized vanadium-catalyst for **A1**$_{HH}$ cleavage. The considered catalyst was VO^{2+} cations supported on a Nafion® SAC-13, an acidic sulfonated resin mixed with silica to increase the surface area (see Fig. II. 25).

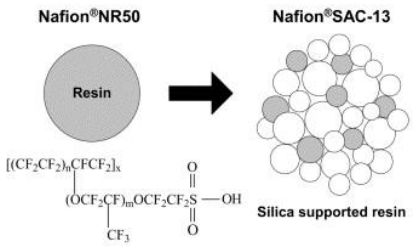

Figure II. 25: Preparation of SAC-13 support

All the protons (0.13 eq H^+/g) were substituted by vanadyl cations, which give rise to a vanadium content of 3.3 wt%. A test was carried out in the conditions described on Table II. 21, entry 20 (**A1**$_{HH}$ 100 mM, O_2 5 bar before heating, 120°C, 6 h in MeCN – 10 vol% AcOH) with a loading of vanadium of 15 mol%. The conversion of **A1**$_{HH}$ was 35% with a selectivity for C-O (PhOH) and C-C (PhCHO and PhCOOH) cleavage of 18% and 21%, and the yield of **K1**$_{HH}$, **Est**$^{\alpha}$**A1**$_{HH}$ and **D1**$_{HH}$ were 9.6, 6.8 and 8.6% respectively. So, the

heterogenized catalyst is still less active than V_3-HT in the same conditions, but it give rise to similar selectivity for C-C cleavage and even the selectivity for C-O cleavage was better in presence of the heterogenized catalyst.

Last but not least, due to the resistance of the alcohol model, $PMoV_x$ having a high vanadium content should be more adapted but the hydrothermal procedure was not the most suitable for the synthesis of such of catalyst. So, an alternative synthetic route will be considered. Cleavage optimization should progressively enable to perform real lignin aerobic oxidative cleavage.

References:

[1]: R. Behling, S. Valange, G. Chatel, *Green Chem.* **2016**, 18, 1839-1854.
[2]: M. B. Hocking, *J. Chem. Educ.*. 1997, 74, 9, 1055-1059.
[3]: H. Lange, S. Decina, C. Crestini, *Eur. Polymer J.* **2013**, 49, 1151-1173.
[4]: R. Ma, M. Guo, X. Zhang, *Catal. Today* **2018**, 302, 50-60.
[5]: W. Schutyser, J. S. Kruger, A. M. Robinson, R. Katahira, D. G. Brandner, N. S. Cleveland, A. Mittal, D. J. Peterson, R. Meilan, Y. Román-Leshkov, G. T. Beckham, *Green Chem.* **2018**, 16, 3828-3844.
[6]: J. Mottweiller, M. Puche, C. Räuber, T. Schmidt, P. Concepción, A. Corma, C. Bolm *ChemSusChem* **2015**, 8, 2106-2113.
[7]: S. Liu, Z. Shi, L. Li, S. Yu, C. Xiec, Z. Song, *RSC Adv.* **2013**, 3, 5789-5793.
[8]: H. Werhan, N. Assmann, P. R. von Rohr, *Chem. Eng. Process.* **2013**, 73, 29-37.
[9]: H. Werhan, J. M. Mir, T. Voitl, P. R. von Rohr, *Holzforschung* **2011**, 65, 703-710.
[10]: T. N. Lugovitskaya, K. N. Bolatbaeva, S. S. Naboichenko, *Russ. J. Gen. Chem.* **2014**, 84, 2, 309-312.
[11]: Ch. Díaz-Urrutia, B. B.Hurisso, P. M .P. Gauthier , B. Sedai, R. D. Singer, R. T. Baker, *J. Mol.. Catal. A* **2016**, 423, 414-422.
[12]: E. Amadio, R. Di Lorenzo, C. Zonta, G. Licini, *Coord. Chem. Rev.* **2015**, 301, 147-162.
[13]: Y. Zhao, Q. Xu, T. Pan, Y. Zuo, Y. Fu, Q-X. Guo, *Appl. Catal. A.* **2013**, 467, 504-508.
[14]: G. F. De Gregorio, R. Prado, C. Vriamont, X. Erdocia, J. Labidi, J. P. Hallett, T. Welton, *ACS Sustainable Chem. Eng.* **2016**, 4, 11, 6031-6036.
[15]: F. Cheng, H. Wang, R. D. Rogers, *ACS Sustainable Chem. Eng.* **2014**, 2, 12, 2859-2865.
[16]: I. A. Weinstock, *Pat. US5302248* **1994**.
[17]: A. R. Gaspar, J. A. F. Gamelas, D. V. Evtuguin, C. Pascoal Neto, *Green Chem.* **2007**, 9, 717-730.
[18]: L. El Aakel, F. Launay, J-M. Brégeault, A. Atlamsani, *Chem. Commun.* **2001**, 2218-2219.
[19]: B. El Ali, A. M. El-Ghanam, M. Fettouhi, *J. Mol. Catal. A.* **2001**, 165, 283-290.
[20]: N. Ballarini, L. Casagrandi, F. Cavani, T. D'Alessandro, A. Frattini, P. Accorinti, S. Alini, P. Babini, *Appl. Catal. A* **2011**, 391, 118-124.
[21]: R. Rinaldi, R. Jastrzebski, M. T. Clough, J. Ralph, M. Kennema, P. C. A. Bruijnincx, B. M. Weckhuysen, *Angew. Chem. Int. Ed.* **2016**, 55, 8164-8215.
[22]: A. Azarpira, J. Ralph, F. Lu, *Bioenerg. Res.* **2014**, 7, 78–86.
[23]: B. Sedai, T. Baker, *Adv. Synth. Catal.* **2014**, 356, 3563-3574.
[24]: M. Wang, J. Lu, L. Li, H. Li, H. Liu, F. Wang, *J. Catal.* **2017**, 348, 160-167.
[25]: B. Sedai, C. Diaz-Urrutia, R. T. Baker, R. Wu, L. A. Silks, S. K. Hanson, *ACS Catal.* **2011**, 1, 794-804.
[26]: S. K. Hanson, R. T. Baker, J. C. Gordon, B. L. Scott, D. L. Thorn, *Inorg. Chem.* **2010**, 49, 5611-5618.
[27]: S. Son, F. D. Toste, *Angew. Chem. Int. Ed.* **2010**, 49, 3791-3794.
[28]: G. Zhang, B. L. Scott, R. Wu, L. A. Silks, S. K. Hanson, *Inorg. Chem.* **2012**, 51, 7354-7361.
[29]: S. K. Hanson, R. Wu, L. A. Silks, *Angew. Chem. Int. Ed.* **2012**, 51, 3410-3413.
[30]: Y. Ma, Z. Du, J. Liu, F. Xia, J. Xu, *Green Chem.* **2015**, 17, 4968-4973.
[31]: Y-Y Jiang, L. Yan, H-Z. Yu, Q. Zhang, Y. Fu, *ACS Catal.* **2016**, 6, 4399-4410.
[32]: H. J. Parker, C. J. Chuck, T. Woodman, M. D. Jones, *Catal. Today* **2016**, 269, 40-47.

[33]: S. Gazi, M. Đokić, A. Mangala P. Moeljadi, R. Ganguly, H. Hirao, H. Sen Soo, *ACS Catal.* **2017**, 7, 4682-4691.
[34]: D. V. Evtuguin, A. I. D. Daniel, A. J. D. Silvestre, F. M. L. Amado, C. Pascoal Neto, *J. Mol. Catal. A*, **2000**, 154, 217-224.
[35]: G. A. Tsigdinos, J. Hallada, *Inorg. Chem.* **1968**, 7, 3, 437-441.
[36]: R.G. Derwent, M.E. Jenkin, N.R. Passant, M.J. Pilling, *Atmos. Environ.* **2007**, 41, 12, 2570-2579.
[37]: A. Atlamsani, M. Ziyad, J.-M. Brégeault, *J. Chem. Phys.* **1995**, 92, 1344-1364.
[38]: V. F. Odyakov, E. G. Zhizhina, *Russ. J. Inorg. Chem.* **2009**, 54, 3, 361-367.
[39]: G. Süss-Fink, L. Gonzalez, G. B. Shul'pin, *Appl. Catal. A* **2001**, 217, 111-117.
[40]: F. Kern, S. Ruf, G. Emig, *App. Catal. A* **1997**, 150, 143-151.
[41]: M. Otake, T. Onoda, *Pat. FR 7715134*, 1977.
[42]: J. M. Nichols, L. M. Bishop, R. G. Bergman, J. A. Ellman, *J. Am. Chem. Soc.* **2010**, 132, 12554-12555.
[43]: F. Abdelkafi, H. Ammar, B. Rousseau, M. Tessier, R. El Gharbi, A. Fradet, *Biomacromol.* **2011**, 12, 3895-3902.
[44]: C. Marchal-Roch, R. Bayer, J. F. Moisan, A. Tezé, G. Hervé, *Top. Catal.* **1996**, 407-419.
[45]: L. Pettersson, *Mol. Eng.* **1993**, 3, 29-42.
[46]: P. Villabrille, G. Romanelli, P. Vázquez, C. Cáceres, *Appl. Catal. A.* **2004**, 270, 101-111.
[47]: S. T. Perisanu, *J. Solution. Chem.* **2001**, 30, 183-192.
[48]: M. Quaranta, M. Murkovic, I. Klimant, *Analyst* **2013**, 138, 6243-6245.
[49]: X. Wu, Z. Deng, J. Yan, Z. Zhang, F. Zhang, Z. Zhang, *Ind. Eng. Chem. Rev.* **2014**, 53, 9932-9937.
[50]: Y. Ma, Z. Du, J. Liu, F. Xia, J. Xu, *Green Chem.* **2015**, 17, 4968-4973.
[51]: T. Voitl, M. V. Nagel, P. R. von Rohr, *Holzforschung* **2010**, 64, 13-19
[52]: K. H. Kim, T. Dutta, E. D. Walter, N. G. Isern, J. R. Cort, B. A. Simmons, S. Singh, *ACS Sustainable Chem. Eng.* **2017**, 5, 3913-3919.
[53]: J. Zhu, P-C. Wang, M. Lu, *Chempluschem* **2014**, 79, 8265-8268.
[54]: J. T. Muckerman, J. H. Skone, M. Ning, Y. Wasada-Tsutsui, *Biochim. Biophys Acta* **2013**, 1827, 882-891.
[55]: T. Sato, Y. Hamada, M. Sumikawa, S. Araki, H. Yamamoto, *Ind. Eng. Chem. Res.* **2014**, 53, 19331-19337.
[56]: P. S. Bailey, Y-G. Chang, *J. Org. Chem.* **1962**, 27, 1192-1197
[57]: F. Cavani, L. Ferroni, A. Frattini, C. Lucarelli, A. Mazzini, K. Raabova, S. Alini, P. Accorinti, P. Babini, *Appl. Catal. A* **2011**, 391, 118-124.
[58]: G. F. De Gregorio, C. C. Weber, J. Gräsvik, T. Welton, A. Brandt, J. P. Hallett, *Green Chem* **2016**, 20, 5456-5465.
[59]: R. Neumann, A. M. Khenkin, *Chem Commun.* **2006**, 2529-2538.
[60]: R. Ben-Daniel, P. Alsters, R. Neumann, *J. Org. Chem.* **2001,** 66, 8650-8653.
[61]: H. Guo, D. M. Miles-Barrett, A. R. Neal, T. Zhang, C. Li, N. J. Westwood, *Chem. Sci.* **2018**, 9, 702-711.
[62]: M. Wang, J. Lu, X. Zhang, L. Li, H. Li, N. Luo, F. Wang, *ACS Catal.* **2016**, 6, 6086-6090.
[63]: M. L. Andersen, W. Long, D. M. Wayner, *J. Am. Chem. Soc.* **1997**, 119, 6590-6595.
[64]: T. Imai, T. Yokoyama, Y. Matsumoto, *J. Wood. Sci.* **2011**, 57, 219-225.
[65]: X-F. Zhou, X-J. Lu, *J. Appl. Polym. Sci.* **2016**, 44, 44133-44141.

Appendix part II

* *Synthesis of dimeric lignin models* (cf experimental part II. 2.2)

⇒ List of reactants

2-bromoacetophenone (98%), phenol (>99%), guaiacol (97%), sodium borohydrure and acetic anhydride were purchased from Sigma-Aldrich. Potassium carbonate (anhydrous) and formaldehyde (37% in water, stabilized by methanol) were purchased from Acros Organics.

⇒ Cases of **K1**$_{HH}$ and **K1**$_{HG}$

2-bromoacetophenone (16.85 g, 84 mmol) and an excess of phenol (9.56 g, 101 mmol) were dissolved in 200 mL of acetone. 20 g of K_2CO_3, used as a catalyst and as an acid (HBr) trap, were added to the solution. The mixture may take a pink coloration due to the formation of phenolate anions that disappears with time. Reflux is needed during 6 h to get **K1**$_{HH}$. Initially pale yellow, the coloration became yellow and then orange, meaning that all the brominated reactant is consumed and phenol begins to be oxidized by air. The reaction was monitored by TLC using cyclohexane/diethylether 80/20 as the eluent. After filtration and acetone evaporation, **K**1$_{HH}$ was recrystallized in a minimum amount of heated (65-70°C) absolute ethanol. **K1**$_{HH}$ was then recovered by filtration and dried by pressing. The formation of the ether bond was checked by FT-IR by the presence of a band at 1240 cm^{-1}. **K1**$_{HH}$ was characterized more deeply by ^{1}H NMR according to Ref S1.

^{1}H NMR (CD_3CN, 300 MHz) : 8.05 (m, 2H), 7.66 (m, 1H), 7.54 (m, 2H), 7.33 (m, 2H), 7.00 (m, 3H), 5.31 (s, 2H).

This above-mentioned procedure was repeated several times at different scales affording yields of **K1**$_{HH}$ of c.a. 80%.

K1$_{HG}$ was also synthesized with a yield of 80% through a similar procedure starting from 2-bromoacetophenone and an excess of guaiacol. **K1**$_{HH}$ was characterized by ^{1}H NMR (according to Ref S1).

^{1}H NMR (CD_3CN, 300 MHz): 8.05 (m, 2H), 7.66 (m, 1H), 7.54 (m, 2H), 7.33 (m, 2H), 7.00 (m, 3H), 5.31 (s, 2H).

⇒ Case of **K2**$_{HH}$

K2$_{HH}$ was synthesized from the attack of **K1**$_{HH}$ (1.00 g, 4.7 mmol) by 780 µL (10 mmol) of aqueous formaldehyde (Acros Organics, 37% in water stabilized by 10-15% of methanol) during 1.5 h in presence of 0.71 g of K_2CO_3 (5.1 mmol). The reaction was monitored by TLC (eluent: pentane/diethylether 1/1) and **K2**$_{HH}$ was purified on a silica gel chromatographic column and then characterized by ^{1}H NMR according to Ref S1. 0.254 g of **K2**$_{HH}$ was obtained (yield: 22%).

^{1}H NMR (300 MHz, $CDCl_3$): 7.96-7.99 (2H, m), 7.52-7.54 (1H, m), 7.39-7.44 (2H, m), 7.16-7.21 (2H, m), 6.82-6.93 (3H, m), 5.47-5.51 (1H, t), 4.01-4.14 (2H, m), 2.22 (1H, brs).

⇒ Case of **A1**$_{HH}$

To get **A1**$_{HH}$, **K1**$_{HH}$ (4.98 g, 23 mmol) was solubilized in 52 mL of THF and 13 mL of H_2O and reduced by $NaBH_4$ (1.32 g, 35 mmol) for 5 h. The reaction was monitored by TLC using a binary (80/20) cyclohexane/diethylether mixture. Afterwards, the reaction was quenched by 120 mL of saturated NH_4Cl (added slowly because of H_2 emission) and then diluted by 120 mL of water. Later, **A1**$_{HH}$ was extracted by diethyl ether (250 + 120 mL). After washing the diethylether fractions by brine (120 mL) and drying by anhydrous $MgSO_4$, the solvent was evaporated to get **A1**$_{HH}$ as a white solid with a yield of 90% on average. FT-IR spectroscopy enabled to check the disappearance of the strong signal at 1700 cm^{-1} due to the carbonyl group reduction. **A1**$_{HH}$ was deeply characterized by ^{1}H NMR (according to Ref S1).

^{1}H NMR (CD_3CN, 300 MHz): 7.39 (m, 7H), 6.97 (m, 3H), 5.04 (dd, 1H), 4.13 (dd, H), 4.05 (dd, 1H).

⇒ Case of **Est$^\alpha$A1**$_{HH}$ (inspired from Ref. S2)

A1$_{HH}$ was esterified by acetic anhydride in pyridine giving rise to **Est$^\alpha$A1**$_{HH}$. Hence, 505 mg of the alcohol dimer, **A1**$_{HH,}$ were dissolved in 5 mL of pyridine in a round-bottom flask and 5 mL of acetic anhydride were dropped. The resulting mixture was stirred during 17 h and the total consumption of **A1**$_{HH}$ monitored by TLC with a 80/20 cyclohexane/diethylether eluent. Excess of anhydride was quenched by 20 mL of methanol (Be careful! This quenching reaction is very exothermic and the mixture may boil). After cooling, the solvent was evaporated. Then, the concentrated residue was

dissolved again in methanol (≈5 mL) and the mixture was dropped in a 20 mL volumetric flask. The first flask was washed by methanol. The washing fraction was poured also in the volumetric flask. Then, the volume was completed to 20 mL. The solution was injected by HPLC to check the retention time. Afterwards, the solvent was evaporated then to eliminate the most possible the pyridine. The obtained ester noted **Est$^{\alpha}$A1**$_{HH}$ was then purified on a chromatographic column (eluent: pentane/diethylether 1/1). After evaporation of the solvent, 489 mg (yield 97%) of pure **Est$^{\alpha}$A1**$_{HH}$ were collected as a colorless oil and characterized according a predicted spectrum.

RMN ^{1}H ($CDCl_3$, 300 MHz): 7.37 (m, 7H), 6.96 (m, 3H), 6.18 (dd, 1H), 4.30 (dd, H), 4.18 (dd, 1H), 2.14 (s, 3H).

**Calibration curves*

The main products of dimer cleavage reactions were quantified by HPLC using the following external calibration curves established at the UV absorption wavelengths most favorable for detection (see also the exp Part in II. 2.5). The injection loop used had a volume of 20 µL.

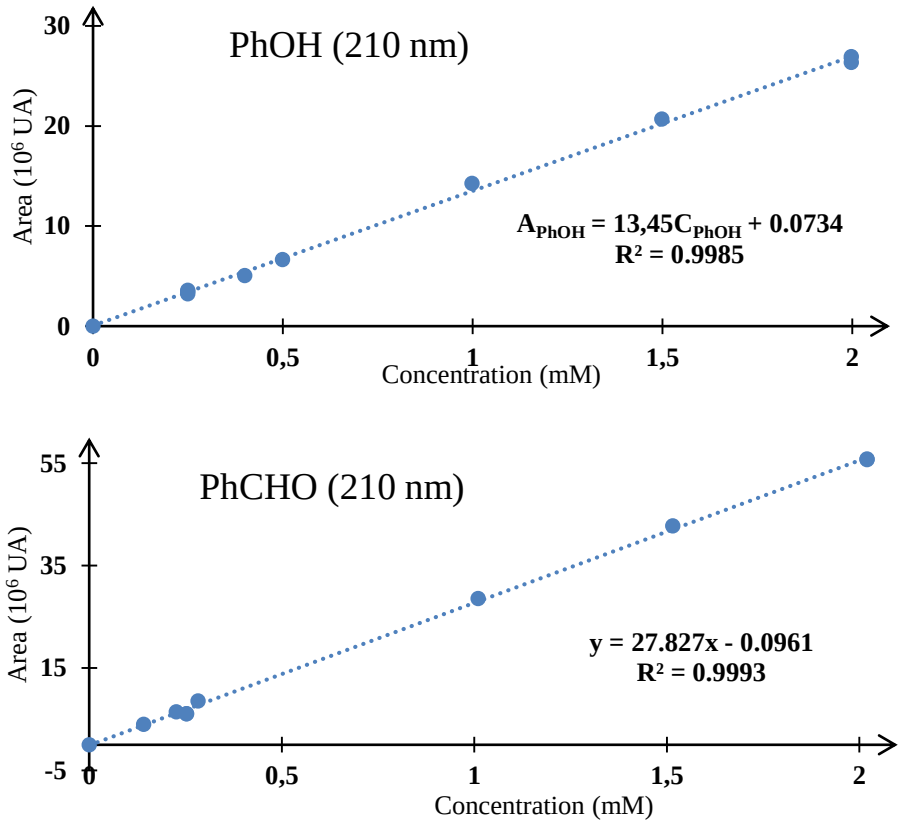

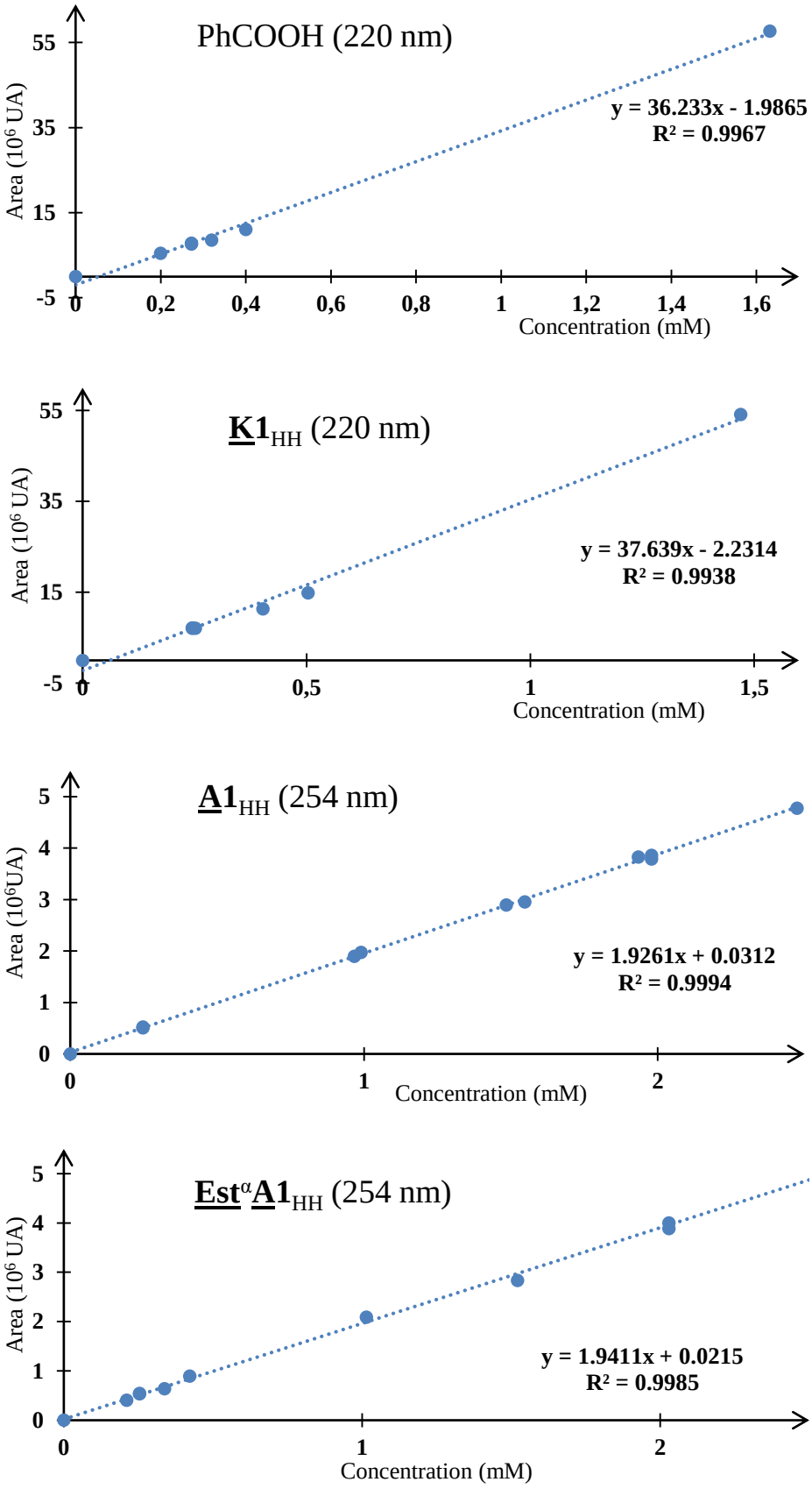

Figure SII. 1: Calibration curves of the products and reactants in HPLC

** Quantification of **D1**$_{HH}$ (cf experimental part, paragraph II. 2.5)*

The mixture of reaction media containing **D1**$_{HH}$ was concentrated into a yellow oil and then analyzed by ^{1}H NMR (300 MHz, $CDCl_3$). The obtained spectra (red) was compared to the models **K1**$_{HH}$ (green), **A1**$_{HH}$ (brown) and **Est**$^{\alpha}$**A1**$_{HH}$ (blue).

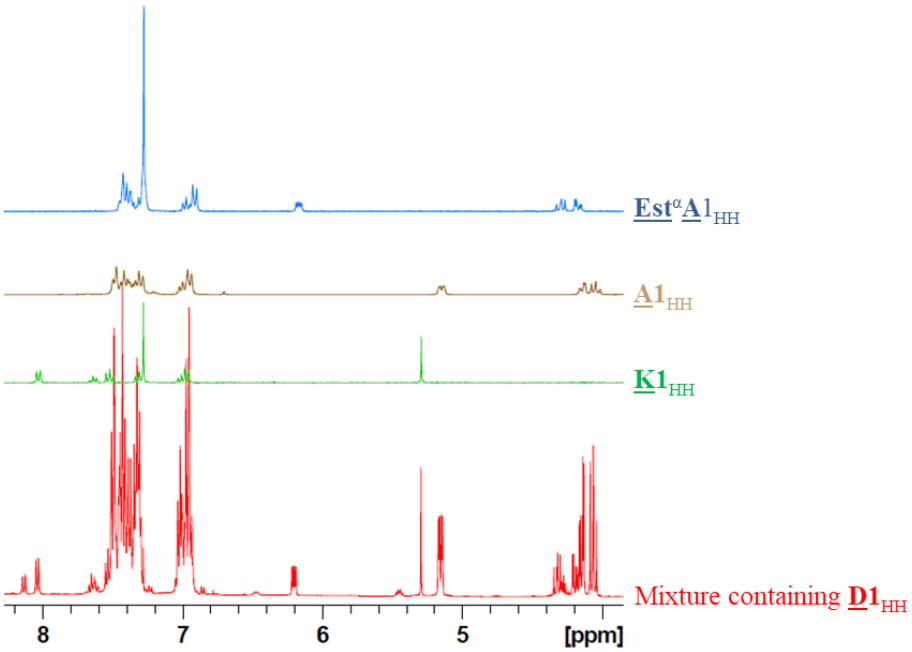

*Figure SII. 2: ^{1}H NMR spectra of the concentrated mixture containing **D1**$_{HH}$, **K1**$_{HH}$, **A1**$_{HH}$ and **Est**$^{\alpha}$**A1**$_{HH}$*

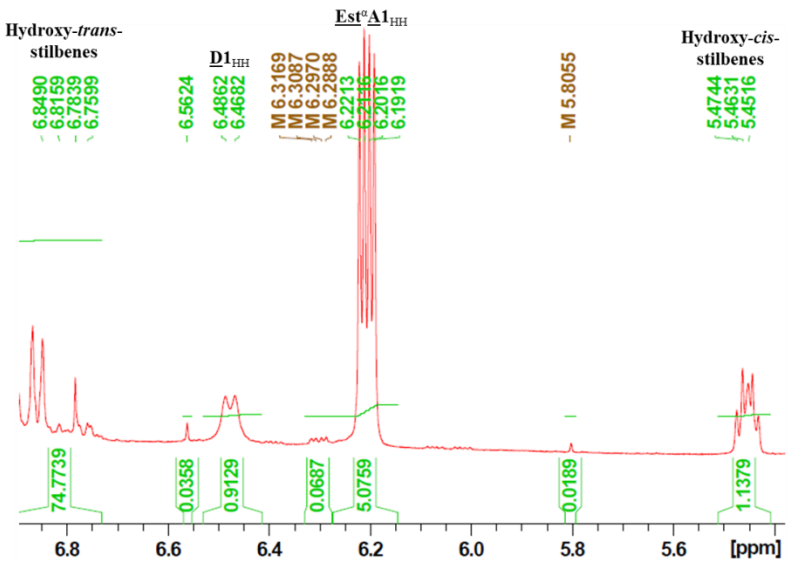

*Figure SII. 3: Characterization of **D1**$_{HH}$ by ^{1}H NMR (according to Ref S3)*

On Fig. SII. 2 were characterized the contribution of the models **A1**$_{HH}$, **K1**$_{HH}$ and of **Est**$^{\alpha}$**A1**$_{HH}$ in the spectrum of the concentrated mixture. Then, the peaks of **D1**$_{HH}$ were attributed (Fig; SII. 3) according to Ref S7. **D1**$_{HH}$ is the isomer *trans* of vinyl styryl ether. Moreover, hydroxystilbenes (attribution according to Ref S4) were also detected in the mixture so as by GC-MS (see paragraph II. 5, GC-MS characterization).

**Diffraction profiles of V_1-HT and V_3-HT vs JCPDS 00-043-0317 ($H_3PMo_{12}O_{40}$, $13H_2O$) (cf. II. 3, Fig. II. 9)*

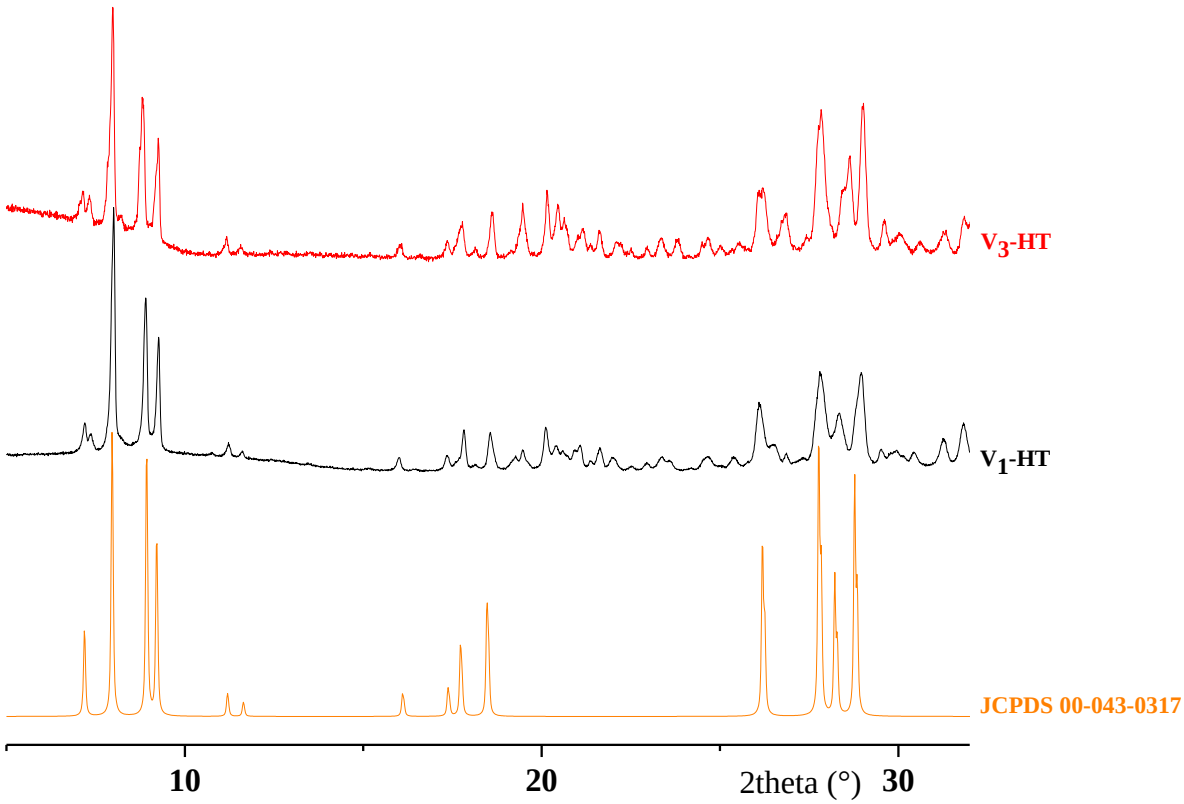

Figure SII. 4: XRD profiles of V_1-Ht and V_3-HT vs JCPDS 00-043-0317

The diffraction profiles of V_1-HT (black line) and V_3-HT (red line) are compared to the JCPDS 00-043-0317 (orange line). The peaks characteristic to KEGGIN structure (JCPDS) are observed as the main peaks in the diffractograms of V_1-HT and V_3-HT. So, it can be concluded the hydrothermal $PMoV_x$ (see experimental part, paragraph II. 2.1 and results in paragraph II. 3)

** Refinement on Fullprof Suite (cf II. 3, Table II. 4)*

```
 ➔ CONDITIONS OF THIS RUN FOR PATTERN No.:  1
  => Global Refinement of X-ray powder diffraction data
  => Global Refinement of X-ray powder diffraction data
     Bragg-Brentano(X-rays) or Debye-Scherrer
geometry(Neutrons)
  => The    5th default profile function was selected
  => Data supplied in free format for pattern:  1
  => Wavelengths:  1.54056 1.54439
  => Cos(Monochromator angle)=   1.0000
  => Absorption correction (AC), muR-eff =   0.0000  0.0000
  => Base of peaks: 2.0*HW*    8.00
  ➔ Angular range, step and number of points:
      2Thmin:       5.000000  2Thmax:      49.994240  Step:
0.009190  No. of points:   4897
  =>-----→ Pattern#  1
  => Profile Matching (fixed scale) for phase: 1
  => Score: 2.8614

  ➔ RESULTS OF REFINEMENT:

  => No. of fitted parameters:   10

  => Phase No.  1 49.994240                                P -1
```

```
  =>  No. of reflections for pattern#:   1:  1492/2

  ➔ PROFILE PARAMETERS FOR PATTERN#  1

  => Cell parameters      :   14.07430   0.00054 (a)
                              14.16135   0.00050 (b)
                              13.57723   0.00040 ©
                             112.24306   0.00248 (α)
                             109.78651   0.00243 (β)
                              60.60961   0.00230 (γ)

  => overall scale factor :    0.001000000     0.000000000
  => Eta(p-v) or m(p-vii) :    0.51855   0.01111
  => Overall tem. Factor  :    0.00000   0.00000
  => Halfwidth parameters :    0.00590   0.00000
                              -0.00191   0.00000
             0.00229   0.00000
  => Preferred orientation:    0.00000   0.00000
                               0.00000   0.00000
  => Asymmetry parameters :    0.00000   0.00000
                               0.00000   0.00000
                               0.00000   0.00000
                               0.00000   0.00000
```

```
 => X and y parameters   :    0.01781   0.00039
                              0.00000   0.00000
 => Strain parameters    :    0.00000   0.00000
                              0.00000   0.00000
                              0.00000   0.00000
 => Size parameters (G,L):    0.01058   0.00015
                              0.00000   0.00000

 ➔ GLOBAL PARAMETERS FOR PATTERN#  1

 => Zero-point:     0.0127    0.0003
 => Cos( theta)-shift parameter :   0.0000  0.0000
 => Sin(2theta)-shift parameter :   0.0000  0.0000

 ➔ RELIABILITY FACTORS WITH ALL NON-EXCLUDED POINTS FOR
PATTERN: 1

 => Cycle :  5 => MaxCycle :  5
 => N-P+C :  4887
 => R-factors (not corrected for background) for Pattern:  1
 => Rp :  2.48     Rwp :  3.66     Rexp :    1.74 Chi2 :  4.43
L.S. refinement
 => Conventional Rietveld R-factors for Pattern:  1
 => Rp :  8.67     Rwp :  9.84     Rexp :    4.68 Chi2 :  4.43
 => Deviance :  0.215E+05     Dev* :   4.391
 => DW-Stat.:    0.5235     DW-exp:     1.9154
 => N-sigma of the GoF:  169.491

 ➔ RELIABILITY FACTORS FOR POINTS WITH BRAGG CONTRIBUTIONS
FOR PATTERN:  1
 => N-P+C:  4737
 =>  R-factors (not corrected for background) for Pattern:  1
 => Rp :  2.51     Rwp :  3.71     Rexp :    1.74 Chi2 :  4.53
L.S. refinement
 => Conventional Rietveld R-factors for Pattern:  1
 => Rp :  8.50     Rwp :  9.80     Rexp :    4.60 Chi2 :  4.53
 => Deviance :  0.213E+05     Dev* :   4.486
 => DW-Stat.:    0.5285     DW-exp:     1.9141
 => N-sigma of the GoF:      171.574
 => Global user-weigthed Chi2 (Bragg contrib.):   4.57
```

Figure SII.5: Extract of the refinement results on Fullprof Suite for V_1-HT

A RIETVIELD analysis of the diffractograms of V_1-HT and V_3-HT was carried out on Fullprof Suite using the JCPDS file 00-043-0317 corresponding to tridecahydrated phosphomolybdic acid (triclinic crystalline structure (P-1)). The main phase of each $PMoV_x$ has the same crystalline structure. The content of the Figure SII.2 is an extract of the results obtained for V_1-HT.

** Choice of the ^{31}P NMR relaxation delay for P quantification in V_3-HT (cf II. 3, Fig. II. 10)*

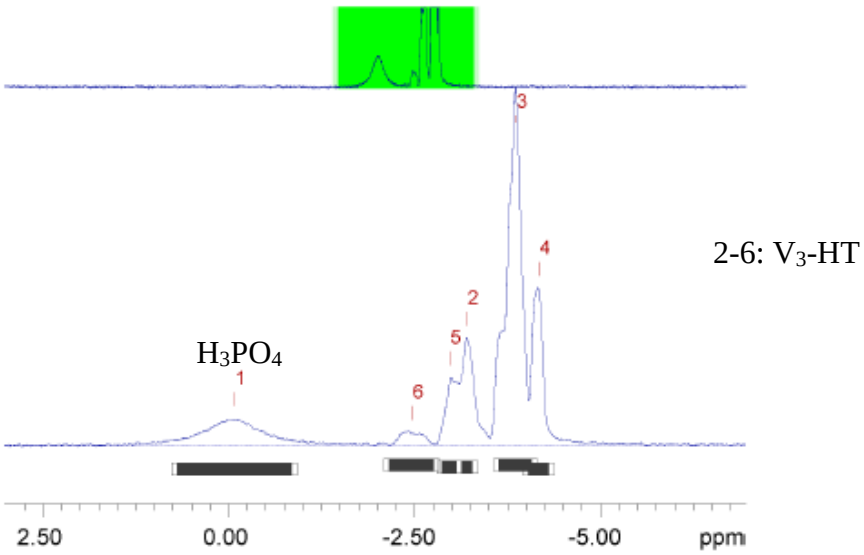

NB: The pH is more acidic as 300 mg of V_3-HT was used instead of 30 mg. Since the position of the peaks depends on the pH, the phosphorous center in $PMoV_x$ in those conditions was more deshielded (*vs* Fig. II.9).

Figure SII. 6a: Peak attributions

Fitted function:	f(t) = Io * [1 - a*exp (-t/T1)]
Random error estimation of data:	RMS per spectrum (or trace/plane)
Systematic error estimation of data:	worst case per peak scenario
Fit parameter Error estimation method:	from fit using arbitray y uncertainties
Confidence level:	95%
Used peaks:	
Used integrals:	area integral
Used Mixing time:	all values (including replicates) used

Peak name	F2 [ppm]	T1 [s]	error
1	-0.080	0.00	0.000
2	-3.209	0.824	0.1096
3	-3.864	0.857	0.1271
4	-4.171	1.02	0.1137
5	-2.969	0.00	0.000
6	-2.464	0.00	0.000

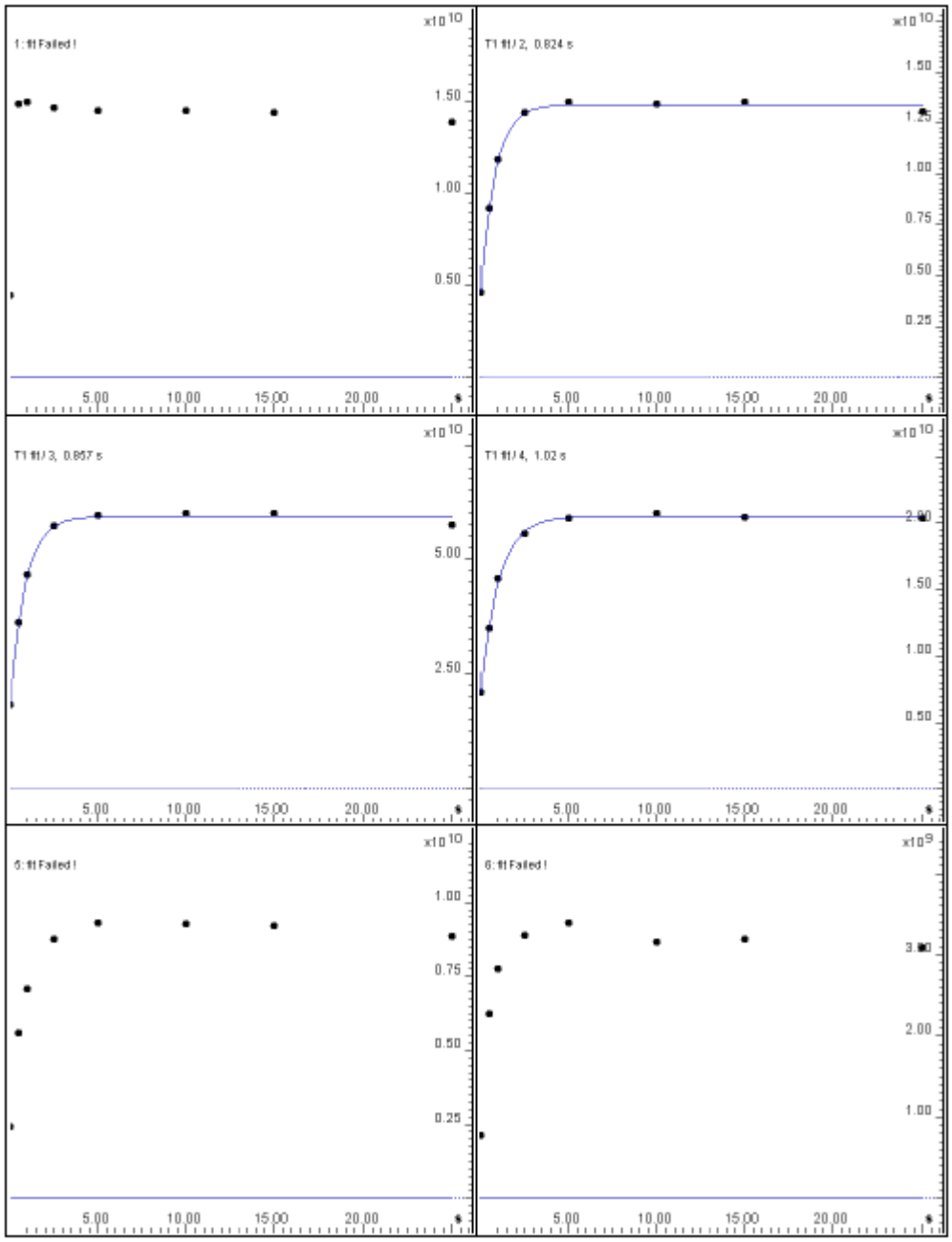

Figure SII. 6b: Relaxation delays

The peak at 0 ppm corresponds to H_3PO_4. The peak n°6 corresponds to $H[PMo_9V_3O_{40}]^{5-}$ and the peaks 2-5 correspond to $[PMo_9V_3O_{40}]^{6-}$. The order of the peaks is unchanged compared to typical ^{31}P NMR analysis (30 mg $PMoV_x$, see Fig II.9). The longest relaxation time is 1.02 s.

** Determination of the formula of the synthesized $PMoV_x$ - Calculation of x and n in $H_{3+x}PMo_{12-x}V_xO_{40}, nH_2O$ (cf II. 3, Fig. II. 11)*

$PMoV_x$ TG profiles are characterized by two weight losses related to hydration and constitutive water [S5, S6].

- The first weight loss takes place until the temperature reaches a value noted T_1 (around 220°C) as shown by the DSC curves and proved to be a two-step processus in the case of V_1-HT. The evolution of crystalline structure between r.T. and 100°C is given in Table SII.1.

Table SII. 1: Crystalline structure evolution of the $PMoV_x$ during hydration water loss [S7]

Hydration index n	T (°C)	Crystalline structure
12-13	r. T.	Triclinic
6	60	Cubic
0	200	Quadratic

In some cases, there are more than two steps because the solid to be analyzed may be composed by a mixture of $PMoV_x$ having different hydration indexes. Since the evaporation of the hydration water is an endothermic reaction, the heat flow is negative (exo up) and reaches a local maximum for $T = T_1$. At this time, the $PMoV_x$ is totally dehydrated. This heat flow corresponds to the heating of the sample and the value of the first derivative reaches a local minimum (0 in theory) as there should not be weight loss as no water is evaporated. The global equation is:

$$H_{3+x}PMo_{12-x}V_xO_{40}, nH_2O_{(s)} = H_{3+x}PMo_{12-x}V_xO_{40}{}_{(s)} + nH_2O_{(g)} \text{ (Eq. SII. 1)}$$

- The second loss is due to constitutive water[1]. It takes places until $T = T_2$. The equation of the involved reaction is as follows:

  $$H_{3+x}PMo_{12-x}V_xO_{40}{}_{(s)} = \frac{1}{2}P_2O_5 + (12-x)MoO_3 + \frac{x}{2}V_2O_5 \text{ (Eq. SII. 2)}$$

  The heat flow decreases again when the evaporation of the constitutive water starts. It is maximized when the temperature reaches a value noted T_2, so after completion of constitutive water evaporation, as confirmed by the local minimum of the derivative curve.

[1] A TGA-DSC analysis was carried out on a commercial phosphomolybdic acid (noted PMo_{12}). The second loss corresponding to the constitutive water was 1.6 wt% meaning that P_2O_5 does not evaporate. Otherwise, the weight loss should have been 5.4 wt%. Thus, it can be asserted that the weight loss between T1 and T2 would be due only to water evaporation in our conditions of TGA analysis (cf part exp).

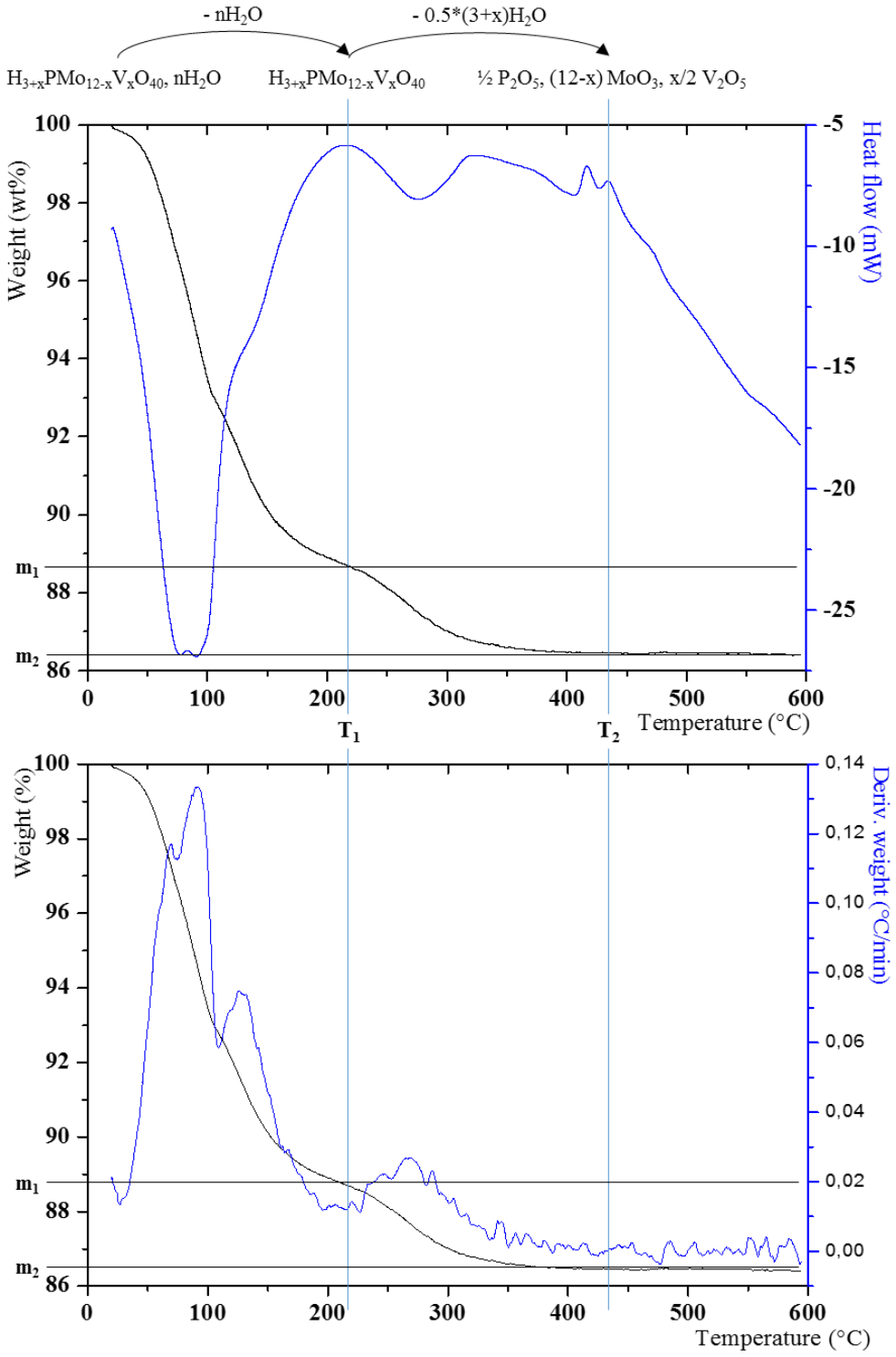

Figure SII. 7: Graphical determination of T_1 and T_2 by TGA

If there is still some residual phosphoric acid, the following reaction can take place:

$H_3PO_4 = \frac{1}{2}P_2O_5 + \frac{3}{2}H_2O$ (Eq SII. 3)

For the $PMoV_x$ with high x values, the heat flow declines maybe as the result of the proximity of the melting point of V_2O_5 (T_{fus} = 690°C). In V_3-HT (see Fig. II. 11) some

isomers containing vicinal vanadium atoms exist with V-O-V bonds weaker than the Mo-O-M (M = Mo or V) ones [S8]. As a consequence, the loss of the constitution water takes place in several steps. As the substitution of Mo by V degrades the thermal stability of the $PMoV_x$, the first loss is due to the presence of the vanadium which gives rise to a mixture of phosphomolybdic acid, lacunar phosphomolybdic acid and V_2O_5 (eq. SII. 2).

$H_{3+x}PMo_{12-x}V_xO_{40} = H_3PMo_{12-x}O_{40-3x} + \frac{x}{2}(V_2O_5 + H_2O)$ (Eq SII. 4)

Lacunar phosphomolybdates are not stable upon heating. As a consequence, they are degraded into phosphomolybdic acid and phosphoric acid as follows:

$H_3PMo_{12-x}O_{40-3x} = \left(1 - \frac{x}{12}\right)H_3PMo_{12}O_{40} + \frac{x}{12}H_3PO_4$ (Eq SII. 5)

Phosphomolybdic acid is later thermally decomposed into phosphoric acid and molybdenum trioxide. Finally, phosphoric acid is dehydrated into P_2O_5 (Eq SII. 3).

As a result, the following equations can be written allowing the determination of x and n values. The yield of $PMoV_x$ (cf Fig II. 10 and Table II.5) are noted η and $PMoV_x$ designates the protonated form ($H_{3+x}PMo_{12-x}V_xO_{40}$). Here, $\Delta m\%_2$ corresponds to the loss of constitutive water with the dehydrated $PMoV_x$ as the reference instead of the second loss observed on the TG profiles (hydrated $PMoV_x$ as the reference).

$$\frac{\Delta m\%_1}{100} = \frac{m_1 - m_0}{m_0} = \frac{m_{H_2O,hydration}}{m_{PMoV_x,nH_2O} + m_{H_3PO_4}} = \frac{nM_{H_2O}}{M_{PMoV_x,nH_2O} + \left(\frac{100-\eta}{\eta}\right)M_{H_3PO_4}}$$

$$\frac{\Delta m\%_2}{100} = \frac{m_2 - m_1}{m_1} = \frac{100(\Delta m\%_t - \Delta m\%_1)}{100 - \Delta m\%_1} = \frac{m_{H_2O,constitutive}}{m_{dehydrated\ PMoV_x} + m_{H_3PO_4}} = \frac{\left(\frac{3+x}{2}\right)M_{H_2O}}{M_{PMoV_x} + \left(\frac{100-\eta}{\eta}\right)M_{H_3PO_4}}$$

Moreover, $M_{PMoV_x} = M_{PMo_{12}} - \alpha x$, where $\alpha = M_{Mo} - (M_H + M_V) = 43.992\ g/mol$ given that a molybdenum atom is substituted by a vanadium atom of an hydrogen atom.

So, $x = \frac{\left(M_{PMo_{12}} + \left(\frac{100-\eta}{\eta}\right)M_{H_3PO_4}\right)\frac{\Delta m\%_2}{100} - \left(\frac{3}{2}\right)M_{H_2O}}{\frac{M_{H_2O}}{2} + \alpha\frac{\Delta m\%_2}{100}}$ and $n = \left(\frac{M_{PMoV_x} + \left(\frac{100-\eta}{\eta}\right)M_{H_3PO_4}}{(100 - \Delta m\%_1)M_{H_2O}}\right)\Delta m\%_1$

However, ICP was preferred for the determination of x as it is easier and more precise. Indeed, for high values of x, the evaporation of hydration and constitutive water may take place at the same temperature, which makes the calculation of x from TG results more difficult and less precise. Provided that the final solid is constituted of $PMoV_x$ and residual H_3PO_4, the equation linking the values of the weight fractions of Mo (w_{Mo}) and V (w_V) to the x parameter can be written as follows: $\frac{n_{Mo}}{n_V} = \frac{12-x}{x} = \frac{w_{Mo}M_V}{w_V M_{Mo}}$ which is equivalent to $x = \frac{12}{1 + \frac{w_{Mo}M_V}{w_V M_{Mo}}}$.

So, the error Δx may be given by the equation:

$\frac{\Delta x}{x} = \frac{\Delta w_V}{w_V} + \frac{\Delta w_{Mo}}{w_{Mo}} + \frac{\Delta M_V}{M_V} + \frac{\Delta M_{Mo}}{M_{Mo}}$ where $\Delta w_V = \Delta w_{Mo} = 0.0001$ and

$M_V = 50.9415 \pm 0.0001\ g/mol$; $\Delta M_{Mo} = 95.95 \pm 0.02\ g/mol$

So, $\Delta x = x\left(0.0001 * \left(\frac{1}{w_V} + \frac{1}{w_{Mo}}\right) + 0.0002\right)$

Moreover, the yield of the POM synthesis can be obtained by ICP. Indeed, if the KEGGIN POM is pure, $\frac{w_{Mo}/M_{Mo} + w_V/M_V}{w_P/M_P} = 12$ and in case of presence of residual H_3PO_4: $\frac{w_{Mo}/M_{Mo} + w_V/M_V}{w_P/M_P} = 12 * \frac{\eta}{100}$ where η stands for the yield of the $PMoV_x$.

* *Demonstration of the effect of acetic acid on dioxygen solubility (cf II. 4.1, effect of acetic acid)*

In the case of a mixture of acetonitrile (MeCN) and acetic acid (AcOH), intuitively, a raise of the volumic fraction of acetic acid noted v should enhance the dioxygen solubility since dioxygen is more soluble in AcOH. However, a demonstration is relevant. The evolution of the solubility of dioxygen in a solvent *j* can be estimated with the help of HANSEN parameters and more specifically of the radius of the HANSEN sphere noted R_j where j stands for the solvent. The smaller the radius is, the higher the solubility of dioxygen should be. For example, $R^2_{AcOH} < R^2_{MeCN}$.

The starting equation [S9] is:

$$\boxed{R_j^2 = 4(\delta_{d,j} - \delta_{d,O_2})^2 + (\delta_{p,j} - \delta_{p,O_2})^2 + (\delta_{h,j} - \delta_{h,O_2})^2 = \sum_i a_i {R_{j,i}}^2}$$

The δ_d, δ_p and δ_h terms stand for the dispersion forces, the dipole interaction and hydrogen bonding between the solvent j and dioxygen dissolved, $R_{j,i} = (\delta_{d,j} - \delta_{d,O_2})$ denotes the difference of solubility parameters (solvent *vs* dioxygen) and a_i is the multiplying factor of $R_{j,i}^2$. So: $\forall i$, $a_i > 0$

For a mixture of two solvents s_1 (volumic fraction v_1) and s_2 (volumic fraction v_2):

$$\boxed{\forall i, \forall (s_1, s_2), \delta_{i,mix\,(s_1,s_2)} = v_1\delta_{i,s_1} + v_2\delta_{i,s_2} = v_1\left(\delta_{i,s_1} - \delta_{i,s_2}\right) + \delta_{i,s_2}}$$

So, the aim, here, is to prove that the radius of the HANSEN sphere noted $R_{a,mix}(v)$ for the mixture decreases when v increases, that can be otherwise stated by $\frac{d(R_{a,mix}(v))^2}{dv} < 0$.

Let the function noted f_i defined by

$\boxed{f_i(v) = \left(v\left(\delta_{i,AcOH} - \delta_{i,MeCN}\right) + \delta_{i,MeCN} - \delta_{i,O_2}\right)^2, v \in [0;1]}$ (A)

A property of the function f_i is: $R^2_{a,j} = \sum_i a_i f_i(v)$ where $\forall i, a_i > 0$.

The relation (A) can be derivatized as follows:

$\frac{df_i(v)}{dv} = 2\left(\delta_{i,AcOH} - \delta_{i,MeCN}\right)\left(v\left(\delta_{i,AcOH} - \delta_{i,MeCN}\right) + \delta_{i,MeCN} - \delta_{i,O_2}\right)$

$\boxed{\frac{df_i(v)}{dv} = 2v\left(\delta_{i,AcOH} - \delta_{i,MeCN}\right)^2 + 2\left(\delta_{i,AcOH} - \delta_{i,MeCN}\right)\left(\delta_{i,MeCN} - \delta_{i,O_2}\right)}$ (B)

Yet: $\left(\delta_{i,AcOH} - \delta_{i,MeCN}\right)^2 = \left(\left(\delta_{i,AcOH} - \delta_{i,O_2}\right) - \left(\delta_{i,MeCN} - \delta_{i,O_2}\right)\right)^2 =$

$\left(R_{AcOH,i} - R_{MeCN,i}\right)^2$ (C)

And: $\left(\delta_{i,AcOH} - \delta_{i,MeCN}\right)\left(\delta_{i,MeCN} - \delta_{i,O_2}\right) = \left(R_{AcOH,i} - R_{MeCN,i}\right)R_{MeCN,i}$ (D)

So: $\frac{1}{2}\frac{df_i(v)}{dv} = v\left(R_{AcOH,i} - R_{MeCN,i}\right)^2 + \left(R_{AcOH,i} - R_{MeCN,i}\right)R_{MeCN,i}$

$\frac{1}{2}\frac{df_i(v)}{dv} = vR^2_{AcOH,i} + (1-v)R_{AcOH,i}R_{MeCN,i} - R^2_{MeCN,i}$

$\boxed{\frac{1}{2}\frac{df_i(v)}{dv} = v\left(R^2_{AcOH,i} - R_{AcOH,i}R_{MeCN,i}\right) - \left(R^2_{MeCN,i} - R_{AcOH,i}R_{MeCN,i}\right)}$ (E)

(E) is derivatized: $\boxed{\frac{1}{2}\frac{d^2f_i(v)}{dv^2} = R^2_{AcOH,i} - R_{AcOH,i}R_{MeCN,i}}$

As $R^2_{a,AcOH} < R^2_{a,MeCN}$, $R_{AcOH,i}$ *and* $R_{MeCN,i} > 0$

$R^2_{AcOH,i} < R_{AcOH,i}R_{MeCN,i} < R^2_{a,MeCN}$

Consequently $\frac{d^2f_i(v)}{dv^2} < 0$ and therefore $\frac{df_i(v)}{dv}$ decreases with v.

Yet: $\frac{df_i(0)}{dv} = -R^2_{MeCN,i} + R_{AcOH,i}R_{MeCN,i} < 0$

Consequently: $\boxed{\forall v,\ \frac{df_i(v)}{dv} < 0}$

Thus, $\boxed{\frac{d(R_{a,mix}(v))^2}{dv} < 0}$ as $R^2_{a,j} = \sum_i a_i f_i(v)$ and $\forall i$, $a_i > 0$

So, $R_{a,mix}(v)$ decreases when v increases. Therefore, acetic acid has a positive impact on the dioxygen solubility in the binary solvent.

**Tests with added PhOH (cf. paragraph: Why such of difference of reactivity between <u>A1</u>$_{HH}$ and <u>K1</u>$_{HH}$?)*

These tests were carried out in presence of the catalyst V_3-BM_{50} synthesized according ball-milling procedure (see paragraph III. 2.1). Phenols derivatives may deactivate the catalyst for the dimer cleavage [S10]. So, catalytic tests in presence of added phenol (Table SII. 2, entries S2-3 *vs* S1) were carried out at higher pressure (5 bar before heating).

*Table SII. 2: Influence of phenol on **A1**$_{HH}$ cleavage*

Entry	Conc. (mM)		**A1**$_{HH}$ Conv.	Yield (%)							Carbon
	A1$_{HH}$	PhOH	(%)	PhOH	p-Q[a]	PhCHO	PhCOOH	**K1**$_{HH}$	**Est**[α]**A1**$_{HH}$	**D1**$_{HH}$	balance (%)
S1	100	0	33	4.5	5.3	2.2	3.6	9.2	6.7	8.7	99
S2	80	20	32	-0.9	6.4	6.2	6.2	11	12	14	129
S3	100	20	29	-6.1	7.0	4.4	3.5	7.8	6.7	9.5	91

O_2 5 bar, V_3-BM_{50} (Mo + V 15 mol%), MeCN + 10% AcOH, 80°C, 6 h; [a]*p*-quinone

So, the phenol does not influence the conversion of **A1**$_{HH}$ so as the yield of the cleavage products. The yield of phenol was negative. It means that the phenol was converted into *p*-quinone (p-Q) and the production of phenol through cleavage was not enough to compensate the phenol conversion. So, phenol does not deactivate the catalyst. To study more deeply the effect of phenol, a test was carried out on **K1**$_{HH}$ in presence of phenol (Table SII. 3, entries S4-5).

*Table SII. 3: Influence of phenol on **A1**$_{HH}$ cleavage*

Entry	**K1**$_{HH}$	PhOH	**K1**$_{HH}$ Conv. (%)	PhOH	p-Q	PhCHO	PhCOOH	Carbon balance (%)
S4	100	0	78	38	-	16	32	62
S5	100	20	81	45	6.7	29	53	87

Atm. O_2, V_3-BM_{50} (Mo + V 18 mol%), MeCN + 10% AcOH, 80°C, 24 h

There is a notable boost of the C-C cleavage (entry S5 *vs* S4) meaning that the phenol may be a pre-co-catalyst for the oxidative cleavage of the C-C bond. Indeed, quinones proved to be efficient co-catalyst for alcohol aerobic oxidation in presence a $PMoV_x$ catalyst as shown in paragraph IB. 3.1. So, it can be deduced that phenol oxidation gives rise to *p*-quinone that acts as a co-catalyst with V_3-BM_{50} for **K1**$_{HH}$ cleavage.

Attempts for **A1$_{HH}$ oxidation into **K1**$_{HH}$ (cf. II. 7. Conclusions)*

A conclusion from part II is the ketone **K1**$_{HH}$ is cleaved more easily than **A1**$_{HH}$. Moreover, there are fewer side reactions in the case of ketone cleavage. So, a strategy may be to oxidize first the alcohol into the ketone and then to carry out the cleavage of the resulting ketone at atmospheric pressure. TEMPO and derivatives are well-known to be efficient co-catalyst for alcohol oxidation. One efficient example of **A1**$_{HH}$ aerobic oxidation into **K1**$_{HH}$ described by WANG *et al* [S11] deals with the use of $VOSO_4$ (20 mol%) and TEMPO (20 mol%) in acetonitrile at 100°C under 4 bar of oxygen (before heating) during 12 h (see Table SII. 4, entry S6). As the total volume of the autoclave is 100 mL, the molar ratio oxygen/substrate in our case was 11.4. The catalytic system is

active for alcohol oxidation into the ketone as **K1**$_{HH}$ is the main product, but the yield is lower than in Ref S10 (yield 58% *vs* 82% in Ref S10). Moreover, the stability of the catalytic system was assessed. Some fresh substrate was added at the end of the reaction (entry S7).

*Table SII. 4: **A1**$_{HH}$ oxidation catalyzed by VO-TEMPO, stability of TEMPO*

Entry	Conv. (%)	Yield (%)				Carbon balance (%)
		PhOH	PhCHO	PhCOOH	**K1**$_{HH}$	
S6	90	5.3	7.5	12	58	90
S7[a]	67	20	13	10	41	54

A1$_{HH}$ 250 mM, $VOSO_4$, $5H_2O$ 20 mol% + TEMPO 20 mol%, MeCN 20 mL, 100°C, 12 h
[a]Fresh substrate was added on the reaction media from test S6

So, the catalytic system is less active as the conversion (67% *vs* 90%) so as the yield of **K1**$_{HH}$ (41% vs 58%) declined (entry S7 *vs* S6) and there is an enhanced yield of cleavage products. Besides, the carbon balance plummeted (54% *vs* 90%). The TEMPO degradation proved to be the cause of the loss of activity.

References

[S1]: J. M. Nichols, L. M. Bishop, R. G. Bergman, J. A. Ellman, *J. Am. Chem. Soc.* **2010**, 132, 12554-12555
[S2]: G-H. Delmas, B. Benjelloun-Mlayah, Y. Le Bigot, M. Delmas, *J. Appl. Polym. Sci.* **2011**, 121, 491-501
[S3]: C. Zhang, J. Lu, X. Zhang, K. MacArthur, M. Heggen, H. Li, F. Wang, *Green Chem.*, **2016**, 18, 6545-6555
[S4]: C. J. Lion, C. S. Matthews, M. F. G. Stevens, A. D. Westwell, *J. Med. Chem.* **2005**, 48, 1292-1295
[S5]: M. Shi, D. Zhang, X. Yu, Y. Li, X. Wang, W. Yang, *Fuel Process. Technol.* **2017**, 160, 136-142
[S6]: J. Ralph, K. Lundquist, G. Brunow, F. Lu, H. Kim, P. F. Schatz, J. M. Marita, R. D. Hatfield, S. A. Ralph, J. Holst Christensen, W. Boerjan, *Phytochem. Rev.* **2004**, 3, 29-60
[S7]: D. Barats-Damatov, L. J. W. Shimon, Y. Feldman, T. Bendikov, R. Neumann, *Inorg. Chem.* **2015**, 54, 628-634
[S8]: M. J. Janik, B. B. Bardin, R. J. Davis, M. Neurock, *J. Phys. Chem. B* **2006**, 110, 4170-4178
[S9]: T. Sato, Y. Hamada, M. Sumikawa, S. Araki, H. Yamamoto, *Ind. Eng. Chem. Res.* **2014**, 53, 19331-19337
[S10]: T. Imai, T. Yokoyama, Y. Matsumoto, *J. Wood. Sci.* **2011**, 57, 219-225
[S11]: M. Wang, J. Lu, X. Zhang, L. Li, H. Li, N. Luo, F. Wang, *ACS Catal.* **2016**, 6, 6086-6090

III. Alternative ball milling synthesis of $PMoV_x$ for the aerobic cleavage of lignin and its models

These experiments were partly carried out in collaboration with Dr. Martine TESSIER and Dr. Brigitte ROUSSEAU from the IPCM laboratory (Sorbonne Université) in Paris.

III. 1. Introduction

Our choice for the $PMoV_x$ synthesis was based on the use of an hydrothermal procedure which involves the treatment of MoO_3, V_2O_5 and H_3PO_4 in boiling water (see II. 2.1). The main advantage was the simplicity of the protocol and no external reactant was needed. Yet, especially for high values of x, long reaction time (6.5 h minimum) and diluted conditions were required (see II. 3. 1). However, since the alcohol **A1**$_{HH}$ proved to be resistant to cleavage, $PMoV_x$ with a high amount of vanadium are considered to be more suitable for an increased oxidizing power (IB. 1.2). So, an alternative synthetic procedure had to be envisaged.

The interest in ball milling and more generally mechanochemistry techniques is skyrocketing [1]. Such approaches proved to be adequate to prepare heterogeneous catalysts with enhanced performances [2] such as Metal-organic frameworks (MOFs) [1], layered double hydroxides [3], metal containing carbon nanotubes [4] and zeolites [5]. For instance, a mixed oxide, MoV_2O_8, has been synthesized from MoO_3 and V_2O_5 by ZAZHIGALOV *et al* and was used as a catalyst for hydrocarbon oxidation [6]. In presence of the hand mixture of MoO_3 with 2 equivalents of V_2O_5, the conversion of benzene was 1.7% and the selectivity to maleic anhydride was 3% only whereas in presence of ball-milled MoV_2O_8, the conversion raised to 84% in average and the average selectivity of maleic anhydride was 56%. Also, LIU *et al* proved that ball-milling is adapted for the impregnation of a MOF by $PMoV_2$ giving rise to an active catalyst for desulfurization [7]. In this case, the conversion of dibenzothiophene into dibenzosulfolane in presence of impregnated MOF was 100% after 2 h whereas it fell down to 45% in presence of the MOF alone and to 4% in presence of $PMoV_2$. In addition, $PMoV_2$ supported on a mesoporous polymer active for benzene hydroxylation was synthesized by LENG *et al* [8] but, in these two cases, $PMoV_2$ was synthesized before, using conventional procedures. However, MOLCHANOV *et al* showed that $PMoV_x$ catalysts may be also prepared through the hydrothermal attack (80°C) by H_3PO_4 of a

previously ball-milled mixture of V_2O_5 and MoO_3 [9-10]. One important advantage (*vs.* a 100% hydrothermal pathway) is that ball-milling on the starting metal oxides may help their dissolution, especially for V_2O_5 thus facilitating the formation of the desired $PMoV_x$. As a result, it is expected that the yield of $PMoV_x$ will be improved which can be beneficial for the activity per weight of powdered catalyst. In addition, the attack of the mixed oxide by H_3PO_4 should be easier and hence, performed at lower temperature. As a matter of fact, such hybrid pathway (ball-milling conjugated to hydrothermal treatment) may be considered as a greener approach than the 100% hydrothermal one as it should require less energy and no additional reactant. Consequently, wastes should be minimized.

Previously, MOLCHANOV *et al* investigated the influence of the balls/oxides ratio, the milling duration and of the operative conditions of the H_3PO_4 attack in water. However, the synthesized $PMoV_x$ was characterized by XRD, ^{31}P and ^{51}V MAS NMR only. Nothing was published on the speciation in solution. They were focused on the use of mechanochemical activation to save time for $PMoV_x$ synthesis. Similarly, ZAZHIGALOV *et al* [6] performed only XRD and RAMAN spectroscopy characterizations on the mixed oxide, but no BET and granulometry measurements as well as SEM were performed. The energy consumption was not calculated too. Last but not least, $PMoV_x$ hence synthesized was not tested for the catalytic aerobic cleavage of lignin and of its surrogates, a reaction of industrial relevance and more generally not any catalytic test was performed. In the present work, we propose a comparison between the 100% hydrothermal (HT) and the hybrid procedure involving a mechanochemical step (BM) with a focus on the yield of the $PMoV_x$ and the energy consumed.

The activity and the selectivity of the catalysts synthesized through the BM procedure will be compared to those of the materials obtained by the HT one in the aerobic cleavage of 2-phenoxyacetophenone (**K1**$_{HH}$) and 2-phenoxy-1-phenylethanol (**A1**$_{HH}$), two model molecules of lignin. Then preliminary tests on a wheat straw Organosolv lignin will also be performed.

III. 2. Experimental part

The methodology for the characterization of the PMoVx are detailed in II. 2. 3 (atmospheric conditions) and II. 2. 4 (under higher pressure). Here, we will focus on the

ball-milling route for $PMoV_x$ synthesis (III. 2.1 and III. 2.2). As the $PMoV_x$ characterization was detailed in II. 2.1, we will concentrate on the characterization of the intermediate mixed oxide (III. 2.3). Then, the purification of an Organosolv wheat straw lignin and the catalytic tests on the purified lignin will be described.

III. 2.1. Ball-milling route for $PMoV_x$ synthesis

The milling procedure was carried out in a Fritsch Pulverisette 7 planetary miller using zirconium oxide balls (ø = 10 mm, weight set to 68 g for each experiment) according to ref. 9 in a zirconium oxide coated autoclave. The rotation speed was set to 700 rpm (11.7 s^{-1}) and the ZrO_2 balls/oxides weight ratio, noted r, was 20 or 50.

- For r = 50, to get V_x-BM_{50} solids (theoretical x = 1-4), the milling duration (t_{BM}) was 1 h and the obtained mixed oxide was attacked by phosphoric acid in water at 80°C during t_{HT} = 1.5 h (see Table III. 1).
- For r = 20 and a theoretical x of 2, to get V_2-BM_{20}-t_{BM}-t_{HT} solids, t_{BM} was varied from 1 to 4 h and the mixed oxide was attacked during either t_{HT} = 1.5 h or 3 h (see Table III.1). When nothing is otherwise stated, the temperature during the attack step was 80°C. Two samples of this series, V_2-BM_{20}-2x2-1.5 and V_2-BM_{20}-2x2-3, were prepared differently in the sense that ball-milling (t_{BM} = 4 h) was decomposed into two steps. First, V_2O_5 was milled alone during 2 h and then with MoO_3 during 2 h. The mixed oxide was then attacked during t_{HT} = 1.5 h or 3 h.

Generally, the mixture of the starting oxides was initially clear brown and it turned dark brown after milling. When the obtained mixed oxide is added to an aqueous solution containing a stoichiometric amount of H_3PO_4, the mixture initially brown turned red on the first seconds. The suspension was filtered to eliminate the zirconium oxide coming from the abrasion of the balls. Then, likewise to the hydrothermal procedure, the last steps were filtration and then water evaporation to get a red-orange final $PMoV_x$.

A 100% ball-milling synthesis of $PMoV_x$ was also tested (wet BM procedure, wBM) consisting in milling together the oxides and H_3PO_4 in presence of water during 1 h (see Table III.1). The main aim was to use a faster and simpler procedure to get first $PMoV_2$. Stoichiometric amounts of V_2O_5 (0.381 g), MoO_3 (3.019 g) and H_3PO_4 85% (14 µL, 142 mg) were added to the balls in the autoclave (68 g), then 0.2-1 mL of distilled

water was dropped. The milling duration was set to 1 h (r = 20) affording a viscous red suspension contaminated by ZrO_2 coming from the unavoidable abrasion of the balls in these conditions (acidity, high temperature) whose efficient separation could be performed by centrifugation (7500 rpm during 10 min), after dilution with 25 mL of distilled water. The centrifugation step was repeated once after adding some extra water. Afterwards, the last step was water evaporation to get the purified $PMoV_x$ (V_2-wBM_{20}) as a red solid. It has to be noted that this route was adapted for r = 50 and x = 2 (V_2-wBM_{50} solid) using 0.152 g of V_2O_5, 1.208 g of MoO_3, H_3PO_4 85% (5.6 µL, 57 mg) and 0.4 mL of distilled water.

III. 2.2. Materials characterization

The mixed oxide was characterized by XRD (see details in II. 2.1), SEM, RAMAN spectroscopy, granulometry and N_2 sorption. SEM analyses were carried out with a Hitachi SU-70 microscope. The sample was put at 3.2 mm from the source of the current, generated by an electrons flow. The accelerating voltage was set to 1000 V and the intensity of the emission current to 47 µA. Granulometry measurements were performed on a Fristch Analysette 22 Nano Tec. RAMAN analyses were performed with a RamanRXN spectrometer, equipped with an optical microscope (magnification X10) from Kaiser Optical Systems Inc. and a laser working at λ = 785 nm, with a power of 10-12 mW and a resolution of 4 cm^{-1}. The duration of each scan was 10 s and the number of scans was 30. N_2 sorption analyses affording BET data were carried at -196°C out on a Belsorp Mini II apparatus from BEL Japan. Prior to each measurement, synthesized samples (≈ 100 mg) were degassed under vacuum for 3 h at 180°C.

Table III. 1: amounts of the staring oxides, phosphoric acid and conditions used for $PMoV_x$ synthesis

Procedure	x	r	t_{BM} (h)	t_{HT} (h)	Name	MoO_3		V_2O_5		H_3PO_4 85%		Water volume (mL)
						Weight (g)	Quantity (mmol)	Weight (g)	Quantity (mmol)	Weight (g)	Quantity (mmol)	
Hydrothermal	1	-	-	3	**V_1-HT**	14.41	100	0.916	5	1.165	10.1	150
	3	-	-	6.5	**V_3-HT**	3.930	27.3	0.919	5.1	0.385	3.3	200
Dry ball-milling	1	50	1	1.5	**V_1-BM_{50}**	1.286	8.9	0.074	0.41	0.196[a]	0.57	50
	2	50			**V_2-BM_{50}**	1.207	8.4	0.153	0.84	0.257[a]	0.75	
	3	50			**V_3-BM_{50}**	1.123	7.8	0.237	1.3	0.240[a]	0.70	
	4	50			**V_4-BM_{50}**	1.034	7.2	0.326	1.8	0.464[a]	1.3	
	2	20	1	1.5	**V_2-BM_{20}-1-1.5**	3.019	21	0.381	2.1	0.071[b]	0.6	50
			1	3	**V_2-BM_{20}-1-3**							
			2	1.5	**V_2-BM_{20}-2-1.5**							
			2	3	**V_2-BM_{20}-2-3**							
			4	1.5	**V_2-BM_{20}-4-1.5**							
			4	3	**V_2-BM_{20}-4-3**							
			2x2	1.5	**V_2-BM_{20}-2x2-1.5**							
			2x2	3	**V_2-BM_{20}-2x2-3**							
Wet ball-milling	2	20	1	-	**V_2-wBM_{20}-1**	3.019	21	0.381	2.1	0.142	1.2	1
		50	1	-	**V_2-wBM_{50}-1**	1.207	8.4	0.153	0.84	0.057	0.48	0.4

[a] H_3PO_4 was diluted to 28.5% and added in stoichiometric amounts and the mixed oxide was not totally recovered; [b] 1.7 g of mixed oxide was used and H_3PO_4 was added in stoichiometric amounts

III. 2.3. Lignin purification

The lignin from wheat straw we have studied was graciously provided by CIMV (Compagnie Industrielle de la Matière Végétale) and has been extracted using an Organosolv process. Before use, the sample (noted WSL_i) had to be further purified according to the recommendations of MBOTCHAK et al [12]. With an alkaline treatment, hydrophilic impurities such as sugars, formic acid and acetic acid were removed, then the solid (WSL_h) was washed by organic solvents to eliminate the hydrophobic impurities such as fatty acids.

- ***Alkaline treatment***

Hence, *c.a.* 10 g of lignin were dissolved in 300 mL of NaOH 1 M and the resulting mixture heated to 80°C during 3 h. After cooling, fractions of 25 mL of the black liquor were collected in centrifugation vials. In each fraction, 8.4 mL of HCl 37% were added to precipitate the lignin and the resulting mixtures centrifugated (7500 rpm, 10 min). Afterwards, the recovered liquid fractions were combined and filtered (porosity 3). Then, *c.a.* 30 mL of water were added to the solid in the centrifugation vial. The residual lignin was suspended and the suspension shaken. The suspension was dark brown after shaking. The centrifugation and the suspension steps were repeated until the centrifugation did not impact the color of the liquid phase (dark brown after centrifugation). Once the centrifugation done, the suspension was filtered and the solid was washed by water until pH = 6. Initially, the filtrate was clear, then, after several centrifugation and suspension steps, it became darker and darker. The lignin, hence recovered, was dried in an oven at 50°C affording 8.39 g of material (hydrolyzed lignin) that was noted WSL_h (71% yield).

- ***Washing with organics***

WSL_h was washed twice by refluxing with CH_2Cl_2 and then three times by refluxing with AcOEt. Each washing step lasted 1 h. Finally, the recovered solid was treated by CH_2Cl_2 to remove completely ethyl acetate and then dried in a dessicator under vacuum affording 6.83 g of purified lignin noted WSLp (81% yield).

The global yield of the purification procedure was 68 %.

III. 2.4. Procedure of the catalytic tests performed on lignin and monitoring

Preliminary cleavage tests were carried out on WSLp in the presence of a V_3-BM_{50} catalyst. The targeted products are *p*-hydroxybenzaldehyde, vanillin, syringaldehyde and their corresponding acids. Experiments were carried out directly under 5 bars of dioxygen at either 80 or 120°C.

Hence, 0.854 g of lignin and 59.6 mg of V_3-BM_{50} (Mo+V 15 mol% according to the substrate) were weighted and contacted with 25 mL of MeCN - 10 vol% AcOH in an autoclave. The procedure used was then similar to that of **A1**$_{HH}$ oxidation under pressure (II. 5). At the end of the reaction, since lignin is barely soluble, the mixture had to be filtered on a sintered filter (porosity n° 4).

- An aliquot of the filtrate (20 µL) containing the targeted phenolic aldehydes and acids was poured in a test tube capped by a septum that was later connected to a vacuum pump in order to evaporate the solvent. Then, 20 µL of pyridine, 10 µL of a solution of an internal standard (biphenyle, 10 mM in acetonitrile) and 250 µL of BSTFA (N,O-Bis(trimethylsilyl)trifluoroacetamide) were added and the mixture was stirred overnight. Afterwards, the obtained solution was analyzed by GC-MS in duplicate (cf II. 2.6). The lone modification (*vs* II. 2.6) is the mass spectra were recorder in a larger range of m/z ($35 \leq m/z \leq 400$ every 0.4 s).
- The solid phase constituted of lignin / oxidized lignin was analyzed directly by liquid ^{1}H NMR or after phosphorylation by ^{31}P NMR on a Bruker spectrometer (400 MHz).
    - For ^{1}H NMR, 10 mg of the solid "lignin" sample was dissolved in 500 µL of DMSO-d_6. However, since the oxidized samples turned out to be poorly soluble in DMSO (*c.a.* 10%), some analyses had to be carried out using NaOD 1 M in D_2O. 256 scans were recorded with a relaxation delay of 2 s.
    - For ^{31}P NMR, phosphorylated lignin samples were dissolved in pyridine-$CDCl_3$ (see the Appendix, *Lignin phosphorylation*, Fig SIII. 12). An average number of 10000 scans were recorded with a relaxation delay of 25 s.

III. 3. Results and discussion

The $PMoV_x$ obtained using the hybrid ball milling / hydrothermal procedure (BM) are characterized and compared to V_1-HT and V_3-HT (see II. 2. 3).

III. 3.1. Characterization of the $PMoV_x$ from ball-milling

A first series of $PMoV_x$ were synthesized using the hybrid ball milling / hydrothermal procedure (BM) with r = 50, a milling duration of 1 h and an attack duration of the mixed oxide of 1.5 h. The resulting solids noted V_x-BM_{50} (x = 1-4) were compared to V_1-HT and V_3-HT used as references for the 100% hydrothermal synthesis (HT, see II. 2. 3).

KEGGIN structure of the new materials was checked by XRD (Fig. III. 1 and Fig SIII.1).

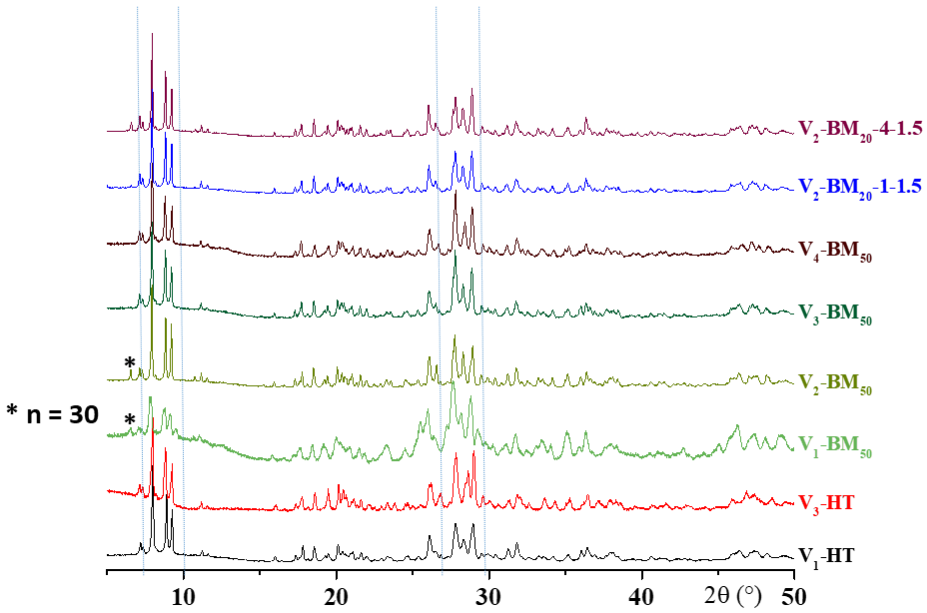

Figure III. 1: XRD profiles of $PMoV_x$ catalysts

As in the XRD profiles of V_1-HT and V_3-HT, the peaks at *c.a* 8° and 28° are present in the diffractograms of all the V_x-BM_{50} solids (see Fig III. 1). The V_1-BM_{50} solid turned out to be more amorphous than other samples. Actually, prior to its utilization in catalytic tests, V_1-BM_{50} had to be further purified by centrifugation to remove completely zirconium oxide in spite of the filtration which might be responsible of the presence of an amorphous phase. Otherwise, using the EVA software, V_1-BM_{50} and V_2-BM_{50} catalysts seem to be constituted of at least two $PMoV_x$ crystalline phases differing by

their hydration index. The main crystalline phase corresponds to n = 13, also present in the reference $PMoV_x$ and the minor one corresponds a hydration index of n = 30 (peaks *, see Fig III. 1). V_3-BM_{50} is constituted of only one crystalline phase as shown by the RIETVIELD refinement (R_P = 10.1 and Chi_2 = 2.39), which differentiates it from V_3-HT (R_P = 15.1 and Chi_2 = 13.1, see Table II. 4).

XRD was completed by liquid ^{31}P NMR to estimate the yield of $PMoV_x$, hypothesizing that H_3PO_4 is the lone impurity (see the results for the materials obtained by the HT and BM pathways in Fig. III. 2). For r = 50, remaining amounts of H_3PO_4 were rather low excepted for V_4-BM_{50} for which the KEGGIN structure could not be validated. This seems antagonist to XRD conclusion, but H_3PO_4 is not crystalline and consequently not detectable by XRD. Looking more precisely to V_3-BM_{50} (*vs* V_3-HT) and V_1-BM_{50} (*vs* V_1-HT), we have noticed that ball milling led to a higher yield of $PMoV_x$, especially for x = 3 (^{31}P NMR). Moreover, the synthesis time was considerably reduced. ^{1}H NMR spectra of V_3-HT and V_3-BM_{50} samples (Fig. III. 2) are complex as the result of the partial protonation of $PMoV_3$ at pH ~ 1 due to its weaker acid than $PMoV_1$ and $PMoV_2$ ($pK_a \approx 0.2$) [13] and the co-existence of $PMoV_x$ with different x values [14]. Thus, a deeper study will be carried out only for $PMoV_1$ and $PMoV_2$ solids.

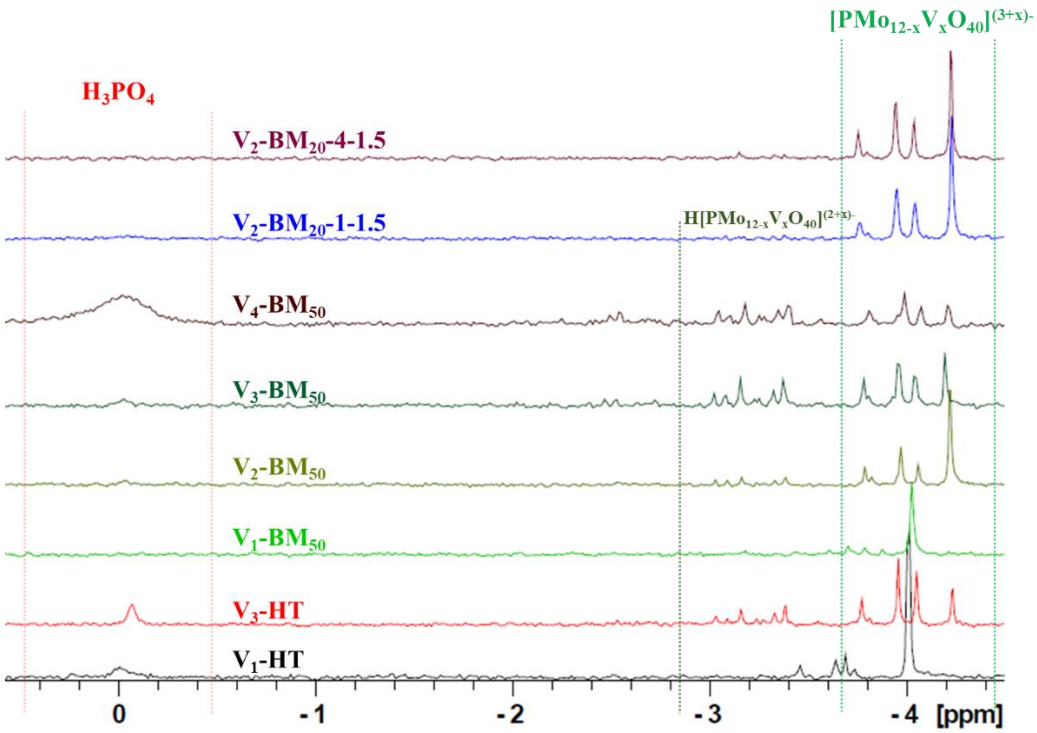

Figure III.2: ^{31}P NMR spectra of V_x-HT and V_x-BM materials

Both V_1-BM_{50} and V_1-HT (x = 1) solutions are characterized by the presence mainly of the isomer α of $PMoV_1$ (see II. 3, Fig II. 10) as indicated by the major peak at -4.10 ppm. V_2-BM_{50} solution contains the isomers α-1,2 (peak 4), α-1,4 and α-1,5 (peak 3), α-1,6 and α-1,11 and the isomers β (whose proportions are given in Table SIII. 1). Among them, α-1,2 was the major one (37.4-58.5%) and the estimated abundancy of the other isomers was 12.6% minimum. Such determination shows that the α-1,2 and α-1,5 isomers, *i.e.* those containing vicinal vanadium atoms, correspond to roughly 76% of all the isomers meaning that V_2-BM_{50} should be a good oxidation catalyst [13, 14].

The values of x_{exp} were determined from ICP and the hydration index was further calculated using TGA (Table III.3).

Generally, the experimental value of x is close to the nominal value. This is due to the enhanced dissolution of the oxides. Indeed, during the hydrothermal synthesis of V_x-HT, a residue enriched in vanadium oxide had to be filtered off. So, the x is unavoidably lower. The deviation (Table III. 3) between the experimental and the theoretical x was always higher than 10% in the case of hydrothermal $PMoV_x$ (V_1-HT: 14%, V_3-HT: 11%) whereas the deviation was lower than 10% for V_1-BM_{50} (4%), V_2-BM_{50} (6%) and V_3-BM_{50} (7%).

The TGA-DSC curves of V_x-HT and V_x-BM_{50} are given in Fig. SIII. 6 and their characteristic temperatures reported in Table III.2. Profiles obtained for V_x-BM_{50} are similar to the references V_1-HT and V_3-HT which agrees with KEGGIN structures. However, for x = 1, T_1 and T_2 values of V_1-BM_{50} and V_1-HT are quite different which could be linked to contaminations either of phosphoric acid in V_1-HT or of ZrO_2 in V_1-BM_{50}.

The calculated hydration index value (n) was between 12 and 15 as expected from XRD data except for V_1-HT (see Table III. 3). It should be noted that the phase corresponding to n = 30 is a minor phase and so has a minor impact on the average n. The losses of hydration (T_1) and constitutive water (T_2) took place at the same temperature for both $PMoV_1$ catalysts so as for both $PMoV_3$ solids, thus confirming the similarity of the number of vanadium equivalents in V_1-BM_{50} (*vs* V_1-HT) and V_3-BM_{50} (*vs* V_3-HT). Besides, the values of T_1 and T_2 for V_2-BM_{50} and V_3-BM_{50} are similar.

Table III. 2: Values of T_1 and T_2 for V_x-HT and V_x-BM_{50} catalysts from TGA

x	r	t_{BM} (h)	t_{HT} (h)	Name	T_1 (°C)	T_2 (°C)
1	-	0	3	**V_1-HT**	261.1	466.3
3	-	0	6.5	**V_3-HT**	222.1	420.6
1		1	1.5	**V_1-BM_{50}**	240.8	444.7
2	50	1	1.5	**V_2-BM_{50}**	218.7	429.1
3		1	1.5	**V_3-BM_{50}**	215.8	416.4
2	20	1	1.5	**V_2-BM_{20}-1-1.5**	222.6	428.4
			3	**V_2-BM_{20}-1-3**	214.7	428.4
		2	1.5	**V_2-BM_{20}-2-1.5**	232.9	430.9
			3	**V_2-BM_{20}-2-3**	214.0	428.3
		4	1.5	**V_2-BM_{20}-4-1.5**	213.7	428.0
			3	**V_2-BM_{20}-4-3**	211.2	427.4
		2x2	1.5	**V_2-BM_{20}-2x2-1.5**	215.1	428.7
			3	**V_2-BM_{20}-2x2-3**	222.2	431.2

Furthermore, the energy consumption of the two synthesis procedures was calculated for all the materials synthesized (see details in Table SIII. 2) showing that, after normalization, the hybrid protocol (BM) is more energy-saving than the hydrothermal (HT) one for $PMoV_3$ synthesis (422 kW.h for V_3-BM_{50} *vs* 618 kW.h for V_3-HT). For V_3-HT synthesis, the duration of the attack had to be raised from 3 h to 6.5 h to dissolve the residual oxides (cf. II. 2.1), which leads to a raise of the energy consumption from 287 to 618 kW.h. Therefore BM procedure is more suitable for x = 3.

Table III. 3: Comparison of the materials obtained by the HT or BM procedures

Procedure (temperature)	Hydrothermal (HT) (100°C)		Ball milling (BM) r = 50 (80°C)			
Name	**V_1-HT**	**V_3-HT**	**V_1-BM_{50}**	**V_2-BM_{50}**	**V_3-BM_{50}**	-
w(P) (%)	1.77	2.01	2.24	1.67	1.80	-
w(Mo) (%)	49.25	46.16	58.65	53.20	49.92	-
w(V) (%)	2.75	7.06	2.98	5.23	8.02	-
x_{exp} (x_{th})	1.14 (1)	2.68 (3)	1.04 (1)	1.88 (2)	2.79 (3)	No Keggin (4)
Δx (%)	14	11	4	6	7	
Yield (%)	81 ± 8	79 ± 8	97 ± 10	95 ± 10	97 ± 10	-
n	8.4	13	12	15	12	-
Global energy consumption (kW.h/mol)	85.3	618[a]	451	439	422	

[a]The duration of the attack was raised to 6.5 h

A second series of $PMoV_x$ were synthesized using the hybrid ball milling / hydrothermal procedure (BM) with r = 20, *i.e.* increasing the amount of vanadium and molybdenum oxides (V_2-BM_{20}). The idea was to synthesize a higher amount of $PMoV_x$

per autoclave in order to start to intensify the procedure. For every value of x, a milling time of 1 h and a subsequent attack by H_3PO_4 at 80°C during 1.5 h (conditions of the first series) did not lead to the desired KEGGIN structure with a correct yield (H_3PO_4 signal too intense in ^{31}P NMR). However, due to the use of higher amounts of oxides, the heat generated by the friction between the balls might be not enough to generate the mixed oxide. Indeed, SCHMIDT *et al* showed that an increased amount of powder leads to a dramatic decrease of the local temperature in the autoclave. The elasticity of the collisions is modified and "the grinding stock acts as a heat sink" [15]. Therefore, the milling step might give rise to a lower temperature and be less beneficial for the generation of the mixed oxide as well as for the contact between molybdenum and vanadium oxides. As a consequence, in the present case, the duration of ball milling and H_3PO_4 attack were further modified.

Firstly, for x = 2, the attack by phosphoric acid was optimized by raising either the temperature to 100°C (V_2-BM_{20}-1-1.5) or the attack duration (V_2-BM_{20}-1-3) keeping 1 h for the milling step. Then, a longer duration of this step was tested too (either 2 or 4 h) affording V_2-BM_{20}-**2**-1.5, V_2-BM_{20}-**4**-1.5, V_2-BM_{20}-**2**-3 and V_2-BM_{20}-**4**-3 samples, the general notation being V_2-BM_{20}-t_{BM}-t_{HT}.

The characterization figures (XRD, NMR and TGA) of the materials obtained after a 3h-attack by phosphoric acid are given in the supplementary information section as a longer attack did not give rise to a notable modification.

- Keeping a 1 h-ball-milling time and increasing the temperature from 80°C to 100°C (V_2-BM_{20}-1-1.5) or the duration of the attack (V_2-BM_{20}-1-3) resulted in the successful synthesis of the KEGGIN $PMoV_x$ as shown by XRD data (Fig. III. 1 and SIII. 1). Moreover, the NMR characterization of V_2-BM_{20}-1-1.5 and V_2-BM_{20}-1-3 (Fig. III.2 and SIII. 3) showed that an optimization of the H_3PO_4 attack was beneficial for the synthesis of the $PMoV_2$. Indeed, the peak of phosphoric acid (δ = 0 ppm) is almost absent as for the reference V_2-BM_{50}.
- A longer milling step also gave rise to similar results (Fig. III. 1-2, SIII. 1 and SIII. 3). The XRD profiles of the materials obtained through a longer milling step are compared to that of V_2-BM_{50} chosen as a reference (Fig. III. 1 and SIII. 1) showing exactly the same peaks. The yield of $PMoV_2$ was almost 100% for V_2-BM_{20}-2-1.5, V_2-BM_{20}-4-1.5, V_2-BM_{20}-2-3 and V_2-BM_{20}-4-3 (Fig 3. 2 and Fig. SIII. 3) as shown by NMR

analysis by the peak of H_3PO_4 being almost absent.

So, for all the V_2-BM_{20} materials prepared with adapted conditions, the KEGGIN structure could be validated and the obtained yields were in between 92 and 97% (*vs* 79% for V_3-HT). However, it can be mentioned that the proportion of α-1,2 isomer was lower in the V_2-BM_{20} materials compared to V_2-BM_{50}, but yet still the major one (37.4-47.9%), β-isomers being in minority and the amount of isomers containing vicinal vanadium atoms between 61 and 71%. It is noteworthy that the proportion of the α-1,2 isomer was particularly high in the case of V_2-BM_{50} (58.5%). Yet, the combined proportion of vicinal isomers (α-1,2, α-1,4 and α-1,5) are lower in the catalysts obtained after a milling step of 4 h (V_2-BM_{20}-4-1.5: 59.9% and V_2-BM_{20}-4-3: 61.2%) and in V_2-BM_{20}-1-1.5 (60.4% *vs* 71.1% in V_2-BM_{50}) are particularly low. They may be less reactive for the catalytic oxidation of **K1**$_{HH}$ and **A1**$_{HH}$. So, a longer milling step may be not beneficial for the synthesis of active $PMoV_x$. So, for r = 20, a milling step of 2 h may be more adequate. This has to be confirmed by the catalytic tests on **K1**$_{HH}$.

Furthermore, since V_2O_5 appeared to be in principle more difficult to attack, we thought that there might be a positive influence of milling first this oxide prior to the mixing with MoO_3. Consequently, two other solids (V_2BM_{20}-2x2-1.5 and V_2-BM_{20}-2x2-3) were synthesized by milling previously V_2O_5 for 2 h and adding afterwards MoO_3 for a subsequent ball-milling step of another 2 h followed by a 1.5h or a 3h-attack by aqueous H_3PO_4. Actually, such milling strategy had a low impact on the structure as shown by XRD (Fig. SIII. 2) and the yield of $PMoV_x$ for a hydrothermal attack of 1.5 h was 95% (*vs* 92% for V_2-BM_{20}-4-1.5) and 98% for V_2-BM_{20}-2x2-3 (*vs* 98% for V_2-BM_{20}-4-3) (NMR, Fig. SIII. 4). Moreover, the experimental value of x was lower than that of the materials prepared with a 4h-milling performed in one step (Table III. 4). As a matter of fact, such procedure was not more successful and the key step seems to be the milling of the starting oxides together.

The ICP results showed that x_{exp} value was generally higher for longer H_3PO_4 attack duration and seemed to not be affected by the milling duration (Table III. 4). TGA-DSC analysis of V_2-BM_{20} catalysts (Fig. SIII. 7-8) were carried out and their results compared to those of V_2-BM_{50}. The loss of constitutive water took place at the same temperature (*c.a.* T_2 = 428°C) in agreement with the similar amounts of vanadium of all these solids. The hydration index, n, is between 12 and 15, which is in good accordance

with the estimations given by XRD (Table III. 4).

These results are gathered in Table III. 4. Briefly, the hybrid / ball-milling (BM) procedure showed to be efficient for the synthesis of $PMoV_x$ catalysts with an improved yield, especially those with high values of x (Table III. 4). However, the energy consumption after a long milling step (4 h or 2x2 h, Table III. 4) is still lower (*vs* V_3-HT, 618 kW.h, Table III.3).

All of the catalysts (of which the KEGGIN structure was validated) will be tested for aerobic oxidative cleavage of lignin dimeric models.

III. 3.2. Characterization of the mixed oxides resulting from ball-milling

To better understand the influence of ball-milling, mixed oxides from the synthesis of V_2-BM_{50} and of V_2-BM_{20} catalysts were recovered from the autoclave and further characterized. The mixed oxide from V_2-BM_{50} and V_2-BM_{20} catalysts synthesis were characterized by XRD and the mean size of the crystallite, noted τ, was estimated using the SCHERRER equation (Eq. III.1) applied to the (110) diffraction plane (Table III. 5).

$\tau = \frac{K\lambda}{L_{FWHM}cos\theta}$ (Eq. III.1) *where K = 0.888 is the shape factor, λ = 1.5418 Å, L_{FWHM} (Full Width at Half Maximum intensity), 2θ = position of the peak.*

Entry 1 corresponds to the hand-mixture from which all of these mixed oxides were synthesized. The solid is crystalline as shown by the narrow peaks on the diffractogram (Fig SIII. 9). The mixed oxides were compared to the hand mixtures (entries 2-6 *vs* 1). As expected, the mixed oxides are more amorphous and for r = 50, there is a shift of the peak towards lower angles. An increase of r (in other words a decrease of the weight of the starting oxides, entry 3 *vs* 2) and a longer milling step (entries 3-5) led to smaller crystallites (Table III. 5) and to less crystalline mixed oxide (see Fig SIII. 9). The mixed oxide from a stepwise milling (2 x 2 h, entry 6) was compared to the mixed oxide from V_2-BM_{20}-4 catalysts synthesis (4 h, entry 5). The mixed oxide from V_2-BM_{20}-2x2 catalysts is less crystalline than the oxide from V_2-BM_{20}-4 synthesis and similar to the oxide from V_2-BM_{20}-2 catalysts synthesis.

Table III. 4: Comparison of the materials obtained by the BM procedure for r = 20 and x = 2

Name	V_2-BM_{20}-1-1.5	V_2-BM_{20}-1-3	V_2-BM_{20}-2-1.5	V_2-BM_{20}-2-3	V_2-BM_{20}-4-1.5	V_2-BM_{20}-4-3	V_2-BM_{20}-2x2-1.5	V_2-BM_{20}-2x2-3
Milling duration (h)	1		2		4		2*2[b]	
Attack duration[a] (h)	1.5 (100°C)	3	1.5	3	1.5	3	1.5	3
x_{exp} (ICP)	2.1	2.3	2.0	2.3	2.3	2.3	2.0	2.1
n (TGA)	12	13	15	12	13	14	15	12
Energy consumption (kW.h/mol)	210	257	304	374	539	608	539	608

MoO_3 3.019 g; V_2O_5 0.381 g; 700 rpm; [a]T = 80°C if not specified, [b]V_2O_5 was first milled alone (2 h) and then with MoO_3 (2 h)

Table III. 5: Crystallite size of a BM and of a hand mixture of oxides

Entry	**r**	**t(BM) (h)**	**L_{FWHM} (°)**	**Position of the peak (110) (°)**	**Crystallites size (Å)**
1	-	-	0.1434	23.31	9.7
2	50	1	0.9486	23.08	2.8
3	20	1	1.4469	23.49	1.4
4	20	2	1.3897	23.80	1.3
5	20	4	1.1693	23.49	1.7
6	20	2x2	2.1583	23.21	1.1

Figure III. 3 shows one example of XRD profile for a ball-mixture of oxides (pink) precursor of V_2-BM_{50} as well as those of the starting oxides (V_2O_5: red, MoO_3: blue) and of a hand-mixture in same Mo/V proportions obtained by conventional grinding (purple). MoO_3 and V_2O_5 are crystallized according to an orthorhombic structure. As expected, the XRD profile of the hand mixture of oxides corresponds to the sum of the the X-Ray diffractograms of both oxides with minor peaks for V_2O_5. Concerning the mixture resulting from ball-milling,

- the superposition of the XRD profiles confirms that the crystallite size in the ball-milled mixture is much smaller than in the hand-mixed material (wider peaks of the XRD diagram).
- the crystalline structure of the ball-milled mixture is close to that of MoO_3 but with reflections sometimes shifted to lower 2θ values, meaning that the crystalline structure of MoO_3 changes slightly. It was suggested by MOLCHANOV *et al* that the crystal lattice of the "mixed oxide" could be constituted on alternated MoO_3 and V_2O_5 layers. For x = 2, the peaks of vanadium oxide are difficult to observe in the hand-mixture diffractogram. However, as milling gave rise to larger and smaller peaks, nothing clear could be concluded on the structure of the powder from the vanadium point of view.

The Raman analysis (Fig. III. 4) of the precursor of V_2-BM_{20}-2 catalyst tends to show that the peaks corresponding to the bonds between molybdenum and oxygen atoms did not shift, meaning that the molecular structure of MoO_3 is preserved in the mixed oxide. The widening of the peaks can be explained by the amorphization of the material. Moreover, is it very likely that the profile of RAMAN spectrum of the ball-milled material is not only due to the amorphization of the solid and some peaks due to the mixed oxide V_2MoO_8 showing that the milling procedure gave rise to chemical reactions.

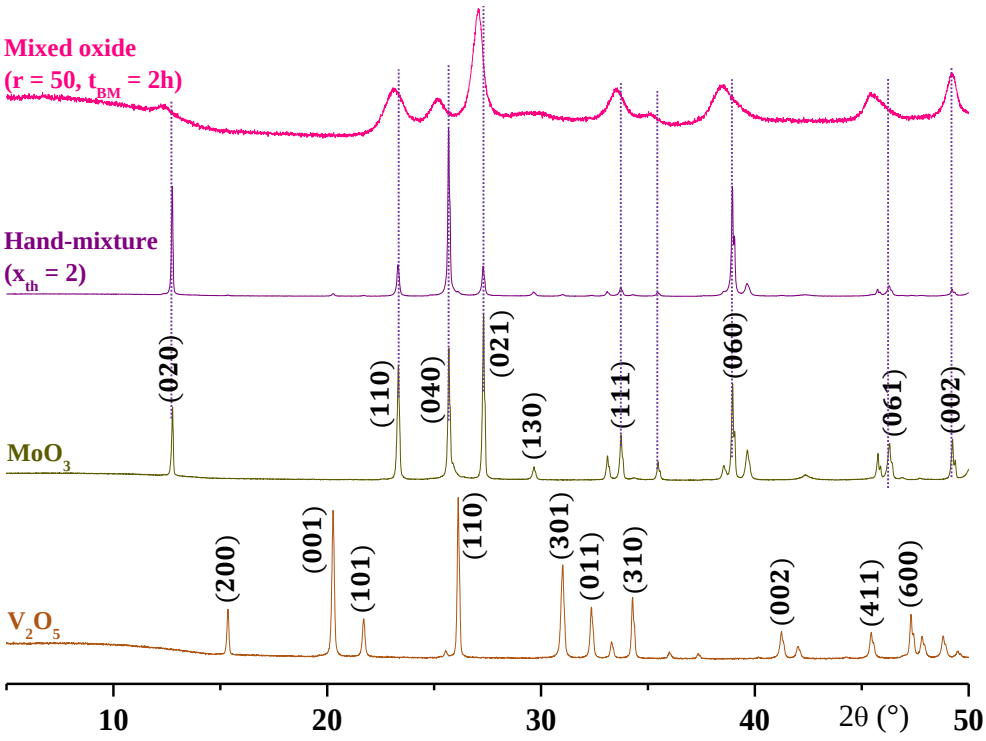

Figure III. 3: Diffractograms of the pure oxides, their hand-mixture and of the mixed oxide precursor of V_2-BM_{20}-2.

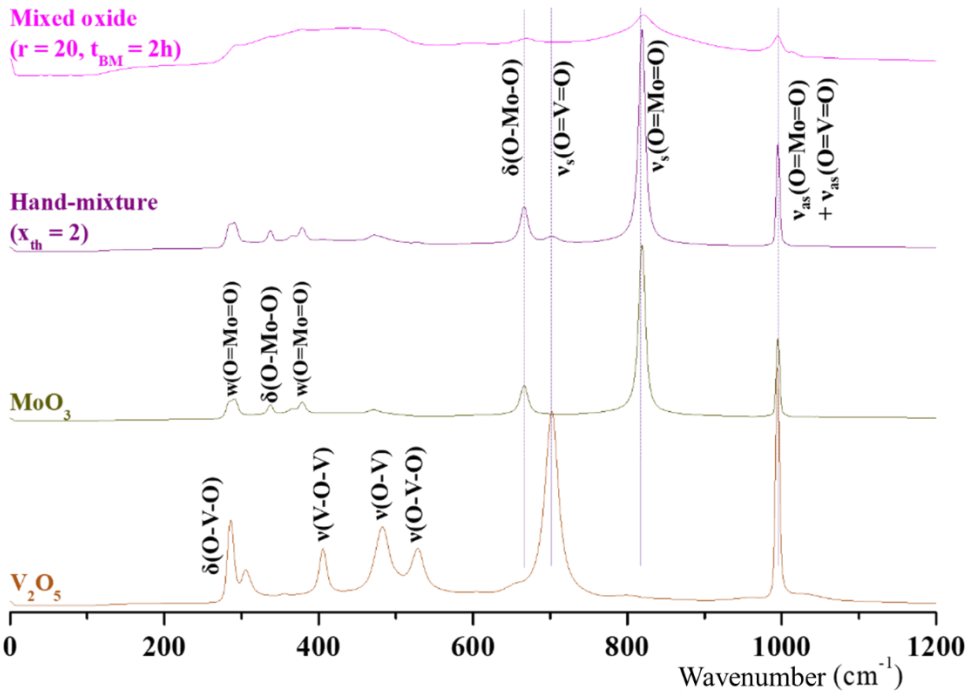

Figure III. 4: Raman spectra of the starting materials and of the mixed oxide precursor of V_2-BM_{20}-2

During the milling step, a color change of the powder from clear brown to dark brown could be observed with the naked eye.

SEM images (magnification x2k - x30k) of the starting oxides (here the precursor of V_2-BM_{20}-2) in the hand mixture after conventional grinding (Fig. III. 5a and c) and of the mixed oxide resulting from the milling step (Fig. III. 5b and d) were also useful to get a better idea of the morphology of the powder grains.

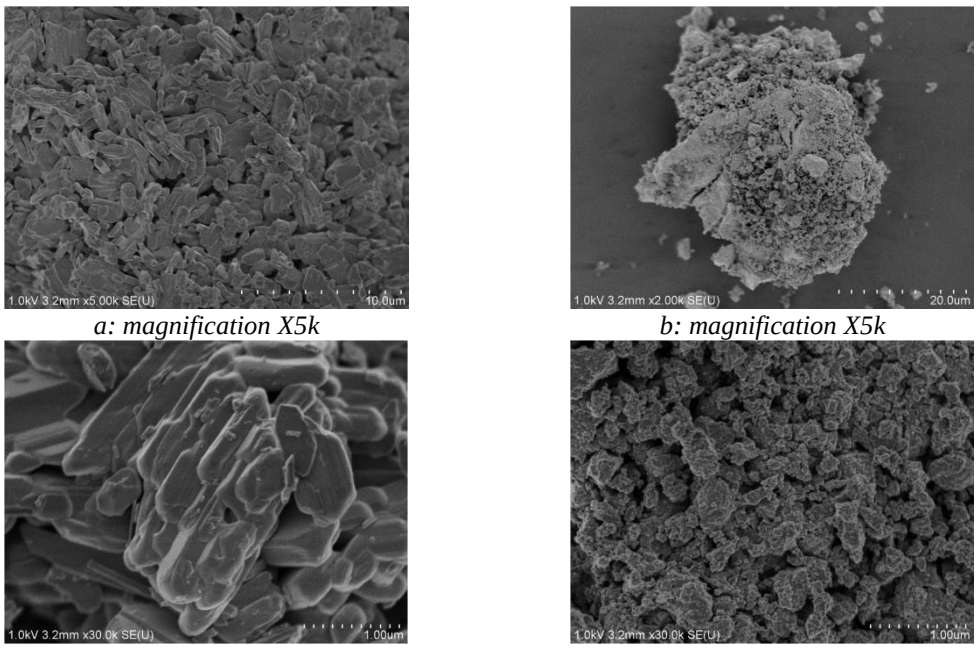

a: magnification X5k *b: magnification X5k*

c: magnification X30k *d: magnification X30k*

Figure III. 5: SEM images of the hand-mixture (left) and of the mixed oxide precursor of V_2-BM_{20}-2 (right). More images are presented on the Appendix (Fig. SIII. 10a-b).

Actually, the hand mixture was composed of smooth particles with quite regular elongated shapes and an average size estimated to 2 x 0.6 µm (Fig. III. 5a / 5c). After the milling step, according to SEM, the grains became less well-defined with more irregular and alveolar surfaces and now look like as an aggregation of small pieces (0.6 x 0.4 µm) on the surface of larger particles (Fig. III. 5b / 5d). Indeed, articles with dimensions from 5 to 35 µm were observed. Ball-milling was expected to give rise to smaller particles as shown by XRD, then, SEM images information could appear to be in contradiction with the XRD data, but it has to be recalled that those later are averaged ones.

The size of the grains of the mixed oxide obtained during V_2-BM_{20}-1-1.5 (blue line) and V_2-BM_{20}-4-1.5 (orange curve) synthesis (with r = 20) was further investigated by granulometry (Fig. III.6) and compared with those of the starting oxides (MoO_3 in green and V_2O_5 in orange) and of their hand-mixture (purple).

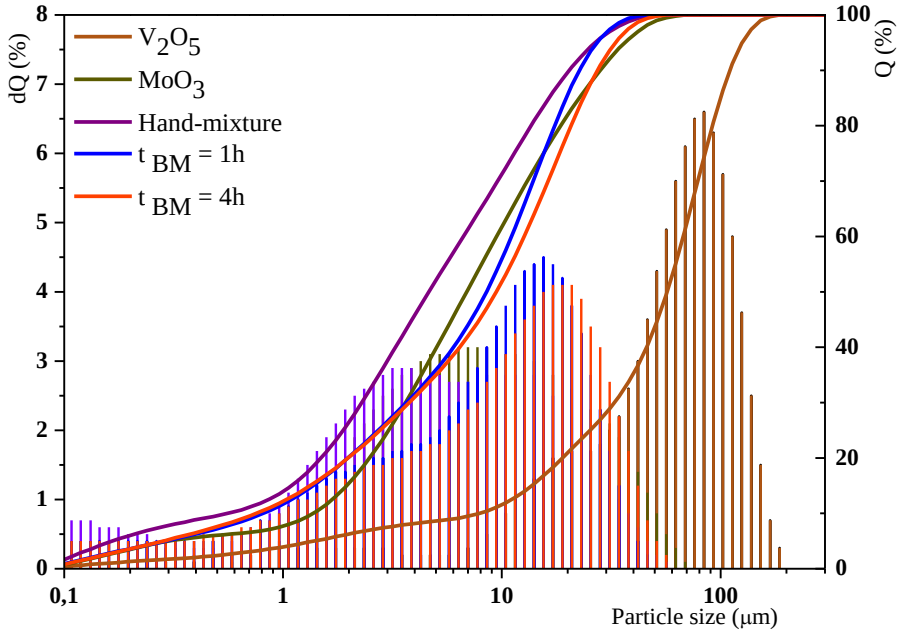

Figure III. 6: Distribution of the grain size in the starting oxides, the hand mixture and the mixed oxide (precursors of V_2-BM_{20} catalysts) by granulometry measurements

At first, it can be noticed that, for starting oxides so as the conventional mixture, the experimental distributions of the particle sizes fit with Gaussian curves.

- The average grain sizes of MoO_3 and V_2O_5 before grinding were around 7 µm and 80 µm respectively.
- Conventional grinding of a mixture of those oxides shifted the distribution curve to less than 1 µm (like MoO_3 alone) with one of the maximum at 3 µm and no more maximum observed at all around 80 µm like for V_2O_5 alone.
- The mixed oxides resulting from both a 1 h and a 4 h ball-milling time (r = 20) were characterized by very similar distributions of the grain sizes meaning that milling duration has almost any influence beyond 1 h. Two well-defined maximum are observed on the distribution curve, respectively at 3 and 15 µm in those cases.

To sum up, RAMAN spectroscopy showed that the solid resulting from the ball-milling step is actually composed of at least two different compounds: MoO_3 and the mixed oxide. Moreover, SEM emphasized the presence of aggregates. So, MoO_3 < mixed oxide < V_2O_5 where < refers to smaller average grain size. The peak at 15 µM (Fig III. 6) is less represented in the distribution of the grain size of the starting oxides and is therefore

characteristic of the mixed oxide. The milling step should have generated smaller particles. However, due to the high temperature during the milling step, the particles agglomerated as observed by SEM analysis and therefore to bigger particles having irregular surfaces.

Nitrogen adsorption-desorption isotherms of the hand-mixture of the oxides (Fig. SIII. 11a), the mixed oxide obtained after 1 h (Fig SIII. 11a-b) and 4 h of milling (Fig. SIII. 11b) were recorded. All of them corresponded to type III isotherms according to IUPAC, meaning that these materials are non-porous or characterized by weak interaction between N_2 and the adsorbent. However, it is noteworthy that the mixed oxides obtained after a short (Fig. SIII. 11a) or a long milling step (Fig. SIII. 11b) adsorb more nitrogen than the hand-mixture of the starting oxides (3.6 vs. 0.8 mmol N_2/g) which should be explained by the raise of the BET surface area after ball-milling (between 5 and 6 m²/g, instead of 1.5 m²/g (Table III. 6)). As ball-milled samples did not show significant hysteresis, such enhancement of nitrogen adsorption would be due to the irregular surface of the particles of the mixed oxide confirming the SEM data (Fig. 5b/5d, right).

Table III. 6: Textural properties of the mixed oxide vs the hand-mixture for x = 2

Sample	**S_{BET} (m^2/g)**	**V_{total} (cm^3/g)**	**V_{BJH} (cm^3/g)**	**V_{micro} (cm^3/g)**	**Av. pore size (nm)**
Hand-mixture	1.5	0.007	0.007	0	18.3
Mixed oxide r = 20, t_{BM} = 1h	5.9	0.037	0.036	0	23.9
Mixed oxide r = 20, t_{BM} = 4h	4.9	0.035	0.0034	0	30.6

All of these features confirm that the mixed oxide is a new compound obtained by the inclusion of V_2O_5 in the structure of MoO_3 and having an enhanced contact thanks to an irregular surface. This may explain the higher efficiency of the ball-milling route for the synthesis of $PMoV_x$.

To conclude, the dry ball-milling route (BM) is a hybrid protocol, which makes it more complicated than the hydrothermal procedure and, sometimes (with r = 20), a long milling step gave rise to a higher energy consumption than the 100% hydrothermal synthetic procedure of V_3-HT. A solution to make it simpler and faster would be to adapt this route for a wet one-pot procedure. In the literature, wet ball-milling proved to be

suitable for the synthesis of nanomaterials [14] and of the mixed oxide V_2MoO_8 [6]. But, to the best of our knowledge, this was not reported for the synthesis of $PMoV_x$.

III. 3.3. One-pot wet ball-milling synthesis of $PMoV_2$

Preliminary essays for a 100% ball milling procedure (no hydrothermal treatment) for $PMoV_2$ synthesis were carried out with the following parameters: r = 20 or 50; t_{BM} = 1 h. In addition to the stoichiometric amount of H_3PO_4, water had to be added in the autoclave (0.4 mL for r = 50 or 1 mL for r = 20). The resulting $PMoV_x$ noted V_2-wBM_{20}-1 and V_2-wBM_{50}-1 were characterized by XRD (Fig. III. 7) before purification, ^{31}P NMR (Fig III. 8) before purification and by TGA (Fig III. 9) after purification (because residual zirconium oxide has to be eliminated).

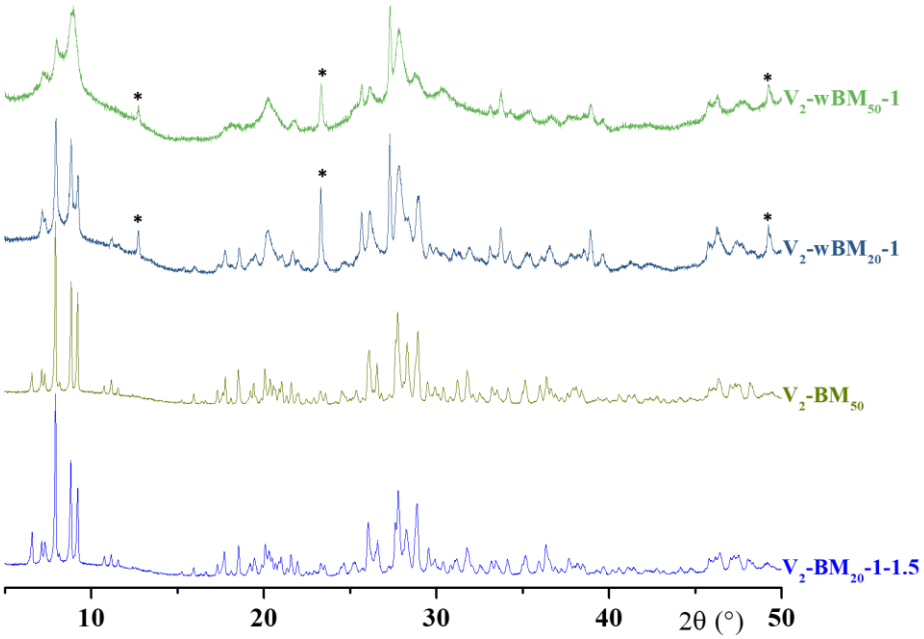

Figure III. 7: X-Ray profiles of the $PMoV_2$ prepared by wet ball-milling vs dry ball-milling synthesis

Clearly, V_2-wBM_{20}-1 and V_2-wBM_{50}-1 materials displayed the characteristic XRD patterns of the KEGGIN structure of polyoxometallates but with broader peaks than those of the reference solids (V_2-BM_{50} and V_2-BM_{20}-1-1.5) co-existing with amorphous phases, especially for V_2-wBM_{50}. Besides, extra narrow peaks at 12.75, 23.30 and 49.24 (see * in Fig. III.8) are present on the XRD profiles of the new materials due to the presence of hydrated zirconium phosphate (JCPDS 01-082-1422) formed by the attack of the zirconium oxide from the balls by phosphoric acid. Already after 1 h of milling, the

zirconium oxide balls started to be destructed. As a consequence, in the future, for r = 20, balls made of other materials more resistant to abrasion as carbon nitride should be preferred.

Liquid ^{31}P NMR studies emphasized the presence of free phosphoric acid in the case of V_2-wBM_{20}-1 probably as the result of a too short milling step. For r = 50, the peak of phosphoric acid was very weak meaning that the reaction would be almost quantitative. Otherwise, the appearance of the V_2-wBM_{20}-1 and V_2-wBM_{50}-1 spectra were found to be quite similar to those of V_2-BM_{50} and V_2-BM_{20}-1-1.5.

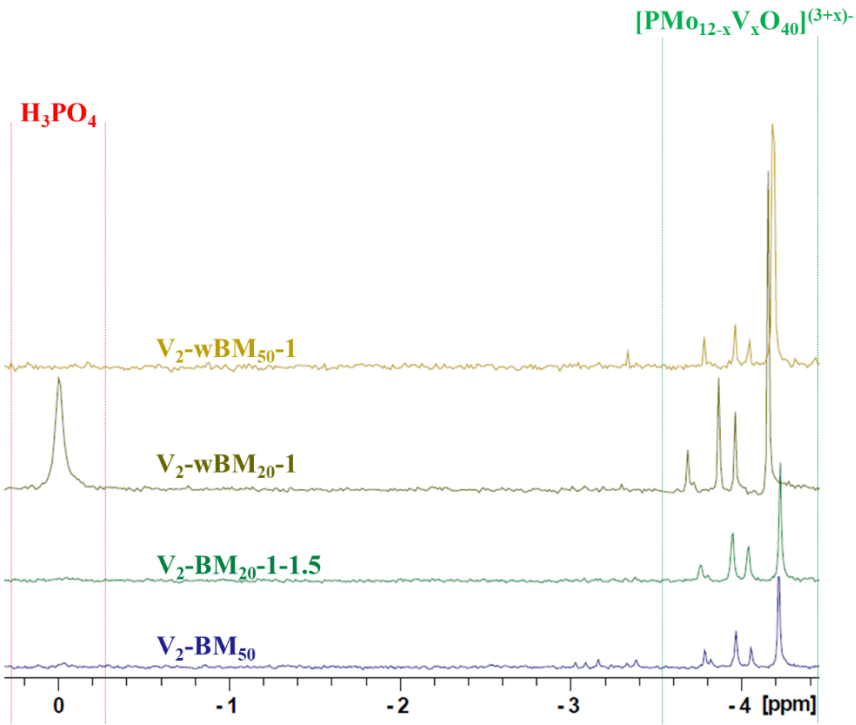

Figure III. 8: ^{31}P NMR spectra of the $PMoV_2$ prepared by wet ball-milling vs dry ball-milling synthesis

Then, it has also to be noted that, in the TGA profiles, the second weight loss (at T_2 = 448.5°C, due to constitutive water) of the V_2-wBM_{20}-1 obtained by wet and dry ball-milling took place at similar temperatures.

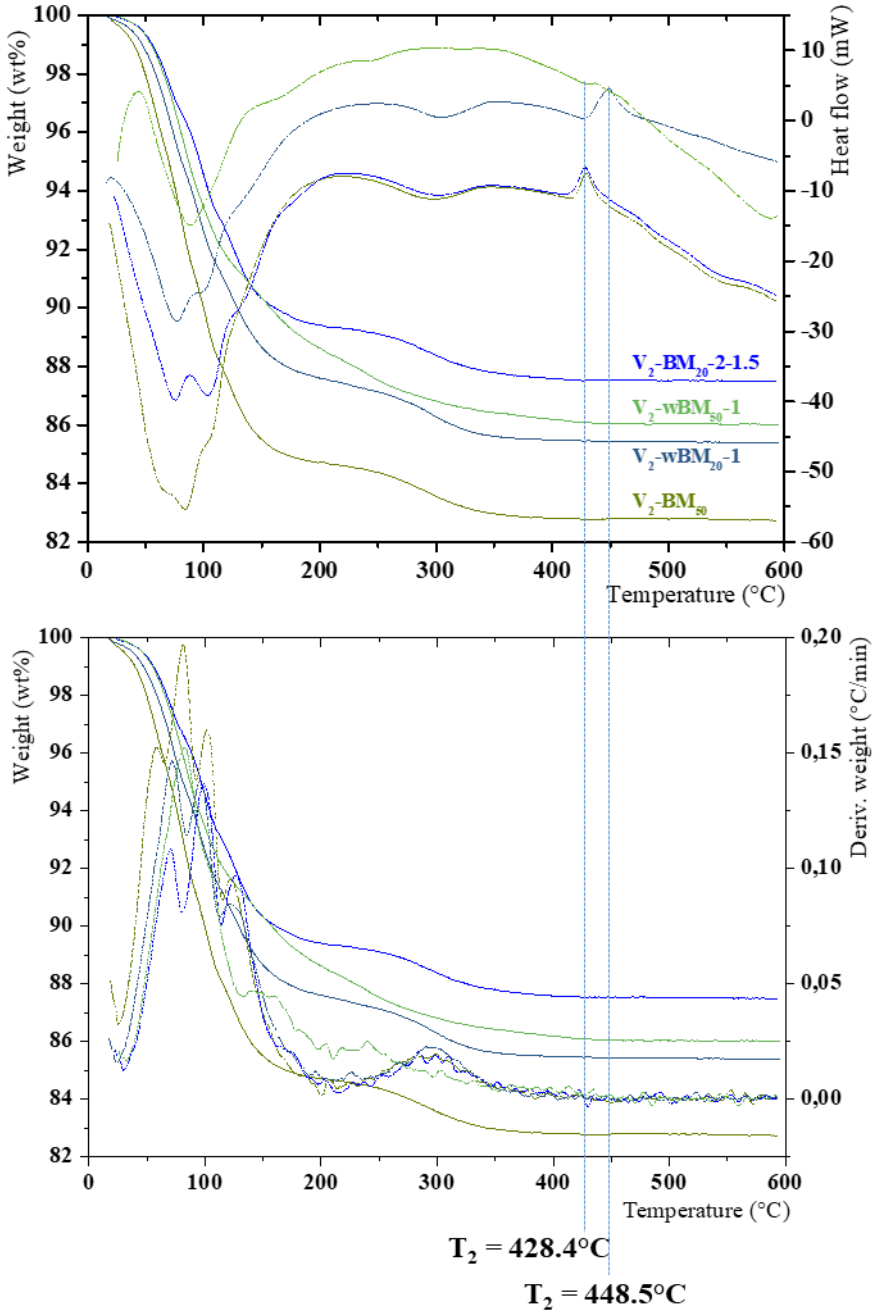

Figure III. 9: TGA-DSC profiles of the $PMoV_2$ prepared by wet ball-milling vs dry ball-milling synthesis

The TGA-DSC profile of V_2-wBM_{50}-1 seemed to be different from the others, meaning that there might be some zirconium oxide even after purification by centrifugation.

This procedure consists in performing a milling step of 1 h and then, the obtained $PMoV_x$ had to be purified by centrifugation at 7500 rpm during 10 min. The required power for the centrifugation (Eppendorf Centrifuge 5804 R, P_{max} = 1650 W) is calculated

using Eq SIII. 2. The global required power is 229 kW.h/mol. The synthesis of $PMoV_x$ using a 100% ball-milling procedure is more energy-saving than the hydrothermal procedure for V_3-HT synthesis (618 kW.h/mol) and V_2-BM_{50} synthesis (422 kW.h/mol) in spite of the centrifugation step needed to eliminate the zirconium oxide.

III. 4. Aerobic cleavage of the dimeric lignin models **K1**$_{HH}$ and **A1**$_{HH}$

Here, the KEGGIN $PMoV_x$ synthesized by a hybrid ball-milling / hydrothermal procedure will be compared to reference V_1-HT and V_3-HT for **K1**$_{HH}$ cleavage. The chosen operative conditions were defined from our previous work (see II. 4.1). Then, the V_3-HT and V_3-BM_{50} will be compared for **A1**$_{HH}$ cleavage

III. 4.1. **K1**$_{HH}$ cleavage

K1$_{HH}$ cleavage (Fig. III. 10) was used as a reference test in order to investigate the catalytic activity of all the $PMoV_x$ materials prepared following the hybrid procedure (BM). The reaction was performed in acetonitrile/acetic acid 90/10 during 24 h at 82°C with Mo + V 18 mol% under atmospheric pressure of O_2.

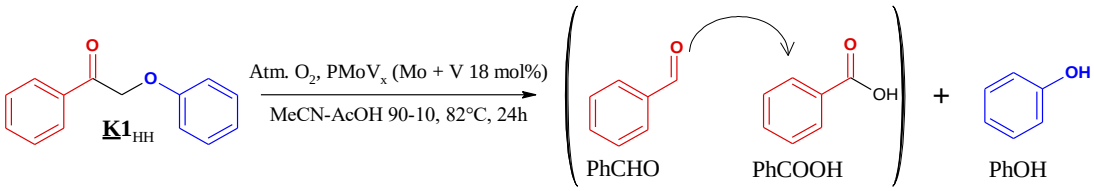

*Figure III. 10: Targeted products from **K1**$_{HH}$ aerobic oxidative cleavage in presence of $PMoV_x$ catalysts*

As in part II, the goal of our work was to maximize the yield of phenol from C-O cleavage, as well as of benzaldehyde and benzoic acid from C-C cleavage (Table III. 7).

The catalytic activity of the materials of the first series (r = 50) was compared to that of V_1-HT and V_3-HT (Table III.7, entries 1-5). At first sight, it could be noted that results of the tests carried out with the V_3 materials (Table III. 7, entries 2 and 4) showed strong similarities with, on average, 77% conversion *(standard deviation of 1.4%)*, yields of 38% *(standard deviation of 0%)* in phenol, 15.5% *(standard deviation of 0.7%)* in benzaldehyde and 31% *(standard deviation of 1.4%)* in benzoic acid, the carbon balance

being equal to 68% *(standard deviation of 7%, CB_{max} = 95%)*[2]. Slightly larger differences were found between V_1-type materials that could be attributed to experimental errors. On average, V_1 catalysts (Table III. 7, entries 1 and 3) would lead to 74.5% conversion *(standard deviation of 7.8%)*, yields of 46.5% *(standard deviation of 16%)* to phenol, 21.5% *(standard deviation of 7.8%)* to benzaldehyde and 38.5% *(standard deviation of 4.9%)* to benzoic acid, the material balance being 73% *(standard deviation of 2.8%, CB_{max} = 95%)*. As for the V_2 catalyst series, only one was synthesized (V_2-BM_{50}) and led, under the same reaction conditions as V_1 and V_3 materials, to 84% conversion, yields of 54% in phenol, 19% in benzaldehyde and 49% in benzoic acid, the material balance being equal to 62% (CB_{max} = 94%). Considering only the series of materials from V_1 to V_3 prepared by ball milling (Table III.7, entries 3-5) or including materials prepared by the 100% hydrothermal route (Table III.7, entries 1-2), it appears that one of the best catalysts was V_2-BM_{50}. Indeed, the conversion and yield of cleavage products were high while keeping a good carbon balance. $PMoV_3$ catalysts may be less stable than $PMoV_2$ and so may deactivate earlier.

It is noteworthy that the tests carried out with the V_2-BM_{20} series of materials (Table III.7, entries 6-13) led on average to a conversion of **<u>K1</u>**$_{HH}$ at 24 h of *c.a.* 77% *(standard deviation of 3.8%)* with a phenol yield of 51% *(standard deviation of 9.6%)*, a benzaldehyde yield of 13.5% *(standard deviation of 5.1%)* and a benzoic acid yield of 39% *(standard deviation of 4.4%)*. The mean value of the carbon balance was equal to 71% *(standard deviation of 4.5%)*. Such results imply that, on average, the materials of the second series prepared with r = 20 are slightly less efficient than V_2-BM_{50}. Among the solids in the second series, some seem to stand out, with lower conversion values (70% for V_2-BM-2-1.5) or phenol deficiencies probably due to over-oxidation (42% for V_2-BM-1-3 or even 37% for V_2-BM-2-3). However, this difference is rather low because of the similarities between V_2-BM_{20} and V_2-BM_{50} as shown by ^{31}P NMR. Yet, the catalysts obtained after long milling and attack steps seemed to be more selective for C-O cleavage. These catalysts have generally (except V_2-BM_{20}-2x2-3) a lower amount of

[2] In the case of V_3-HT (Table III.7, entry 2), one of the catalyst, contaminated with H_3PO_4, the experimental loading of H_3PO_4 was only 0.31 mol% which is too low to have any significant influence on the activity of the catalyst.

isomers having vicinal vanadium atoms and so are less reactive and therefore as less active for oxidative C-C cleavage (Table SIII. 1).

This can be explained by the similarities between V_2-BM_{20} and V_2-BM_{50} catalysts as shown by NMR. Yet, ^{31}P NMR analysis did not show that V_2-BM_{20} from a long milling-step are not significantly richer than the others V_2-BM_{20} in a certain isomer. So, more research is needed.

Whatever the series of materials, the O_2 consumption per mol of **K1**$_{HH}$ converted was about 1.3. So, the mechanism is likely not impacted neither by the synthetic route of the PMoV$_x$, nor the value of x (see II. 4. 3).

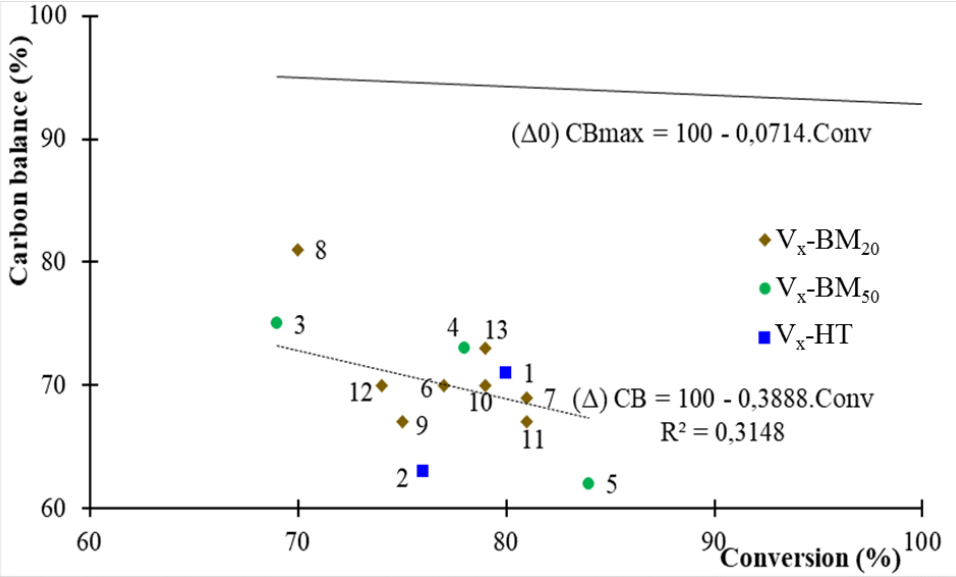

*Figure III. 11: Carbon balance versus **K1**$_{HH}$ in presence of V_x-HT (entries 1-2), V_x-BM_{50} (entries 3-5) and V_x-BM_{20} (entries 6-13) catalysts*

The evolution of carbon balance in function of conversion is given. Nevertheless, a trend cannot be given here as the regression coefficient R^2 is low (0.3148, see Fig III. 11). As on II. 4.2, a raise of the conversion leads to a decrease of carbon balance and to an increase of the gap between the theoretical carbon balance (CB_{max}, materialized by the line (Δ_0)) and the experimental mass balance (dashed line (Δ)).

*Table III. 7: Aerobic cleavage of **K1**$_{HH}$ in presence of $PMoV_x$ from hydrothermal and mixed ball-milling/hydrothermal pathway*

Entry	Catalyst	Conv. (%)	Yield (%) PhOH	Yield (%) C-C cleavage PhCHO	Yield (%) C-C cleavage PhCOOH	Carbon balance[a] (%)	Maximal carbon balance[b] (%)	Oxygen consumption /mol converted **K1**$_{HH}$	$\frac{n_{PhCHO}+n_{PhCOOH}}{n_{PhOH}}$
1	V_1-HT	80	58	27	35	71	94	1.4	1.1
2	V_3-HT	76	38	15	30	63	95	1.3	1.2
3	V_1-BM_{50}	69	35	16	42	75	95	1.4	1.7
4	V_3-BM_{50}	78	38	16	32	73	94	1.3	1.3
5	V_2-BM_{50}	84	54	19	49	62	94	1.1	1.3
6	V_2-BM_{20}-1-1.5	77	48	14	38	70	95	1.4	1.1
7	V_2-BM_{20}-1-3	81	42	17	47	69	94	1.3	1.5
8	V_2-BM_{20}-2-1.5	70	57	23	31	81	95	1.5	0.9
9	V_2-BM_{20}-2-3	75	37	15	38	67	95	1.3	1.4
10	V_2-BM_{20}-4-1.5	79	52	12	41	70	94	1.2	1.0
11	V_2-BM_{20}-4-3	81	59	7	39	67	94	1.3	0.8
12	V_2-BM_{20}-2x2-1.5	74	45	12	37	70	95	1.2	1.1
13	V_2-BM_{20}-2x2-3	79	66	8	40	73	94	1.2	0.7

K1$_{HH}$ 100 mM, Atm. O_2, Mo + V 18 mol%, MeCN – 10 vol% AcOH, 82°C, 24 h [a] $CB = \frac{6\eta_{PhOH}+7(\eta_{PhCHO}+\eta_{PhCOOH})+14(100-Conv)}{14}$; [b] $CB_{max} = 100 - \frac{Conv}{14}$

*Table III. 8: Aerobic oxidative cleavage of **A1**$_{HH}$ in presence of V_3-HT or V_3-BM_{50}*

Entry	Catalyst	Conv. (%)	Yield (%) PhOH	Yield (%) C-C cleavage PhCHO	Yield (%) C-C cleavage PhCOOH	Yield (%) Dimeric by-products **K1**$_{HH}$	Yield (%) Dimeric by-products **Est**[a]**A1**$_{HH}$	Yield (%) Dimeric by-products **D1**$_{HH}$	Carbon balance [a](%)	$\frac{n_{PhCHO}+n_{PhCOOH}}{n_{PhOH}}$	Selectivity in monomers (%) C-O cleavage[b]	Selectivity in monomers (%) C-C cleavage[c]
14	V_3-HT	33	3.6	2.9	3.5	8.7	9.9	10	100	1.8	11	19
15	V_3-BM_{50}	33	4.5	2.2	3.6	9.2	6.7	10	98	1.3	14	18

A1$_{HH}$ 100 mM, O_2 5 bar, MeCN – 10 vol% AcOH 82°C

[a] $CB = \frac{6\eta_{PhOH}+7(\eta_{PhCHO}+\eta_{PhCOOH})+14(100-Conv)}{14}$; [b] $Sel(C-C\ cleavage) = \frac{\eta_{PhCHO}+\eta_{PhCOOH}}{Conv}$; [c] $Sel(C-O\ cleavage) = \frac{\eta_{PhOH}}{Conv}$

III. 4.2. A1HH cleavage

Some tests were also carried out on a model closer to lignin, **A1**$_{HH}$ using V_3-HT (Table III. 8, entry 14) and V_3-BM_{50} (entry 15) catalysts in acetonitrile/acetic acid 90/10 during 6 h at 82°C with Mo + V 15 mol% under 5 bar of O_2 (Fig III. 12). As shown in part II (II. 5 and II. 6), due to the presence of the alcohol functionality, three additional side reactions: dehydration (**D1**$_{HH}$ product), esterification by acetic acid (**Est$^{\alpha}$A1**$_{HH}$ product) and alcohol oxidation into ketone **K1**$_{HH}$ also occur.

The ball-milling derived catalyst V_3-BM_{50} (entry 15) exhibited similar activity (33% conversion for both catalysts) and selectivity (C-O cleavage : 14 *vs* 11% and C-C cleavage : 18 *vs* 19%) compared to V_3-HT (entry 14). Yet, the formation of **Est$^{\alpha}$A1**$_{HH}$ took place but to slightly lower extent (6.7 vs 9.9%) whereas **K1**$_{HH}$ yield increased slightly (9.2 vs 7.1%). This might be due to the presence of a lower amount of phosphoric acid that boost the esterification (H_3PO_4 loading = 0.8 mol% in presence of V_3-BM_{50} *vs* 3.6 mol% in presence of V_3-HT). Generally, there is no carbon loss as the minimal carbon balance in presence of V_3-HT was 100% (entry 14) and 98% in presence V_3-BM_{50} (entry 15).

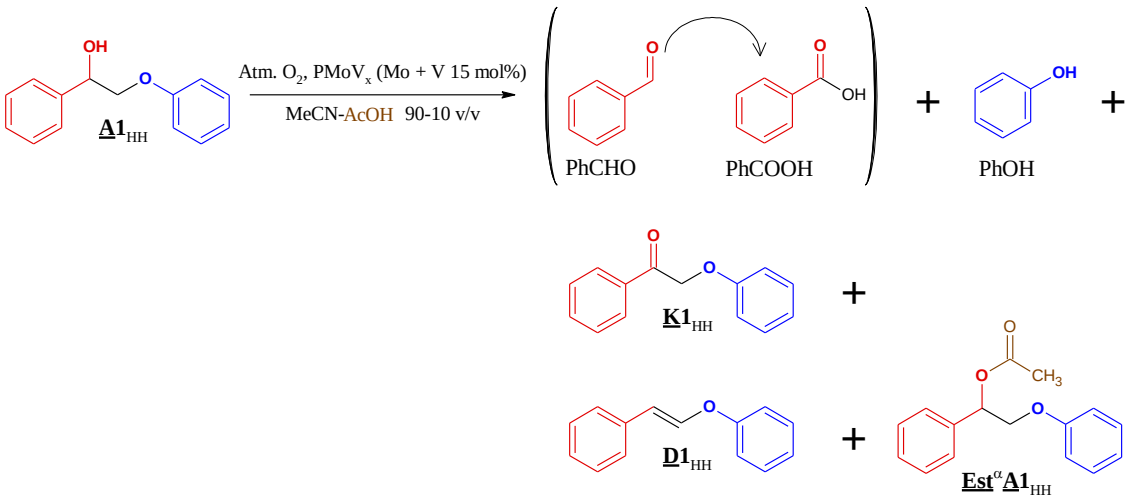

*Figure III. 12: Products from the **A1**$_{HH}$ aerobic cleavage catalyzed by $PMoV_3$*

III. 5. Preliminary tests of aerobic cleavage of a wheat straw lignin

On the basis of results from lignin dimeric model catalytic cleavage, preliminary tests are carried out on an Organosolv Wheat straw lignin. As a strong oxidant will be needed, a $PMoV_x$ with a high amount of vanadium will be preffered. As ball-milling (for

r = 50) is more energy-saving than the hydrothermal procedure, V_3-BM_{50} will be used as the catalyst for lignin aerobic cleavage.

III. 5.1. Characterization of the lignin used

Wheat straw Organosolv lignin extracted according to the patent FR 8551747 [17] was used in this work. The main advantage of this lignin compared to others (technical lignins such as kraft lignin and lignosulfonates, see IA. 2.1) is the absence of sulphur. Indeed, this element may involve safety problems (bad smell, caustic wastes…), may poison the catalysts [18] and has to be eliminated during the depolymerization. Another advantage of Organosolv lignin is that it should contain more β-O-4 bonds than technical lignins and so, it should be less recalcitrant to oxidation, which should facilitate aromatic platform molecules production. Indeed, Organosolv lignin is extracted in softer conditions which should avoid the formation of recalcitrant C-C bonds [19] during the extraction process.

The Organosolv Wheat straw lignin, noted WSLi, as it is produced by the extraction process, still contains residual saccharides (δ = 5-5.3 ppm) and fatty acids (δ = 5.4 ppm) as shown by ^{1}H NMR (Fig III. 13) as well as acetic and formic used in the extraction process. Narrow peaks correspond to low-molecular weight compounds such as *p*-coumaric and ferulic acids. Furthermore, due to the extraction process, the alcohol functions present in lignin are partly esterified by the organic acids.

As mentioned in the experimental part (III. 2.3), WSLi had to be purified by saponification affording WSLh (after acidification) followed by an extraction treatment with lipophilic organic solvents affording WSlp [20]. The aim was to cleave the ester and ether linkages between lignin and the saccharides from hemicellulose, then to get rid of the fatty acids. On each step, lignin was characterized by ^{1}H NMR (400 MHz) in DMSO (Fig. III. 14).

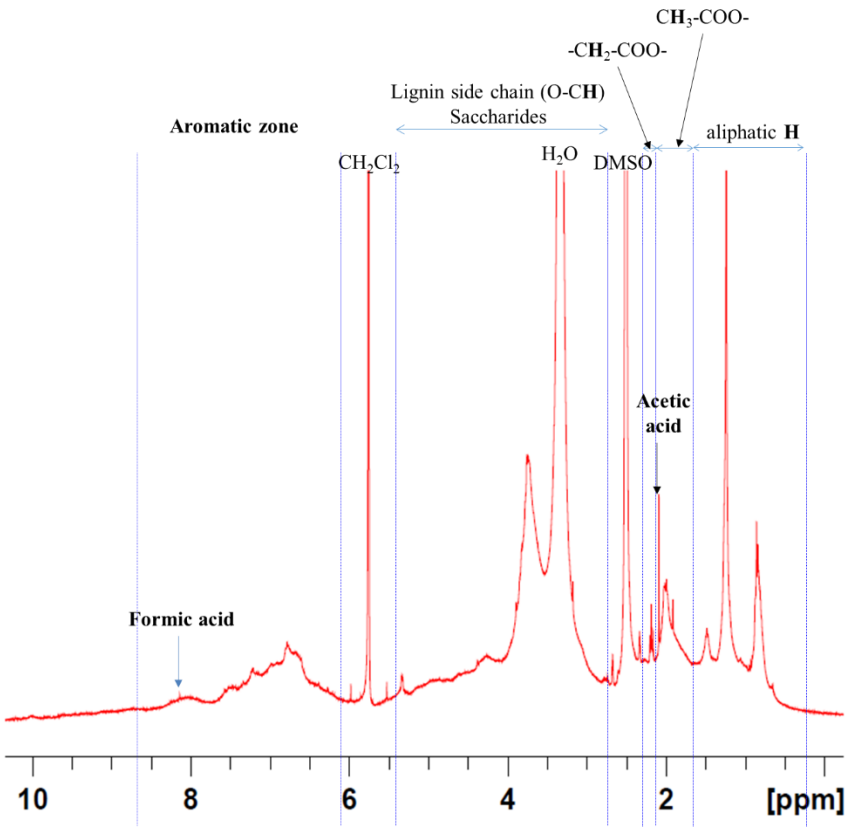

Figure III. 13: ^{1}H NMR (DMSO-d^6, 400 MHz) spectrum of the wheat straw lignin (WSL_i) before purification

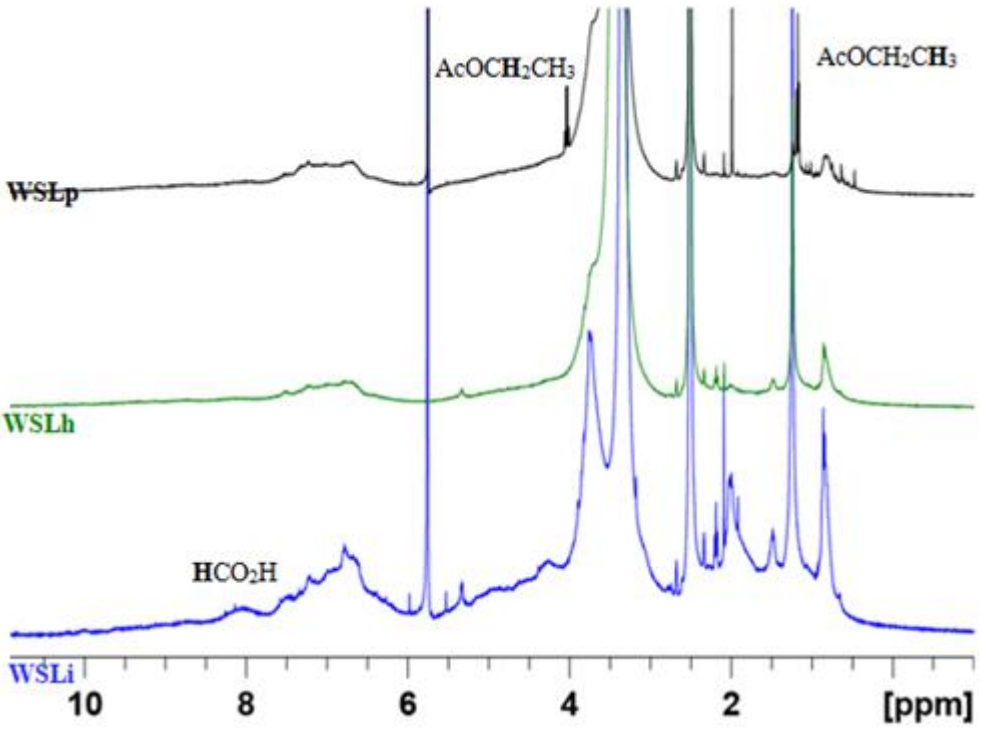

Figure III. 14: Evolution of ^{1}H NMR spectra of lignin during the purification procedure

The proportions of the different components were estimated from the above-mentioned ^{1}H NMR spectra (Table III. 9). In the case of the estimation of methoxy groups, as the corresponding peak coalesced with the peak of water (Fig III. 14), a ^{1}H NMR analysis in NaOD 1 M in water was carried out.

Table III. 9: Proportion of functional groups in lignin estimated by ^{1}H NMR during the purification steps

Function	Chemical shift (ppm)	WSLi	WSLp
Aromatics[a]	7.8-6.5	16	22
Saccharides and lignin side chains[a]	4.6-3.4	14	14
Methoxy groups in lignin[b]	4.0-3.4	29	36
Acids and esters[a]	2.2-1.7	13	14
Aliphatics[a]	1.7-0.8	27	13

[a]Estimated by NMR in DMSO-d^6 ; [b]Estimated by NMR in NaOD 1 M in D_2O

Saponification enabled to eliminate the hydrophilic impurities as residual sugars (5.3-5.5 ppm), the carboxylic acids (8.1 and 1.8-2.1 ppm) and some light compounds. Indeed, the spectrum of WSL_h displayed already much fewer narrow peaks (low molecular weight compounds) in the region of the aromatic signals and the integration in the region of the signals attributed to saccharides decreased (4.6-3.4 ppm). Washing treatment of WSLh by organic solvents (CH_2Cl_2 and ethyl acetate) showed to be able to eliminate the last traces of sugars and hydrophobic impurities (decrease of the signals in the aliphatic region from 27% in WSL_i to 13% in WSL_i). This is confirmed by the variation of the proportions of the different functions. The proportion of methoxy groups in lignin raised from 29 to 36%. The relative integration in the zone of the saccharides and lignin side chains and of acids and esters did not change in the end. The proportion of aromatics raise a little, but less significantly than methoxy groups as aromatic monomers were eliminated [20]. In the end, the spectrum of WSLp should be composed of only broad peaks corresponding to polymeric species.

Another important characterization of lignin consists in the quantification of its different types of OH groups *i.e.* the aliphatic ones, phenolic ones (with a possible distinction between those of G, H and S units) and carboxylic ones. Since the work of ARGYROPOULOS and GRANATA (see Appendix *Lignin phosphorylation*), an elegant way to achieve this is based on the phosphorylation of all OH groups in lignin with 2-chloro-4,4,5,5-tetramethyl-1,3,2-dioxaphospholane (Aldrich, 95%) and, then the

quantification of the different resulting P species by ^{31}P NMR [12] (see *e.g.* the spectrum of the phosphorylated WSLp sample, Fig. III. 15). It has to be noted that this method allows indirectly the determination of the proportions of the H, G and S units of lignin too.

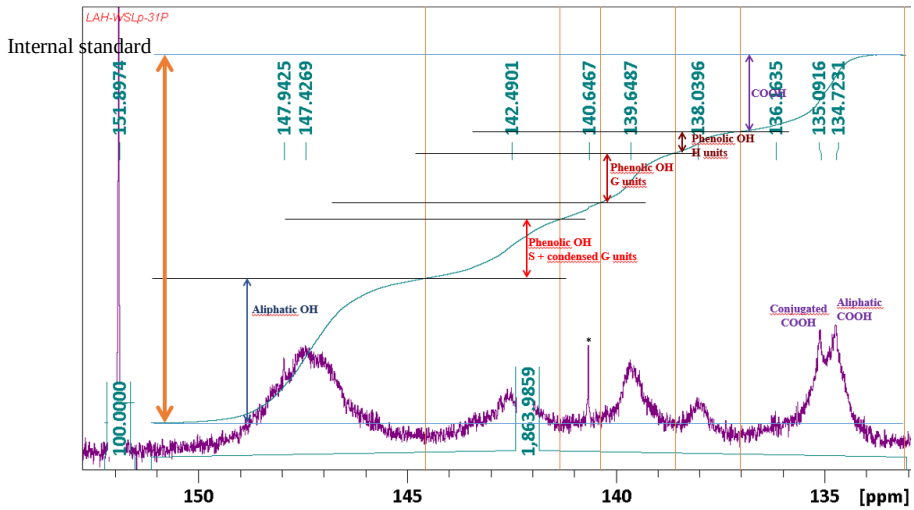

Figure III. 15: Division of the interesting region of the 31P NMR spectrum of phosphorylated lignin for the quantification of the different types of OH groups (The internal standard was N-hydroxy-6-norbornene-2,3-dicarboximide)

The interesting signals, *i.e.* those of phosphorylated lignin, are located in the 130-150 ppm region (Fig. III. 15, see also their attribution in Table SIII. 4).

The evolution of the OH distribution from WSLi to WSLp (Table III.10) shows that the the purification led to a small increase of the total OH content that hides a stronger increase of the carboxylic groups (+0.65 mmol/g) due to the saponification of esters whereas OH groups from H, G, S units and aliphatic alcohols decreased (0.41mmol/g in total). Such observations may be understood as the result of the removal of low molecular weight aromatic molecules and oligomeric compounds that were chemically bond to the carboxylic acid function present in lignin. In WSLp, the proportion of monomers is assimilated to the proportions of phenolic OH functions, *i.e.* the H/G/S is equal to 17/38/45.

Table III. 10: Proportion of OH functions in lignin before and after purification

Lignin sample	Total OH (mmol/g)	Aliphatic OH (mmol/g)	Phenolic OH (mmol/g)			COOH (mmol/g)
			H	Uncondensed G	S + Condensed G	
WSLi	4.53	2.08	0.38	0.77	0.90	0.40
WSLp	4.78	1.96	0.29	0.67	0.80	1.05
Variation	+0.25	-0.12	-0.09	-0.1	-0.1	+0.65

III. 5.2. Aerobic oxidative cleavage of lignin

In the continuity of what was presented before for the models (III. 4. 2), we have sought to introduce, in the lignin cleavage tests, as many β-O-4 bonds as there were in the tests performed on **A1**$_{HH}$ **(**100 mM). So, the adequate weight of lignin had to be calculated assuming that, WSLp is essentially constituted of β-O-4 bonds, the others such as β-5 and 5-5 linkages, being neglected[3].

The catalytic tests were performed directly under 5 bars of O_2 (measured at R.T.) at 80°C since lignin is more inert than **A1**$_{HH}$. Furthermore, some of them were carried out at higher temperature too (120°C) while shortening the duration (2 h instead of 6 h) to maintain a high carbon balance. The targeted oxidative cleavage reaction is described below (Fig. III. 16).

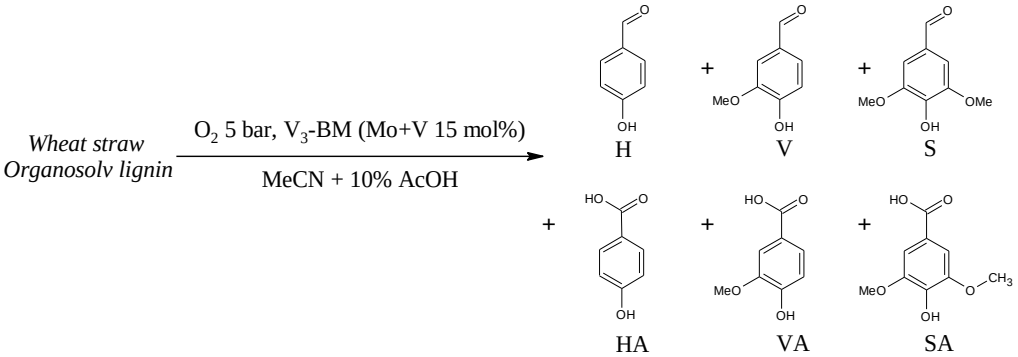

Figure III. 16: Aerobic oxidative cleavage of WSLp catalyzed by V_3-BM_{50}

The aromatic aldehydes noted H, V and S were effectively detected by GC-MS (Table III. 11). However, the expected phenolic acids were barely not detected by GC-MS as shown on Table III. 11. Since they are not stable at high temperature and tend to undergo a decarboxylation reaction [21], the reaction mixture had to be treated overnight by an excess of N,O-Bis(trimethylsilyl)trifluoroacetamide (BSTFA) for quantification of the trimethylsilyl derivatives by GC-MS. Alcohols and acids are both transformed. In some cases (120°C, 2 h) the reaction media was injected without silylation to check the presence of by-products such as 2,6-DMBQ or acetosyringone. The retention time of the main oxidation products identified is given in Table III. 11.

[3] The molecular weight of the average dimeric unit ($C_{18}H_{16.2}O_5(CH_3)_{1.3}$ was estimated at 364.7 g/mol from ^{31}P NMR data

The GC-MS analyses of the reaction media before silylation showed also the formation of *p*-quinones derivatives such as 2,6-DMBQ (19.66 min) which are products of C(Ar)-C cleavage as shown in Fig. III. 17. Such reaction can take place due to the presence of phenolic functions in the para position of C(Ar)-C bonds. Indeed, such products were not observed in the case of the oxidative cleavage of the non-phenolic dimeric models, especially for **A1**$_{HH}$. The phenol moiety would be firstly transformed into a quinone methide intermediate.

Table III. 11: List of V_3-BM_{50} catalyzed lignin aerobic oxidative cleavage detected by GC-MS

RT (min)	Compound (Match%)	GC-MS area (/vanillin)	Structure	Comments
4.01	*p*-quinone (83%)	0.03	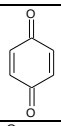	From C(Ar)-C cleavage
11.3	methoxy-*p*-quinone	0.36	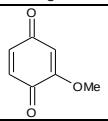	Supposed from MS data
14.25	*p*-hydroxybenzaldeyde (H) (97%)	0.28	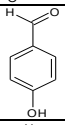	From C^{α}-C^{β} cleavage
15.3	Vanillin (V) (97%)	1	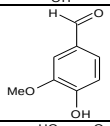	From C^{α}-C^{β} cleavage
19.54	Vanillic acid (VA)	0.05	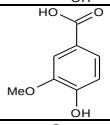	From C^{α}-C^{β} cleavage
19.66	2,6-dimethoxybenzoquinone (2,6-DMBQ) (92%)	1.3	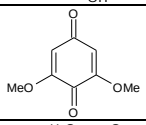	From C(Ar)-C cleavage
20.06	Acetovanillone (84%)	0.3	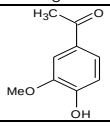	From C^{β}-O cleavage

Lignin 0.854 g, V_3-BM_{50} (Mo + V 15 mol%), O_2 5 bar, 120°C, 6 h (Table III. 13, entry 4)

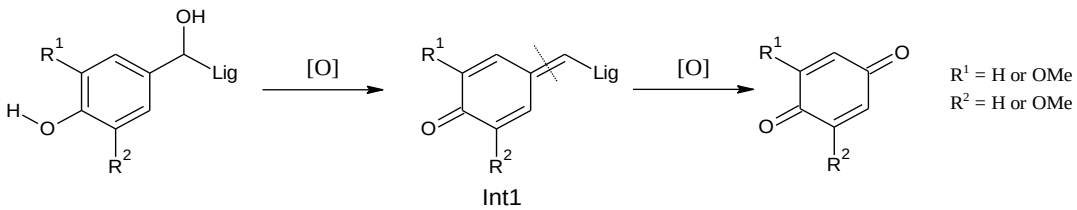

Figure III. 17: C(Ar)-C cleavage in lignin leading to p-quinones derivatives

In addition, acetovanillone (20.06 min) was produced. It is originated from a non-oxidative C-O cleavage, accelerated by the acidity brought by the catalyst.

The yields of the targeted soluble products, determined by GC-MS (Table III. 12 et SIII. 14) were rather low with a sum for H, HA, V, VA , S and SA (expressed in mol%[4]) lower than 3% in the best case 120°C, 6 h, Table III.12, entry 4). On one hand, a high temperature proved to be required for lignin aerobic cleavage since, for T = 80°C (Table III. 12, entry 1), the yields of those soluble aldehydes and acids proved to be extremely low (maximum 0.7% for V). On the other hand, the catalyst turned out to be necessary for lignin aerobic cleavage (Table III. 12, entries 2 vs. 3) since V, VA and HA monomers were not detected after 2 h at 120°C in the absence of V_3-BM_{50}. Moreover, the extent of lignin dissolution is rather unchanged by the catalyst. The temperature did not seem to have any influence (Table III. 12, entries 1 vs 4). At 120°C, the duration had a positive impact on the yield of cleavage products (Table III.12, entries 2 vs 4).

Table III. 12: Results of V_3-BM_{50} catalyzed lignin aerobic cleavage

Entry	T (°C)	t (h)	Lignin dissolution (wt%)	Liquid phase (GC-MS after silylation) Yield of monomers (mol%)[b]						Residual lignin (^{31}P NMR) Function ratio	Monomer type proportions[b]		
				Units H		Units G		Units S					
				H	HA	V	VA	S	SA	Aliph/ArOH/COOH	H	G	S
1	80	6	0	0.2	0	0.3	0	0.1	0	n. d.	n. d.	n. d.	n. d.
2	120	2	9	0.4	0.1	1.2	0.3	0.2	0	40/30/30	16	36	48
3[a]	120	2	9	0	0	0.1	0	0.2	0	39/21/40	12	38	50
4	120	6	10	0.6	0.3	0.7	0.4	0.3	0	n. d.	n. d.	n. d.	n. d.
WSL_p	-	-	-	-	-	-	-	-	-	36/40/24	16	38	46

WSL_p 0.854 g ; V_3-BM_{50} (Mo + V 15.9 mol% according dimeric units) ; stirring by a magnet ; [a]Without catalyst, [b]According to moles of each monomer type calculated from ^{31}P NMR data (entry WSL_p)

One reason to explain the low yields of the expected monomers would be related to the esterification of the alcohol functions during the reaction as for **A1**$_{HH}$ cleavage. Indeed, it can be noticed that the fractions of phenolic OH functions (21 *vs* 40%) decreased in the run performed without the V_3BM_{50} catalyst (Table III. 12, entry 3). This may mean that, in the absence of oxidation, esterification took place at a significant extent. The distribution of H (46-50%), G (36-38%) and S (12-16%) monomers was rather unchanged, meaning that the different monomers had similar reactivities.

The temperature has a positive impact on lignin solubilization (Table III. 12, entries 1 vs 2-3). Indeed, at 120°C, the dissolution was maximized, even without catalyst.

[4] The quantity of monomeric units is 5 mmol, so the quantity of H, G and S monomers (see entry WSL_p, Table III. 13) is 0.16 x 5 = 0.8 mmol of H, 0.38 x 5 = 1.9 mmol of G and 0.46 x 5 = 2.3 mmol of S.

However, the dissolution is too high to be due to monomers only. Consequently, the enhanced solubility may be due to soluble oligomers formation.

It should also be noted that lignin is almost insoluble under the conditions used. In addition to the analysis of the products in solution, we have also focused our attention on the characterization of the insoluble fraction of lignin by applying the same techniques as those described in III.5.1. As evocated in the experimental part, the lignin sample treated at 120°C (Table III. 12, entry 2) had to be analyzed in NaOD 1 M in D_2O instead of DMSO because the solubility in DMSO plummeted from 100% to 10% only. As mentioned before, a partial esterification of lignin by acetic acid may have occurred that might influence the solubility of the lignin sample in DMSO. However, such sample should be very soluble in THF (usual solvent for SEC analysis of acetylated lignin).

SEC analysis is suitable for the estimation of the average molecular weight of lignin before and after the oxidative cleavage test. Usually, acetylation of lignin in the presence of acetic anhydride in excess enables to dissolve WSLp in THF but the same procedure applied to $WSLp^{ox}$ showed that the lignin recovered from the 2 h test in MeCN/AcOH (9/1) at 120°C under 5 bar of O_2 (Table III. 12, entry 2) became almost totally unsoluble. Hopefully, lignin samples issued from the test at 80°C during 6 h (Table III.12, entry 1) had an intermediate behavior. They may be not totally soluble in THF unlike the WSLp, but it is much more soluble than the lignin treated at higher temperature.

Another, more plausible explanation of the low solubility of lignin in DMSO and acetylated lignin in THF would be related to other phenomena such as condensation reactions which could explain that lignin treated at 120°C has a structure much more different to that of the initial lignin compared to that of the samples treated at lower temperature [23]. As the oxidized lignin contains less phenolic groups (^{31}P NMR analysis (Table III. 12, entry 2)), this may be explained by a higher reactivity of phenol moieties [24] that can be oxidized into quinone methide groups (see Fig. III. 17). Such reaction should initiate oxidative condensation, which leads to unsoluble and less reactive polymerized lignin formation [25-26].

Furthermore, the cleavage of lignin also generates formaldehyde from CH_2OH groups that can be at the origin of condensation reactions, leading to diphenylmethane functions that are recalcitrant to cleavage and have a negative impact on lignin cleavage [23]. In brief, an oxidative treatment at high temperature leads to a lignin recalcitrant to

cleavage and much less soluble in conventional solvents in spite of treatment by acetic anhydride because of oxidative condensation.

Lignin ($WSLp^{ox}$) recovered from a previous test performed during 2 h at 120°C (from table III.12, entry 2) was submitted again to O_2 under the same conditions with a new batch of V_3BM_{50} catalyst. The dissolution of $WSLp^{ox}$ proved to be even inexistant (-1.3% *vs* 10% for WSL_p). One explanation would be that $WSLp^{ox}$ has become more recalcitrant to cleavage than the purified lignin [25-27]. This could be explained by lignin repolymerization mechanisms favored in harsh conditions, leading unfortunately to recalcitrant C-C bonds [22, 27] and the β-O-4 bond are destructed. We tried to analyze the phosphorylated solid residues (see Table III. 12, entries 2-3) by ^{31}P NMR in $CDCl_3$-pyridine 1-1.6 but oxidized lignin turned out to be only partially soluble on the contrary to the starting WSLp, so the OH content could not be determined. Yet, the ratio of each functions and monomers type can be calculated.

III.6 Conclusions

Ball-milling gave rise to better yields of $PMoV_x$ and can be more energy-saving than the hydrothermal procedure, especially for x = 3. The key step is the formation of a mixed oxide, which is actually a new compound obtained by the inclusion of vanadium oxide in the structure of the molybdenum oxide. However, ball-milling and hydrothermal $PMoV_3$ catalysts exhibited similar activity and similar selectivity for **K1**$_{HH}$ and **A1**$_{HH}$ cleavage. So, ball-milling has a low impact on the catalytic properties of the $PMoV_3$. Therefore, the impact of ball-milling is mainly a saving of energy and the most adapted parameters are r = 50 and a short milling step (1 h) and a short attack (1.5 h).

V_3-BM_{50} catalyst was tested for lignin aerobic cleavage. The yields of the targeted platform molecules were really low, even lower compared to those of the **A1**$_{HH}$ cleavage products. A temperature of 120°C and a reaction time of 6 h proved to be the most efficient reaction conditions for lignin aerobic cleavage (yield of monomers: 2.8 mol%). Lignin being rather unsoluble in the MeCN/AcOH (90/10), the mass transfers of dioxygen and of the substrate have to be improved. Yet, one may deduce that operating at high temperature and high pressure may be a double-edged sword.

Thus, a solution could be found by the implementation of a sonochemical process intensification. Besides, the well-known cavitation which takes place in presence of

ultrasounds and more generally a mechanical wave, local raises of temperature and pressure are known to be in favor of the generation of strong radicals oxidants that may be helpful to cleave the C-C and C-O bonds

References:

[1]: J. Qu, L. Sha, C. Wu, Q. Zhang, *Nanomater.* **2019**, 9, 80-94.
[2]: K. Ralphs, C. Hardacre, S. L. James, *Chem. Sc. Rev.* **2013**, 42, 7701-7718.
[3]: D. Chen, J. Zhao, P. Zhang, S. Dai, *Polyhedron* **2019**, 162, 59-64.
[4]: R. A. Buyanov, V. V. Molchanov, V. V. Boldyrev, *Catal. Today* **2009**, 212-218.
[5]: G. Majano, L. Borchardt, S. Mitchell, V. Valtchev, J. Pérez-Ramírez, *Microporous Mesoporous Mater.* **2014**, 194, 106-114.
[6]: V. A. Zazhigalov, S. V. Khalameida, N. S. Litvin, I. V. Bacherikova, J. Stoch, L. Depero, *Kinet. Catal.* **2008**, 49, 5, 692-701.
[7]: L. Xu, Y. Wang, T. Xu, S. Liu, J. Tong, R. Chu, X. Hou, B. Liu, *ChemCatChem* **2018**, 10, 5386-5390.
[8]: Y. Leng, Y. Jiang, H. Peng, Z. Zhang, M. Liu, K. Jie, P. Zhang, S. Dai, *Catal. Sci. Technol.* **2019**, 9, 2173-2179.
[9]: V. V. Molchanov, R. A. Buyanov, *Kinet. Catal.* **2001**, 42, 3, 366-374.
[10]: V. V. Molchanov, G. M. Maksimov, R. I. Maksimovskaya, V. V. Goidin, R. A. Buyanov, *Inorg. Mater.* **2003**, 39, 7, 687-693.
[11]: V. F. Odyakov, E. G. Zhizhina, Y. A. Rodikova, L. L. Gogin, *Eur. J. Inorg. Chem.* **2015**, 3618-3631.
[12]: L. Mbotchak, C. Le Morvan, K. Linh Duong, B. Rousseau, M. Tessier, A. Fradet, *J. Agric. Food Chem.* **2015**, 63, 5178-5188.
[13]: L. Pettersson, *Mol. Eng.* **1993**, 3, 29-42.
[14]: R. Neumann, A. Khenkin, *Chem. Commun.* 2006, 2529-2538.
[15]: R. Schmidt, H. M. Scholze, A. Stolle, *Int. J. Ind. Chem* **2016**, 7, 181-186.
[16]: T. P. Yadav, R. M. Yadav, D. P. Singh, *Nanosci. and Nanotechnol.* **2012**, 2, 3, 22-48.
[17]: M. Delmas, B. Benjelloun-Mlayah, *Pat. Fr 2926824* **2008.**
[18]: J.-P. Lange, *Angew. Chem. Int. Ed.* **2015**, 54, 13186-13197.
[19]: S. Van den Bosch, S.-F. Koelewijn, T. Renders, G. Van den Bossche, T. Vangeel, W. Schutyser, B. F. Sels, *Chem. Soc. Rev.* **2018**, 47, 852-908.
[20]: F. Abdelkafi, H. Ammar, B. Rousseau, M. Tessier, R. El Gharbi, A. Fradet, *Biomacromolecules* **2011**, 12, 3895-3902.
[21]: R. H. Stadler, D. H. Welti, A. A. Stämpfli, L. B. Fay, *J. Agric. Food Chem.* **1996**, 44, 898-905.
[22]: W. Schutyser, T. Renders, S. Van den Bosch, S.-F. Koelewijn, G. T. Beckham, B. F. Sels, *Chem. Soc. Rev.* **2018**, 47, 852-908.
[23]: L. G. Akim, J. L. Colodette, D. S. Argyropoulos, *Can. J. Chem.* **2001**, 79, 201-210.
[24]: R. Parthasarathi, R. A. Romero, A. Redondo, S. Gnanakaran, *J. Phys. Chem. Lett.* **2011**, 2, 20, 2660-2666.
[25]: S. Kim, S. C. Chmely, M. R. Nimlos, Y. J. Bomble, T. D. Foust, R. S. Paton, G. T. Beckham, *J. Phys. Chem. Lett.* **2011**, 2, 22, 2846-2852.
[26]: S. Guadix-Montero, M. Sankar, *Top. Catal.* **2018**, 61, 183-198.
[27]: Z. Sun, B. Fridrich, A. de Santi, S. Elangovan, K. Barta, *Chem. Rev.* **2018**, 118, 614−678.7

Appendix: part III

***** *XRD profiles of V_2-BM_{20} catalysts (see III. 3.1, Fig. III. 1)*

The XRD profiles of the V_2-BM_{20}-t_{BM}-t_{HT} series (Fig SIII. 1) and the V_2-BM_{20}-2x2-t_{HT} series (*vs* V_2-BM_{20}-2-t_{HT}, Fig SIII. 2) are given here.

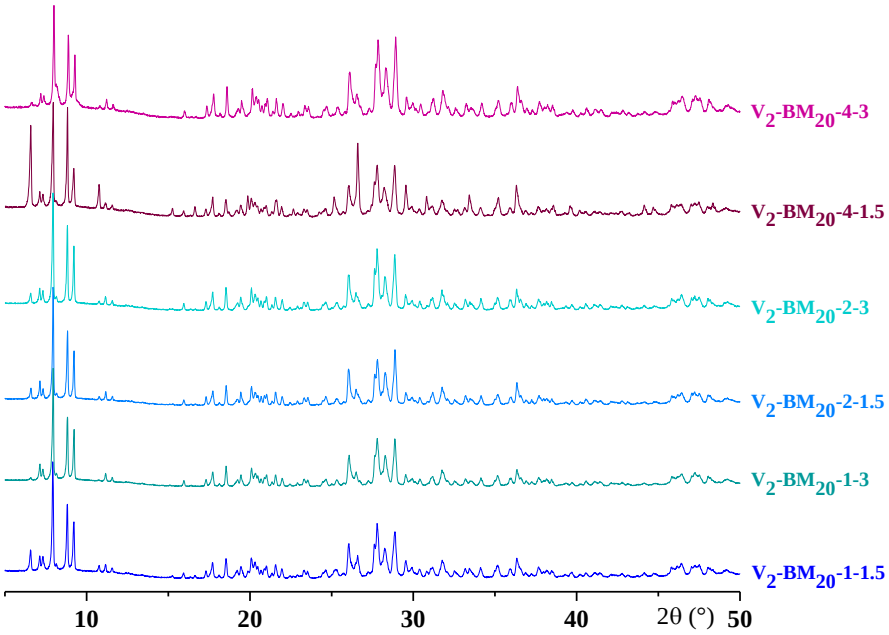

Figure SIII. 1: Influence of the milling (t_{BM}) and attack duration (t_{HT}) on XRD profiles of V_2-BM_{20} materials

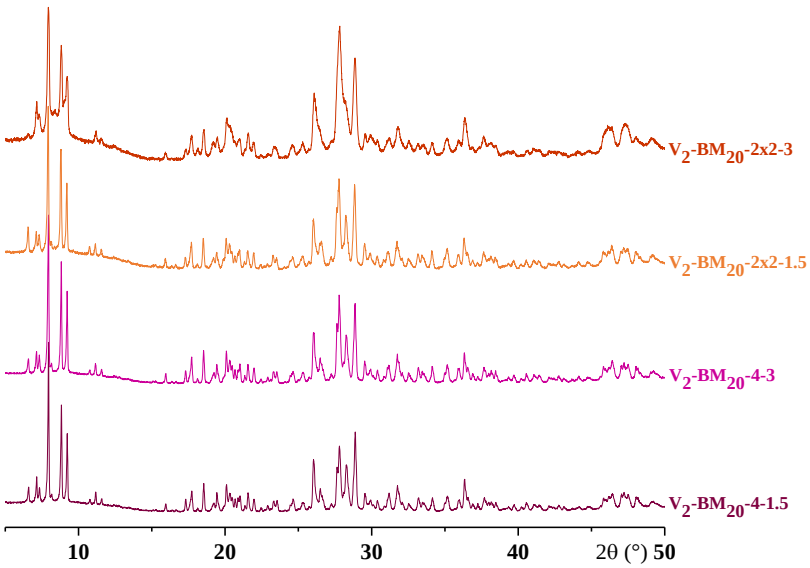

Figure SIII. 2: Impact of a stepwise milling on the XRD profiles of V_2-BM_{20} materials after a 4 h-milling step

**NMR spectra of V_x-BM_{20} materials (V_x-HT and V_x-BM_{50} series, see III. 1, Fig. III. 2)*

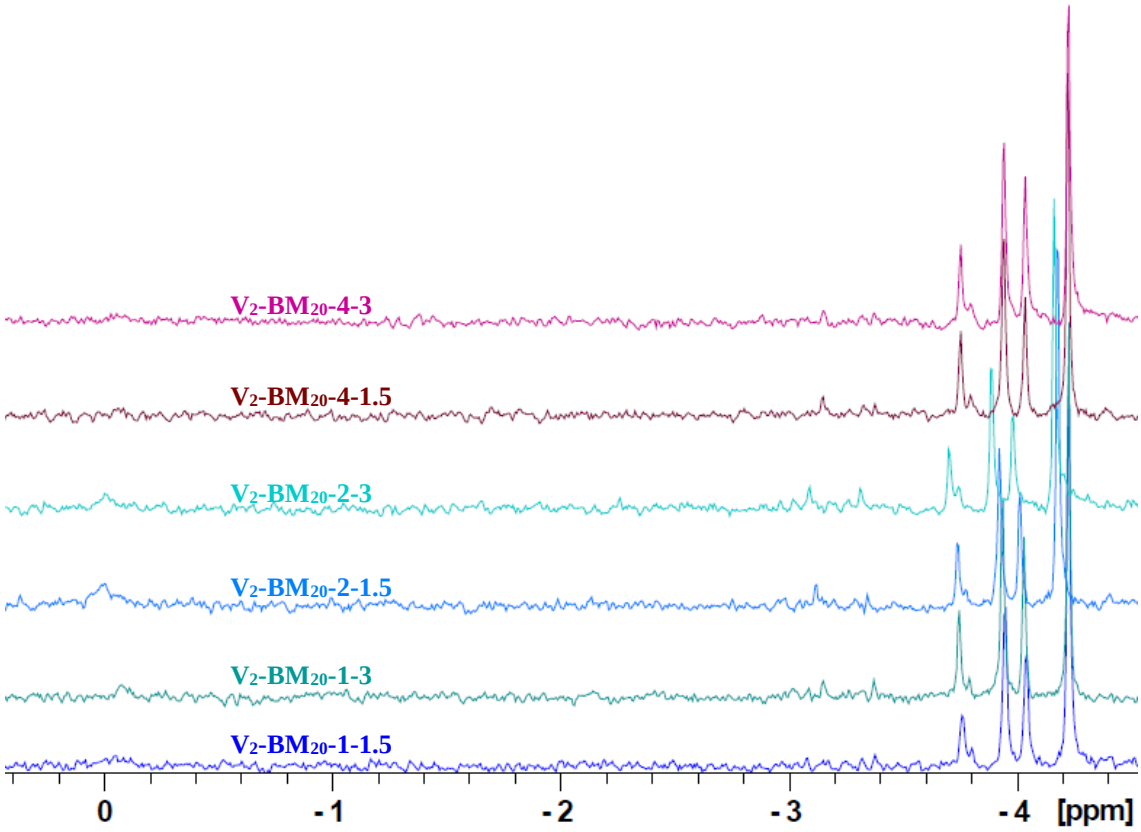

Figure SIII. 3: ^{31}P NMR spectra of V_2-BM_{20} materials in D_2O-H_2O 50-50

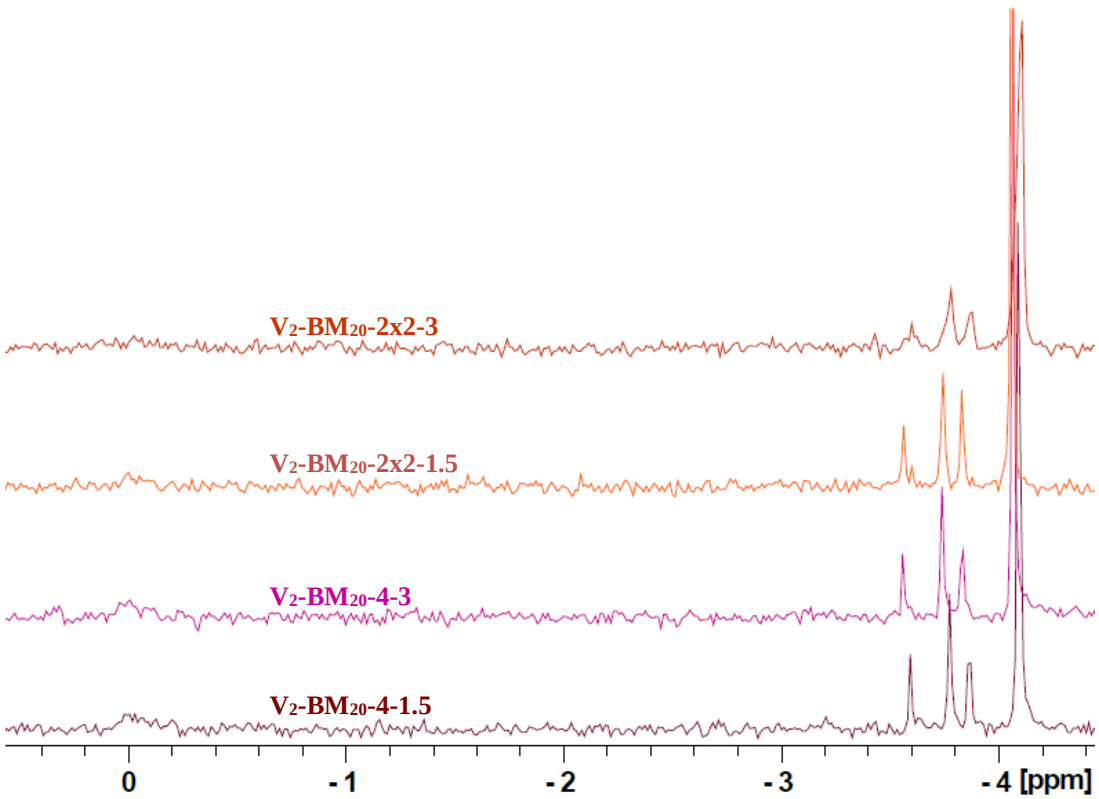

Figure SIII. 4: Influence of a stepwise 4h-milling step on the ^{31}P NMR spectra of the resulting materials

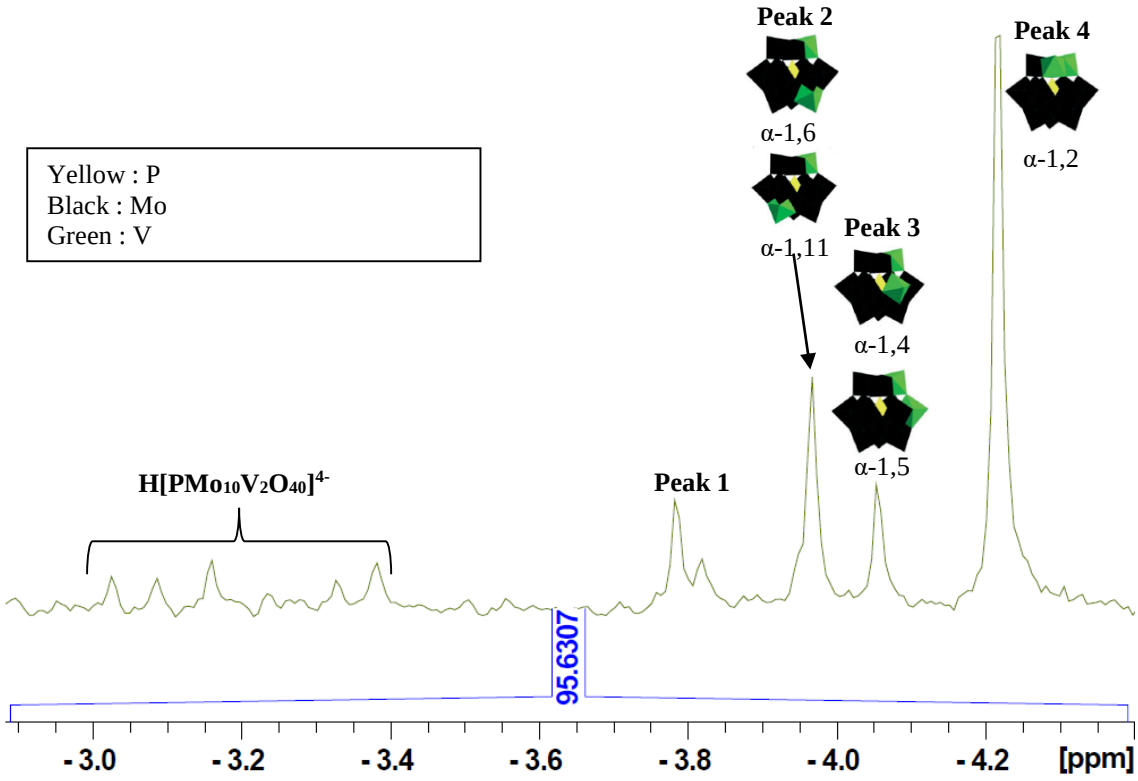

Figure SIII. 5: Attribution of the ^{31}P NMR signals in the case of $PMoV_2$-BM_{50}

Table SIII. 1: Isomers proportions in $PMoV_2$ catalysts

Peak n°	1	2	3	4
Isomer	β	α-1,6 α-1,11	α-1,4 α-1,5	α-1,2
Location of vanadium atoms	n. i.	Not vicinal	Vicinal, on different triads	On the same triad
Oxygen type in V-O-V bond	-	-	O_e (*e = edge-sharing)*	O_c (*c = corner-sharing)*
	Chemical shift in ppm (proportion in %)			
V_2-BM_{50}	-3.80 (12.7)	-3.97 (16.3)	-4.06 (12.6)	-4.22 (58.5)
V_2-BM_{20}-1-1.5	-3.78 (11.0)	-3.95 (24.0)	-4.04 (17.1)	-4.23 (47.9)
V_2-BM_{20}-1-3	-3.77 (12.1)	-3.94 (27.0)	-4.03 (18.7)	-4.23 (42.2)
V_2-BM_{20}-2-1.5	-3.75 (13.3)	-3.92 (23.3)	-4.01 (14.3)	-4.18 (49.1)
V_2-BM_{20}-2-3	-3.72 (14.2)	-3.89 (20.6)	-3.98 (19.1)	-4.16 (46.0)
V_2-BM_{20}-4-1.5	-3.77 (14.6)	-3.94 (25.5)	-4.04 (14.7)	-4.22 (45.2)
V_2-BM_{20}-4-3	-3.78 (17.7)	-3.94 (21.1)	-4.04 (23.8)	-4.23 (37.4)
V_2-BM_{20}-2x2-1.5	-3.78 (13.3)	-3.94 (19.5)	-4.04 (22.3)	-4.23 (44.8)
V_2-BM_{20}-2x2-3	-3.78 (9.4)	-3.95 (22.5)	-4.04 (15.6)	-4.23 (52.5)

$PMoV_2$ 30 mg in H_2O-D_2O 1:1 500 µL + 7.5 µL dioxane; 400 MHz, 16 scans, relaxation delay : 32 s

**TGA analysis (discussion & T_1 and T_2 values, see III. 1, Table III. 3)*

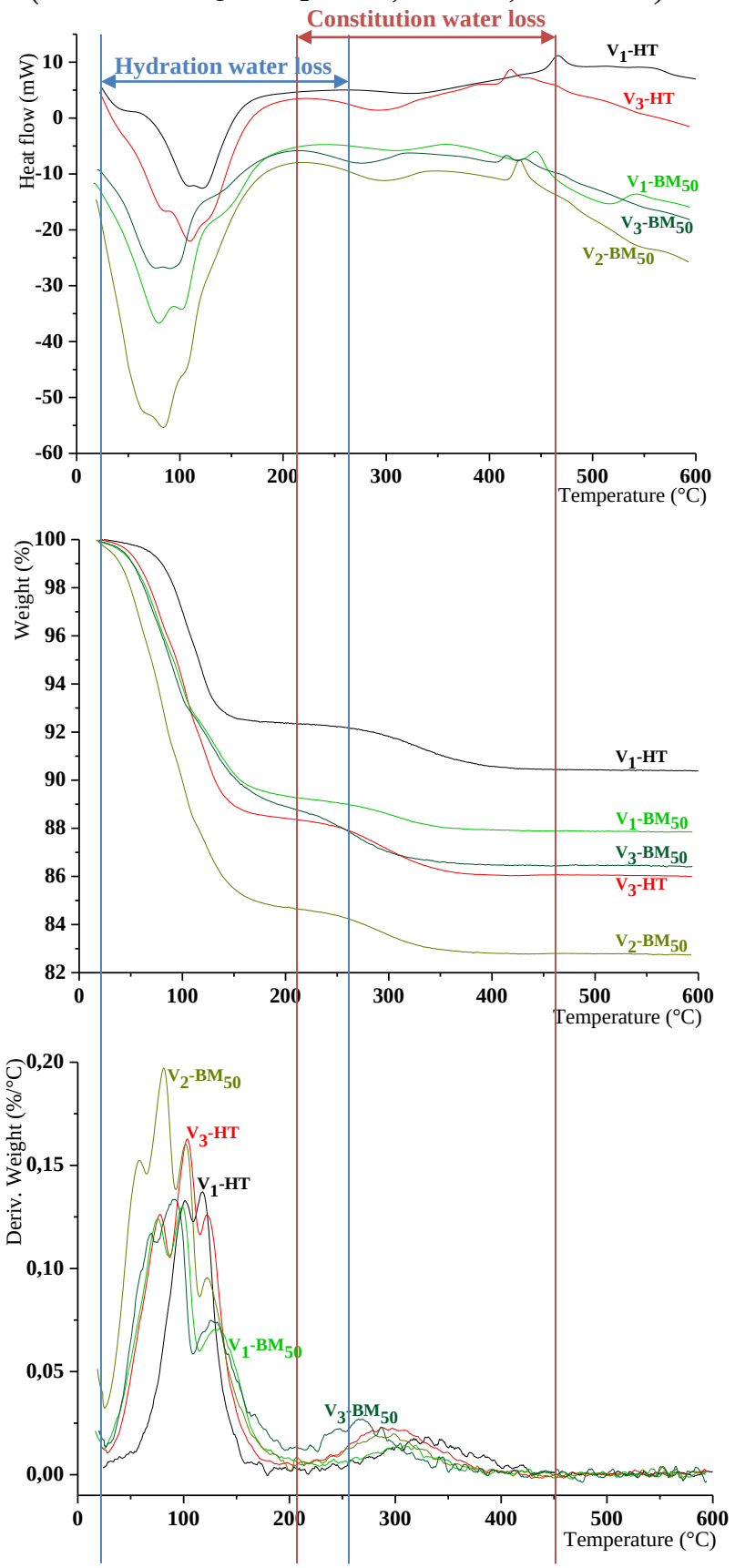

Figure SIII. 6: Influence of x and of the synthetic procedure (series n°1 and references PMoV$_x$)

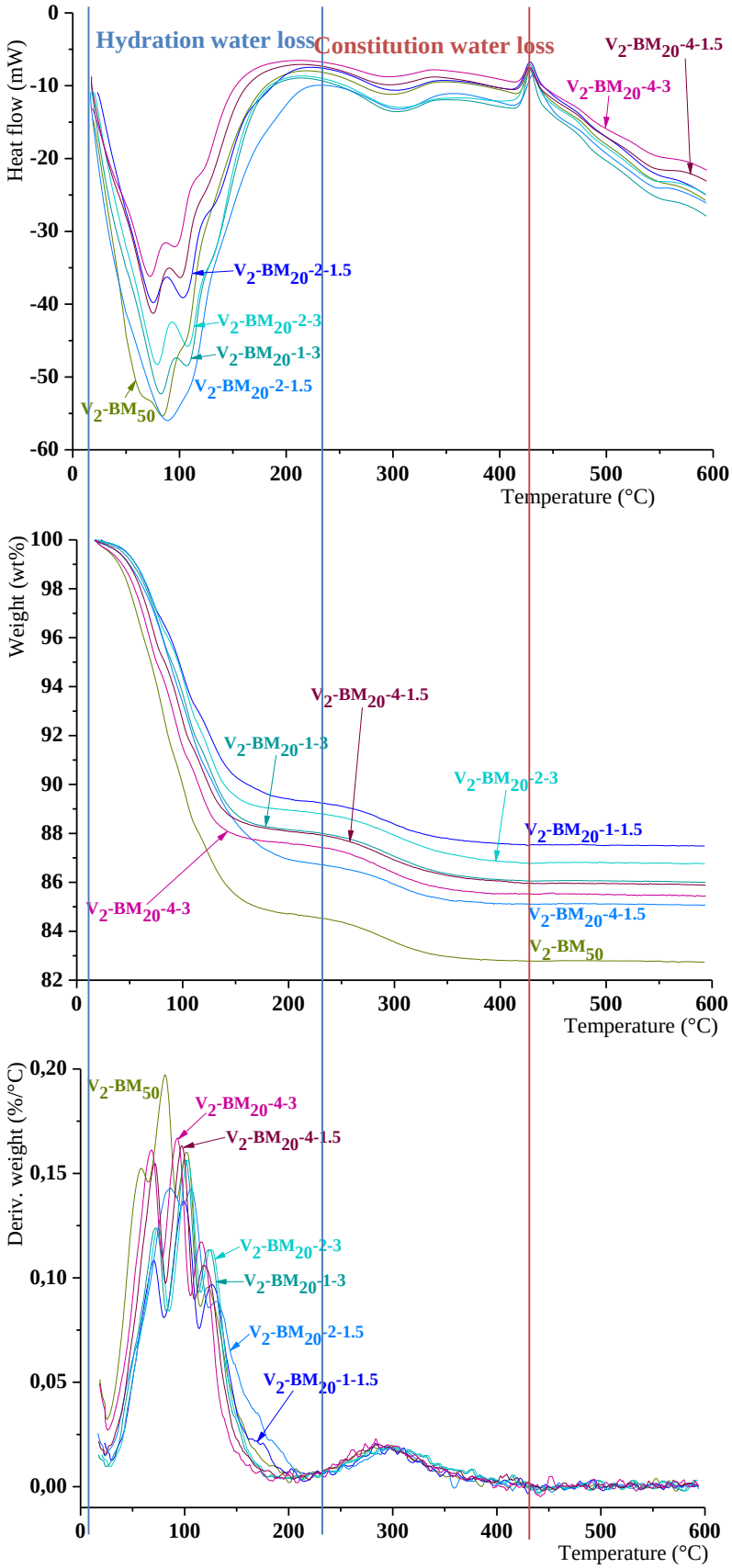

Figure SIII. 7: Influence of the ball-milling parametration (r, t_{HT}, t_{BM}, series n°2 and V_2-BM_{50})

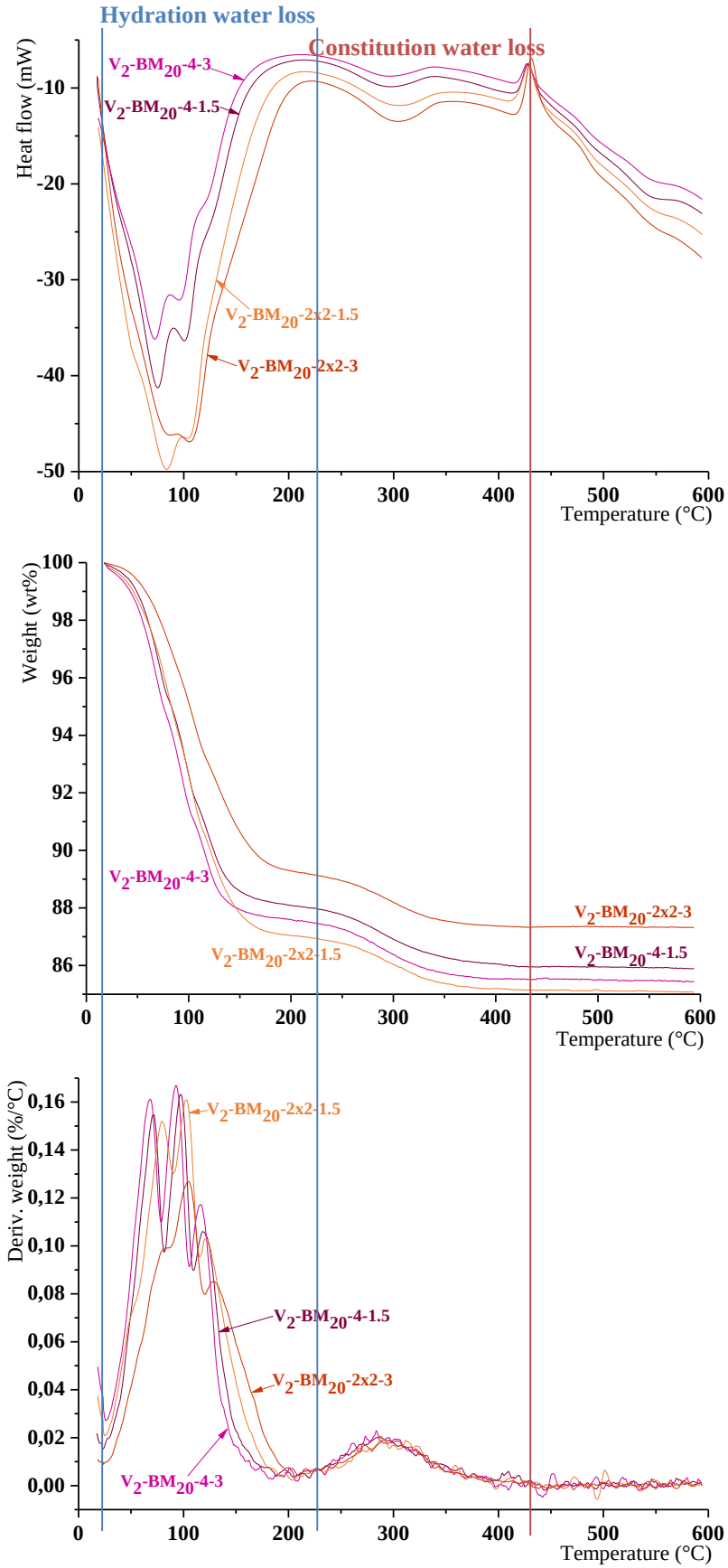

Figure SIII. 8: Two-step milling procedure vs direct milling procedure (r = 20, 4 h)

**Energy consumption: detailed calculation (cf. III. 1, Tables III. 3 and III. 4)*

- 100% hydrothermal treatment (HT)

The maximal power of the heater was $P_{th,max}$ = 825 W and the maximal temperature noted T_{max} wass 300°C. Since the energy delivered is proportional to the rise of the temperature and, assuming that the starting temperature is 20°C, the average power noted P_{th} required for the thermal heating until a temperature T would be given by Eq SIII. 1 as follows: $\boxed{P_{th} = \left(\frac{T-20}{T_{max}-20}\right) P_{max}}$ (Eq SIII. 1).

- hybrid treatment (BM)

The range of the rotation speed (noted ω) during the milling step was 100-1100 rpm and the maximal power (ω_{max} = 1100 rpm) was $P_{BM,max}$ = 1100W. Assuming that the power is proportional to the square of the rotation speed, the required power P_{BM} can be calculated according to Eq SIII. 2: $\boxed{P_{th} = \left(\frac{\omega}{\omega_{max}}\right)^2 P_{BM,max}}$ (Eq SIII. 2).

Since then, the energy consumption was calculated. The obtained values are given in the tables hereafter:

**XRD profiles of the different mixed oxides (cf III. 3.2)*

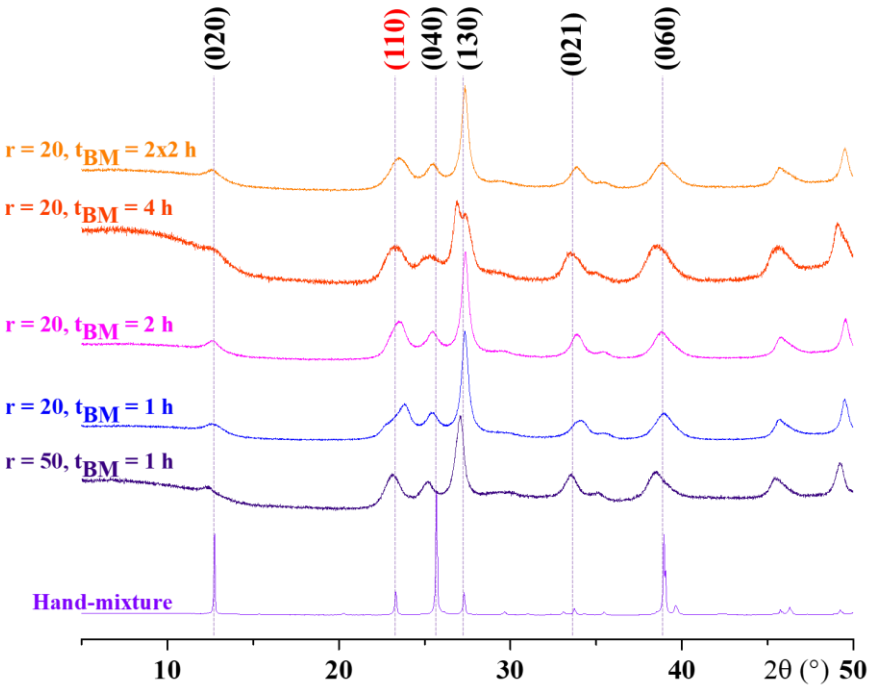

Figure SIII. 9: XRD profiles of the mixed oxides (x = 2) prior to hydrothermal attack (The (100) signal was used for DEBYE-SCHERRER calculations)

Table SIII. 2: Calculation of the energy consumption of V_x-HT and V_x-BM_{50} synthesis procedures

Catalyst	V_1-HT	V_3-HT	V_1-BM_{50}	V_2-BM_{50}	V_3-BM_{50}
Procedure (temperature)	Hydrothermal		Ball milling r = 50		
Milling duration (h)	0	0	1		
Energy consumption during the milling step (kW.h)	0	0	0.45		
Attack duration (h)	3	6.5	1.5		
Temperature (°C)	100	100	80		
Energy consumption by heating (kW.h)	0.71	1.53	0.27		
Global energy consumption (kW.h)	**0.71**	**1.53**	**0.72**		
Maximum anhydrous $PMoV_x$ weight (g)	16.41	5.345	2.895	2.897	2.937
$PMoV_x$ Yield (%)	81	79	95-97		
Global energy consumption (kW.h/mol)	**85.3**	**618**	**451**	**439**	**422**

Table SIII. 3: Calculation of the energy consumption of V_x-BM_{20} synthesis procedures

	V_2-BM_{20}-1-1.5	V_2-BM_{20}-1-3	V_2-BM_{20}-2-1.5	V_2-BM_{20}-2-3	V_2-BM_{20}-4-1.5	V_2-BM_{20}-4-3	V_2-BM_{20}-2x2-1.5	V_2-BM_{20}-2x2x-3
Milling duration (h)	1	1	2	2	4	4	2x2	2x2
Energy consumption during the milling step (kW.h)	0.45	0.45	0.89	0.89	1.78		1.78	
Attack duration (h)	1.5	3	1.5	3	1.5		3	
Temperature (°C)	100	80	80	80	80		80	
Energy consumption by heating (kW.h)	0.35	0.53	0.27	0.53	0.27		0.53	
Global energy consumption (kW.h)	**0.80**	**0.98**	**1.16**	**1.52**	**2.05**		**2.31**	
Global energy consumption (kW.h/mol)	**210**	**257**	**304**	**374**	**539**	**608**	**539**	**608**

Maximum anhydrous $PMoV_x$ weight : 6.950 g, yield = 92-97 %

**SEM (Magnification X2k et X30k, see III. 2.3, Fig III. 6)*

Measurements on both the mixed oxide and the hand-mixture of molybdenum and vanadium oxides were made at different magnifications.

Mixed oxide (x5k) Hand-mixture (x5k)

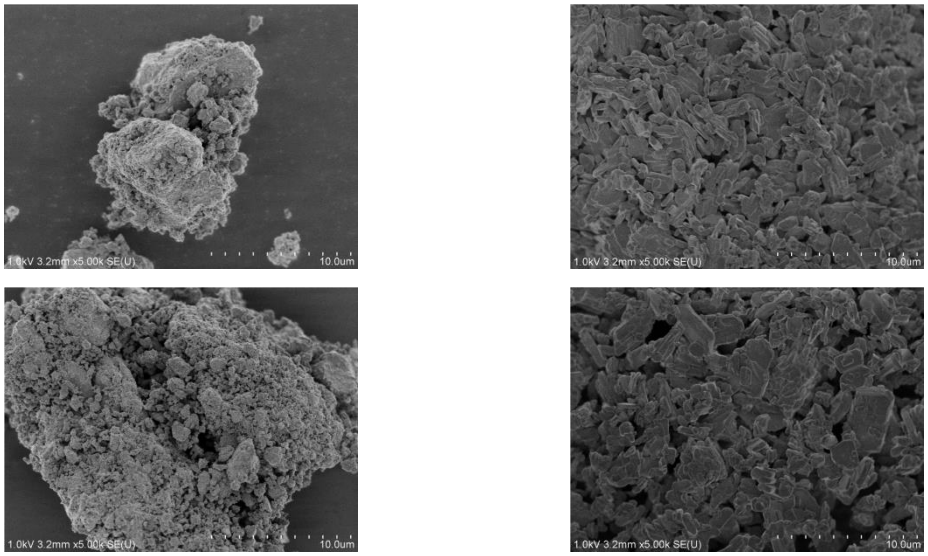

Figure SIII. 10a: SEM images of the mixed oxide (r = 20, t_{BM} = 2 h) (left) and of the hand-mixture (right), magnification x5k

Mixed oxide (x10k) Hand-mixture (x10k)

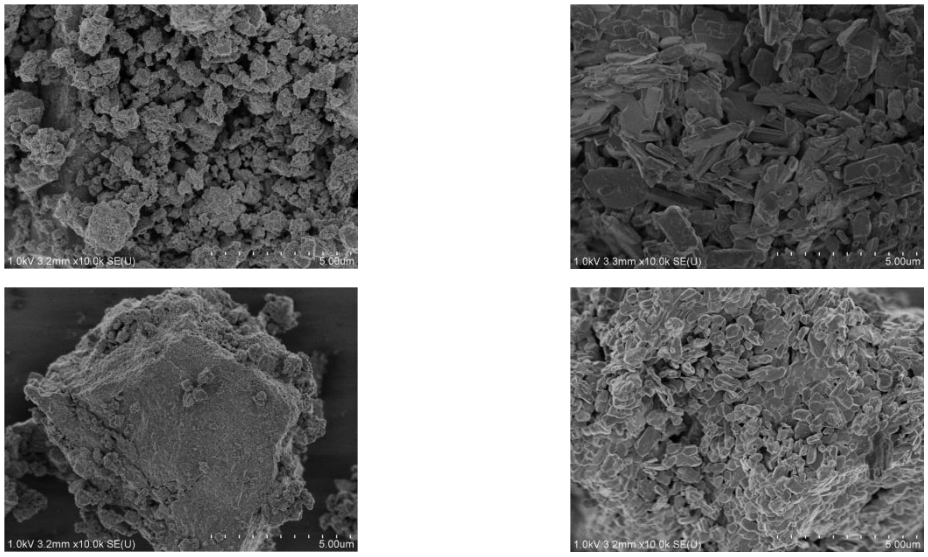

Figure SIII. 10b: SEM images of the mixed oxide (r = 20, t_{BM} = 2 h) (left) and of the hand-mixture (right), magnification x10k

**N_2 sorption isotherms at 77 K (results detailed on III. 3.2, Table III. 6)*

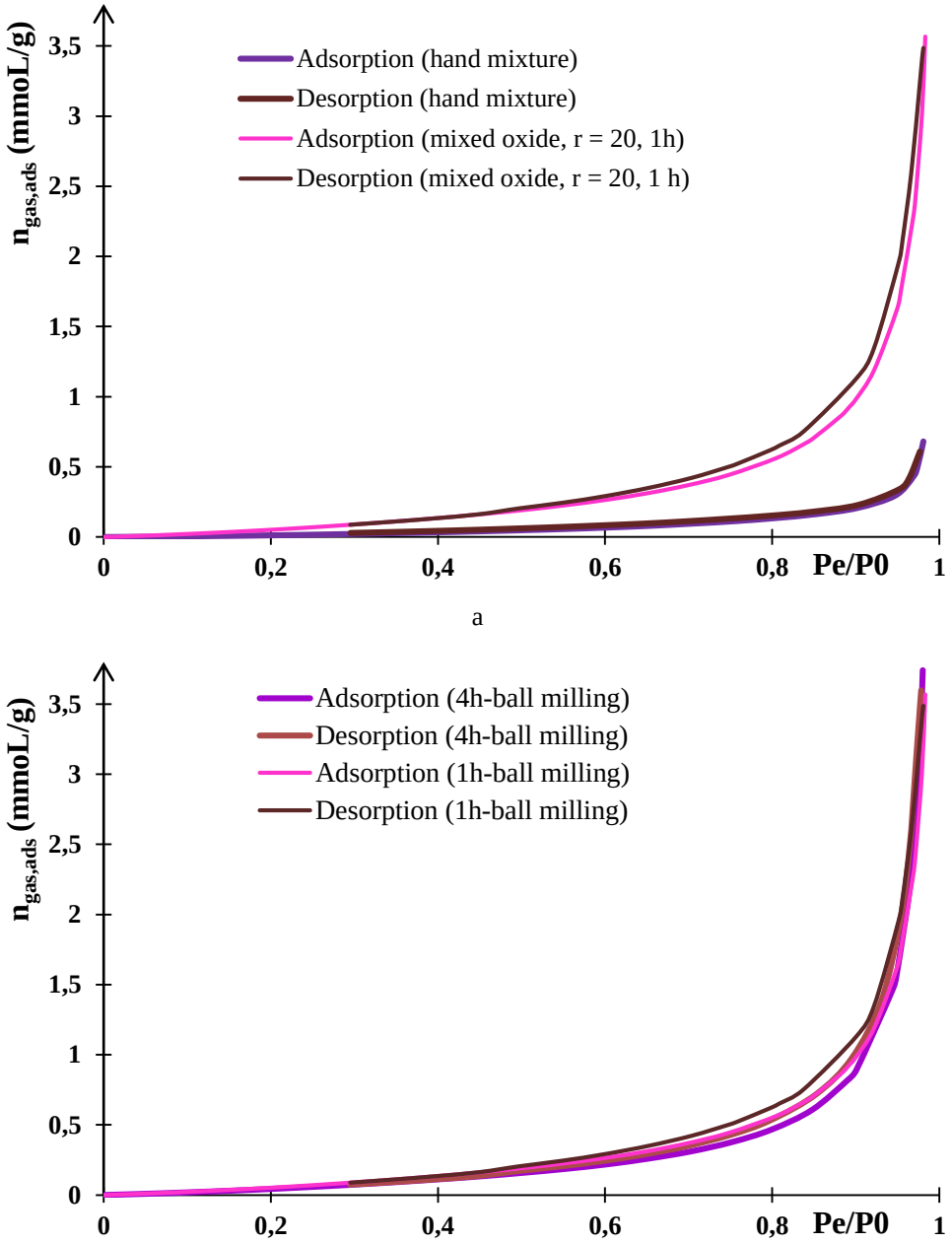

Figure SIII. 11: Adsorption-desorption isotherms of the a) hand-mixture b) the mixed oxide used as precursor of V_2-BM_{20}-1 and V_2-BM_{20}-4 materials

**Lignin extraction (cf III. 2.3, lignin purification)*

Lignin was impregnated by a ternary acetic acid-formic acid-water 50/30/20 mixture heated to 95-110°C during 3 h under atmospheric pressure. Lignocellulose was destructured by formic acid and the role of acetic acid was to dissolve lignin and hemicellulose, which enables to recover the cellulose pulp by filtration. Water and the acids were evaporated until reaching 60% of dry matter, thus enabling the recycling of the organic solvents. The resulting thick liquor

was diluted by water to precipitate lignin that was separated by membrane filtration and then pressed in order to concentrate it [S1, S2].

**Lignin phosphorylation (cf. III. 5, Fig. III. 16)*

The phosphorylation was carried out according to the method of GRANATA and ARGYROPOULOS with slight modifications [S3, S4] using pyridine-$CDCl_3$ 1.6-1 as the solvent.

30 mg of lignin were dissolved in 500 µL of pyridine-$CDCl_3$ 1.6-1. Then, 100 µL of chromium acetylacetonate (III) 0.014 M and 100 µL of N-hydroxy-6-norbornene-2,3-dicarboximide 0.1 M (internal standard) both in pyridine-$CDCl_3$ 1.6-1 were added followed by 150 µL of 2-chloro-4,4,5,5-tetramethyl-1,3,2-dioxaphospholane to start the phosphorylation reaction. The mixture was stirred overnight. The involved reaction is described in Figure SIII.12.

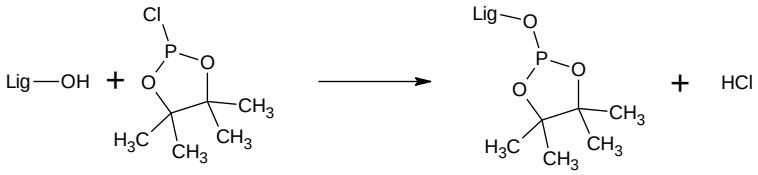

Figure SIII. 12: Equation of lignin phosphorylation

Before the reaction starts, the lignin sample is not totally soluble in the solvent but usually the reaction leadd to the dissolution of the solid, excepted for $WSLp^{ox}$ in this study. So, as indicated in the main text, the total content of OH functions could not be determined in these conditions. The peaks of phosphorylated lignin are in the region from

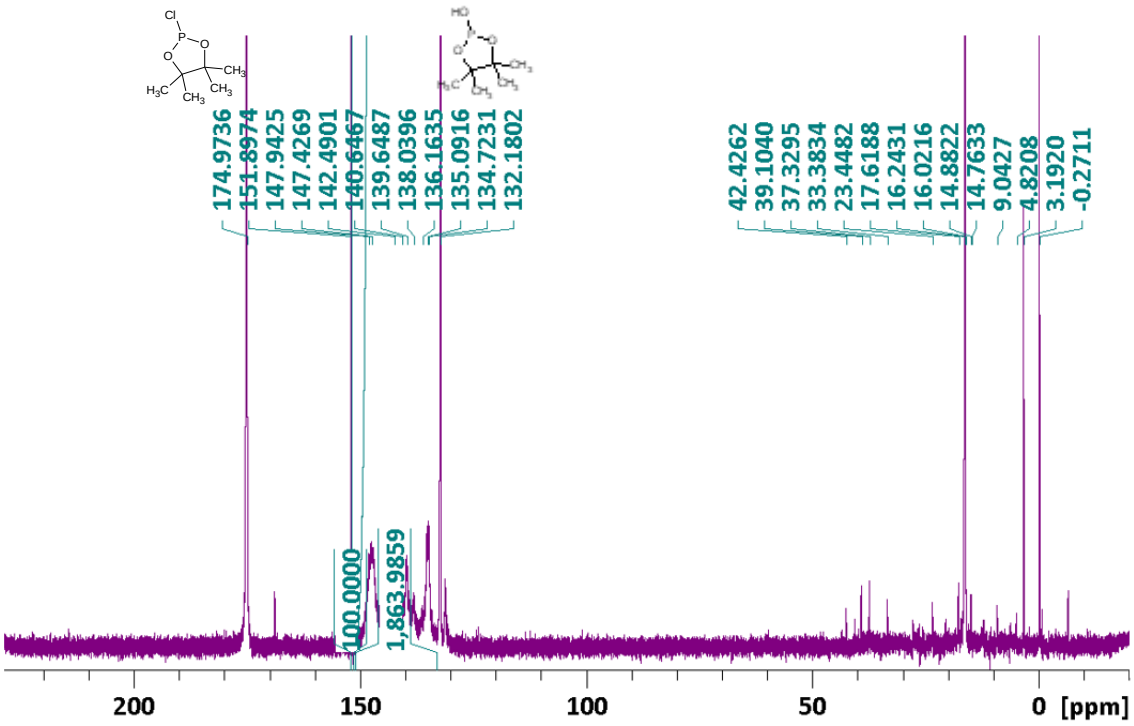

Figure SIII. 13: ^{31}P NMR spectrum of phosphorylated purified lignin (WSL_p)

Table SIII. 4: Attribution of OH function in ^{31}P NMR spectra

Chemical shift (ppm)	OH type
144.5-151	Aliphatic
141-144.5	Phenolic (S + condensed G units)
138.5-140.5	Phenolic (uncondensed G units)
137-138.5	Phenolic (H units)
133-137	Carboxylic acid (unconjugated 134.5 ppm and conjugated 134 ppm)

**Calibration of silylated phenolic aldehydes and acids*

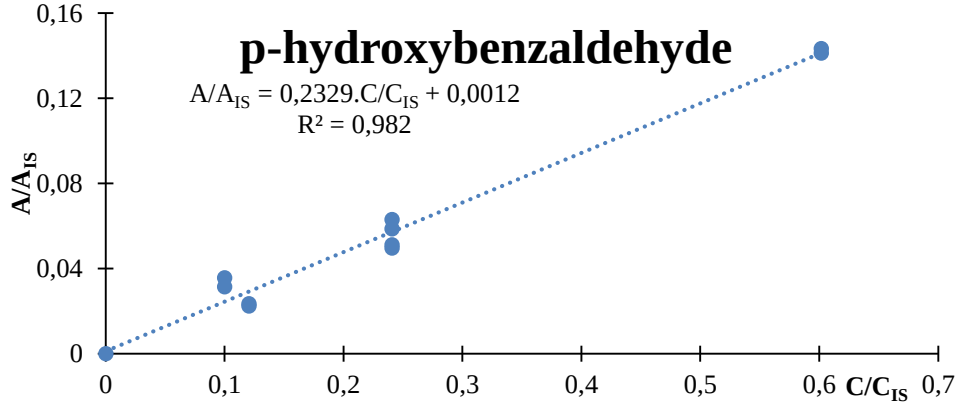

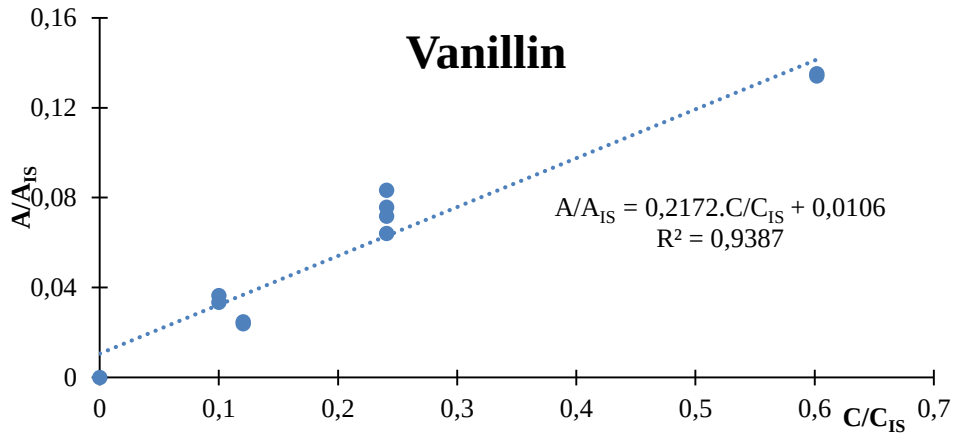
Vanillin
A/A$_{IS}$ = 0,2172.C/C$_{IS}$ + 0,0106
R² = 0,9387
A/A$_{IS}$
C/C$_{IS}$
0,16
0,12
0,08
0,04
0
0
0,1
0,2
0,3
0,4
0,5
0,6
0,7

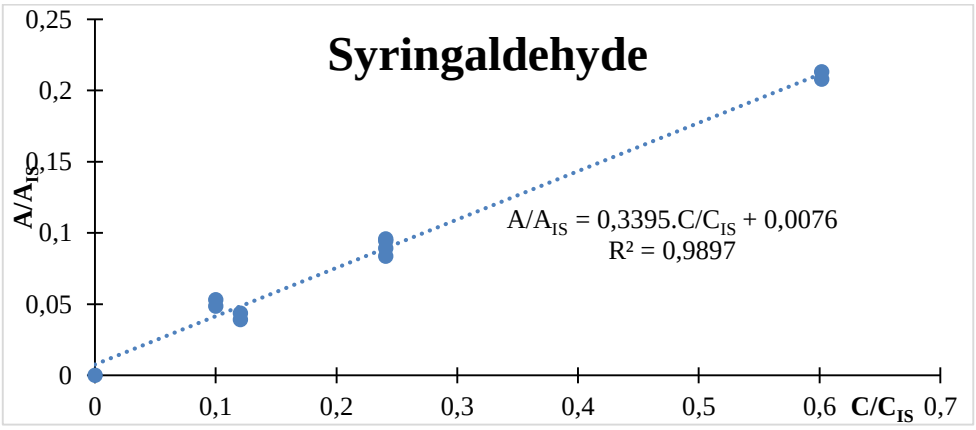
Syringaldehyde
A/A$_{IS}$ = 0,3395.C/C$_{IS}$ + 0,0076
R² = 0,9897
A/A$_{IS}$
C/C$_{IS}$
0,25
0,2
0,15
0,1
0,05
0
0
0,1
0,2
0,3
0,4
0,5
0,6
0,7

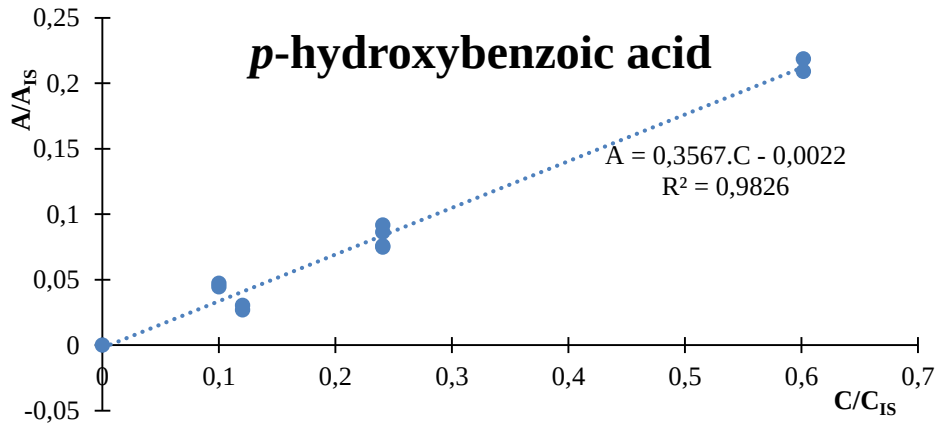
p-hydroxybenzoic acid
A = 0,3567.C - 0,0022
R² = 0,9826
A/A$_{IS}$
C/C$_{IS}$
0,25
0,2
0,15
0,1
0,05
0
-0,05
0
0,1
0,2
0,3
0,4
0,5
0,6
0,7

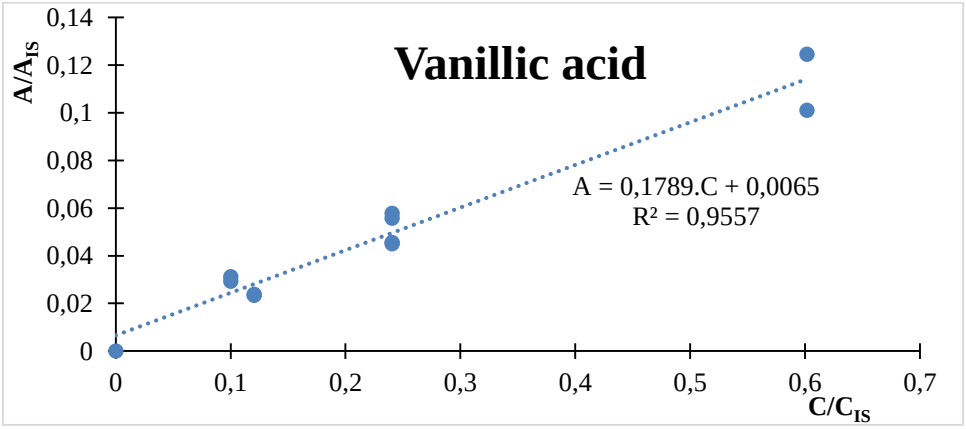
Vanillic acid
A = 0,1789.C + 0,0065
R² = 0,9557
A/A$_{IS}$
C/C$_{IS}$
0,14
0,12
0,1
0,08
0,06
0,04
0,02
0
0
0,1
0,2
0,3
0,4
0,5
0,6
0,7

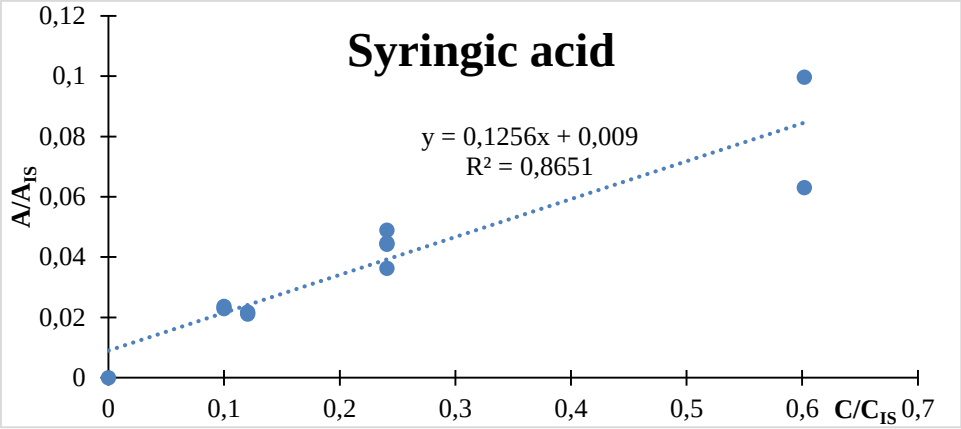

Figure SIII. 14: Calibration curves of the targeted silylated phenolic aldehydes and acids

Table SIII. 5: Retention time of silylated phenolic cleavage products (GC-MS)

RT (min)	Compound
14.6	Silylated H
18.8	Silylated V
21.0	Silylated HA
22.8	Silylated S
24.2	Silylated VA
27.1	Silylated SA

References

[S1]: M. Delmas, B. Benjelloun-Mlayah, *Pat. Fr 2926824* **2008**.
[S2]: G-H. Delmas, B. Benjelloun-Mlayah, Y. Le Bigot, M. Delmas, *J. Appl. Polym. Sci.* **2011**, 121, 491-501.
[S3]: A. Granata, D. S. Argyropoulos, *J. Agric. Food. Chem.* **1995**, 43, 1538−1544.
[S4]: L. Mbotchak, C. Le Morvan, K. Linh Duong, B. Rousseau, M. Tessier, A. Fradet, *J. Agric. Food Chem.* **2015**, 63, 5178−5188.

IV. Process intensification strategies: sonochemistry

These experiments were partly carried out in collaboration with Dr. Sabine VALANGE and Dr. Prince AMANIAMPONG in the IC2MP laboratory in Poitiers.

IV. 1. Introduction

In part III, two catalyst synthesis procedures were compared: mixed ball-milling/hydrothermal pathway and a 100% hydrothermal pathway. Though the first one enabled better yield, the activity of the resulting catalysts is not significantly different to their hydrothermal encounters. Yet, such a procedure allows some energy saving. An intensification of the oxidation process was attempted by raising both temperature and pressure (II. 6). The yield of phenol could not be higher than 16% (80°C, 24 h, 5 bar) and the maximized combined yield of benzaldehyde and benzoic acid was 22% (120°C, 6 h, 5 bar). However, stringent conditions (120°C, 6 h, 5 bar) leads to a minimized carbon balance (only 55%). In presence of a co-oxidant as TEMPO, the yield of phenol the yield of C-C cleavage products reached 18% and 23% and the esterification and dehydration of **A1**$_{HH}$ were both cut down. The main drawback is the use of a supplementary co-catalyst that shows to be less active after recycling.

Therefore, we thought that ultrasonic intensification may lead to better results in terms of selectivity for cleavage. Indeed, lignin aerobic cleavage catalyzed by $PMoV_x$ is a radical oxidation process. It relies either on substrate by oxidized $PMoV_x$ or on oxygen activation by reduced $PMoV_x$ (see IB.3). During irradiation by ultrasound, cavitation takes place. Bubbles are formed, oscillate and may then collapse, leading to the formation of "hot spots" where temperature and pressure may increase until 5000 K and 1000 bars. Such conditions may be favorable for bond homolytic dissociation. It proved to be adequate for generation of hydrogen peroxide and other active oxygen species as superoxide ($O_2^{\cdot -}$) and hydroxyl radicals ($HO^{\cdot}$) from dioxygen. Moreover, as discussed before (IC. 3), ultrasonic cavitation leads to enhanced mass transfer. Consequently, these effects may work in synergy with the $PMoV_x$ catalysts. Ultrasonic cavitation was already tested for lignin oxidative cleavage with hydrogen peroxide. It proved to favor oxidative condensation [1] leading to recalcitrant C-C bonds (see IC.1), which may explain the negative influence of ultrasounds for lignin depolymerization. It is well-known that hydrogen peroxide may be cleaved to hydroxyl radicals that are one of the strongest oxidants but they are not selective for cleavage. Using dioxygen instead of hydrogen peroxide leads to moderate oxidative strength that may be more suitable of lignin cleavage into aromatic platform

molecules. Besides, to the best of our knowledge, ultrasound-assisted oxidative cleavage of lignin and its surrogates was never reported elsewhere.

Ultrasonic intensification has a growing interest as a clean energy activation tool compared to conventional processes [2, 3]. Ultrasonic-assisted procedures proved to be efficient for aerobic oxidation of benzyl alcohol oxidation [4-6]. Working at low frequencies (< 100 kHz) generally favor the physical effects of cavitation, such as bubble formation and collapse leading to good mixing, high degree of turbulence and enhanced mass and heat transfer (see IC.2.2). At high frequencies, the oscillation and implosion of bubbles of smaller diameter (less than 0.5 mm) leads to chemical effects. This may result in the sonolysis of the reaction media, leading to the formation of radical and active species [7, 8]. The frequency of the ultrasounds used is thus an important parameter that needs to be explored. Therefore, the intensification of the **A1**$_{HH}$ aerobic oxidative cleavage was assayed in the presence of i) high (540 kHz), ii) medium (100 kHz) and iii) low frequency (20 kHz) ultrasounds. As a binary acetonitrile-acetic acid proved to be the most suitable for **A1**$_{HH}$ aerobic cleavage, such solvent will be used for sonochemical cavitation tests.

IV. 2. Experimental part

The substrate used in the ultrasound-assisted experiments was **A1**$_{HH}$, since the **K1**$_{HH}$ aerobic oxidative cleavage proved to be feasible and led to high product yields even at atmospheric pressure in silent conditions. The preparation of the reaction media, as well as the monitoring of the experiments in silent conditions have been previously detailed (II. 2. 5). Only the reaction volume was changed, in order to keep the liquid to gas ratio constant and equal to the previous experiments performed in absence of ultrasonic intensification (V_{liq}/V_{gas} = 3). Moreover, the work-up after reaction is already detailed on II.2. 5. Therefore, the particular procedure for these ultrasound-assisted experiments will be uniquely detailed in this part. All the experiments performed are summarized in the general scheme (Fig IV. 5) provided at the end of the experimental part.

IV. 2. 1. Tests at 540 kHz

A designed double layered cylindrical steel reactor in a cup-horn configuration was fixed on the top of a 540 kHz transducer (Sinaptec Ultrasonic Technology). The transducer was connected to a power generator (NextGen Lab 1000) immerged in water. The power was consequently fixed to 30 W. In the reactor was poured 50 mL of the reaction media and then it

was sealed. It was purged 3 times by oxygen (3 bar). Then, the oxygen pressure was adjusted to 3 bar and the reaction media was heated to 80°C by a water flow (Fig IV. 1). Once the targeted temperature reached, the mixture was irradiated by ultrasounds at 535 kHz (0.6 W/mL) during 6 h.

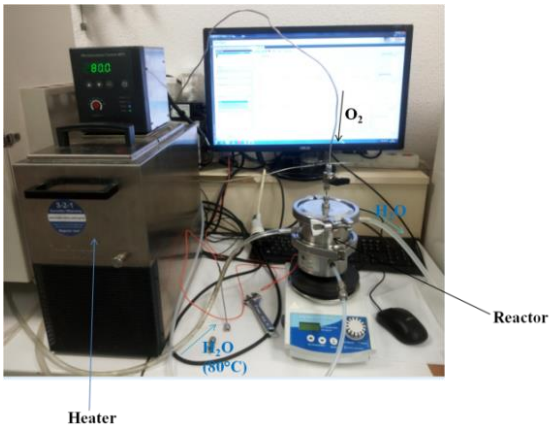

Figure IV. 1: Experimental set-up for reactions under irradiation by high frequency ultrasounds (550 kHz)

IV. 2. 2. Tests at 100 kHz

The experiments on the reaction media composed of **A1**$_{HH}$ 100 mM in MeCN – 10 vol% AcOH, V_3-BM_{50} (Mo + V 15 mol%, synthesis procedures see III. 4.2) were performed using a 250 mL stainless steel reactor containing in a cup-horn configuration fixed on a 100 kHz transducer (Sinaptec, 88 cm², 73 W). The reactor was sealed by a steel piston, keeping a gas volume of around 185 mL (see Fig. IV. 2). The closed reactor was purged five times using oxygen (2 bar) in order to evacuate nitrogen. Upon confirming the absence of leaks, *i.e.* checking pressure stability, the dioxygen pressure was finally adjusted to 3 bar once the reaction media was heated up to 80°C using a heating mantle. After that, the reaction media was irradiated using ultrasounds at a frequency of 95 kHz (0.6 W/mL) during 6 h generated by a transducer (Sinaptec NextGen 750, 30 W). The ultrasonic power in the reaction media was 0.6 W/mL.

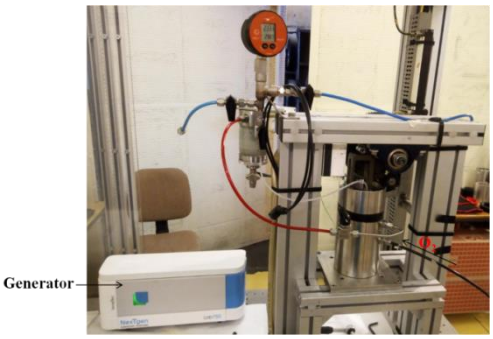

Figure IV. 2: Experimental set-up for catalytic tests under irradiation by ultrasounds (100 kHz) under oxygen pressure (3 bar)

IV. 2. 3. Tests at 20 kHz at atmospheric pressure

A customized double-layered glass reactor was used in these experiments (Fig IV. 3). This reactor contained 15 mL of the reaction media and was equipped by a refrigerant capped by a septum for oxygen flowing (through a needle). The reactor cooled down by a water flow (72°C) in presence of ultrasounds or heated to 82°C without ultrasounds. The reaction media was irradiated by a tapered probe (Bioblock Scientific Vibra-Cell 75115, 20 kHz, d = 13 mm, P_{elec} = 200 W, amplitude 40%). The resulting acoustic power, estimated by calorimetry was 0.93 W/mL. Concerning the tests without bubbling, there is still an oxygen flow in the gaseous phase that leads to oxygen turnover.

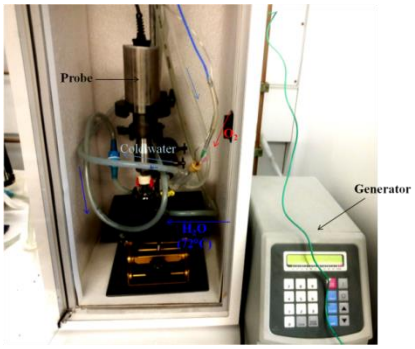

Figure IV. 3: Experimental set-up for the catalytic aerobic cleavage of ***A1***$_{HH}$ *at atmospheric pressure under irradiation by 20 kHz-ultrasounds*

IV. 2. 4. Tests at 20 kHz at higher pressure

In a 25 mL-double-layered reactor (Fig. IV. 4) are poured 12.5 mL of the reaction media. Because of the transducer (Digital Sonifer), the volumic ratio gas/liquid was 1 instead of 3. It was purged 3 times by oxygen (5 bar) three times to evacuate nitrogen [9]. Then, the oxygen pressure was adjusted to 5 bar and the reaction media was heated to 80°C by a water flow. Once the aimed temperature reached, the mixture was irradiated by ultrasounds at 20 kHz (2 W/mL) during 6 h. Then, the work-up was similar to the tests in silent conditions at higher pressure (II. 5. 1).

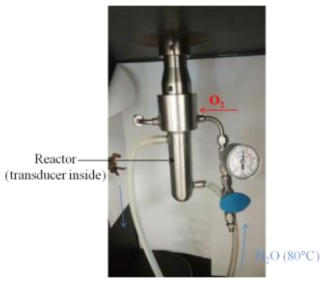

Figure IV. 4 : Experimental set-up for ***A1***$_{HH}$ *cleavage at higher pressure under irradiation by 20 kHz-ultrasounds*

All the experiments performed are summarized in the general scheme (Fig IV. 5).

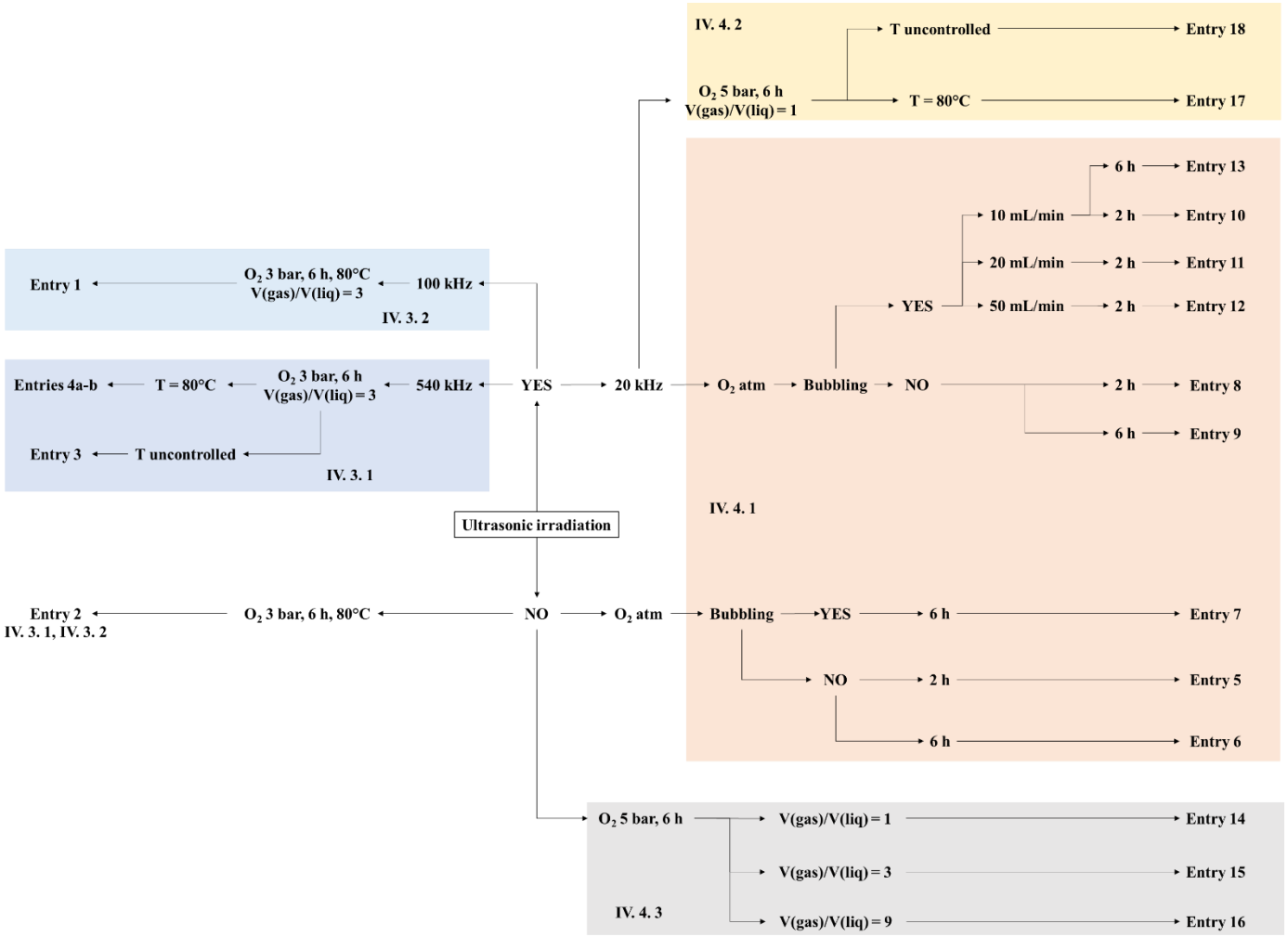

Figure IV. 5: General scheme of the tests carried out in presence under ultrasonic irradiation and/or bubbling

IV. 3. Influence of high (540 kHz) and medium (100 kHz) frequency ultrasounds on $\underline{\mathbf{A1}}_{HH}$ cleavage

IV. 3. 1. Tests at 540 kHz

A test under high frequency ultrasounds irradiation (535 kHz, 0.6 W/L) was carried out during 6 h (Table IV.1, entry 1). The reactor was externally heated to 80°C. The results gathered in Table IV.1 show that the conversion increases from 24% in the absence of ultrasounds (Table IV. 1, entry 2) to 31% upon ultrasound irradiation at 540 kHz. However, the yield of the C-O and C-C cleavage products so as of $\underline{\mathbf{K1}}_{HH}$, $\underline{\mathbf{Est}}^{\alpha}\underline{\mathbf{A1}}_{HH}$ and $\underline{\mathbf{D1}}_{HH}$ were lower. For instance, exposition to ultrasounds gave rise to a combined yield of benzaldehyde and benzoic acid 2.5 times lower compared to the test in silent conditions (entry 1 *vs* 2) and the selectivity to C-O cleavage (phenol + *p*-quinone) was 6.4% (entry 1) whereas the yield of phenol was 8.8% in silent conditions (entry 2). So, **side reactions took place to a higher extent as conversion raised**. Therefore, high frequency ultrasounds have a **negative impact on the production of C-C and C-O cleavage products**. This may mean that side reactions as carbon dioxide production by pyrolysis and condensation reactions took place to a higher extent.

Using high-frequency ultrasounds favors sonolysis of the solvent, which was largely proved to occur in water, however, the sonolysis of acetonitrile has not been extensively studied. As shown by WEISSLER [10], acetonitrile can be homotically cleaved into methyl and cyanide radicals. Methyl radicals give rise to methylation reactions. By an analogy with $HO^{\cdot}$ radicals, cyanide radicals ($CN^{\cdot}$) can be considered as strong oxidants [11] and cyanogen $(CN)_2$ through recombination and cyanates through oxidation by $HO^{\cdot}$ can be produced *in situ*. By an analogy with the radicals $HO^{\cdot}$ and $HO_2^{\cdot}$, it can be deduced that such reactions may give rise also to side reactions with $\underline{\mathbf{A1}}_{HH}$ leading to a degraded mass balance.

IV. 3. 2. Tests at 100 kHz

Since using high-frequency ultrasounds (540 kHz) led to non selective oxidation and to the activation of parallel and undesired reactions, the cleavage of $\underline{\mathbf{A1}}_{HH}$ was assayed in the presence of medium-frequency (100 kHz) ultrasounds. Using medium-frequency ultrasound irradiation may help controlling the extent and the selectivity of the reaction, leading to higher cleavage products yields. Moreover, at 100 kHz, bigger size bubbles will be excited contributed to the enhancement of physical and mass transfer phenomena. An experiment was carried out

without any external heating, under pseudo-adiabatic conditions (Table IV. 1, entry 3). **After 6 h, the temperature reached only 50°C. The conversion reached 3.6% and the oxidative cleavage was barely observed**. It was therefore decided to heat up the reactor using an external heating mantle at 80°C. In this case, after 6 h of irradiation, the temperature of the reaction media reached 85°C that is close to the temperature set by the heating system. This experiment (test 4) resulted in a high conversion (62%). However, the yield of cleavage products showed to be not significantly enhanced compared to the test in silent conditions (PhOH: 8.8%, PhCHO + PhCOOH: 10.7%, entry 2). Although the use of medium-frequency ultrasounds may be positive for the intensification of this oxidative cleavage reaction, its impact on the conversion and selectivity deserves further investigation. It remains true that at 100 kHz, some radical formation cannot be excluded. However, this it not yet clear when using acetonitrile as reaction media. Dioxygen mass transfer under ultrasonic irradiation may be the main reason for achieving higher conversion in comparison to silent tests.

IV. 4. Influence of low frequency ultrasounds (20 kHz) on A1$_{HH}$ cleavage

The tests at atmospheric pressure were carried out in presence of low-frequency ultrasounds at 20 kHz. Besides, it is well-known that oxygen transfer is one of the main limiting factors for lignin aerobic cleavage. Adequate oxygen diffusion in the liquid phase contributes to its saturation, making it available for the oxidation reaction, and enhances the elimination of other eventual gaseous compounds, such as the carbon dioxide formed during the reaction. Therefore, enhancing oxygen diffusion and mass transfer in the liquid phase may lead to improved oxidative cleavage. Low frequency ultrasound is known for highly contributing to enhancing mass transfer through the implosion of bubbles of relatively bigger size resulting in good mixing and turbulence. Moreover, the influence of oxygen bubbling in the absence and in the presence of low frequency ultrasounds was also assessed, since it may also contribute to improved oxygen transfer.

Table IV. 1: Tests carried out with irradiation by a high frequency ultrasound

Entry	Frequency (kHz)	Control of temperature ?	Conversion (%)	Yield (%)							Carbon balance (%)
				PhOH	p-quinone	PhCHO	PhCOOH	**K1**$_{HH}$	**Est**$^{\alpha}$**A1**$_{HH}$	**D1**$_{HH}$	
1	540	Yes	31	2.6	3.8	2	2.3	4.5	6.3	9.6	94
2[a]	-	Yes	24	8.8	-	7.6	3.1	7.2	5.9	8.7	110
3[b]	100	No	3.6	0	-	0	0	2.9	1.7	1.3	104
4	100	Yes	62	9.4	-	5.3	6.4	9.8	12	13	62

O_2 3 bar, V_3-BM_{50} (Mo+V 15 mol%), MeCN + 10% AcOH 80°C, 6 h, volumic ratio gas/liq = 3
[a]Test without ultrasound, stirring by a magnet (see II. 6); [b]The temperature reached 50°C at the end of the test

Table IV. 2: Catalytic tests in atmospheric pressure

Entry	Ultrasonic power (mW/mL)	Duration (h)	Oxygen flow (mL/min)	Bubbling ?	Conversion (%)	Yield (%)						Selectivity (%)		Carbon balance (%)
						PhOH	PhCHO	PhCOOH	**K1**$_{HH}$	**Est**$^{\alpha}$**A1**$_{HH}$	**D1**$_{HH}$	C-O cleavage	C-C cleavage	
5	0	2	10	No	18	0.7	1.2	2.4	4.1	5.2	6.5	3.7	20	99
6		6		No	28	1.5	1.6	3.0	6.3	6.3	8.1	5.1	16	98
6bis		6		No	26	2.0	1.3	2.9	6.2	6.4	7.8	7.9	16	101
7		6		Yes	31	1.2	1.7	3.0	7.1	6.0	7.4	3.9	15	95
8[a]	0.93	2	10	No	21	1.0	1.0	2.2	2.6	2.6	5.2	5.0	15	92
9[a]		6	10	No	33	6.1	3.1	3.3	4.3	5.4	6.4	19	19	89
10[a]		2	10	Yes	24	1.7	1.1	2.5	3.4	6.1	5.6	7.0	15	93
11[a]		2	20	Yes	28	3.6	1.7	3.0	3.8	4.2	5.5	13	16	89
12[a]		2	50	Yes	33	3.9	2.7	3.2	4.2	4.6	4.5	12	18	87
13[a]		6	10	Yes	46	13	4.8	5.0	4.3	4.5	5.2	27	21	78

Atm. O_2, **A1**$_{HH}$ 100 mM, V_3-HT (Mo+V 15 mol%), MeCN- 10 vol% AcOH 15 mL, 80°C
[a]Cooling by water (72°C)

IV. 4.1. Tests at atmospheric pressure

Firstly, the effect of the experiment duration without bubbling and without ultrasound was studied (Table IV. 2, entries 5-6bis). The conversion reached 18% after 2 h (entry 5) of reaction and 28% after 6 h (entry 6 and 6bis). However, the yield of phenol (0.7% after 2 h and 1.5 % after 6 h) so as the combined yield of benzaldehyde and benzoic acid (3.6% after 2 h and 4.6% after 6 h) are very low though the conversion. So, the selectivity to C-O cleavage was very low (5.1% after 6 h, entry 6). Yet, other C-O cleavage products, such as phenylglyoxylic acid (see II. 2) are not quantified. The selectivity for C-C cleavage products was 15% after 6 h (entry 6). Dimeric products (**D1**$_{HH}$ at a higher extent with a yield of 8.1% after 6 h, entry 2) were favored. Moreover, a repetition of the test 6 enabled to show the results are reproducible. Indeed, for an 80% confidence limit, the incertitude on the conversion and the yield of phenol is 16%, 7% on the yield of benzaldehyde and 1% and even lower on the yield of the other products. The effect of bubbling was assessed (entry 7 vs 6) after 6 h. Under silent conditions bubbling did not had a noticeable impact on conversion, so as on the yield of oxidative cleavage products and dimeric by-products. Indeed, the conversion was 31% (entry 7, *vs* 26% without bubbling) and the selectivity to cleavage products did not raise (C-O cleavage: 3.9% with bubbling *vs* 7.9% without bubbling, C-C cleavage: 15% *vs* 16%).

Afterwards, the effect of 20 kHz ultrasound was studied in the absence of bubbling (entries 8-9 vs 5-6). After 2 h of reaction, 20 kHz ultrasound irradiation had almost no impact on the activity and selectivity of the cleavage reaction. For instance, after 2 h, the conversion was 21% under irradiation (entry 8) and 18% in silent conditions (entry 5) and the yields of phenol, benzaldehyde and benzoic acid were 1, 1 and 2.2% respectively under irradiation (entry 8) and 0.7, 1.2 and 2.4% in silent conditions (entry 5). Also, after 6 h (entry 9 *vs* entry 6), the conversion was neither significantly higher in presence of ultrasounds (33% under irradiation, entry 9 *vs* 26% in silent conditions, entry 6), but the selectivity to C-O cleavage was improved (C-O cleavage: 19% (entry 9) *vs* 5% (entry 6)). The combined effect of bubbling and ultrasound was then assessed (Table IV. 2, entries 10-12). The duration was set to 2 h. The oxygen flow was adjusted either to 10 (entry 10), 20 (entry 11) or 50 mL/min (entry 12). The conversion (from 24 to 33%) and the combined yield of benzaldehyde and benzoic acid (from 3.6 to 5.9%) increased with the oxygen flow (entries 10-12). However, it had not a significant impact on the selectivity to C-C cleavage. Moreover, the yield of phenol was not impacted significantly (1.7-3.9%). Consequently, the duration was raised to 6 h and the oxygen flowing set to 10 mL/min. In presence of bubbling (entry 13), there is a notable boost of conversion (46% vs 33% without bubbling) and of phenol production (13% vs 6.1%). The combined yield of benzaldehyde and

benzoic acid rose from 6.4% (entry 9) to 9.8% (entry 13). There was only a slight decrease of the yield of **Est**$^{\alpha}$**A1**$_{HH}$ (4.5% with bubbling (entry 9) *vs* 5.4% without bubbling (entry 13)) and **D1**$_{HH}$ (5.2% with bubbling (entry 13) *vs* 6.4% without bubbling (entry 13)) and the carbon balance decreased from 89% (entry 9) to 78% (entry 13). It can be therefore concluded that the carbon balance was only a little impacted, in spite of the important increase of the conversion observed (from 33% to 46%). Consequently, bubbling boosted both the activity and the selectivity to cleavage products. Low frequency ultrasound proved then to be efficient for the intensification of this oxidative cleavage reaction. This is due to the particular conditions created by ultrasound irradiation at 20 kHz resulting in the excitation and implosion of bubbles of relatively big diameters, *i.e.* the ones created upon bubbling of gaseous oxygen in the liquid reaction media. The cavitation and collapse of these bubbles induced by the low frequency ultrasounds may lead to improved oxygen diffusion and to increased reaction rate and favored cleavage. Ultrasonic irradiation at 20 kHz and bubbling act therefore in synergy with V_3-BM_{50} catalyst for aerobic oxidative cleavage of **A1**$_{HH}$. In addition, without bubbling, the cavitation bubbles contain only a slight amount of oxygen and are composed mainly of solvent vapor (acetonitrile mainly as it is the most volatile). So, oxygen activation is slowed down. Bubbling enabled on the one hand generation of bubbles than can cavitate and on the other hand to trap more oxygen in the cavitation bubbles, which led to an enhanced production of oxygen active species. As a consequence of these encouraging results, catalytic tests under a higher pressure were carried out.

IV. 4.2. Influence of the gas to liquid volumic ratio

As detailed in the experimental part (IV. 2.4), the volumic ratio gas/liquid in the experiments performed at higher pressure conditions is lower than in the tests under atmospheric pressure (1 instead of 3). Therefore, the influence of this parameter had to be studied first for interpretation of the results in the following sections. Also, it has to be specified that the area of the interface gas-liquid is lower in the tests under higher pressure (9 cm²) than in the case of tests in silent conditions (≈102 cm²), as detailed in section 2. 6. 1. Consequently, catalytic tests varying the ratio gas to liquid were carried out. Also, the oxygen to substrate molar ratio was calculated. It was hypothesized that oxygen is a perfect gas and the solvent is incompressible. So: $\boxed{\frac{n_{O_2}}{n_{subs}} = \frac{\frac{P_{O_2}V_{gas}}{RT}}{C_{subs}V_{liq}} = \frac{P_{O_2}}{RTC_{subs}}\frac{V_{gas}}{V_{liq}}}$ (Eq IV. 7)

Therefore, P(O_2) = 5 bar and T = 20°C, $\boxed{\frac{n_{O_2}}{n_{subs}} \approx 2.05\frac{V_{gas}}{V_{liq}}}$ (Eq IV. 8)

This parameter showed to have a low impact on the conversion of the substrate (Table IV. 3, entries 14-16, 24-32%) and the yield of cleavage products so as of the dimeric by-products. For instance, the yield of benzaldehyde varied from 2.1 to 2.9% and the yield of benzoic acid from 3.1 to 3.9%. The yield of **Est**$^{\alpha}$**A1**$_{HH}$ decreased slightly from 7.9 (entry 14) to 6.0% (entry 16) and the yield of **K1**$_{HH}$ decreased from 12 (entry 14) to 9.3% (entry 16).
At the sight of these results, one can conclude that bubble formation inside the liquid is more important than the gas to liquid volumic ratio. Under reaction conditions, it is the contact surface between the gas phase and the liquid and not the volumic ratio that determines the yield of oxidation products. Indeed, the presence of bubbles will increase the effective surface for transferring the dioxygen to the liquid medium.

IV. 4.3. Tests at higher pressure

The dioxygen pressure was raised to 5 bar (before heating) and the volumic ratio gas to liquid was 1. Here, *p*-quinone was quantified even if the yield is not very precise (see II. 3). A first test with control of temperature was carried out (Table IV. 4, entry 17) and compare to the test without ultrasound and with the same ratio gas to liquid. The conversion showed to be much lower (4% under irradiation (entry 17) *vs* 26% without irradiation (entry 14)). Actually, the interface surface gas-liquid is much smaller in the 20 kHz ultrasonic reactor than in the autoclave used in silent tests. Therefore, the oxygen transfer was more hindered, which is detrimental for the cleavage reaction.

Consequently, the temperature was not controlled. In such conditions, the temperature was most probably largely higher than 80°C. The final oxygen pressure at room temperature was 2 bar meaning that 60% of the oxygen was consumed. The conversion was consequently very high (94%, entry 18) and the combined yield of phenol and *p*-quinone reached 29%. The yield of phenol was 17% (*vs* 0.8% with a temperature control (entry 17) and 2.7% without ultrasound (entry 14)) and unlike the tests with temperature control (entry 17) and without irradiation (entry 14), *p*-quinone was obtained with a yield of 12%. Therefore, phenol over-oxidation took place at a higher extent due to a higher temperature. The yield of **K1**$_{HH}$ was 7.2%, which is three times higher than in the test with a control of temperature (entry 17), but is slight lower than in the test without irradiation. This means **K1**$_{HH}$ cleavage was accelerated under ultrasounds, which is the cleavage of the ketone substrate already proved to be easy (see II. 4.1 and III. 4.1) Moreover, such conditions led to an enhancement of selectivity to C-O (including *p*-quinone). The production of **D1**$_{HH}$ was not significantly modified compared to the

test in silent conditions (entry 14) and the production of **Est**$^{\alpha}$**A1**$_{HH}$ did not rise much (11% *vs* 7.9%) compared to products from C-O and C-C cleavage, which is encouraging as the acetyl ester of **A1**$_{HH}$ is more resistant to cleavage than **A1**$_{HH}$. This was consequently beneficial for the selectivity to C-C cleavage and especially for C-O cleavage (30% (entry 18) *vs* 10% (entry 14)). However, the carbon balance showed to be poor (61%), which means the side reactions as in the experiments under irradiation by a high-frequency ultrasound were accelerated. At 20kHz the reason for this poor carbon balance may be different and mostly related to the higher temperature at which these experiments were performed.

The test under a higher pressure (Table IV. 4, entry 18) without control of temperature and without bubbling is compared to the test at atmospheric conditions with oxygen flowing of 10 mL/min (Table IV. 2, entry 13). Additionally, both tests were compared to the test carried out under 5 bars of dioxygen during 24 h and with a stirring by an helicoidal stirrer without (entry 19) and with of 30 mol% of TEMPO (entry 20) on Table IV. 5. These tests were chosen as references as they were carried out with the same ratio gas to liquid and they gave rise to the best yield of cleavage products. Under higher pressure, the conversion was much higher (94% *vs* 46%). The combined yield of benzaldehyde and benzoic acid was 22% at the end of the test under 5 bar of dioxygen (without control of temperature, entry 18). It has to be noted that similar yields were obtained in silent conditions in presence of 30 mol% TEMPO (ratio gas to liquid = 3, 24 h, see Table IV. 5, entry 20), but the duration had to be lengthened to 24 h.

*Table IV. 3 : Influence of volumic ratio liquid-gas on **A1**$_{HH}$*

Test n°	Volumic ratio gas/liq	n(O_2)/n(**A1**$_{HH}$)	Conv. (%)	Yield (%)						Selectivity (%)		Carbon balance (%)
				PhOH	PhCHO	PhCOOH	**K1**$_{HH}$	Est$^{\alpha}$**A1**$_{HH}$	**D1**$_{HH}$	C-O cleavage	C-C cleavage	
14	1	2	26	2.7	2.1	3.1	12	7.9	11	10	20	113
15	3	6	32	4.5	2.2	3.6	9.2	6.7	8.7	14	18	100
16	9	18	24	3.0	2.9	3.7	9.3	6.0	9.3	13	28	109

A1$_{HH}$ 100 mM, O_2 5 bar, V_3-BM_{50} (Mo+V 15 mol%), MeCN + 10% AcOH 80°C, 6 h

Table IV. 4: Tests carried out with irradiation by a low frequency ultrasound under a higher pressure of oxygen

Entry	US ?	Conv. (%)	Yield (%)							Selectivity (%)		Carbon balance (%)
			PhOH	p-quinone	PhCHO	PhCOOH	**K1**$_{HH}$	Est$^{\alpha}$**A1**$_{HH}$	**D1**$_{HH}$	C-O cleavage	C-C cleavage	
14	No	26	2.7	0	2.1	3.1	12	7.9	11	10	20	113
17	Yes	4	0.8	0	1.3	2.2	3.5	3.3	5.7	20	88	111
18[a]	Yes	94	17	12	8.3	14	7.2	11	13	30	24	61

A1$_{HH}$ 100 mM, O_2 5 bar, n_{oxygen}/n_{subs} = 2, V_3-BM_{50} (Mo + V 15 mol%), MeCN - 10 vol% AcOH; [a]Without control of temperature

Table IV. 5: ultrasonic irradiation vs silent conditions (without and with TEMPO) for $PMoV_3$-catalyzed cleavage

Entry	US[a]	P (O_2) (bar)	Duration (h)	Bubbling[b]	Conv. (%)	Yield (%)							Selectivity (%)		Carbon balance (%)
						PhOH	*p*-quinone	PhCHO	PhCOOH	**K1**$_{HH}$	Est$^{\alpha}$**A1**$_{HH}$	**D1**$_{HH}$	C-O cleavage	C-C cleavage	
9	V	1	6	Yes	46	13	n. d.	4.8	5.0	4.3	4.5	5.2	27	21	78
18[a]	V	5	6	No	94	17	12	8.3	14	7.2	11	13	30	24	61
19	X	5	24	No	54	16	n. d.	7.1	9.8	10	18	21	30	31	118
20[a]	X	5	24	No	45	18	n. d.	9.2	15	7	0	0	40	54	82

Atm. O_2, **A1**$_{HH}$ 100 mM, V_3-HT (Mo + V 15 mol%), MeCN- 10 vol% AcOH, 80°C, volumic ratio gas/liquid = 3; [a]20 kHz, [b]Temperature was not controlled and volumic ratio gas/liquid = 1, [c]With 30 mol% and V_3-HT catalyst instead of V_3-BM_{50} (Mo + V 15 mol%)

At atmospheric conditions with oxygen bubbling; the combined yield of benzaldehyde and benzoic acid was 9.8%. The selectivity to C-O (phenol and *p*-quinone) and C-C cleavage (benzaldehyde and benzoic acid) were respectively 30% and 24% under a higher pressure without temperature control and without bubbling (entry 18) and at atmospheric conditions with oxygen bubbling, they were respectively 27% and 21%. Thus, these two conditions led to similar selectivity for C-O and C-C cleavage. However, *p*-quinone was not detected in atmospheric conditions. Finally, the carbon balance was more degraded under a higher pressure (61%, entry 18) than in atmospheric conditions (78%, entry 13). This is due to an uncontrolled temperature in the case of the test under a higher pressure, which unavoidably leads to favored side conditions due to too harsh conditions. As a result, an atmospheric pressure while using an oxygen bubbling (10 mL/min) are the most adequate conditions for **A1**$_{\text{HH}}$. They gave rise to similar conversion (45-54%) the yield of phenol does not vary significantly (13-18%). The carbon balance obtained under irradiation by ultrasounds (78%, Table IV. 5, entry 9) was similar to the test in presence of TEMPO (82%, entry 20) but much lower compared to the test under 5 bar of oxygen in silent conditions without TEMPO. However, under irradiation by ultrasounds, the combined yield of benzaldehyde and benzoic acid was 9.8% only while it was 17% under a higher pressure and without TEMPO and even 24% in presence of TEMPO. It has to be noted that the duration of the test under irradiation was 6 h instead of 24 h. Yet, without TEMPO, in silent conditions (entry 19) the production of **D1**$_{\text{HH}}$ (21%) and **Est**$^{\alpha}$**A1**$_{\text{HH}}$ (18%) was notably boosted. As a result, parasite reactions are slow down under irradiation by ultrasounds (because of a shorther duration), but they are not cut down contrary to the test in presence of TEMPO. In brief, yields of cleavage products similar to a 24 hour-oxidation can be obtained after irradiation by an ultrasonic wave during 6 h. A limitation is the lower carbon balance in presence of ultrasounds (78% (atm O_2) and 61% (O_2 5 bar) *vs* 118% and 82%). This is due to conversion and side reactions. Atmospheric conditions with oxygen bubbling showed to be the most suitable conditions because of the carbon balance, but it should be noted that the yields of C-C cleavage products have to be improved. Indeed, a higher pressure was more beneficial for C-C cleavage, as it was already showed in II. 6 dealing with preliminary optimization essays for **A1**$_{\text{HH}}$ cleavage.

IV. 5. GC-MS studies

From the tests under irradiation by ultrasonic wave, it can be asserted that side reactions took place during irradiation by ultrasounds. Therefore, GC-MS analyses were performed on

samples of the reaction media from the test i) with oxygen bubbling only (Table IV. 2, entry 3), ii) under irradiation by a 20 kHz-ultrasound, with bubbling (Table IV. 2, entry 9), iii) under irradiation by a 20 kHz ultrasound at higher pressure (5 bar), iv) under irradiation by a 540 kHz-ultrasound under 3 bars of dioxygen. Except 2-hydroxybenzaldehyde (in the case of the test under irradiation by a low-frequency ultrasound at a higher pressure), all the oxidation products were detected (Table IV. 6). The positive impact of ultrasound and bubbling on oxidative cleavage was confirmed by the selectivity for C-C (27% under 5bar + ultrasound, 12% with ultrasound + bubbling) and C-O cleavage (18% under 5bar + ultrasound, 13% with ultrasound + bubbling), which was expected from HPLC data. Moreover, the proportions of phenylacetaldehyde and acetophenone from dehydration-hydrolysis of **A1**$_{HH}$ (see II. 5) so as of *p*-quinone from phenol over-oxidation and phenyl formate and benzoic acid from direct C-C cleavage (see Fig. II. 18) were higher under pressure. Moreover, the test under irradiation by a high frequency-ultrasound stands out by a higher proportions of condensation products and the formation of 4-phenanthrenol from cis-hydroxystilbene thus confirming the results from HPLC. Besides, the proportion of **K1**$_{HH}$ after irradiation by a 540 kHz-ultrasound is lower compared to the test with bubbling only in spite these conditions both give rise to the same conversion. Besides, it can be noticed that the proportions of phenylglyoxylic acid decreases with the conversion. As a result, ultrasonic cavitation accelerates the decarboxylation of phenylglyoxylic acid leading to benzaldehyde and carbon dioxide. Also, the ratio benzaldehyde to benzoic acid is higher than in the tests in silent conditions without bubbling (II. 4.2 and II. 5.2). Therefore, bubbling and ultrasounds led to a boost of direct C-C cleavage in **A1**$_{HH}$ as benzaldehyde and phenyl formate production were favored and it can be hypothesized the irradiation by a low-frequency boost the C-C cleavage in **A1**$_{HH}$ without oxidation into a ketone, which is consistent with the mechanism proposed on Fig II. 23.

Table IV. 6: Products detected by GC-MS after irradiation by ultrasounds

Frequence (kHz)			-	20	20	540
Pressure (bar)			Atm.	Atm.	5	3
Bubbling			Yes	Yes	No	No
Conversion			31	46	94	31
Retention time (min)	Compound	Match (%)	Relative area (%)			
4.0	*p*-quinone 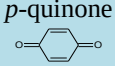	97	0.17	0.18	3.17	0.11
4.9	Phenol (PhOH)	98	8.05	12.1	11.2	10.0
6.3	Phenylacetaldehyde 	98	0.03	0.08	0.17	0.01
6.8	Acetophenone 	88	0.03	0.27	0.66	0.03
6.9	Phenylglyoxylic acid 	91	0.59	0.32	0.12	0.48
12.6	2-hydroxyacetopheneone 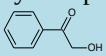	93	0.00	0.00	0.12	0.00
19.6	2-acetoxyacetophenone 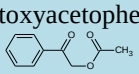	94	0.13	0.23	2.24	0.10
TOTAL C-O CLEAVAGE			9.00	13.2	17.6	10.8
4.7	Benzaldehyde (PhCHO)	98	1.69	3.79	3.69	1.62
4.8	Phenyl formate 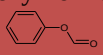	91	1.97	7.68	12.1	1.34
9.3	Benzoic acid (PhCOOH)	95	0.75	0.77	11.0	0.65
17.2	N-acetylbenzamide 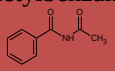	91	0.20	0.04	0.32	0.01
TOTAL C-C CLEAVAGE			4.61	12.3	27.1	4.95
25.8	Phenyl benzoate 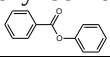		0.16	0.36	1.65	0.17
ESTIMATED SELECTIVITY TO C-O CLEAVAGE			9.16	13.6	19.3	11.0
ESTIMATED SELECTIVITY TO C-C CLEAVAGE			4.77	12.7	28.8	5.12
22.0	Hydroxystilbene 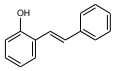	90	1.13	1.58	0.12	1.49
22.8	**D1**$_{HH}$ 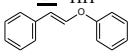	-	13.5	16.6	1.30	17.9
23.3	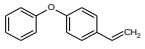	81	6.17	7.91	0.81	7.76
24.8	4-phenanthrenol 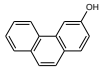	96	0.00	0.00	0.00	0.15
25.6	**K1**$_{HH}$ 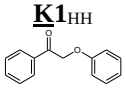		42.4	31.3	29.3	29.4
27.8	**Est**$^{\alpha}$**A1**$_{HH}$ 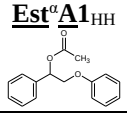		23.1	16.7	22.1	27.3
Proportions of **K1**$_{HH}$+**D1**$_{HH}$+**Est**$^{\alpha}$**A1**$_{HH}$ in dimeric products			86.2	74.1	53.7	84.1

IV. 6. Preliminary tests of ultrasound-assisted lignin aerobic cleavage

Preliminary tests were carried out on a wheat straw Organosolv lignin under irradiation by either a 20 kHz-ultrasound (atmospheric conditions and bubbling, Table IV. 7, entry 23) and a 100 kHz-ultrasound (3 bar, entry 22). The reference is a test carried out under 5 bar of dioxygen at 80°C (entry 21, 6 h). The duration was set to 6 h and the temperature was 80°C. A striking result is ultrasonic cavitation assisted oxidation led to syringaldehyde only with very low yields (0.05-0.06 %). The other aromatic platform molecules were produced only as traces and were barely detected by GC-MS. As a result, ultrasonic cavitation has a negative effect on the production of phenolic aldehydes and acids. Further characterization of lignin has to be done to check the content of β-O-4 linkage and of the proportion of tars among others in order to determinate the reactivity of lignin in these operative conditions.

Table IV. 7: Results of V_3-BM_{50} catalyzed lignin aerobic cleavage

Entry	P (bar)	US ?	f (kHz)	Liquid phase (GC-MS after silylation) Yield of monomers (mol%)[b]					
				Units H		Units G		Units S	
				H	HA	V	VA	S	SA
21	5	No	-	0.16	0	0.29	0	0.12	0
22	3	Yes	100	0	0	0	0	0.06	0
23[a]	1	Yes	20	0	0	0	0	0.05	0

WSL_p 34.2 g/L, V_3-BM_{50} (Mo + V 15.9 mol% according dimeric units), MeCN – 10 vol% AcOH, 80°C, 6 h
[a]O_2 bubbling (10 mL/min), [b]According to moles of each monomer type calculated from ^{31}P NMR data

IV. 7. Conclusions

Ultrasound-assisted oxidation of **A1**$_{HH}$ in presence of a $PMoV_3$ catalyst was assessed. High frequency irradiation (540 and 100 kHz) resulted in moderate conversion and favored condensation reactions due to strong oxidative conditions, which was confirmed by GC-MS analysis.

At low frequencies (20 kHz), high yields of C-C cleavage products can be obtained at both atmospheric pressure and under 5 bars of oxygen after 6 h only instead of 24 h in silent conditions. The conversion was 46% in atmospheric conditions and higher than 90% under a higher pressure. These operative conditions led to similar selectivites to C-O (27-30%) and C-C (21-24%) cleavage. However, the carbon balance at higher pressure was 60% only whereas the minimal carbon balance in silent conditions at 80°C was 82% (test in presence of TEMPO 30 mol%, Table IV. 5, entry 20). It may be explained by pyrolysis and CO_2 formation. The effect of ultrasonic cavitation was to boost the C-C cleavage in **A1**$_{HH}$ as shown by GC-MS studies.

A solution can be to perform a test under pressure to boost C-C cleavage and with bubbling as the conjunction of bubbling and ultrasounds proved to boost **A1**$_{HH}$ cleavage in atmospheric conditions while mitigating the formation of the ester **Est**$^{\alpha}$**A1**$_{HH}$. Also, a major drawback of the test under pressure is the smaller gas-liquid contact surface, which may be detrimental for oxygen transfer. Moreover, the temperature could not be controlled during the test for **A1**$_{HH}$ cleavage and it was presumably much higher than 80°C.

References:

[1]: F. Napoly, N. Kardos, L. Jean-Gérard, C. Goux-Henry, B. Andrioletti, M. Draye, *Ind. Eng. Chem. Res.* **2015**, 5422, 6046-6051.
[2]: G. Chatel, K. de Olivera Vigier, F. Jerôme, *ChemSusChem* **2014**, 7, 2274-2287.
[3]: Y. Liu, Y. Nie, X. Lu, X. Zhang, H. He, F. Pan, L. Zhou, X. Liu, X. Ji, S. Zhang, *Green Chemistry* **2019**, 21, 3499-3535.
[4]: M. Mirza-Aghayana, N. Ganjbakhsha, M. Molaee Tavanaa, R. Boukherroub, *Ultrasonics Sonochemistry* **2016**, 32, 37-43.
[5]: M. Mirza-Aghayan, M. Molaee Tavana, R. Boukherroub, *Tetrahedron Lett.* **2012**, 53, 4962-4965.
[6]: A. Maleki, *Ultrasonics Sonochemistry* **2018**, 40, 460-464.
[7]: R. J. Wood, J. Lee, M. J. Bussemaker, *Ultrasonics Sonochemistry* **2017**, 38, 351-370.
[8]: T. G. McKenzie, F. Karimi, M. Ashokkumar, G. G. Qiao, *Chem. Eur. J.* **2019**, 25, 5372-5388.
[9]: R. Behling, Thèse de doctorat, Université de Poitiers, **2017**
[10]: A. Weissler, I. Pecht, M. Anbar, *Science* **1965**, 150, 1288-1289.
[11]: T. L. Rose, C. Nanjundiah, *J. Phys. Chem.* **1985**, 89, 3766-3771.

CONCLUSION GENERALE / PERSPECTIVES

La lignine et plus largement la biomasse lignocellulosique est l'alternative majeure aux ressources fossiles pour la synthèse des molécules plateformes aromatiques telles que la vanilline. Dans ce travail, l'oxydant choisi pour sa dépolymérisation est le dioxygène, d'une part en raison de sa grande disponibilité et d'autre part, pour des questions de développement durable.

La lignine a une structure très complexe et hétérogène, ce qui fait que des modèles sont très souvent utilisés lors des études préliminaires réalisées en vue de tester de nouvelles formulations de catalyseurs (notamment à base de vanadium, de cuivre ou de cobalt) ou des conditions opératoires différentes. La revue bibliographique présentée au début de ce manuscrit a permis de souligner la masse importante de travail déjà réalisée dans le domaine de la seule dépolymérisation oxydante de la lignine et de ses modèles en présence de O_2. Dans les publications d'origine, la corrélation n'est pas toujours faite entre le comportement des modèles et celui de la, ou mieux des lignines s'y l'on tient compte de l'influence du mode d'extraction. Nous avons cherché à le faire au niveau de la partie IB. Cette étude de l'état de l'art a permis de mettre en exergue de fortes diminutions des rendements en produits de clivage lors du passage des modèles à la lignine (maximum de 30% pour la lignine). Nous avons retenu notamment qu'une des causes est que la lignine est altérée par les procédés d'extractions et devient ainsi plus récalcitrante à l'oxydation. Il apparaît donc plus judicieux de choisir une **lignine extraite dans les conditions les plus douces possibles**. Les différences entre lignines et modèles ont bien évidemment des origines structurelles mais il s'agit également de problématiques de mises en œuvre des réactions qui apparaissent plus du ressort du génie des procédés (solubilité du dioxygène, notamment). **Le transfert de matière est en effet un des paramètres cruciaux** des processus de dépolymérisation.

Des catalyseurs déjà utilisés au niveau de l'étape en amont que constitue la délignification au dioxygène et qui ont été encore peu testés jusqu'à présent pour le clivage de la lignine en molécules aromatiques plateformes sont les molybdovanadophosphates **$PMoV_x$ de KEGGIN ($H_{3+x}PMo_{12-x}V_xO_{40}$)** évoqués au niveau du point bibliographie **IB**. Ces derniers ont déjà donné des résultats prometteurs pour le clivage de liaisons simples C-C et C-O dans les molécules simples telles que les α-hydroxycétones lors des travaux réalisés dans notre laboratoire ainsi que pour l'oxydation des dérivés de l'alcool benzylique. Les $PMoV_x$ peuvent être synthétisés par plusieurs voies conventionnelles, dont les voies étherates qui sont celles qui reviennent le plus souvent dans la littérature. Cependant, ces dernières impliquent un solvant organique

(éther) nocif pour l'environnement et pour l'homme et des acides forts (acide sulfurique par exemple), ce qui nous a orientés vers une voie plus simple à mettre en œuvre, **la voie hydrothermale**.

Comme indiqué plus tôt, le **transfert du dioxygène au sein du milieu réactionnel est important**, ce qui nous a amené à proposer pour la première fois dans le cadre de la dépolymérisation oxydante de la lignine une assistance **sono-chimique.** Le point bibliographique IC laisse penser en effet que les **phénomènes de cavitation** devraient permettre d'intensifier le processus, ce qui a été démontré notamment grâce à l'étude de tests d'oxydation de l'alcool benzylique et dérivés rapportés dans la littérature. Les rendements obtenus en benzaldéhyde ont été accrus. Cette voie reste néanmoins marginale (3 occurrences seulement depuis 2 décennies !) et seules des basses fréquences ont été utilisées. Or, des hautes fréquences peuvent être plus adaptées pour favoriser le phénomène sono-chimique qui aboutit à la formation d'espèces actives du dioxygène ($O_2^{\cdot -}$, $HO^{\cdot}$) *in situ* à partir du dioxygène. Ainsi, au vu des modes d'action des $PMoV_x$ mis en évidence dans la partie IB, nous avons souhaité étudier la possibilité d'une synergie entre **la voie sono-chimique et les $PMoV_x$ pour la dépolymérisation oxydante de la lignine.**

Lors de ce travail, des $PMoV_x$ ($PMoV_1$ et $PMoV_3$) synthétisés « classiquement », par voie hydrothermale, ont d'abord été testés comme catalyseurs de clivage oxydant aérobie sur deux modèles des liaisons β-O-4 de la lignine, à savoir sur **K1**$_{HH}$ (2-phénoxyacétophénone) et **A1**$_{HH}$ (1-phényléthanol). Les $PMoV_x$ retenus ont été synthétisés par attaque acide (H_3PO_4) des oxydes de départ dans l'eau. Ils ont été caractérisés par DRX, RMN ^{31}P, ICP et ATG. Une structure de KEGGIN tridécahydratée a été confirmée pour les deux $PMoV_x$ (DRX + ATG) et les rendements obtenus sont de 89% ($PMoV_1$) et 79% ($PMoV_3$) respectivement. **La voie hydrothermale est donc apparue plus adaptée à la synthèse des $PMoV_x$ à faible taux de vanadium**. Ces deux solides ont ensuite été testés comme catalyseurs pour le clivage oxydant du modèle **K1**$_{HH}$ (100 mM) sous pression atmosphérique de dioxygène (82°C, 24 h). Une optimisation préliminaire des conditions opératoires a permis de montrer que le solvant le plus adapté est **l'acétonitrile acidifié par de l'acide acétique (10 vol%)** et que la charge **optimale de métaux (Mo + V) est de 15 mol%**. Dans ces conditions, la **conversion de K1**$_{HH}$ **est de 82% en 24 h avec un rendement en phénol de l'ordre de 52% tout comme le rendement combiné en benzaldéhyde et en acide benzoïque (bilan carbone de 79%).**

Néanmoins, la structure de **K1**$_{HH}$ est peu similaire à celle de la lignine. Ainsi, le modèle **A1**$_{HH}$ a aussi été oxydé dans les mêmes conditions. Ce dernier s'est **révélé être plus résistant au**

clivage que <u>K1</u>$_{HH}$ et trois produits issus de réactions secondaires ont été mis en évidence : **<u>K1</u>**$_{HH}$, **<u>Est</u>$^{\alpha}$<u>A1</u>**$_{HH}$ (ester acétique de **<u>A1</u>**$_{HH}$) et **<u>D1</u>**$_{HH}$ (2-phenoxystyrène), produit de déshydratation de **<u>A1</u>**$_{HH}$). Des tests catalytiques à pression et température plus élevées ont donc été réalisés**. La sélectivité combinée en benzaldéhyde et acide benzoïque a été maximisée** (32%) à pression plus élevée (**O_2 5 bar**) et pour une température de **120°C pendant 2 h (bilan carbone de 96%)**. Aussi, nous avons réalisé des tests en présence d'un co-oxydant destiné à favoriser une pré-oxydation de **<u>A1</u>**$_{HH}$ en **<u>K1</u>$_{HH}$. L'ajout de 30 mol% de TEMPO s'est révélé être bénéfique pour la sélectivité en produits de clivage des liaisons C-O (phénol, 40%) et C-C (benzaldéhyde + acide benzoïque, 54%)**. Cependant, le TEMPO perd en partie son activité après recyclage.

Etant donné que **<u>A1</u>**$_{HH}$ est résistant à l'oxydation, il nous est apparu plus judicieux de privilégier des **voies de synthèse des $PMoV_x$ plus adaptées aux valeurs de x élevés**, ce qui nous a orientés vers une voie **hybride « ball-milling/hydrothermale »**. Les oxydes de départ (MoO_3 et V_2O_5) ont donc été broyés dans un broyeur à billes, ce qui a donné un oxyde mixte dont **l'attaque, plus courte** (1,5 h *vs* 6,5 h pour $PMoV_3$), peut se faire à **température plus basse** (80°C) que dans le cas de la seule voie hydrothermale (100°C). Plusieurs paramètres (ratio billes/oxydes, temps de broyage et d'attaque hydrothermale) ont été testés. Cette approche a donné lieu à des **rendements en $PMoV_x$ plus élevés** ($PMoV_3$: 97% *vs* 79% pour la voie hydrothermale) et est aussi plus **économe en énergie**, notamment pour la synthèse des $PMoV_3$ (422 *vs* 618 kW.h). Les $PMoV_x$ obtenus par une telle voie ont montré une **activité peu différente de celle des $PMoV_x$ obtenus par la voie hydrothermale** que ce soit pour le clivage de **<u>K1</u>**$_{HH}$ ou de **<u>A1</u>**$_{HH}$. Cette étude a montré par ailleurs qu'il est préférable de **privilégier des étapes de broyage et d'attaques courtes**. Noter également que des travaux préliminaires visant à synthétiser des $PMoV_x$ selon une voie 100% ball-milling ont été entrepris avec un relatif succès. En fin de cette partie, un $PMoV_3$ synthétisé par la voie hybride « ball-milling/hydrothermale » a été testé comme catalyseur pour le clivage oxydant (O_2 5 bar) d'une lignine de paille de blé Organosolv. Les produits visés (aldéhydes et acides aromatiques) ont été obtenus avec de **très faibles rendements (120°C, 6 h)** à défaut d'un transfert de matière suffisant (solubilité modérée de O_2 et insolubilité de la lignine).

Ceci nous a incités à mettre en œuvre une assistance sono-chimique. Afin d'améliorer le clivage de **<u>A1</u>**$_{HH}$, nous avons testé plusieurs fréquences (20, 100 et 540 kHz) en présence du $PMoV_3$ synthétisé par la voie hybride « ball-milling/hydrothermale » (Mo + V 15 mol%, 80°C, 6 h). Sous irradiation par des **ultrasons à moyenne et à haute fréquence, les conversions**

obtenues sont modérées et les réactions secondaires ont été favorisées. Les tests en présence d'ultrasons à basse fréquence (20 kHz) ont été réalisés soit à pression atmosphérique avec et sans bullage, soit sous 5 bar de dioxygène (température non contrôlée). La **conjonction bullage et ultrasons a permis de multiplier les rendements en phénol et en produits de clivage de la liaison C-C (benzaldéhyde et acide benzoïque) par 6 et 2 respectivement**. Sous pression, le phénol (17% *vs* 18%) ainsi que le benzaldéhyde et l'acide benzoïque (somme : 22% *vs* 24%) ont été obtenus avec des **rendements similaires aux tests sans irradiation** (O_2 5 bar, 120°C, 24 h, présence de 30 mol% de TEMPO) **mais après 6 h au lieu de 24 h.**

Nos travaux ont permis d'établir que ***K1****$_{HH}$ est plus facile à oxyder que* ***A1****$_{HH}$. Aussi, il pourrait être intéressant de procéder à un clivage en deux étapes au moyen de deux systèmes catalytiques différents. Ainsi, i)* ***A1****$_{HH}$ pourrait être* ***oxydé au préalable en K1$_{HH}$ en l'absence d'acide acétique*** *pour éviter la formation de l'ester* ***Est$^{\alpha}$A1$_{HH}$*** *résistant au clivage et en présence d'un* ***co-oxydant tel que le TEMPO*** *puis ii)* ***K1****$_{HH}$ serait alors* ***oxydé sous atmosphère de dioxygène en présence de O_2/PMoV$_3$*** *comme décrit dans ce manuscrit. Pour aller dans ce sens, nous avons reproduit des conditions de la littérature (****VOSO$_4$/TEMPO 20 mol%****). Ce système s'est révélé être efficace pour oxyder l'alcool en cétone, mais le TEMPO a perdu en activité après recyclage et opère en homogène. Nous pensons que, dans la suite, il pourrait être intéressant d'utiliser une forme de* ***TEMPO hétérogénéisé.***

Il faut également signaler que les PMoV$_x$ opèrent en homogène et que les composés du vanadium (V) sont réputés pour avoir une certaine toxicité. Des tests impliquant des ***cations VO^{2+} ancrés sur du SAC-13*** *partiellement échangé (Nafion supporté sur silice) ont été réalisés sur* ***A1****$_{HH}$ (O_2 5 bar, VO^{2+} 15 mol% par rapport au substrat, MeCN + 10 vol% AcOH, 120°C, 6 h). Une* ***conversion de 35% ainsi qu'une sélectivité en produits de clivage (C-O : 18%, C-C : 21%) ont été obtenus****. Cette voie mérite donc d'être exploitée davantage. Un tel catalyseur pourrait être associé au TEMPO pour l'oxydation de* ***A1****$_{HH}$ en* ***K1****$_{HH}$.*

En ce qui concerne les tests en présence d'ultrasons à basse fréquence et sous pression (5 bar), il n'y avait pas de contrôle de température dans les essais préliminaires. Afin d'améliorer le bilan matière, vu que la ***conjonction bullage et ultrasons s'est révélée être efficace pour le clivage oxydant de A1$_{HH}$****, il pourrait être pertinent de réaliser des tests* ***sous bullage et sous pression.***

Résumé : Du fait de l'épuisement des ressources fossiles, l'intérêt de la lignine en tant qu'alternative durable est grandissant. Ainsi, le but principal de cette thèse était de mettre au point un procédé de clivage oxydant de la lignine par le dioxygène qui implique des voies non conventionnelles (sonochimie, ball-milling). Les catalyseurs utilisés sont des molybdovanadophosphates de KEGGIN. D'abord, nous avons optimisé les conditions opératoires (solvant, charge catalytique et taux de vanadium) pour le clivage, à pression atmosphérique de deux modèles, *la* 2-phénoxyacétophénone (**K1**$_{HH}$) et le 2-phénoxy-1-phenyléthanol (**A1**$_{HH}$) en phénol, en benzaldéhyde et en acide benzoïque. Pour **A1**$_{HH}$, des conditions plus dures se sont avérées être nécessaires (O_2 5 bar, 120°C). Le catalyseur est synthétisé conventionnellement par la voie hydrothermale qui consiste à attaquer MoO_3 et V_2O_5 dans l'eau à reflux en présence de H_3PO_4. Une longue durée de chauffage est souvent requise pour des rendements modérés. La synthèse par ball-milling a donc été envisagée. Elle consiste à préparer un oxyde mixte par broyage. L'attaque de ce dernier est alors plus courte, se déroule à plus faible température et donne lieu à des rendements en catalyseur plus élevés. Leur activité pour le clivage des modèles est similaire à celle de leurs homologues synthétisés par voie hydrothermale. Des tests préliminaires sur une lignine Organosolv issue de la paille de blé dans des conditions optimisées ont donné des faibles rendements en produits de clivage. L'assistance sonochimique a donc été testée montrant, dans le cas de **A1**$_{HH}$, qu'une basse fréquence en conjonction avec un bullage de dioxygène constitue la meilleure option.

Mots-clés : Valorisation de la biomasse, lignine, oxydation aérobie, molybdovanadophosphates, ball-milling, intensification sono-chimique.

Abstract: Due to the depletion of fossil resources, the interest of lignin as a sustainable alternative to petroleum is growing. Thus, the main purpose of this thesis was to develop a process for oxidative cleavage of lignin by dioxygen that involves unconventional methodologies like sonochemistry and ball-milling. The catalysts used here were KEGGIN molybdovanadophosphates ($PMoV_x$). First, the operating conditions (solvent, catalytic charge and vanadium content) were optimized to afford the cleavage of two models, 2-phenoxyacetophenone (**K1**$_{HH}$) and 2-phenoxy-1-phenylethanol (**A1**$_{HH}$), at atmospheric O_2 pressure, into phenol, benzaldehyde and benzoic acid. For **A1**$_{HH}$, harsher conditions were found to be necessary (O_2 5 bar, 120°C). The catalysts were conventionally synthesized using a hydrothermal pathway, which consists in the H_3PO_4 attack of MoO_3 and V_2O_5 in reflux water. A long heating period is often required to get moderate yields of $PMoV_x$. Ball-milling synthesis was therefore considered. It consisted in preparing a mixed oxide by grinding MoO_3 and V_2O_5. The latter's attack by H_3PO_4 was then shorter, took place at a lower temperature and resulted in higher yields of $PMoV_x$. The activity of thus obtained $PMoV_x$ for model cleavage was similar to that of their hydrothermally synthesized counterparts. Preliminary tests on an Organosolv lignin from wheat straw under optimized conditions yielded low yields of cleavage products. Sonochemical assistance was therefore tested showing, in the case of **A1**$_{HH}$, that a low frequency in conjunction with dioxygen bubbling was the best option.

Keywords: Biomass valorization, lignin, aerobic oxidation, molybdovanadophosphates, ball-milling, sonochemical intensification